

University of Southampton Research Repository ePrints Soton

Copyright © and Moral Rights for this thesis are retained by the author and/or other copyright owners. A copy can be downloaded for personal non-commercial research or study, without prior permission or charge. This thesis cannot be reproduced or quoted extensively from without first obtaining permission in writing from the copyright holder/s. The content must not be changed in any way or sold commercially in any format or medium without the formal permission of the copyright holders.

When referring to this work, full bibliographic details including the author, title, awarding institution and date of the thesis must be given e.g.

AUTHOR (year of submission) "Full thesis title", University of Southampton, name of the University School or Department, PhD Thesis, pagination

UNIVERSITY OF SOUTHAMPTON

FACULTY OF CHEMISTRY

Department of Chemistry - Faculty of Organic Chemistry: Synthesis, Catalysis
and Flow

Volume 1 of 1

**“Synergistic catalysis: merging amino catalysis and metal Lewis acid
activation of azaarenes; Green chemistry: first organophotocatalytic
approach to the synthesis of phosphoramidates”**

Section 1

**“Synergistic catalysis: merging amino catalysis and metal Lewis acid activation of
azaarenes”**

Section 2

**“Green chemistry: first organophotocatalytic approach to the synthesis of
phosphoramidates”**

by

Marta Meazza

Thesis for the degree of Doctor of Philosophy

February 2016

ABSTRACT – Section 1

FACULTY OF NATURAL AND ENVIRONMENTAL SCIENCES

Organic Chemistry

Thesis for the degree of Doctor of Philosophy

**DEPARTMENT OF CHEMISTRY - FACULTY OF ORGANIC CHEMISTRY: SYNTHESIS,
CATALYSIS AND FLOW**

Marta Meazza

The art of building complex chemical scaffolds in a totally stereoselective manner is one of the cornerstones for Organic Chemists. The quest for new catalytic methodologies that fulfil the requirements of efficiency, green chemistry and predictable stereochemical outcome have become the Holy Grail for synthetic chemists.

In the present thesis we investigated new catalytic strategies for the enantioselective synthesis of azaarene scaffolds. Alkyl-azaarenes are common motifs in natural products and pharmaceutical compounds, however few methodologies are devoted to their functionalisation in an enantioselective manner. The major part of the approaches are based on the use of stoichiometric strategies and chiral auxiliaries due to the difficulty to activate the methylene position of alkylazaarenes. Our innovative approach relies on the use of a synergistic strategy where a Lewis acid activates the azaarene moiety making it a nucleophile while a Lewis base catalyst activates the electrophile. This dual activation presents several advantages such as an easy optimisation of each catalytic cycle and a greater decrease of the activation energy required for the reaction, allowing the use of low temperatures and soft conditions.

In Chapter 4 we demonstrate the proof of concept of this approach by joining transition metal catalysis (Lewis acid) and secondary amine catalysis (Lewis base, iminium activation) achieving the enantioselective addition of alkyl-benzoxazoles and related heterocycles to enals in good yields and reasonable stereoselectivity levels. In Chapter 5 we expanded this new concept in the application of cascade reactions. We designed a cascade reaction consisting in the Michael addition of chloromethylbenzoxazoles to enals followed by a 3-exo-trig cyclisation to furnish cyclopropanes in good yields and enantioselectivities.

The value of the present work is not only the development of these methodologies for the synthesis of chiral azaarenes (aldehyde derivatives and cyclopropanes) but also to demystify some misconceptions such as that metal Lewis acid could not coexist with secondary amine catalysis.

This pioneering work is an open gate to generate new methodologies using a synergistic approach that tries to take the best of two of the pillars of catalysis: the high activity and rich chemistry of transition metal catalysis with the affordable and easy stereochemical prediction of secondary amine catalysis, avoiding the use of extreme reaction conditions or the use of chiral ligands.

UNIVERSITY OF SOUTHAMPTON

ABSTRACT- Section 2

FACULTY OF NATURAL AND ENVIRONMENTAL SCIENCES

Organic Chemistry

Thesis for the degree of Doctor of Philosophy

**DEPARTMENT OF CHEMISTRY - FACULTY OF ORGANIC CHEMISTRY:
SYNTHESIS, CATALYSIS AND FLOW**

Marta Meazza

Photocatalysis has become lately a common strategy for the synthesis of new atom-atom bond. Light is a renewable source that should be witnessed as the future for industrial processes.

Our research group started a quest of new green procedures and, for this reason, we turned our attention to photocatalysis. The use of light as the initiator of a chemical reaction presents several advantages in terms of renewable source of energy, cost and generation of waste.

On the other hand, atom economy should be one of the main driving forces in the design of new strategies for the synthesis of organic compounds. In this area, Cross Dehydrogenative Couplings have emerged as a useful approach. Formally, in CDC reactions two unfunctionalised molecules react together generating a new atom-atom bond and obtaining hydrogen as the only by-product. In this part of my thesis are described our last efforts in the green chemistry area joining the two concepts of photocatalysis and CDC reactions to generate new green protocols for the formation of atom-atom bonds.

Fascinated by the widely use of phosphoramidates as catalysts, flame retardants or even in biological applications, we focused the attention on their synthesis. All the methodologies previously reported in the literature are based on the use of halogens, phosphoryl chlorides, stoichiometric oxidants or transition metal catalysts. We studied the reaction between phosphites and amines to generate phosphoramidates in a CDC process using a photocatalytic oxidation with oxygen acting as a stoichiometric oxidant.

The reaction was catalysed by an organic dye (Rose Bengal), and the phosphoramidates were obtained in excellent yields in reasonable reaction times when irradiated with green LED light. Importantly, we developed a protocol to isolate the final products without the use of any chromatographic technique making all the process a clear example of green methodology. Moreover we designed a homemade photoreactor that improved reaction times.

DECLARATION OF AUTHORSHIP

I, Marta Meazza

declare that the thesis entitled

“Synergistic catalysis: merging amino catalysis and metal Lewis acid activation of azaarenes;
Green chemistry: first organophotocatalytic approach to the synthesis of phosphoramidates”

and the work presented in the thesis are both my own, and have been generated by me as the result of my own original research. I confirm that:

- this work was done wholly or mainly while in candidature for a research degree at this University;
- where any part of this thesis has previously been submitted for a degree or any other qualification at this University or any other institution, this has been clearly stated;
- where I have consulted the published work of others, this is always clearly attributed;
- where I have quoted from the work of others, the source is always given. With the exception of such quotations, this thesis is entirely my own work;
- I have acknowledged all main sources of help;
- where the thesis is based on work done by myself jointly with others, I have made clear exactly what was done by others and what I have contributed myself;
- parts of this work have been published as:
 - M. Meazza, V. Ceban, M. B. Pitak, S. J. Coles and R. Rios, *Chem. Eur. J.* **2014**, *20*, 16853-16857. **(Highlighted in Synfacts; 01, 2015)**
 - M. Meazza, M. E. Light; A. Mazzanti, R. Rios, *Chem. Sci.* **2016**, *7*, 984-988.
 - M. Meazza, A. Kowalczyk, L. Shirley, J. W. Yang, H. Gao, R. Rios, *Adv. Synth. Catal.*, **2016**, *358*, 719-723.

Signed:

Date:.....

UNIVERSITY OF SOUTHAMPTON

FACULTY OF CHEMISTRY

Department of Chemistry - Faculty of Organic Chemistry: Synthesis, Catalysis
and Flow

Volume 1 of 1

Section 1

**“Synergistic catalysis: merging amino catalysis and metal Lewis acid
activation of azaarenes”**

by

Marta Meazza

Thesis for the degree of Doctor of Philosophy

February 2016

UNIVERSITY OF SOUTHAMPTON

ABSTRACT

FACULTY OF NATURAL AND ENVIRONMENTAL SCIENCES

Organic Chemistry

Thesis for the degree of Doctor of Philosophy

**DEPARTMENT OF CHEMISTRY - FACULTY OF ORGANIC CHEMISTRY: SYNTHESIS,
CATALYSIS AND FLOW**

Marta Meazza

The art of building complex chemical scaffolds in a totally stereoselective manner is one of the cornerstones for Organic Chemists. The quest for new catalytic methodologies that fulfil the requirements of efficiency, green chemistry and predictable stereochemical outcome have become the Holy Grail for synthetic chemists.

In the present thesis we investigated new catalytic strategies for the enantioselective synthesis of azaarene scaffolds. Alkyl-azaarenes are common motifs in natural products and pharmaceutical compounds, however few methodologies are devoted to their functionalisation in an enantioselective manner. The major part of the approaches are based on the use of stoichiometric strategies and chiral auxiliaries due to the difficulty to activate the methylene position of alkylazaarenes. Our innovative approach relies on the use of a synergistic strategy where a Lewis acid activates the azaarene moiety making it a nucleophile while a Lewis base catalyst activates the electrophile. This dual activation presents several advantages such as an easy optimisation of each catalytic cycle and a greater decrease of the activation energy required for the reaction, allowing the use of low temperatures and soft conditions.

In Chapter 4 we demonstrate the proof of concept of this approach by joining transition metal catalysis (Lewis acid) and secondary amine catalysis (Lewis base, iminium activation) achieving the enantioselective addition of alkyl-benzoxazoles and related heterocycles to enals in good yields and reasonable stereoselectivity levels. In Chapter 5 we expanded this new concept in the application of cascade reactions. We designed a cascade reaction consisting in the Michael addition of chloromethylbenzoxazoles to enals followed by a 3-exo-trig cyclisation to furnish cyclopropanes in good yields and enantioselectivities.

The value of the present work is not only the development of these methodologies for the synthesis of chiral azaarenes (aldehyde derivatives and cyclopropanes) but also to demystify some misconceptions such as that metal Lewis acid could not coexist with secondary amine catalysis.

This pioneering work is an open gate to generate new methodologies using a synergistic approach that tries to take the best of two of the pillars of catalysis: the high activity and rich chemistry of transition metal catalysis with the affordable and easy stereochemical prediction of secondary amine catalysis, avoiding the use of extreme reaction conditions or the use of chiral ligands.

Contents

Contents.....	i
List of tables	v
List of figures	vii
List of Schemes	xi
DECLARATION OF AUTHORSHIP	xvii
Acknowledgements	xix
Definitions and Abbreviations.....	xxi
1. Introduction	1
1.1 Asymmetric synthesis.....	1
1.1.1 Methods of asymmetric synthesis	2
1.1.1.1 Chiral pool strategy	2
1.1.1.2 Chiral resolution	3
1.1.1.3 Chiral auxiliaries	5
1.1.1.4 Enantioselective catalysis.....	8
1.2 Organocatalysis	12
1.2.1 Historical development of organocatalysis.....	12
1.2.2 Classification of the organic catalysts	15
1.2.3 Modes of activation: aminocatalysis	18
1.2.3.1 Iminium catalysis	18
1.2.3.2 Enamine catalysis	21
1.2.3.3 Sequential iminium-enamine catalysis.....	23
1.3 Multicatalysis.....	25
1.3.1 Synergistic catalysis.....	26
2. Objectives	31
3. Azaarenes	33
3.1 Synthesis of azaarenes: alkylazaarenes as pronucleophiles	35
3.2 Strategies for the activation of alkyl-azaarenes.....	39
4. Synergistic catalysis: enantioselective addition of alkylbenzoxazoles to enals	43
4.1 Michael addition.....	43

4.1.1	Introduction	43
4.1.2	Enantioselective organocatalytic Michael addition with α,β -unsaturated aldehydes as Michael acceptor	45
4.2	Project aim.....	49
4.3	Research hypothesis and proposed mechanism.....	51
4.4	Results and discussions	53
4.4.1	Synthesis of the starting materials	53
4.4.1.1	Synthesis of the benzoxazoles.....	53
4.4.1.2	Synthesis of the aldehydes.....	55
4.4.2	Optimisation of the reaction conditions.....	59
4.4.2.1	Derivatisation	59
4.4.2.2	Screening of solvents.....	59
4.4.2.3	Screening of metal Lewis acids.....	62
4.4.2.4	Screening of different loading of Pd(OAc) ₂	63
4.4.2.5	Screening of bases and of different loading of base	65
4.4.2.6	Synthesis of organic catalysts.....	66
4.4.2.7	Screening of organic catalyst and temperature.....	68
4.4.3	Scope of the reaction with enals	71
4.4.4	Scope of the reaction with azaarenes.....	75
4.4.5	Relative and absolute configuration	79
4.5	Conclusion	80
5.	Synergistic catalysis: <i>cis</i>-cyclopropanation of benzoxazoles	81
5.1	One-pot reactions.....	81
5.1.1	Telescoping reactions	81
5.1.2	Multicomponent reactions	82
5.1.3	Domino/Cascade/Tandem reactions	83
5.1.3.1	Anionic domino reaction	84
5.1.3.2	Cationic domino reaction	84
5.1.3.3	Radical domino reaction.....	85
5.1.3.4	Pericyclic domino reaction	85
5.1.3.5	Transition metal catalysed domino reaction	86
5.1.3.6	Enzymatic domino reaction.....	87
5.1.3.7	Organocatalytic enantioselective domino reactions	87
5.2	Cyclopropanes	90
5.2.1	Simmons-Smith reaction.....	90

5.2.1.1	Chiral auxiliaries	91
5.2.1.2	Chiral ligands	91
5.2.1.3	Chiral catalysts.....	92
5.2.2	Cyclopropanation with diazomethane.....	93
5.2.3	Michael Initiated Ring Closure	94
5.3	Project aim.....	99
5.4	Research hypothesis and proposed reaction mechanism	99
5.5	Results and discussions	102
5.5.1	Synthesis of the starting materials	102
5.5.2	Optimisation of the reaction conditions.....	103
5.5.2.1	Screening of solvents.....	104
5.5.2.2	Screening of organic catalysts	105
5.5.2.3	Screening of bases.....	106
5.5.2.4	Screening of metal Lewis acids.....	107
5.5.2.5	Screening of temperatures.....	108
5.5.2.6	Screening of metal Lewis acids with 2,6-lutidine as a base	109
5.5.3	Scope of the reaction with enals.....	110
5.5.4	Scope of the reaction with benzoxazoles	112
5.5.5	Relative and absolute configuration	114
5.6	Conclusion	116
6.	Experimental section	117
6.1	Synergistic catalysis: enantioselective addition of alkylbenzoxazoles to enals 118	
6.1.1	Synthesis of the starting materials: α,β -unsaturated aldehydes (80)	118
6.1.2	Synthesis of the starting materials: azaarenes	118
6.1.3	Synthesis of the catalysts: derivatives of the Jorgensen-Hayashi catalyst 121	
6.1.4	Synthesis of 3-(6-nitrobenzoxazol-2-yl)-2-phenylbutanal (235a)	122
6.1.5	General procedure	123
6.1.6	Crystallographic data (259f major diastereomer)	159
6.2	Synergistic catalysis: <i>cis</i> -cyclopropanation of benzoxazoles.....	161
6.2.1	Synthesis of the starting material: benzoxazoles (391)	161
6.2.2	Synthesis of the starting material: α,β -unsaturated aldehydes (80).....	165
6.2.3	General procedure for the synthesis of cyclopropanes (392, 402)	166
6.2.4	Final products characterisation	167

6.2.5	Crystallographic data and experimental 392d minor diastereomer obtained with (<i>R</i>)-catalyst	197
6.2.6	Conformational analysis and absolute configuration	200
6.2.6.1	Absolute configuration	202
6.2.6.2	Major diastereomer	207
6.2.6.3	Absolute configuration of 392d-major	213
List of References		220

List of tables

Table 1. Results obtained in the synthesis of enals	57
Table 2. Screening of solvents	60
Table 3. Screening of metals.....	62
Table 4. Screening of loading of Pd(OAc) ₂	64
Table 5. Screening of bases.....	65
Table 6. Screening of organic catalysts and temperature	68
Table 7. Scope of the reaction with several enals	73
Table 8. Scope of the reaction with different benzoxazoles and pyridines	77
Table 9. Screening of solvents	104
Table 10. Screening of organic catalysts.....	105
Table 11. Screening of bases	106
Table 12. Screening of metal Lewis acids	107
Table 13. Screening of temperatures	108
Table 14. Screening of metal Lewis acids with 2,6-lutidine as base.....	109
Table 15. Scope of the reaction with several enals	110
Table 16. Scope of the reaction with several benzoxazoles.....	112
Table 17. Relative energies of the four conformations of 392d-minor	201
Table 18. Relative energies of the four conformations of 392d-minor	201
Table 19. Relative energies of the four conformations of 392a-major	209
Table 20. Calculated and experimental coupling constants for the four diastereomers of 392d	210

Table 21. Relative energies of the four conformations of 392d-major	214
---	-----

List of figures

Figure 1. Enantiomers of limonene.....	1
Figure 2. Enantiomers of Thalidomide.....	2
Figure 3. Dynamic kinetic resolution	4
Figure 4. Structure of BINAP	9
Figure 5. Organocatalytic cycles	15
Figure 6. Transition state models for the electrophilic attack to the enamine. (A) List-Houk model, (B) Seebach-Eschenmoser model, (C) steric model.	23
Figure 7. Classification of multicatalysis	26
Figure 8. Traditional/Synergistic catalysis	26
Figure 9. Examples of biologically active azaarenes	35
Figure 10. Mode of activation A	40
Figure 11. Activation of benzoxazoles with an EWG	40
Figure 12. Activation of benzoxazoles with a Lewis acid	41
Figure 13. Modes of activation of azaarenes.....	49
Figure 14. Results obtained in the synthesis of benzoxazoles with triethoxyalkanes ...	54
Figure 15. Results obtained in the synthesis of benzoxazoles with acid	55
Figure 16. Azaarenes that did not react with the enals.....	78
Figure 17. Crystal structure of product 259f . For more information about the crystal see Chapter 6	79
Figure 18. Example of Horeau principle applied to domino reactions.....	88
Figure 19. Examples of interesting cyclopropanes	90

Figure 20. Chloromethylenebenzoxazole acting as nucleophile (389) and then as electrophile (390).....	99
Figure 21. New synergistic approach: two catalysts, three catalytic cycles and the formation of two new C-C bonds.....	100
Figure 22. Results obtained in the synthesis of chloro-alkylbenzoxazoles	103
Figure 23. Proposed epimerisation of the minor diastereomer of the product 392i ..	111
Figure 24. X-ray structure of compound 392d	114
Figure 25. Stereochemistry of the products for each enantiomer of the catalyst.....	166
Figure 26. Thermal ellipsoids drawn at the 50 % probability level	197
Figure 27. 3D view of the four conformations of the model compound 392d-minor .	202
Figure 28. ECD (blue trace) and UV (red trace) spectra of 392d-minor (R)-catalyst . Spectra were recorded in acetonitrile, $6 \cdot 10^{-5}$ M, 0.5 cm cell path	203
Figure 29. TD-DFT simulated spectra calculated for conformation d of 392d-minor ..	204
Figure 30. TD-DFT simulated spectra calculated for the four conformations of 392d-minor	205
Figure 31. Simulations of the experimental ECD spectrum of 392d-minor (obtained with (R)-catalyst)	206
Figure 32. ^1H spectrum of the aliphatic region of 392a-major (600 MHz, CD_3CN)	208
Figure 33. Geometries of the four conformations of 392a-major	209
Figure 34. DPGSE NOE spectra of 392a-major (600 MHz in CD_3CN).	212
Figure 35. ECD (blue trace) and UV (red trace) spectra of 392d-major (obtained with (S)-catalyst) . Spectra were recorded in acetonitrile, $1 \cdot 10^{-4}$ M, 0.2 cm cell path.	213
Figure 36. Calculated ECD for each conformation of 392d-major with different functionals and the same 6-311++G(2d,p) basis set.....	215

Figure 37. View of the dipoles of 392d-major acting in the generation of the UV spectrum in the 250-350 nm region.	215
Figure 38. DPGSE-NOE of 392d-major recorded on saturation of the CH(CHO) signal and using 4 s mixing time.....	217
Figure 39. Simulations of the experimental ECD spectrum of 392d-major	219

List of Schemes

Scheme 1. Synthesis of Aspartame	2
Scheme 2: Total synthesis of (-)-Deoxoprosopphylline	3
Scheme 3. Sharpless' kinetic resolution of allylic alcohols	3
Scheme 4. Dinamic kinetic resolution of Duloxetine	4
Scheme 5. Enantioselective synthesis <i>via</i> DKR	5
Scheme 6. General scheme for a chiral auxiliary	5
Scheme 7. Example of alkylation with Evans oxazolidinone	6
Scheme 8. Example of a nucleophilic addition with Ellman's auxiliary	7
Scheme 9. Example of alkylation with Enders' auxiliary	7
Scheme 10. Example of allylic addition with Oppolzer's auxiliary	8
Scheme 11. Synthesis of L-Dopa using Knowles' asymmetric dehydrogenation	8
Scheme 12. Asymmetric hydrogenation of ketones.....	9
Scheme 13. Sharpless epoxidation	10
Scheme 14. Sharpless dihydroxylation	10
Scheme 15. Bredig's work.....	13
Scheme 16. Pracejus' work	13
Scheme 17. Hajos-Parrish-Eder-Sauer-Wiechert reaction	14
Scheme 18. Julia-Colonna epoxidation.....	14
Scheme 19. Pioneering works of List and MacMillan	15
Scheme 20. Lewis base catalysis.....	16
Scheme 21. Lewis acid catalysis.....	16

Scheme 22. Brønsted base and acid bifunctional catalyst	17
Scheme 23. Takemoto bifunctional catalyst.....	17
Scheme 24. Enamine and iminium intermediates.....	18
Scheme 25. Catalytic cycle of iminium catalysis.....	19
Scheme 26. Stereochemical outcome of amine-catalysed addition to enals	20
Scheme 27. Examples of organocatalytic nucleophilic addition	20
Scheme 28. Generalised mechanism for the amine-catalysed α -functionalisation of carbonyls	22
Scheme 29. Sequential iminium-enamine catalysis	23
Scheme 30. Intramolecular sequential iminium-enamine catalysis.....	24
Scheme 31. MacMillan cyclopropanation of α,β -unsaturated aldehydes by β - oxosulfonium ylides	24
Scheme 32. Córdova's enantioselective silyl addition to enals catalysed by copper and a chiral amine	28
Scheme 33. Proposed mechanism of benzoxazole addition to MBH carbonates.....	29
Scheme 34. Mechanism of Córdova's DYKAT between α,β -unsaturated aldehydes and propargylated carbon acids to form enantiomerically pure cyclopentenones	30
Scheme 35. Synthesis of piperidines	33
Scheme 36. Rios' synthesis of α -methylene- γ -lactone.....	33
Scheme 37. Addition of pyrazolones and oxazolones to maleimides	34
Scheme 38. Guo's amination of 2-alkylazaarenes.....	36
Scheme 39. Rueping's and Huang's racemic addition of azaarenes to <i>N</i> -sulfonyl aldimines	36

Scheme 40. Li's and Fossey's addition of 2-methylazaarenes to isatines and ethyl glyoxylates.....	37
Scheme 41. Matsunaga's addition of alkylazaarenes to C=C double bonds of enones .	37
Scheme 42. Lam's activation of azaarenes with metal Lewis acid	38
Scheme 43. Melchiorre's first organocatalytic synthesis of azaarenes.....	38
Scheme 44. Wang's enantioselective Michael addition of 4-methyl-3-nitropyridine to α,β -unsaturated aldehydes	39
Scheme 45. Alkylazaarenes as pronucleophiles	39
Scheme 46. First examples of Michael additions reported by Michael in 1887 and 1894	43
Scheme 47. Wu's 1,4-Michael addition of allyltrimethylsilanes to α,β -carbonyl compounds.....	44
Scheme 48. Jørgensen's metal catalysed Michael addition addition of O-benzylhydroxylamines to α,β -unsaturated carbonyl compounds	44
Scheme 49. 1,4-addition of chiral imidazolidinones to α,β -unsaturated aldehydes	45
Scheme 50. Hayashi's Michael addition of nitroalkanes to α,β -unsaturated aldehydes	46
Scheme 51. Asymmetric addition of malonates to aromatic α,β -unsaturated aldehydes	46
Scheme 52. Melchiorre's addition of oxindoles to α,β -unsaturated aldehydes	47
Scheme 53. Jørgensen's addition of oxazolones to enals	47
Scheme 54. Jørgensen's addition of β -keto sulfones to α,β -unsaturated aldehydes	48
Scheme 55. Highly diastereoselective benzoxazole addition to Morita-Baylis-Hillman carbonates.....	50
Scheme 56. Proposed reaction mechanism for the enantioselective addition of alkylbenzoxazoles to enals	51
Scheme 57. First reaction tested	52

Scheme 58. Synthesis of the benzoxazoles as starting materials.....	53
Scheme 59. Mechanism of benzoxazoles' synthesis from triethoxyalkane	53
Scheme 60. Mechanism of benzoxazoles' synthesis from acids	54
Scheme 61. General scheme of the synthesis of starting aldehydes	55
Scheme 62. Mechanism of the Wittig reaction	56
Scheme 63. Rationalisation of the formation of <i>E</i> -alkene with stabilised ylides	56
Scheme 64. Synthesis of disubstituted aldehyde in β position	58
Scheme 65. Wittig derivatisation.....	59
Scheme 66. Synthesis of the organic catalysts	67
Scheme 67. Scope of the reaction with several enals. a) DIPEA as the base; b) reaction conducted at 30 °C; c) 189 as the catalyst; d) 103 as the catalyst.	72
Scheme 68. Explanation of the epimerisation at the β -position.....	74
Scheme 69. Attempted reactions with aliphatic aldehydes	75
Scheme 70. Scope of the reaction with different benzoxazoles and pyridines. a) TMS catalyst 103 used; b) TES catalyst 189 used; c) the reaction was performed at 45 °C...	76
Scheme 71. Synthesis of 235d	80
Scheme 72. Telescopic reaction for the synthesis of 7-hydroxyquinoline.....	82
Scheme 73. Multicomponent reactions	83
Scheme 74. Evans' synthesis of Salvinorin A through an anionic Michael/Michael cascade reaction	84
Scheme 75. Cationic domino reaction reported for total synthesis of (-)-Dysibetaine PP85	
Scheme 76. Takahashi's radical domino reaction for the synthesis of steroids	85
Scheme 77. Winkler's pericyclic Diels-Alder domino reaction	86

Scheme 78. Pfeffer's Pd catalysed domino reaction	86
Scheme 79. Synthesis of Precorrin through an enzymatic domino reaction	87
Scheme 80. Enders' Michael/Michael/aldol enantioselective cascade reaction	88
Scheme 81. Rios' cascade reactions for the synthesis of spiropyrazolones and spiroxindoles	89
Scheme 82. Furukawa modification of Simmons Smith cyclopropanation and mechanism	91
Scheme 83. Bull's cyclopropanes synthesis with hydroxyl as directing group.....	91
Scheme 84. Charette's asymmetric cyclopropanation of allylic alcohols with dioxaborolane ligands	92
Scheme 85. Charette's cyclopropanation of allylic alcohols with chiral phosphoric acid	92
Scheme 86. Cyclopropanation with diazometane and olefines	93
Scheme 87. Noyori's synthesis of cyclopropanes.....	93
Scheme 88. Mechanism of the transition-metal catalysed decomposition of diazoalkenes.....	94
Scheme 89. Fu's cyclopropanation with bidentate chiral ferrocene copper ligand.....	94
Scheme 90. Mechanism of Aggarwal's asymmetric cyclopropanation of alkenes mediated by a chiral sulphide	95
Scheme 91. Gaunt's cyclopropanation via ammonium ylides.....	95
Scheme 92. Nitrocyclopropanation of 1-bromonitroalkanes with α,β -unsaturated aldehydes	96
Scheme 93. Cyclopropanation of enals with malonates and ketoesters	96
Scheme 94. Organocatalytic enantioselective synthesis of spirocyclopropanes	97

Scheme 95. Cobb's cyclopropanation of conjugated cyanosulfones with bromomalonates.....	98
Scheme 96. First reaction tested for the addition of 2-(chloromethyl)-6-nitrobenzoxazole with cinnamaldehyde	100
Scheme 97. Proposed mechanism for the cyclopropanation	101
Scheme 98. Synthesis of the chloromethylenebenzoxazoles as starting materials.....	102
Scheme 99. Katzuki and Mezzetti's <i>cis</i> -cyclopropanation.....	115
Scheme 100. MacMillan's enantioselective synthesis of <i>trans</i> -trisubstituted cyclopropanes	115
Scheme 101. General scheme of the Michael addition step.....	122
Scheme 102. General scheme of the Michael addition and subsequent Wittig derivatisation	123

DECLARATION OF AUTHORSHIP

I, Marta Meazza

declare that the thesis entitled

“Synergistic catalysis: merging amino catalysis and metal Lewis acid activation of azaarenes”

and the work presented in the thesis are both my own, and have been generated by me as the result of my own original research. I confirm that:

- this work was done wholly or mainly while in candidature for a research degree at this University;
- where any part of this thesis has previously been submitted for a degree or any other qualification at this University or any other institution, this has been clearly stated;
- where I have consulted the published work of others, this is always clearly attributed;
- where I have quoted from the work of others, the source is always given. With the exception of such quotations, this thesis is entirely my own work;
- I have acknowledged all main sources of help;
- where the thesis is based on work done by myself jointly with others, I have made clear exactly what was done by others and what I have contributed myself;
- parts of this work have been published as:
 - M. Meazza, V. Ceban, M. B. Pitak, S. J. Coles and R. Rios, *Chem. Eur. J.* **2014**, *20*, 16853-16857. **(Highlighted in Synfacts; 01, 2015)**
 - M. Meazza, M. E. Light; A. Mazzanti, R. Rios, *Chem. Sci.* **2016**, *7*, 984-988.

Signed:

Date:.....

Acknowledgements

Undertaking this PhD would not have been possible without the support and guidance that I received from many people. Thanks to all the people with whom I shared this season of my life.

First of all, I would like to express my appreciation and sincere thanks to my supervisor, Dr Ramon Rios, for his teachings and support and for allowing me to grow as a research scientist. His passion for research is highly contagious and encouraging, I greatly benefit from his huge scientific experience. I would also like to thank my advisor Prof Bruno Linclau for motivating me to do my best.

I would especially like to thank my colleagues and friends: Dr Victor Ceban, for the three years spent together as PhD students, thanks for the help in the lab and for the pleasant discussions at the tea room, Maria Ashe for the friendship. Both of you are not only colleagues but also friends. Thanks also to the other past and present members of Rios' research group, in particular: Michael Potter, Dr Piotr Putaj, Dr Tope Olomola, Dr Jiri Tauchman, India Willans, Luke Kidwell, Greg Gallagher, Aga Kowalczyk, Kane Hands, Luke Shirley and Cameron Ross. Thanks to Prof Andrea Mazzanti for the optical rotation analysis and NMR studies reported in this thesis.

I wish to thank the University of Southampton for providing the facilities and in particular Dr Neil Wells for the NMR service, Dr Mark Light, Dr Mateusz Pitak and Dr Simon Coles for the single crystal X-ray diffraction, Dr John Langley and Julie Herniman for the mass spectrometry service and HRMS analysis. Thanks also to Mr Karl and Mr Keith of the store for their kindness and Ms Anne of the tea room where I could relax when I was tired but also where I had interesting discussions with my friends and colleagues.

I would like to acknowledge the AI-CHEM INTERREG IVb for the fellowships and the financial support.

Finally I thank my beloved animals Birillo, Sandokan, Maggie and Notte for their friendship while growing up and Pio and particularly Sera for her unconditional love

and for supervising the writing of many parts of this thesis from my lap and behind the laptop.

Last I thank my family and my friends: I owe a lot to my family and in particular to my parents and grandmother Diana, who encouraged and helped me at every stage of my personal and academic life, for always being there for me and for their unconditional love.

Definitions and Abbreviations

$[\alpha]_D$	Specific rotation
Ac	Acetyl
AC	Brønsted acid
aq	Aqueous
Ar	Aryl
β -ICPD	β -Isocupreidine
bd	Broad doublet
BINAP	2,2'-bis(diphenylphosphino)-1,1'-binaphthyl
BINOL	1,1'-binaphthyl-2,2'-diol
Bn	Benzyl
Boc	<i>tert</i> -butyloxycarbonyl
br	broad
<i>n</i> -Bu	Normal butyl
<i>t</i> -Bu	Tertiary butyl
c	concentration
°C	degrees centigrade
Cbz	Carbobenzyloxy
COSY	Correlated spectroscopy
Cq	Quaternary carbon
δ	Chemical shift
d	Doublet

dd	Doublet of doublets
ddd	Doublet of doublets of doublets
dddd	Doublet of doublets of doublets of doublets
DABCO	1,4-diazabicyclo[2.2.2]octane
DCM	Dichloromethane
D-(-)-DET	(-)-Diethyl D-Tartrate
DFT	Density functional theory
(DHQD) ₂ PHAL	1,4-bis[(S)-[(2R,4S,5R)-5-ethylquinuclidin-2-yl]-(6-methoxy-4-quinolyl)methoxy]phthalazine
DIBALH	diisobutylaluminium hydride
DIPEA	Diisopropylethylamine
DMF	N,N Dimethylformamide
DMSO	Dimethylsulfoxide
2D-NMR	Two-dimensional Nuclear Magnetic Resonance
DPFGSE NOE	Double Pulse Field Gradient Spin Echo Nuclear Overhauser Effect
dq	Doublet of quartets
dr	Diastereomeric ratio
dt	Doublet of triplets
dtd	Doublet of triplets of doublets
E, E ⁺	Electrophile
ECD	Electronic circular dichroism

<i>ee</i>	Enantiomeric excess
equiv.	Equivalents
ESI+	Electrospray ionization (positive mode)
Et	Ethyl
EtOAc	Ethyl Acetate
EWG	Electron withdrawing group
g	gram
h	hour
Het	Heterocycle
HMBC	Heteronuclear multiple bond correlation
HOMO	Highest Occupied Molecular Orbital
HPLC	High Performance Liquid Chromatography
HRMS	High resolution mass spectrometry
HSQC	Heteronuclear Single Quantum Correlation
Hz	Hertz
IR	Infra Red
<i>J</i>	Coupling constant
L	Ligand
LCMS	Liquid Chromatography Mass Spectrometry
LDA	Lithium diisopropylamide
L-(+)-DET	(+)-Diethyl L-Tartrate
LUMO	Lowest Unoccupied Molecular Orbital

M	Metal catalyst
m	Multiplet
MacMillan II catalyst	(2S,5S)-(-)-2-tert-butyl-3-methyl-5-benzyl-4-imidazolidinone
MBH	Morita-Baylis-Hillman
Me	Methyl
mg	Milligram
MHz	Mega Hertz
mL	Millilitre
mmol	Millimoles
mp	Melting point
MS	Mass Spectroscopy
MTBE	Methyl <i>tert</i> butyl ether
<i>m/z</i>	mass / charge ratio
NMO	<i>N</i> -methylmorpholine- <i>N</i> oxide
NMR	Nuclear Magnetic Resonance
NOE	nuclear Overhauser Effect
Nu	Nucleophile
OR	Optical rotation
PCM	Polarizable continuum model
Pin	4,4,5,5-Tetramethyl-[1,3,2]dioxaborolane (pinacolborane)
PG	protecting group
Ph	Phenyl

ppm	Parts per million
PPA	Polyphosphoric Acid
<i>i</i> -Pr	Isopropyl
q	Quartet
qd	Quartet of doublets
rt	Room Temperature
s	Singlet
t	Triplet
TADDOL	$\alpha,\alpha,\alpha,\alpha$ -tetraaryl-1,3-dioxolane-4,5- dimethanols
TBAF	Tetrabutylammonium fluoride
TBDMS	tert-butyldimethylsilyl
TBS	<i>tert</i> -butyldimethylsilyl
TCM	Chloroform
td	Triplet of doublets
TD-DFT	Time-Dependent formalism
TEA	Triethylamine
TES	Triethylsilyl
Tf	Trifluoromethanesulfonyl
TFA	Trifluoroacetic acid
THF	Tetrahydrofuran
TLC	Thin Layer Chromatography
TMS	Trimethylsilyl

TOF	Time of Flight
t_r	Retention time
Ts	Tosyl
<i>p</i> -TSA	<i>p</i> -Toluensulfonic acid
UV	Ultraviolet
VDC	Vibrational circular dichroism

1. Introduction

1.1 Asymmetric synthesis

In Nature, most of the compounds are chiral (for example hormones, enzymes, DNA ...). Two enantiomers can have different biological activities. For example the enantiomers of Limonene **1** smell differently: the enantiomer (*S*)-Limonene smells of lemons, while the (*R*)-Limonene smells of oranges (**Figure 1**). We are able to distinguish between the enantiomers because the nasal receptors are made of chiral molecules.

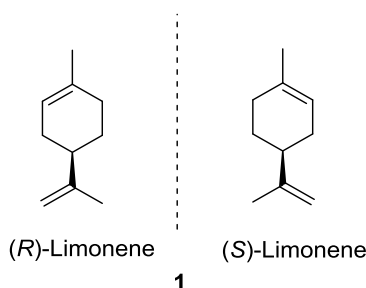


Figure 1. Enantiomers of limonene

This can also be appreciated in the context of drug receptors: as the receptors in the cells are chiral, the drug used should match the receptor. The activity of the drugs depends on which enantiomer is used. For example, while one enantiomer possesses the required activity, the other can be ineffective as in the case of Dopa. Dopa is a chiral amino acid used to treat patients with Parkinson disease, only *L*-Dopa (*S*) **51** is effective as a psychoactive while *D*-dopa (*R*) is biologically inactive.

In other cases one of the enantiomers can be toxic (**Figure 2**). In the early 1960s, the drug Thalidomide **2** was manufactured as a racemic mixture of two enantiomers and was prescribed primarily as a sedative for women suffering morning sickness during pregnancy. Whilst the (*R*)-Thalidomide proved to be the active molecule, the (*S*)-Thalidomide caused birth defects such as deformities in the limbs.^{[1][2]} Recent reports show that the strongly acidic hydrogen atom at the asymmetric centre epimerises under physiological conditions, for example in the stomach.^[3]

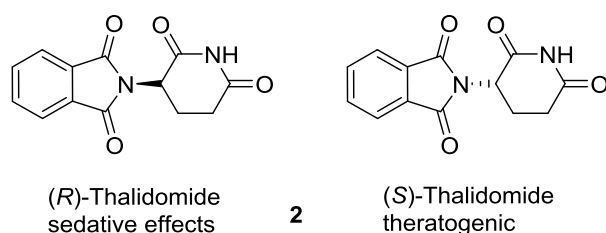


Figure 2. Enantiomers of Thalidomide

Strategies to develop drugs that can have the beneficial effect of Thalidomide without the teratogenic effects have been developed. Shibata and co-workers synthesised 3-fluorothalidomide,^[4] an isosteric analogue of Thalidomide. Fluorine was chosen because of its high electronegativity and strong C-F bond and it was shown that this increased the resistance to racemisation.

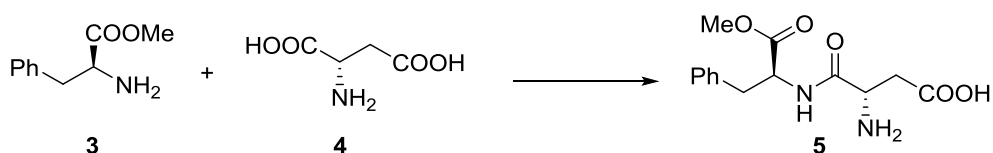
This was an extreme example that highlighted the need for new strategies for the synthesis of enantiopure products.

1.1.1 Methods of asymmetric synthesis

1.1.1.1 Chiral pool strategy

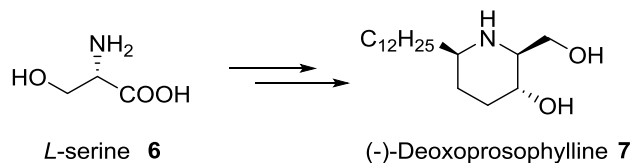
One possibility to obtain an enantiopure product is to start from an enantiomerically pure starting material. The chiral pool is a collection of cheap and available pure natural products, usually amino acids or sugars, which contain the chiral center needed in the final product.

One example is the synthesis of Aspartame **5**: it is a dipeptide and is made using two constituents of the chiral pool, the natural (*S*) amino acids phenylalanine **3** and aspartic acid **4** (**Scheme 1**).^[5]



Scheme 1. Synthesis of Aspartame

Chiral pool strategy is applied to the total synthesis of pharmaceutical products for example (-)-Deoxoprosophylline **7**,^[6] synthesised starting from the natural amino acid L-serine **6** (**Scheme 2**).

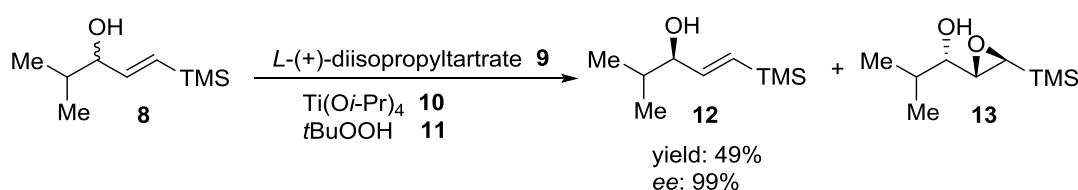


Scheme 2: Total synthesis of (-)-Deoxoprosophylline

1.1.1.2 Chiral resolution

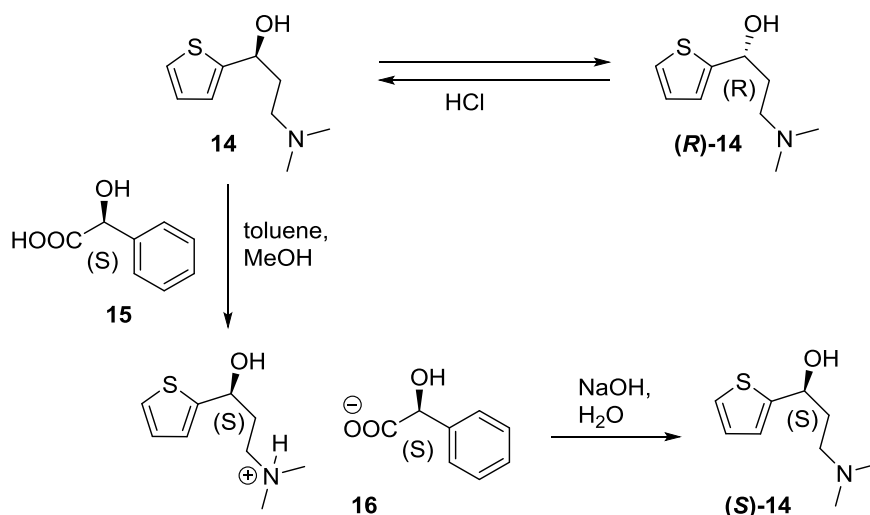
Chiral resolution is a technique to separate two enantiomers from a racemic mixture, through the precipitation of one enantiomer or converting them into diastereomers, using a resolving agent. In this way the diastereomers can be separated based on their different physical properties.

Kinetic resolution is based on the differences between the two enantiomers, as only one will react in an enantioselective way. For this reason, the enantioselectivity of the starting material will increase until only one enantiomer will remain unreacted. One example is the kinetic resolution of allylic alcohols **8** using the Sharpless epoxidation^[7,8] as shown in **Scheme 3**.



Scheme 3. Sharpless' kinetic resolution of allylic alcohols

The dynamic kinetic resolution (DKR) happens when the starting material is able to epimerise rendering, in this way, a theoretical yield of 100% of enantiomerically pure product. One example is the dynamic kinetic resolution of the drug Duloxetine, prescribed for depressive disorders, anxiety disorder, fibromyalgia and neurotic pain (**Scheme 4**).^[9]



Scheme 4. Dynamic kinetic resolution of Duloxetine

To a solution of the racemic alcohol **14** (S)-mandelic acid **15** is added. The (S)-enantiomer of the alcohol forms an insoluble salt with the mandelic acid and is then recovered by filtration. After deprotonation with NaOH the free alcohol is obtained, with 93% of enantiomeric excess (ee). The (R)-enantiomer remains in solution and is treated with HCl to epimerise and form again the racemic mixture.

In the DKR^[10] the enantiomers of a racemic substrate are induced to equilibrate at a rate that is faster than that of the reaction of the slow-reacting enantiomer with the chiral agent (**Figure 3**). The theoretical yield of this process is of 100%.

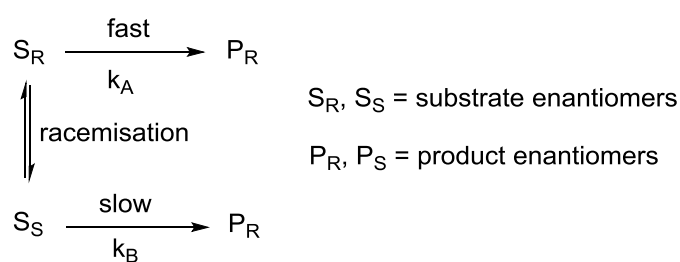
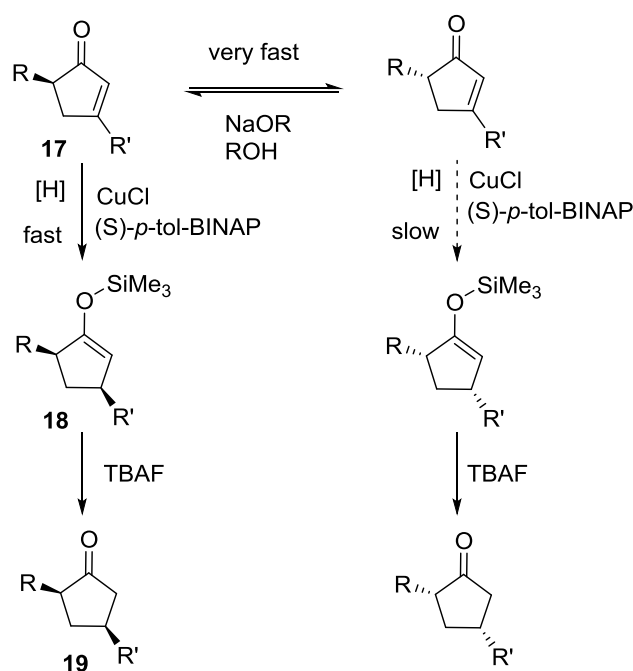


Figure 3. Dynamic kinetic resolution

When the reaction occurs with the creation of a new stereogenic centre, the DKR can be applied for the enantioselective synthesis of a diastereomer. An example reported by Buchwald^[11] deals with the diastereoselective synthesis of 3,5-dialkylcyclopentenones **19** (**Scheme 5**).

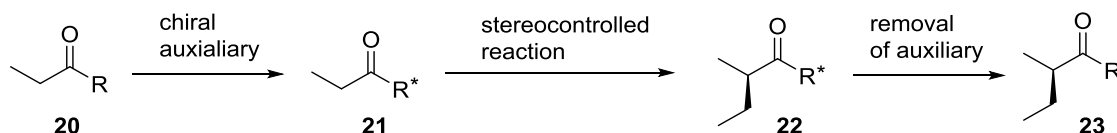


Scheme 5. Enantioselective synthesis *via* DKR

As the reaction is performed under basic conditions, a rapid racemisation of the starting material occurs. The ketone product **17** is masked as silyl enol ether **18** so that the epimerisation at the α -stereocenter is obviated.

1.1.1.3 Chiral auxiliaries

A chiral auxiliary is a molecule that is temporarily covalently bonded to a substrate of interest to control the stereochemical outcome of the reaction. As shown in **Scheme 6**, the chiral auxiliary is incorporated in the initial substrate **20** and can influence the stereochemistry of one or more following reactions. Then it can be removed, recycled and reused.



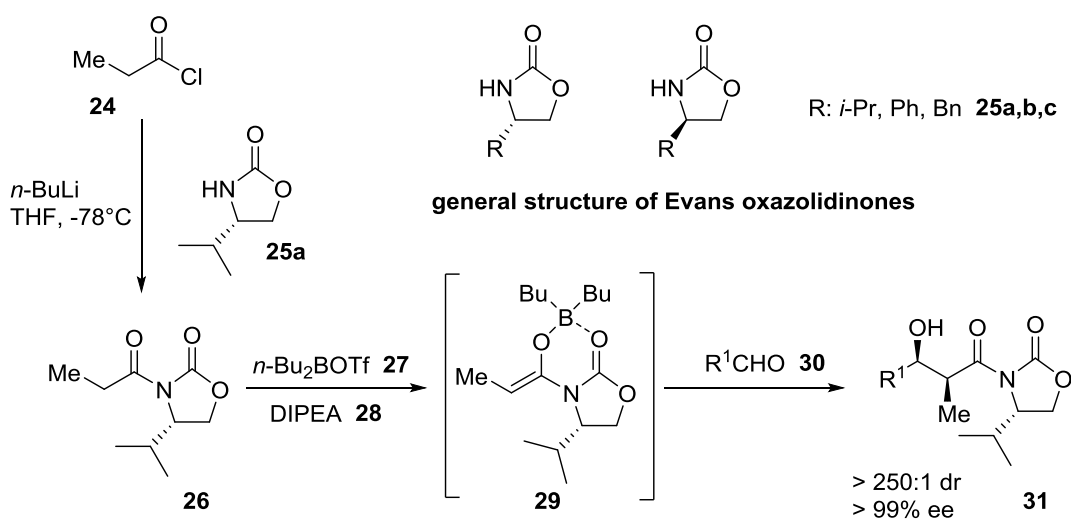
Scheme 6. General scheme for a chiral auxiliary

An efficient chiral auxiliary should possess the following characteristics: (a) cheap and readily available, (b) easy to attach to the substrate, (c) able to induce the correct

stereochemistry, (d) chemically inert under the reaction conditions and (e) easy to remove.

The most common chiral auxiliaries are: Evans's oxazolidinones, Ellman's, Enders' and Oppolzer's auxiliaries.

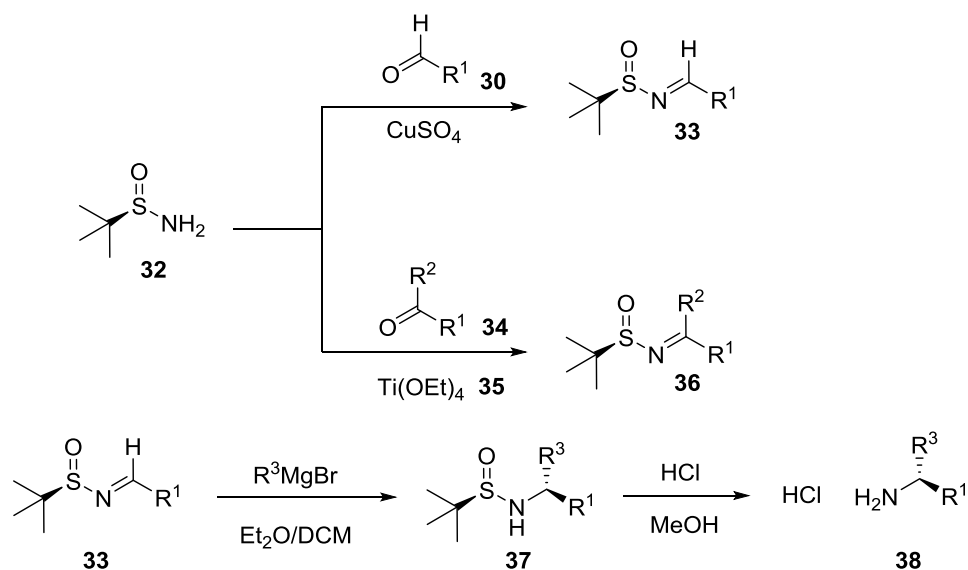
Evans' auxiliaries **25** are oxazolidinones applied to different stereoselective reactions, including aldol reactions,^[12] alkylation reactions (**Scheme 7**)^[13] and Diels-Alder reactions.^[14]



Scheme 7. Example of alkylation with Evans oxazolidinone

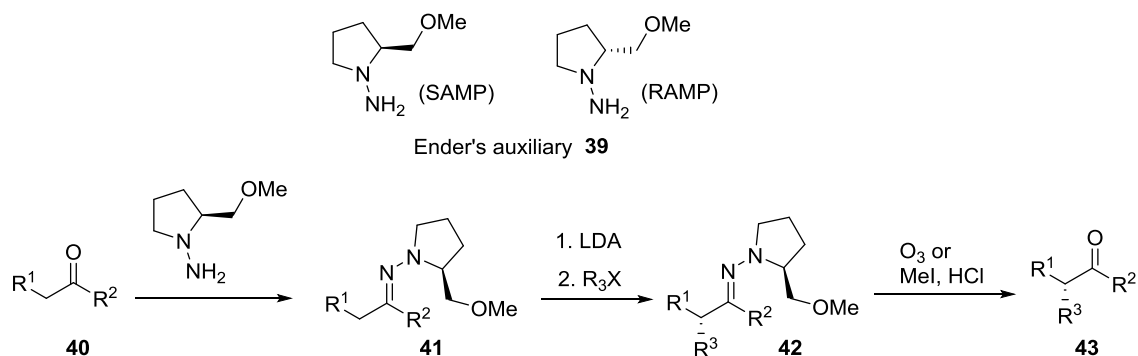
The intermediate **29** is the (Z) -enolate formed under kinetic conditions. A nucleophilic addition to the aldehyde **30** gives the syn product **31** as the aldehyde reacts preferentially with one face of the enolate due to steric hindrance of the substituent on the oxazolidinone. An additional advantage of the oxazolidinones is the fact that the products are easy to crystallise, making it easier to obtain enantioenriched compounds.

Ellman's auxiliaries are N -*tert*-butanesulfinyl aldimines **33** and ketimines **36** and are useful intermediates for the asymmetric synthesis of amines **38**.^[15] The *tert*-butanesulfinyl group activates the imine for the addition of different nucleophiles and acts as a chiral directing group. After the addition it is cleaved by treatment with acid (**Scheme 8**).



Scheme 8. Example of a nucleophilic addition with Ellman's auxiliary

Ender's auxiliaries 39 is a chiral hydrazine that reacts with an aldehyde or ketone forming an hydrazone 41.^[16] Then it is deprotonated with lithium diisopropylamide (LDA) forming an azaenolate that reacts with an electrophile and after ozonolysis or hydrolysis the final alkylated product 43 is obtained (**Scheme 9**).



Scheme 9. Example of alkylation with Enders' auxiliary

Oppolzer's auxiliary 44 is a camphorsultam that has become a common auxiliary demonstrating its utility in enantioselective Diels-Alder^[17] or allylic addition reactions (**Scheme 10**).^[18]

Noyori developed the field of asymmetric hydrogenations reporting the discovery of an atropoisomeric chiral diphosphine **52** (BINAP) (**Figure 4**). Rhodium(I) complexes with BINAP were effective to perform enantioselective reactions, including an enantioselective hydrogenation of α -(acylamino)acrylic acids or esters, rendering amino acid derivatives.^[21]

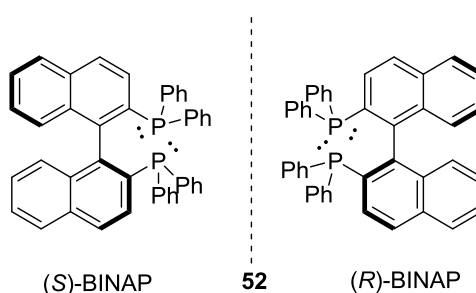
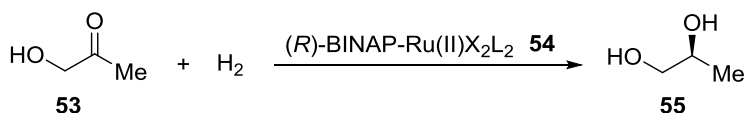


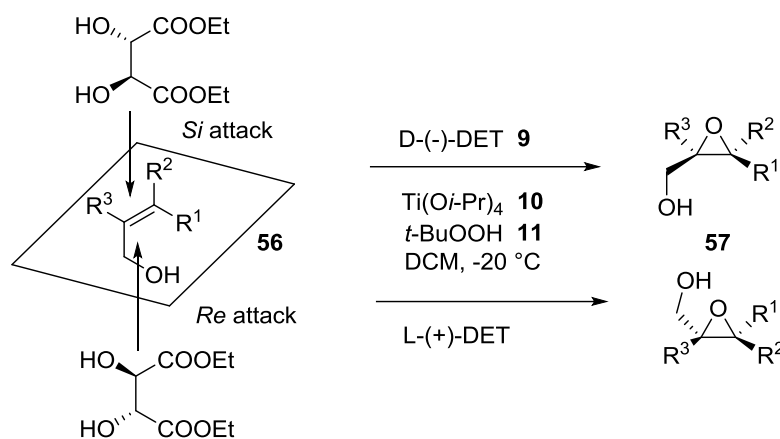
Figure 4. Structure of BINAP

Subsequently Noyori discovered the BINAP-Ru(II) complex catalyst **54**, active in the enantioselective hydrogenation of unsaturated carboxylic acids^[22] and differently functionalized ketones **53** (**Scheme 12**).^[23]



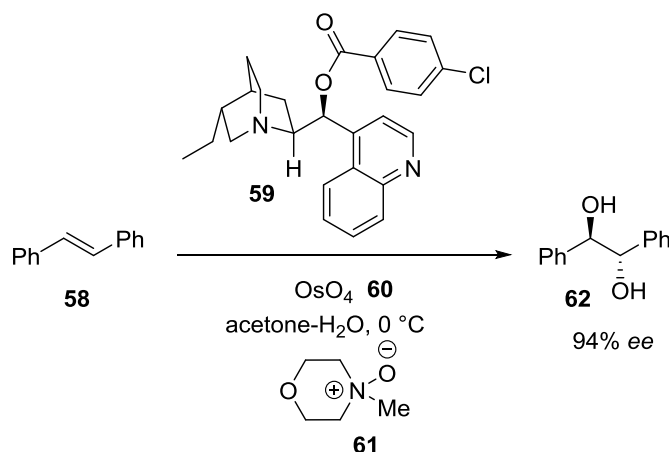
Scheme 12. Asymmetric hydrogenation of ketones

In parallel with the development of asymmetric hydrogenations, Sharpless developed a chiral catalyst for oxidation reactions. In 1980 Sharpless and Katsuki reported an asymmetric epoxidation of allylic alcohols **56**, using titanium(IV) tetraisopropoxide **10**, *tert*-butyl hydroperoxide **11** and enantiomerically pure dialkyl tartrate **9** (**Scheme 13**).^[24]



Scheme 13. Sharpless epoxidation

Sharpless also developed a catalytic asymmetric dihydroxylation using *N*-methylmorpholine *N*-oxide (NMO) **61** as stoichiometric oxidant, osmium tetroxide **60** (OsO₄) as catalytic oxidant and a cinchona alkaloid **59** as ligand (**Scheme 14**).^[25]



Scheme 14. Sharpless dihydroxylation

For their discoveries in the field of asymmetric catalysis, Knowles,^[26] Noyori^[27] and Sharpless^[28] were rewarded with the Nobel Prize in 2001.

Another method of enantioselective catalysis is biocatalysis,^[29] that is based on the use of enzymes as catalysts. The advantages of biocatalysis are (a) high stereo-selectivity, chemo-selectivity and regioselectivity, (b) reduced use of protecting groups, (c) minimised side reactions and (d) fewer environmental problems compared to organometallic catalysis. The drawbacks are (a) limited substrate scope for each

enzyme and (b) the fact that most of the reactions are carried out in water as solvent and most organic substrates have limited solubility in water.

An example of such methodology is the work reported by Rosenthaler regarding the preparation of (*R*)-mandelonitrile by treating benzaldehyde with HCN in the presence of the enzyme emulsin, extracted from bitter almonds.^[30]

The third pillar is organocatalysis, the use of small, chiral, organic molecules to catalyse asymmetric organic reactions. This topic is developed in depth in Chapter 1.2.

1.2 Organocatalysis

The name 'organocatalysis' was coined by MacMillan in 2000, even if some reactions catalysed by small, organic molecules were known since the beginning of the XX century. From the beginning of this century organocatalysis has become a powerful tool, added to other well established techniques such as biocatalysis and metal catalysis. Organocatalysis relies on the capability of small organic molecules to catalyse organic transformations, the most useful of which belong to the area of asymmetric synthesis. Today most of the reactions in asymmetric catalysis still rely on organometallic complexes, but organocatalysis is becoming more and more important because it presents a series of advantages: (a) reactions can be performed in an aerobic atmosphere (the presence of water is often beneficial), (b) the catalysts used are more stable and less expensive as often they are obtained from natural compounds, (c) organocatalysis is best suited for the synthesis of more complex structures through domino reactions thanks to the easy prediction of stereoselectivity and (d) it presents fewer toxicity issues being safer, cheaper and not requiring expensive waste treatment.

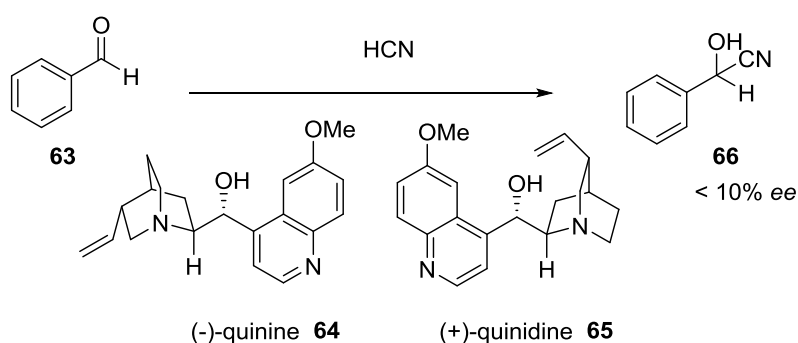
Despite the advantages offered by organocatalysis, there are also some drawbacks as, for example, the high catalyst loading needed in most of the reactions and the limited substrate scope for a particular organocatalyst in a particular transformation.

1.2.1 Historical development of organocatalysis

The initial experiments in this field dated back to the end of the XIX century. It takes a long time for asymmetric organocatalysis to become a practical synthetic paradigm. For a long time it was considered to be limited both in efficiency and scope if compared to organometallic catalysis.

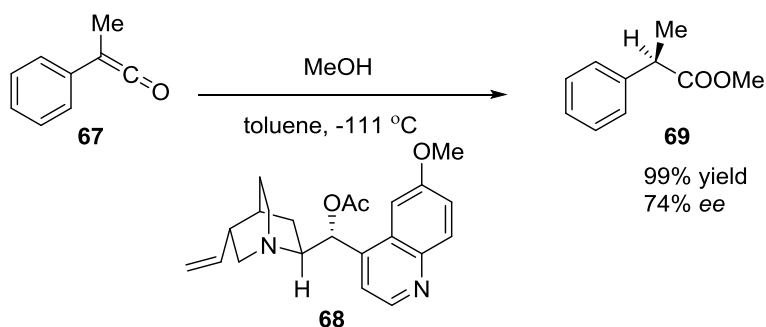
Organocatalysis seems to have operated in the formation of prebiotic fundamental chiral organic molecules such as sugars (for example *L*-isovaline, found in meteorites, was able to catalyse reactions that lead to the formation of sugars).^[31–33] Then, the discovery of the catalytic properties of enzymes played an important role in the

development of asymmetric catalytic reactions (biocatalysis).^[34] It has to be noted that more than half of the enzymes work without the presence of a metal. Combining these two concepts, the potential role of small optically active organic molecules as asymmetric catalysts becomes evident. To name just a few examples: the first asymmetric carbon-carbon bond formation was described by Bredig, that obtained mandelonitrile **66**, with an enantiomeric excess of less than 10%, by the addition of HCN to benzaldehyde **63** using the alkaloids quinine **64** and quinidine **65** as catalysts (**Scheme 15**).^[35] This work was inspired by the previous achievement of Rosenthaler, who prepared mandelonitrile, by the same reaction catalysed by the isolated enzyme emulsin.^[30]



Scheme 15. Bredig's work

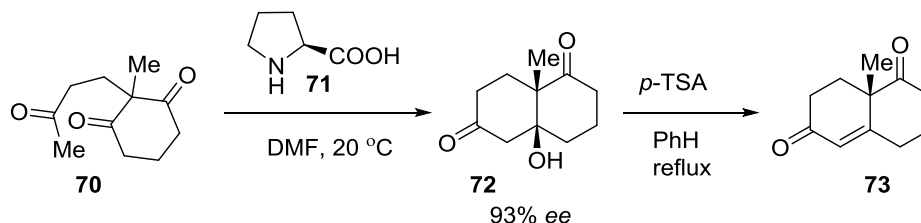
In the late 1950s Pracejus converted methyl phenyl ketene **67** to (-)- α -phenyl methylpropiolate **69** in 99% yield, with 74% ee, employing *O*-acetylquinine **68** as catalyst (**Scheme 16**).^[36]



Scheme 16. Pracejus' work

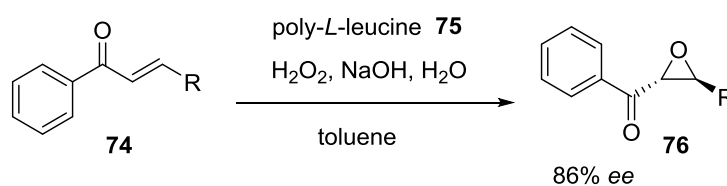
In the early 1970s, the Hajos-Parrish-Eder-Sauer-Wiechert reaction, a (*S*)-proline **71** catalysed asymmetric desymmetrisation by aldol reaction, led to the preparation of

the Wieland-Miescher ketone **73**, a useful intermediate in the synthesis of natural compounds. The bicyclic ketol **72** was obtained in 93% *ee*, using only 3% of (*S*)-proline catalyst (**Scheme 17**).^[37,38]



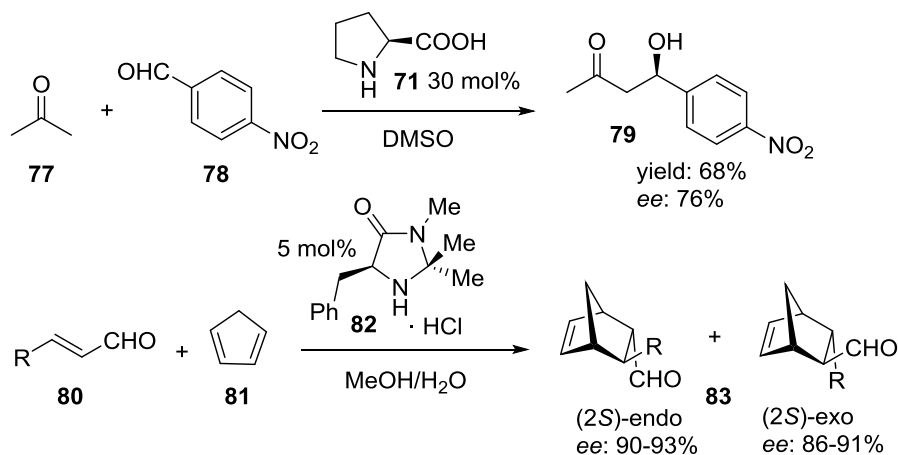
Scheme 17. Hajos-Parrish-Eder-Sauer-Wiechert reaction

In the 1980s, the Julia-Colonna epoxidation of enones **74** with H_2O_2 catalysed by poly-*L*-leucine **75**, represented the first example of hydrogen-bonding catalysis, another important tool in asymmetric synthesis (**Scheme 18**).^[39,40]



Scheme 18. Julia-Colonna epoxidation

The year 2000 can be considered the start of the “Renaissance” of organocatalysis thanks to the pioneering works of List^[41] and MacMillan.^[42] List published an intermolecular asymmetric aldol reaction catalysed by proline **71**, while MacMillan studied the first enantioselective organocatalytic Diels-Alder reaction (**Scheme 19**).



Scheme 19. Pioneering works of List and MacMillan

Since then a plethora of asymmetric reactions have been developed.^[43–47]

1.2.2 Classification of the organic catalysts

According to List^[43] it is possible to classify most of the organic catalysts in four classes: Lewis bases, Lewis acids, Brønsted bases, Brønsted acids (**Figure 5**).

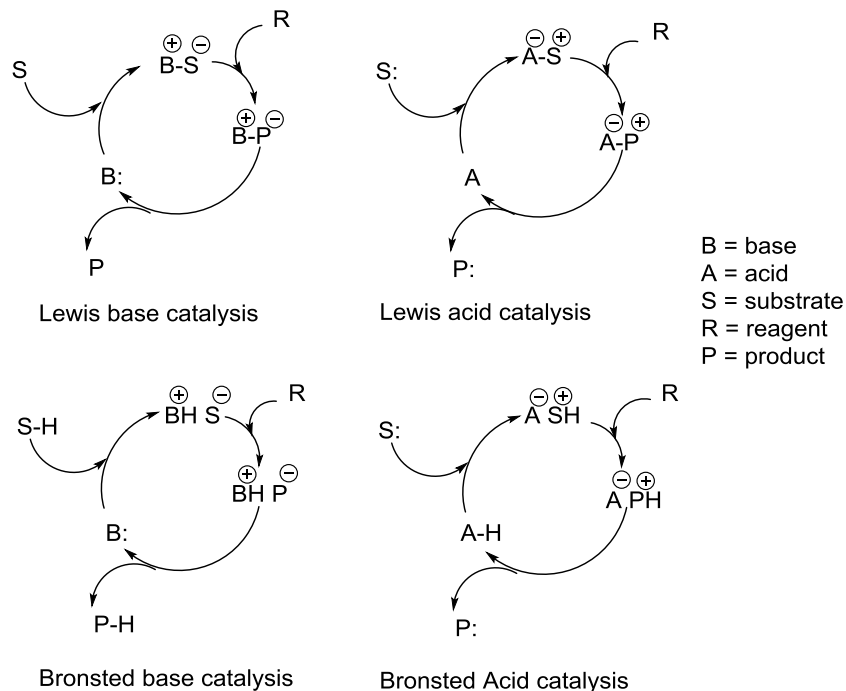
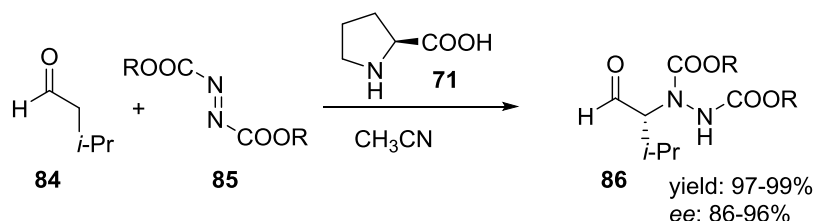


Figure 5. Organocatalytic cycles

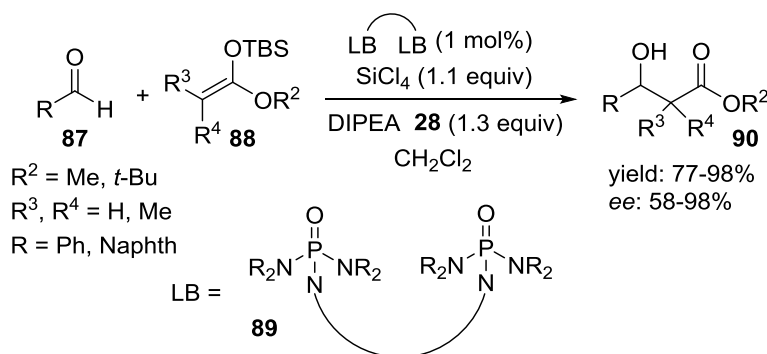
In the case of Lewis base catalyst (B:) the cycle starts with the nucleophilic addition of the catalyst to the substrate (S). The complex undergoes a reaction and then releases

the product (P) and the catalyst, ready to participate in another catalytic cycle. An example of Lewis base catalysis is the enamine catalysis that involves an enamine intermediate generated *via* deprotonation of an iminium ion that can react with an electrophile. An example of this type of catalysis is presented in the work of List,^[48] shown in **Scheme 20**.



Scheme 20. Lewis base catalysis

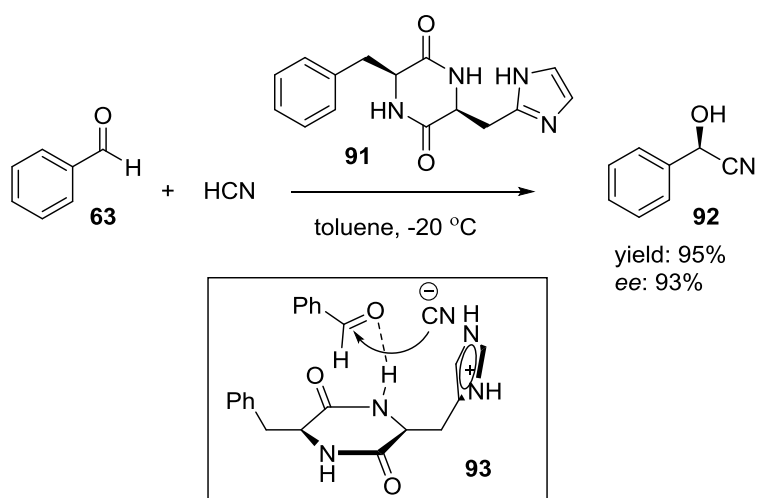
In the case of the Lewis acid (A) there are the addition of the nucleophilic substrate (S:) to the catalyst, the formation of the product and the release of the product (P:) and the catalyst as in the previous case. It is characterised by the electrophilic activation of functional groups towards a nucleophilic attack. An example is given by the work of Denmark that used a chiral bidentate Lewis base and SiCl_4 to create a Lewis acid in situ (**Scheme 21**).^[49]



Scheme 21. Lewis acid catalysis

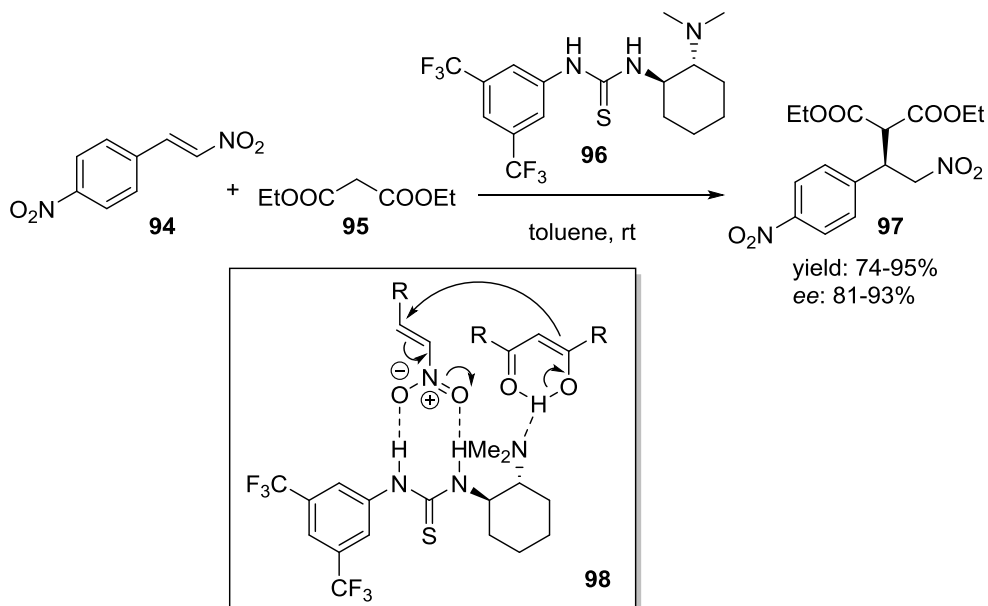
Brønsted acid and base catalytic cycles start with a partial deprotonation or protonation of the substrate, respectively. Typical examples of Brønsted base catalysed reactions are the hydrocyanation reactions as shown in Inoue work in **Scheme 22**.^[50] This catalyst **91** can act as a bifunctional catalyst as not only the imidazolyl moiety deprotonates HCN forming the cyanide anion (that then interacts

with the same moiety) but also the oxygen of the benzaldehyde forms a hydrogen bond with the hydrogen of the istidine residue.



Scheme 22. Brønsted base and acid bifunctional catalyst

The Takemoto catalyst **96** is a bifunctional organic catalyst that can act as a Brønsted acid and as a Brønsted base catalyst: the thiourea interacts with the nitro group *via* hydrogen-bonding activation, while the tertiary amine activates the nucleophile acting as a Brønsted base (**Scheme 23**).^[51]

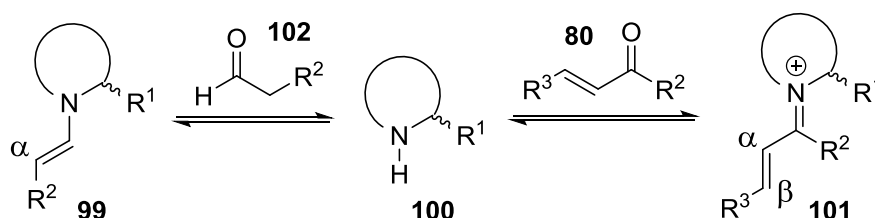


Scheme 23. Takemoto bifunctional catalyst

One of the limitations of this classification is the lack of information on the mechanisms of most of the organocatalytic reactions due to the lack of kinetic data.

1.2.3 Modes of activation: aminocatalysis

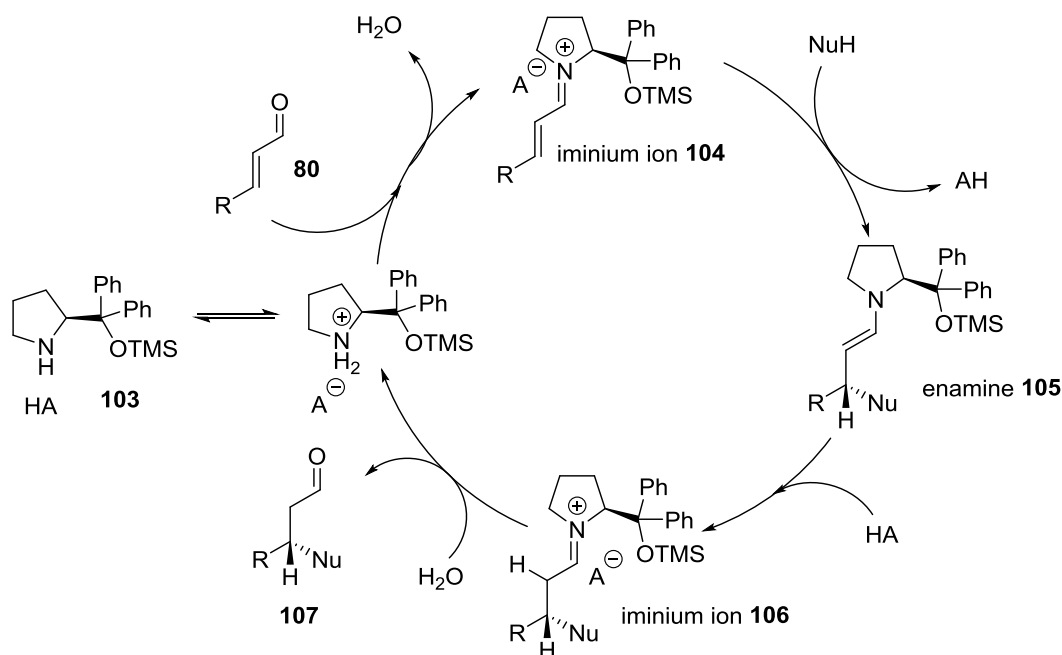
For the purpose of this thesis, only the Lewis base catalysis will be discussed in depth, in particular the **aminocatalysis**. This term was first used by List in 2001^[44] to designate reactions catalysed by secondary and primary amines, taking place via enamine and iminium ion intermediates (**Scheme 24**). Enamine activation **99** produces an increased electron density at the α -carbon atom, while the iminium activation **101** results in a decreased electron density at the carbonyl carbon atom, thus activating the β -position of the aldehyde **80**. In both cases there is an amplified reactivity of the reaction center.



Scheme 24. Enamine and iminium intermediates

1.2.3.1 Iminium catalysis

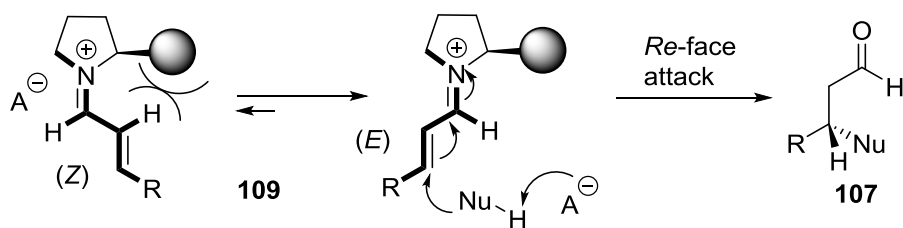
Iminium catalysis is now an established strategy for the asymmetric addition of nucleophiles at the β position of enals. An example of a catalytic cycle is shown in **Scheme 25**.



Scheme 25. Catalytic cycle of iminium catalysis

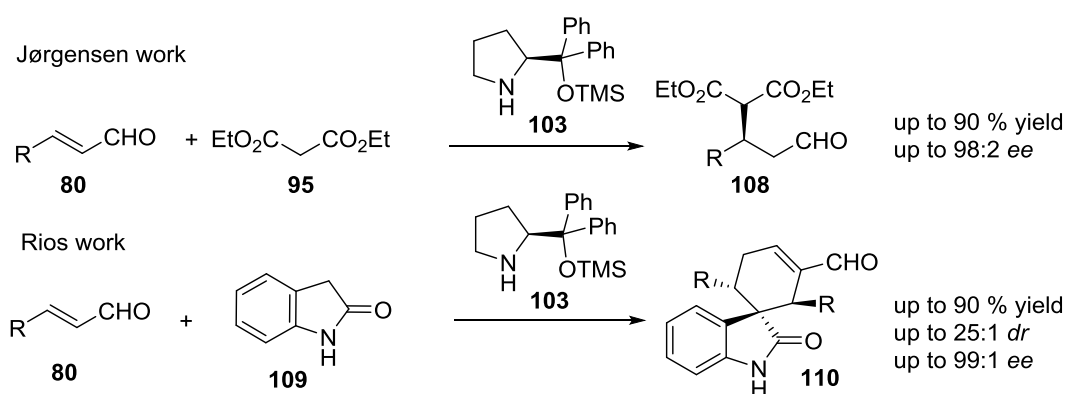
The cycle starts with the acid-promoted condensation of the carbonyl **80** with the amine **103** to form the iminium ion **104**, more electrophilic than the starting enal. The equilibrium between the *E*-iminium ion and the *Z*-iminium ion is shifted heavily towards the *E* form as it is the more stable one. The nucleophile then attacks the β -position with the formation of the *anti*-enamine **105** in equilibrium with the iminium ion **106**. The hydrolysis of the iminium releases the product **107** and the catalyst which can re-enter the catalytic cycle.

The facial selectivity of the attack is determined by the chirality of the secondary amine. The bigger the substituents on the pyrrolidine the better the selectivity will be, but conversely the rate of the reaction will decrease. The stereochemistry can be predicted from the transition state depicted in **Scheme 26**: the attack of the nucleophile will be from the face opposite to the bulky amine substituent in the energetically favoured *trans* conformer of the (*E*)-iminium ion.



Scheme 26. Stereochemical outcome of amine-catalysed addition to enals

Some examples of C-C bond formation based on the iminium activation are: the addition of malonates **95** to α,β -unsaturated aldehydes **80** developed by Jørgensen,^[52] the addition of fluorobis(phenylsulfonyl)methane to enals^[53–55] or the synthesis of spirocyclic compounds developed by Melchiorre^[56] and Rios^[57] (**Scheme 27**).



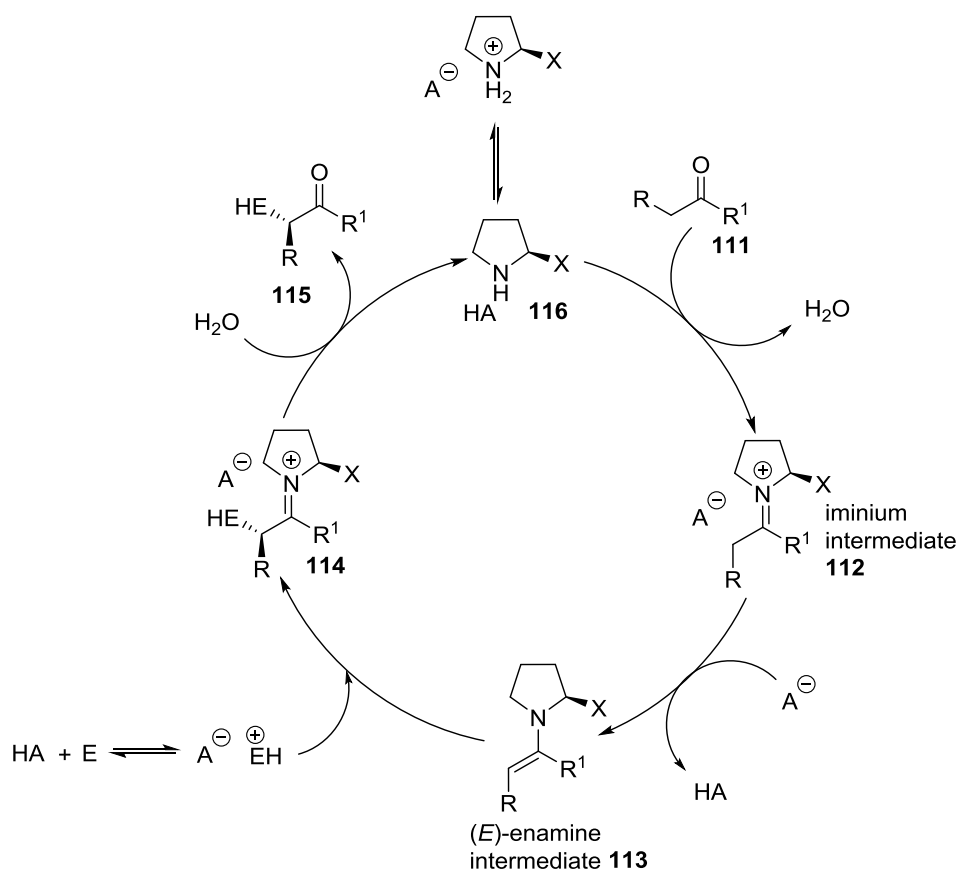
Scheme 27. Examples of organocatalytic nucleophilic addition

There are still big challenges in this area of organocatalysis such as the fact that the addition of enals requires the use of good nucleophiles like malonates or, in general, dicarbonyl compounds containing acidic hydrogens. There are only two examples in the literature on the addition of benzylic nucleophiles to enals: Melchiorre reported the addition of diarylmethylenes to the β position of the enals but this reaction has some limits such as the very low diastereoselectivity and the need to use two activated aryl groups bearing electro-withdrawing groups.^[58] In 2010 Ruano reported the addition of nitrophenylacetonitriles to enals catalysed by secondary amines with good enantioselectivity.^[59]

1.2.3.2 Enamine catalysis

Enamine catalysis has become one of the most employed organocatalytic mode of activation, allowing the enantioselective α -functionalisation of enolisable aldehydes and ketones with a variety of electrophiles.^[60]

In **Scheme 28** is presented the general mechanism. A chiral 2-substituted pyrrolidine **116** is the most representative catalyst, acting with a Brønsted acid co-catalyst AH. The acid can be a protic solvent (water, alcohols), an added external acid or a functional group present in the amine catalyst. The first step of the catalytic cycle is the acid promoted condensation of the carbonyl **111** with the amine forming an iminium ion **112**. One of the α -acidic protons of the iminium ion is removed by the conjugate base of the Brønsted acid, forming the nucleophilic enamine intermediate **113**. The reaction with an electrophile generates an iminium ion **114** that, after hydrolysis, liberates the final product **115**, the acid and the amine catalyst. The efficiency of this catalytic cycle is based on the fast and quantitative generation of the iminium ion, its interconversion in the (*E*)-enamine intermediate and a high stereochemical control over the electrophilic attack. Finally it is important that the possible reaction between the amine and the electrophile is slow or reversible.



Scheme 28. Generalised mechanism for the amine-catalysed α -functionalisation of carbonyls

The stereochemical outcome of the reaction can be predicted based on the substituent present in position 2 of the pyrrolidine. If the chiral amine bears a hydrogen-bond directing group (carboxylic acid, amide) the attack of the electrophile takes place *via* a cyclic transition state (List-Houk model, **Figure 6 A**). Seebach and Eschenmoser^[61] proposed an alternative transition state based on the protonation of the electrophile followed by an electrophilic attack directed by an intramolecular reaction of the conjugate base of the substituent on the amine (**Figure 6 B**). If the amine substituent is bulky and without acidic protons, the attack of the electrophile is directed by steric effect, leading to the opposite facial stereoselectivity (**Figure 6 C**).

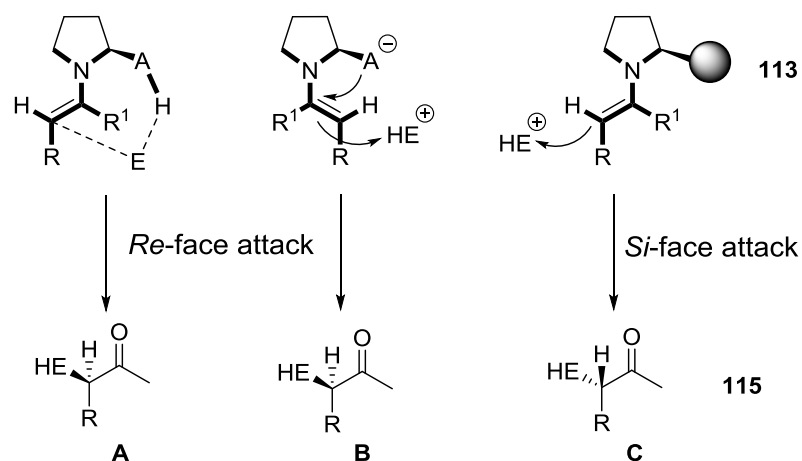
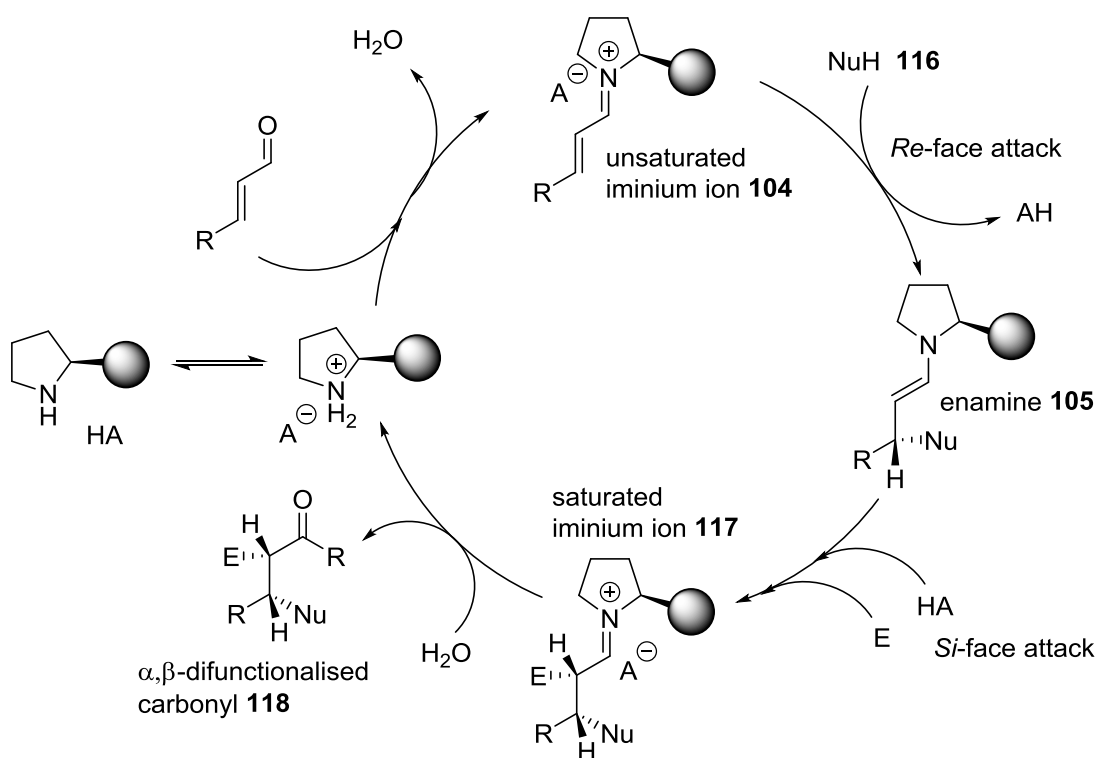


Figure 6. Transition state models for the electrophilic attack to the enamine. (A) List-Houk model, (B) Seebach-Eschenmoser model, (C) steric model.

1.2.3.3 Sequential iminium-enamine catalysis

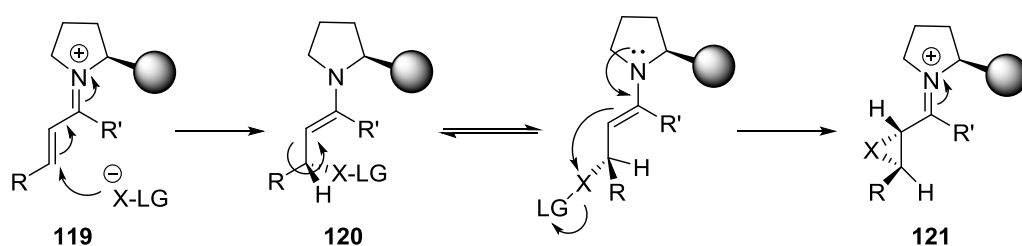
Iminium catalysis proceeds, after the addition of the nucleophile, *via* an (*E*)-enamine **105**. In the presence of a suitable electrophile, an electrophilic addition occurs, forming an iminium ion **117** that, after hydrolysis, releases the catalyst and an α,β-difunctionalised carbonyl product **118** (Scheme 29).



Scheme 29. Sequential iminium-enamine catalysis

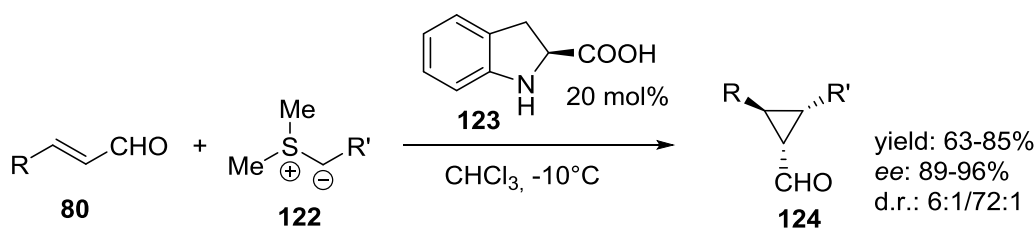
Some examples are reported in 2005 by List,^[62] MacMillan^[63] and Jørgensen.^[64] The absolute stereochemistry can be predicted by the application of the steric model for the Michael addition to iminium ions and of the steric model for the electrophilic attack to enamines.

A limitation is that the electrophile and the nucleophile must be simultaneously present in the reaction mixture without reacting with each other. A way to overcome this limitation is the use of a reagent that exhibits sequentially nucleophilic and electrophilic character. As it is shown in **Scheme 30**, a good reagent could be one with a nucleophilic center attached to a leaving group; after the initial addition of the nucleophile to the iminium ion, an intramolecular attack of the enamine will form a cyclic product **121**.



Scheme 30. Intramolecular sequential iminium-enamine catalysis

An example of an intramolecular sequential iminium-enamine catalysis is the work of MacMillan on the amine-catalysed cyclopropanation of α,β -unsaturated aldehydes **80** by β -oxosulfonium ylides **122** (**Scheme 31**).^[65]



Scheme 31. MacMillan cyclopropanation of α,β -unsaturated aldehydes by β -oxosulfonium ylides

1.3 Multicatalysis

The development of organocatalysis has recently regarded its use in combination with transition metal complexes to take advantage of both catalysts. The driving force is to discover more efficient approaches to synthesise complex molecules with good chemo and stereoselectivity, inaccessible with the use of a single catalytic system.^[66]

The advantages of combining organo- and transition metal catalysts are: (a) enabling the development of new transformations and new reactivity, (b) creating or improving enantioselectivity by using an appropriate combination of an organocatalyst and a chiral or achiral transition metal catalyst, (c) improving the efficiency and expanding the substrate scope.

The main challenges are to ensure the compatibility of the catalysts, substrates, intermediates and solvents.^[67]

As presented in a review of MacMillan^[68] there are four type of multicatalysis mechanisms (**Figure 7**):

1. Bifunctional catalysis when both the nucleophile and electrophile are activated separately by functional groups present on the same catalyst.
2. Double activation catalysis when both catalysts work in concert to activate one of the substrates.
3. Cascade catalysis when both catalysts activate the same substrate in a sequential way.
4. Synergistic catalysis when the nucleophile and the electrophile are simultaneously activated by two separate and distinct catalysts.

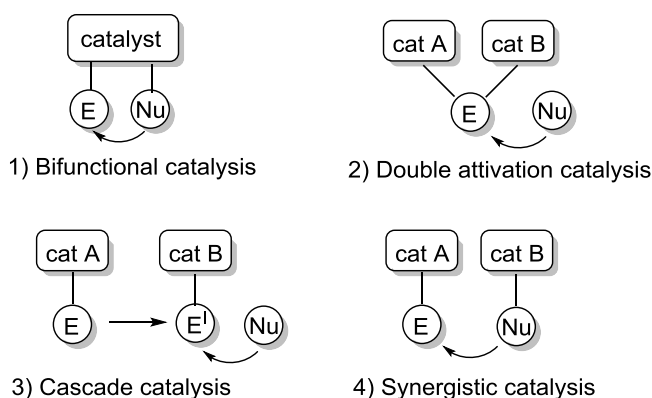


Figure 7. Classification of multicatalysis

1.3.1 Synergistic catalysis

Synergistic catalysis is prevalent in nature as most enzymes work through the cooperation of two or more catalytic moieties to afford one transformation. In organic chemistry is now beginning to emerge as a powerful tool for the formation of new bonds, especially carbon-carbon bonds.

Traditional catalysis is based on the interaction of a single catalyst with a single substrate lowering the energetic barrier to favour the reaction with a second, not activated, substrate. Synergistic catalysis is based on the activation of both the nucleophile and the electrophile creating two reactive species, respectively one with a higher HOMO (highest occupied molecular orbital) and one with a lower LUMO (lowest unoccupied molecular orbital) (**Figure 8**).

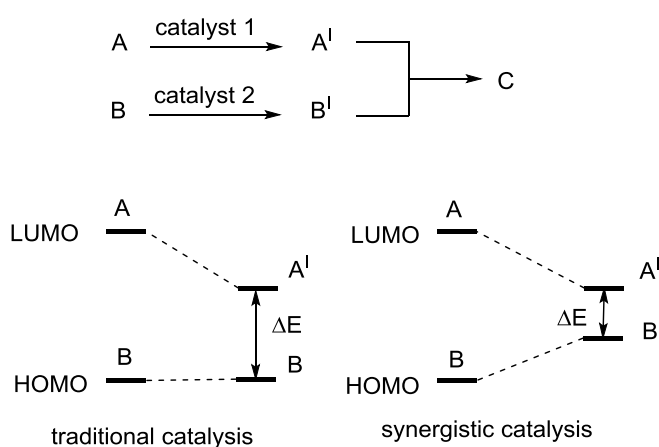


Figure 8. Traditional/Synergistic catalysis

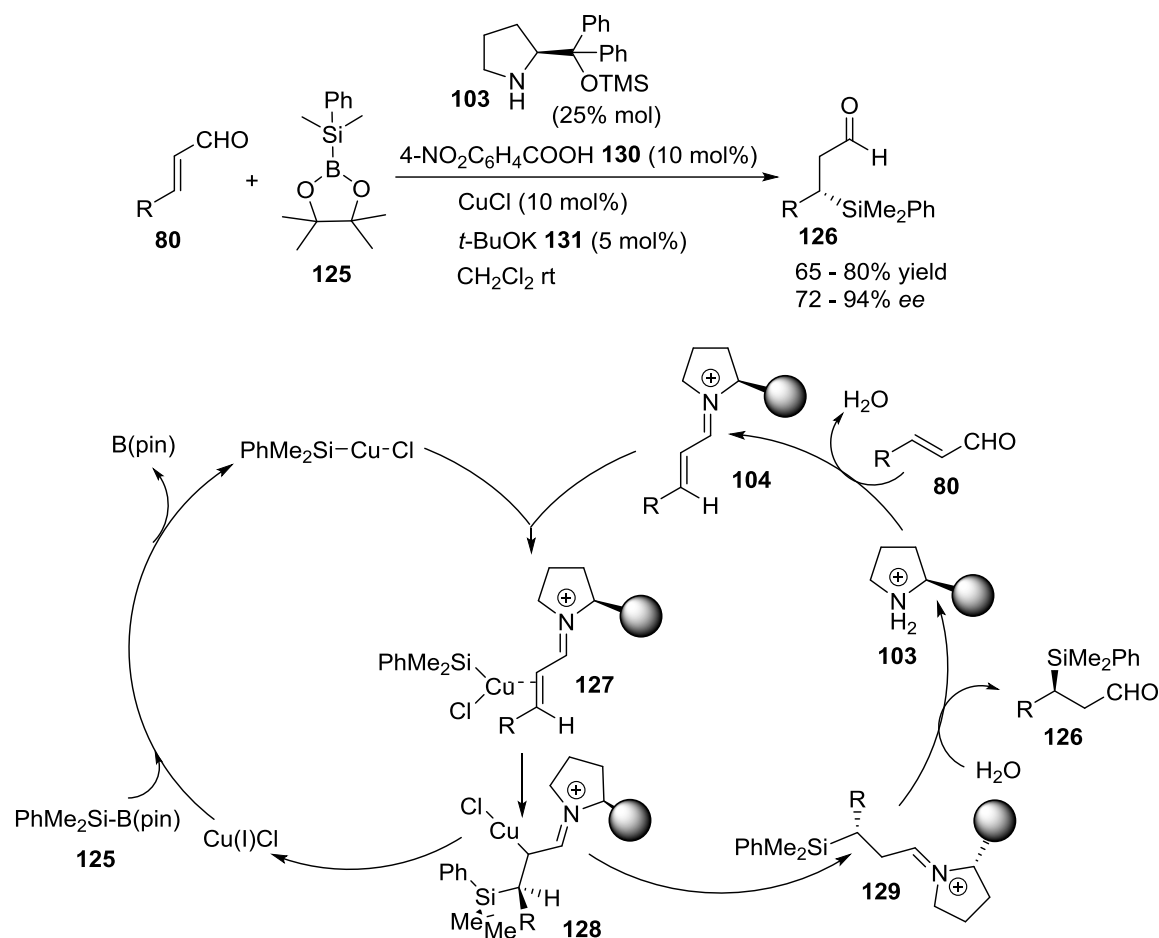
One of the most common approaches in organocatalysis has been the bifunctional catalysis for example the use of tertiary amine/thiourea catalysts as in the Takemoto catalyst. This catalyst activates the nucleophile *via* the amine while the two hydrogen atoms of the thiourea activate the electrophile *via* hydrogen bond-activation as presented before in **Scheme 23**. The main drawback of this type of catalysis is the need to synthesise a new catalyst each time one of the subunits is modified; this will cost money and time and the results could be difficult to predict.

Synergistic catalysis, on the other hand, allows the optimisation of each catalyst independently from the other co-catalyst and allows the use of more varied sources of chirality in each of the catalysts. This increased flexibility leads to an enhancement of the chemical reactivity, allowing the synthesis of more complex products.

A drawback of this type of catalysis is the possible auto-quenching of the two catalysts, rendering them inactive. The solution is to carefully choose an appropriate combination of catalysts, for example a hard Lewis acid and a soft Lewis base that will avoid the formation of strongly coordinated complexes.

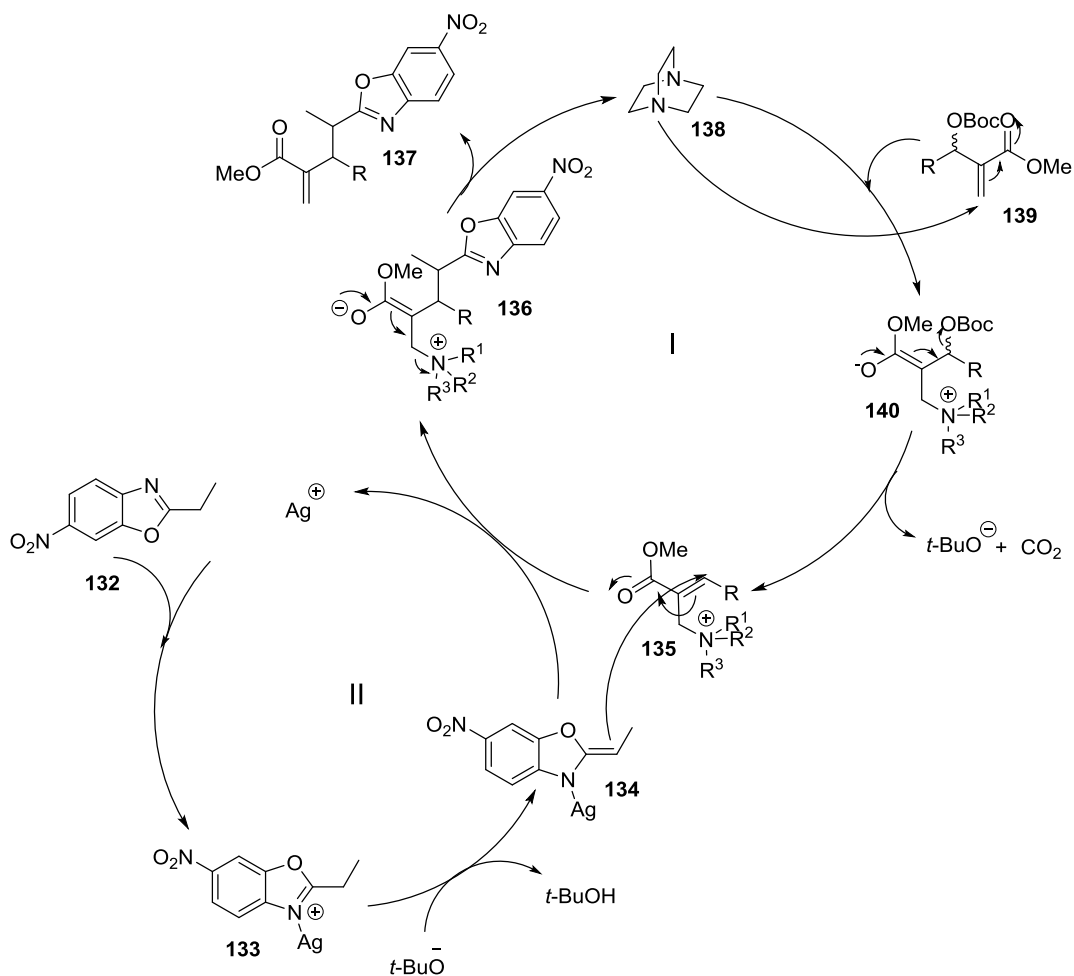
Another apparent drawback is related to the kinetic of the reaction. As the two catalysts are present in substoichiometric concentrations, the concentrations of the two active intermediates will be low and the reaction rate should be low. But this does not take into consideration the rate constant k of the kinetic equation. Compared to traditional catalysis, there is a narrower gap between HOMO and LUMO (**Figure 8**). This causes a decrease in the activation energy, increasing the rate constant (k) of the reaction and overcoming the kinetic effect.

An example of this type of catalysis is the enantioselective silyl addition to enals **80** catalysed by copper and a chiral amine **103**, reported by Córdova in 2011.^[69] As shown in **Scheme 32**, $\text{Me}_2\text{PhSi-B(pin)}$ (pin = pinacolborane) **125** acts as a nucleophile after treatment with CuCl. CuCl induces transmetallation to form the nucleophilic Cu(I)-SiMe₂Ph. This complex attacks the β position of the iminium ion **104**. After the subsequent protonation and hydrolysis of the amine catalyst the desired β -silyl aldehyde **126** is obtained with good yields and selectivities although selectivities are higher with aromatic enals.



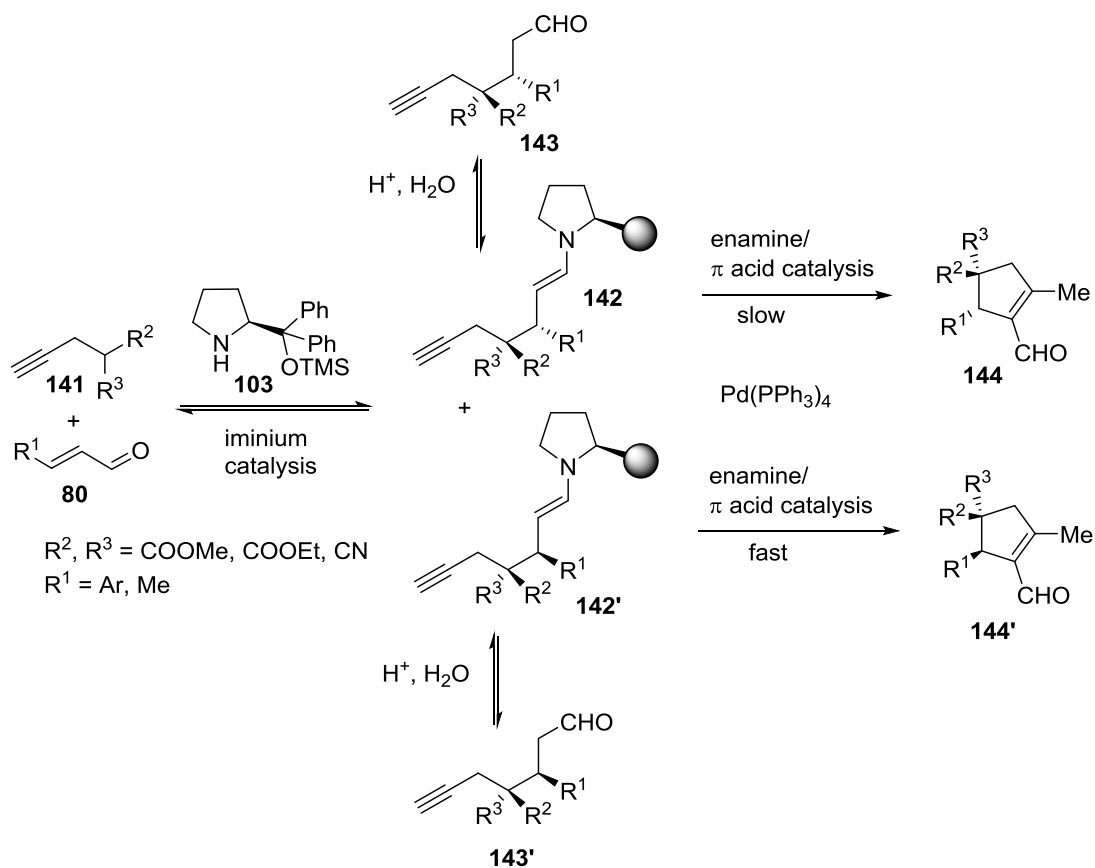
Scheme 32. Córdova's enantioselective silyl addition to enals catalysed by copper and a chiral amine

Recently our research group developed a diastereoselective addition of benzoxazoles **132** to Morita-Baylis-Hillman carbonates (MBH) **139** using the concurrent activation with a Lewis acid and a tertiary amine respectively.^[70] This is the first synergistic catalysis example of alkyl-azaarenes addition to MBH carbonates. As presented in the proposed mechanism in **Scheme 33**, the metal Lewis acid (AgOAc) interacts with the alkyl-azaarene *via* nitrogen coordination, thus increasing the acidity of the α carbon that can be deprotonated by a base. A simultaneous reaction happens between an organic Lewis base (DABCO) **138** and an MBH carbonate **139** *via* $\text{S}_{\text{N}}2$ addition with the formation of the intermediate **135** and the release of carbonic acid. This intermediate reacts with the previously activate nucleophilic intermediate **134** to obtain the intermediate **136**. After the release of the catalyst the final product **137** is obtained with very good diastereoselectivities.



Scheme 33. Proposed mechanism of benzoxazole addition to MBH carbonates

Córdova and co-workers also successfully combined transition metal catalysis with the iminium and enamine catalysis.^[71] They developed a highly enantioselective dynamic kinetic asymmetric transformation (DYKAT) between α,β -unsaturated aldehydes **80** and propargylated carbon acids **141** to form enantiomerically pure cyclopentenones **144'** with good diastereoselectivities and high enantioselectivities (**Scheme 34**).



Scheme 34. Mechanism of Córdoba's DYKAT between α,β -unsaturated aldehydes and propargylated carbon acids to form enantiomerically pure cyclopentenones

This reaction proceeds through a Michael addition catalysed by the secondary amine organocatalyst **103**, followed by a cycloisomerisation catalysed by Pd(0)/enamine, rendering cyclopentenones **144'**. The intermediates **143** and **143'** are formed in equal amounts, but the cyclisation step is irreversible and proceeds with different rates for the two diastereomers.

2. Objectives

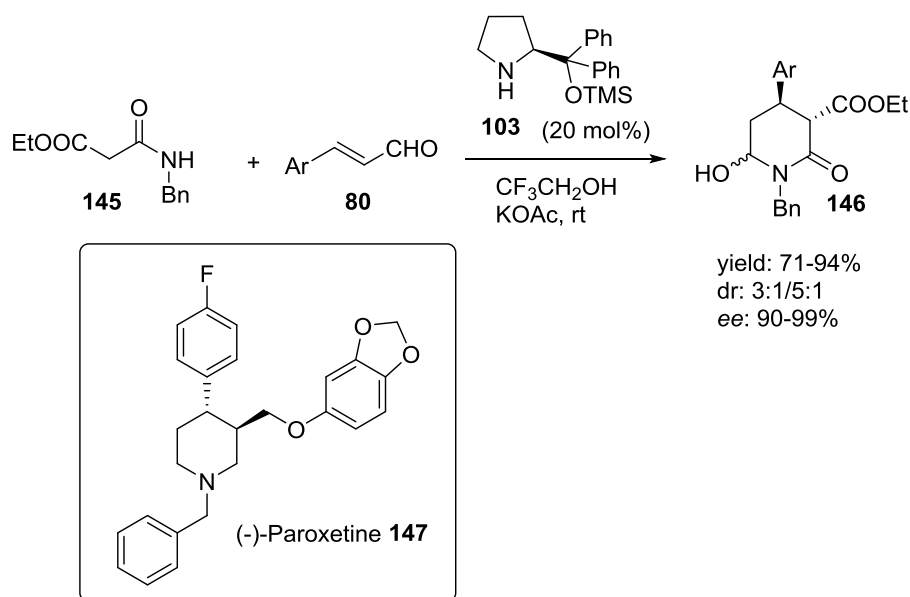
The synthesis of new scaffolds based on alkyl-*N*-heteroaromatics is of paramount importance in medicinal chemistry and agrochemistry. There are very few methodologies for the enantioselective synthesis of *N*-heterocyclic compounds because of the lack of synthetic options currently available.

The objectives of this thesis involve the development of new enantioselective methodologies for the synthesis of alkyl-azaarenes. In particular we want to study the activation of the pseudo benzylic position of alkyl-azaarenes in nucleophilic additions to enals.

- The aim of the first project (Chapter 4) is to study the activation of alkyl-azaarenes through the application of synergistic catalysis. In particular a metal Lewis acid activates the alkyl-azaarenes and an organocatalyst activates the enals.
- The aim of the second project (Chapter 5) is to expand the concept developed in Chapter 4 to a cascade reaction for the synthesis of cyclopropanes and to push the boundaries of synergistic catalysis joining together 3 catalytic cycles for the formation of 2 new C-C bonds.

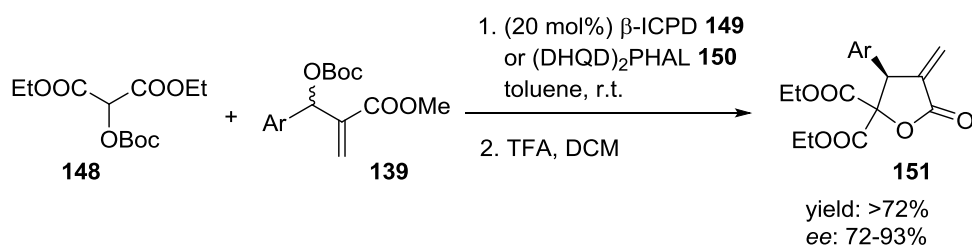
3. Azaarenes

Our research group has developed different organocatalytic methodologies for the enantioselective synthesis of useful and valuable products. For example the organocatalytic synthesis of piperidines for the synthesis of (-)-Paroxetine **147** (Scheme 35).^[72]



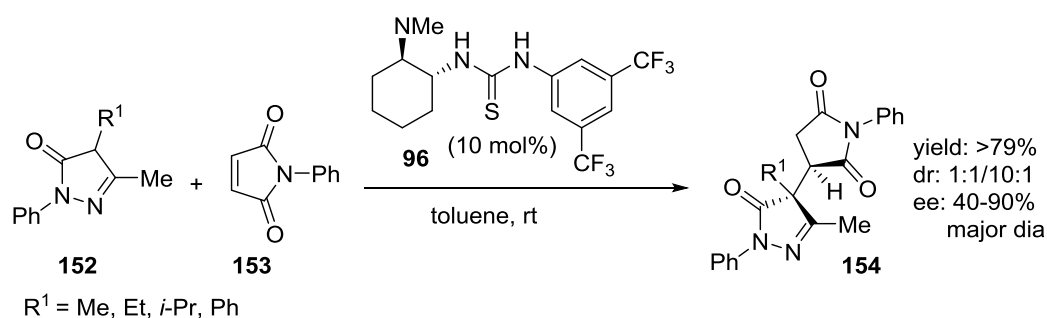
Scheme 35. Synthesis of piperidines

Rios and co-workers developed a reaction between protected 2-hydroxymalonates **148** and MBH carbonates **139** for the synthesis of α -methylene- γ -lactone **151**,^[73] obtained in excellent yields and enantioselectivities (Scheme 36).



Scheme 36. Rios' synthesis of α -methylene- γ -lactone

Other representative examples are the enantioselective addition of pyrazolones **152** to maleimides **153** (Scheme 37).^[74]



Scheme 37. Addition of pyrazolones and oxazolones to maleimides

Recently we became interested in the development of new methodologies for the synthesis of azaarene derivatives.

The synthesis of natural products or metabolites with biological activities has always been an important part of organic chemistry. Despite the advances obtained so far, the synthesis of natural products still requires multiple reaction steps and purifications. For these reasons it is important to study and develop new stereoselective methodologies that can avoid the use of protecting groups and simplify the reactions and the purifications.

The synthesis of azaarenes has attracted a lot of attention due to their importance as they are ubiquitous structures in biologically active pharmaceuticals, agrochemicals and natural products, as shown in **Figure 9**. Azaarenes are used for the treatment of diabetes as inhibitors of dipeptidyl peptidase 4 (DPP-4) **155**,^[75] for the treatment of schizophrenia as GlyT-1 inhibitor **156**,^[76] as fungicide **157**,^[77] as inotropic agent **158**,^[78] as psychoactive drug **159**.^[79]

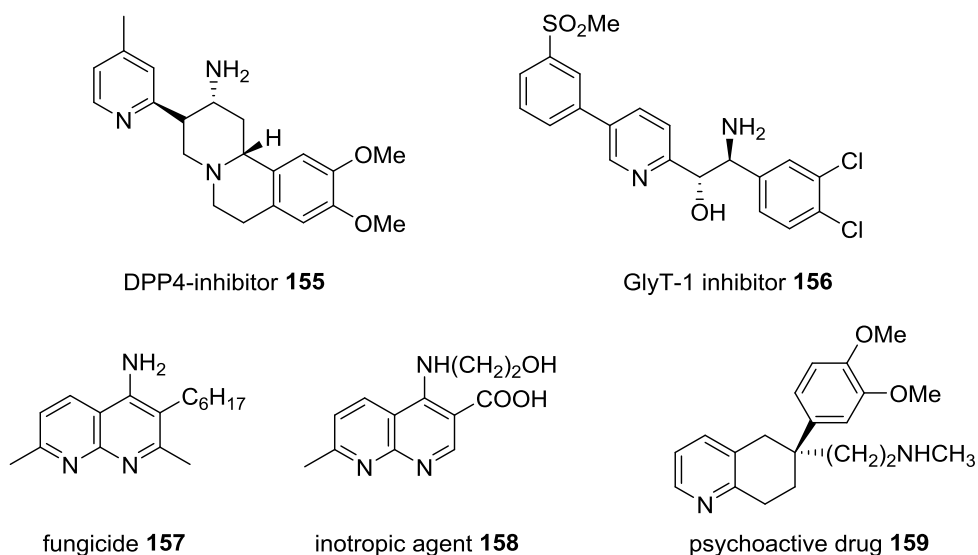


Figure 9. Examples of biologically active azaarenes

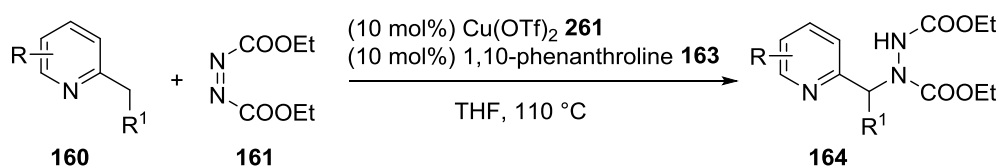
During the last few decades approaches for the synthesis of azaarenes using chiral auxiliaries, employing transition metal catalysts, or using organolithium reagents to deprotonate the acidic proton of the azaarene, have been studied. These methodologies require the use of harsh conditions such as high temperatures, thus presenting problems of compatibility with some functional groups.

3.1 Synthesis of azaarenes: alkylazaarenes as pronucleophiles

The majority of the methodologies reported in literature for the synthesis of azaarenes are non-asymmetric and mainly based on the direct C-H activation and functionalisation using transition metal catalysts.

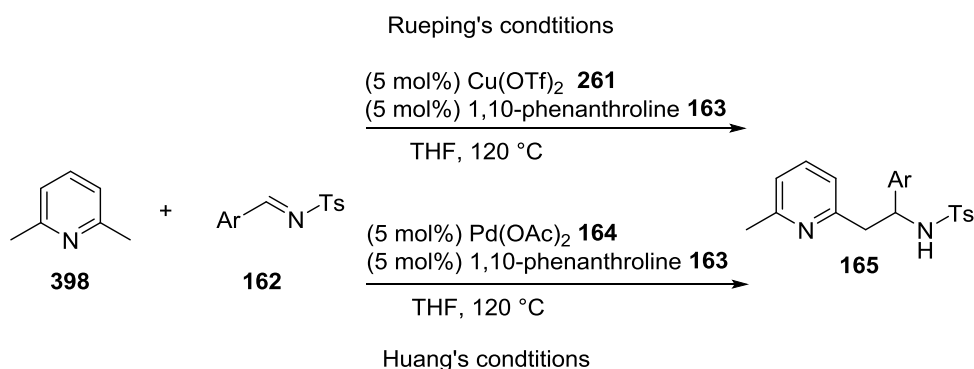
Some examples of synthesis of azaarenes are the following:^[80]

Azaarenes addition to N=N bonds: Guo and Qu reported a Cu(II) catalysed racemic amination of 2-alkylazaarenes **160**. They obtained the products with good yields but using high temperatures (**Scheme 38**).^[81]



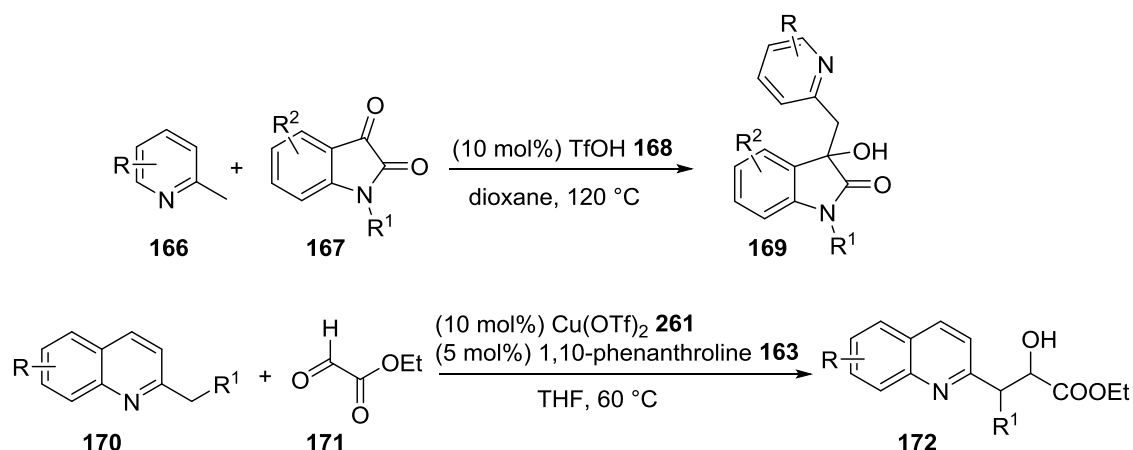
Scheme 38. Guo's amination of 2-alkylazaarenes

Azaarenes addition to C=N bonds: Rueping and Huang studied the addition of azaarenes **398** to *N*-sulfonyl aldimines **162** catalysed by copper **261** and palladium **164** salts respectively (**Scheme 39**).^[82,83] The final products **165** are racemic and the reactions still require the use of high temperatures.



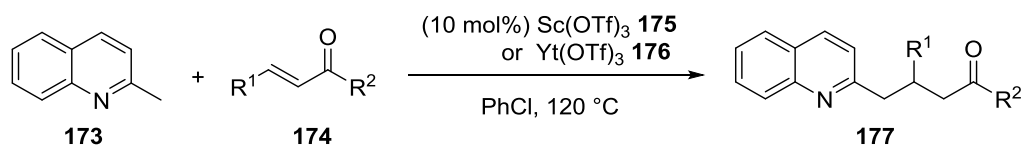
Scheme 39. Rueping's and Huang's racemic addition of azaarenes to *N*-sulfonyl aldimines

Azaarenes addition to C=O bonds: Li^[84] and Fossey^[85] reported the addition of 2-methylazaarenes to isatines **167** and ethyl glyoxylates **171** respectively, using high temperatures (**Scheme 40**).



Scheme 40. Li's and Fossey's addition of 2-methylazaarenes to isatines and ethyl glyoxylates

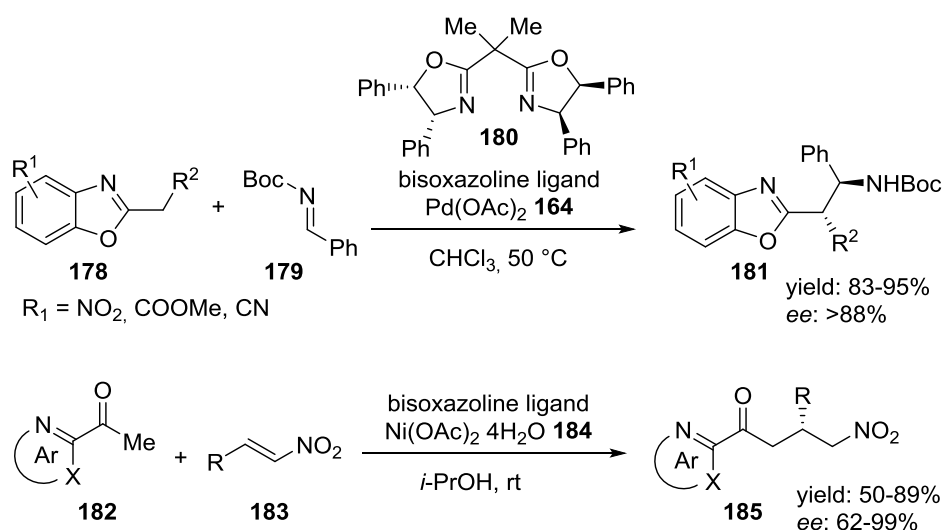
Azaarenes addition to C=C bonds: Huang and co-workers have developed the addition of 2-alkylazaarenes to methylenemalononitriles, using ytterbium salts as catalysts, achieving the products in good yields.^[86] Matsunaga and Kanai studied the direct addition of alkylazaarenes to C=C double bonds of enones **174** catalysed by Lewis acid (**Scheme 41**).^[87]



Scheme 41. Matsunaga's addition of alkylazaarenes to C=C double bonds of enones

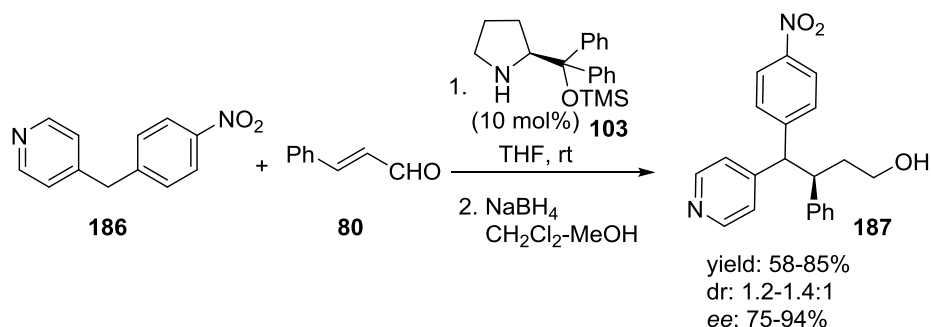
All these methodologies are non-asymmetric and require high temperatures.

Recently, some enantioselective methodologies have been developed. In 2012 Lam and co-workers reported the enantioselective addition of alkylazaarenes **178** to *N*-Boc imines^[88] **179** using Pd(II) salts **164** as catalysts and in 2013 an enantioselective nickel-catalysed Michael addition of 2-acetylazaarenes **182** to nitroalkenes **183**.^[89] The choice of ligand (in this case bisoxazolines **180**) becomes crucial to obtain good enantioselectivities (**Scheme 42**).



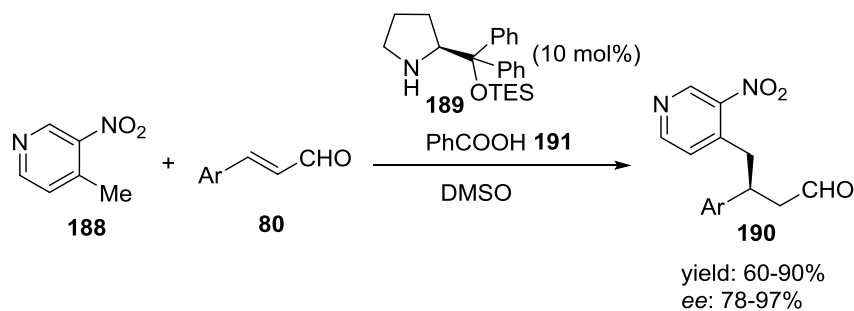
Scheme 42. Lam's activation of azaarenes with metal Lewis acid

Melchiorre and co-workers reported the only organocatalysed methodology for the synthesis of azaarenes. They developed a methodology for the addition of (4-nitrobenzyl)pyridine **186** to enals **80** catalysed by chiral secondary amines **103** (**Scheme 43**). The products **187** are obtained with good yields and enantioselectivities but low diastereoselectivities.^[58]



Scheme 43. Melchiorre's first organocatalytic synthesis of azaarenes

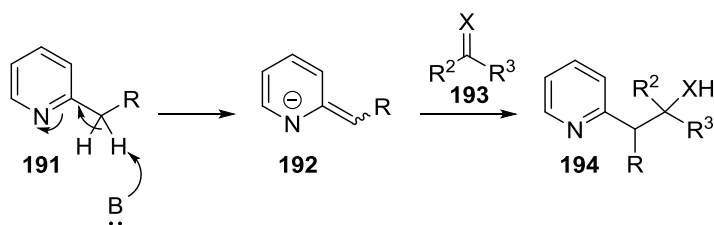
While working on the development of the project reported in Chapter 4, another work in the organocatalytic synthesis of azaarenes was reported by Wang and co-workers.^[90] They described the enantioselective Michael addition of 4-methyl-3-nitropyridine **188** to α,β -unsaturated aldehydes **80**, catalysed by a chiral secondary amine **189** (**Scheme 44**). The final products **190** are obtained with good yields and excellent enantioselectivities (> 90% ee).



Scheme 44. Wang's enantioselective Michael addition of 4-methyl-3-nitropyridine to α,β -unsaturated aldehydes

3.2 Strategies for the activation of alkyl-azaarenes

There are different methods for the activation of these compounds to allow enantioselective reaction. They all use the ability of the C=N of the azaarenes to acidify the protons in α position of the 2-alkylazaarenes **191**, enabling the formation of an azaallyl anion^[91] **192** that can act as a nucleophile in the addition to a π electrophile **193**. The α -deprotonation of 2-alkylazaarenes can be compared to the enolisation of carbonyl compounds (**Scheme 45**).



Scheme 45. Alkylazaarenes as pronucleophiles

The main limitation in the development of these reactions is the low acidity of the 2-alkylazaarenes compared with the carbonyl compounds, so there is the need to find a way to activate the 2-alkylazaarenes, increasing the acidity of the methylene position.

(A) Activation with an electron withdrawing group (EWG) in the alkyl chain.

By adding an EWG at the α -carbon of the alkyl chain, the two hydrogens of the alkyl chain become more acidic (**Figure 10**). In this way the CH_2 can be deprotonated more easily and the azaarene becomes a better nucleophile.

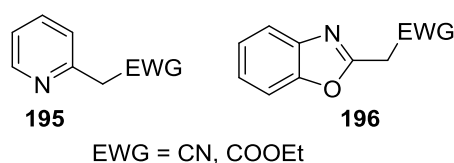


Figure 10. Mode of activation A

(B) Activation with an EWG on the aromatic ring of the azaarenes:

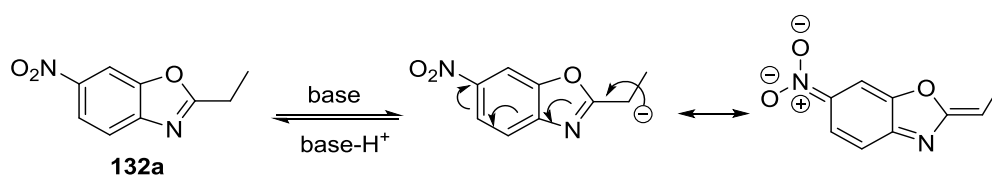


Figure 11. Activation of benzoxazoles with an EWG

We envisaged that incorporation of electron-withdrawing groups (such as nitro, cyano, and ester) into an azaarene **132** would decrease the pKa, increasing the acidity of the α -protons of a pendant alkyl substituent by stabilisation of the conjugate base through conjugation (**Figure 11**). This extended conjugation will allow deprotonation of azaarenes in milder conditions (using weaker bases and lower temperatures). For this reason this will be more compatible with the organocatalytic activation step of the enal and hence more suited to obtain higher stereoselectivities. Moreover, the use of these functional groups would provide highly useful functional handles for subsequent elaboration of the products.

(C) Activation with a metal Lewis acid that coordinates with the *N*-atom.

The equilibrium between the 2-alkylazaarene and its enamine counterpart could be easily shifted once the acidity of the benzylic proton had been enhanced by a suitable metal catalyst. Moreover, a Lewis acid could coordinate with the nitrogen atom of the C=N double bond on the heteroaryl ring and could increase the acidity of the α -carbon position, facilitating the deprotonation (**Figure 12**).

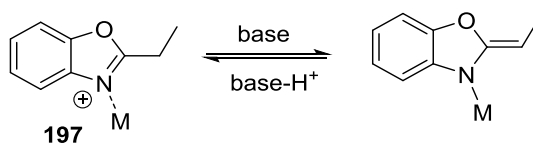


Figure 12. Activation of benzoxazoles with a Lewis acid

We decided to study the stereoselective addition of azaarenes to α,β -unsaturated aldehydes. In order to achieve this goal we plan to use a synergistic approach (as explained in Chapter 1) that consist in the activation of the azaarene with a transition metal salt and the activation of the enal with a chiral secondary amine catalyst.

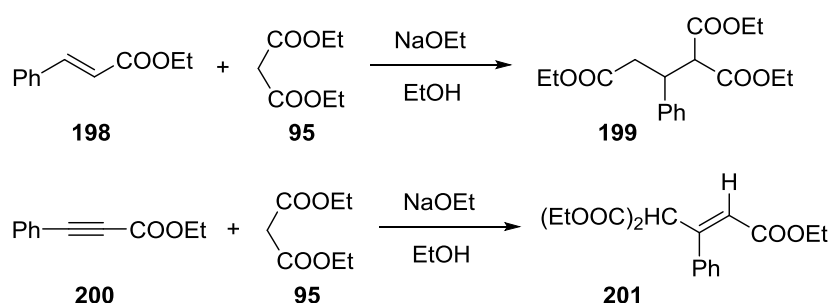
4. Synergistic catalysis: enantioselective addition of alkylbenzoxazoles to enals

4.1 Michael addition

4.1.1 Introduction

The Michael addition is a 1,4-addition (conjugate addition) of a nucleophile to an activated π system. The nucleophile (Michael donor) derives from the deprotonation of a CH-activated compound for example aldehydes, ketones, nitriles, β -dicarbonyl compounds or from the deprotonation of heteroatoms. If the EWG present in the Michael donor is strong enough, it is possible to use relatively weak bases (e.g., Et_3N). The Michael acceptor is an alkene or alkyne activated by an EWG.

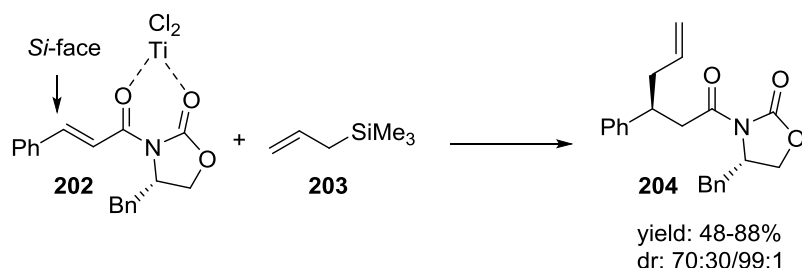
Komnenos, in 1883, published the first example of a carbon nucleophile adding to an electron-deficient double bond^[92] with the addition of the anion of diethyl malonate to ethylidene malonate. In 1887 Michael systematically studied the reaction of stabilised anions with α,β -unsaturated systems^[93,94] and reported the addition of diethyl malonate **95** to the double bond of ethyl cinnamate **198** in the presence of a base to afford a pentanedioic acid diester **199**. Some years later Michael reported that also electron deficient triple bonds **200** can work as Michael acceptors with diethyl malonate as Michael donors (**Scheme 46**).^[95]



Scheme 46. First examples of Michael additions reported by Michael in 1887 and 1894

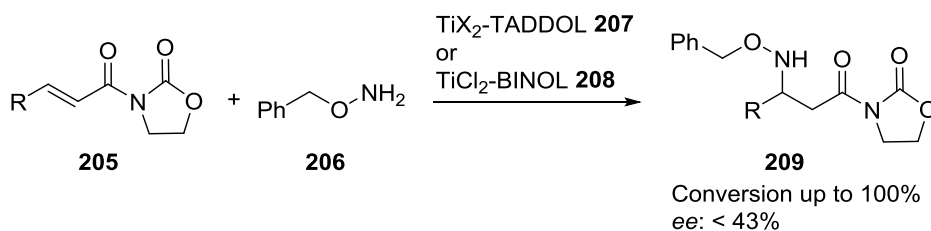
Evans auxiliary was efficiently used by Wu and co-workers to promote a 1,4-Michael addition of allyltrimethylsilanes **203** to α,β -unsaturated carbonyl compounds.^[96] After

the addition of the oxazolidinone auxiliary, an *N*-acylamide **202** is formed and the subsequent Michael addition is promoted by TiCl_4 as Lewis acid, obtaining the allylation products **204** with good yields and diastereoselectivities (**Scheme 47**).



Scheme 47. Wu's 1,4-Michael addition of allyltrimethylsilanes to α,β -carbonyl compounds

Several transition metal-catalysed Michael addition reactions have been developed. One nice example was reported by Jørgensen *et al.* with the addition of *O*-benzylhydroxylamines **206** to α,β -unsaturated carbonyl compounds using chiral Lewis acids (TiX_2 -TADDOL **207** or TiCl_2 -BINOL **208**) as catalysts (**Scheme 48**).^[97]



Scheme 48. Jørgensen's metal catalysed Michael addition of *O*-benzylhydroxylamines to α,β -unsaturated carbonyl compounds

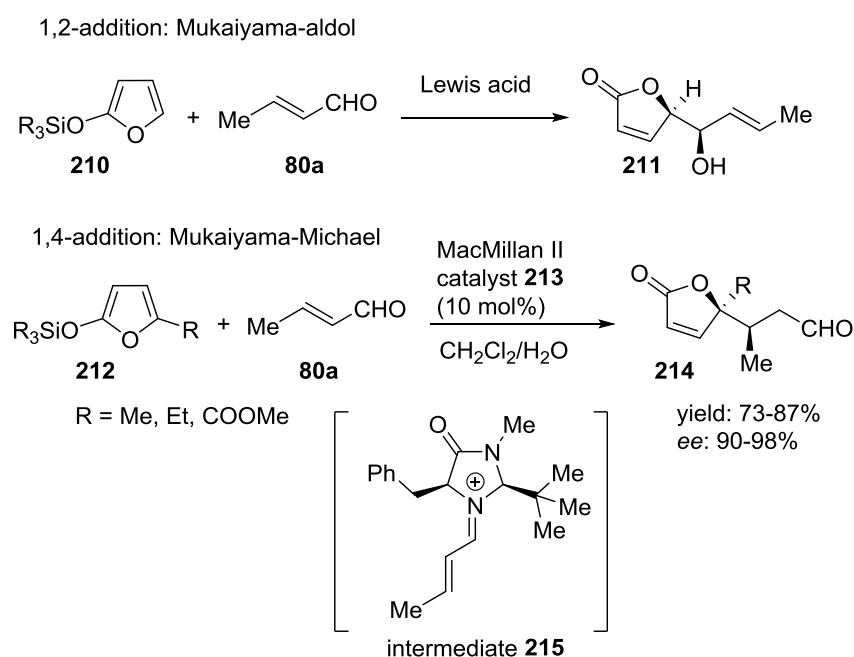
After the development of organocatalysis since 2000, the organocatalytic asymmetric Michael addition has gained a lot of success.^[98–101]

For the purpose of this thesis only the enantioselective organocatalytic Michael addition to α,β -unsaturated aldehydes as Michael acceptor will be covered.

4.1.2 Enantioselective organocatalytic Michael addition with α,β -unsaturated aldehydes as Michael acceptor

The catalytic cycle involving the formation of the iminium ion and the activation of the enal as a Michael acceptor is explained in **Scheme 25** and **Scheme 29**.

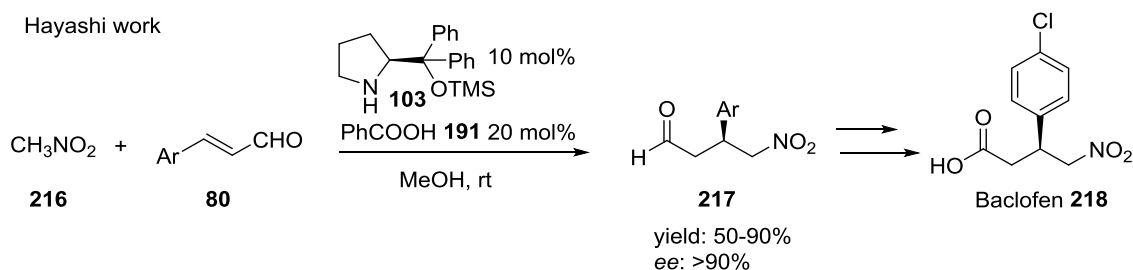
After the formation of the iminium ion, due to the high reactivity, the competitive 1,2-addition could be a major limitation of this reaction. In this regards, MacMillan *et al.* in 2003 reported the first enantioselective organocatalytic Mukaiyama-Michael reaction for the synthesis of γ -butenolide products **214** through the addition of chiral imidazolidinones **215** to α,β -unsaturated aldehyde **80a**.^[102] The same reaction reported in literature (Mukaiyama-aldol) uses metal salts to promote the 1,2-addition. While MacMillan proved that iminium organocatalysis using chiral imidazolidinones promotes the 1,4-addition due to the bulkiness of the catalyst (**Scheme 49**).



Scheme 49. 1,4-addition of chiral imidazolidinones to α,β -unsaturated aldehydes

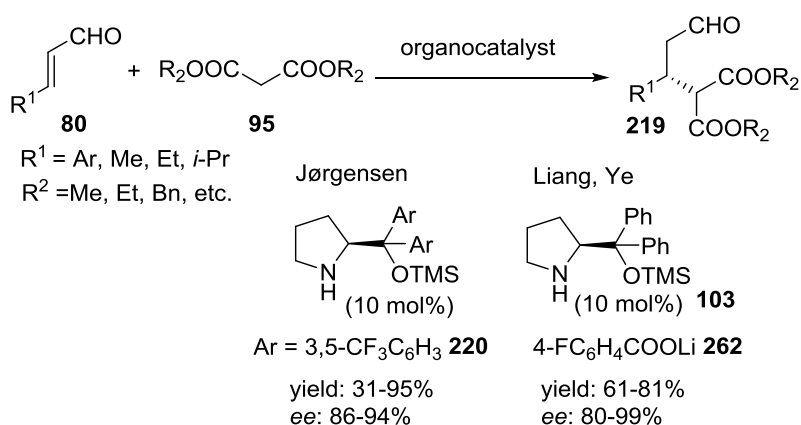
An important reaction based on iminium chemistry is the use of enals as Michael acceptors in the reaction with nitroalkanes as Michael donors, as a strategy to synthesise γ -nitro aldehyde compounds **217**. For example the works of Hayashi *et al.*^[103] (**Scheme 50**) and Wang *et al.*^[104] that use diphenylprolinol silyl ether **103** as a catalyst and benzoic acid **191** as additive, or the work of Ye and Liang *et al.*^[105] using

LiOAc as additive, allow to obtain the final products with excellent enantioselectivities and good yields. This reaction was used in the enantioselective synthesis of the drug Baclofen **218**.



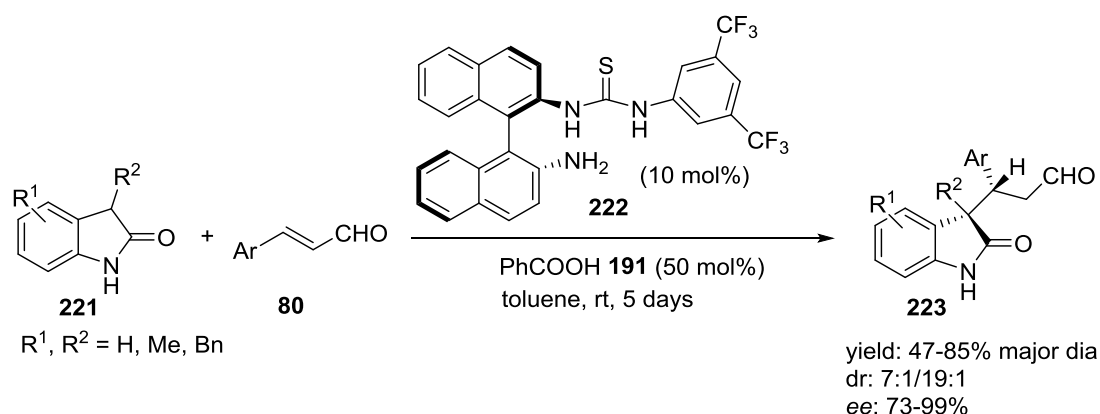
Scheme 50. Hayashi's Michael addition of nitroalkanes to α,β -unsaturated aldehydes

In the same year Jørgensen and co-workers^[106] reported the first organocatalytic asymmetric addition of malonates **95** to aromatic α,β -unsaturated aldehydes **80**. The products **219** were obtained in high yields and excellent enantioselectivities. Later on Liang, Ye and co-workers^[107] found that the reaction proceed faster with the use of a base additive **262** (**Scheme 51**). This reaction is useful for the synthesis of the drugs (-)-Paroxetine and (-)-Femoxetine. Another enantioselective organocatalytic Michael addition applied for the synthesis of (-)-Paroxetine **147** was reported by Rios, Moyano, Vesely *et al.* through the addition of amidomalonates to α,β -unsaturated aldehydes (**Scheme 35**).^[72]



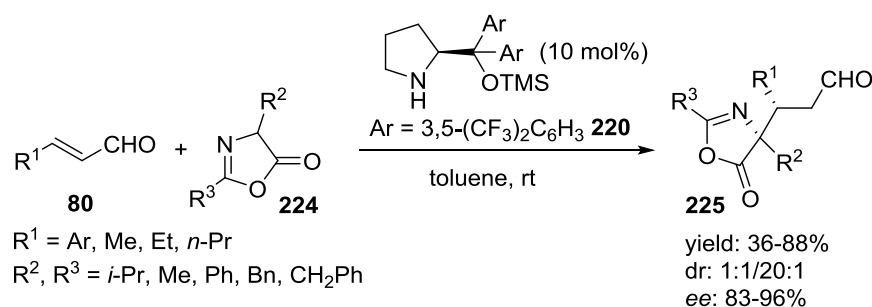
Scheme 51. Asymmetric addition of malonates to aromatic α,β -unsaturated aldehydes

In 2009 Melchiorre and co-workers^[108] reported the first asymmetric conjugate addition of oxindoles **221** to α,β -unsaturated aldehydes **80** (**Scheme 52**). With the use of diarylprolinol, proline or MacMillan catalyst the product was obtained with good enantioselectivity but without diastereoselectivity. For this reason they developed a new bifunctional chiral thiourea catalyst **222** to increase the diastereoselectivity.



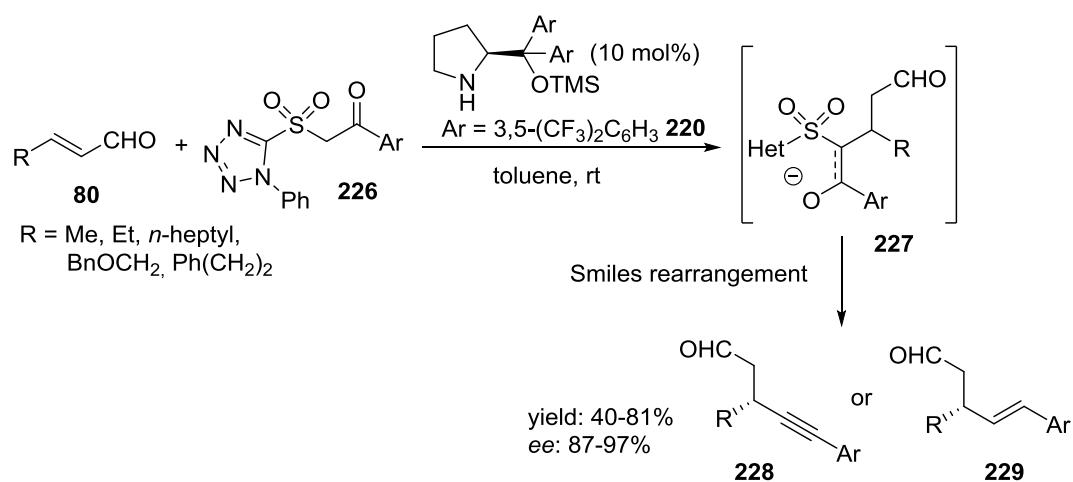
Scheme 52. Melchiorre's addition of oxindoles to α,β -unsaturated aldehydes

Jørgensen *et al.*^[109] reported the addition of oxazolones **224** to enals **80** obtaining the products **225** with moderate to good diastereoselectivity and excellent enantioselectivity (**Scheme 53**). Oxazolones are important reagents for the synthesis of chiral quaternary amino acids and their derivatives.



Scheme 53. Jørgensen's addition of oxazolones to enals

Recent developments report the use of β -carbonyl heteroaryl sulfones as nucleophiles in the addition to enals. Jørgensen and co-workers^[110] reported the Michael addition of β -keto sulfones **226** to α,β -unsaturated aldehydes **80** catalysed by diphenylprolinol silylether **220**, obtaining the final products **228** in good yields and excellent enantioselectivities (**Scheme 54**).



Scheme 54. Jørgensen's addition of β -keto sulfones to α,β -unsaturated aldehydes

4.2 Project aim

The aim of the project is to develop an enantioselective synthesis of alkylazaarenes. In particular to study the activation of 2-alkylazaarenes as nucleophiles to a Michael addition with α,β -unsaturated aldehydes, through the application of the synergistic catalysis concept.

As stated in the introduction in Chapter 1, azaarenes are common structures in biologically active molecules such as pharmaceuticals, agrochemicals and natural products. In spite of their huge importance only few enantioselective methodologies for their synthesis have been developed so far. We have been inspired by Lam and co-workers^[88] that reported the addition of alkyl-azaarenes to nitrostyrenes catalysed by Pd-bisoxazoline complexes with excellent results (**Scheme 42**, Chapter 3).

We planned to activate the benzylic position of the alkyl-azaarenes (a) placing an EWG on the aromatic ring and (b) adding a metal Lewis acid that would work as a catalyst, by coordination with the nitrogen atom. Only the combination of these two strategies can decrease the pKa of the α protons in the methylene position, facilitating the deprotonation in the presence of a weak base, such as a tertiary amine. After the deprotonation, the formation of the enolate form, stabilised through conjugation thanks to the nitro group, would make the benzoxazole a suitable nucleophile.

In **Figure 13** are schematised the strategies of activation of azaarenes that we planned to use in the project.

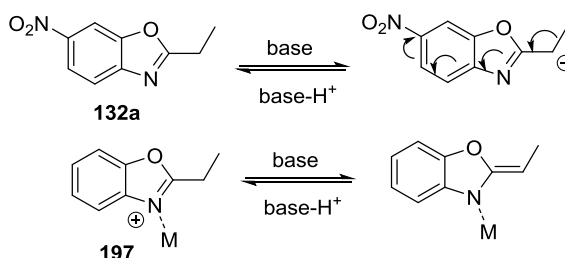
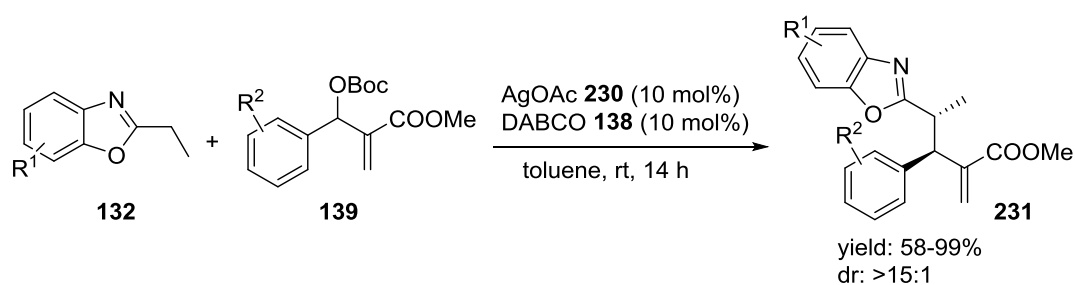


Figure 13. Modes of activation of azaarenes

Recently, our research group demonstrated the feasibility of this synergistic approach reporting the addition of alkylbenzoxazoles to MBH carbonates^[70] based on synergistic

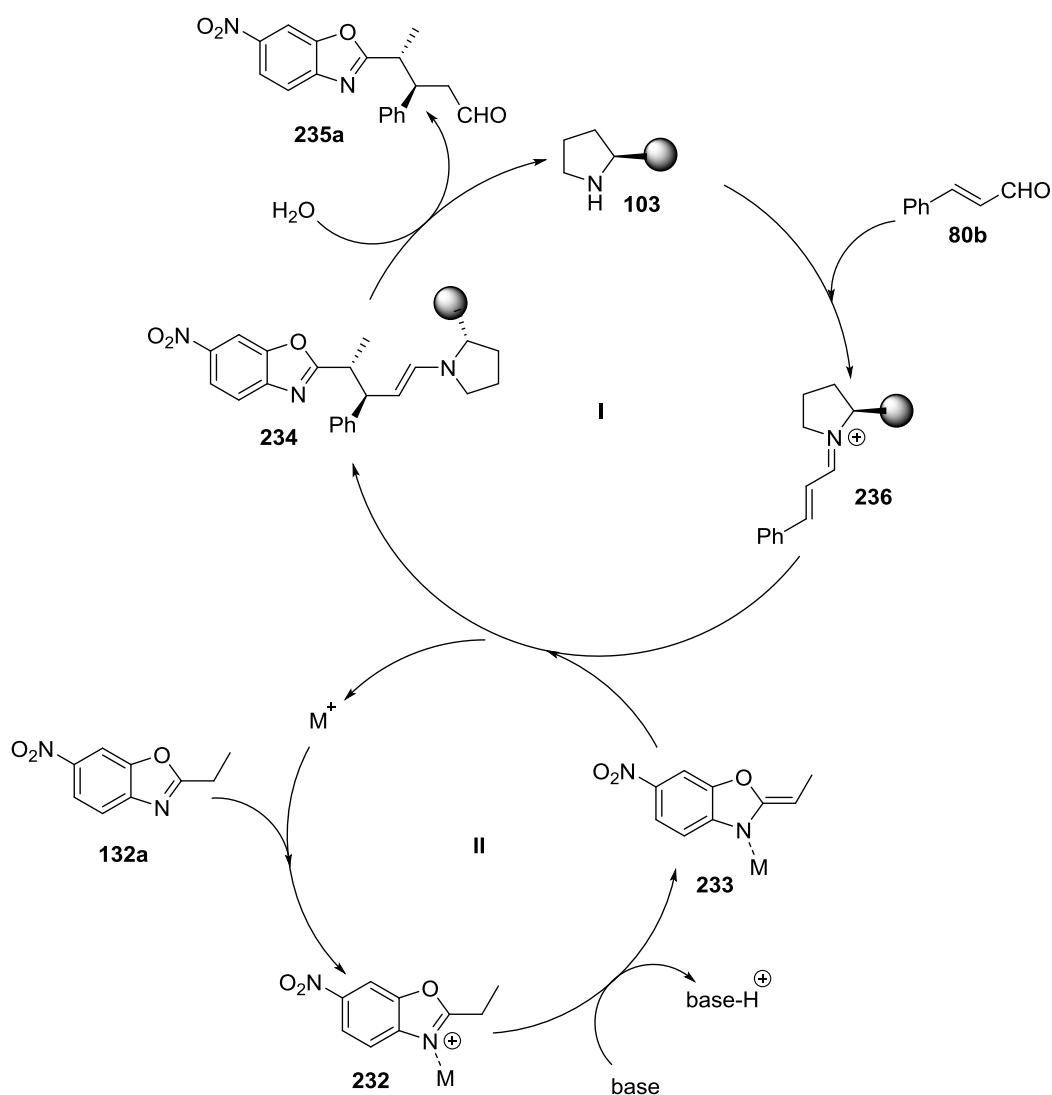
approach in a diastereoselective fashion (**Scheme 33** and **Scheme 55**). The benzoxazole **132** is activated with AgOAc **230** that acts as a metal Lewis acid while the MBH **139** is activated by DABCO **138** and the final products **231** are obtained with good to excellent yields, completely diastereoselective.



Scheme 55. Highly diastereoselective benzoxazole addition to Morita-Baylis-Hillman carbonates

4.3 Research hypothesis and proposed mechanism

In **Scheme 56** is presented the proposed mechanism for the reaction described in the project aim.



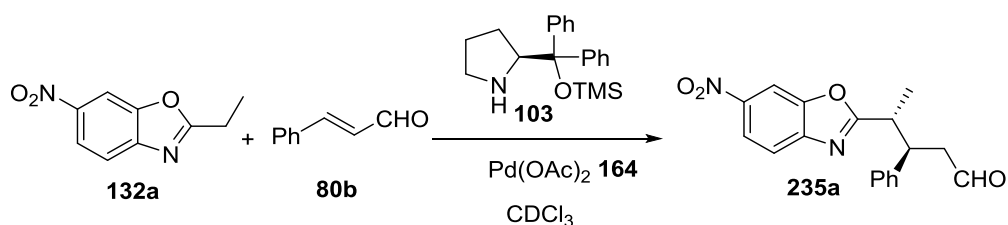
Scheme 56. Proposed reaction mechanism for the enantioselective addition of alkylbenzoxazoles to enals

As is it shown in **Scheme 56**, we envisioned that the metal Lewis acid could interact with the alkyl benzoxazole **132a** coordinating to the nitrogen and increasing the acidity of the α -carbon hydrogens **232**. After treatment with the base, it forms a suitable nucleophile **233** that can react with the electrophile **236**. The enal **80b** reacts with the secondary amine of the organic catalyst **103** to form the activated iminium species **236**. The catalyst efficiently shields one face of the enal, so the benzoxazole is mostly

forced to attack the opposite face. The activated benzoxazole attacks the β position of the aldehyde and releases the metal catalyst. After the addition took place, hydrolysis of the compound **234** leads to the product **235a** and releases the organic catalyst.

We studied the addition reaction between alkyl-benzoxazoles and enals as presented in section **4.2**. To our delight the reaction between **132a** and **80b** rendered the final compound **235a** by using a mixed activation of the azaarene *via* Lewis acid metal coordination catalysis and the activation of the enal using an organocatalyst (**Scheme 57**). The product **235a** was obtained in low yield and selectivity and the reaction was difficult to reproduce in the same conditions.

As this reaction is difficult to monitor and follow by TLC, due to spots overlapping, we checked the reaction by the NMR of the crude. The first reaction was performed in deuterated chloroform in order to easily check the crude by NMR and follow the progress of the reaction. From the integration of the aldehyde signals it is possible to observe the formation of the final product and calculate the reaction conversion. In fact the signal of the starting aldehyde is a doublet while the signal of the final product is a characteristic triplet with a small coupling constant.



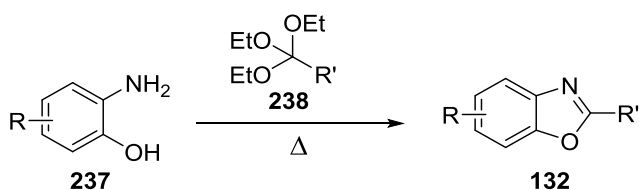
Scheme 57. First reaction tested

4.4 Results and discussions

4.4.1 Synthesis of the starting materials¹

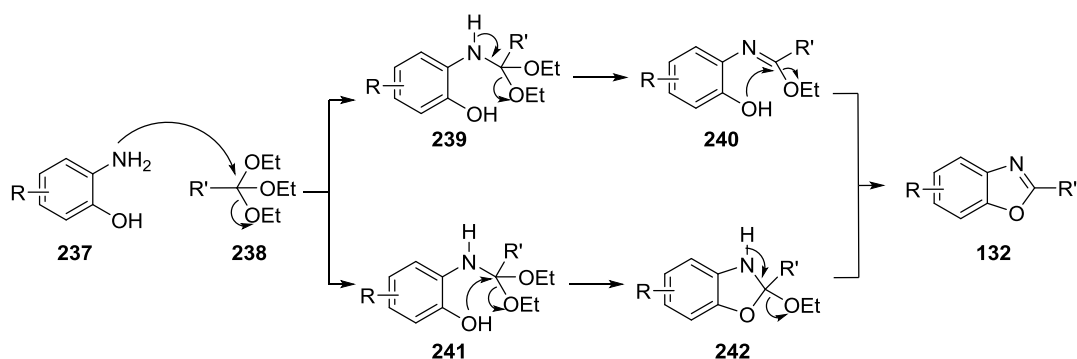
4.4.1.1 Synthesis of the benzoxazoles

Most of the azaarenes were synthesised following the procedure reported in the article of Lam and co-workers^[88] as shown in **Scheme 58**.



Scheme 58. Synthesis of the benzoxazoles as starting materials

The mechanism of the reaction between an aminoalcohol **237** and triethoxyalkane **238** is depicted in **Scheme 59**.



Scheme 59. Mechanism of benzoxazoles' synthesis from triethoxyalkane

The mechanism starts with the attack of the amine to the triethoxyalkane with the elimination of EtOH. Then the reaction can follow two pathways: (a) elimination of ethanol and formation of the iminoether **240** followed by the nucleophilic attack of the phenolic OH with elimination of another molecule of EtOH; (b) nucleophilic attack of

¹ The azaarenes **132** and aldehydes **80** were synthesised by me, India Willans and Michael Potter, project students that I supervised, and azaarenes **132h** and **132j** by Victor Ceban.

the OH with elimination of EtOH **242**, followed by a second elimination of EtO⁻ and formation of the double bond.

The results obtained in the synthesis of the starting benzoxazoles are presented in **Figure 14**, with isolated yields ranging from 73 to 95%.

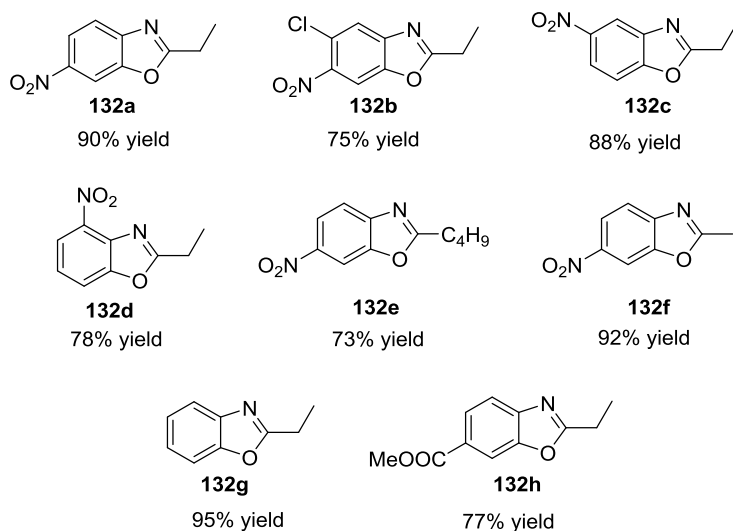
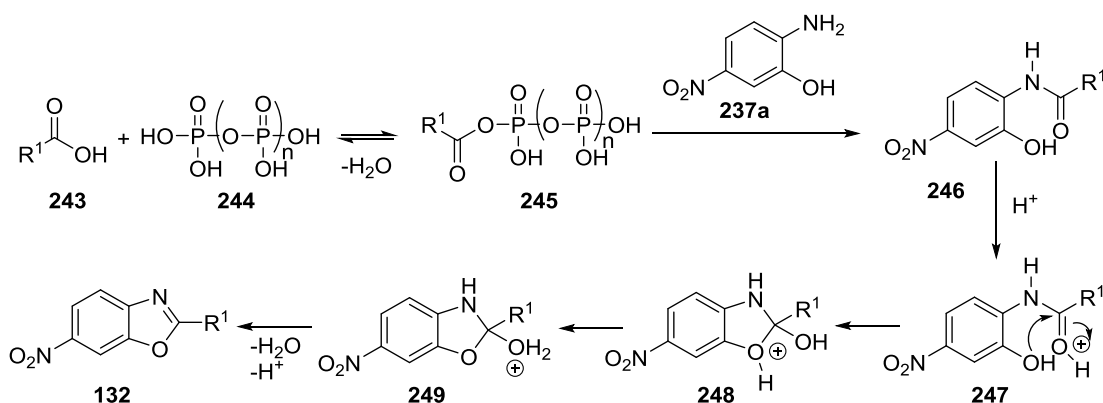


Figure 14. Results obtained in the synthesis of benzoxazoles with triethoxyalkanes

Benzoxazoles **132i** and **132j** are synthesised according to the route reported in **Scheme 60**.



Scheme 60. Mechanism of benzoxazoles' synthesis from acids

The acid **243** reacts with PPA (polyphosphoric acid) **244** forming a mixed anhydride **245** that reacts with 2-amino-5-nitrophenol **237a** to give the corresponding amide **246**. This

intermediate cyclises with elimination of water to render the desired benzoxazole **132**. The results are presented in **Figure 15**.

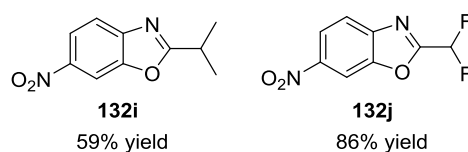
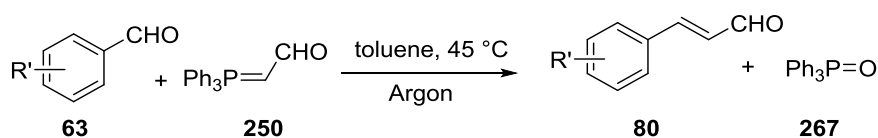


Figure 15. Results obtained in the synthesis of benzoxazoles with acid

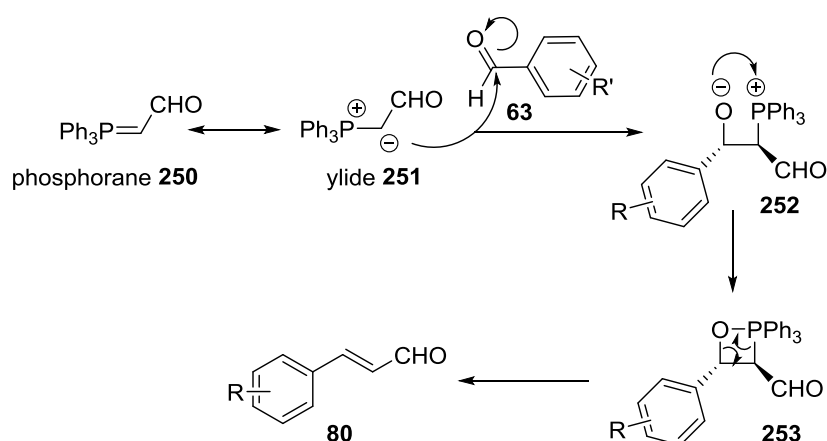
4.4.1.2 Synthesis of the aldehydes

Cinnamaldehyde **80b** and crotonaldehyde **80a** are commercially available, while the other α,β -unsaturated aldehydes were synthesised. This was achieved through a Wittig reaction leading to the *E* form of the aldehydes (**Scheme 61**).



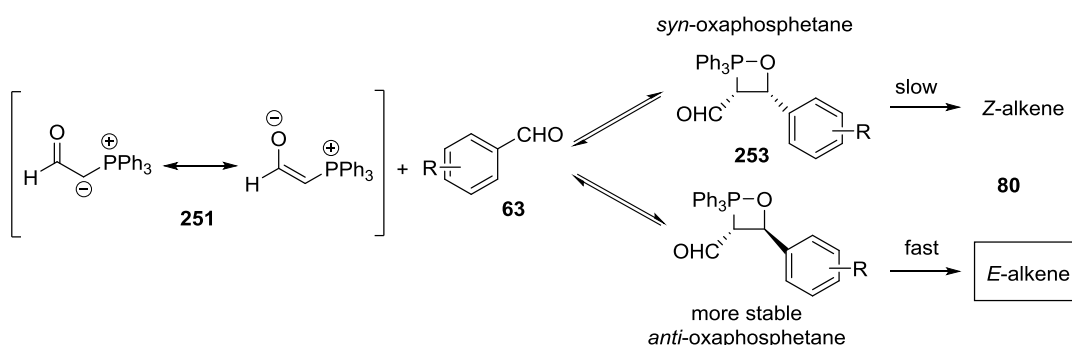
Scheme 61. General scheme of the synthesis of starting aldehydes

The mechanism of the reaction is presented in **Scheme 62**: the first step is the attack of the carbonyl group of the benzaldehyde **63** by the carbanion of the phosphonium ylide **251**. Then the negatively charged oxygen attacks the positively charged phosphorous, forming a four-membered ring oxaphosphetane intermediate **252**. This intermediate goes through an elimination reaction, rendering the alkene **80** and the phosphine oxide **267** as products.



Scheme 62. Mechanism of the Wittig reaction

The Wittig reaction is stereoselective and all the aldehydes were obtained in the *E* form and this depends from the nature of the substituent on the carbon atom of the ylide. The (triphenylphosphoranyldiene)acetaldehyde **251** is an ylide stabilised through conjugation thanks to the carbonyl group substituent: an *E*-selectivity is observed when a stabilised ylide is used in the Wittig reaction (**Scheme 63**). The stereochemistry is determined by the intermediate oxaphosphetane **253** that, in the case of stabilised ylides, is *anti*. The reason is that the stabilised ylide is less reactive and more stable and makes the formation of the oxaphosphetane reversible. The *anti*-oxaphosphetane is the more thermodynamically stable diastereomer due to the bulkier substituents being on the opposite side of the four-member ring.



Scheme 63. Rationalisation of the formation of *E*-alkene with stabilised ylides

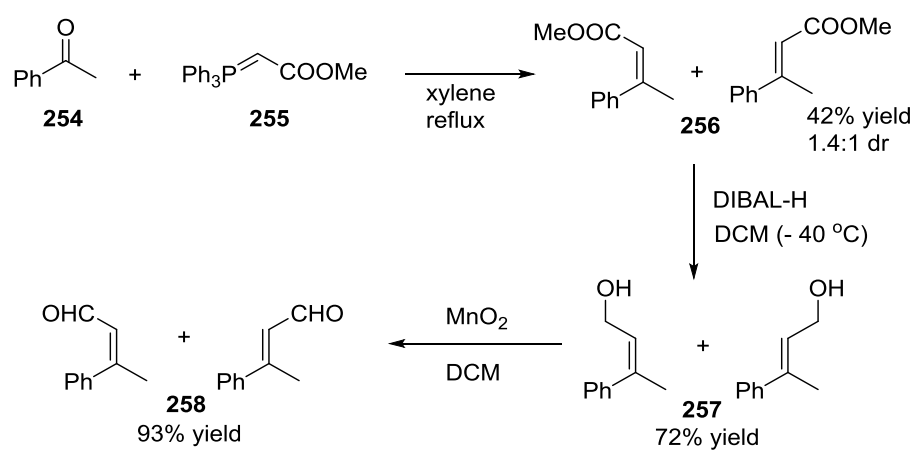
The results obtained in the synthesis of the starting aldehydes are presented in **Table 1**, with yields ranging from 50 to 72%.

Table 1. Results obtained in the synthesis of enals

Entry	Number	R	Yield ^[a] (%)
1	80c	2-Br	51
2	80d	3-Br	74
3	80e	4-Cl	70
4	80f	3-Cl	58
5	80g	4-CN	57
6	80h	4-Br	66
7	80i	4-NO ₂	72
8	80j	4-F	50
9	80k	4-Me	65

[a] Yields are of pure isolated products

Then, to be able to avoid the epimerisation of the final product **235a**, we synthesised a disubstituted enal **258**, following the procedure reported in literature^[111] as depicted in **Scheme 64**. The first step is a Wittig reaction, followed by reduction of the ester **256** to alcohol **257** with di-isobutyl aluminium hydride and finally the oxidation of the alcohol to aldehyde by manganese dioxide. A mixture of *E* and *Z* aldehydes was obtained, but this is not an issue because the iminium intermediate formed between the aldehyde and the organic catalyst is more stable as the *trans* isomer, so that all the activated aldehydes will be in the *E* form.



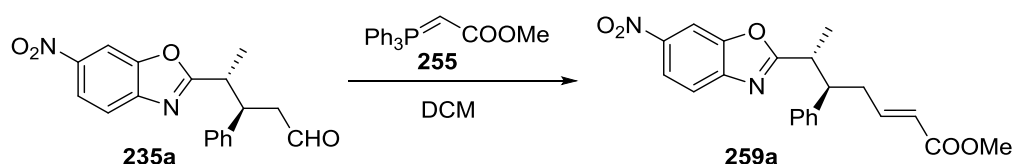
Scheme 64. Synthesis of disubstituted aldehyde in β position

4.4.2 Optimisation of the reaction conditions

Interested by the result obtained, we worked on the optimisation of the reaction screening different solvents, metal Lewis acids, bases and organocatalysts.

4.4.2.1 Derivatisation

As the product **235a** is not stable (degradation occurred after 48 hours even if it is kept in the fridge) we decided to derivatise it. Moreover the aldehyde is not stable even in the HPLC columns. For these reasons, we needed a derivatisation reaction that was possible to apply directly on the crude reaction mixture. The first reaction tried was a reduction of the aldehyde to alcohol. Only traces of the desired product were obtained, plus a mixture of by-products comprising the reduced form of the nitro group: this is due to the presence of $\text{Pd}(\text{OAc})_2$ in the reaction mixture. The Wittig reaction suited well for our purpose: it is easy to perform on the crude product of the Michael addition step, after solvent evaporation, by adding DCM and methyl (triphenylphosphoranylidene)acetate **255** (Scheme 65). After 48 hours the product **235a** is completely converted in the product **259a** in quantitative yield.

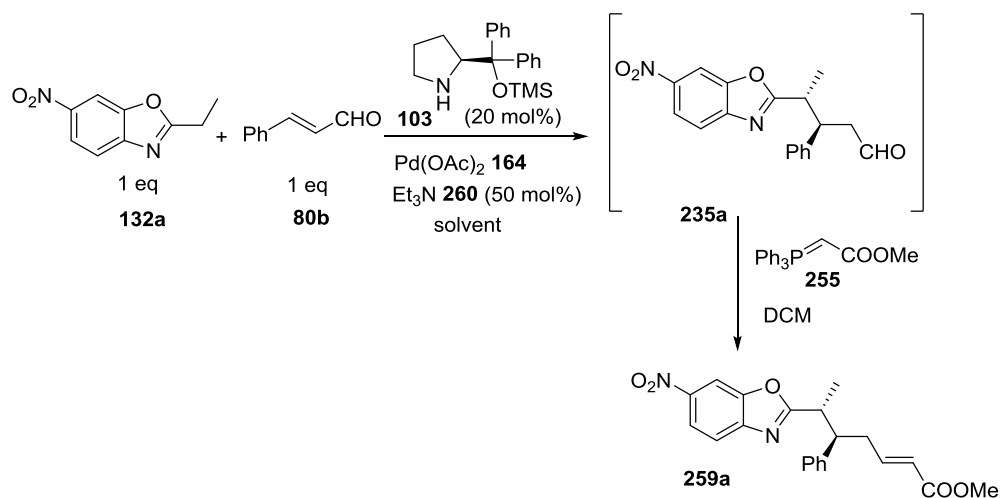


Scheme 65. Wittig derivatisation

4.4.2.2 Screening of solvents

Table 2 collects the results obtained from the screening of solvents. The reaction was performed using 50 mol% of trimethylamine **260**, 20 mol% of the organic Jorgensen-Hayashi catalyst **103** and employing $\text{Pd}(\text{OAc})_2$ **164** as the Lewis acid catalyst in 20 mol% or 10 mol% equivalents. Entries 1 to 8 were performed to check the conversion and dr on the crude NMR, without purification of the product **235a**. All the reactions were carried out at 45 °C.

Table 2. Screening of solvents



Entry	T (°C)	Lewis acid	Solvent	dr ^[a]	ee dia1 % ^[b]	ee dia2 % ^[b]	Conversion % (24 h) ^[a]
1	45	Pd(OAc) ₂ 20%	EtOAc	1.2:1	---	---	70
2	45	Pd(OAc) ₂ 20%	DMF	1:1	---	---	62
3	45	Pd(OAc) ₂ 20%	1,4-dioxane	---	---	---	No conversion
4	45	Pd(OAc) ₂ 20%	DMSO	1:1	---	---	75
5	45	Pd(OAc) ₂ 20%	CHCl ₃	---	---	---	no conversion
6	45	Pd(OAc) ₂ 20%	toluene	---	---	---	no conversion
7	45	Pd(OAc) ₂ 20%	CH ₃ CN	1:1	nd	nd	89
8	45	Pd(OAc) ₂ 20%	THF	1:1	nd	nd	39
9	40	Pd(OAc) ₂ 10%	EtOAc	2:1	53	47	32
10	40	Pd(OAc) ₂ 10%	DMF	1.2:1	rac	rac	67
11	40	Pd(OAc) ₂ 10%	DMSO	1.2:1	rac	rac	72
12	40	Pd(OAc) ₂ 10%	CH ₃ CN	1.3:1	rac	rac	85
13	40	Pd(OAc) ₂ 10%	THF	1.4:1	rac	rac	74
14	40	Pd(OAc) ₂ 10%	DCM	1.3:1	5	6	70 (20h)

15	50	Pd(OAc) ₂ 20%	CH ₃ CN	---	---	---	degradation
----	----	-----------------------------	--------------------	-----	-----	-----	-------------

[a] dr and conversions are calculated from the crude NMR comparing the aldehydes signals of **80b** and **235a**

[b] ee are calculated on product **259a** through HPLC analysis (column IE; 90:10 hexane:IPA; 1 ml/min; 230 nm)

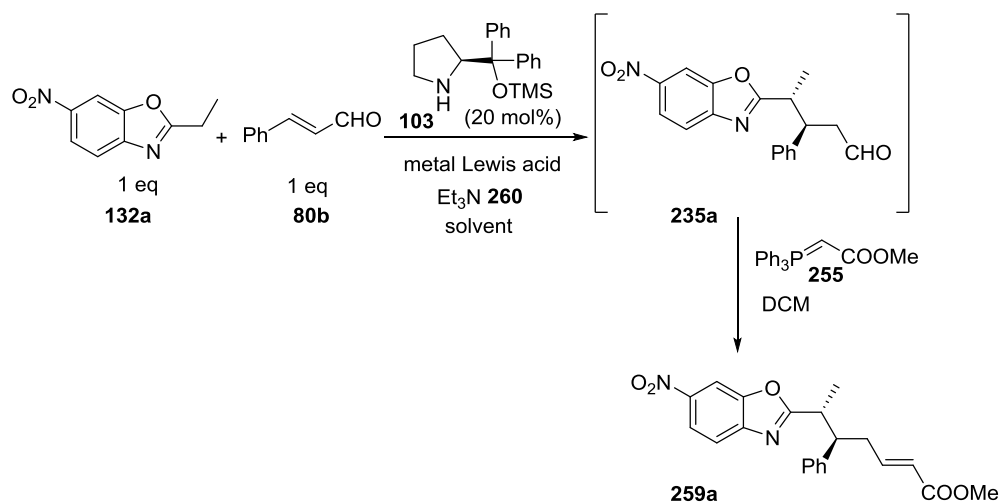
The results show that there was no conversion in CHCl₃, dioxane and toluene (**Table 2**, entries 3, 5 and 6). The reaction in EtOAc, DMF, DMSO, CH₃CN (**Table 2**, entries 1, 2, 4 and 7) had a good conversion after 24 hours but the reactions in DMF, DMSO and CH₃CN at 45 °C gave only by-products due to the degradation of the starting materials. The reaction in THF (**Table 2**, entry 8) had a low conversion. From these first 8 entries, EtOAc seemed to be the best solvent giving a slightly better diastereoselectivity of 2:1 compared to the 1:1 of the other solvents tested.

Then we checked the enantioselectivity of the derivatised product **259a**. The reactions were performed at 40 °C (**Table 2**, entries 9-14). The reactions in DMF, DMSO, CH₃CN, THF and DCM after 24 hours presented a good conversion, between 67% and 85% (**Table 2**, entries 10-14) but low diastereoselectivity (less than 2:1) and low ee (racemics or lower than 10%). With EtOAc (**Table 2**, entry 9) the reaction has a dr of 2:1 and an ee of 53% and 47%. EtOAc seemed to be the only solvent that, in these conditions, gave low diastereoselectivity and moderate enantioselectivity. We tried the reaction in CH₃CN at 50 °C (**Table 2**, entry 15) but it only rendered degradation products after 24 hours. We believe that the reaction is temperature sensitive: at room temperature the conversion is low but at temperatures higher than 45 °C only the degradation of the starting materials was observed.

4.4.2.3 Screening of metal Lewis acids

We proceeded in the optimisation by screening different metal Lewis acids as listed in **Table 3**.

Table 3. Screening of metals



Entry	T (°C)	Metal catalysts	Base	Solvent	dr [a]	ee dia1 % [b]	ee dia2 % [b]	Conversion % (20 h) [a]
1	40	$(\text{CF}_3\text{SO}_3)_2\text{Cu}$ (II) 20% 261	TEA 50%	EtOAc	---	---	---	16
2	40	$(\text{CF}_3\text{SO}_3)_3\text{Yb}$ (III) 20% 176	TEA 50%	EtOAc	---	---	---	no conversion
3	40	CuCl_2 (II) 20% 263	TEA 50%	EtOAc	---	---	---	7
4	40	$\text{Cu}(\text{OAc})_2$ (II) 20% 264	TEA 50%	EtOAc	---	---	---	no conversion
5	40	CH_3COOAg 20% 130	TEA 50%	EtOAc	---	---	---	8
6	40	PdCl_2 (II) 20% 266	TEA 50%	EtOAc	1:1	22	13	9 (45 after 4 days)
7	40	Co/Ti 20 % 265	TEA 50%	EtOAc	---	---	---	degradation
8	40	$\text{Ni}(\text{OAc})_2 \cdot 4\text{H}_2\text{O}$ (III) 5% 184	TEA 10%	EtOAc	---	---	---	traces
9	40	K_2PdCl_4 (II) 5% 268	TEA 10%	EtOAc	---	---	---	no conversion
10	40	K_2PtCl_4 (II) 5% 269	TEA 10%	EtOAc	---	---	---	no conversion
11	40	$\text{HAuCl}_4 \cdot \text{H}_2\text{O}$ (III) 5% 270	TEA 10%	EtOAc	---	---	---	no conversion

Entry	T (°C)	Metal catalysts	Base	Solvent	dr [a]	ee dia1 % [b]	ee dia2 % [b]	Conversion % (20 h) [a]
12	50	AgOAc 10% 230	TEA 5%	toluene	---	---	---	no conversion
13	35	AgOAc 5% 230 Pd(OAc) ₂ 5% 164	TEA 50%	EtOAc	---	---	---	degradation

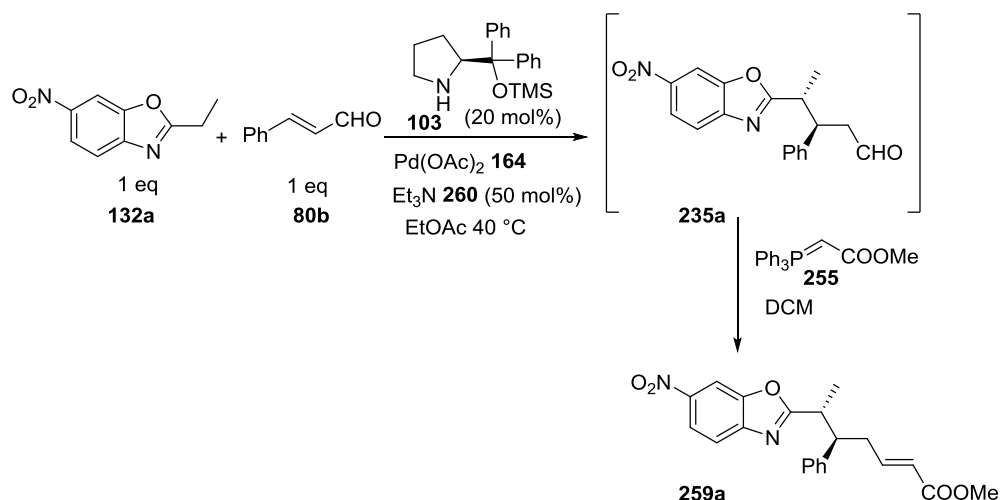
[a] dr and conversions are calculated from the crude NMR comparing the aldehydes signals of **80b** and **235a**

[b] ee are calculated on product **259a** through HPLC analysis (column IE; 90:10 hexane:IPA; 1 ml/min; 230 nm)

As presented in the table above, most of the metals tested did not give any conversion at all (**Table 3**, entries 2, 4, 9, 10, 11, 12 and 13) or gave only degradation products (**Table 3**, entries 7 and 13). With some of the metals, the crude NMR showed traces of the desired aldehydes (**Table 3**, entries 1, 3, 5 and 8) after 20 hours. Prolonged reaction time did not lead to conversion improvement. The only metal Lewis acid that showed an improved conversion after 4 days was PdCl₂ **266** (**Table 3**, entry 6). The dr and the ee were not good, as we mainly obtained racemic products. From those results the only Lewis acid that gave acceptable conversions and enantioselectivity is Pd(OAc)₂ **164** (**Table 2**, entry 9).

4.4.2.4 Screening of different loading of Pd(OAc)₂

The subsequent step was to screen different loading of Pd(OAc)₂ **164** as reported in **Table 4**. The reactions were performed using 20 mol% of the organic catalyst **103**, 50 mol% of triethylamine **260** as the base and EtOAc as the solvent at 40 °C.

Table 4. Screening of loading of Pd(OAc)₂

Entry	Pd(OAc) ₂	dr ^[a]	ee dia1 % ^[b]	ee dia2 % ^[b]	Conversion % ^[a]
1	---	---	---	---	no conversion
2	5%	1.5:1	56	43	40 (42 h) 60 (65 h)
3	1%	1.2:1	51	22	20 (42 h) 27 (65 h) 64 (7 days)

[a] dr and conversions are calculated from the crude NMR comparing the aldehydes signals of **80b** and **235a**

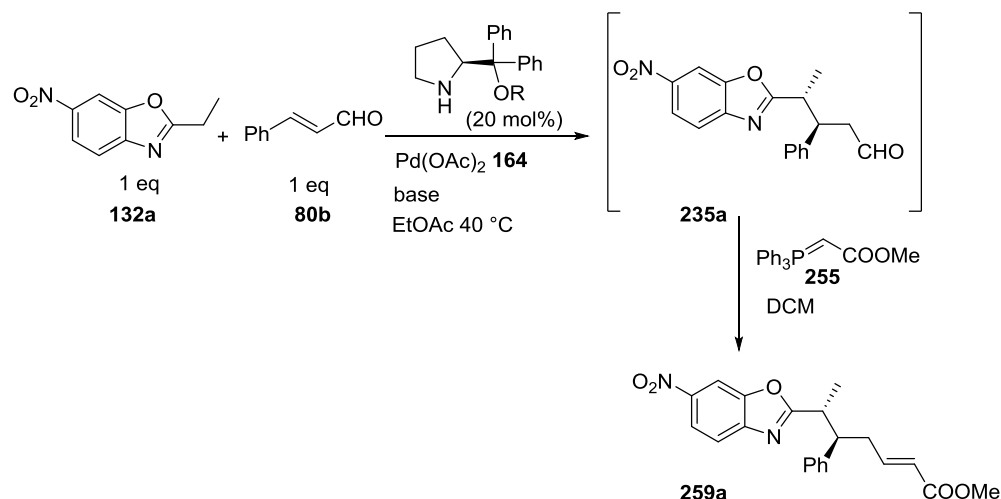
[b] ee are calculated on product **259a** through HPLC analysis (column IE; 90:10 hexane:IPA; 1 ml/min; 230 nm)

The reaction requires the presence of Pd(OAc)₂ as it did not give any conversion without the presence of the Lewis acid (**Table 4**, entry 1). The reaction worked well with 5 mol% as well as with 1 mol% of the catalyst (**Table 4**, entries 2 and 3). This is the demonstration that the synergistic catalysis is necessary to make the reaction work. The reaction with 1 mol% of metal catalyst is however too slow, an acceptable conversion is reached only after 7 days. The best loading of Pd(OAc)₂ resulted to be 5 mol%, as it gave a comparable enantioselectivity as using 10 mol% of it (**Table 5**, entry 5), but producing less metal waste.

4.4.2.5 Screening of bases and of different loading of base

We also tested different bases and different loading of them as shown in **Table 5**.

Table 5. Screening of bases



Entry	Organic catalyst 20% (R)	Metal	Base	Solvent	dr ^[a]	ee dia1 % ^[b]	ee dia2 % ^[b]	Conversion % ^[a]
1	TMS	$\text{Pd}(\text{OAc})_2$ 10%	quinine 64 10%	EtOAc	---	----	----	No conversion
2	TMS	$\text{Pd}(\text{OAc})_2$ 10%	quinidine 65 10%	EtOAc	---	----	----	No conversion
3	TMS	$\text{Pd}(\text{OAc})_2$ 10%	DIPEA 28 10%	EtOAc	2:1	43	54	75 (46 h)
4	TMS	$\text{Pd}(\text{OAc})_2$ 20%	DABCO 138 50%	DCM	---	----	----	No conversion
5	TMS	$\text{Pd}(\text{OAc})_2$ 10%	TEA 260 20%	EtOAc	1.5:1	26	---	75 (42 h)
6	TMS	$\text{Pd}(\text{OAc})_2$ 10%	TEA 260 10%	EtOAc	1.2:1	41	21	55 (42 h)
7	TMS	$\text{Pd}(\text{OAc})_2$ 10%	TEA 260 5%	EtOAc	1.2:1	38	19	63 (42 h)
8 ^[c]	TBDMS 271	$\text{Pd}(\text{OAc})_2$ 10%	---	CH_3CN	---	---	---	No conversion

[a] dr and conversions are calculated from the crude NMR comparing the aldehydes signals of **80b** and **235a**

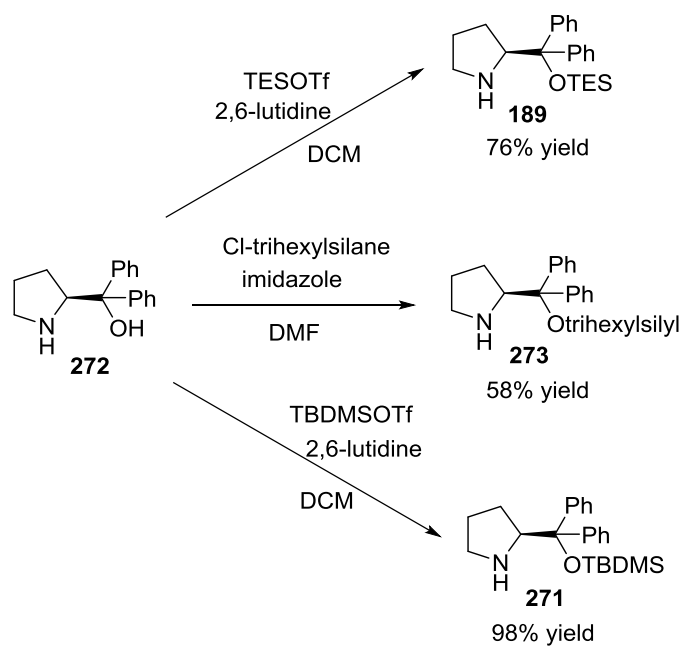
[b] *ee* are calculated on product **259a** through HPLC analysis (column IE; 90:10 hexane:IPA; 1 ml/min; 230 nm)

[c] This entry was performed at 20 °C

The reaction did not work with quinine **64**, quinidine **65** and DABCO **138** (**Table 5**, entries 1, 2 and 4) probably because they can chelate the metal catalyst. The reaction worked well using DIPEA **28** (**Table 5**, entry 3) and it gave a slightly better dr and *ee* compared to the reaction performed using the same amount of TEA **260** (**Table 5**, entry 6). The reaction gave a worse enantioselectivity using 20 mol% or only 5 mol% of TEA (**Table 5**, entries 5 and 7). The reaction does not work in the absence of the base (**Table 5**, entry 8).

4.4.2.6 Synthesis of organic catalysts

As the enantioselectivities obtained with the commercial Jorgensen-Hayashi catalyst were not excellent, we decided to synthesise more bulky catalysts starting from the commercial (*S*)-diphenyl(pyrrolidin-2-yl)methanol by reaction with triflates or chloro silanes to obtain the derivatised products **189**, **271**, **273**, following the procedures reported in literature (**Scheme 66**).^[112]

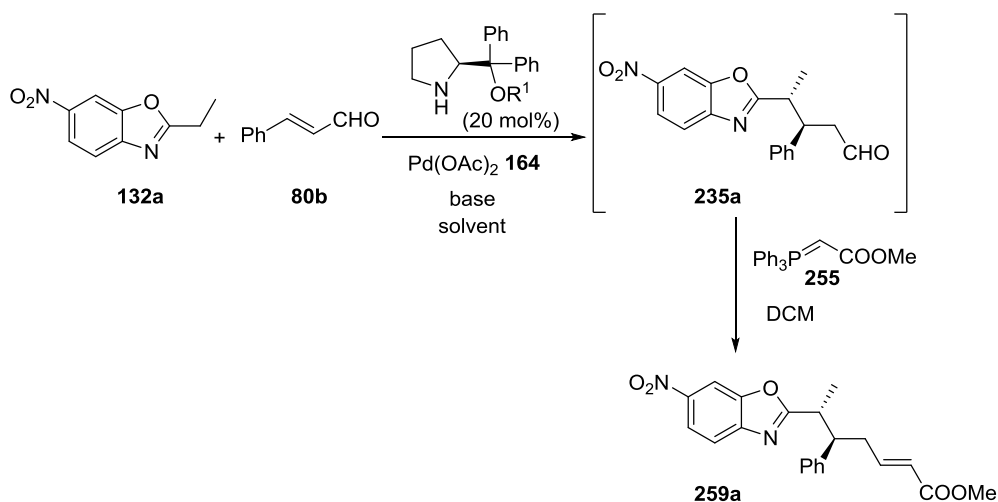


Scheme 66. Synthesis of the organic catalysts

4.4.2.7 Screening of organic catalyst and temperature

Then we tested different organic catalysts and different conditions as shown in **Table 6**.

Table 6. Screening of organic catalysts and temperature



Entry	Ald. (eq)	T (°C)	Organic catalyst 20% (R ¹)	Pd(OAc) ₂ %	Base/ Acid	Solv	dr ^[a]	ee dia1 % ^[b]	ee dia2 % ^[b]	Conversion % ^[a]
1	1	45	pyrrolidine 274	20	TEA 50%	DCM	---	---	---	no conversion
2	1	rt- 40	TMS 103	---	PhCO ₂ H	DMSO	---	---	---	traces after adding base
3	1	45	TMS (CF ₃) 220	5	TEA 5%	EtOAc	---	---	---	no conversion
4	1	45	TES 189	5	TEA 5%	EtOAc	1.2:1	61	19	80 (4 days)
5	1	25	TMS 103	5	TEA 5%	EtOAc	1.8:1	71	61	17 (24 h) 87 (4 days)
6	1	50	TMS 103	5	TEA 5%	EtOAc	1.1:1	35	10	61 (24 h)
7	1	45	TBDMS	5	TEA 5%	EtOAc	1.2:1	9	1	66 (4 days)
8	1	25	TES 189	5	TEA 10%	EtOAc	1.6:1	86	50	51 (3 days)

Entry	Ald. (eq)	T (°C)	Organic catalyst 20% (R ¹)	Pd(OAc) ₂ %	Base/Acid	Solv	dr ^[a]	ee dia1 % ^[b]	ee dia2 % ^[b]	Conversion % ^[a]
9	1	25	TBDMS 271	5	TEA 10%	EtOAc	---	---	---	no conversion
10	1	25	trihexylsilyl 273	5	TEA 10%	EtOAc	1:1	44	4	70 (5days)
11	1.5	25	TES 189	5	DIPEA 50%	DCM	1.5:1	82	55	66 (3 days)
12	1.5	25	TES 189	5	DIPEA 50%	EtOAc	1.3:1	77	42	81 (3 days)
13	1.5	25	TES 189	5	DIPEA 50%	EtOAc	1.2:1	26	14	71 (7 days)
14	2	25	TBDMS 271	5	DIPEA 50%	CN ₃ CN	1.3:1	88	68	45 (1 day)
15	2	25	TES 189	5	DIPEA 50%	EtOAc	1.2:1	26	14	>71 (7 days)
16	2	4	TBDMS 271	5	TEA 50%	CH ₃ CN	1:1	68	26	>70 (6 days)
17	2	30	TBDMS 271	5	TEA 50%	CH ₃ CN	1.3:1	88	68	full (40 h)
18	2	30	---	5	TEA 50%	CH ₃ CN	---	---	---	complex mixtures

[a] dr and conversions are calculated from the crude NMR comparing the aldehydes signals of **80b** and **235a**

[b] ee are calculated on product **259a** through HPLC analysis (column IE; 90:10 hexane:IPA; 1 ml/min; 230 nm)

When we performed the reaction using pyrrolidine **274**, as the organic catalyst, in order to obtain more easily the racemic compound, the NMR of the crude showed no conversion (**Table 6**, entry 1). To prove the need of the synergistic catalysis activation, we tested the reaction in the same conditions reported by Wei Wang's and co-workers, where they presented an addition of α,β -unsaturated aldehydes to dinitrotoluene and to nitropyridines.^[90] In this case we did not use Pd(OAc)₂ and instead of the base we used benzoic acid according to Wang's conditions (**Table 6**, entry 2). The NMR of the crude showed traces of conversion only after the addition of TEA.

Then we tested the reaction using different organic catalysts: the reaction with the commercial catalyst (*R*)- α,α -bis[3,5-bis(trifluoromethyl)phenyl]-2-pyrrolidinemethanol trimethylsilyl ether **220** (Table 6, entry 3) did not work and no conversion was observed in the NMR of the crude. Among the three catalysts synthesised, the (*R*)-2-((trihexylsilyl)oxy)pyrrolidine **273** gave low selectivities (Table 6, entry 10) and (*S*)-2-(((*tert*-butyldimethylsilyl)oxy)diphenylmethyl)pyrrolidine **271** in EtOAc did not show any conversion at 25 °C (Table 6, entry 9). With the catalysts **271** the reaction worked only by heating at 45 °C (Table 6, entry 7). The reaction worked well with the (*S*)-2-(diphenyl((triethylsilyl)oxy)methyl)pyrrolidine **189** especially at room temperature (Table 6, entries 4, 8 and 15). These results confirmed the fact that the reaction is temperature sensitive: with higher temperatures the reaction proceeds faster but the enantioselectivity decreases. The same reduction of enantioselectivity occurs with longer reaction times (Table 6, entry 12 and 13). When the reaction was left stirring for more than 7 days an epimerisation and degradation of the final compound occurred. We tested again the reaction in DCM and it showed good results since the reaction was faster and less epimerisation occurred (Table 6, entry 11). Then we tested again the reaction with OTBDMS the bulkiest catalyst that, in theory, should give the best enantioselectivity. We used CH₃CN as the solvent, as it showed the best conversion in this reaction (Table 2, entries 7 and 12) and we obtained good enantioselectivities (Table 6, entry 14). The next reactions were performed using TEA **260**, the base that gave the fastest reaction as we need a good *ee* but also an acceptable conversion and yield in a short period of time to prevent further epimerisation. The reaction was also tested at 4 °C but, since it took 6 days to give an acceptable conversion, the enantioselectivities obtained were lower (Table 6, entry 16). When the reaction was tested without the organic catalyst (Table 6, entry 18) a complex mixture was seen in the NMR of the crude, confirming in this way the synergistic aspect of the reaction.

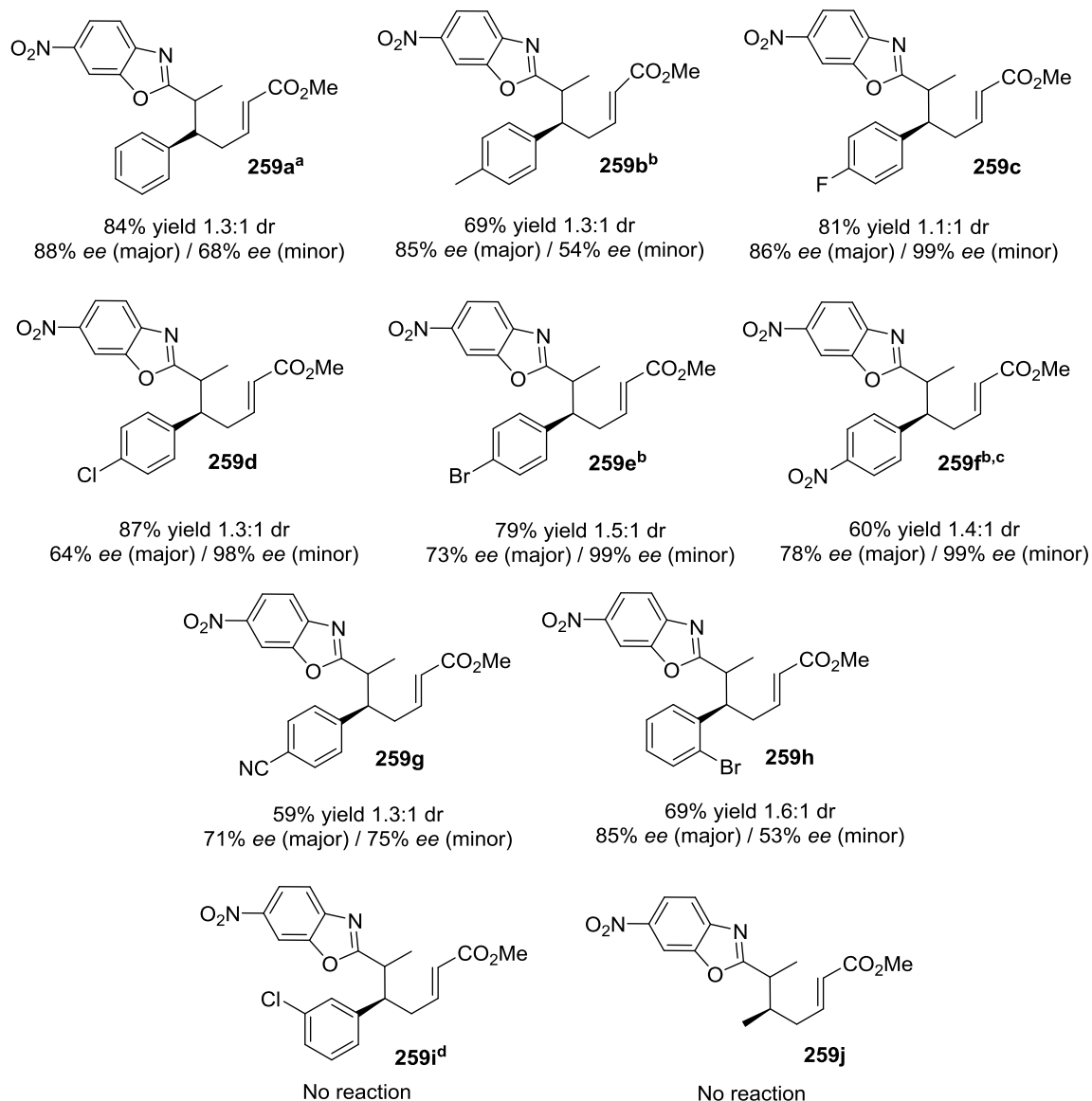
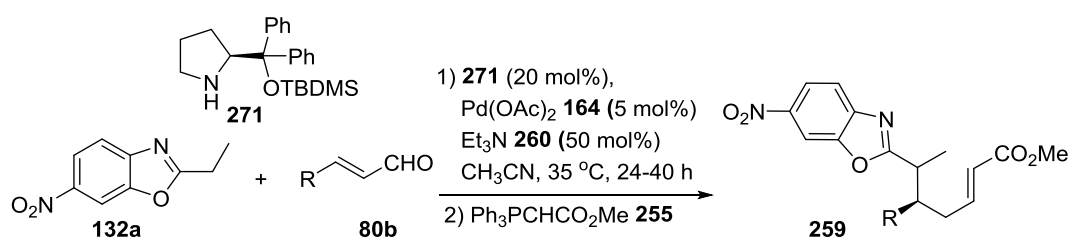
After this extensive screening, in our hands, the best conditions are the use of CH₃CN as the solvent, at 30-35 °C, 20 mol% of amine organocatalyst, 5 mol% of Pd(OAc)₂ **164** and 50 mol% of Et₃N **260**. TBDMS **271** derivative is the secondary amine that gives the best stereoselectivities (Table 6, entry 17).

We also tested two ligands for $\text{Pd}(\text{OAc})_2$, phenantroline and 2,2-bipyridyl, in order to better solubilise the metal catalyst. The crude NMR of the first reaction showed only traces of conversion while with 2,2-bipyridyl we had 60% of conversion only after 10 days.

The current reaction presents some drawbacks. The reaction time becomes crucial, higher reaction times result in lower enantioselectivities: this data induces us to think that there is an epimerisation process that led to racemic mixtures. Good enantioselectivities can be obtained only if the reaction is stopped after a maximum of 40 hours by adding the Wittig reagent. Temperature also has a pivotal importance: in order to speed up the reaction, heating is required; however, high temperatures render low enantioselectivities.

4.4.3 Scope of the reaction with enals

Once we optimised the reaction, we decided to investigate the scope of the reaction in terms of the enals.



Scheme 67. Scope of the reaction with several enals. a) DIPEA as the base; b) reaction conducted at 30 °C; c) **189** as the catalyst; d) **103** as the catalyst.

Some more information are reported in the **Table 7**.

Table 7. Scope of the reaction with several enals

Number	Organic Catalyst (R ¹)	T (°C)	Yield % ^[a]	dr ^[b]	ee dia 1 % ^[c]	ee dia 2 % ^[c]	Time before Wittig
259a	TBDMS 271	30	84	1.3:1	88	68	24 h
259e	TBDMS 271	30	79	1.5:1	73	99	40 h
259f	TBDMS 271	30	96	1.4:1	27	19	2 days
259f	TES 189	30	60	1.4:1	78	67	24 h
259b	TBDMS 271	30	69	1.3:1	85	54	2 days
259c	TBDMS 271	35	81	1.1:1	86	99	40 h
259d	TBDMS 271	35	87	1.3:1	64	99	24 h
259h	TBDMS 271	35	69	1.6:1	84	53	24 h
259g	TBDMS 271	35	59	1.3:1	71	75	40 h

[a] Yields are of pure isolated diastereomers

[b] dr are calculated from the crude NMR comparing the aldehydes signals

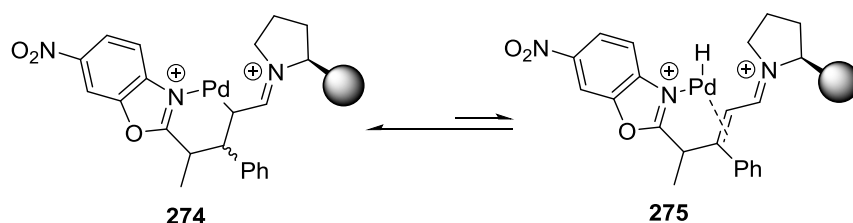
[c] ee were determined by chiral HPLC analysis

As it is shown in **Table 7** and **Scheme 67**, the reaction gave the final products in good yields and enantioselectivities when different aromatic enals were used. However in almost all the examples the diastereoselectivity of the reaction is very low. This could be explained by the epimerisation of the final adduct at the carbon in the α position of the azaarene, due to its high acidity in the reaction conditions. The best results were obtained with the 4-halogen substituted cinnamaldehydes, for example the fluoro derivative **259c** was obtained in 81% yield 1.5:1 dr and in 86% and 99% ee. Compounds **259e** and **259d** (4-Br and 4-Cl derivatives respectively) were afforded in similar yields and stereoselectivities. Electron withdrawing groups in the aromatic ring gave lower enantioselectivities (**259f** and **259g**). The reaction with the halogen in the *ortho* position of the aromatic ring of the aldehyde was faster and it gave good yield and enantioselectivity (**259h**). However the reaction with the halogen in the *meta* position

of the aromatic ring of the aldehyde did not work, the NMR of the crude showed only traces of the final product (**259i**).

As already stated before, for longer reaction times, the enantioselectivity of the final adducts dropped dramatically as shown in **Table 7**, entry 2 compared to **Table 7**, entry 3. This data suggests an epimerisation in the β -position of the aldehyde in the reaction conditions and could explain the low enantioselectivity in the compounds **259f** and **259g** as the electron withdrawing groups favour the epimerisation.

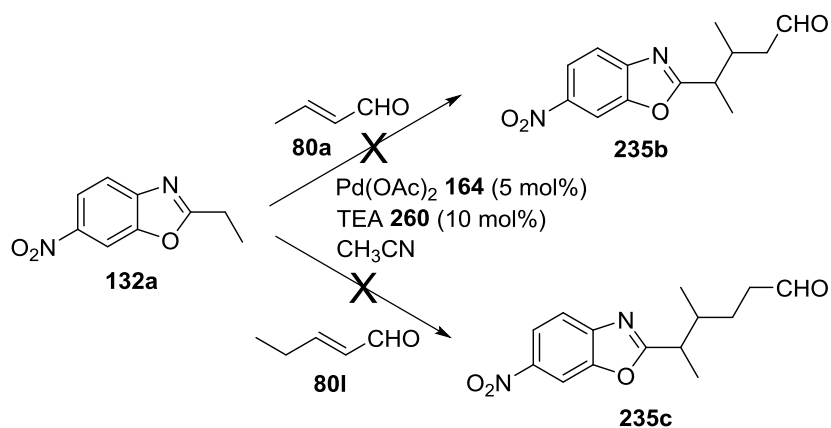
The epimerisation observed at longer reaction times is one of the most important challenges that we face in this reaction: in order to explain this phenomenon we propose that there is the formation of a Pd enolate with the enamine intermediate **274** that equilibrates through a β -elimination and an H insertion **275** (**Scheme 68**).



Scheme 68. Explanation of the epimerisation at the β -position

To avoid the epimerisation, we tested the reaction with (*E*)-3-phenylbut-2-enal an α,β -unsaturated aldehyde, disubstituted at the β position (**Scheme 64**, **258**). Unfortunately this reaction did not work, most likely because of the steric hindrance.

We also expanded the scope of the reaction with aliphatic aldehydes as shown in **Scheme 69**, but they only rendered complex mixtures due to the aldehyde's decomposition probably by polymerisation through a dienamine process.

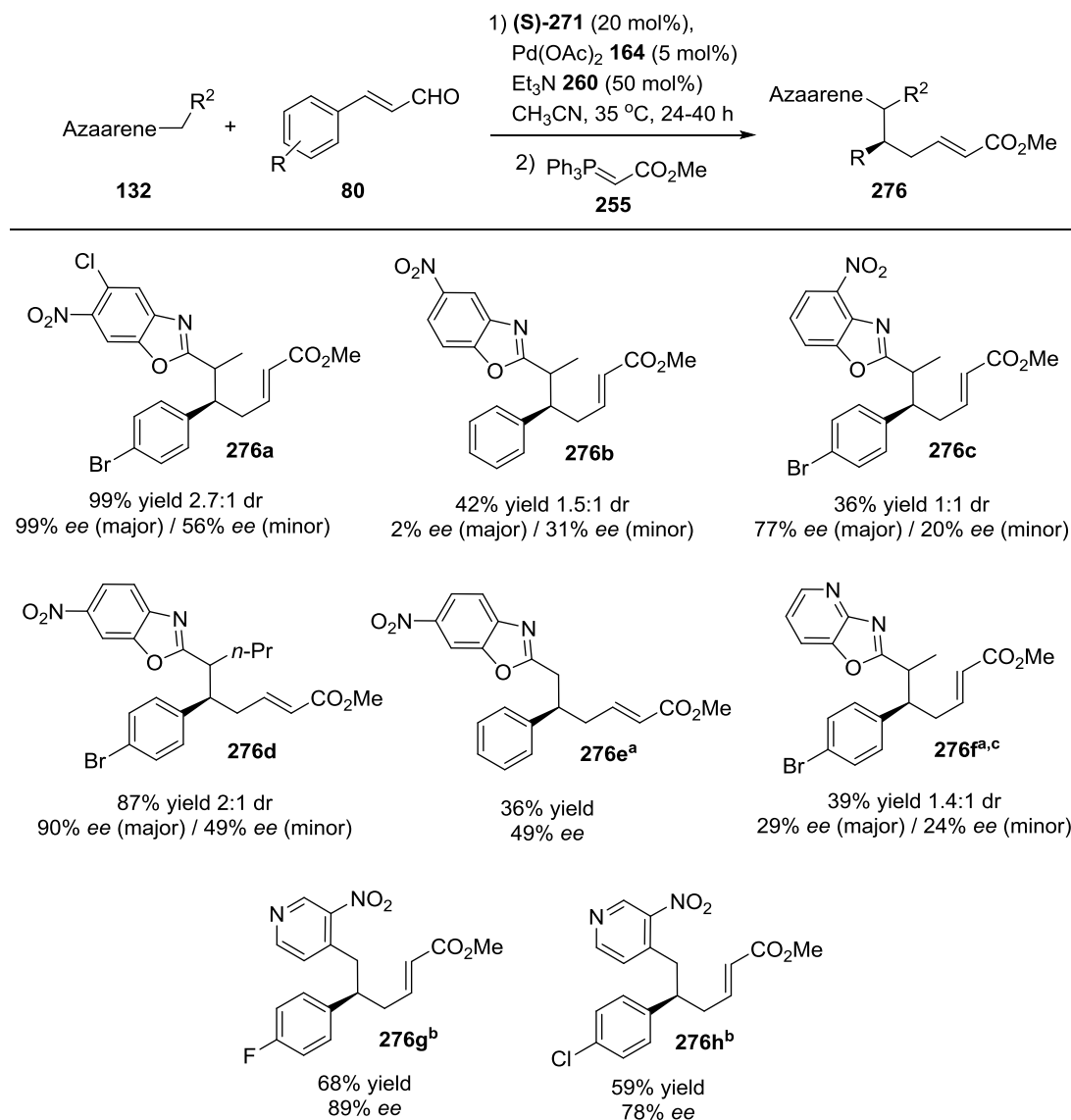


Scheme 69. Attempted reactions with aliphatic aldehydes

4.4.4 Scope of the reaction with azaarenes

Then we proceeded to expand the scope of the reaction testing different azaarenes as presented in

Table 8 and Scheme 70.



Scheme 70. Scope of the reaction with different benzoxazoles and pyridines. a) TMS catalyst **103** used; b) TES catalyst **189** used; c) the reaction was performed at 45 °C

More information are reported in the

Table 8.

Table 8. Scope of the reaction with different benzoxazoles and pyridines

Entry	number	T (°C)	R	organic cat	Yield % [a]	dr ^[b]	ee dia1 % [c]	ee dia2 % [c]	Time before Wittig
1	276a	35	4-Br 80h	TBDMS 271	99	2.7:1	99	56	24 h
2	276f	45	4-Br 80h	TMS 103	39	1.4:1	29	24	5 days
3	276d	35	4-Br 80h	TBDMS 271	87	2:1	90	49	40 h
4	276e	30	H 80b	TMS 103	36/56	---	49	---	48 h
5	276b	35	H 80b	TBDMS 271	42	1.5:1	12	rac	10 days
6	276c	35	4-Br 80h	TBDMS 271	36	1:1	77	20	72 h
7	276h	35	4-Cl 80e	TES 189	59	---	78	---	24h
8	276g	35	4-F 80j	TES 189	68/52	---	89	---	24 h

[a] Yields are of pure isolated diastereomers

[b] dr are calculated from the crude NMR comparing the aldehydes signals

[c] ee were determined by chiral HPLC analysis on the product isolated from flash column chromatography

To generate more complex scaffold that can be further derivatised, we tested a benzoxazole bearing a nitro group and a chlorine as substituents on the aromatic ring (**276a**); the product was obtained with excellent yields and enantioselectivities in the major diastereomer and good diastereoselectivities. Then we investigated the effect of the substituents on the alkyl chain of the benzoxazole. Larger substituents (*n*-butyl, **276d**) can be used and render the final product in good yield and *ee* and moderate *dr*, while smaller substituents (Me, **276e**) made the reaction slower when the bulky catalyst (*S*)-2-(((*tert*-butyldimethylsilyl)oxy)diphenylmethyl)pyrrolidine **271** was used, therefore the catalyst **103** was used. Next, we tested two benzoxazoles with the nitro group in positions 5 or 4 and both products **276b** and **276c** were obtained in moderate yields and with moderate to low stereoselectivity. These not so good results can be attributed to the steric effect of the nitro group that cause difficulty in the coordination of the Pd to the nitrogen atom of the benzoxazole ring. The reaction with

the enal and the 2-ethyloxazolo[4,5]pyridine gave the final product **276f** in moderate yields and selectivities. The reaction also works with 4-methyl pyridine, with the final products **276g** and **276h** obtained in moderate yields and good *ee*. In the case of the pyridines, the catalyst (*R*)-2-((trihexylsilyl)oxy)pyrrolidine **189** was used.

The following benzoxazoles (**Figure 16**) did not undergo any conversion or, in the case of 2-isopropyl-6-nitrobenzoxazole **132i**, only traces of product were observed. As **132i** did not work, it is not surprising that also 2-(difluoromethyl)-6-nitrobenzoxazole **132j** did not work. In fact a fluorine atom stabilises a carbocation in the α position by resonance effect but it destabilises a carbocation in the β position. On the contrary, a fluorine atom stabilises a β carbanion, by the inductive effect, and destabilises an α carbanion. Although α -F could, in theory, stabilise by the inductive effect, its opposing electron-pair repulsion predominates and the carbanion stability is determined by the degree of this repulsion, which increases in the order Br > Cl > F.

The reaction with the benzoxazoles **132g**, **132k**, **132h** and **132l** did not proceed because the methylene hydrogens are not sufficiently acidic without the contribution of the nitro group to the carbanion stabilisation through the delocalisation of the negative charge formed by the base. This demonstrates that the presence of an EWG on the aromatic ring of the azaarene is crucial for the reactivity and it shows a limitation of the reaction reported in this chapter.

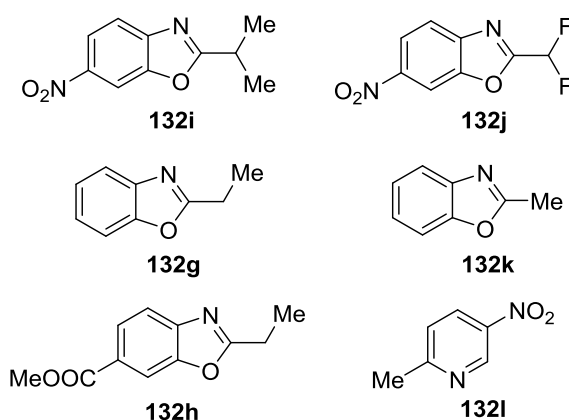


Figure 16. Azaarenes that did not react with the enals

4.4.5 Relative and absolute configuration

In order to determine the stereochemistry of the compounds obtained, an X-ray diffraction study of the minor isomer of **259f** was performed.² The relative stereochemistry was obtained, as shown in **Figure 17**.

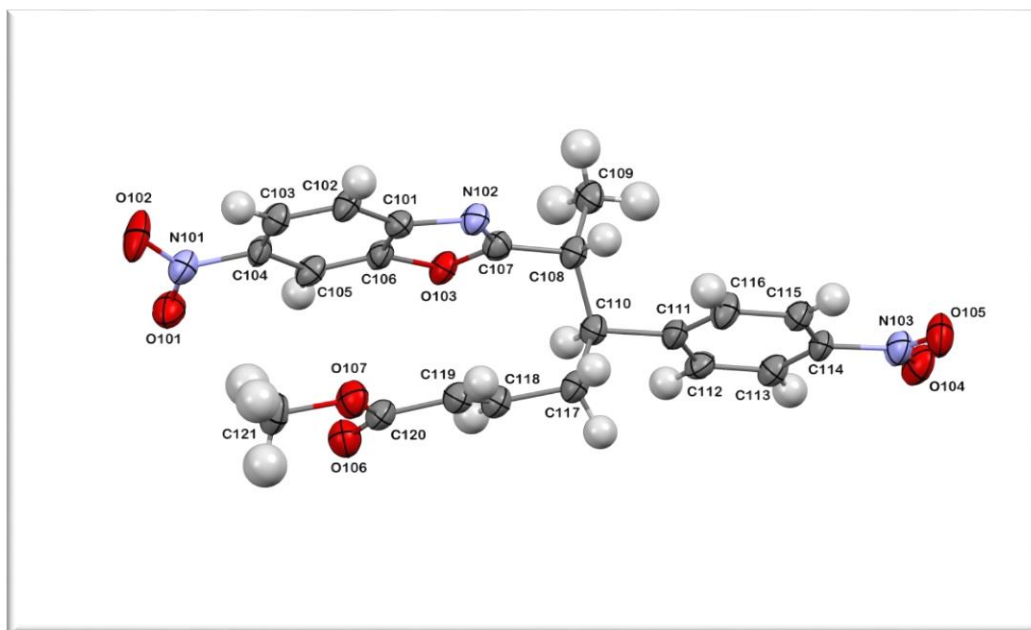
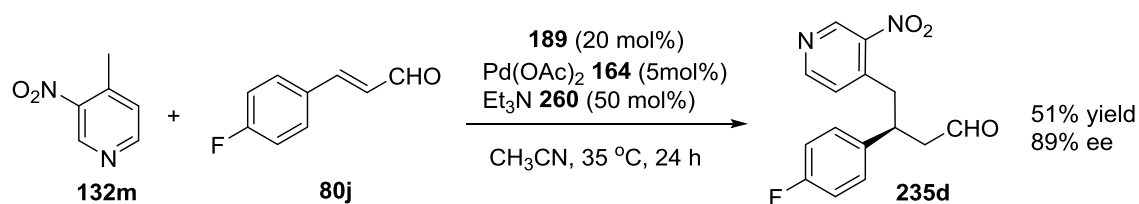


Figure 17. Crystal structure of product **259f**. For more information about the crystal see Chapter 6

The absolute configuration cannot be assigned reliably, based on anomalous dispersion effect since the molecule does not possess any heavy element. However, the relative configuration can be assigned as *S**, *R** on C108 and C110. The analysis of the crystal shows that the compound **259f** tends to crystallise as a racemic form. For this reason, it could be difficult to obtain an enantiomeric crystal.

It has to be noted that the Michael addition products derived from the pyridines are stable after isolation (**Scheme 71**).

² The X-ray analysis was done by Dr Mateusz B. Pitak and Dr. Simon Coles



Scheme 71. Synthesis of **235d**

The absolute configuration of these compounds was determined by comparison of the compound **235d** with the same compound reported by Wang and co-workers.^[90] Using the same (*S*)-secondary amine catalyst, the product obtained had the same specific rotation as reported in Wang's paper. Assuming that our reaction follows a homogeneous mechanism, we could assign the absolute configuration of the stereocenter in the β position of the aldehyde. With the information obtained from the X-ray we could assign the absolute configuration to all the compounds synthesised.

4.5 Conclusion

In conclusion we developed a chiral synthesis of alkylazaarenes through an addition reaction of azaarenes to enals. We proposed one of the first examples of synergistic catalysis in which one of the catalysts is a secondary amine and the other is a metal Lewis acid. We obtained the final products in good yields, enantioselectivity ranging from low to excellent, based on the substrate, but low diastereoselectivity.

5. Synergistic catalysis: *cis*-cyclopropanation of benzoxazoles

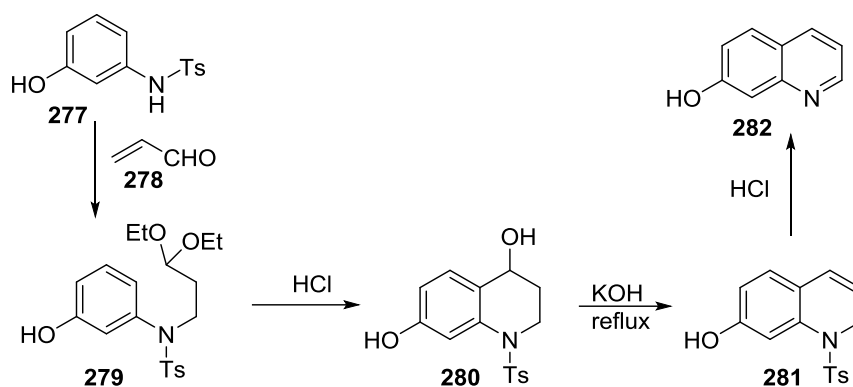
5.1 One-pot reactions

In the last decades there has been growing importance of environmental issues related to synthetic chemistry. The most important problems addressed are the handling of waste, the search for environmentally tolerable procedures, atom economy related to the increase of the efficiency of the procedures. Most of the synthesis of pharmaceutical products require multistep synthesis and this means the use of solvents, reagents and energy for each step and especially for the work-up or the purification of the intermediate product after each step.^[113,114] The traditional method in organic synthesis is the formation of a single bond in each step. In Nature, though, most of the reactions are one-pot reactions or multistep synthesis,^[115] for example the reactions catalysed by the enzymes in the human body. In the search for greener procedures, synthetic chemists developed one-pot synthesis.

There are different types of one-pot reaction: telescoping, multicomponent, cascade/domino/tandem.

5.1.1 Telescoping reactions

A telescopic reaction is a synthetic route where the reagents are added one at a time, without doing the work-up after each step. One example is reported by Cameron, Hoerrner and co-workers for the synthesis of 7-hydroxyquinoline **282** (**Scheme 72**).^[116]

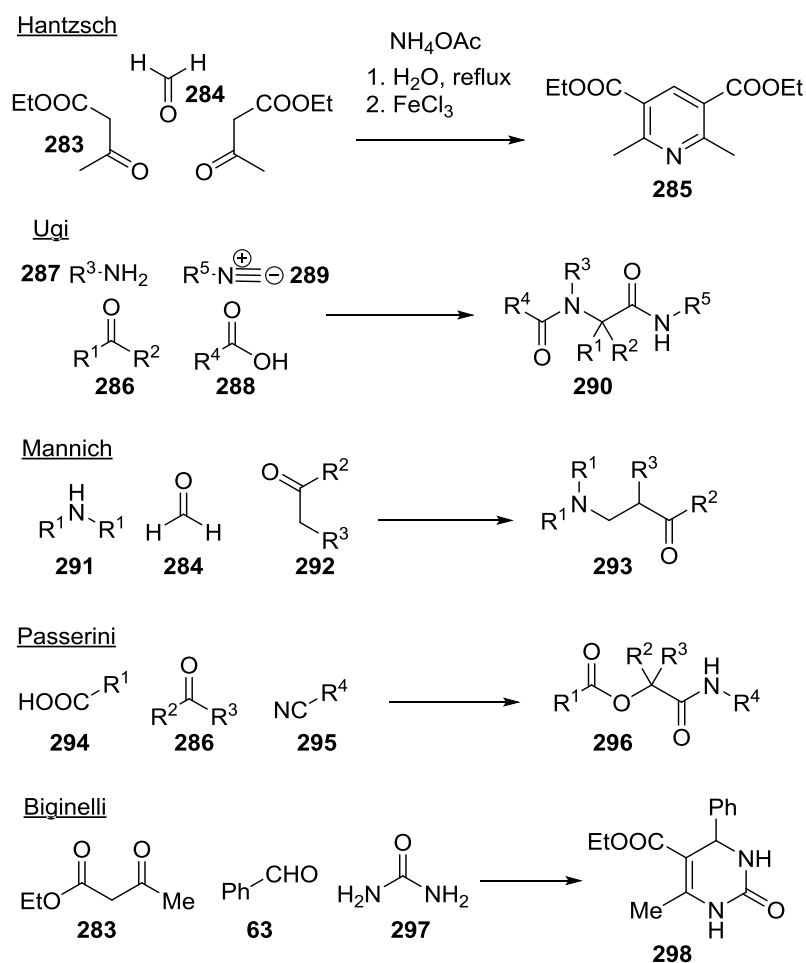


Scheme 72. Telescopic reaction for the synthesis of 7-hydroxyquinoline

One simple example of this reaction can be considered the Michael addition/Wittig reaction presented in Chapter 4, as the Wittig reagent was added to the reaction mixture without the need to purify the Michael addition product.

5.1.2 Multicomponent reactions

Multicomponent reactions convert more than two simple reagents in one complex final product. These reactions meet the request of atom economy of green chemistry, avoiding the necessity of protecting groups and the isolation of the intermediates. Some of the most famous reactions of this type are the Hantzsch pyridine synthesis,^[117] Ugi,^[118] Mannich,^[119] Passerini^[120] and Biginelli^[121] reactions (**Scheme 73**).



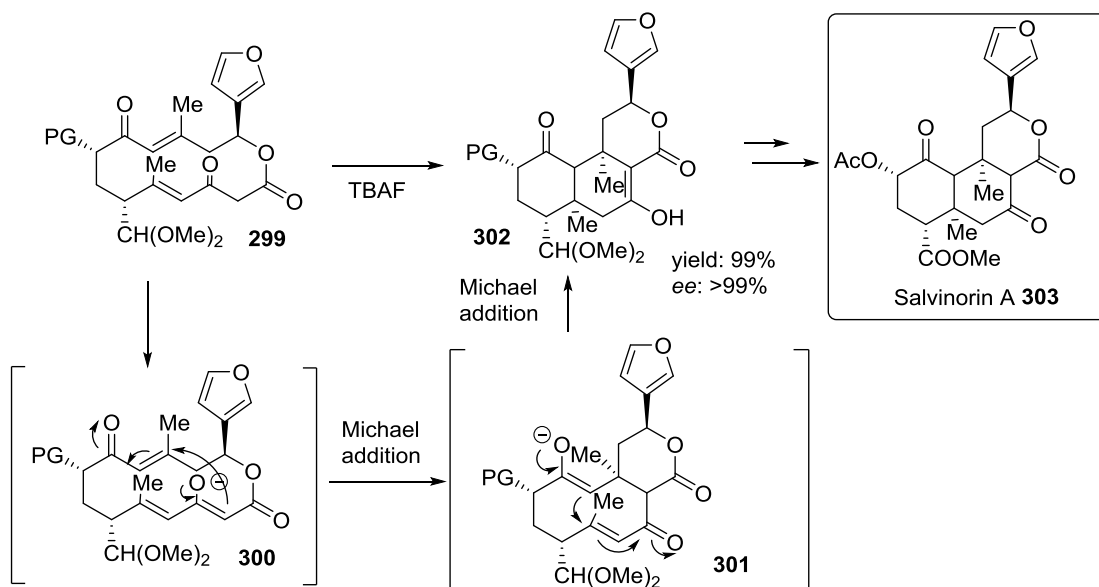
Scheme 73. Multicomponent reactions

5.1.3 Domino/Cascade/Tandem reactions

In the last decades there has been a huge development of cascade reactions^[122–124] and reviews have been written on this topic.^[123,125] Citing Tietze, as he defines in his review: “a domino reaction is a process involving two or more bond-forming transformations (usually C-C bonds) which take place under the same reaction conditions without adding additional reagents and catalysts, and in which the subsequent reactions result as a consequence of the functionality formed in the previous step”. Domino reactions can be classified in: anionic, cationic, radical, pericyclic and transition metal induced.

5.1.3.1 Anionic domino reaction

The anionic domino reaction is the most common in literature, especially when combining two Michael/Michael reactions. The first step is the attack of an anion or a nucleophile to an electrophilic position. A lot of natural products have been synthesised in this way, for example Evans *et al.* published the synthesis of Salvinorin A **303**,^[126] a diterpene that acts as an agonist on the κ opioid receptors (**Scheme 74**).

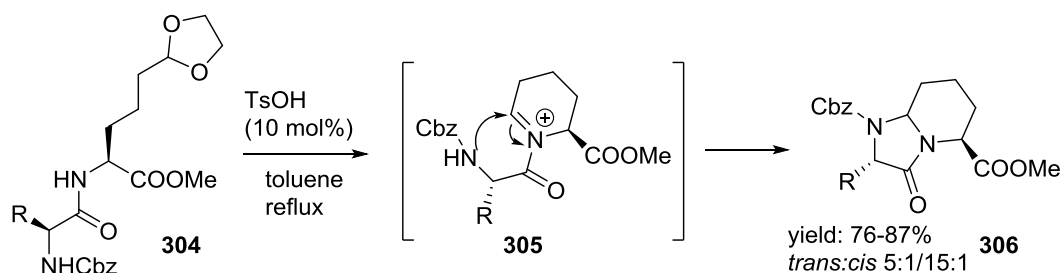


Scheme 74. Evans' synthesis of Salvinorin A through an anionic Michael/Michael cascade reaction

5.1.3.2 Cationic domino reaction

The cationic domino reactions are characterised by the formation of a carbocation that reacts with a nucleophile, generating another carbocation that undergoes the same transformation until the carbocation is trapped by a nucleophile.

One example of this reaction is reported by Blaauw and co-workers as the key step in the synthesis of *N*-heterocyclic scaffolds and applied for the total synthesis of (-)-Dysibetaine PP.^[127] The final products **306** were obtained in good yields and diastereoselectivities ranging from good to excellent based on the nature of the substituent R (**Scheme 75**).

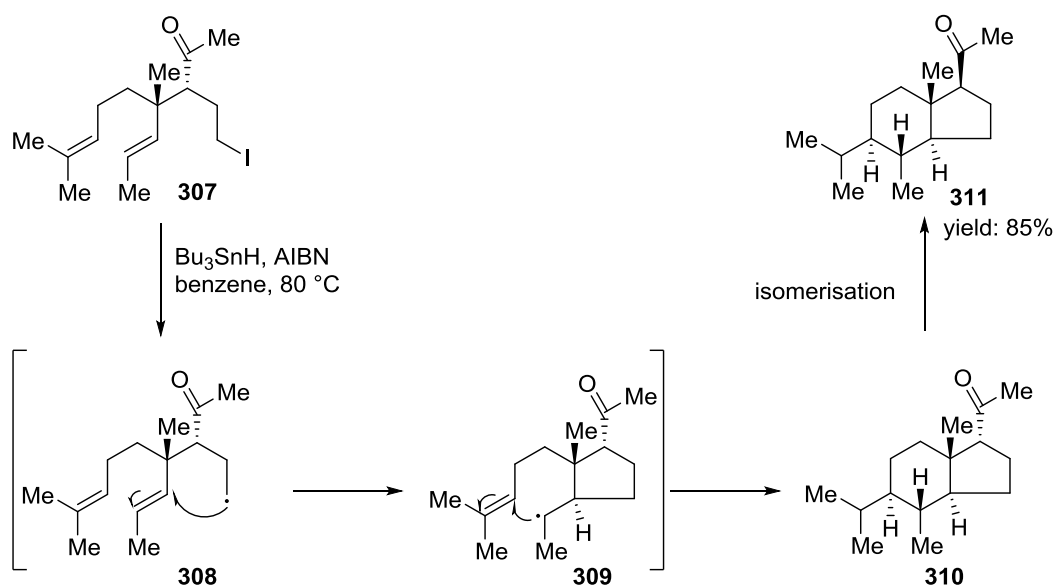


Scheme 75. Cationic domino reaction reported for total synthesis of (-)-Dysibetaine PP

5.1.3.3 Radical domino reaction

The radical domino reactions have been applied to the synthesis of polycyclic compounds and, in most cases, they are one-component intramolecular reactions.

One application of this reaction is presented by Takahashi and co-workers for the formation of the C and D rings of the steroids, obtaining the product **311** in good yield and stereoselectivity (**Scheme 76**).^[128]



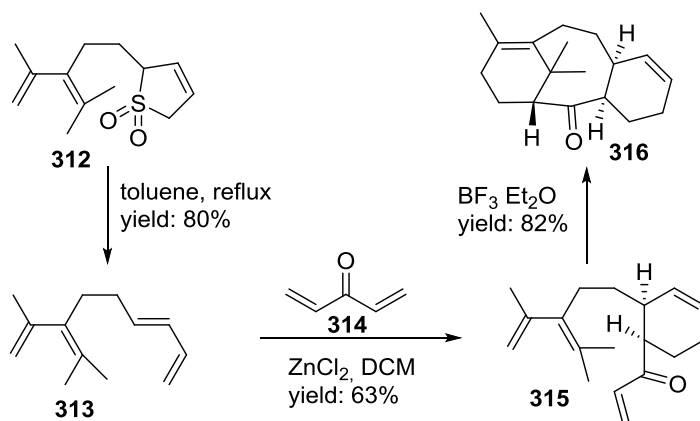
Scheme 76. Takahashi's radical domino reaction for the synthesis of steroids

5.1.3.4 Pericyclic domino reaction

Pericyclic reactions are very useful transformations in organic chemistry, for example the Diels-Alder reactions, sigmatropic and electrocyclic reactions. Combining two or more of these reactions can amplify the effect and they have been used for the

synthesis of many natural products.^[129] Most of the pericyclic domino reactions include a Diels-Alder at least in the first step.

Winkler and co-workers reported an example of this type of reaction even if it is not strictly a domino reaction as the solvent and Lewis acid have to be changed for the two cycloadditions. The first step is a cycloreversion followed by two [4+2] Diels-Alder, the first intermolecular and the second intramolecular (**Scheme 77**).^[130]

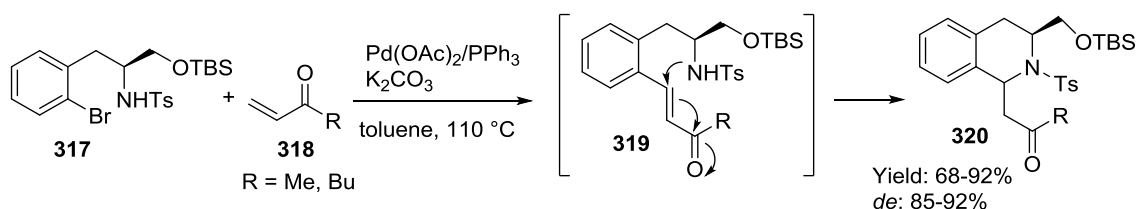


Scheme 77. Winkler's pericyclic Diels-Alder domino reaction

5.1.3.5 Transition metal catalysed domino reaction

The transition metal-catalysed domino reactions are of increasing interest in organic chemistry. Several Pd catalysed domino reactions were already present in literature before the term 'cascade' or 'domino' were coined, representing some domino Heck reactions.^[131,132]

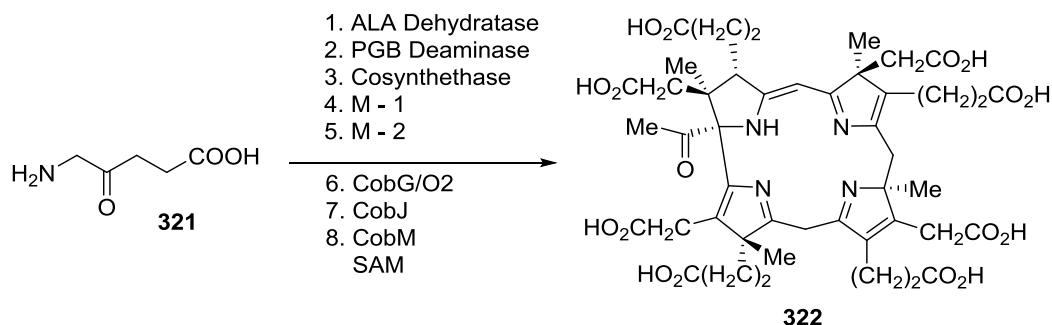
One more recent example is the enantioselective Heck reaction followed by an intramolecular aza-Michael addition reported by Pfeffer *et al.* for the synthesis of 1,3-disubstituted tetrahydroisoquinolines **320** (**Scheme 78**).^[133]



Scheme 78. Pfeffer's Pd catalysed domino reaction

5.1.3.6 Enzymatic domino reaction

In this type of reaction a multienzyme cocktail is used to catalyse different reactions. One example is the synthesis of Precorrin **322** starting from aminolevulinic acid and using eight different enzymes (**Scheme 79**).^[134]



Scheme 79. Synthesis of Precorrin through an enzymatic domino reaction

5.1.3.7 Organocatalytic enantioselective domino reactions

Since the advent of organocatalysis in 2000, efforts have been put to apply the concept of domino reaction^[122,135] to organocatalysis, thus maximising the advantages from a green chemistry point of view. The general scheme of iminium-enamine activation was already presented and explained in Chapter 1, **Scheme 29**.

As stated by the Horeau principle,^[136] the combination of sequential asymmetric reactions will render the final product in higher enantioselectivity compared to the product obtained by the single transformations. An example is reported in **Figure 18**: assuming, for example, that the first and second catalytic cycles each gave 86% *ee*, if they are performed in a cascade reaction the final product will be obtained with 7:1 *dr* and 99% *ee*.

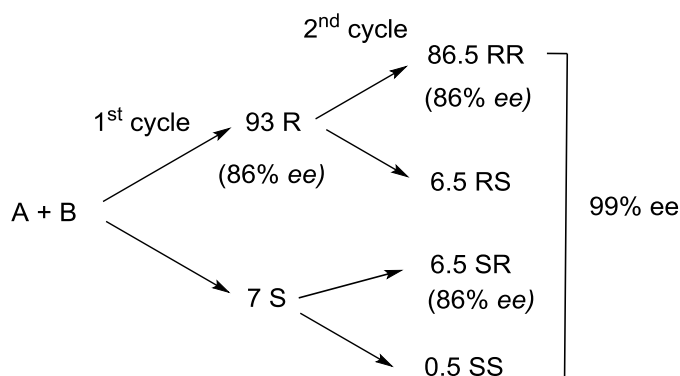
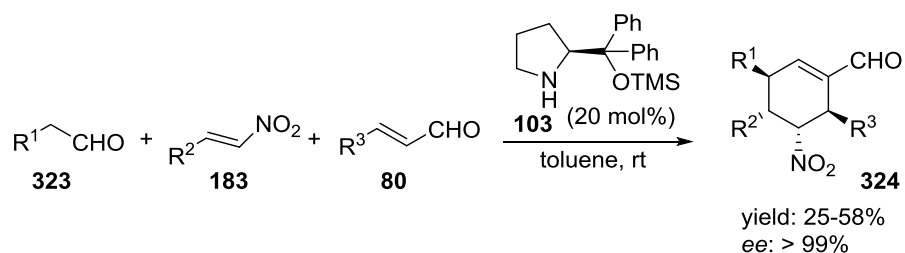


Figure 18. Example of Horeau principle applied to domino reactions

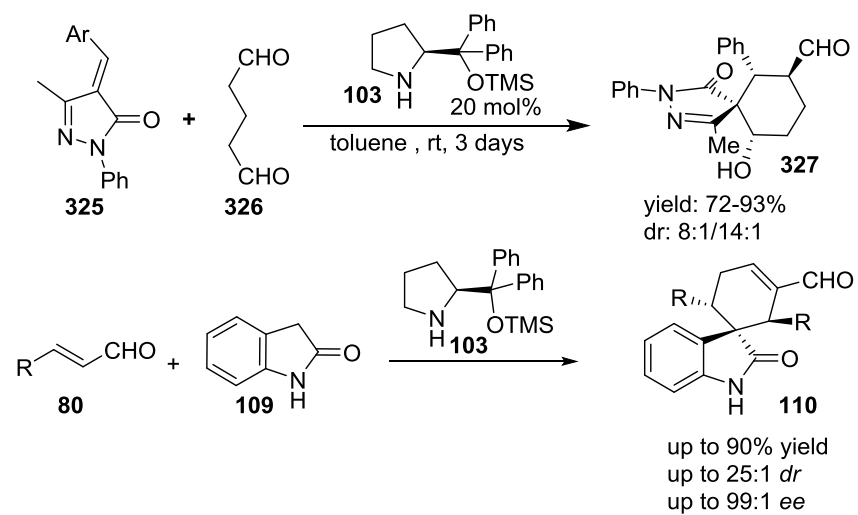
Enders proposed one of the first enantioselective triple organocascade reaction for the synthesis of tetra-substituted cyclohexene carbaldehydes.^[137] This reaction proceeds through a Michael/Michael/aldol reaction rendering the products **324** with moderate yields but excellent enantioselectivity (**Scheme 80**).



Scheme 80. Enders' Michael/Michael/aldol enantioselective cascade reaction

More examples of cascade reactions for the synthesis of cyclopropanes will be presented in the next section of this Chapter.

Recently our research group developed a highly diastereoselective synthesis of spiropyrazolones **327**^[138] and an enantioselective synthesis of spiroxindoles **110**^[57] (**Scheme 81**).



Scheme 81. Rios' cascade reactions for the synthesis of spiropyrazolones and spiroxindoles

5.2 Cyclopropanes

The synthesis of chiral cyclopropanes has always attracted the attention of the organic chemists^[139,140] due to the fact that they are often found in natural products and biologically active compounds. Cyclopropanes can be found in nature for example in terpenes, pheromones, fatty acid metabolites, amino acids.^[141–147] Natural occurring and synthetic cyclopropanes also show pharmaceutical activities for example as antidepressants **329**,^[148] HIV-inhibitors,^[149] antipsychotics^[146] and marine lactones **328**.^[150] The pyrethrins from the Chrysanthemum flowers **330** are potent insecticide and represented lead compounds for the synthetic pyrethroid, the most important class of insecticide on the market (**Figure 19**).^[151] Moreover the cyclopropanes are useful intermediates than can undergo ring-opening and ring-expansion reactions to form differently substituted products.^[152–158]

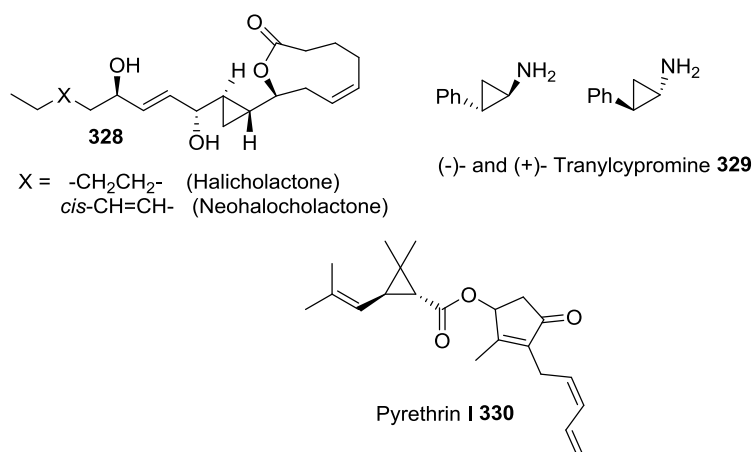


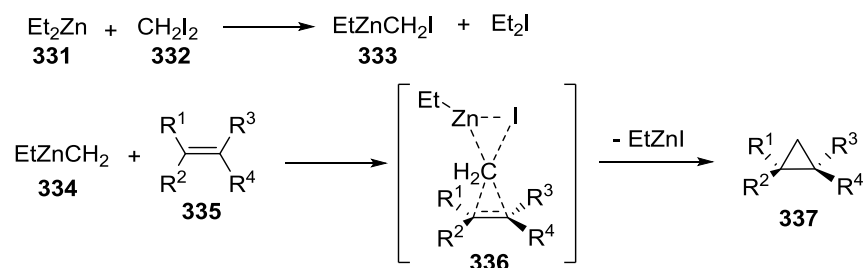
Figure 19. Examples of interesting cyclopropanes

The most common method to synthesise cyclopropanes is the Simmons-Smith reaction, the cyclopropanation with diazomethane and the Michael initiated ring closure catalysed by transition metals or organocatalysts.

5.2.1 Simmons-Smith reaction

In 1958 Simmons and Smith developed a cyclopropanation reaction using diiodomethane **332** in the presence of zinc-copper to convert unfunctionalised alkenes **335**.^[159,160] This reaction is a concerted process, through a [2+1] methylene transfer *via*

a three-centred transition state **336** as shown in **Scheme 82**. The reaction is stereospecific and it retains the configuration of the starting alkene; if the diiodomethane is substituted there is a preference for the *cis* configuration of the final product **337**. There have been several modifications to prepare the starting reagent, for example the use of diethylzinc **331** and diiodomethane (Furukawa modification, **Scheme 82**).^[161,162]

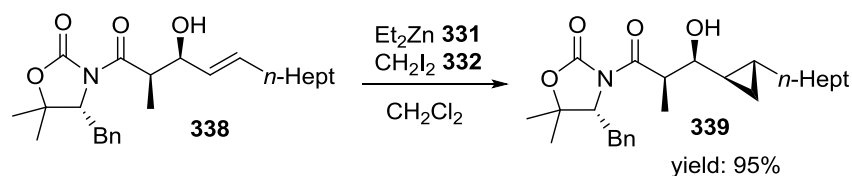


Scheme 82. Furukawa modification of Simmons Smith cyclopropanation and mechanism

The asymmetric version of the Simmons Smith cyclopropanation can be achieved through the use of chiral auxiliaries or chiral catalysts.

5.2.1.1 Chiral auxiliaries

When the alkene has one functional group containing a heteroatom, a directing effect happens and the attack of the alkylidene takes place from the less hindered face of the double bond. One example is reported by Bull *et al.* that uses an oxazolidinone ligand, and the directing effect of the hydroxyl group in the allylic position allows the formation of the *syn* cyclopropane **339** (**Scheme 83**).^[163]

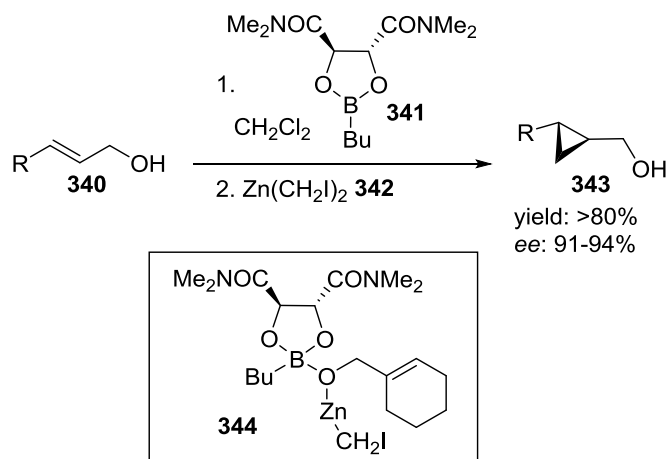


Scheme 83. Bull's cyclopropanes synthesis with hydroxyl as directing group

5.2.1.2 Chiral ligands

Another way to achieve an asymmetric cyclopropanation is the use of stoichiometric chiral additives as in the asymmetric modification described by Charette *et al.* in

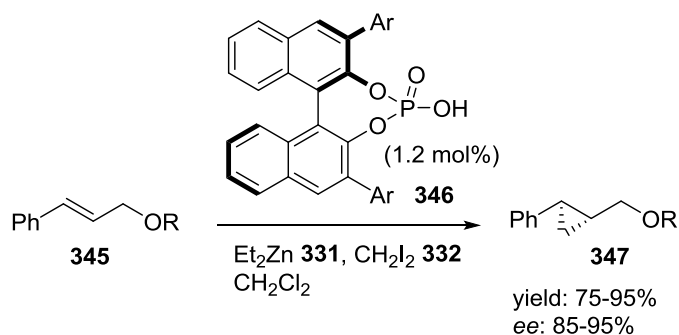
1998.^[164] They reported the cyclopropanation of allylic alcohols **340** with dioxaborolane ligands **341** (Scheme 84) obtaining the products in high yields and enantioselectivity. The chiral ligand is based on the presence of a boron atom that forms a complex with the acidic halomethylzinc reagent.



Scheme 84. Charetté's asymmetric cyclopropanation of allylic alcohols with dioxaborolane ligands

5.2.1.3 Chiral catalysts

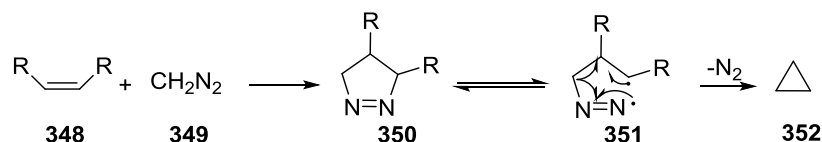
Several catalytic systems have been published for the asymmetric Simmons-Smith cyclopropanation, though most of the catalysts have to be used in stoichiometric amounts. Again Charetté reported a nice example using a chiral phosphoric acid **346** derived from a disubstituted BINOL derivative.^[165] This allows the formation of an intermediate chiral zinc phosphate that would allow the cyclopropanation of protected allylic alcohols **345** (Scheme 85).



Scheme 85. Charetté's cyclopropanation of allylic alcohols with chiral phosphoric acid

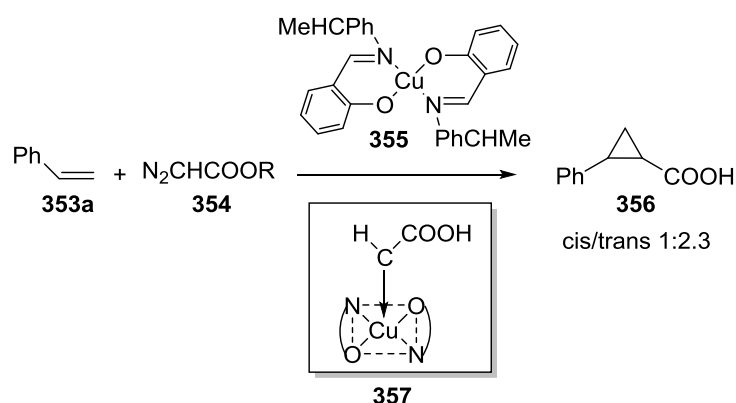
5.2.2 Cyclopropanation with diazomethane

Diazomethane **349** reacts with olefins **348** to render cyclopropanes **352**. The first step is a 1,3-cycloaddition to form a pyrazoline **350** and the second step is a denitrogenation, by thermal or photochemical decomposition (**Scheme 86**).^[166,167]



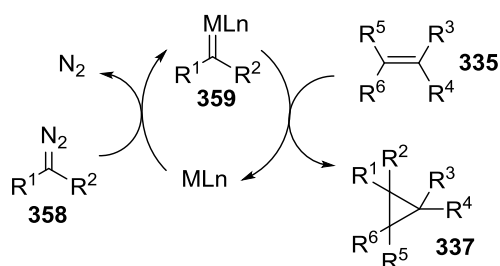
Scheme 86. Cyclopropanation with diazomethane and olefins

A safer way to use the diazocompounds is in combination with transition-metal catalysts **355**, for example the work of Noyori and Nozaki (**Scheme 87**).^[168]



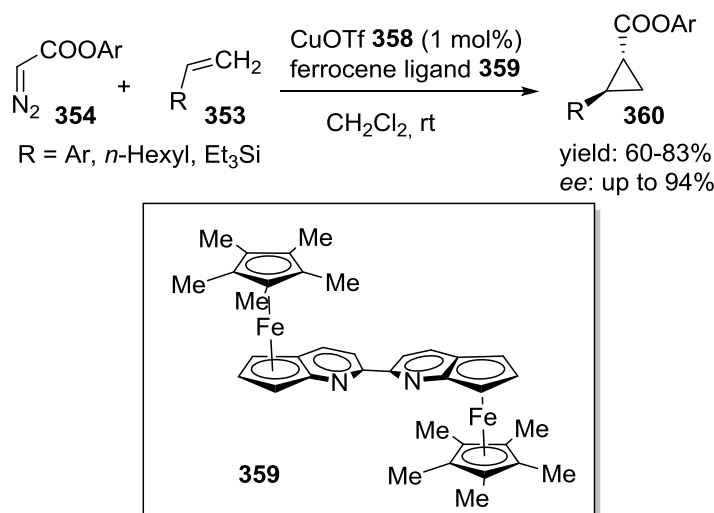
Scheme 87. Noyori's synthesis of cyclopropanes

The mechanism of these reactions (**Scheme 88**) goes through a carbenoid formation: the metal catalyst interacts with the diazo compound **358** to form a metalcarbene complex **359** and then the carbene is transferred to the alkene **335**. The enantiocontrol is due to the careful choice of chiral ligand for the metal catalyst.



Scheme 88. Mechanism of the transition-metal catalysed decomposition of diazoalkenes

Fu *et al.* reported a copper(I) catalysed cyclopropanation of olefins **353** and diazocompounds **354** using a novel bidentate chiral ferrocene ligand **359** (**Scheme 89**).^[169]

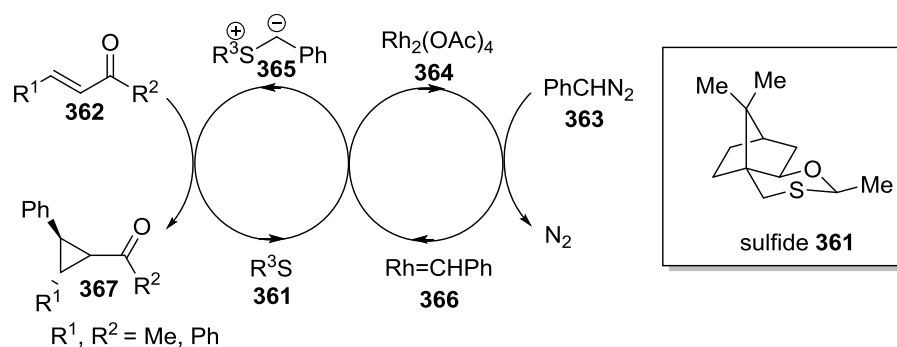


Scheme 89. Fu's cyclopropanation with bidentate chiral ferrocene copper ligand

5.2.3 Michael Initiated Ring Closure

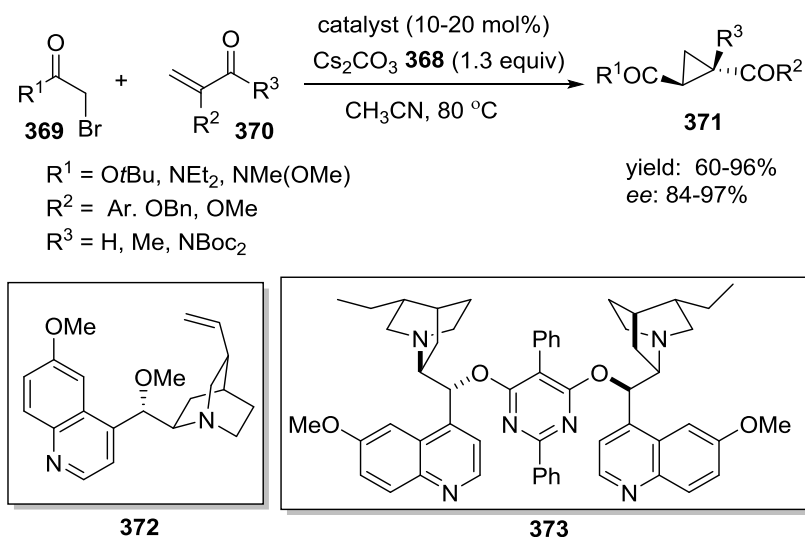
Michael initiated ring closure (MIRC) involves a conjugate addition of a nucleophile to an alkene to produce an enolate that undergoes an intramolecular ring closure.

A good example of this methodology was reported by Aggarwal *et al.* using the sulfoxonium ylides **365** synthesised by Corey and Chaykovsky^[170] in 1962. Aggarwal and co-workers developed an asymmetric cyclopropanation of electron deficient alkenes **362** catalysed by a chiral sulphide **361**, obtaining the final products **367** in moderate yields and excellent enantioselectivities (yield: 14-60%; dr: 4:1; ee: >97%) (**Scheme 90**).^[171]



Scheme 90. Mechanism of Aggarwal's asymmetric cyclopropanation of alkenes mediated by a chiral sulphide

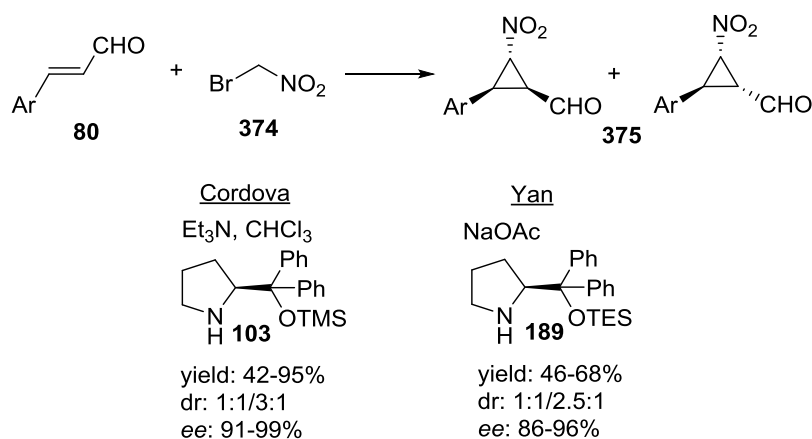
Organocatalytic versions using ylides were later proposed by MacMillan and Gaunt. MacMillan *et al.* presented the amine-catalysed cyclopropanation of α,β -unsaturated aldehydes **80** by β -oxosulfonium ylides **122**, using a 2-carboxylic acid dihydroindole catalyst **123**, as previously reported in the **Scheme 31**, Chapter 1.^[65] Gaunt *et al.* presented an enantioselective cyclopropanation of an α -bromo carbonyl compound **369** and electron poor alkenes **370** *via* ammonium ylides using chiral tertiary amines **372** and **373** as catalysts (**Scheme 91**).^[172]



Scheme 91. Gaunt's cyclopropanation via ammonium ylides

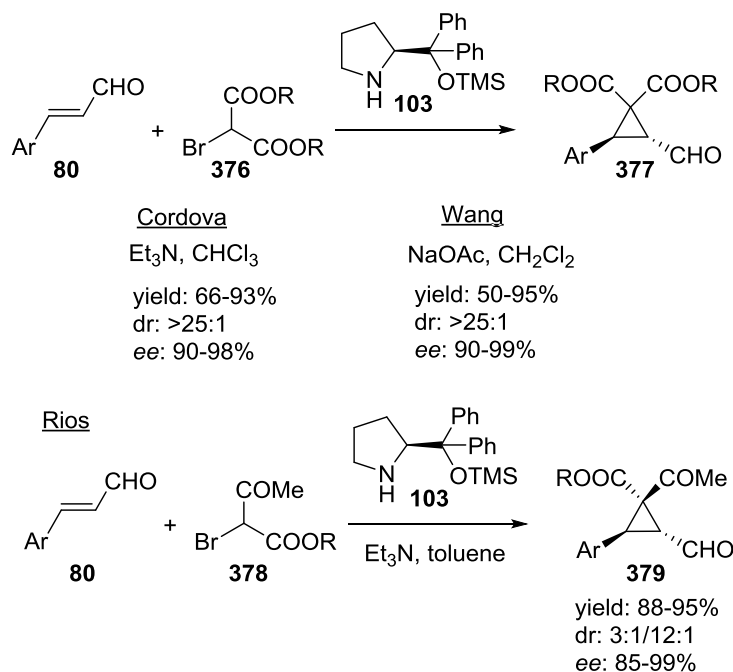
With the advent of organocatalysis, several MIRC domino reactions catalysed by diphenylprolinol catalysts have been developed. An example is the nitrocyclopropanation reported by Cordova *et al.*^[173] and Yan *et al.*^[174] through the

reaction of bromonitromethane **374** with α,β -unsaturated aldehydes **80** as shown in the **Scheme 92**.



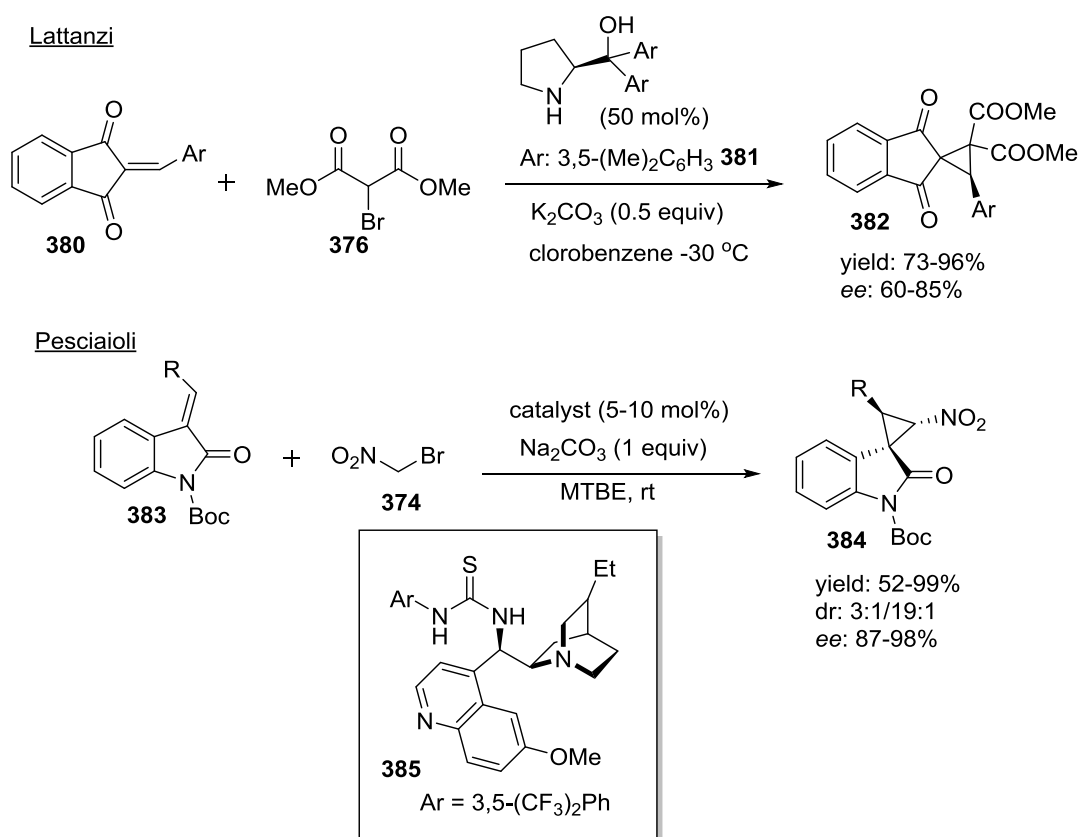
Scheme 92. Nitrocyclopropanation of 1-bromonitroalkanes with α,β -unsaturated aldehydes

Other examples of organocascade reactions leading to the formation of cyclopropanes were reported by Cordova *et al.*,^[175,176] Wang *et al.*^[177] and Rios *et al.*^[178] They use enals **80** as electrophiles, activated by the secondary amine catalyst **103**, and bromomalonates **376** or bromoketoesters **378** as nucleophiles respectively (**Scheme 93**).



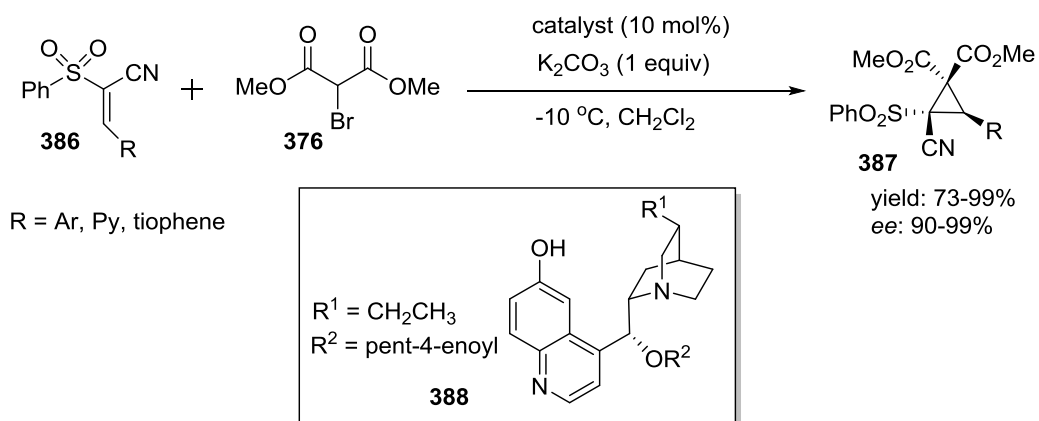
Scheme 93. Cyclopropanation of enals with malonates and ketoesters

In 2011 Lattanzi and co-workers and Pesciaioli and co-workers developed an organocatalytic enantioselective synthesis of spirocyclopropanes through a MIRC reaction. In particular Lattanzi^[179] reported the cyclopropanation of 2-arylidene-1,3-indandiones **380** with bromomalonates **376**, using diphenylprolinol **381** as catalyst and Pesciaioli^[180] reported the cyclopropanation of *N*-Boc protected oxindoles **383** with bromonitroalkane **374** using a quinine derivative **385** as catalyst (**Scheme 94**).



Scheme 94. Organocatalytic enantioselective synthesis of spirocyclopropanes

In 2015 Cobb and co-workers explored an asymmetric cyclopropanation of conjugated cyanosulfones **386** with bromomalonates **376** catalysed by a derivatised cupreine catalyst **388**, obtaining highly functionalised cyclopropanes **387** in good yields and enantioselectivities (**Scheme 95**).^[181]



Scheme 95. Cobb's cyclopropanation of conjugated cyanosulfones with bromomalonates

5.3 Project aim

Despite the advantages and progress of synergistic catalysis presented in Chapter 1, 3 and 4, there are still some limitations as, for example, the fact that only one C-C bond is formed using two catalytic cycles. This fact makes the process expensive from an atom economy point of view as there is the need to use two catalysts to create only one new bond. This drawback attracted our interest, together with the idea to study a way to improve the results obtained in the previous project (Chapter 4) and to obtain higher diastereo- and enantioselectivities.

For this reasons, the aim of this second project is to expand the synergistic catalysis approach, presented in Chapter 4, to a cascade reaction. Inspired by the previous experience in our research group in the synthesis of cyclopropanes^[176] and interested to explore the possibility to combine a metal Lewis acid and an organocascade reaction in a synergistic approach, we designed a cascade reaction that could trap the enamine *in situ*, forming two C-C bonds with three catalytic cycles, pushing the boundaries of synergistic catalysis.

5.4 Research hypothesis and proposed reaction mechanism

We decided to study the reaction of chloromethylenebenzoxazoles with enals to obtain formyl cyclopropanes in a highly enantioselective fashion. The choice of the chloromethylenebenzoxazoles is related to the need to have a compound that could act as a nucleophile at the start of the reaction (**Figure 20, 389**) and subsequently as an electrophile with the loss of chlorine anion as a leaving group (**Figure 20, 390**).

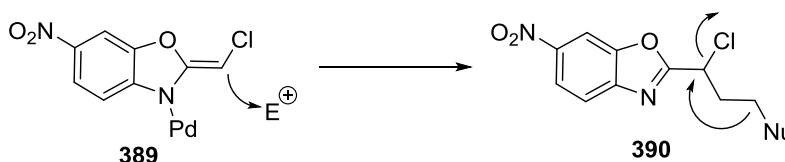


Figure 20. Chloromethylenebenzoxazole acting as nucleophile (**389**) and then as electrophile (**390**)

One of the three catalytic cycles is the activation of a chloromethylenebenzoxazole by a metal Lewis acid, the second cycle is the activation of the enal by the secondary

amine catalyst through an iminium activation while the third cycle is still promoted by the organocatalyst, but this time, through the enamine catalysis (**Figure 21**).

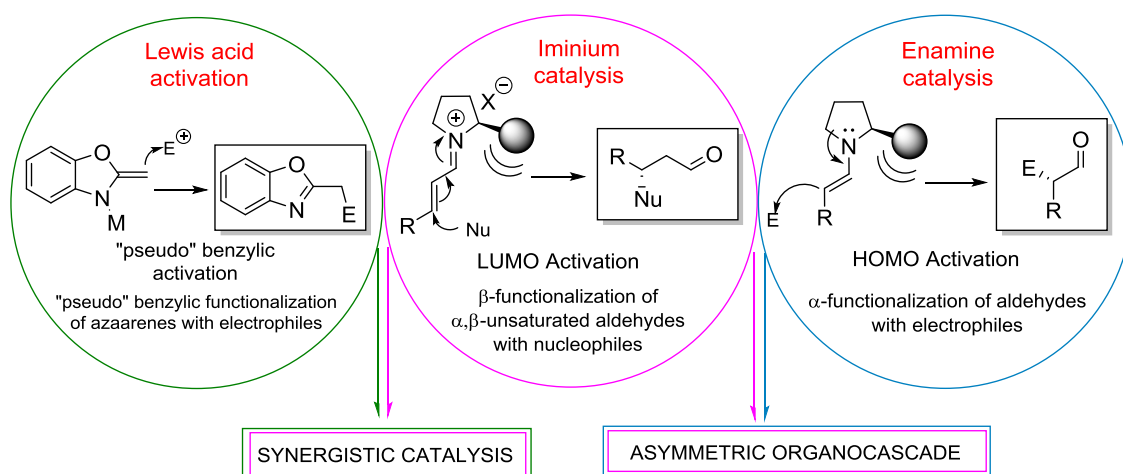
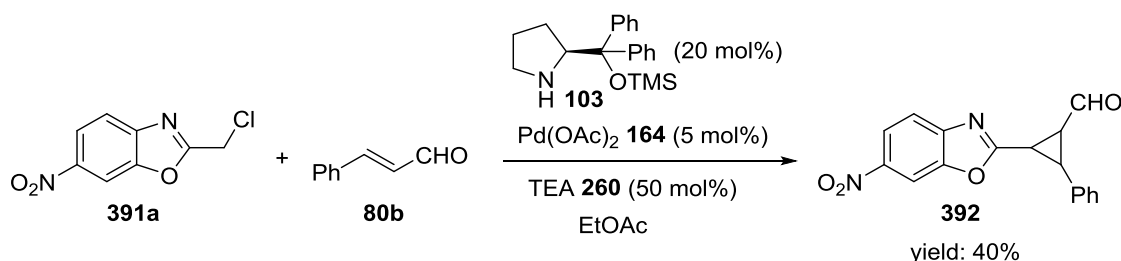


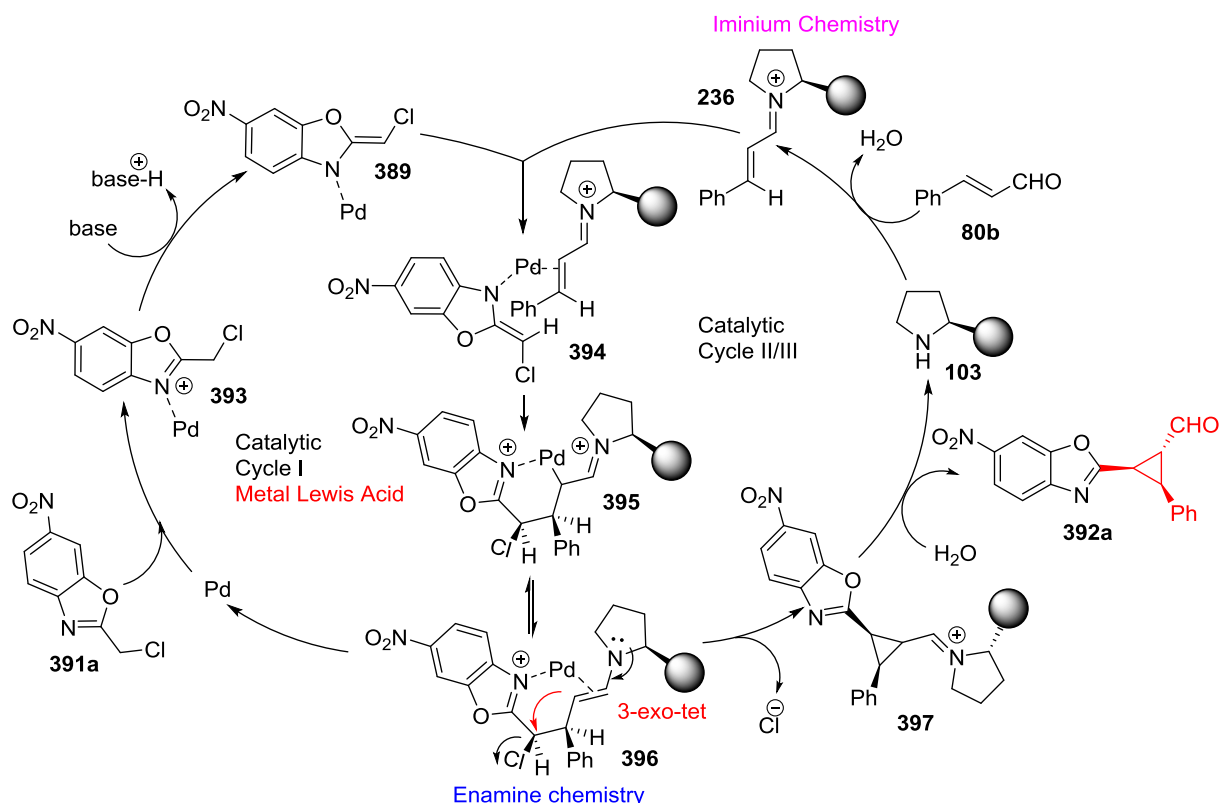
Figure 21. New synergistic approach: two catalysts, three catalytic cycles and the formation of two new C-C bonds

To prove the viability of this approach, we tested the reaction of addition of 2-(chloromethyl)-6-nitrobenzoxazole **391a** with cinnamaldehyde **80b** as shown in **Scheme 96** and, to our delight, the final product **392** was obtained in moderate yield.



Scheme 96. First reaction tested for the addition of 2-(chloromethyl)-6-nitrobenzoxazole with cinnamaldehyde

The proposed reaction mechanism is shown in **Scheme 97**.



Scheme 97. Proposed mechanism for the cyclopropanation

As suggested by Lam,^[88] Pd interacts with the alkylbenzoxazole **391a** by coordinating to the nitrogen, thus increasing the acidity of the protons in the methylene position. After treating the metallated alkylbenzoxazole **393** with a base, a nucleophile **389**, suitable to react with the electrophile, was obtained. In the other catalytic cycle, the enal **80b** reacts with the secondary amine organocatalyst **103** to form the corresponding activated iminium form **236**. The (*S*)-catalyst efficiently shields one face of the enal. Then the coordination between the Pd enolate and the double bond of the imine occurs to form the intermediate **394**. After the addition of the intermediate to the β -position of the iminium intermediate, the enamine intermediate **396** reacts intramolecularly with the alkyl halide through a 3-exo-tet cyclisation to form the cyclopropane ring. Hydrolysis of compound **397** affords the final product **392a** and releases the catalyst, thus completing the catalytic cycle.

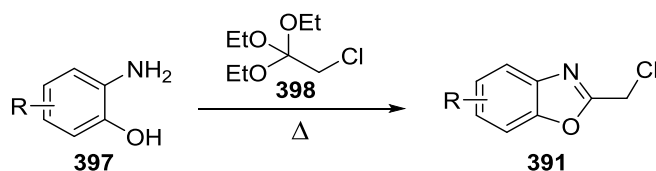
Some stereochemical considerations have to be done. As shown in the **Scheme 97**, we suggest the formation of an intermediate Pd enolate **394**: the coordination of the Pd to

the double bond of the iminium intermediate **236** happens on the *Si*-face, as the bulky substituents of the organic catalyst efficiently shield the *Re*-face. The azaallyl ligand in the intermediate **394** possess an *E*-stereochemistry to minimise the steric interactions between the Cl substituent and the iminium. This is the crucial step for the determination of the stereochemistry: the nucleophilic attack on the β position of the aldehyde happens on the *Si*-face with the formation of a 6 membered ring intermediate **395** with the new Pd enolate formed in the α position of the iminium. Then an intramolecular alkylation between the Pd enolate and the methylene chloride, followed by an inversion of the configuration, renders the product **397** with the *cis* configuration between the two aromatic substituents.

5.5 Results and discussions

5.5.1 Synthesis of the starting materials

The azaarenes **391** were synthesised following the procedure presented in the article of Lam and co-workers^[88] using differently substituted 2-aminophenol **397** and 2-chloro-1,1,1-triethoxyethane **398** as shown in **Scheme 98**. The mechanism is the same as the one reported in Chapter 4, **Scheme 59**.



Scheme 98. Synthesis of the chloromethylenebenzoxazoles as starting materials

The results obtained in the synthesis of the starting chloro-alkylbenzoxazoles are presented in **Figure 22**, with yields ranging from 54 to 95%.

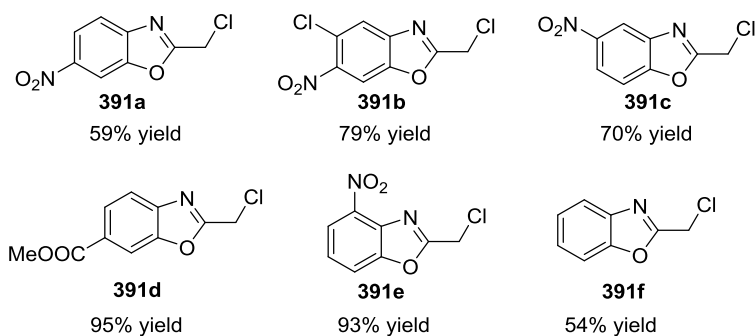


Figure 22. Results obtained in the synthesis of chloro-alkylbenzoxazoles

The α,β -unsaturated aldehydes **80** were synthesised through a Wittig reaction leading to the *E* form of the aldehydes as already shown in Chapter 4, **Scheme 61** and **Scheme 62**.³

5.5.2 Optimisation of the reaction conditions

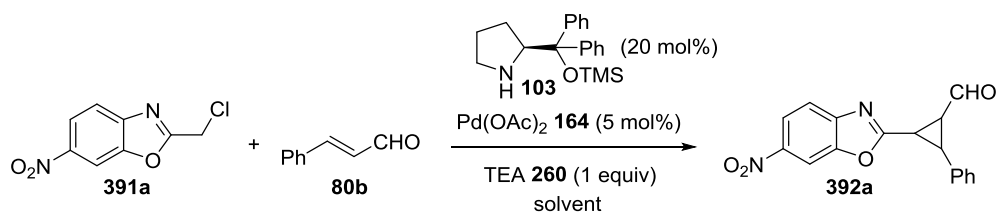
It has to be noted that the final cyclopropane **392** is stable so there is no need to further derivatise as required in the project presented in Chapter 4.

Spurred by the result obtained, we studied the optimisation of the reaction screening different solvents, metal Lewis acids, bases and organocatalysts.

³ The azaarenes **391** and aldehydes **80** were synthesised by me and Cameron Ross, a summer project students that I supervised.

5.5.2.1 Screening of solvents

Table 9. Screening of solvents



Entry	Solvent	Conversion % (24 h)	dr (crude) ^[a]	ee major dia (%) ^[b]
1	EtOAc	52	2.1 : 1.7 : 1	94
2	CH ₃ CN	59	4 : 3.2 : 1	99
3	DMF	33	3.5 : 2.4 : 1	---
4	MeOH	97	2 : 1	> 90
5	DCM	57	2 : 1.2 : 1	> 90
6	CHCl ₃	29	2.4 : 1.6 : 1	> 70

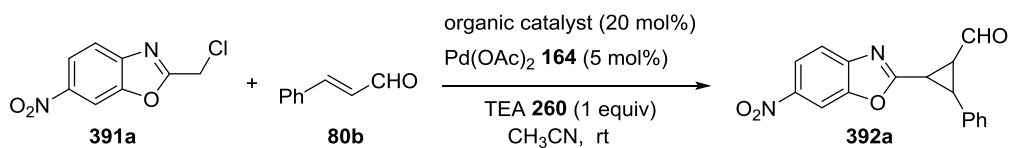
[a] dr are calculated from the crude NMR comparing the aldehydes signals

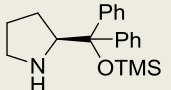
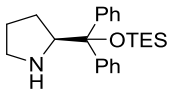
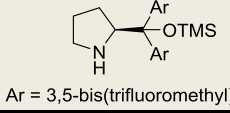
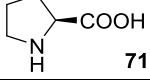
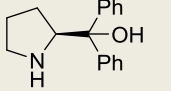
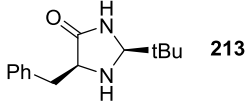
[b] ee were determined by chiral HPLC analysis

At first a screening of solvents was performed as shown in **Table 9**. With all the solvents tested, three diastereomers were present in the crude NMR after 24 hours except with MeOH (**Table 9**, entry 4). MeOH was not chosen as a solvent for the next reactions as the crude NMR was less clean than with the other solvents and showed a degradation of the reagents. Mostly degradation of the reagents was seen in the reaction performed in DMF (**Table 9**, entry 3). In CDCl₃ (**Table 9**, entry 6) the conversion was too low after 24 hours. The best solvent was found to be CH₃CN (**Table 9**, entry 2) as regards the diastereoselectivity, compared to EtOAc and DCM (**Table 9**, entries 1 and 5).

5.5.2.2 Screening of organic catalysts

Table 10. Screening of organic catalysts



Entry	Catalyst	Conversion % (24 h)	dr (crude) ^[a]	ee major dia (%) ^[b]
1	 103	59	4 : 3.2 : 1	99
2	 189	82	2.5 : 1.1 : 1	99
3	 220 Ar = 3,5-bis(trifluoromethyl)phenyl	traces	---	---
4	 71	traces	---	---
5	 272	--	---	---
6	 213	traces	---	---
7	No organic catalyst	---	---	---

[a] dr are calculated from the crude NMR comparing the aldehydes signals

[b] ee were determined by chiral HPLC analysis

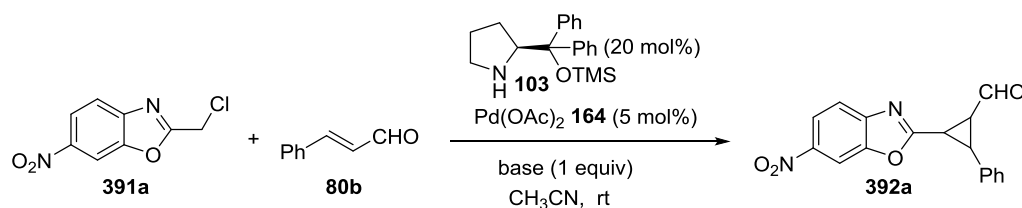
Then a screening of organic catalysts was performed (**Table 10**). Entries 3, 4, 5 and 6, **Table 10**, did not show any conversion or traces of the product in the NMR of the crude. The lack of reactivity observed with trifluoromethyl-substituted diarylprolinol **220** (**Table 10**, entry 3) is in agreement with Hayashi's findings.^[182] Diarylprolinol catalysts lower the LUMO of the iminium ion intermediate facilitating the Michael addition but the formation of the iminium ion in absence of an acid co-catalyst is possible, at acceptable rate, only with the more basic/nucleophilic diphenylprolinols.

Good results were obtained with the commercial Jorgensen-Hayashi catalyst **103** (**Table 10**, entry 1) and with the modified version of it with a bulkier substituent **189**

(**Table 10**, entry 2). The conversion with the last catalyst is better, however the diastereoselectivity is worse so that the commercial catalyst was chosen as the best organic catalyst. To prove the need of the organic catalyst the reaction was performed without any secondary amine (**Table 10**, entry 7) and from the NMR of the crude no formation of the products was seen.

5.5.2.3 Screening of bases

Table 11. Screening of bases



Entry	Base	Conversion % (24 h)	dr (crude) ^[a]	ee major dia (%) ^[b]
1	TEA 260	59	4 : 3.2 : 1	99
2	DIPEA 28	full	1.6 : 0.8 : 1	99
3	2,6-lutidine 398	93	4.1 : 2.4 : 1	99
4	CS ₂ CO ₃ 368	---	---	---
5	DABCO 138	34	2.5 : 1.1 : 1	> 90
6	No base	29	2.4 : 1 : 1	---

[a] dr are calculated from the crude NMR comparing the aldehydes signals

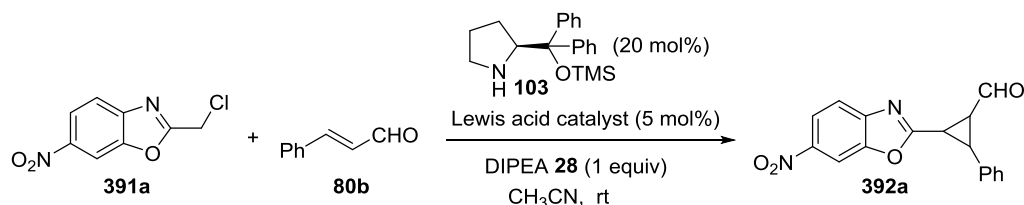
[b] ee were determined by chiral HPLC analysis

Table 11 shows the screening of bases that was performed using the best solvent and organic catalyst found before. The best results were obtained with 2,6-lutidine **398** (**Table 11**, entry 3): the conversion is better than with TEA **260** (**Table 11**, entry 1) with a similar dr from the NMR of the crude. The reaction with DIPEA **28** (**Table 11**, entry 2) gave full conversion but the dr is worse. With an inorganic base **368** (**Table 11**, entry 4) the reaction did not work, while with DABCO **138** (**Table 11**, entry 5) the conversion and dr are worse compared to the first three entries. The reaction was tested without

any base (**Table 11**, entry 6), rendering only 29% conversion after 24 hours, with some degradation of the starting aldehyde. So we prove the need of a base and the best was found to be 2,6-lutidine.

5.5.2.4 Screening of metal Lewis acids

Table 12. Screening of metal Lewis acids



Entry	Lewis acid	Conversion % (24 h)	dr (crude) ^[a]	ee major dia (%) ^[b]
1	Pd(OAc) ₂ 164	full	1.6 : 0.8 : 1	99
2	AgOBz 399	92	2 : 1 : 1	20
3	AgOAc 230	79	2.7 : 1.3 : 1	> 90
4	Cu(OAc) ₂ 264	61	1.7 : 0.6 : 1	> 90
5	Yb(SO ₃ CF ₃) ₂ 176	---	---	---
6	Cu(SO ₃ CF ₃) ₂ 261	50	2.5 : 2.2 : 1	> 90
7	PdCl ₂ 266	29	1 : 0.6 : 1	> 90
8	No Lewis Acid	traces	---	---

[a] dr are calculated from the crude NMR comparing the aldehydes signals

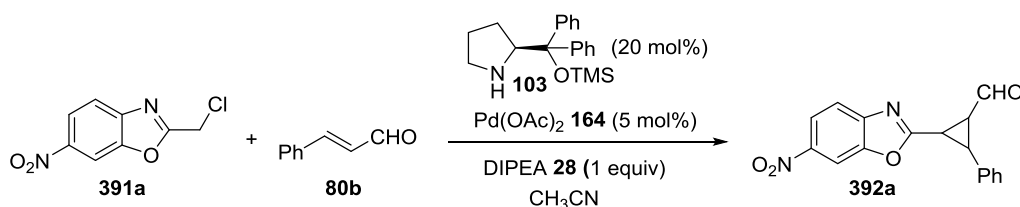
[b] ee were determined by chiral HPLC analysis

Next, different metal Lewis acids were tested using acetonitrile as the solvent and DIPEA **28** as the base (**Table 12**). The best results were obtained with AgOAc **230** and Pd(OAc)₂ **164** (**Table 12**, entries 1 and 3), both of them showing good conversion and good selectivities: in particular Pd(OAc)₂ rendered a better enantioselectivity while AgOAc rendered a better diastereoselectivity. Nevertheless, comparing with those of the previous table, these results are worse than the ones obtained with 2,6-lutidine

and Pd(OAc)₂. The reaction with Yb(SO₃CF₃)₂ **176** (Table 12, entry 5) did not work as a degradation of the starting materials occurred. With the other Lewis acid tested, the reaction worked but all of them showed worse results compared to AgOAc and Pd(OAc)₂. With AgOBz **399** (Table 12, entry 2) low enantioselectivity was obtained, with Cu(OAc)₂ **264**, Cu(SO₃CF₃)₂ **261** and PdCl₂ **266** (Table 12, entries 4, 6 and 7) lower conversions and dr were obtained. When the reaction was performed without any Lewis acid (Table 12, entry 8) no conversion was observed in the NMR of the crude. This demonstrated the need of both catalysts and consequentially confirms the mechanism of the synergistic catalysis.

5.5.2.5 Screening of temperatures

Table 13. Screening of temperatures



Entry	Temperature (°C)	Conversion %	dr (crude) ^[a]	ee major dia (%) ^[b]
1	30	63 (24 h)	1.7 : 1.1 : 1	> 95
2	4	61 (60 h)	2 : 0.8 : 1	> 95
3	rt	full (24h)	1.6 : 0.8 : 1	> 95

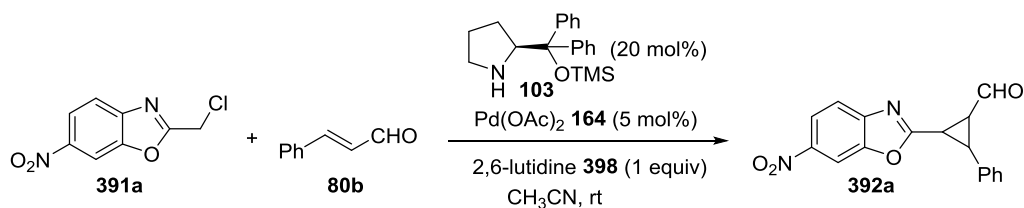
[a] dr are calculated from the crude NMR comparing the aldehydes signals

[b] ee were determined by chiral HPLC analysis

The reaction was tested at higher and lower temperatures as shown in Table 13. In both cases the conversion was lower than at room temperature (Table 13, entry 3). In the first case (Table 13, entry 1) the heating probably caused some degradation of the catalyst. In the second case (Table 13, entry 2) the low temperature is the cause of the lower reaction rate.

5.5.2.6 Screening of metal Lewis acids with 2,6-lutidine as a base

Table 14. Screening of metal Lewis acids with 2,6-lutidine as base



Entry	Metal	Conversion % (24 h)	dr (crude) ^[a]
1	Pd(OAc) ₂ 164	full	5.2 : 2.6 : 1
2	Cu(OAc) ₂ 264	traces-degradation	---
3	AgOAc 230	full (NMR less clean than with Pd)	2.2 : 1.4 : 1

[a] dr are calculated from the crude NMR comparing the aldehydes signals

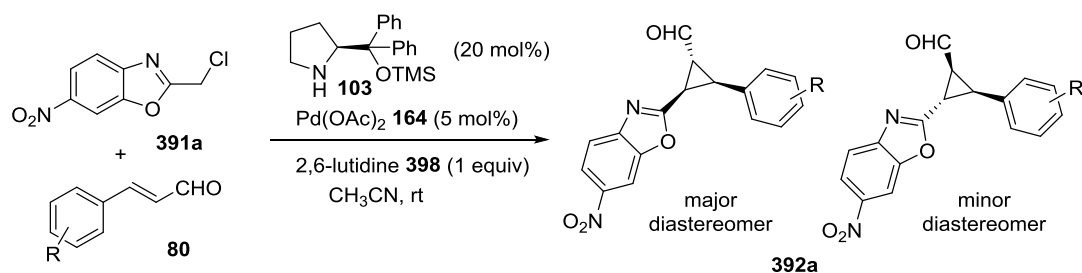
As 2,6-lutidine was found to be the most suitable base, the best Lewis acids found with DIPEA **28** were tested again with 2,6-lutidine **398** as presented in **Table 14**. Cu(OAc)₂ **264** gave only traces of the final products (**Table 14**, entry 2), due to the degradation of the starting materials. Compared to AgOAc **230** (**Table 14**, entry 3), Pd(OAc)₂ **164** gave a better conversion, a cleaner NMR of the crude and especially a better diastereoselectivity (**Table 14**, entry 1).

We found that the best reaction conditions were the use of one equivalent of benzoxazole **391**, two equivalents of aldehyde **80**, Pd(OAc)₂ **164** (5 mol%) as metal Lewis acid, Jorgensen-Hayashi catalyst **103** (20 mol%) as secondary amine, 2,6-lutidine **398** (1 equivalent) as the base and CH₃CN as the solvent.

Then we proceeded to study the scope of the reaction testing different enals and differently substituted benzoxazoles. In all the examples reported, the major diastereomer could be easily isolated after column chromatography, while the two minor diastereomers are often an inseparable mixture.

5.5.3 Scope of the reaction with enals

Table 15. Scope of the reaction with several enals



Product	Aldehyde (R)	Yield ^[a] (%)	dr ^[b]	ee major (%) ^[c]	ee minor (%) ^[c]
392a	H 80b	89	4.5 : 1.2 : 1	96 (R catalyst) 99 (S catalyst)	not determined
392b	4-Br 80h	70	7 : 2.2 : 1	97 (R catalyst) 98 (S catalyst)	not determined
392c	4-Cl 80e	74	2:1	98 (R catalyst) 97 (S catalyst)	not determined
392d	4-NO ₂ 80i	79	14 : 5.6 : 1	>99 (R catalyst) >99 (S catalyst)	81 (R catalyst) 89 (S catalyst)
392e	4-CN 80g	89	4.8 : 3 : 1	>99 (R catalyst) >99 (S catalyst)	not determined
392f	4-F 80j	86	6.6 : 2.6 : 1	98 (R catalyst) 98 (S catalyst)	not determined
392g	4-Me 80k	66	5.3 : 1.6 : 1	99 (R catalyst) 99 (S catalyst)	not determined
392h	2-Br 80c	81	13.4 : 2.3 : 1	>99 (R catalyst) >99 (S catalyst)	not determined
392i	80m	85	> 15:1	81 (R catalyst) 87 (S catalyst)	-----
392j	80a	---	---	---	---

[a] yields are from the sum of the isolated diastereomers after column chromatography

[b] dr are calculated from the isolated diastereomers after column chromatography

[c] ee were determined by chiral HPLC analysis

In **Table 15** is presented the study of the scope of the reaction testing several enals. All the products were obtained in good to excellent yields with moderate to good diastereoselectivities and excellent enantioselectivities regarding the major diastereomer. We tested different substituents on the aromatic ring of the enal. Employing aryl compounds substituted with halogens in the *para* position (4-Br, 4-Cl and 4-F) the products **392b**, **392c** and **392f** respectively, were obtained in good yields and dr (86 -70% yield, 3:1 dr, up to 99% *ee*). When the Br is in the *ortho* position **392h**, even if the aldehyde was sterically hindered, the reaction worked with good yields, *ee* and dr. When electron-withdrawing substituents were present (4-NO₂ and 4-CN) the products **392d** and **392e** were obtained in good yields (79 – 63%), good dr and excellent *ee* (> 99%).

Then we tested the aldehyde derived from the glyoxylate **80m**, obtaining the final product **392i** in good yield and excellent diastereoselectivity (only one diastereomer) but with lower enantioselectivity. The reason for the epimerisation is explained in **Figure 23**: on the carbon bearing the ester group, the proton is more acidic compared to the other cyclopropanes synthesised. As in the reaction mixture is present a base, this could deprotonate this position and an epimerisation would occur rendering the more stable *cis* product **401**, stabilised by the coordination of Pd with the nitrogen atom of the benzoxazole ring and the carbonyl of the ester group.

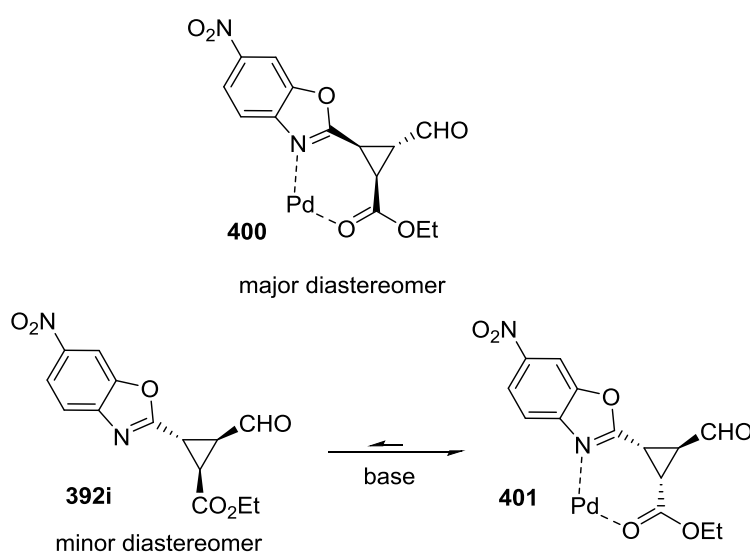
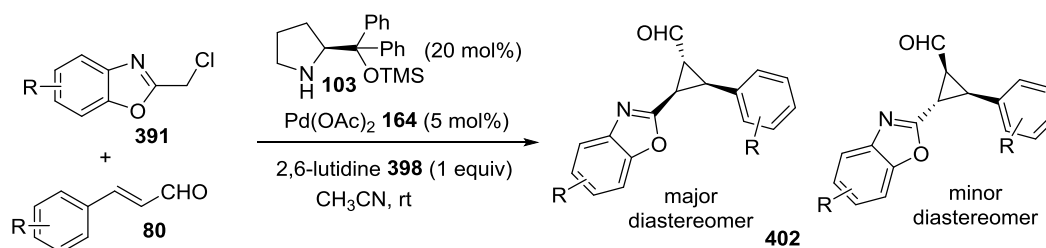


Figure 23. Proposed epimerisation of the minor diastereomer of the product **392i**

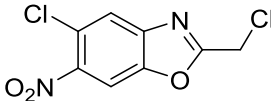
One of the limit of the reaction is that it is not suitable for aliphatic aldehydes as it gave only complex mixtures in the crude.

5.5.4 Scope of the reaction with benzoxazoles

Table 16. Scope of the reaction with several benzoxazoles



Product	Benzoxazole	R	Yield ^[a] (%)	dr ^[b]	ee major (%) ^[c]	ee minor (%) ^[c]
392a		H 80b	89	4.5 : 1.2 : 1	96 (R cat.) 99 (S cat.)	not determined
402a		H 80b	68	10.5 : 3.3 : 1	>99 (R cat.) >99 (S cat.)	90 (R cat.)
402g		H 80b	traces	---	---	---
402b		H 80b	78	4.5 : 1.9 : 1	98 (R cat.) 98 (S cat.)	not determined
402c		H 80b	55	6.2 : 1.3 : 1	99 (R cat.) 98 (S cat.)	not determined
402d		H 80b	51	2.3 : 1.6 : 1	>99 (R cat.) >99 (S cat.)	not determined
402e		4-Br 80h	85	8.1 : 4.8 : 1	98 (R cat.) 97 (S cat.)	not determined

Product	Benzoxazole	R	Yield ^[a] (%)	dr ^[b]	ee major (%) ^[c]	ee minor (%) ^[c]
402f		3-Br 80d	66	17.4 : 6.3 : 1	91 (R cat.) 97 (S cat.)	not determined

[a] yields are from the sum of the isolated diastereomers after column chromatography

[b] dr are calculated from the isolated diastereomers after column chromatography

[c] ee were determined by chiral HPLC analysis

In **Table 16** is presented the study of the scope of the reaction testing several benzoxazoles. With the 5-Cl,6-NO₂ substituted benzoxazole **391b**, the products **402a**, **402e** and **402f** were obtained in good yields, dr and excellent ee (91-99%). When benzoxazoles with the nitro group in different position of the aromatic ring **391c** and **391e** were tested, lower yields but good dr and excellent ee were observed (**402c** and **402d**). When an ester group is present in position 6 **391d**, the final product **402b** was obtained in excellent yield and ee and good dr.

The limitation of the reaction is that the presence of an electron-withdrawing group on the benzoxazole ring is crucial for the reactivity, as previously noted in Chapter 4. In fact the reaction with the unsubstituted benzoxazole **391f** did not give any product (**Table 16**, compound **402g**).

5.5.5 Relative and absolute configuration

The relative configuration of the minor diastereomer was determined by X-ray crystallography as shown in **Figure 24**.⁴

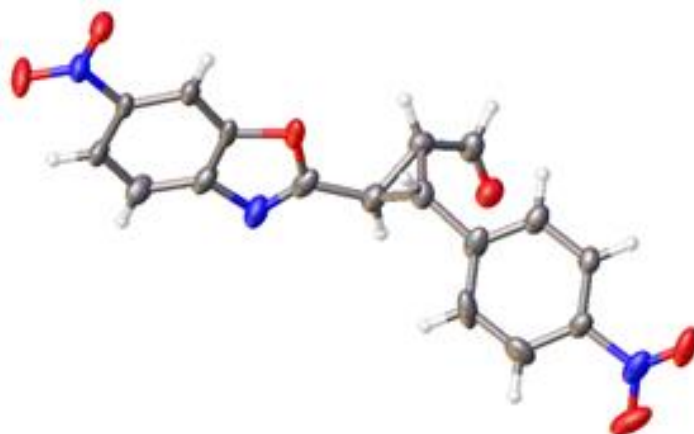


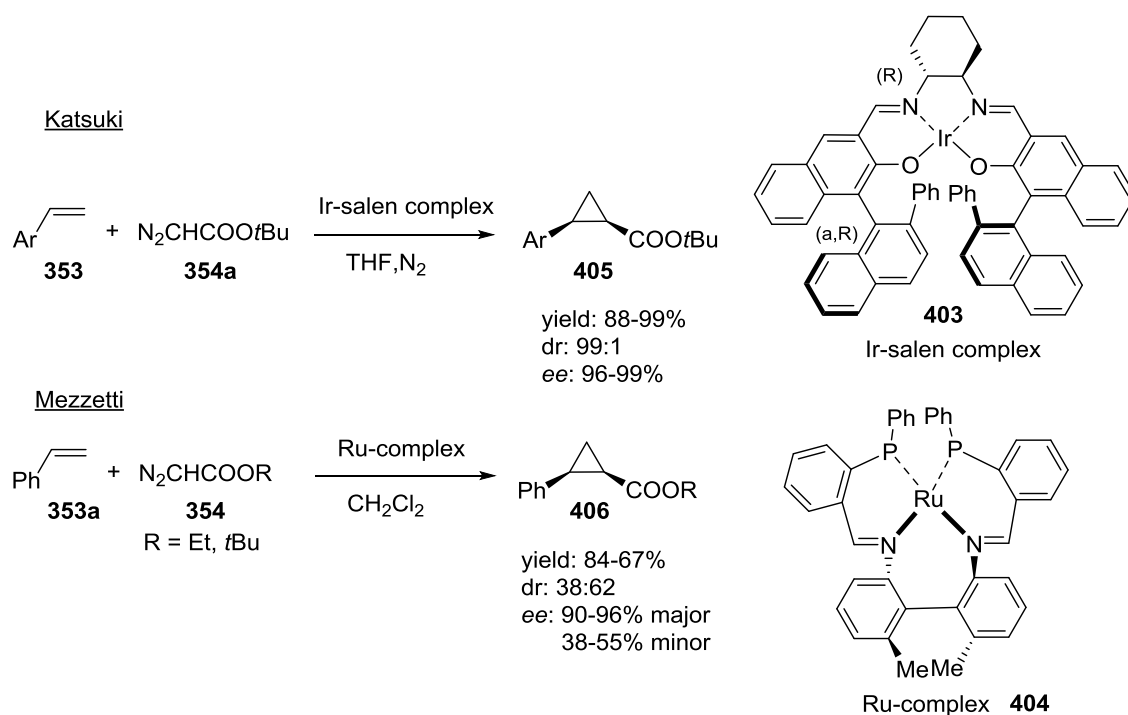
Figure 24. X-ray structure of compound **392d**

The absolute configuration of the minor diastereomer and the relative and absolute configuration of the major diastereomer were determined by 2D-NMR and by TD-DFT simulation of the Electronic Circular Dichroism (ECD) spectra.⁵ The absolute configuration was determined to be 1*R*,2*R*,3*S* for the major diastereomer **392d** (using (*S*)-**301** as catalyst) and 1*R*,2*R*,3*R* for the minor diastereomer **392d'** (using (*R*)-**301** as catalyst). (See Chapter 6 for a detailed explanation)

The major diastereomers have a *cis* configuration between the aryl substituent and the benzoxazole. This adds an even more important value to the methodology described in this chapter as the synthesis of *cis* diaromatic cyclopropanes *via* an intermolecular reaction is very challenging. Only Katzuki *et al.*^[183] and Mezzetti *et al.*^[184] reported the enantioselective synthesis of *cis*-cyclopropanes using iridium and ruthenium catalysts **403** and **404** respectively in the reaction of styrenes **353** with diazoacetates **354** (**Scheme 99**).

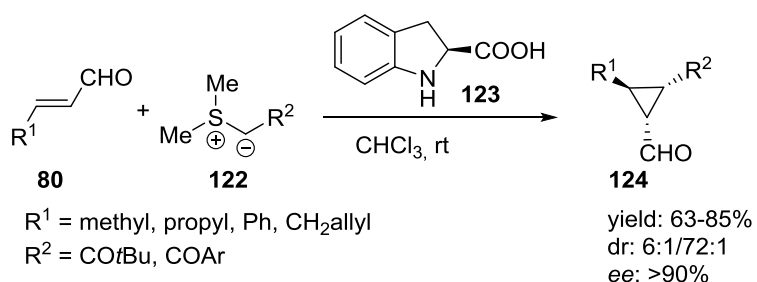
⁴ The X-ray analysis was done by Dr Mark E. Light

⁵ The NMR analysis and TD-DFT simulation of the Electronic Circular Dichroism (ECD) spectra were done by Professor Andrea Mazzanti



Scheme 99. Katsuki and Mezzetti's *cis*-cyclopropanation

The methodology reported in this chapter can be considered stereocomplementary to the organocatalytic cyclopropanation of MacMillan *et al.*^[65] They reported the cyclopropanation of enals **80** catalysed by a secondary amine organocatalyst **123** mediated by a sulphur ylide **122**, obtaining the final *trans*-trisubstituted cyclopropanes **124** in good yields and excellent diastereo- and enantioselectivities (**Scheme 100**).



Scheme 100. MacMillan's enantioselective synthesis of *trans*-trisubstituted cyclopropanes

5.6 Conclusion

In conclusion we demonstrated that the concept of synergistic catalysis, presented in Chapter 4, can be applied to a cascade reaction. We developed an organocascade highly enantioselective cyclopropanation of enals with chloroalkylbenzoxazoles, using a metal Lewis acid to activate the benzoxazole and a secondary amine catalyst to activate the enals with a cascade iminium and then enamine activation. The final products were obtained in good yields, moderate to good diastereoselectivity and excellent enantioselectivity in the major diastereomer. Moreover the major diastereomer has a *cis* configuration that is otherwise difficult to obtain and gives more importance to the methodology reported in this chapter.

6. Experimental section

Thin layer chromatography (TLC) was performed on Merck TLC Silicagel 60 F₂₅₄. Product spots were visualized by UV-light at 254 nm. Column chromatography was effectuated using silica gel (Geduran Si60, 40-63 µm). Melting points were measured with a Gallenkamp Electrothermal apparatus and are uncorrected. Infra-red spectra were recorded on a Nicolet 380 FT-IR; the IR analysis were performed with the compounds dissolved in CHCl₃. ¹H-NMR, ¹³C-NMR, ¹⁹F-NMR, 2D-NMR were recorded with a Bruker DPX400 NMR. High resolution mass spectra were recorded using a MaXis (Bruker Daltonics, Bremen, Germany) mass spectrometer equipped with a Time of Flight (TOF) analyser. Optical rotations were performed on an Optical Activity PolAAR 2001 machine. The HPLC analysis were performed on a Perkin Elmer Flexar HPLC and an Agilent 1220 Infinity LC system HPLC.

6.1 Synergistic catalysis: enantioselective addition of alkylbenzoxazoles to enals

6.1.1 Synthesis of the starting materials: α,β -unsaturated aldehydes (**80**)

The starting aldehydes were synthesised through a Wittig reaction, following the procedure described in literature. In a 250 mL round bottom flask a substituted benzaldehyde derivative **63** (2 equiv) and (triphenylphosphoranyldiene)acetaldehyde **250** (1 equiv) were stirred in anhydrous toluene at 45 °C in an atmosphere of argon. Yields were obtained after column chromatography.

The aldehydes **80a** and **80b** are commercially available (Sigma-Aldrich).

The ^1H -NMR of the aldehydes **80k**, **80e**, **80i** are consistent with the ones provided in literature.^[185]

The ^1H -NMR of the aldehydes **80j** and **80f** are consistent with the ones provided in literature.^[186]

The ^1H -NMR of the aldehyde **80h** is consistent with the one provided in literature.^[187]

The ^1H -NMR of the aldehyde **80g** is consistent with the one provided in literature.^[188]

The ^1H -NMR of the aldehyde **80c** is consistent with the one provided in literature.^[189]

6.1.2 Synthesis of the starting materials: azaarenes

The starting benzoxazoles were synthesised following the procedure described in literature.^[88]

2-ethyloxazolo-[4,5-b]-pyridine (**132n**), 2-methylbenzoxazole (**132k**), 2-methyl-5-nitropyridine (**132l**) and 4-methyl-3-nitropyridine (**132m**) are commercially available (Acros and Sigma-Aldrich).

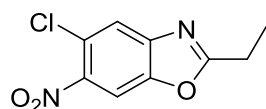
The ^1H -NMR of 2-ethyl-6-nitrobenzoxazole (**132a**), 2-methyl-6-nitrobenzoxazole (**132f**) are consistent with the ones provided in literature.^[190]

The ^1H -NMR of 2-ethylbenzoxazole (**132g**) is consistent with the one provided in literature.^[191]

The ^1H -NMR of 2-ethyl-4-nitrobenzoxazole (**132d**), 2-butyl-6-nitrobenzoxazole (**132e**) and methyl 2-ethylbenzoxazole-6-carboxylate (**132h**) are consistent with the ones provided in literature.^[88]

The ^1H -NMR of 2-ethyl-5-nitrobenzoxazole (**132c**) is consistent with the one provided in literature.^[192]

5-chloro-2-ethyl-6-nitrobenzoxazole (**132b**)



A mixture of 2-amino-4-chloro-5-nitrophenol (5 g, 26.4 mmol, 1 equiv) and triethyl orthopropionate (5.8 mL, 29.0 mmol, 1.1 equiv) was stirred at 50 °C for 48 hours. The crude was purified by flash column chromatography (hexane/EtOAc 5:1) to obtain 4.5 g of a yellow solid. The yield is 75%.

mp: 83-85 °C

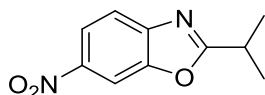
IR: 3106, 3035, 2992, 1560, 1523, 1446, 1324, 1255, 1209, 822 cm^{-1} .

^1H NMR (400 MHz, CDCl_3) δ 8.07 (s, 1H, Het), 7.82 (s, 1H, Het), 3.04 (q, J = 7.6 Hz, 2H, CH_2), 1.48 (t, J = 7.6 Hz, 3H, CH_3).

^{13}C NMR (101 MHz, CDCl_3) δ 173.6 (Cq), 148.3 (Cq), 145.2 (Cq), 144.5 (Cq), 123.4 (Cq), 122.1 (CH), 108.4 (CH), 22.4 (CH_2), 10.6 (CH_3).

HRMS (ESI+) Exact mass calculated for $\text{C}_9\text{H}_8\text{Cl}^{35}\text{N}_2\text{O}_3$ $[\text{M}+\text{H}]^+$: 227.0218, found: 227.0217.

2-isopropyl-6-nitrobenzoxazole (132i)



In a round bottom flask charged with 2-amino-5-nitrophenol (3.0 g, 19.5 mmol, 1 equiv) isobutyric acid (1.8 mL, 19.5 mmol, 1 equiv) and polyphosphoric acid (38 g, 390 mmol, 20 equiv) were added. The reaction mixture was stirred for 7 hours at 50 °C. Then the mixture was cooled at room temperature and a solution of sodium hydroxide was added until the mixture had a basic pH. The solid formed was filtered and washed with ice-water to afford 2.4 g of a brown solid. The yield is 59%.

mp: 86-87 °C

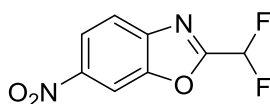
IR: 3107, 2970, 1568, 1520, 1344, 1276, 1139, 1088, 886, 818 cm⁻¹.

¹H NMR (400 MHz, CDCl₃) δ 8.41 (d, *J* = 2.1 Hz, 1H, Het), 8.29 (dd, *J* = 8.7, 2.1 Hz, 1H, Het), 7.78 (d, *J* = 8.7 Hz, 1H, Het), 3.40 – 3.26 (m, 1H, CH), 1.51 (d, *J* = 7.0 Hz, 6H, CH₃).

¹³C NMR (101 MHz, CDCl₃) δ 176.2 (Cq), 149.9 (Cq), 146.7 (Cq), 144.9 (Cq), 120.3 (CH), 119.5 (CH), 107.0 (CH), 29.2 (CH), 20.1 (CH₃).

HRMS (ESI+) Exact mass calculated for C₁₀H₁₁N₂O₃ [M+H]⁺: 207.0764, found: 207.0764.

2-(difluoromethyl)-6-nitrobenzoxazole (132j)



In a round bottom flask charged with 2-amino-5-nitrophenol (3.6 g, 23.36 mmol, 1 equiv) 2,2-difluoroacetic acid (2.24 g, 23.36 mmol, 1 equiv) and polyphosphoric acid (45 g, 467 mmol, 20 equiv) were added. The reaction mixture was stirred for 24 hours at 80 °C. Then the mixture was cooled at room temperature and a solution of sodium hydroxide was added until the mixture had a basic pH. The solid formed was filtered and washed with ice-water to afford 4.3 g of a brown solid. The yield is 86%.

mp: 102-104 °C

IR: 3105, 1526, 1354, 1304, 1255, 1109, 1056, 844, 835 cm⁻¹.

¹H-NMR (400 MHz, CDCl₃): 8.51 (d, *J* = 2.0 Hz, 1H, Het), 8.34 (dd, *J* = 8.8 Hz, *J* = 2.1 Hz, 1H, Het), 7.92 (d, *J* = 8.9 Hz, 1H, Het), 6.93-6.65 (t, *J* = 52.2 Hz, 1H, CH).

¹⁹F-NMR (CDCl₃, 300 MHz): -119.9 ppm.

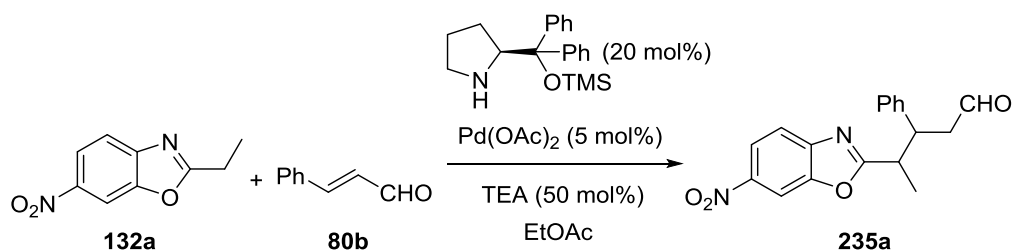
¹³C NMR (101 MHz, CDCl₃) δ 149.8 (Cq), 144.62 (Cq), 121.85 (CH), 121.36 (CH), 109.02 (Cq), 108.38 (CH), 106.61 (CH), 104.20 (Cq).

MS (ESI+) *m/z*: 215.0708 [M+H]⁺; **HRMS (ESI+)** Exact mass calculated for C₈H₅F₂N₂O₃ [M+H]⁺: 215.0724, found: 215.0719.

6.1.3 Synthesis of the catalysts: derivatives of the Jorgensen-Hayashi catalyst

The catalysts were synthesised following the procedure described in literature.^[112] The ¹H-NMR of the catalysts are consistent with the ones provided in literature.

6.1.4 Synthesis of 3-(6-nitrobenzoxazol-2-yl)-2-phenylbutanal (235a)



Scheme 101. General scheme of the Michael addition step

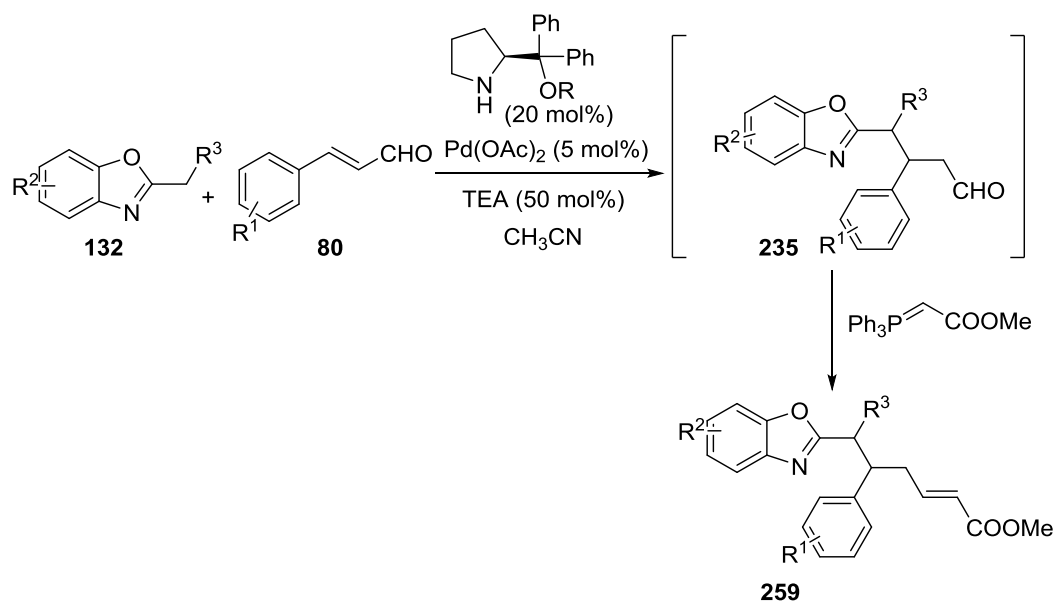
In a vial the following reagents were sequentially added: (S)-2-(diphenyl((trimethylsilyl)oxy)methyl)pyrrolidine (20 mol% equiv, 17 mg, 0.052 mmol), cinnamaldehyde (34 mg, 0.260 mmol, 1 equiv), 2-ethyl-6-nitrobenzoxazole (50 mg, 0.260 mmol, 1 equiv), Pd(OAc)₂ (5 mol% equiv, 3 mg, 0.013 mmol) and TEA (50% equiv, 13 mg, 0.130 mmol) and finally EtOAc (0.5 mL). The reaction mixture was stirred at 40 °C for 3 days and then concentrated *in vacuo*. The crude was purified by flash column chromatography (hexane/EtOAc 10:1) to obtain the desired product.

Diastereomer 1 (major): ¹H-NMR (400 MHz, CDCl₃) δ 9.52 (t, *J* = 1.6 Hz, 1H, CHO), 8.46 (d, *J* = 2.1 Hz, 1H, Het), 8.33 (dd, *J* = 8.8, 2.1 Hz, 1H, Het), 7.81 (d, *J* = 8.8 Hz, 1H, Het), 7.39-7.23 (m, 5H, Ph), 3.75 (m, 1H, CHPh), 3.47 (dq, *J* = 14.0, 7.0 Hz, 1H, CHCH₃), 2.93 (dddd, *J* = 17.0, 8.7, 1.8 Hz, 1H, CH₂), 2.80 (dddd, *J* = 17.0, 5.6, 1.5 Hz, 1H, CH₂), 1.29 (d, *J* = 7.0 Hz, 3H, CH₃).

Diastereomer 2 (minor): ¹H-NMR (400 MHz, CDCl₃) δ 9.62 (t, *J* = 1.5 Hz, 1H, CHO), 8.28 (d, *J* = 2.1 Hz, 1H, Het), 8.19 (dd, *J* = 8.7, 2.1 Hz, 1H, Het), 7.66 (d, *J* = 8.7 Hz, 1H, Het), 7.17-7.00 (m, 5H, Ph), 3.82-3.75 (m, 1H, CHPh), 3.48 (dq, *J* = 13.9, 7.0 Hz, 1H, CHHet), 3.07-2.89 (m, 2H, CH₂), 1.41 (d, *J* = 7.0 Hz, 3H, CH₃).

The instability of this final compound did not allow further characterisation. The derivatised products were fully characterised in the next section.

6.1.5 General procedure

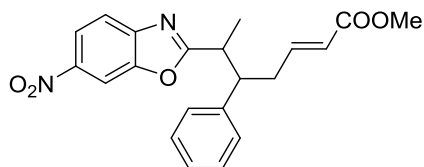


Scheme 102. General scheme of the Michael addition and subsequent Wittig derivatisation

In a vial the following reagents were sequentially added: the organic catalyst (20 mol% equiv), α,β -unsaturated aldehyde (2 equiv), azaarene (1 equiv), $\text{Pd}(\text{OAc})_2$ (5 mol% equiv) and CH_3CN (1 mL). To the crude solution was finally added TEA (50 mol% equiv). The reaction mixture was stirred at the temperature and time reported in **Table 7** and

Table 8 and then concentrated *in vacuo*. In a vial were then added: the crude obtained after the first reaction, an excess of methyl triphenylphosphoranylidene acetate (>3 equiv) and DCM as the solvent. The reaction mixture was stirred at rt for 48 hours and then concentrated *in vacuo*. The crude product was purified by flash column chromatography (hexane/EtOAc) to obtain the desired product.

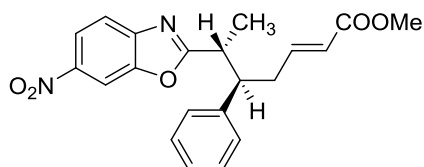
methyl (*E*)-6-(6-nitrobenzoxazol-2-yl)-5-phenylhept-2-enoate (259a)



The reaction was performed following the general procedure adding: the organic catalyst (*S*)-2-(((*tert*-butyldimethylsilyl)oxy)diphenylmethyl)pyrrolidine (19 mg, 0.052 mmol, 20 mol% equiv), cinnamaldehyde (69 mg, 0.520 mmol, 2 equiv), 2-ethyl-6-nitrobenzoxazole (50 mg, 0.260 mmol, 1 equiv), Pd(OAc)₂ (3 mg, 0.013 mmol, 5 mol% equiv) and CH₃CN (1 mL). To the crude solution DIPEA (17 mg, 0.130 mmol, 50 mol% equiv) was finally added. The first reaction was stirred for 24 hours before performing the Wittig. The final crude was purified by flash column chromatography (hexane/EtOAc 5:1) to obtain 83 mg of the desired products as a yellow oil. Yield: 84%. The diastereomeric ratio was determined by the crude NMR: 1.3:1

Diastereomer 1 (major):

methyl (*5R,6R,E*)-6-(6-nitrobenzoxazol-2-yl)-5-phenylhept-2-enoate



IR (CHCl₃, liquid film): 2924, 2854, 2168, 1720 (ester), 1655, 1562, 1524 (aromatic NO₂), 1454, 1435, 1346 (aromatic NO₂), 1269, 1165, 1041, 825 cm⁻¹.

¹H-NMR (400 MHz, CDCl₃) δ 8.36 (d, *J* = 2.1 Hz, 1H, Het), 8.24 (dd, *J* = 8.8, 2.1 Hz, 1H, Het), 7.71 (d, *J* = 8.8 Hz, 1H, Het), 7.32 – 7.06 (m, 5H, Ph), 6.55 (ddd, *J* = 15.4, 7.7, 6.8 Hz, 1H, =CHCH₂), 5.49 (dt, *J* = 15.6, 1.3 Hz, 1H, =CHCO₂Me), 3.48 (s, 3H, OCH₃), 3.37 (dq, *J* = 9.8, 6.9 Hz, 1H, CHCH₃), 3.26 – 3.14 (m, 1H, CHCH₂), 2.53 (dddd, *J* = 15.3, 8.4, 6.7, 1.5 Hz, 1H, CH₂), 2.46 – 2.33 (m, 1H, CH₂), 1.17 (d, *J* = 6.7 Hz, 3H, CH₃).

¹³C-NMR (101 MHz, CDCl₃) δ 173.2 (Cq), 165.3 (Cq), 148.6 (Cq), 145.4 (Cq), 144.6 (CH), 144.2 (Cq), 139.5 (Cq), 127.9 (CH), 126.9 (CH), 126.4 (CH), 121.5 (CH), 119.5 (CH), 118.8 (CH), 106.2 (CH), 50.3 (CH₃), 48.7 (CH), 39.2 (CH), 36.3 (CH₂), 16.0 (CH₃).

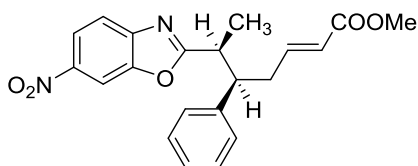
The enantiomeric excess was determined by **HPLC** using a Chiralpak IE column (hexane/*i*PrOH = 90:10, flow rate 1.0 mL/min, λ = 230 nm): t_r (major) = 29.5, t_r (minor) = 33.6, 88% *ee*.

$[\alpha]_D^{20} = -1.1^\circ$ ($c = 0.75$, CHCl_3)

MS (ESI+) m/z : 381.1 $[\text{M}+\text{H}]^+$; **HRMS (ESI+)** Exact mass calculated for $\text{C}_{21}\text{H}_{21}\text{N}_2\text{O}_5$ $[\text{M}+\text{H}]^+$: 381.1445, found: 381.1445.

Diastereomer 2 (minor):

methyl (5*R*,6*S*,*E*)-6-(6-nitrobenzoxazol-2-yl)-5-phenylhept-2-enoate



IR (CHCl_3 , liquid film): 2924, 2854, 2172, 1720 (ester), 1659, 1562, 1524 (aromatic NO_2), 1454, 1435, 1346 (aromatic NO_2), 1269, 1161, 1038, 825 cm^{-1} .

$^1\text{H-NMR}$ (400 MHz, CDCl_3) δ 8.26 (d, $J = 2.1$ Hz, 1H, Het), 8.18 (dd, $J = 8.8, 2.1$ Hz, 1H, Het), 7.64 (d, $J = 8.8$ Hz, 1H, Het), 7.18 – 6.95 (m, 5H, Ph), 6.69 (dt, $J = 15.5, 7.2$ Hz, 1H, $=\text{CHCH}_2$), 5.73 (dt, $J = 15.6, 1.3$ Hz, 1H, $=\text{CHCO}_2\text{Me}$), 3.56 (s, 3H, OCH_3), 3.50 – 3.38 (m, 1H, CHCH_3), 3.29 (dt, $J = 9.2, 6.1$ Hz, 1H, CHCH_2), 2.81 – 2.60 (m, 2H, CH_2), 1.43 (d, $J = 7.0$ Hz, 3H, CH_3).

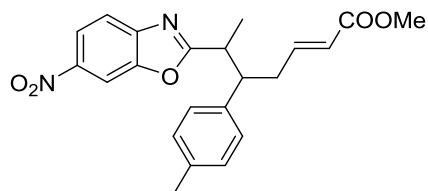
$^{13}\text{C-NMR}$ (101 MHz, CDCl_3) δ 173.5 (Cq), 166.5 (Cq), 149.5 (Cq), 146.3 (Cq), 146.0 (CH), 145.0 (Cq), 140.1 (Cq), 128.6 (CH), 127.9 (CH), 127.3 (CH), 123.0 (CH), 120.4 (CH), 119.6 (CH), 107.0 (CH), 51.4 (CH_3), 48.9 (CH), 40.1 (CH), 34.3 (CH_2), 15.2 (CH_3).

The enantiomeric excess was determined by **HPLC** using a Chiralpak IE column (hexane/*i*PrOH = 90:10, flow rate 1.0 mL/min, λ = 230 nm): t_r (major) = 34.0, t_r (minor) = 31.3, 68% *ee*.

$[\alpha]_D^{20} = -3.9^\circ$ ($c = 0.50$, CHCl_3)

MS (ESI+) m/z : 381.1 $[M+H]^+$; **HRMS (ESI+)** Exact mass calculated for $C_{21}H_{21}N_2O_5$ $[M+H]^+$: 381.1445, found: 381.1441.

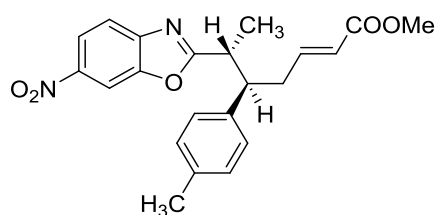
methyl (*E*)-6-(6-nitrobenzoxazol-2-yl)-5-(*p*-tolyl)hept-2-enoate (259b)



The reaction was performed following the general procedure adding: the organic catalyst (*S*)-2-(((*tert*-butyldimethylsilyl)oxy)diphenylmethyl)pyrrolidine (38 mg, 0.104 mmol, 20 mol% equiv), (*E*)-3-(*p*-tolyl)acrylaldehyde (152 mg, 1.040 mmol, 2 equiv), 2-ethyl-6-nitrobenzoxazole (100 mg, 0.520 mmol, 1 equiv), $Pd(OAc)_2$ (6 mg, 0.026 mmol, 5 mol% equiv) and CH_3CN (1 mL). To the crude solution was finally added TEA (26 mg, 0.260 mmol, 50 mol% equiv). The first reaction was stirred for 48 hours at 30 °C before performing the Wittig. The final crude was purified by flash column chromatography (hexane/EtOAc 10:1) to obtain 141 mg of the desired product as a yellow oil. Yield: 69%. The diastereomeric ratio was determined by the crude NMR: 1.3:1

Diastereomer 1, major:

methyl (5*R*,6*R*,*E*)-6-(6-nitrobenzoxazol-2-yl)-5-(*p*-tolyl)hept-2-enoate



IR ($CHCl_3$, liquid film): 2978, 2947, 1720 (ester), 1655, 1562, 1524 (aromatic NO_2), 1435, 1342 (aromatic NO_2), 1269, 1119, 1041 cm^{-1} .

1H -NMR (400 MHz, $CDCl_3$) δ 8.35 (d, J = 2.1 Hz, 1H, Het), 8.22 (dd, J = 8.7, 2.1 Hz, 1H, Het), 7.70 (d, J = 8.8 Hz, 1H, Het), 7.06 (d, J = 7.9 Hz, 2H, Ar), 6.97 (d, J = 8.1 Hz, 2H, Ar), 6.55 (ddd, J = 15.4, 7.8, 6.8 Hz, 1H, $=CHCH_2$), 5.49 (dt, J = 15.5, 1.4 Hz, 1H, $=CHCO_2Me$),

3.47 (s, 3H, OCH₃), 3.33 (dq, $J = 9.6, 6.9$ Hz, 1H, CHCH₃), 3.16 (td, $J = 9.1, 5.7$ Hz, 1H, CHCH₂), 2.51 (dddd, $J = 15.4, 8.5, 6.7, 1.5$ Hz, 1H, CH₂), 2.38 (dddd, $J = 15.4, 7.9, 6.1, 1.5$, 1H, CH₂), 2.25 (s, 3H, CH₃Ar), 1.16 (d, $J = 6.9$ Hz, 3H, CH₃).

¹³C-NMR (101 MHz, CDCl₃) δ 174.3 (Cq), 166.3 (Cq), 149.6 (Cq), 146.4 (Cq), 145.8 (CH), 145.1 (Cq), 137.3 (Cq), 136.98 (Cq), 129.6 (CH), 127.8 (CH), 122.4 (CH), 120.5 (CH), 119.7 (CH), 107.2 (CH), 51.3 (CH₃), 49.3 (CH), 40.2 (CH), 37.4 (CH₂), 21.1 (CH₃), 16.9 (CH₃).

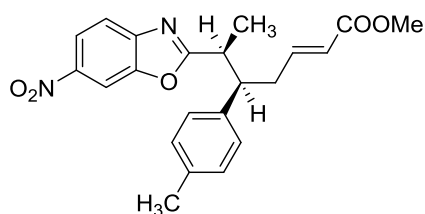
The enantiomeric excess was determined by **HPLC** using a Chiralpak IE column (hexane/*i*PrOH = 90:10, flow rate 1.0 mL/min, $\lambda = 230$ nm): t_r (major) = 29.5, t_r (minor) = 32.6, 85% *ee*.

$[\alpha]_D^{20} = -1.8^\circ$ ($c = 1.29$, CHCl₃)

MS (ESI+) m/z : 395.1 [M+H]⁺; **HRMS (ESI+)** Exact mass calculated for C₂₂H₂₃N₂O₅ [M+H]⁺: 395.1601, found: 395.1603.

Diastereomer 2, minor:

methyl (5*R*,6*S*,*E*)-6-(6-nitrobenzoxazol-2-yl)-5-(*p*-tolyl)hept-2-enoate



IR (CHCl₃, liquid film): 2982, 2947, 1720 (ester), 1659, 1562, 1524 (aromatic NO₂), 1435, 1346 (aromatic NO₂), 1269, 1119, 1041 cm⁻¹.

¹H-NMR (400 MHz, CDCl₃) δ 8.57 (d, $J = 2.1$ Hz, 1H, Het), 8.47 (dd, $J = 8.8, 2.1$ Hz, 1H, Het), 7.94 (d, $J = 8.8$ Hz, 1H, Het), 7.23 (d, $J = 8.0$ Hz, 2H, Ar), 7.16 (d, $J = 8.1$ Hz, 2H, Ar), 6.99 (dt, $J = 15.5, 7.2$ Hz, 1H, =CHCH₂), 6.03 (dt, $J = 15.6, 1.2$ Hz, 1H, =CHCO₂Me), 3.86 (s, 3H, OCH₃), 3.72 (dt, $J_1 = J_2 = 6.9$ Hz, 1H, CHCH₃), 3.55 (dt, $J = 9.3, 6.0$ Hz, 1H, CHCH₂), 3.06 – 2.89 (m, 2H, CH₂), 2.48 (s, 3H, CH₃Ar), 1.71 (d, $J = 7.0$ Hz, 3H, CH₃).

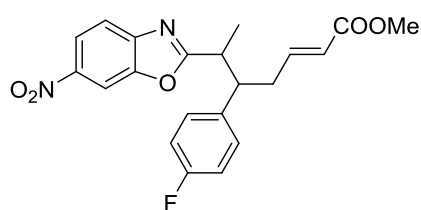
¹³C-NMR (101 MHz, CDCl₃) δ 173.6 (Cq), 166.5 (Cq), 149.5 (Cq), 146.3 (Cq), 146.2 (CH), 145.0 (Cq), 137.0 (Cq), 136.8 (Cq), 129.3 (CH), 127.8 (CH), 122.9 (CH), 120.4 (CH), 119.6 (CH), 107.0 (CH), 51.4 (CH₃), 48.5 (CH), 40.2 (CH), 34.4 (CH₂), 21.0 (CH₃), 15.1 (CH₃).

The enantiomeric excess was determined by **HPLC** using a Chiralpak IE column (hexane/*i*PrOH = 90:10, flow rate 1.0 mL/min, λ = 230 nm): t_r (major) = 31.2, t_r (minor) = 29.5, 54% *ee*.

$[\alpha]_D^{20}$ = -12.2° (*c* = 0.51, CHCl₃)

MS (ESI+) *m/z*: 395.1 [M+H]⁺; **HRMS (ESI+)** Exact mass calculated for C₂₂H₂₃N₂O₅ [M+H]⁺: 395.1601, found: 395.1606.

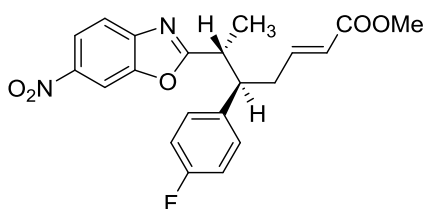
methyl (*E*)-5-(4-fluorophenyl)-6-(6-nitrobenzoxazol-2-yl)hept-2-enoate (259c)



The reaction was performed following the general procedure adding: the organic catalyst (*S*)-2-(((*tert*-butyldimethylsilyl)oxy)diphenylmethyl)pyrrolidine (38 mg, 0.104 mmol, 20 mol% equiv), (*E*)-3-(4-fluorophenyl)acrylaldehyde (234 mg, 1.560 mmol, 2 equiv), 2-ethyl-6-nitrobenzoxazole (100 mg, 0.520 mmol, 1 equiv), Pd(OAc)₂ (6 mg, 0.026 mmol, 5 mol% equiv) and CH₃CN (1 mL). To the crude solution was finally added TEA (26 mg, 0.260 mmol, 50 mol% equiv). The first reaction was stirred for 40 hours at 35 °C before performing the Wittig. The final crude was purified by flash column chromatography (hexane/EtOAc 5:1) to obtain 168 mg of the desired product as yellow oil. Yield: 81%. The diastereomeric ratio was determined by the crude NMR: 1.1:1

Diastereomer 1:

methyl (5*R*,6*R*,*E*)-5-(4-fluorophenyl)-6-(6-nitrobenzoxazol-2-yl)hept-2-enoate



IR (CHCl₃, liquid film): 2922, 2852 (stretch *HC=C*), 1721 (stretch *C=O*, ester), 1564, 1526 (aromatic NO₂), 1437, 1346 (aromatic NO₂), 1269 cm⁻¹

¹H NMR (400 MHz, CDCl₃) δ 8.61 (d, *J* = 2.0 Hz, 1H, Het), 8.49 (dd, *J* = 8.8, 2.0 Hz, 1H, Het), 7.97 (d, *J* = 8.8 Hz, 1H, Het), 7.33 (dd, *J* = 8.5, 5.4 Hz, 2H, Ar), 7.23 – 7.19 (m, 2H, Ar), 6.80 (dt, *J* = 15.5, 7.4 Hz, 1H, =CHCH₂), 5.76 (d, *J* = 15.6 Hz, 1H, =CHCO₂Me), 3.74 (s, 3H, OCH₃), 3.59 (dq, *J* = 9.7, 6.9 Hz, 1H, CHCH₃), 3.47 (td, *J* = 9.1, 5.7 Hz, 1H, CHCH₂), 2.83 – 2.60 (m, 2H, CH₂), 1.42 (d, *J* = 6.9 Hz, 3H, CH₃).

¹³C NMR (101 MHz, CDCl₃) δ 173.9 (Cq), 166.2 (Cq), 162.0 (*J* = 246.0 Hz, Cq), 149.6 (Cq), 146.3 (Cq), 145.3 (CH), 145.2 (Cq), 136.1 (*J* = 3.3 Hz, Cq), 129.4 (*J* = 7.9 Hz, CH), 122.7 (CH), 120.6 (CH), 119.8 (CH), 115.9 (*J* = 21.3 Hz, CH), 107.2 (CH), 51.4 (CH₃), 48.9 (CH), 40.2 (CH), 37.3 (CH₂), 16.9 (CH₃).

¹⁹F NMR (376 MHz, CDCl₃) δ -114.92.

The enantiomeric excess was determined by **HPLC** using a Chiralpak IE column (hexane/*i*PrOH = 93:7, flow rate 1.0 mL/min, λ = 230 nm): *t_r* (major) = 38.5, *t_r* (minor) = 43.1, 86% *ee*.

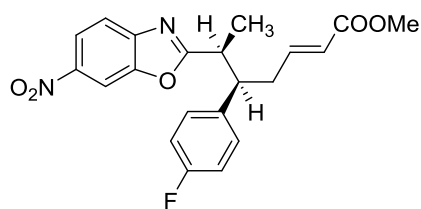
[α]_D¹⁹ = -6.3° (*c* = 0.8, CHCl₃)

MS (ESI⁺) *m/z*: 399.1 [M+H]⁺

HRMS (ESI⁺) Exact mass calculated for C₂₁H₂₀FN₂O₅ [M+H]⁺: 399.1351, found: 399.1360; Exact mass calculated for C₂₁H₁₉FN₂NaO₅ [M+Na]⁺: 421.1170, found: 421.1181.

Diastereomer 2:

methyl (5*R*,6*S*,*E*)-5-(4-fluorophenyl)-6-(6-nitrobenzoxazol-2-yl)hept-2-enoate



IR (CHCl₃, liquid film): 2921, 2852 (stretch HC=C), 1721 (stretch C=O, ester), 1564, 1526 (aromatic NO₂), 1437, 1345 (aromatic NO₂), 1269 cm⁻¹

¹H NMR (400 MHz, CDCl₃) δ 8.51 (d, J = 2.0 Hz, 1H, Het), 8.42 (dd, J = 8.8, 2.1 Hz, 1H, Het), 7.88 (d, J = 8.8 Hz, 1H, Het), 7.20 (dd, J = 8.5, 5.4 Hz, 2H, Ar), 7.08 - 7.04 (m, 2H, Ar), 6.91 (dt, J = 14.9, 7.2 Hz, 1H, =CHCH₂), 5.96 (d, J = 15.6 Hz, 1H, =CHCO₂Me), 3.81 (s, 3H, OCH₃), 3.66 (dq, J = 13.09, 7.0 Hz, 1H, CHCH₃), 3.56 – 3.46 (m, 1H, CHCH₂), 3.05 – 2.94 (m, 1H, CH₂), 2.92 – 2.79 (m, 1H, CH₂), 1.67 (d, J = 7.0 Hz, 3H, CH₃).

¹³C NMR (101 MHz, CDCl₃) δ 173.2 (Cq), 166.4 (Cq), 161.8 (J = 246.0 Hz, Cq), 149.5 (Cq), 146.2 (Cq), 145.6 (CH), 145.0 (Cq), 135.8 (J = 3.3 Hz, Cq), 129.4 (J = 8.0 Hz, CH), 123.2 (CH), 120.5 (CH), 119.7 (CH), 115.5 (J = 21.3 Hz, CH), 107.0 (CH), 51.5 (CH₃), 48.3 (CH), 40.2 (CH), 34.6 (CH₂), 15.5 (CH₃).

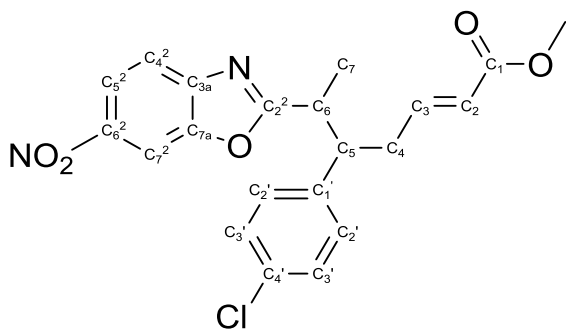
¹⁹F NMR (376 MHz, CDCl₃) δ -115.08.

The enantiomeric excess was determined by **HPLC** using a Chiralpak IE column (hexane/*i*PrOH = 93:7, flow rate 1.0 mL/min, λ = 230 nm): t_r (major) = 40.4, t_r (minor) = 42.3, 99% *ee*.

$[\alpha]_D^{19}$ = -1.65° (c = 1, CHCl₃)

MS (ESI+) m/z : 399.1 [M+H]⁺; **HRMS (ESI+)** Exact mass calculated for C₂₁H₂₀FN₂O₅ [M+H]⁺: 399.1351, found: 399.1349; Exact mass calculated for C₂₁H₁₉FN₂NaO₅ [M+Na]⁺: 421.1170, found: 421.1169.

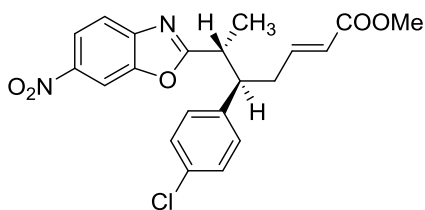
methyl (*E*)-5-(4-chlorophenyl)-6-(6-nitrobenzoxazol-2-yl)hept-2-enoate (259d)



The reaction was performed following the general procedure adding: the organic catalyst (*S*)-2-(((*tert*-butyldimethylsilyl)oxy)diphenylmethyl)pyrrolidine (38 mg, 0.104 mmol, 20 mol% equiv), (*E*)-3-(4-chlorophenyl)acrylaldehyde (173 mg, 1.040 mmol, 2 equiv), 2-ethyl-6-nitrobenzoxazole (100 mg, 0.520 mmol, 1 equiv), Pd(OAc)₂ (6 mg, 0.026 mmol, 5 mol% equiv) and CH₃CN (1 mL). To the crude solution was finally added TEA (26 mg, 0.260 mmol, 50 mol% equiv). The first reaction was stirred for 24 hours at 35 °C before performing the Wittig. The final crude was purified by flash column chromatography (hexane/EtOAc 10:1) to obtain 187 mg of the desired product as orange oil. Yield: 87%. The diastereomeric ratio was determined by the crude NMR: 1.3:1

Diastereomer 1, major:

methyl (5*R*,6*R*,*E*)-5-(4-chlorophenyl)-6-(6-nitrobenzoxazol-2-yl)hept-2-enoate



IR (CHCl₃, liquid film): 2924 (stretch HC=C), 1721 (stretch C=O, ester), 1564, 1526 (aromatic NO₂), 1436, 1345 (aromatic NO₂), 1269 cm⁻¹.

¹H NMR (400 MHz, CDCl₃) δ 8.37 (d, *J* = 1.7 Hz, 1H, H₇²), 8.24 (dd, *J* = 8.8, 1.7 Hz, 1H, H₅²), 7.72 (d, *J* = 8.8 Hz, 1H, H₄²), 7.25 (d, *J* = 8.3 Hz, 2H, H₃[']), 7.04 (d, *J* = 8.3 Hz, 2H, H₂[']), 6.53 (dt, *J* = 15.2, 7.3 Hz, 1H, H₃), 5.51 (d, *J* = 15.6 Hz, 1H, H₂), 3.50 (s, 3H, OCH₃), 3.33

(dq, $J = 14.0, 6.9$ Hz, 1H, H_6), 3.21 (td, $J = 9.1, 5.7$ Hz, 1H, H_5), 2.49 (ddd, $J = 14.7, 7.5$ Hz, 1H, H_4), 2.40 (ddd, $J = 14.7, 7.1$ Hz, 1H, H_4), 1.17 (d, $J = 6.9$ Hz, 3H, CH_3).

^{13}C NMR (101 MHz, CDCl_3) δ 173.8 (C_2^2), 166.2 (C_1), 149.6 (C_{7a}), 146.3 (C_{3a}), 145.2 (C_6^2), 145.1 (C_3), 138.9 (C_1'), 133.2 (C_4'), 129.3 (C_2' or C_3'), 129.1 (C_2' or C_3'), 122.9 (C_2), 120.6 (C_5^2), 119.8 (C_4^2), 107.3 (C_7^2), 51.4 (OCH_3), 49.0 (C_5), 40.1 (C_6), 37.1 (C_4), 16.9 (C_7).

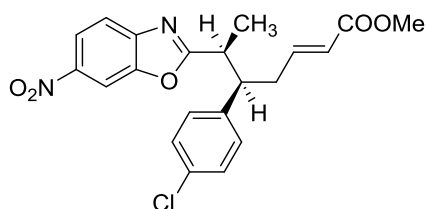
The enantiomeric excess was determined by **HPLC** using a Chiralpak IE column (hexane/*i*PrOH = 95:5, flow rate 1.0 mL/min, $\lambda = 230$ nm): t_r (major) = 58.7, t_r (minor) = 69.0, 64% *ee*.

$[\alpha]_D^{19} = -8.3^\circ$ ($c = 1.2$, CHCl_3)

MS (ESI+) m/z : 415.0 $[\text{M}+\text{H}]^+$; **HRMS (ESI+)** Exact mass calculated for $\text{C}_{21}\text{H}_{19}\text{Cl}^{35}\text{N}_2\text{NaO}_5$ $[\text{M}+\text{Na}]^+$: 437.08747, found: 437.08850; Exact mass calculated for $\text{C}_{21}\text{H}_{19}\text{Cl}^{35}\text{KN}_2\text{O}_5$ $[\text{M}+\text{K}]^+$: 453.06141, found: 453.06224.

Diastereomer 2:

methyl (5*R*,6*S*,*E*)-5-(4-chlorophenyl)-6-(6-nitrobenzoxazol-2-yl)hept-2-enoate



IR (CHCl_3 , liquid film): 2950 (stretch $\text{HC}=\text{C}$), 1722 (stretch $\text{C}=\text{O}$, ester), 1562, 1526 (aromatic NO_2), 1436, 1345 (aromatic NO_2), 1269 cm^{-1}

^1H NMR (400 MHz, CDCl_3) δ 8.59 (s, 1H, Het), 8.50 (d, $J = 8.7$ Hz, 1H, Het), 7.95 (d, $J = 8.7$ Hz, 1H, Het), 7.42 (d, $J = 7.8$ Hz, 2H, Ar), 7.24 (d, $J = 7.9$ Hz, 2H, Ar), 6.97 (dt, $J = 7.1, 15.1$ Hz, 1H, $=\text{CHCH}_2$), 6.03 (d, $J = 15.6$ Hz, 1H, $=\text{CHCO}_2\text{Me}$), 3.88 (s, 3H, OCH_3), 3.7 (dt, $J = 6.7, 13.8$ Hz, 1H, CHCH_3), 3.63 – 3.54 (m, 1H, CHCH_2), 3.11 – 3.00 (m, 1H, CH_2), 2.99 – 2.87 (m, 1H, CH_2), 1.73 (d, $J = 6.9$ Hz, 3H, CH_3).

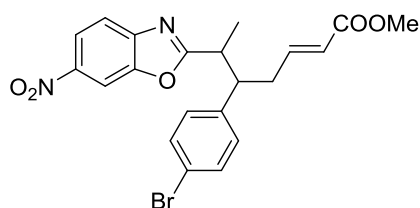
¹³C NMR (101 MHz, CDCl₃) δ 173.1 (Cq), 166.4 (Cq), 149.5 (Cq), 146.2 (Cq), 145.4 (CH), 145.1 (Cq), 138.6 (Cq), 133.1 (Cq), 129.3 (CH), 128.8 (CH), 123.4 (CH), 120.5 (CH), 119.7 (CH), 107.1 (CH), 51.5 (CH₃), 48.3 (CH), 40.0 (CH), 34.4 (CH₂), 15.4 (CH₃).

The enantiomeric excess was determined by **HPLC** using a Chiralpak IB column (hexane/*i*PrOH = 95:5, flow rate 1.0 mL/min, λ = 230 nm): *t_r* (major) = 30.3, *t_r* (minor) = 27.1, 98% *ee*.

[α]_D²⁰ = −9.9° (c = 1.1, CHCl₃)

MS (ESI+) *m/z*: 415.0 [M+H]⁺; **HRMS (ESI+)** Exact mass calculated for C₂₁H₁₉Cl³⁵N₂NaO₅ [M+Na]⁺: 437.08747, found: 437.08842; Exact mass calculated for C₂₁H₁₉Cl³⁵KN₂O₅ [M+K]⁺: 453.06141, found: 453.06249.

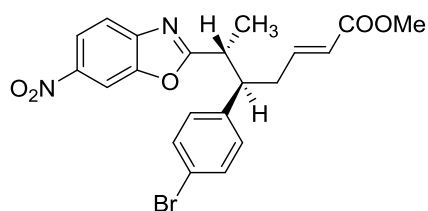
methyl (*E*)-5-(4-bromophenyl)-6-(6-nitrobenzoxazol-2-yl)hept-2-enoate (259e)



The reaction was performed following the general procedure adding: the organic catalyst (*S*)-2-(((*tert*-butyldimethylsilyl)oxy)diphenylmethyl)pyrrolidine (38 mg, 0.104 mmol, 20 mol% equiv), (*E*)-3-(4-bromophenyl)acrylaldehyde (329 mg, 1.560 mmol, 2 equiv), 2-ethyl-6-nitrobenzoxazole (100 mg, 0.520 mmol, 1 equiv), Pd(OAc)₂ (6 mg, 0.026 mmol, 5 mol% equiv) and CH₃CN (1 mL). To the crude solution was finally added TEA (26 mg, 0.260 mmol, 50 mol% equiv). The first reaction was stirred for 40 hours at 30 °C before performing the Wittig. The final crude was purified by flash column chromatography (hexane/EtOAc 5:1) to obtain 188 mg of the desired product as yellow oil. Yield: 79%. The diastereomeric ratio was determined by the crude NMR: 1.5:1

Diastereomer 1, major:

methyl (5*R*,6*R*,*E*)-5-(4-bromophenyl)-6-(6-nitrobenzoxazol-2-yl)hept-2-enoate



IR (CHCl₃, liquid film): 3105, 2924, 2854, 1729 (ester), 1659, 1562, 1524 (aromatic NO₂), 1435, 1346 (aromatic NO₂), 1315, 1269 cm⁻¹

¹H-NMR (400 MHz, CDCl₃) δ 8.37 (d, *J* = 2.0 Hz, 1H, Het), 8.24 (dd, *J* = 8.8, 2.0 Hz, 1H, Het), 7.72 (d, *J* = 8.8 Hz, 1H, Het), 7.40 (d, *J* = 8.3 Hz, 2H, Ar), 6.99 (d, *J* = 8.3 Hz, 2H, Ar), 6.53 (dt, *J* = 7.4, 15.2, 1H, =CHCH₂), 5.51 (bd, *J* = 15.6 Hz, 1H, =CHCO₂Me), 3.50 (s, 3H, OCH₃), 3.33 (dq, *J* = 8.9, 6.9 Hz, 1H, CHCH₃), 3.20 (td, *J* = 9.2, 5.7 Hz, 1H, CHCH₂), 2.55 – 2.35 (m, 2H, CH₂), 1.17 (d, *J* = 8.5 Hz, 3H, CH₃).

¹³C-NMR (101 MHz, CDCl₃) δ 173.7 (Cq), 166.2 (Cq), 149.6 (Cq), 146.3 (Cq), 145.2 (Cq), 145.0 (CH), 139.4 (Cq), 132.1 (CH), 129.6 (CH), 122.9 (CH), 121.3 (Cq), 120.6 (CH), 119.9 (CH), 107.3 (CH), 51.4 (CH₃), 49.1 (CH), 40.0 (CH), 37.1 (CH₂), 16.9 (CH₃).

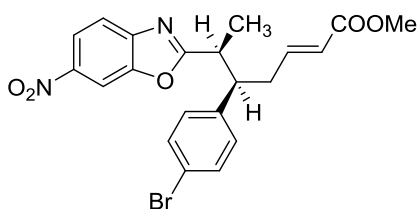
The enantiomeric excess was determined by **HPLC** using a Chiralpak IE column (hexane/*i*PrOH = 90:10, flow rate 1.0 mL/min, λ = 230 nm): *t_r* (major) = 32.1, *t_r* (minor) = 36.0, 73% *ee*.

[α]_D²⁰ = -7.6° (*c* = 1.75, CHCl₃)

MS (ESI+) *m/z*: 459.0 [M+H]⁺; **HRMS (ESI+)** Exact mass calculated for C₂₁H₂₀Br⁷⁹N₂O₅ [M+H]⁺: 459.0550, found: 459.0545.

Diastereomer 2, minor:

methyl (5*R*,6*S*,*E*)-5-(4-bromophenyl)-6-(6-nitrobenzoxazol-2-yl)hept-2-enoate



IR (CHCl₃, liquid film): 3105, 2924, 2854, 1720 (ester), 1659, 1562, 1520 (aromatic NO₂), 1435, 1346 (aromatic NO₂), 1315, 1269 cm⁻¹.

¹H-NMR (400 MHz, CDCl₃) δ 8.28 (d, *J* = 2.0 Hz, 1H, Het), 8.19 (dd, *J* = 8.8, 2.0 Hz, 1H, Het), 7.65 (d, *J* = 8.8 Hz, 1H, Het), 7.27 (d, *J* = 8.4 Hz, 2H, Ar), 6.88 (d, *J* = 8.4 Hz, 2H, Ar), 6.65 (dt, *J* = 15.2, 7.1, 1H, =CHCH₂), 5.72 (d, *J* = 15.6 Hz, 1H, =CHCO₂Me), 3.58 (s, 3H, OCH₃), 3.42 (dq, *J*₁ = *J*₂ = 6.8 Hz, 1H, CHCH₃), 3.31 – 3.22 (m, 1H, CHCH₂), 2.79 – 2.69 (m, 1H, CH₂), 2.67 – 2.56 (m, 1H, CH₂), 1.42 (d, *J* = 7.0 Hz, 3H, CH₃).

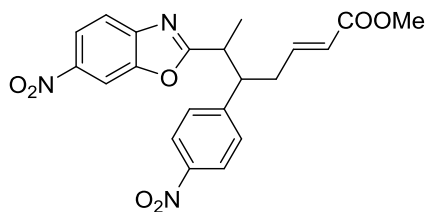
¹³C-NMR (101 MHz, CDCl₃) δ 173.0 (Cq), 166.4 (Cq), 149.5 (Cq), 146.2 (Cq), 145.3 (Cq), 145.1 (CH), 139.2 (Cq), 131.8 (CH), 129.6 (CH), 123.4 (CH), 121.2 (Cq), 120.5 (CH), 119.8 (CH), 107.1 (CH), 51.5 (CH₃), 48.4 (CH), 39.9 (CH), 34.4 (CH₂), 15.4 (CH₃).

The enantiomeric excess was determined by **HPLC** using a Chiralpak IE column (hexane/*i*PrOH = 95:5, flow rate 1.0 mL/min, λ = 230 nm): *t_r* (major) = 23.6, *t_r* (minor) = 22.5, 99% *ee*.

[α]_D²⁰ = –20.3° (*c* = 1.38, CHCl₃)

MS (ESI+) *m/z*: 458.9 [M+H]⁺; **HRMS (ESI+)** Exact mass calculated for C₂₁H₂₀Br⁷⁹N₂O₅ [M+H]⁺: 459.0550, found: 459.0556.

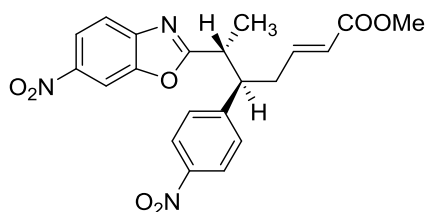
methyl (*E*)-6-(6-nitrobenzoxazol-2-yl)-5-(4-nitrophenyl)hept-2-enoate (259f)



The reaction was performed following the general procedure adding: the organic catalyst (*S*)-2-(diphenyl((triethylsilyl)oxy)methyl)pyrrolidine (38 mg, 0.104 mmol, 20 mol% equiv), (*E*)-3-(4-nitrophenyl)acrylaldehyde (184 mg, 1.040 mmol, 2 equiv), 2-ethyl-6-nitrobenzoxazole (100 mg, 0.520 mmol, 1 equiv), Pd(OAc)₂ (6 mg, 0.026 mmol, 5 mol% equiv) and CH₃CN (1 mL). To the crude solution was finally added TEA (26 mg, 0.260 mmol, 50 mol% equiv). The first reaction was stirred at 30 °C for 24 hours before performing the Wittig. The final crude was purified by flash column chromatography (hexane/EtOAc 5:1) to obtain 133 mg of the desired product as an orange oil (major diastereomer) and orange solid (minor diastereomer). Yield: 60%. The diastereomeric ratio was determined by the crude NMR: 1.4:1

Diastereomer 1, major:

methyl (5*R*,6*R*,*E*)-6-(6-nitrobenzoxazol-2-yl)-5-(4-nitrophenyl)hept-2-enoate



IR (CHCl₃, liquid film): 2954, 2924, 2854, 2360, 2341, 1720 (ester), 1601, 1562, 1524 (aromatic NO₂), 1435, 1346 (aromatic NO₂), 1269 cm⁻¹.

¹H-NMR (400 MHz, CDCl₃) δ 8.37 (d, *J* = 1.8 Hz, 1H, Het), 8.25 (dd, *J* = 8.8, 1.1 Hz, 1H, Het), 8.15 (d, *J* = 8.5 Hz, 2H, Ar), 7.73 (d, *J* = 8.8 Hz, 1H, Het), 7.31 (d, *J* = 8.7 Hz, 2H, Ar), 6.53 (dt, *J* = 15.4, 7.3 Hz, 1H, =CHCH₂), 5.53 (d, *J* = 15.6 Hz, 1H, =CHCO₂Me), 3.50 (s, 3H, OCH₃), 3.48 – 3.36 (m, 2H, CHCH₃, CHCH₂), 2.61 – 2.45 (m, 2H, CH₂), 1.19 (d, *J* = 6.3 Hz, 3H, CH₃).

¹³C-NMR (101 MHz, CDCl₃) δ 173.0 (Cq), 166.0 (Cq), 149.6 (Cq), 148.0 (Cq), 147.3 (Cq), 146.2 (Cq), 145.3 (Cq), 144.2 (CH), 129.0 (CH), 124.2 (CH), 123.4 (CH), 120.7 (CH), 120.0 (CH), 107.3 (CH), 51.5 (CH₃), 49.3 (CH), 39.8 (CH), 36.8 (CH₂), 16.9 (CH₃).

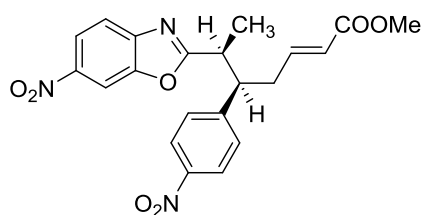
The enantiomeric excess was determined by **HPLC** using a Chiralpak IC column (hexane/*i*PrOH = 70:30, flow rate 1.0 mL/min, λ = 230 nm): *t_r* (major) = 70.7, *t_r* (minor) = 76.9, 78% *ee*.

[α]_D²⁰ = −3.4° (c = 1.53, CHCl₃)

MS (ESI+) *m/z*: 426.0 [M+H]⁺; **HRMS (ESI+)** Exact mass calculated for C₂₁H₂₀N₃O₇ [M+H]⁺: 426.1296, found: 426.1288; Exact mass calculated for C₂₁H₁₉N₃NaO₇ [M+Na]⁺: 448.1115, found: 448.1107.

Diastereomer 2, minor:

methyl (5*R*,6*S*,*E*)-6-(6-nitrobenzoxazol-2-yl)-5-(4-nitrophenyl)hept-2-enoate



mp: 151 °C

IR (CHCl₃, liquid film): 2955, 2924, 2854, 2361, 2341, 1720 (ester), 1601, 1562, 1524 (aromatic NO₂), 1439, 1346 (aromatic NO₂), 1269 cm^{−1}.

¹H-NMR (400 MHz, CDCl₃) δ 8.28 (d, *J* = 2.0 Hz, 1H, Het), 8.19 (dd, *J* = 8.8, 2.1 Hz, 1H, Het), 8.02 (d, *J* = 8.8 Hz, 2H, Ar), 7.64 (d, *J* = 8.8 Hz, 1H, Het), 7.20 (d, *J* = 8.0 Hz, 2H, Ar), 6.64 (dt, *J* = 15.4, 7.2 Hz, 1H, =CHCH₂), 5.73 (bd, *J* = 15.6 Hz, 1H, =CHCO₂Me), 3.58 (s, 3H, OCH₃), 3.54 – 3.39 (m, 2H, CHCH₃, CHCH₂), 2.89 – 2.77 (m, 1H, CH₂), 2.73 – 2.61 (m, 1H, CH₂), 1.47 (d, *J* = 6.8 Hz, 3H, CH₃).

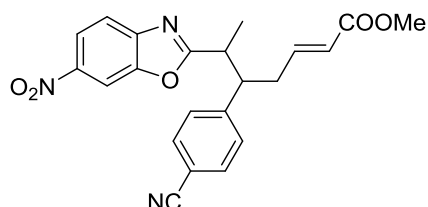
¹³C-NMR (101 MHz, CDCl₃) δ 172.4 (Cq), 166.2 (Cq), 149.5 (Cq), 147.9 (Cq), 147.2 (Cq), 146.0 (Cq), 145.2 (Cq), 144.4 (CH), 128.9 (CH), 123.89 (CH), 123.86 (CH), 120.6 (CH), 119.9 (CH), 107.1 (CH), 51.6 (CH₃), 48.7 (CH), 39.7 (CH), 34.4 (CH₂), 15.8 (CH₃).

The enantiomeric excess was determined by **HPLC** using a Chiralpak IC column (hexane/*i*PrOH = 70:30, flow rate 1.0 mL/min, λ = 230 nm): t_r (major) = 68.1, t_r (minor) = 56.0, 99%.

$[\alpha]_D^{20} = -2.5^\circ$ ($c = 1.55$, CHCl_3)

MS (ESI+) m/z : 426.1 $[\text{M}+\text{H}]^+$; **HRMS (ESI+)** Exact mass calculated for $\text{C}_{21}\text{H}_{20}\text{N}_3\text{O}_7$ $[\text{M}+\text{H}]^+$: 426.1296, found: 426.1296.

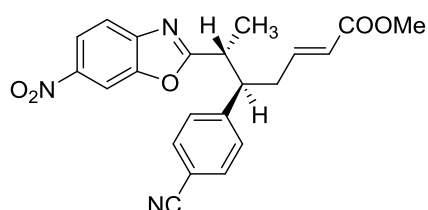
methyl (*E*)-5-(4-cyanophenyl)-6-(6-nitrobenzoxazol-2-yl)hept-2-enoate (259g)



The reaction was performed following the general procedure adding: the organic catalyst (*S*)-2-(((*tert*-butyldimethylsilyl)oxy)diphenylmethyl)pyrrolidine (38 mg, 0.104 mmol, 20 mol% equiv), (*E*)-4-(3-oxoprop-1-en-1-yl)benzonitrile (163 mg, 1.040 mmol, 2 equiv), 2-ethyl-6-nitrobenzoxazole (100 mg, 0.520 mmol, 1 equiv), $\text{Pd}(\text{OAc})_2$ (6 mg, 0.026 mmol, 5 mol% equiv) and CH_3CN (1 mL). To the crude solution was finally added TEA (26 mg, 0.260 mmol, 50 mol% equiv). The first reaction was stirred for 40 hours at 35 °C before performing the Wittig. The final crude was purified by flash column chromatography (hexane/EtOAc 10:1) to obtain 124 mg of the desired product as dark orange oil. Yield: 59%. The diastereomeric ratio was determined by the crude NMR: 1.3:1

Diastereomer 1:

methyl (*5R,6R,E*)-5-(4-cyanophenyl)-6-(6-nitrobenzoxazol-2-yl)hept-2-enoate



IR (CHCl₃, liquid film): 2951 (stretch HC=C), 2928, 2229 (stretch C=N), 1720 (stretch C=O, ester), 1562, 1524 (aromatic NO₂), 1435, 1346 (aromatic NO₂), 1269 cm⁻¹.

¹H NMR (400 MHz, CDCl₃) δ 8.70 (s, 1H, Het), 8.58 (d, *J* = 8.8 Hz, 1H, Het), 8.06 (d, *J* = 8.7 Hz, 1H, Het), 7.92 (d, *J* = 7.8 Hz, 2H, Ar), 7.58 (d, *J* = 7.6 Hz, 2H, Ar), 6.85 (dt, *J* = 14.9, 7.2 Hz, 1H, =CHCH₂), 5.85 (d, *J* = 15.6 Hz, 1H, =CHCO₂Me), 3.84 (s, 3H, OCH₃), 3.78 – 3.61 (m, 2H, CHCH₃, CHCH₂), 2.91 – 2.74 (m, 2H, CH₂), 1.51 (d, *J* = 6.5 Hz, 3H, CH₃).

¹³C NMR (101 MHz, CDCl₃) δ 173.1 (Cq), 166.0 (Cq), 149.6 (Cq), 146.2 (Cq), 146.0 (Cq), 145.3 (Cq), 144.3 (CH), 132.8 (CH), 128.9 (CH), 123.3 (CH), 120.7 (CH), 120.0 (CH), 118.4 (Cq), 111.6 (Cq), 107.3 (CH), 51.5 (CH₃), 49.6 (CH), 39.8 (CH), 36.8 (CH₂), 16.9 (CH₃).

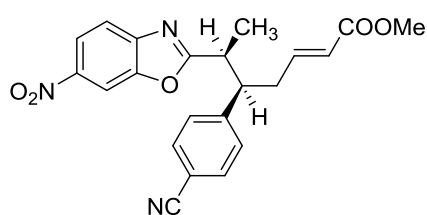
The enantiomeric excess was determined by **HPLC** using a Chiralpak IE column (hexane/*i*PrOH = 75:25, flow rate 1.0 mL/min, λ = 230 nm): *t_r* (major) = 49.0, *t_r* (minor) = 57.7, 71% *ee*.

[α]_D¹⁹ = –10.4° (*c* = 1, CHCl₃)

MS (ESI+) *m/z*: 406.0 [M+H]⁺; **HRMS (ESI+)** Exact mass calculated for C₂₂H₂₀N₃O₅ [M+H]⁺: 406.1397, found: 406.1393.

Diastereomer 2:

methyl (5*R*,6*S*,*E*)-5-(4-cyanophenyl)-6-(6-nitrobenzoxazol-2-yl)hept-2-enoate



IR (CHCl₃, liquid film): 2951 (stretch HC=C), 2928, 2229 (stretch C=N), 1720 (stretch C=O, ester), 1658, 1562, 1527 (aromatic NO₂), 1435, 1342 (aromatic NO₂), 1269 cm⁻¹.

¹H NMR (400 MHz, CDCl₃) δ 8.19 (d, *J* = 2.1 Hz, 1H, Het), 8.11 (dd, *J* = 8.8, 2.1 Hz, 1H, Het), 7.56 (d, *J* = 8.8 Hz, 1H, Het), 7.36 (bd, *J* = 8.3 Hz, 2H, Ar), 7.05 (bd, *J* = 8.3 Hz, 2H, Ar), 6.54 (dt, *J* = 15.4, 7.3 Hz, 1H, =CHCH₂), 5.63 (dt, *J* = 15.7, 1.4 Hz, 1H, =CHCO₂Me),

3.49 (s, 3H, OCH₃), 3.41 – 3.33 (m, 1H, CHCH₃), 3.28 (ddd, *J* = 9.8, 7.1, 5.2 Hz, 1H, CHCH₂), 2.76 – 2.66 (m, 1H, CH₂), 2.61 – 2.50 (m, 1H, CH₂), 1.36 (d, *J* = 7.0 Hz, 3H, CH₃).

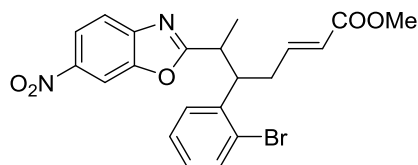
¹³C NMR (101 MHz, CDCl₃) δ 172.5 (Cq), 166.2 (Cq), 149.5 (Cq), 146.0 (Cq), 145.8 (Cq), 145.2 (Cq), 144.5 (CH), 132.4 (CH), 128.8 (CH), 123.8 (CH), 120.6 (CH), 119.8 (CH), 118.4 (Cq), 111.4 (Cq), 107.1 (CH), 51.6 (CH₃), 49.0 (CH), 39.7 (CH), 34.3 (CH₂), 15.6 (CH₃).

The enantiomeric excess was determined by **HPLC** using a Chiralpak IE column (hexane/*i*PrOH = 80:20, flow rate 1.0 mL/min, λ = 230 nm): *t_r* (major) = 74.8, *t_r* (minor) = 70.6, 75% *ee*.

[α]_D¹⁹ = −0.8° (*c* = 1, CHCl₃)

MS (ESI+) *m/z*: 406.1 [M+H]⁺; **HRMS (ESI+)** Exact mass calculated for C₂₂H₂₀N₃O₅ [M+H]⁺: 406.1397, found: 406.1398.

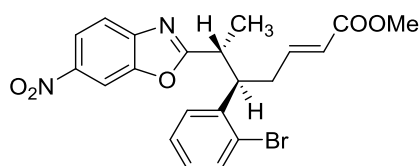
methyl (*E*)-5-(2-bromophenyl)-6-(6-nitrobenzoxazol-2-yl)hept-2-enoate (259h)



The reaction was performed following the general procedure adding: the organic catalyst (*S*)-2-(((*tert*-butyldimethylsilyl)oxy)diphenylmethyl)pyrrolidine (38 mg, 0.104 mmol, 20 mol% equiv), (*E*)-3-(2-bromophenyl)acrylaldehyde (329 mg, 1.560 mmol, 2 equiv), 2-ethyl-6-nitrobenzoxazole (100 mg, 0.520 mmol, 1 equiv), Pd(OAc)₂ (6 mg, 0.026 mmol, 5 mol% equiv) and CH₃CN (1 mL). To the crude solution was finally added TEA (26 mg, 0.260 mmol, 50 mol% equiv). The first reaction was stirred for 24 hours at 35 °C before performing the Wittig. The final crude was purified by flash column chromatography (hexane/EtOAc 10:1) to obtain 165 mg of the desired product as dark yellow oil. Yield: 69%. The diastereomeric ratio was determined by the crude NMR: 1.6:1

Diastereomer 1:

methyl (5*R*,6*R*,*E*)-5-(2-bromophenyl)-6-(6-nitrobenzoxazol-2-yl)hept-2-enoate



IR (CHCl₃, liquid film): 2949 (stretch *HC=C*), 1721 (stretch *C=O*, ester), 1564, 1525 (aromatic NO₂), 1436, 1345 (aromatic NO₂), 1269 cm⁻¹.

¹H NMR (400 MHz, CDCl₃) δ 8.66 (d, *J* = 2.0 Hz, 1H, Het), 8.54 (dd, *J* = 8.8, 2.0 Hz, 1H, Het), 8.03 (d, *J* = 8.8 Hz, 1H, Het), 7.84 (d, *J* = 8.0 Hz, 1H, Ar), 7.56 (t, *J* = 7.5 Hz, 1H, Ar), 7.46 – 7.41 (m, 1H, Ar), 7.40 – 7.34 (m, 1H, Ar), 6.85 (dt, *J* = 15.0, 7.2 Hz, 1H, =*CHCH*₂), 5.77 (d, *J* = 15.6 Hz, 1H, =*CHCO*₂Me), 4.37 – 4.15 (m, 1H, *CHCH*₂), 3.77 (s, 3H, OCH₃), 3.76 – 3.65 (m, 1H, *CHCH*₃), 2.86 – 2.67 (m, 2H, CH₂), 1.53 (d, *J* = 6.9 Hz, 3H, CH₃).

¹³C NMR (101 MHz, CDCl₃) δ 173.6 (Cq), 166.2 (Cq), 149.7 (Cq), 146.4 (Cq), 145.2 (Cq), 144.9 (CH), 140.0 (Cq), 133.5 (CH), 128.8 (CH), 128.1 (CH), 127.5 (CH), 126.0 (Cq), 122.7 (CH), 120.5 (CH), 119.9 (CH), 107.3 (CH), 51.3 (CH₃), 46.9 (CH), 40.1 (CH), 36.8 (CH₂), 17.1 (CH₃).

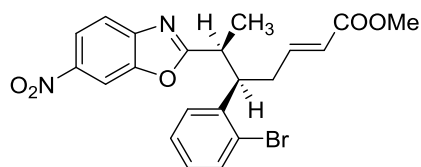
The enantiomeric excess was determined by **HPLC** using a Chiralpak IE column (hexane/*i*PrOH = 93:7, flow rate 1.0 mL/min, λ = 230 nm): *t_r* (major) = 38.3, *t_r* (minor) = 43.0, 85% *ee*.

[α]_D¹⁹ = –12.8° (*c* = 1, CHCl₃)

MS (ESI⁺) *m/z*: 459.0 [*M*+*H*]⁺; **HRMS (ESI⁺)** Exact mass calculated for C₂₁H₂₀Br⁷⁹N₂O₅ [*M*+*H*]⁺: 459.0550, found: 459.0546.

Diastereomer 2:

methyl (5*R*,6*S*,*E*)-5-(2-bromophenyl)-6-(6-nitrobenzoxazol-2-yl)hept-2-enoate



IR (CHCl₃, liquid film): 2924 (stretch HC=C), 1722 (stretch C=O, ester), 1563, 1525 (aromatic NO₂), 1436, 1345 (aromatic NO₂), 1269 cm⁻¹.

¹H NMR (400 MHz, CDCl₃) δ 8.32 (d, J = 1.8 Hz, 1H, Het), 8.19 (dd, J = 8.8, 2.0 Hz, 1H, Het), 7.67 (d, J = 8.8 Hz, 1H, Het), 7.47 (d, J = 7.9 Hz, 1H, Ar), 7.16 (d, J = 7.4 Hz, 1H, Ar), 7.08 – 6.95 (m, 2H, Ar), 6.65 (dt, J = 15.2, 7.1 Hz, 1H, =CHCH₂), 5.68 (d, J = 15.7 Hz, 1H, =CHCO₂Me), 4.11 – 3.99 (m, 1H, CHCH₂), 3.59 – 3.56 (m, 1H, CHCH₃), 3.53 (s, 3H, OCH₃), 2.68, 2.65 (m, 2H, CH₂), 1.40 (d, J = 7.1 Hz, 3H, CH₃).

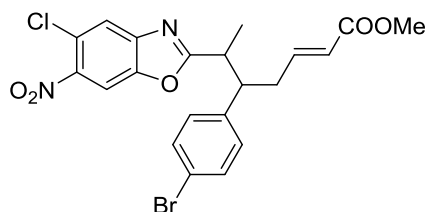
¹³C NMR (101 MHz, CDCl₃) δ 173.3 (Cq), 166.3 (Cq), 149.7 (Cq), 146.3 (Cq), 145.2 (CH), 145.1 (Cq), 139.2 (CH), 133.5 (CH), 128.7 (CH), 128.6 (Cq), 127.5 (CH), 125.4 (Cq), 123.2 (CH), 120.4 (CH), 119.7 (CH), 107.2 (CH), 51.4 (CH₃), 46.0 (CH), 38.1 (CH), 32.8 (CH₂), 13.7 (CH₃).

The enantiomeric excess was determined by **HPLC** using a Chiralpak IE column (hexane/*i*PrOH = 93:7, flow rate 1.0 mL/min, λ = 230 nm): t_r (major) = 30.2, t_r (minor) = 33.1, 53% *ee*.

$[\alpha]_D^{19}$ = –69.3° (c = 0.3, CHCl₃)

MS (ESI+) m/z : 459.0 [M+H]⁺; **HRMS (ESI+)** Exact mass calculated for C₂₁H₂₀Br⁷⁹N₂O₅ [M+H]⁺: 459.0550, found: 459.0540.

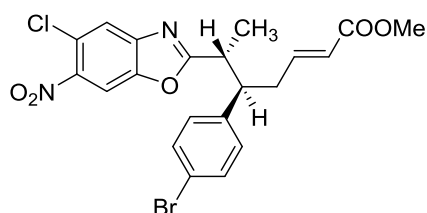
methyl (*E*)-5-(4-bromophenyl)-6-(5-chloro-6-nitrobenzoxazol-2-yl)hept-2-enoate (276a)



The reaction was performed following the general procedure adding: the organic catalyst (*S*)-2-(((*tert*-butyldimethylsilyl)oxy)diphenylmethyl)pyrrolidine (32 mg, 0.088 mmol, 20 mol% equiv), (*E*)-3-(4-bromophenyl)acrylaldehyde (186 mg, 0.882 mmol, 2 equiv), 5-chloro-2-ethyl-6-nitrobenzoxazole (100 mg, 0.441 mmol, 1 equiv), Pd(OAc)₂ (5 mg, 0.022 mmol, 5 mol% equiv) and CH₃CN (1 mL). To the crude solution was finally added TEA (23 mg, 0.221 mmol, 50 mol% equiv). The first reaction was stirred for 24 hours at 35 °C before performing the Wittig. The final crude was purified by flash column chromatography (hexane/EtOAc 6:1) to obtain 216 mg of the desired product as orange oil. Yield: 99% (122 mg dia1 and 94 mg dia2). The diastereomeric ratio was determined by the crude NMR: 2.7:1

Diastereomer 1, major:

methyl (5*R*,6*R*,*E*)-5-(4-bromophenyl)-6-(5-chloro-6-nitrobenzoxazol-2-yl)hept-2-enoate



IR (CHCl₃, liquid film): 2987 (stretch HC=C), 2360, 1720 (stretch C=O, ester), 1560, 1534, 1446, 1348 (aromatic NO₂).

¹H NMR (400 MHz, CDCl₃) δ 8.06 (s, 1H, Het), 7.81 (s, 1H, Het), 7.44 (d, *J* = 8.3 Hz, 2H, Ar), 7.04 (d, *J* = 8.4 Hz, 2H, Ar), 6.57 (dt, *J* = 15.0, 7.3 Hz, 1H, =CHCH₂), 5.55 (bd, *J* = 15.6 Hz, 1H, =CHCO₂Me), 3.56 (s, 3H, OCH₃), 3.37 (dq, *J* = 9.3, 6.9 Hz, 1H, CHCH₃), 3.23 (td, *J* = 8.9, 6.1 Hz, 1H, CHCH₂), 2.61 – 2.37 (m, 2H, CH₂), 1.21 (d, *J* = 6.9 Hz, 3H, CH₃).

¹³C NMR (101 MHz, CDCl₃) δ 174.2 (Cq), 166.1 (Cq), 147.9 (Cq), 145.0 (CH), 144.7 (Cq), 139.4 (Cq), 132.1 (CH), 131.7 (Cq), 129.6 (CH), 123.5 (Cq), 122.8 (CH), 122.4 (CH), 121.3 (Cq), 108.7 (CH), 51.4 (CH₃), 49.0 (CH), 39.9 (CH), 37.1 (CH₂), 16.8 (CH₃).

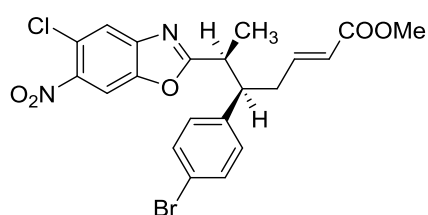
The enantiomeric excess was determined by **HPLC** using a Chiralpak IE column (hexane/*i*PrOH = 80:20, flow rate 1.0 mL/min, λ = 254 nm): *t_r* (major) = 17.1, *t_r* (minor) = 14.6, 99% *ee*.

[α]_D¹⁹ = −3.7° (c = 4, CHCl₃)

MS (ESI+) *m/z*: 494.7 [M+H]⁺; **HRMS (ESI+)** Exact mass calculated for C₂₁H₁₉Br⁷⁹Cl³⁵N₂O₅ [M+H]⁺: 493.0160, found: 493.0154.

Diastereomer 2, minor:

methyl (5*R*,6*S*,*E*)-5-(4-bromophenyl)-6-(5-chloro-6-nitrobenzoxazol-2-yl)hept-2-enoate



IR (CHCl₃, liquid film): 2949 (stretch HC=C), 2361, 1720 (stretch C=O, ester), 1557, 1534, 1446, 1327 (aromatic NO₂).

¹H NMR (400 MHz, CDCl₃) δ 8.00 (s, 1H, Het), 7.76 (s, 1H, Het), 7.34 (d, *J* = 8.4 Hz, 2H, Ar), 6.93 (d, *J* = 8.4 Hz, 2H, Ar), 6.70 (dt, *J* = 14.8, 7.2 Hz, 1H, =CHCH₂), 5.78 (bd, *J* = 15.6 Hz, 1H, =CHCO₂Me), 3.64 (s, 3H, OCH₃), 3.47 (p, *J* = 7.0 Hz, 1H, CHCH₃), 3.30 (ddd, *J* = 9.5, 7.0, 5.4 Hz, 1H, CHCH₂), 2.79 (ddd, *J* = 12.5, 6.8, 1.1 Hz, 1H, CH₂), 2.73 – 2.59 (m, 1H, CH₂), 1.47 (d, *J* = 7.0 Hz, 3H, CH₃).

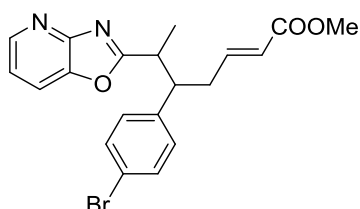
¹³C NMR (101 MHz, CDCl₃) δ 173.6 (Cq), 166.3 (Cq), 147.8 (Cq), 145.2 (CH), 144.6 (Cq), 139.1 (Cq), 131.8 (CH), 129.6 (CH), 129.2 (Cq), 123.5 (Cq), 123.4 (CH), 122.3 (CH), 121.3 (Cq), 108.5 (CH), 51.5 (CH₃), 48.4 (CH), 39.8 (CH), 34.4 (CH₂), 15.5 (CH₃).

The enantiomeric excess was determined by **HPLC** using a Chiralpak IA column (hexane/*i*PrOH = 75:25, flow rate 1.0 mL/min, λ = 254 nm): t_r (major) = 9.5, t_r (minor) = 11.1, 56% *ee*.

$[\alpha]_D^{19} = -18.5^\circ$ ($c = 1.9$, CHCl_3)

HRMS (ESI+) Exact mass calculated for $\text{C}_{21}\text{H}_{19}\text{Br}^{79}\text{Cl}^{35}\text{N}_2\text{O}_5$ $[\text{M}+\text{H}]^+$: 493.0160, found: 493.0148.

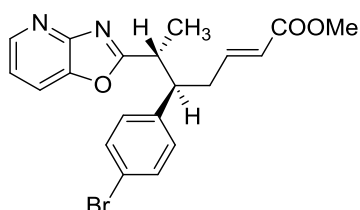
methyl (*E*)-5-(4-bromophenyl)-6-(oxazolo[4,5- β]pyridin-2-yl)hept-2-enoate (276f)



The reaction was performed following the general procedure adding: the organic catalyst 2-(diphenyl((trimethylsilyl)oxy)methyl)pyrrolidine (22 mg, 0.067 mmol, 20 mol% equiv), (*E*)-3-(4-bromophenyl)acrylaldehyde (142 mg, 0.674 mmol, 2 equiv), 2-ethyloxazolo[4,5- β]pyridine (50 mg, 0.337 mmol, 1 equiv), $\text{Pd}(\text{OAc})_2$ (4 mg, 0.017 mmol, 5 mol% equiv) and CH_3CN (1 mL). To the crude solution was finally added TEA (17 mg, 0.169 mmol, 50 mol% equiv). The first reaction was stirred for 4 days at 40 °C and 24 hours at 50 °C before performing the Wittig. The final crude was purified by flash column chromatography (hexane/EtOAc 5:1) to obtain 55 mg of the desired products as yellow oil. Yield: 39%. The diastereomeric ratio was determined by the crude NMR: 1.4:1

Diastereomer 1:

methyl (5*R*,6*R*,*E*)-5-(4-bromophenyl)-6-(oxazolo[4,5- β]pyridin-2-yl)hept-2-enoate



IR (CHCl₃, liquid film): 2983 (stretch HC=C), 1720 (stretch C=O, ester), 1560, 1408, 1259 (aromatic NO₂).

¹H NMR (400 MHz, CDCl₃) δ 8.69 (dd, J = 4.9, 1.3 Hz, 1H, Het), 7.93 (dd, J = 8.1, 1.3 Hz, 1H, Het), 7.58 (d, J = 8.4 Hz, 2H, Ar), 7.41 (dd, J = 8.1, 4.9 Hz, 1H, Het), 7.19 (d, J = 8.4 Hz, 2H, Ar), 6.72 (dt, J = 15.3, 7.3 Hz, 1H, =CHCH₂), 5.70 (d, J = 15.6 Hz, 1H, =CHCO₂Me), 3.70 (s, 3H, OCH₃), 3.55 – 3.47 (m, 1H, CHCH₃), 3.40 (td, J = 9.2, 5.3 Hz, 1H, CHCH₂), 2.73 – 2.55 (m, 2H, CH₂), 1.35 (d, J = 6.9 Hz, 3H, CH₃).

¹³C NMR (101 MHz, CDCl₃) δ 171.9 (Cq), 166.3 (Cq), 155.6 (Cq), 146.5 (CH), 145.4 (CH), 142.7 (Cq), 139.7 (Cq), 132.0 (CH), 129.7 (CH), 122.8 (CH), 121.1 (Cq), 120.0 (CH), 118.2 (CH), 51.4 (CH₃), 49.0 (CH), 40.1 (CH), 37.1 (CH₂), 17.1 (CH₃).

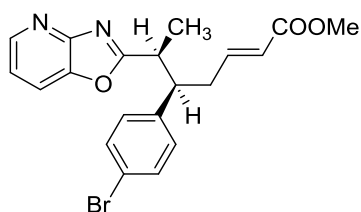
The enantiomeric excess was determined by **HPLC** using a Chiralpak ID column (hexane/*i*PrOH = 80:20, flow rate 1.0 mL/min, λ = 230 nm): t_r (major) = 32.8, t_r (minor) = 37.2, 29% *ee*.

$[\alpha]_D^{19}$ = –0.72° (c = 0.88, CHCl₃)

MS (ESI+) m/z : 416.7 [M+H]⁺; **HRMS (ESI+)** Exact mass calculated for C₂₀H₂₀Br⁷⁹N₂O₃ [M+H]⁺: 415.0652, found: 415.0641.

Diastereomer 2:

methyl (5*R*,6*S*,*E*)-5-(4-bromophenyl)-6-(oxazolo[4,5- β]pyridin-2-yl)hept-2-enoate



IR (CHCl₃, liquid film): 2921 (stretch HC=C), 2361, 1720 (stretch C=O, ester), 1557, 1408, 1260 (aromatic NO₂).

¹H NMR (400 MHz, CDCl₃) δ 8.63 (d, J = 4.8 Hz, 1H, Het), 7.83 (dd, J = 8.1, 1.3 Hz, 1H, Het), 7.45 (d, J = 8.4 Hz, 2H, Ar), 7.35 (dd, J = 8.1, 4.9 Hz, 1H, Het), 7.10 (d, J = 8.4 Hz, 2H, Ar), 6.85 (dt, J = 14.9, 7.2 Hz, 1H, =CHCH₂), 5.91 (d, J = 15.6 Hz, 1H, =CHCO₂Me),

3.77 (s, 3H, OCH₃), 3.60 (dd, *J* = 9.0, 4.8 Hz, 1H, CHCH₃), 3.51 – 3.44 (m, 1H, CHCH₂), 3.00 – 2.89 (m, 1H, CH₂), 2.87 – 2.76 (m, 1H, CH₂), 1.60 (d, *J* = 7.0 Hz, 3H, CH₃).

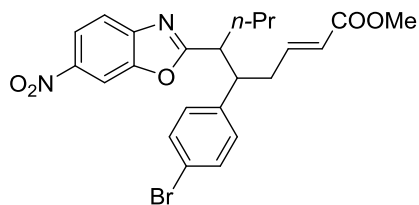
¹³C NMR (101 MHz, CDCl₃) δ 171.3 (Cq), 166.5 (Cq), 155.5 (Cq), 146.4 (CH), 145.7 (CH), 142.5 (Cq), 139.4 (Cq), 131.7 (CH), 129.8 (CH), 123.2 (CH), 121.0 (Cq), 119.9 (CH), 118.0 (CH), 51.5 (CH₃), 48.2 (CH), 39.9 (CH), 34.2 (CH₂), 15.3 (CH₃).

The enantiomeric excess was determined by **HPLC** using a Chiralpak ID column (hexane/*i*PrOH = 80:20, flow rate 1.0 mL/min, λ = 230 nm): *t_r* (major) = 31.1, *t_r* (minor) = 41.3, 24% *ee*.

[α]_D¹⁹ = +14° (c = 0.2, CHCl₃)

MS (ESI+) *m/z*: 416.7 [M+H]⁺; **HRMS (ESI+)** Exact mass calculated for C₂₀H₂₀Br⁷⁹N₂O₃ [M+H]⁺: 415.0652, found: 415.0641.

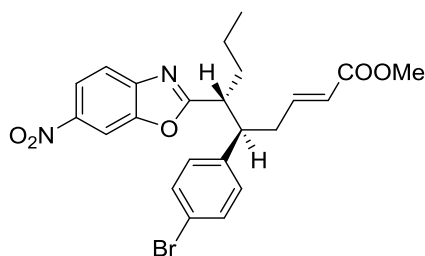
methyl (*E*)-5-(4-bromophenyl)-6-(6-nitrobenzoxazol-2-yl)non-2-enoate (276d)



The reaction was performed following the general procedure adding: the organic catalyst (*S*)-2-(((*tert*-butyldimethylsilyl)oxy)diphenylmethyl)pyrrolidine (15 mg, 0.041 mmol, 20 mol% equiv), (*E*)-3-(4-bromophenyl)acrylaldehyde (86 mg, 0.410 mmol, 2 equiv), 2-butyl-6-nitrobenzoxazole (100 mg, 0.205 mmol, 1 equiv), Pd(OAc)₂ (2 mg, 0.010 mmol, 5 mol% equiv) and CH₃CN (1 mL). To the crude solution was finally added TEA (10 mg, 0.103 mmol, 50 mol% equiv). The first reaction was stirred for 40 hours at 35 °C before performing the Wittig. The final crude was purified by flash column chromatography (hexane/EtOAc 10:1) to obtain 87 mg of the desired product as yellow oil. Yield: 87%. The diastereomeric ratio was determined by the crude NMR: 2:1

Diastereomer 1, major:

methyl (5*R*,6*R*,*E*)-5-(4-bromophenyl)-6-(6-nitrobenzoxazol-2-yl)non-2-enoate



IR (CHCl₃, liquid film): 2955, 2946, 2850 (stretch *HC=C*), 1720 (stretch *C=O*, ester), 1562, 1527 (aromatic NO₂), 1435, 1346 (aromatic NO₂), 1269 cm⁻¹.

¹H NMR (400 MHz, CDCl₃) δ 8.43 (d, *J* = 2.0 Hz, 1H, Het), 8.31 (dd, *J* = 8.8, 2.1 Hz, 1H, Het), 7.79 (d, *J* = 8.8 Hz, 1H, Het), 7.47 (dd, *J* = 8.7, 2.0 Hz, 2H, Ar), 7.07 (d, *J* = 8.4 Hz, 2H, Ar), 6.53 (dt, *J* = 15.4, 7.4, 1H, =CHCH₂), 5.49 (dt, *J* = 15.5, 1.4 Hz, 1H, =CHCO₂Me), 3.53 (s, 3H, OCH₃), 3.26 (dtd, *J* = 15.4, 10.3, 4.4 Hz, 2H, CHCH₂, CHCH₂), 2.54 – 2.44 (m, 1H, CH₂CHAR), 2.38 – 2.29 (m, 1H, CH₂CHAR), 1.71 (tdd, *J* = 14.3, 9.7, 7.0 Hz, 1H, CH₂CH₂CH₃), 1.46 – 1.35 (m, 1H, CH₂CH₂CH₃), 1.14 – 1.02 (m, 2H, CH₂CH₃), 0.75 (t, *J* = 7.3 Hz, 3H, CH₃).

¹³C NMR (101 MHz, CDCl₃) δ 173.1 (Cq), 166.1 (Cq), 149.6 (Cq), 146.2 (Cq), 145.2 (Cq), 145.0 (CH), 140.1 (Cq), 132.2 (CH), 129.5 (CH), 122.7 (CH), 121.2 (Cq), 120.6 (CH), 119.8 (CH), 107.3 (CH), 51.3 (CH₃), 48.7 (CH), 46.0 (CH), 37.5 (CH₂), 34.1 (CH₂), 20.4 (CH₂), 13.6 (CH₃).

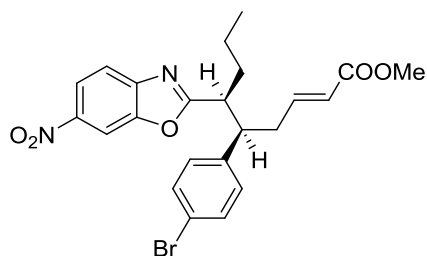
The enantiomeric excess was determined by **HPLC** using a Chiralpak IE column (hexane/*i*PrOH = 70:30, flow rate 1.0 mL/min, λ = 254 nm): *t_r* (major) = 9.5, *t_r* (minor) = 6.6, 90% *ee*.

[α]_D¹⁹ = –2.6 (*c* = 0.5, CHCl₃)

MS (ESI+) *m/z*: 488.8 [M+H]⁺; **HRMS (ESI+)** Exact mass calculated for C₂₃H₂₄Br⁷⁹N₂O₅ [M+H]⁺: 487.0863, found: 487.0855.

Diastereomer 2, minor:

methyl (5*R*,6*S*,*E*)-5-(4-bromophenyl)-6-(6-nitrobenzoxazol-2-yl)non-2-enoate



IR (CHCl₃, liquid film): 2958, 2924, 2854 (stretch HC=C), 1720 (stretch C=O, ester), 1562, 1523 (aromatic NO₂), 1435, 1346 (aromatic NO₂), 1269 cm⁻¹.

¹H NMR (400 MHz, CDCl₃) δ 8.33 (d, *J* = 2.1 Hz, 1H, Het), 8.25 (dd, *J* = 8.8, 2.1 Hz, 1H, Het), 7.69 (d, *J* = 8.7 Hz, 1H, Het), 7.32 – 7.27 (m, 2H, Ar), 6.92 – 6.85 (m, 2H, Ar), 6.72 (dt, *J* = 15.5, 7.2 Hz, 1H, =CHCH₂), 5.79 (dt, *J* = 15.7, 1.3 Hz, 1H, =CHCO₂Me), 3.67 (s, 3H, OCH₃), 3.38 (ddd, *J* = 10.3, 7.8, 4.4 Hz, 1H, CHCH₂), 3.31 – 3.21 (m, 1H, CHCH₂), 2.91 – 2.79 (m, 1H, CHCH₂), 2.69 – 2.58 (m, 1H, CHCH₂), 1.99 – 1.79 (m, 2H, CH₂CH₂CH₃), 1.30 – 1.18 (m, 2H, CH₂CH₃), 0.90 (t, *J* = 7.3 Hz, 3H, CH₃).

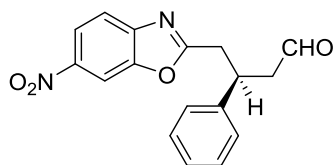
¹³C NMR (101 MHz, CDCl₃) δ 172.4 (Cq), 166.4 (Cq), 149.4 (Cq), 146.1 (Cq), 145.3 (CH), 145.0 (Cq), 139.2 (Cq), 131.7 (CH), 129.6 (CH), 123.4 (CH), 121.1 (Cq), 120.5 (CH), 119.7 (CH), 107.0 (CH), 51.5 (CH₃), 48.0 (CH), 45.7 (CH), 35.4 (CH₂), 33.0 (CH₂), 20.7 (CH₂), 13.8 (CH₃).

The enantiomeric excess was determined by **HPLC** using a Chiralpak IA column (hexane/*i*PrOH = 80:20, flow rate 1.0 mL/min, λ = 254 nm): *t_r* (major) = 8.4, *t_r* (minor) = 13.1, 49% *ee*.

[α]_D¹⁹ = −5.4 (*c* = 0.6, CHCl₃)

MS (ESI+) *m/z*: 488.7 [M+H]⁺; **HRMS (ESI+)** Exact mass calculated for C₂₃H₂₄Br⁷⁹N₂O₅ [M+H]⁺: 487.0863, found: 487.0872.

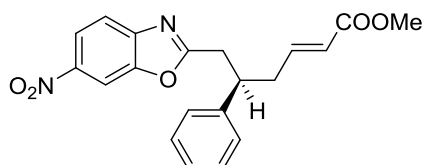
(S)-4-(6-nitrobenzoxazol-2-yl)-3-phenylbutanal (235e) (1st step)



In a vial were added in this sequence: (S)-2-(diphenyl((trimethyl)oxy)methyl)pyrrolidine (18 mg, 0.056 mmol, 20 mol% equiv), cinnamaldehyde (37 mg, 0.281 mmol, 1 equiv), 2-methyl-6-nitrobenzoxazole (50 mg, 0.281 mmol, 1 equiv), Pd(OAc)₂ (13 mg, 0.056 mmol, 20 mol% equiv) and Et₃N (14 mg, 0.141 mmol 50 mol% equiv) and finally CH₃CN (0.5 mL). The reaction mixture was stirred at 30 °C for 24 hours and then concentrated *in vacuo*. The crude was purified by flash column chromatography (hexane/EtOAc 4:1) to obtain 31 mg of the desired product. Yield: 36%

¹H NMR (300 MHz, CDCl₃) δ 9.71 (t, *J* = 1.4 Hz, 1H, CHO), 8.37 (d, *J* = 1.9 Hz, 1H, Het), 8.26 (dd, *J* = 8.8, 2.1 Hz, 1H, Het), 7.73 (d, *J* = 8.9 Hz, 1H), 7.31 – 7.21 (m, 5H, Ph), 4.05 – 3.93 (m, 1H, CHPh), 3.35 (dd, *J* = 7.5, 4.5 Hz, 2H, CH₂Het), 3.04 – 2.95 (m, 2H, CH₂CHO).

methyl (R,E)-6-(6-nitrobenzoxazol-2-yl)-5-phenylhex-2-enoate (276e) (2nd step)



To (S)-4-(6-nitrobenzoxazol-2-yl)-3-phenylbutanal was added methyl(triphenylphosphoranyl)acetate (141 mg, 0.422 mmol, 1.5 equiv) and DCM (0.5 mL) as a solvent. The crude was purified by flash column chromatography (hexane/EtOAc 3:1) to obtain the desired product as yellow oil. Yield: 56%.

IR (CHCl₃, liquid film): 2951, 2920, 2850 (stretch HC=C), 1720 (stretch C=O, ester), 1570, 1527 (aromatic NO₂), 1435, 1346 (aromatic NO₂), 1269 cm⁻¹.

¹H NMR (300 MHz, CDCl₃) δ 8.35 (d, *J* = 2.1 Hz, 1H, Het), 8.26 (dd, *J* = 8.8, 2.1 Hz, 1H, Het), 7.72 (d, *J* = 8.8 Hz, 1H, Het), 7.36 – 7.17 (m, 5H, Ph), 6.88 – 6.74 (m, 1H, =CHCH₂),

5.80 (d, $J = 15.6$ Hz, 1H, $=\text{CHCO}_2\text{Me}$), 3.65 (s, 3H, OCH_3), 3.62 – 3.46 (m, 1H, CHPh), 3.32 (dd, $J = 7.6, 3.8$ Hz, 2H, CH_2Het), 2.69 (td, $J = 7.2, 1.3$ Hz, 2H, CH_2CH).

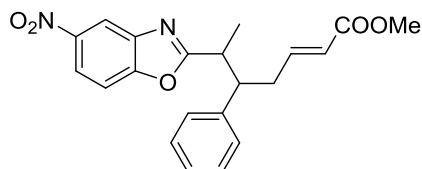
^{13}C NMR (101 MHz, CDCl_3) δ 169.9 (Cq), 166.4 (Cq), 149.8 (Cq), 146.5 (Cq), 145.4 (CH), 145.1 (Cq), 141.7 (Cq), 128.9 (CH), 127.4 (CH), 127.1 (CH), 123.3 (CH), 120.4 (CH), 119.6 (CH), 107.0 (CH), 51.5 (CH_3), 42.9 (CH), 38.6 (CH_2), 35.4 (CH_2).

The enantiomeric excess was determined by **HPLC** using a Chiralpak IE column (hexane/*i*PrOH = 80:20, flow rate 1.0 mL/min, $\lambda = 230$ nm): t_r (major) = 29.7, t_r (minor) = 26.5, 49% *ee*.

$[\alpha]_D^{19} = +8.33^\circ$ ($c = 0.33$, CHCl_3)

MS (ESI+) m/z : 367.0 $[\text{M}+\text{H}]^+$; **HRMS (ESI+)** Exact mass calculated for $\text{C}_{20}\text{H}_{19}\text{N}_2\text{O}_5$ $[\text{M}+\text{H}]^+$: 367.1288, found: 367.1281.

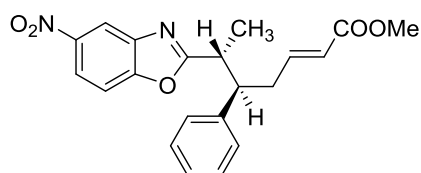
methyl (*E*)-6-(5-nitrobenzoxazol-2-yl)-5-phenylhept-2-enoate (276b)



The reaction was performed following the general procedure adding: the organic catalyst (*S*)-2-(((*tert*-butyldimethylsilyl)oxy)diphenylmethyl)pyrrolidine (38 mg, 0.260 mmol, 20 mol% equiv), cinnamaldehyde (137 mg, 1.040 mmol, 2 equiv), 2-ethyl-5-nitrobenzoxazole (100 mg, 0.520 mmol, 1 equiv), $\text{Pd}(\text{OAc})_2$ (6 mg, 0.026 mmol, 5 mol% equiv) and CH_3CN (1 mL). To the crude solution was finally added TEA (26 mg, 0.260 mmol, 50 mol% equiv). The first reaction was stirred at 35 °C for 10 days before performing the Wittig. The final crude was purified by flash column chromatography (hexane/EtOAc 5:1) to obtain 84 mg of the desired product as yellow oil. Yield: 42%. The diastereomeric ratio was determined by the crude NMR: 1.5:1

Diastereomer 1, major:

methyl (5*R*,6*R*,*E*)-6-(5-nitrobenzoxazol-2-yl)-5-phenylhept-2-enoate



IR (CHCl₃, liquid film): 2955, 2923, 2854 (stretch *HC=C*), 1720 (stretch *C=O*, ester), 1527 (aromatic NO₂), 1454, 1439, 1346 (aromatic NO₂) cm⁻¹.

¹H NMR (400 MHz, CDCl₃) δ 8.58 (d, *J* = 2.1 Hz, 1H, Het), 8.31 (dd, *J* = 8.9, 2.3 Hz, 1H, Het), 7.62 (d, *J* = 8.8 Hz, 1H, Het), 7.36 – 7.30 (m, 3H, Ph), 7.18 (dd, *J* = 5.3, 3.1 Hz, 2H, Ph), 6.62 (ddd, *J* = 15.5, 7.8, 6.8 Hz, 1H, =CHCH₂), 5.56 (dt, *J* = 15.6, 1.3 Hz, 1H, =CHCO₂Me), 3.54 (s, 3H, OCH₃), 3.42 (dq, *J* = 9.6, 7.0 Hz, 1H, CHCH₃), 3.26 (td, *J* = 9.1, 5.8 Hz, 1H, CHCH₂), 2.60 (dddd, *J* = 15.4, 8.5, 6.7, 1.5 Hz, 1H, CH₂), 2.52 – 2.43 (m, 1H, CH₂), 1.23 (d, *J* = 6.9 Hz, 3H, CH₃).

¹³C NMR (101 MHz, CDCl₃) δ 172.5 (Cq), 166.3 (Cq), 154.0 (Cq), 145.7 (CH), 145.3 (Cq), 141.6 (Cq), 140.5 (Cq), 128.9 (CH), 127.9 (CH), 127.4 (CH), 122.5 (CH), 121.0 (CH), 116.3 (CH), 110.8 (CH), 51.3 (CH₃), 49.6 (CH), 40.1 (CH), 37.4 (CH₂), 17.0 (CH₃).

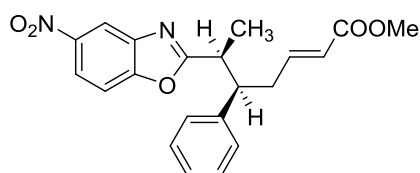
The enantiomeric excess was determined by **HPLC** using a Chiralpak IE column (hexane/*i*PrOH = 90:10, flow rate 1.0 mL/min, λ = 230 nm): *t_r* (major) = 48.3, *t_r* (minor) = 52.2, 12% *ee*.

$[\alpha]_D^{20}$ = –2.8 (*c* = 0.5, CHCl₃)

MS (ESI+) *m/z*: 381.1 [M+H]⁺; **HRMS (ESI+)** Exact mass calculated for C₂₁H₂₁N₂O₅ [M+H]⁺: 381.1445, found: 381.1449.

Diastereomer 2, minor:

methyl (5*R*,6*S*,*E*)-6-(5-nitrobenzoxazol-2-yl)-5-phenylhept-2-enoate



IR (CHCl₃, liquid film): 2954, 2924, 2850 (stretch HC=C), 1720 (stretch C=O, ester), 1531 (aromatic NO₂), 1457, 1439, 1346 (aromatic NO₂) cm⁻¹.

¹H NMR (400 MHz, CDCl₃) δ 8.51 (d, J = 2.2 Hz, 1H, Het), 8.25 (dd, J = 8.9, 2.3 Hz, 1H, Het), 7.51 (d, J = 8.9 Hz, 1H, Het), 7.23 – 7.16 (m, 3H, Ph), 7.08 – 7.04 (m, 2H, Ph), 6.76 (dt, J = 15.5, 7.2 Hz, 1H, =CHCH₂), 5.80 (dt, J = 15.7, 1.4 Hz, 1H, =CHCO₂Me), 3.63 (s, 3H, OCH₃), 3.49 (p, $J_1 = J_2$ = 6.9 Hz, 1H, CHCH₃), 3.39 – 3.31 (m, 1H, CHCH₂), 2.86 – 2.69 (m, 2H, CH₂), 1.49 (d, J = 7.0 Hz, 3H, CH₃).

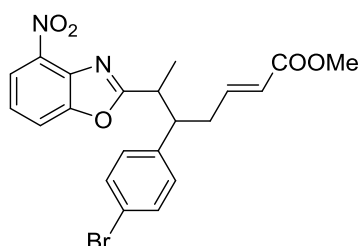
¹³C NMR (101 MHz, CDCl₃) δ 171.8 (Cq), 166.5 (Cq), 153.9 (Cq), 146.0 (CH), 145.2 (Cq), 141.4 (Cq), 140.2 (Cq), 128.6 (CH), 127.9 (CH), 127.2 (CH), 123.0 (CH), 120.8 (CH), 116.2 (CH), 110.5 (CH), 51.4 (CH₃), 48.9 (CH), 40.0 (CH), 34.3 (CH₂), 15.2 (CH₃).

The enantiomeric excess was determined by **HPLC** using a Chiralpak IE column (hexane/*i*PrOH = 90:10, flow rate 1.0 mL/min, λ = 230 nm): t_r (major) = 48.6, t_r (minor) = 50.5, 31% *ee*.

$[\alpha]_D^{20}$ = -1.2 (c = 0.3, CHCl₃)

MS (ESI+) m/z : 381.1 [M+H]⁺; **HRMS (ESI+)** Exact mass calculated for C₂₁H₂₁N₂O₅ [M+H]⁺: 381.1445, found: 381.1450.

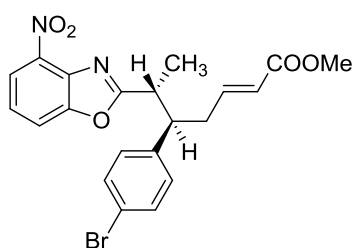
methyl (*E*)-5-(4-bromophenyl)-6-(4-nitrobenzoxazol-2-yl)hept-2-enoate (276c)



The reaction was performed following the general procedure adding: the organic catalyst (*S*)-2-(((tert-butyldimethylsilyl)oxy)diphenylmethyl)pyrrolidine (38 mg, 0.260 mmol, 20 mol% equiv), cinnamaldehyde (220 mg, 1.560 mmol, 3 equiv), 2-ethyl-4-nitrobenzoxazole (100 mg, 0.520 mmol, 1 equiv), Pd(OAc)₂ (6 mg, 0.026 mmol, 5 mol% equiv) and CH₃CN (1 mL). To the crude solution was finally added TEA (26 mg, 0.260 mmol, 50 mol% equiv). The first reaction was stirred at 35 °C for 10 days before performing the Wittig. The final crude was purified by flash column chromatography (hexane/EtOAc 10:1) to obtain 84 mg of the desired product as yellow oil. Yield: 36%. The diastereomeric ratio was determined by the crude NMR: 1:1

Diastereomer 1:

methyl (*5R,6R,E*)-5-(4-bromophenyl)-6-(4-nitrobenzoxazol-2-yl)hept-2-enoate



IR (CHCl₃, liquid film): 2924 (stretch, HC=C), 1720 (stretch, C=O, ester), 1528, 1487, 1435, 1342 (aromatic NO₂) cm⁻¹.

¹H NMR (400 MHz, CDCl₃) δ 8.21 (dd, *J* = 8.2, 0.6 Hz, 1H, Het), 7.85 (dd, *J* = 8.1, 0.7 Hz, 1H, Het), 7.49 (d, *J* = 8.4 Hz, 3H, Ar, Het), 7.10 (d, *J* = 8.4 Hz, 2H, Ar), 6.56 (dt, *J* = 15.2, 7.6 Hz, 1H, =CHCH₂), 5.54 (d, *J* = 15.6 Hz, 1H, =CHCO₂Me), 3.55 (s, 3H, OCH₃), 3.53 (dd, *J* = 7.0, 3.3 Hz, 1H, CHCH₃), 3.27 (td, *J* = 9.4, 5.7 Hz, 1H, CHCH₂), 2.62 – 2.51 (m, 1H, CH₂), 2.48 – 2.38 (m, 1H, CH₂), 1.25 (d, *J* = 7.0 Hz, 3H, CH₃).

¹³C NMR (101 MHz, CDCl₃) δ 171.4 (Cq), 165.2 (Cq), 151.2 (Cq), 144.1 (CH), 138.7 (Cq), 138.1 (Cq), 134.7 (Cq), 131.1 (CH), 128.6 (CH), 123.4 (CH), 121.7 (CH), 120.2 (Cq), 119.8 (CH), 115.7 (CH), 50.3 (CH₃), 48.1 (CH), 39.2 (CH), 36.5 (CH₂), 16.2 (CH₃).

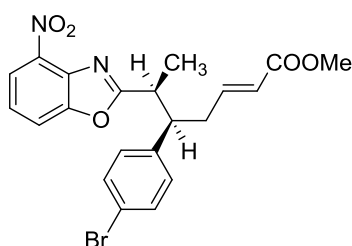
The enantiomeric excess was determined by **HPLC** using a Chiralpak ID column (hexane/*i*PrOH = 90:10, flow rate 1.0 mL/min, λ = 254 nm): *t_r* (major) = 47.1, *t_r* (minor) = 39.0, 77% *ee*.

[α]_D²⁰ = −29.2 (*c* = 0.12, CHCl₃)

HRMS (ESI+) Exact mass calculated for C₂₁H₂₀Br⁷⁹N₂O₅ [M+H]⁺: 459.0550, found: 459.0561.

Diastereomer 2:

methyl (5*R*,6*S*,*E*)-5-(4-bromophenyl)-6-(4-nitrobenzoxazol-2-yl)hept-2-enoate



IR (CHCl₃, liquid film): 2949 (stretch, HC=C), 1720 (stretch, C=O, ester), 1528, 1488, 1435, 1342 (aromatic NO₂) cm^{−1}.

¹H NMR (400 MHz, CDCl₃) δ 8.14 (d, *J* = 8.2 Hz, 1H, Het), 7.74 (d, *J* = 8.1 Hz, 1H, Het), 7.43 (t, *J* = 8.2 Hz, 1H, Het), 7.33 (d, *J* = 8.4 Hz, 2H, Ar), 7.00 (d, *J* = 8.4 Hz, 2H, Ar), 6.72 (dt, *J* = 15.0, 7.2 Hz, 1H, =CHCH₂), 5.79 (d, *J* = 15.6 Hz, 1H, =CHCO₂Me), 3.65 (s, 3H, OCH₃), 3.63 – 3.57 (m, 1H, CHCH₃), 3.38 (ddd, *J* = 9.7, 7.5, 5.1 Hz, 1H, CHCH₂), 2.89 – 2.79 (m, 1H, CH₂), 2.75 – 2.63 (m, 1H, CH₂), 1.53 (d, *J* = 7.0 Hz, 3H, CH₃).

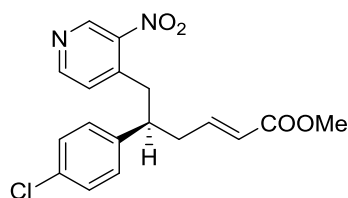
¹³C NMR (101 MHz, CDCl₃) δ 172.5 (Cq), 166.2 (Cq), 152.2 (Cq), 145.1 (CH), 139.8 (Cq), 139.1 (Cq), 135.7 (Cq), 132.1 (CH), 129.6 (CH), 124.4 (CH), 122.8 (CH), 121.3 (Cq), 120.9 (CH), 116.7 (CH), 51.4 (CH₃), 49.1 (CH), 40.2 (CH), 37.5 (CH₂), 17.2 (CH₃).

The enantiomeric excess was determined by **HPLC** using a Chiralpak ID column (hexane/*i*PrOH = 90:10, flow rate 1.0 mL/min, λ = 254 nm): t_r (major) = 38.3, t_r (minor) = 52.1, 20% *ee*.

$[\alpha]_D^{20} = -15.0$ ($c = 0.06$, CHCl_3)

HRMS (ESI+) Exact mass calculated for $\text{C}_{21}\text{H}_{20}\text{Br}^{79}\text{N}_2\text{O}_5$ $[\text{M}+\text{H}]^+$: 459.0550, found: 459.0561.

methyl (*R,E*)-5-(4-chlorophenyl)-6-(4-nitropyridin-3-yl)hex-2-enoate (276h)



The reaction was performed following the general procedure adding: the organic catalyst (*S*)-2-(diphenyl((triethylsilyl)oxy)methyl)pyrrolidine (18 mg, 0.181 mmol, 20 mol% equiv), (*E*)-3-(4-chlorophenyl)acrylaldehyde (121 mg, 0.724 mmol, 2 equiv), 4-methyl-3-nitropyridine (50 mg, 0.362 mmol, 1 equiv), $\text{Pd}(\text{OAc})_2$ (4 mg, 0.018 mmol, 5 mol% equiv) and CH_3CN (1 mL). To the crude solution was finally added TEA (18 mg, 0.181 mmol, 50 mol% equiv). The first reaction was stirred at 35 °C for 24 hours before performing the Wittig. The final crude was purified by flash column chromatography (hexane/EtOAc 5:1) to obtain 77 mg of the desired product as yellow oil. Yield: 59%.

IR (CHCl_3 , liquid film): 2949 (stretch $\text{HC}=\text{C}$), 1717 (stretch $\text{C}=\text{O}$, ester), 1600, 1526, 1492, 1350 (aromatic NO_2) cm^{-1} .

^1H NMR (400 MHz, CDCl_3) δ 9.08 (s, 1H, Het), 8.51 (d, $J = 5.0$ Hz, 1H, Het), 7.22 (d, $J = 8.2$ Hz, 2H, Ar), 6.97 (d, $J = 8.3$ Hz, 2H, Ar), 6.85 (d, $J = 5.1$ Hz, 1H, Het), 6.76 (dt, $J = 15.3, 7.2$ Hz, 1H, $=\text{CHCH}_2$), 5.79 (d, $J = 15.6$ Hz, 1H, $=\text{CHCO}_2\text{Me}$), 3.68 (s, 3H, OCH_3), 3.44 (dd, $J = 12.0, 3.9$ Hz, 1H, CHAr), 3.17 – 3.01 (m, 2H, CH_2Het), 2.65 (t, $J = 7.0$ Hz, 2H, CH_2CH).

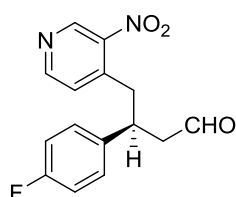
¹³C NMR (101 MHz, CDCl₃) δ 166.4 (Cq), 152.7 (CH), 146.1 (CH), 145.8 (Cq), 145.2 (CH), 143.50 (Cq), 139.8 (Cq), 133.1 (Cq), 129.0 (CH), 128.8 (CH), 126.6 (CH), 123.5 (CH), 51.5 (CH₃), 45.0 (CH), 39.3 (CH₂), 38.6 (CH₂).

The enantiomeric excess was determined by **HPLC** using a Chiralpak IA column (hexane/*i*PrOH = 90:10, flow rate 1.0 mL/min, λ = 254 nm): *t_r* (major) = 19.3, *t_r* (minor) = 21.9, 78% *ee*.

[α]_D¹⁹ = −27.5° (*c* = 1.5, CHCl₃)

MS (ESI+) *m/z*: 361.9 [M+H]⁺; **HRMS (ESI+)** Exact mass calculated for C₁₈H₁₈Cl³⁵N₂O₄ [M+H]⁺: 361.0950, found: 361.0955.

(S)-3-(4-fluorophenyl)-4-(4-nitropyridin-3-yl)butanal (235d) (1st step)

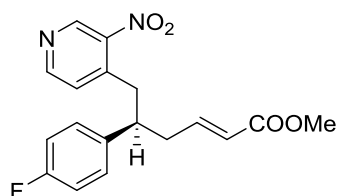


In a vial were added in this sequence:

(S)-2-(diphenyl((triethylsilyl)oxy)methyl)pyrrolidine (26 mg, 0.072 mmol, 20 mol% equiv), (*E*)-3-(4-fluorophenyl)acrylaldehyde (109 mg, 0.724 mmol, 2 equiv), 4-methyl-3-nitropyridine (50 mg, 0.362 mmol, 1 equiv), Pd(OAc)₂ (4 mg, 0.018 mmol, 5 mol% equiv) and TEA (18 mg, 0.181 mmol, 50 mol% equiv) and finally CH₃CN (0.5 mL). The reaction mixture was stirred at 35 °C for 24 hours and then concentrated *in vacuo*. The crude was purified by flash column chromatography (hexane/EtOAc 5:1) to obtain 69 mg of the desired product. Yield: 61%. The ¹H-NMR is consistent with the one provided in literature.^[90]

[α]_D¹⁸ = −4.65 (*c* = 0.01, DCM)

methyl (*R,E*)-5-(4-fluorophenyl)-6-(4-nitropyridin-3-yl)hex-2-enoate (276g) (2nd step)



To (*S*)-3-(4-fluorophenyl)-4-(4-nitropyridin-3-yl)butanal was added an excess of methyl(triphenyl-phosphoranylidene) acetate and DCM (0.5 mL) as a solvent. The crude was purified by flash column chromatography (hexane/EtOAc 5:1) to obtain 40 mg of the desired product as yellow oil. Yield: 52%.

IR (CHCl₃, liquid film): 2951 (stretch HC=C), 2361, 1718 (stretch C=O, ester), 1602, 1527, 1509, 1350 (aromatic NO₂) cm⁻¹.

¹H NMR (400 MHz, CDCl₃) δ 9.27 (s, 1H, Het), 8.70 (d, J = 5.1 Hz, 1H, Het), 7.22 – 7.09 (m, 4H, Ar), 7.04 (d, J = 5.1 Hz, 1H, Het), 6.97 (dt, J = 15.0, 7.3 Hz, 1H, =CHCH₂), 5.99 (d, J = 15.6 Hz, 1H, =CHCO₂Me), 3.88 (s, 3H, OCH₃), 3.63 (dd, J = 12.1, 4.0 Hz, 1H, CHAr), 3.36 – 3.20 (m, 2H, CH₂Het), 2.85 (t, J = 6.7 Hz, 2H, CH₂CH).

¹³C NMR (101 MHz, CDCl₃) δ 166.4 (Cq), 161.8 (d, J = 246 Hz, Cq), 152.7 (CH), 146.1 (CH), 145.9 (Cq), 145.4 (CH), 143.6 (Cq), 137.0 (d, J = 3.3 Hz, Cq), 129.0 (d, J = 8.0 Hz, CH), 126.6 (CH), 123.4 (CH), 115.7 (d, J = 21.3 Hz, CH), 51.5 (CH₃), 44.9 (CH), 39.5 (CH₂), 38.8 (CH₂).

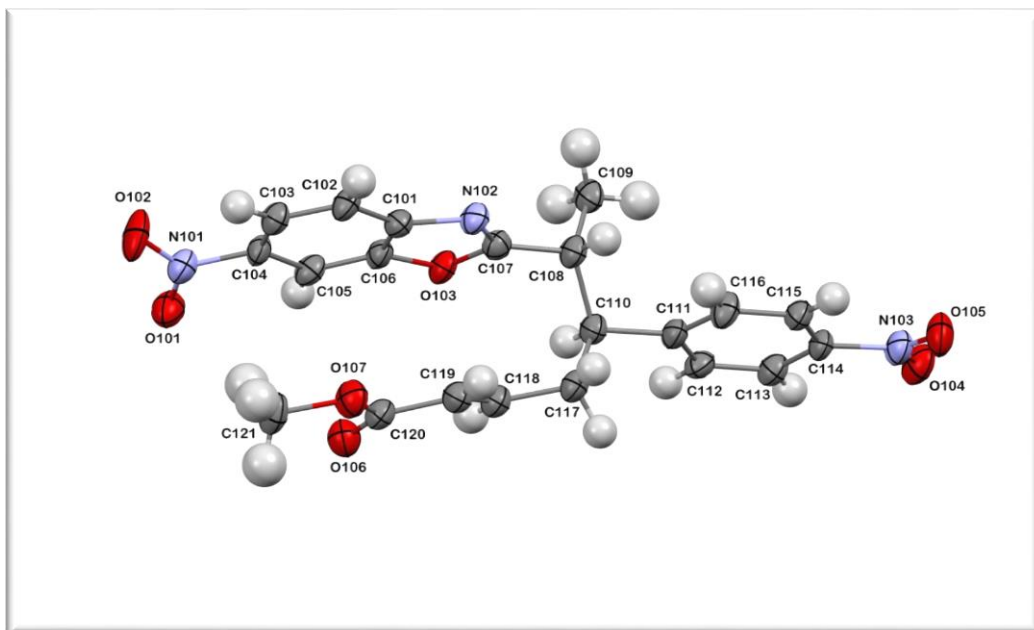
¹⁹F NMR (376 MHz, CDCl₃) δ -115.04.

The enantiomeric excess was determined by **HPLC** using a Chiralpak IA column (hexane/*i*PrOH = 80:20, flow rate 1.0 mL/min, λ = 254 nm): t_r (major) = 9.6, t_r (minor) = 34.3, 89% *ee*.

$[\alpha]_D^{19}$ = +8.5° (c = 1.7, CHCl₃)

MS (ESI+) m/z : 345.1 [M+H]⁺; **HRMS (ESI+)** Exact mass calculated for C₁₈H₁₈FN₂O₄ [M]⁺: 345.1245, found: 345.1255.

6.1.6 Crystallographic data (**259f** major diastereomer)



Single-crystal X-Ray diffraction data of **259f** were collected at 100 K on Rigaku AFC12 goniometer equipped with an enhanced sensitivity (HG) Saturn 724+ detector mounted at the window of an FR-E+ Superbright MoK α rotating anode generator with HF Varimax optics.^[193] Unit cell parameters were refined against all data. An empirical absorption correction was carried out using CrystalClear software (CrystalClear-SM Expert 3.1ba16 (Rigaku, 2012)). The crystal structure of **259f** was solved by charge flipping methods^[194] and refined on F_o^2 by full-matrix least-squares refinements using programs of the SHELX-2013 software.^[195] All non-hydrogen atoms were refined with anisotropic displacement parameters. All hydrogen atoms were added at calculated positions and refined using a riding model with isotropic displacement parameters based on the equivalent isotropic displacement parameter (U_{eq}) of the parent atom.

Crystal data for **259f**: $C_{21}H_{19}N_3O_7$, $M_r = 425.39$, light brown lath, $0.20 \times 0.03 \times 0.01$ mm³, Monoclinic, $C2$, $a = 17.969(2)$, $b = 11.0559(15)$, $c = 19.839(3)$ Å, $\beta = 90.528(6)^\circ$, $V = 3941.0(9)$ Å³, $Z = 8$, $Z' = 2$, $D_c = 1.434$ g cm⁻³, $\mu = 0.110$ mm⁻¹, $T = 100$ K, 25946 collected reflections, 8604 unique reflections ($R_{int} = 0.0895$), 4448 reflections with $F^2 > 2\sigma$, $R(F^2 > 2\sigma) = 0.0596$, $wR2 = 0.1285$, $GoF = 0.893$. Crystallographic data (excluding structure factors) for the structure **259f** have been deposited with the Cambridge Crystallographic Data Centre with CCDC number 1001853. Copies of the

data can be obtained, free of charge, on application to Cambridge Crystallographic Data Centre, 12 Union Road, Cambridge CB2 1EZ, UK, (fax: +44-(0)1223-336033 or e-mail: deposit@ccdc.cam.ac.uk).

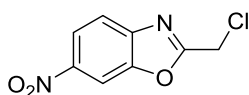
6.2 Synergistic catalysis: *cis*-cyclopropanation of benzoxazoles

6.2.1 Synthesis of the starting material: benzoxazoles (391)

General procedure:

In a round bottom flask, equipped with a condenser, were added 1 equivalent of aminophenol (**237**) followed by 1.1 equivalents of 2-chloro-1,1,1-triethoxyethane (**398**). The reaction mixture is stirred and heated. The reaction is followed by TLC. After the reaction is completed, the crude is purified by recrystallization or by flash column chromatography (*n*-hexane/EtOAc) to obtain the desired benzoxazole.

2-(chloromethyl)-6-nitrobenzoxazole (391a)



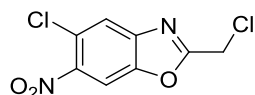
The reaction was performed following the general procedure adding 2-amino-5-nitrophenol (712 mg, 4.623 mmol, 1 equiv) and 2-chloro-1,1,1-triethoxyethane (1 g, 5.085 mmol, 1.1 equiv). The reaction mixture was stirred at 100 °C for 4 hours. The crude was purified by recrystallization with EtOH/H₂O to obtain 584 mg of the desired product as dark orange solid. Yield: 59%.

¹H NMR (400 MHz, CDCl₃) δ 8.49 (s, 1H, Het), 8.35 (d, *J* = 8.6 Hz, 1H, Het), 7.87 (d, *J* = 8.7 Hz, 1H, Het), 4.81 (s, 2H, CH₂).

¹³C NMR (101 MHz, CDCl₃) δ 165.4 (Cq), 150.3 (Cq), 145.9 (Cq), 145.9 (Cq), 120.9 (CH), 120.7 (CH), 107.7 (CH), 35.9 (CH₂).

HRMS *m/z* (ESI+) Exact mass calculated for C₈H₆Cl³⁵N₂O₃ [M+H]⁺: 213.0061, found: 213.0062.

5-chloro-2-(chloromethyl)-6-nitrobenzoxazole (391b)



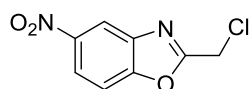
The reaction was performed following the general procedure adding 2-amino-4-chloro-5-nitrophenol (1.66 g, 8.801 mmol, 1 equiv) and 2-chloro-1,1,1-triethoxyethane (1.9 g, 9.681 mmol, 1.1 equiv). The reaction mixture was stirred at 100 °C for 19 hours. The crude was purified by recrystallization with EtOH/H₂O to obtain 1.715 g of the desired product as dark brown solid. Yield: 79%.

¹H NMR (400 MHz, CDCl₃) δ 8.15 (s, 1H, Het), 7.94 (s, 1H, Het), 4.80 (s, 2H, CH₂).

¹³C NMR (101 MHz, CDCl₃) δ 165.9 (Cq), 148.5 (Cq), 145.6 (Cq), 144.3 (Cq), 124.0 (Cq), 123.2 (CH), 109.0 (CH), 35.7 (CH₂).

HRMS *m/z* (ESI+) Exact mass calculated for C₈H₅Cl³⁵N₂O₃ [M+H]⁺: 246.9672, found: 246.9671.

2-(chloromethyl)-5-nitrobenzoxazole (391c)



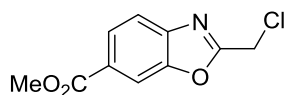
The reaction was performed following the general procedure adding 2-amino-4-nitrophenol (712 mg, 4.623 mmol, 1 equiv) and 2-chloro-1,1,1-triethoxyethane (1 g, 5.085 mmol, 1.1 equiv). The reaction mixture was stirred at 80 °C for 12 hours. The residual solvent was evaporated under *vacuum* to obtain 686 mg of the desired product as brown solid. Yield: 70%.

¹H NMR (400 MHz, CDCl₃) δ 8.65 (d, *J* = 1.9 Hz, 1H, Het), 8.37 (dd, *J* = 9.0, 2.1 Hz, 1H, Het), 7.69 (d, *J* = 9.0 Hz, 1H, Het), 4.80 (s, 2H, CH₂).

¹³C NMR (101 MHz, CDCl₃) δ 164.0 (Cq), 154.5 (Cq), 145.6 (Cq), 141.2 (Cq), 122.0 (CH), 117.1 (CH), 111.3 (CH), 35.9 (CH₂).

HRMS m/z (ESI+) Exact mass calculated for $C_8H_6Cl^{35}N_2O_3$ $[M+H]^+$: 213.0061, found: 213.0062.

methyl 2-(chloromethyl)benzoxazole-6-carboxylate (391d)



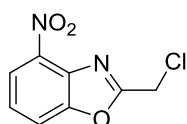
The reaction was performed following the general procedure adding methyl 4-amino-3-hydroxybenzoate (980 mg, 5.862 mmol, 1 equiv) and 2-chloro-1,1,1-triethoxyethane (1.27 g, 6.448 mmol, 1.1 equiv). The reaction mixture was stirred at 100 °C for 19 hours. The crude was purified by recrystallization with EtOH/H₂O to obtain 1.250 g of the desired product as light brown solid. Yield: 95%.

¹H NMR (400 MHz, CDCl₃) δ 8.24 (d, J = 1.0 Hz, 1H, Het), 8.09 (dd, J = 8.4, 1.4 Hz, 1H, Het), 7.77 (d, J = 8.4 Hz, 1H, Het), 4.78 (s, 2H, CH₂), 3.96 (s, 3H, OCH₃).

¹³C NMR (101 MHz, CDCl₃) δ 166.3 (Cq), 163.5 (Cq), 150.8 (Cq), 144.6 (Cq), 128.1 (Cq), 126.5 (CH), 120.2 (CH), 112.6 (CH), 52.5 (CH₃), 36.2 (CH₂).

HRMS m/z (ESI+) Exact mass calculated for $C_{10}H_9Cl^{35}NO_3$ $[M+H]^+$: 226.0265, found: 226.0269.

2-(chloromethyl)-4-nitrobenzoxazole (391e)

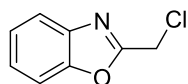


The reaction was performed following the general procedure adding 2-amino-3-nitrophenol (1.355 g, 8.791 mmol, 1 equiv) and 2-chloro-1,1,1-triethoxyethane (1.9 g, 9.670 mmol, 1.1 equiv). The reaction mixture was stirred at 100 °C for 12 hours. The crude was purified by recrystallization with EtOH/H₂O to obtain 720 mg of the desired product as light brown solid. Yield: 93%.

¹H NMR (400 MHz, CDCl₃) δ 8.25 (d, *J* = 8.2 Hz, 1H, Het), 7.94 (d, *J* = 8.2 Hz, 1H, Het), 7.59 (t, *J* = 8.2 Hz, 1H, Het), 4.88 (s, 2H, CH₂).

The ¹H-NMR is consistent with the one provided in literature.^[196]

2-(chloromethyl)benzoxazole (391f)



The reaction was performed following the general procedure adding 2-aminophenol (640 mg, 5.865 mmol, 1 equiv) and 2-chloro-1,1,1-triethoxyethane (1.27 g, 6.451 mmol, 1.1 equiv). The reaction mixture was stirred at 80 °C for 20 hours. The crude was purified by flash column chromatography (*n*-hexane/EtOAc 5:1) to obtain 490 mg of the desired product as light orange oil. Yield: 54%.

¹H NMR (400 MHz, CDCl₃) δ 7.75 (dd, *J* = 6.7, 2.4 Hz, 1H, Het), 7.56 (dd, *J* = 6.9, 2.2 Hz, 1H, Het), 7.43 – 7.32 (m, 2H, Het), 4.76 (s, 2H, CH₂).

The ¹H-NMR is consistent with the one provided in literature.^[197]

6.2.2 Synthesis of the starting material: α,β -unsaturated aldehydes (**80**)

The starting aldehydes were synthesised through a Wittig reaction, following the procedure described in literature. In a round bottom flask a substituted benzaldehyde derivative **63** (2 equiv) and (triphenylphosphoranyldiene)acetaldehyde **250** (1 equiv) were stirred in anhydrous toluene under reflux at 50 °C under argon. The crude mixture was purified by a flash column chromatography.

The aldehydes **80a** and **80b** are commercially available (Sigma-Aldrich).

The ^1H -NMR of the aldehydes (*E*)-3-(4-bromophenyl)acrylaldehyde (**80h**), (*E*)-3-(*p*-tolyl)acrylaldehyde (**80k**) and (*E*)-3-(4-chlorophenyl)acrylaldehyde (**80e**) are consistent with the ones provided in literature.^[185]

The ^1H -NMR of the aldehydes (*E*)-3-(4-nitrophenyl)acrylaldehyde (**80i**) and (*E*)-3-(2-bromophenyl)acrylaldehyde (**80c**) are consistent with the ones provided in literature.^[186]

The ^1H -NMR of the aldehyde (*E*)-3-(4-fluorophenyl)acrylaldehyde (**80j**) is consistent with the ones provided in literature.^[187]

The ^1H -NMR of the aldehyde (*E*)-4-(3-oxoprop-1-en-1-yl)benzonitrile (**80g**) is consistent with the ones provided in literature.^[198]

The ^1H -NMR of the aldehyde ethyl (*E*)-4-oxobut-2-enoate (**80m**) is consistent with the ones provided in literature.^[199]

The ^1H -NMR of the aldehyde (*E*)-3-(3-bromophenyl)acrylaldehyde (**80d**) is consistent with the ones provided in literature.^[200]

6.2.3 General procedure for the synthesis of cyclopropanes (392, 402)

In a closed vial were added in this sequence: the organic catalyst 2-(diphenyl((trimethylsilyl)oxy)methyl)pyrrolidine (20 mol% equiv), α,β -unsaturated aldehyde (2 equiv), azaarene (1 equiv), $\text{Pd}(\text{OAc})_2$ (5 mol% equiv) and CH_3CN (1 mL). To the reaction mixture, was finally added 2,6-lutidine (1 equiv). The reaction mixture was stirred at room temperature and then concentrated *in vacuo*. The crude was purified by flash column chromatography (*n*-hexane/EtOAc) to obtain the desired product.

The stereochemistry of the final compounds was ascertained by X-ray and circular dichroism studies carried out by Andrea Mazzanti. In **Figure 25** is drawn the absolute configuration of the cyclopropanes synthesised.

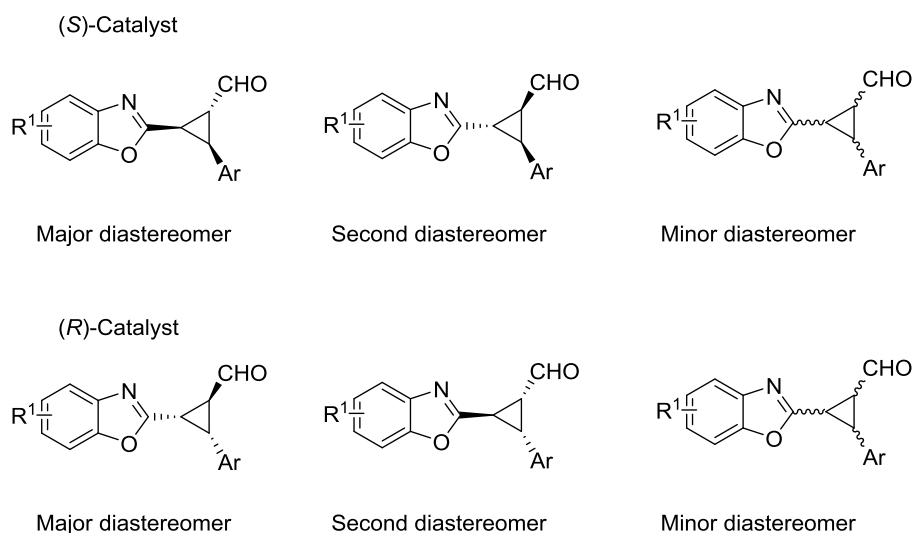
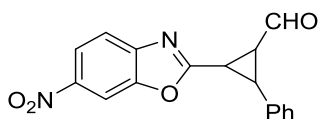


Figure 25. Stereochemistry of the products for each enantiomer of the catalyst

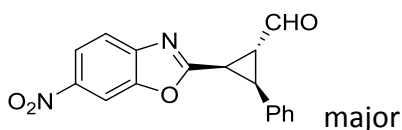
6.2.4 Final products characterisation

Compound 392a



The reaction was performed following the general procedure adding: 2-(diphenyl((trimethylsilyl)oxy)methyl)pyrrolidine (306 mg, 0.941 mmol, 20 mol% equiv), cinnamaldehyde (1.243 g, 9.408 mmol, 2 equiv), 2-(chloromethyl)-6-nitrobenzoxazole (1 g, 4.704 mmol, 1 equiv), Pd(OAc)₂ (53 mg, 0.235 mmol, 5 mol% equiv), CH₃CN (10 mL) and 2,6-lutidine (504 mg, 4.704 mmol, 1 equiv). The crude was purified by flash column chromatography (hexane/EtOAc 10:1) to obtain 1.289 g of the desired products as dark yellow oil. Yield: 89%. The diastereomeric ratio was calculated based on the isolated products after column chromatography. dr: 4.5:1.2:1

(1R,2R,3S)-2-(6-nitrobenzoxazol-2-yl)-3-phenylcyclopropane-1-carbaldehyde



IR (CHCl₃, liquid film): 2922, 2851, 1709 (CHO), 1570 (aromatic NO₂), 1525, 1345 (aromatic NO₂), 758 cm⁻¹.

¹H NMR (400 MHz, CDCl₃) δ 9.89 (d, *J* = 2.8 Hz, 1H, CHO), 8.24 – 8.18 (m, 2H, Het), 7.64 (d, *J* = 8.6 Hz, 1H, Het), 7.24 – 7.16 (m, 5H, Ph), 3.57 (ddd, *J* = 5.6, 5.6, 2.8 Hz, 1H, CHCHO), 3.41 (bd, *J* = 5.5 Hz, 2H, CHHet, CHPh).

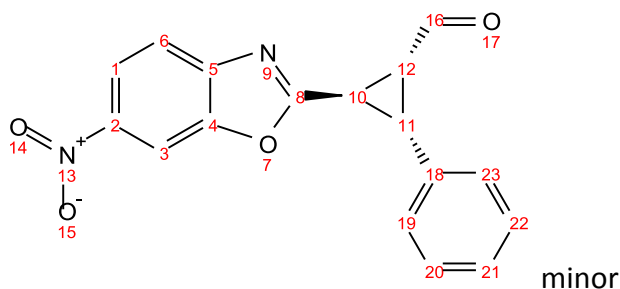
¹³C NMR (101 MHz, CDCl₃) δ 197.4 (CHO), 166.7 (Cq), 150.0 (Cq), 146.3 (Cq), 145.2 (Cq), 133.0 (Cq), 128.8 (CH), 128.7 (CH), 128.0 (CH), 120.7 (CH), 119.7 (CH), 107.0 (CH), 34.9 (CH), 34.5 (CH), 26.24 (CH).

The enantiomeric excess was determined by **HPLC** using a Chiralpak IA column (hexane/*i*PrOH = 85:15, flow rate 1.0 mL/min, λ = 210 nm): *t_r* (S) = 16.1, *t_r* (R) = 17.0, 96% (R) and 99% (S) *ee*.

$[\alpha]_D^{22} = -107.6^\circ$ ($c = 0.1$, CHCl_3) (**S catalyst**)

HRMS m/z (ESI+) Exact mass calculated for $\text{C}_{17}\text{H}_{13}\text{N}_2\text{O}_4$ $[\text{M}+\text{H}]^+$: 309.0870, found: 309.0872.

(1*R*,2*R*,3*R*)-2-(6-nitrobenzoxazol-2-yl)-3-phenylcyclopropane-1-carbaldehyde



^1H NMR (400 MHz, CDCl_3) δ 9.16 (d, $J = 5.0$ Hz, 1H, -CHO), 8.43 (d, $J = 2.1$ Hz, 1H, H^3), 8.32 (dd, $J = 8.8, 2.1$ Hz, 1H, H^1), 7.77 (d, $J = 8.8$ Hz, 1H, H^6), 7.38 (m, $J = 4.4$ Hz, 5H, Ph), 3.66 (m, 2H, $\text{H}^{12}, \text{H}^{11}$), 3.08 (m, 1H, H^{10}).

^{13}C NMR (101 MHz, CDCl_3) δ 197.2 (C^{16}), 166.5 (Cq), 149.8 (Cq), 146.1 (Cq), 145.0 (Cq), 132.8 (Cq), 128.7 (CH), 128.5 (CH), 127.9 (CH), 120.6 (C^1), 119.5 (C^6), 106.9 (C^3), 34.8 (C^{11}), 34.3 (C^{12}), 26.1 (C^{10}).

Proton and carbon were assigned using the COSY and HMBC NMR analysis.

$[\alpha]_D^{21} = +21.4^\circ$ ($c = 0.4$, CHCl_3) (**R catalyst**)

Mixture of minor and minor' :

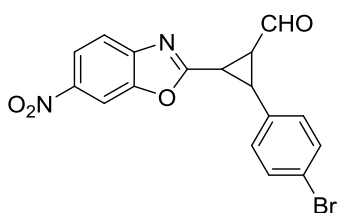
^1H NMR (400 MHz, CDCl_3) δ 9.69 (d, $J = 5.7$ Hz, 1H'), 9.16 (d, $J = 5.0$ Hz, 1H), 8.41 (d, $J = 2.1$ Hz, 2H), 8.30 (dd, $J = 8.8, 2.0$ Hz, 1H + 1H'), 7.77 (dd, $J = 8.8, 4.7$ Hz, 1H + 1H'), 7.43 – 7.23 (m, 11H Ar), 3.77 (t, $J = 6.3$ Hz, 1H'), 3.72 – 3.63 (m, 2H), 3.20 (dd, $J = 8.9, 6.5$ Hz, 1H'), 3.09 (dt, $J = 9.7, 5.0$ Hz, 1H), 2.80 (dt, $J = 8.9, 5.9$ Hz, 1H').

^{13}C NMR (101 MHz, CDCl_3) δ 197.0 (CHO'), 196.0 (CHO), 169.1 (Cq), 167.5 (Cq), 149.9 (Cq), 149.8 (Cq), 146.5 (Cq), 146.3 (Cq), 145.2 (Cq), 145.1 (Cq), 135.8 (Cq), 132.8 (Cq), 129.0 (CH), 129.0 (CH), 128.9 (CH), 128.1 (CH), 128.0 (CH), 126.6 (CH), 120.9 (CH),

120.8 (CH), 119.7 (CH), 119.5 (CH), 107.1 (CH), 107.0 (CH), 39.4 (CH), 38.7 (CH), 35.2 (CH), 32.2 (CH), 26.6 (CH), 22.0 (CH).

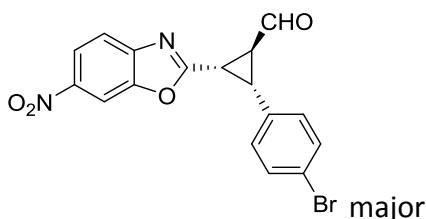
HRMS m/z (ESI+) Exact mass calculated for $C_{17}H_{13}N_2O_4$ $[M+H]^+$: 309.0870, found: 309.0868.

Compound 392b



The reaction was performed following the general procedure adding: 2-(diphenyl((trimethylsilyl)oxy)methyl)pyrrolidine (31 mg, 0.094 mmol, 20 mol% equiv), (*E*)-3-(4-bromophenyl)acrylaldehyde (198 mg, 0.940 mmol, 2 equiv), 2-(chloromethyl)-6-nitrobenzoxazole (100 mg, 0.470 mmol, 1 equiv), $Pd(OAc)_2$ (5 mg, 0.024 mmol, 5 mol% equiv), CH_3CN (1 mL) and 2,6-lutidine (50 mg, 0.470 mmol, 1 equiv). The crude was purified by flash column chromatography (hexane/EtOAc 5:1) to obtain 127 mg of the desired products as light yellow solid. Yield: 70%. The diastereomeric ratio was calculated based on the isolated products after column chromatography. dr: 7:2.2:1

(1*S*,2*R*,3*S*)-2-(4-bromophenyl)-3-(6-nitrobenzoxazol-2-yl)cyclopropane-1-carbaldehyde



IR ($CHCl_3$, liquid film): 2926, 1714 (CHO), 1571 (aromatic NO_2), 1570, 1523, 1344 (aromatic NO_2), 760 cm^{-1} .

1H NMR (400 MHz, $CDCl_3$) δ 9.88 (d, $J = 2.7$ Hz, 1H, CHO), 8.24 (d, $J = 2.1$ Hz, 1H, Het), 8.19 (dd, $J = 8.8, 2.1$ Hz, 1H, Het), 7.64 (d, $J = 8.7$ Hz, 1H, Het), 7.33 – 7.27 (m, 2H, Ar),

7.12 – 7.05 (m, 2H, Ar), 3.53 (ddd, $J = 5.9, 5.3, 2.7$ Hz, 1H, CHCHO), 3.38 (dd, $J = 9.8, 5.2$ Hz, 1H, CH), 3.32 (dd, $J = 9.8, 6.0$ Hz, 1H, CH).

^{13}C NMR (101 MHz, CDCl_3) δ 197.1 (CHO), 166.2 (Cq), 149.9 (Cq), 146.1 (Cq), 145.2 (Cq), 132.0 (Cq), 131.7 (Cq), 130.5 (CH), 122.1 (CH), 120.8 (CH), 119.7 (CH), 107.1 (CH), 34.4 (CH), 34.2 (CH), 26.2 (CH).

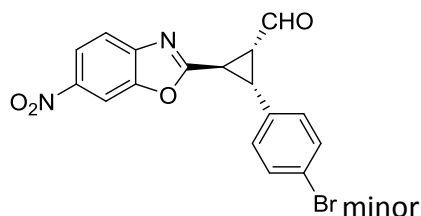
The enantiomeric excess was determined by **HPLC** using a Chiralpak OD-H column (hexane/*i*PrOH = 85:15, flow rate 1.0 mL/min, $\lambda = 210$ nm): t_r (S) = 56.6, t_r (R) = 43.5, 97% (R) and 98% (S) *ee*.

$[\alpha]_D^{22} = +168.0^\circ$ ($c = 0.5$, CHCl_3) (**R catalyst**)

mp: 116-117 °C

HRMS m/z (ESI+) Exact mass calculated for $\text{C}_{17}\text{H}_{12}\text{Br}^{79}\text{N}_2\text{O}_4$ $[\text{M}+\text{H}]^+$: 386.9975, found: 386.9984.

(1*R*,2*R*,3*R*)-2-(4-bromophenyl)-3-(6-nitrobenzooxazol-2-yl)cyclopropane-1-carbaldehyde



^1H NMR (400 MHz, CDCl_3) δ 9.26 (d, $J = 4.3$ Hz, 1H, CHO), 8.42 (d, $J = 2.1$ Hz, 1H, Het), 8.32 (dd, $J = 8.8, 2.1$ Hz, 1H, Het), 7.76 (d, $J = 8.8$ Hz, 1H, Het), 7.51 – 7.48 (m, 2H, Ar), 7.26 – 7.22 (m, 2H, Ar), 3.60 (d, $J = 6.8$ Hz, 2H, CHAr, CHHet), 3.13 (ddd, $J = 7.7, 6.8, 4.3$ Hz, 1H, CHCHO).

^{13}C NMR (101 MHz, CDCl_3) δ 195.5 (CHO), 168.9 (Cq), 150.0 (Cq), 146.6 (Cq), 145.4 (Cq), 132.2 (CH), 131.9 (Cq), 130.8 (CH), 122.4 (Cq), 121.1 (CH), 119.7 (CH), 107.3 (CH), 38.6 (CH), 35.1 (CH), 22.3 (CH).

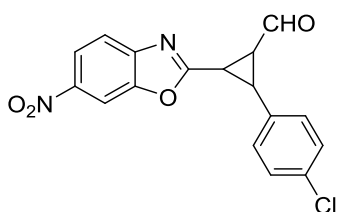
mp: 119-120 °C

HRMS minor *m/z* (ESI+) Exact mass calculated for C₁₇H₁₂Br⁷⁹N₂O₄ [M+H]⁺: 386.9975, found: 386.9982.

Mixture of minor and minor':

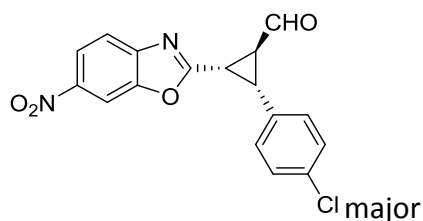
¹H NMR (400 MHz, CDCl₃) δ 9.66 (d, *J* = 5.5 Hz, 1H'), 9.25 (d, *J* = 4.3 Hz, 1H), 8.40 (d, *J* = 1.9 Hz, 1H + 1H'), 8.30 (dd, *J* = 8.8, 2.1 Hz, 1H + 1H'), 7.76 (dd, *J* = 8.7, 6.1 Hz, 1H + 1H'), 7.49 (t, *J* = 7.0 Hz, 2H + 2H'), 7.24 (d, *J* = 8.4 Hz, 2H), 7.13 (d, *J* = 8.4 Hz, 2H'), 3.71 (t, *J* = 6.2 Hz, 1H'), 3.60 (d, *J* = 6.1 Hz, 2H), 3.12 (ddd, *J* = 8.7, 6.0, 4.3 Hz, 1H + m, 1H'), 2.75 (dt, *J* = 9.0, 5.9 Hz, 1H').

Compound 392c



The reaction was performed following the general procedure adding: 2-(diphenyl((trimethylsilyl)oxy)methyl)pyrrolidine (31 mg, 0.094 mmol, 20 mol% equiv), (*E*)-3-(4-chlorophenyl)acrylaldehyde (157 mg, 0.940 mmol, 2 equiv), 2-(chloromethyl)-6-nitrobenzoxazole (100 mg, 0.470 mmol, 1 equiv), Pd(OAc)₂ (5 mg, 0.024 mmol, 5 mol% equiv), CH₃CN (1 mL) and 2,6-lutidine (50 mg, 0.470 mmol, 1 equiv). The crude was purified by flash column chromatography (hexane/EtOAc 4:1) to obtain 120 mg of the desired products as orange solid (major dia) and yellow oil (minor dia). Yield: 74%. The diastereomeric ratio was calculated based on the isolated products after column chromatography. dr: 43:22:1

(1*S*,2*R*,3*S*)-2-(4-chlorophenyl)-3-(6-nitrobenzoxazol-2-yl)cyclopropane-1-carbaldehyde



IR (CHCl₃, liquid film): 3107, 2927, 2924, 2853, 1714 (CHO), 1570 (aromatic NO₂), 1523, 1344 (aromatic NO₂), 751 cm⁻¹.

¹H NMR (400 MHz, CDCl₃) δ 9.89 (d, *J* = 4.5 Hz, 1H, CHO), 8.25 (d, *J* = 2.1 Hz, 1H, Het), 8.21 (dd, *J* = 8.7, 2.1 Hz, 1H, Het), 7.64 (d, *J* = 8.7 Hz, 1H, Het), 7.16 (s, 4H, Ar), 3.56 – 3.52 (m, 1H, CH), 3.41 – 3.33 (m, 2H, CH).

¹³C NMR (101 MHz, CDCl₃) δ 197.2 (CHO), 166.3 (Cq), 149.9 (Cq), 146.1 (Cq), 145.3 (Cq), 134.0 (Cq), 131.5 (Cq), 130.2 (CH), 128.9 (CH), 120.8 (CH), 119.8 (CH), 107.1 (CH), 34.4 (CH), 34.2 (CH), 26.3 (CH).

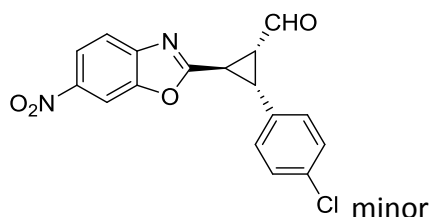
The enantiomeric excess was determined by **HPLC** using a Chiralpak OD-H column (hexane/*i*PrOH = 80:20, flow rate 1.0 mL/min, λ = 250 nm): *t_r* (S) = 41.0, *t_r* (R) = 28.2, 98% (R) and 97% (S) *ee*.

[α]_D²² = +132.4° (*c* = 1.3, CHCl₃) (**R catalyst**)

mp: 86-87 °C

HRMS *m/z* (ESI+) Exact mass calculated for C₁₇H₁₂Cl³⁵N₂O₄ [M+H]⁺: 343.0480, found: 343.0480.

(1*R*,2*R*,3*R*)-2-(4-chlorophenyl)-3-(6-nitrobenzoxazol-2-yl)cyclopropane-1-carbaldehyde



NMR minor diastereomer with traces of the minor':

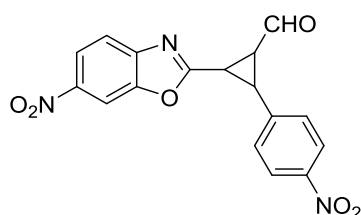
¹H NMR (400 MHz, CDCl₃) δ 9.26 (d, *J* = 4.3 Hz, 1H, CHO), 8.42 (d, *J* = 2.1 Hz, 1H, Het), 8.32 (dd, *J* = 8.8, 2.1 Hz, 1H, Het), 7.76 (d, *J* = 8.8 Hz, 1H, Het), 7.36 – 7.28 (m, 4H, Ar), 3.65 – 3.58 (m, 2H, CHAr, CHHet), 3.13 (ddd, *J* = 8.7, 5.7, 4.4 Hz, 1H, CHCHO).

¹³C NMR (101 MHz, CDCl₃) δ 195.4 (CHO), 169.0 (Cq), 150.0 (Cq), 146.6 (Cq), 145.4 (Cq), 134.3 (Cq), 131.4 (Cq), 130.5 (CH), 129.3 (CH), 121.1 (CH), 119.8 (CH), 107.3 (CH), 38.7 (CH), 35.0 (CH), 22.4 (CH).

[α]_D²¹ = +36.7° (*c* = 0.2, CHCl₃) (***R* catalyst**)

HRMS *m/z* (ESI+) Exact mass calculated for C₁₇H₁₂Cl³⁵N₂O₄ [M+H]⁺: 343.0480, found: 343.0481.

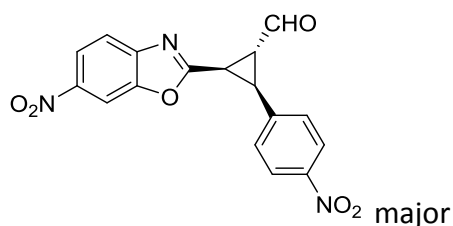
Compound 392d



The reaction was performed following the general procedure adding: 2-(diphenyl((trimethylsilyl)oxy)methyl)pyrrolidine (31 mg, 0.094 mmol, 20 mol% equiv), (*E*)-3-(4-nitrophenyl)acrylaldehyde (166 mg, 0.940 mmol, 2 equiv), 2-(chloromethyl)-6-nitrobenzoxazole (100 mg, 0.470 mmol, 1 equiv), Pd(OAc)₂ (5 mg, 0.024 mmol, 5 mol% equiv), CH₃CN (1 mL) and 2,6-lutidine (50 mg, 0.470 mmol, 1 equiv). The crude was

purified by flash column chromatography (hexane/EtOAc 5:1) to obtain 151 mg of the desired products as orange oil (major dia) and yellow solid (minor dia). Yield: 79%. The diastereomeric ratio was calculated based on the isolated products after column chromatography. dr: 14:5.6:1

(1*R*,2*R*,3*S*)-2-(6-nitrobenzoxazol-2-yl)-3-(4-nitrophenyl)cyclopropane-1-carbaldehyde



IR (CHCl₃, liquid film): 3109, 2924, 2852, 1714 (CHO), 1571 (aromatic NO₂), 1518, 1344 (aromatic NO₂), 735 cm⁻¹.

¹H NMR (400 MHz, CDCl₃) δ 9.96 (d, J = 2.4 Hz, 1H, CHO), 8.25 (d, J = 2.1 Hz, 1H, Het), 8.21 (dd, J = 8.8, 2.1 Hz, 1H, Het), 8.06 (bd, J = 8.7 Hz, 2H, Ar), 7.64 (d, J = 8.8 Hz, 1H, Het), 7.44 (bd, J = 8.7 Hz, 2H, Ar), 3.66 (ddd, J = 5.7, 5.6, 2.4 Hz, 1H, CHCHO), 3.46 (bd, J = 5.7 Hz, 2H, CHAr, CHHet).

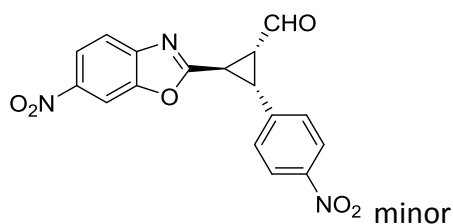
¹³C NMR (101 MHz, CDCl₃) δ 196.6 (CHO), 165.6 (Cq), 149.9 (Cq), 147.6 (Cq), 145.9 (Cq), 145.4 (Cq), 140.5 (Cq), 129.9 (CH), 123.8 (CH), 121.0 (CH), 119.9 (CH), 107.2 (CH), 34.4 (CH), 34.1 (CH), 26.6 (CH).

The enantiomeric excess was determined by **HPLC** using a Chiralpak OD-H column (hexane/*i*PrOH = 55:45, flow rate 0.8 mL/min, λ = 210 nm): t_r (S) = 44.5, t_r (R) = 36.0, >99% (R and S) *ee*.

$[\alpha]_D^{21}$ = -50.1° (c = 1.0, CHCl₃) (S catalyst)

HRMS m/z (ESI+) Exact mass calculated for C₁₇H₁₂N₃O₆ [M+H]⁺: 354.0721, found: 354.0726.

(1*R*,2*R*,3*R*)-2-(6-nitrobenzoxazol-2-yl)-3-(4-nitrophenyl)cyclopropane-1-carbaldehyde



¹H NMR (400 MHz, CDCl₃) δ 9.44 (d, *J* = 3.2 Hz, 1H, CHO), 8.43 (d, *J* = 2.0 Hz, 1H, Het), 8.32 (d, *J* = 8.8 Hz, 1H, Het), 8.22 (d, *J* = 8.7 Hz, 2H, Ar), 7.77 (d, *J* = 8.8 Hz, 1H, Het), 7.54 (d, *J* = 8.6 Hz, 2H, Ar), 3.71 (bd, *J* = 6.8 Hz, 2H, CHAr, CHHet), 3.30 (ddd, *J* = 7.9, 6.7, 3.2 Hz, 1H, CHCHO).

¹³C NMR (101 MHz, CDCl₃) δ 194.7 (CHO), 168.4 (Cq), 150.0 (Cq), 147.8 (Cq), 146.5 (Cq), 145.5 (Cq), 140.2 (Cq), 130.2 (CH), 124.1 (CH), 121.2 (CH), 119.9 (CH), 107.3 (CH), 38.6 (CH), 35.5 (CH), 22.7 (CH).

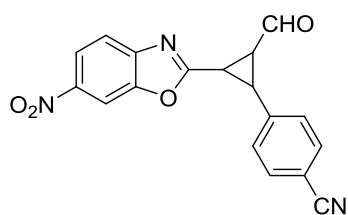
The enantiomeric excess was determined by **HPLC** using a Chiralpak IB column (hexane/*i*PrOH = 70:30, flow rate 1.0 mL/min, λ = 210 nm): *t_r* (S) = 40.3, *t_r* (R) = 38.7, 81% (R) and 89% (S) *ee*.

[α]_D²² = +26.9° (*c* = 0.5, CHCl₃) (***R* catalyst**)

mp: 190 °C decomposition

HRMS *m/z* (ESI+) Exact mass calculated for C₁₇H₁₂N₃O₆ [M+H]⁺: 354.0721, found: 354.0718.

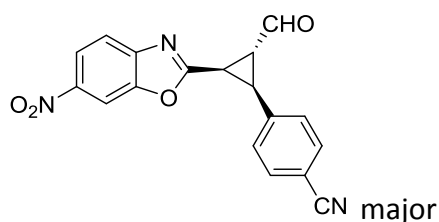
Compound 392e



The reaction was performed following the general procedure adding: 2-(diphenyl((trimethylsilyl)oxy)methyl)pyrrolidine (31 mg, 0.094 mmol, 20 mol% equiv),

(*E*)-4-(3-oxoprop-1-en-1-yl)benzonitrile (148 mg, 0.940 mmol, 2 equiv), 2-(chloromethyl)-6-nitrobenzoxazole (100 mg, 0.470 mmol, 1 equiv), Pd(OAc)₂ (5 mg, 0.024 mmol, 5 mol% equiv), CH₃CN (1 mL) and 2,6-lutidine (50 mg, 0.470 mmol, 1 equiv). The crude was purified by flash column chromatography (hexane/EtOAc 5:1) to obtain 139 mg of the desired products as orange solid (major dia) and yellow oil (minor dia). Yield: 89%. The diastereomeric ratio was calculated based on the isolated products after column chromatography. dr: 4.8:3:1

4-((1*S*,2*R*,3*R*)-2-formyl-3-(6-nitrobenzoxazol-2-yl)cyclopropyl)benzonitrile



IR (CHCl₃, liquid film): 2923, 2838, 2229 (CN), 1714 (CHO), 1571 (aromatic NO₂), 1523, 1345 (aromatic NO₂), 759 cm⁻¹.

¹H NMR (400 MHz, CDCl₃) δ 9.95 (d, *J* = 2.4 Hz, 1H, CHO), 8.27 (d, *J* = 2.0 Hz, 1H, Het), 8.23 (dd, *J* = 8.7, 2.1 Hz, 1H, Het), 7.65 (d, *J* = 8.7 Hz, 1H, Het), 7.51 (bd, *J* = 8.4 Hz, 2H, Ar), 7.37 (bd, *J* = 8.3 Hz, 2H, Ar), 3.62 (ddd, *J* = 5.7, 5.6, 2.4 Hz, 1H, CHCHO), 3.47 – 3.39 (m, 2H, CHAr, CHHet).

¹³C NMR (101 MHz, CDCl₃) δ 196.6 (CHO), 165.7 (Cq), 149.9 (Cq), 145.9 (Cq), 145.4 (Cq), 138.5 (Cq), 132.4 (CH), 129.7 (CH), 120.9 (CH), 119.9 (CH), 118.4 (Cq), 112.0 (Cq), 107.1 (CH), 34.4 (CH), 34.2 (CH), 26.5 (CH).

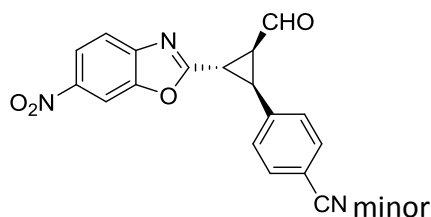
The enantiomeric excess was determined by **HPLC** using a Chiralpak AY-H column (hexane/*i*PrOH = 60:40, flow rate 0.8 mL/min, λ = 210 nm): *t_r* (S) = 33.8, *t_r* (R) = 28.8, >99% (R and S) *ee*.

[α]_D²² = −169.2° (c = 0.7, CHCl₃) (**S catalyst**)

mp: 65 °C decomposition

HRMS *m/z* (ESI+) Exact mass calculated for C₁₈H₁₂N₃O₄ [M+H]⁺: 334.0822, found: 334.0814.

4-((1*R*,2*R*,3*R*)-2-formyl-3-(6-nitrobenzoxazol-2-yl)cyclopropyl)benzonitrile



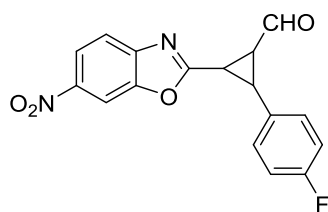
Mixture of minor and minor':

¹H NMR (400 MHz, CDCl₃) δ 9.69 (d, *J* = 5.3 Hz, 1H'), 9.40 (d, *J* = 3.4 Hz, 1H), 8.42 (bs, 1H + 1H'), 8.32 (bd, *J* = 8.8 Hz, 1H + 1H'), 7.79 – 7.75 (m, 1H + 1H'), 7.69 – 7.65 (m, 2H + 2H'), 7.48 (d, *J* = 8.2 Hz, 2H), 7.38 (d, *J* = 8.3 Hz, 2H'), 3.79 (dd, *J* = 6.3, 6.2 Hz, 1H'), 3.68 (bd, *J* = 7.1 Hz, 2H), 3.30 – 3.19 (m, 1H + 1H'), 2.86 – 2.81 (m, 1H').

¹³C NMR (101 MHz, CDCl₃) δ 196.0 (CHO'), 194.8 (CHO), 168.5 (Cq), 166.5 (Cq'), 150.1 (Cq'), 150.0 (Cq), 146.5 (Cq), 146.2 (Cq'), 145.4 (Cq), 141.5 (Cq'), 138.2 (Cq), 133.0 (CH'), 132.7 (CH), 130.0 (CH), 127.6 (CH'), 121.2 (CH), 121.1 (CH'), 120.1 (CH'), 119.8 (CH), 118.39 (Cq), 118.38 (Cq'), 112.3 (Cq), 112.2 (Cq'), 107.4 (CH'), 107.3 (CH), 39.2 (CH'), 38.6(CH), 35.6(CH), 31.6 (CH'), 26.9 (CH'), 22.5 (CH).

HRMS *m/z* (ESI+) Exact mass calculated for C₁₈H₁₂N₃O₄ [M+H]⁺: 334.0822, found: 334.0828.

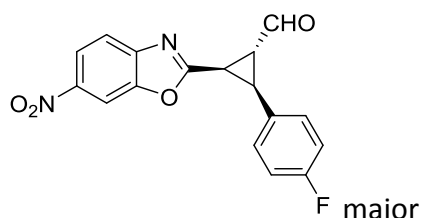
Compound 392f



The reaction was performed following the general procedure adding: 2-(diphenyl((trimethylsilyl)oxy)methyl)pyrrolidine (31 mg, 0.094 mmol, 20 mol% equiv), (*E*)-3-(4-fluorophenyl)acrylaldehyde (141 mg, 0.940 mmol, 2 equiv), 2-(chloromethyl)-6-nitrobenzoxazole (100 mg, 0.470 mmol, 1 equiv), Pd(OAc)₂ (5 mg, 0.024 mmol, 5 mol% equiv), CH₃CN (1 mL) and 2,6-lutidine (50 mg, 0.470 mmol, 1 equiv). The crude

was purified by flash column chromatography (hexane/EtOAc 4:1) to obtain 132 mg of the desired products as yellow oil. Yield: 86%. The diastereomeric ratio was calculated based on the isolated products after column chromatography. dr: 6.6:2.6:1

(1*R*,2*S*,3*R*)-2-(4-fluorophenyl)-3-(6-nitrobenzoxazol-2-yl)cyclopropane-1-carbaldehyde



IR (CHCl₃, liquid film): 3109, 2924, 2850, 1721 (CHO), 1571 (aromatic NO₂), 1513, 1343 (aromatic NO₂), 1232 (aromatic F), 1154 (aromatic F), 757 cm⁻¹.

¹H NMR (400 MHz, CDCl₃) δ 9.89 (d, *J* = 2.7 Hz, 1H, CHO), 8.24 (d, *J* = 1.4 Hz, 1H, Het), 8.23 – 8.18 (m, 1H, Het), 7.64 (d, *J* = 8.7 Hz, 1H, Het), 7.24 – 7.15 (m, 2H, Ar), 6.88 (t, *J* = 8.6 Hz, 2H, Ar), 3.53 (ddd, *J* = 5.5, 5.5, 2.8 Hz, 1H, CHCHO), 3.37 (d, *J* = 5.5 Hz, 2H, CHAr, CHHet).

¹³C NMR (101 MHz, CDCl₃) δ 197.2 (CHO), 166.4 (Cq), 162.4 (d, *J* = 247.3 Hz, Cq), 149.9 (Cq), 146.1 (Cq), 145.2 (Cq), 130.6 (d, *J* = 8.3 Hz, CH), 128.7 (d, *J* = 3.3 Hz, Cq), 120.8 (CH), 119.7 (CH), 115.7 (d, *J* = 21.7 Hz, CH), 107.1 (CH), 34.6 (CH), 34.1 (CH), 26.2 (CH).

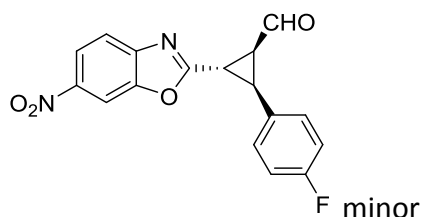
¹⁹F NMR (376 MHz, CDCl₃) δ -113.79.

The enantiomeric excess was determined by **HPLC** using a Chiralpak OD-H column (hexane/*i*PrOH = 80:20, flow rate 1.0 mL/min, λ = 210 nm): *t_r* (S) = 24.8, *t_r* (R) = 18.7, 98% (R and S) *ee*.

[α]_D²¹ = -136.6° (*c* = 1.4, CHCl₃) (**S catalyst**)

HRMS *m/z* (ESI+) Exact mass calculated for C₁₇H₁₂FN₂O₄ [M+H]⁺: 327.0776, found: 327.0771.

(1*R*,2*R*,3*R*)-2-(4-fluorophenyl)-3-(6-nitrobenzoxazol-2-yl)cyclopropane-1-carbaldehyde



Mixture of minor and minor':

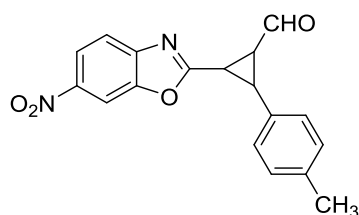
¹H NMR (400 MHz, CDCl₃) δ 9.67 (d, *J* = 5.6 Hz, 1H'), 9.24 (d, *J* = 4.4 Hz, 1H), 8.43 – 8.42 (m, 1H + 1H'), 8.32 (d, *J* = 8.8, 1H + d, *J* = 2.1 Hz, 1H'), 7.78 (d, *J* = 8.7, 1H), 7.76 (d, *J* = 6.2 Hz, 1H'), 7.34 (dd, *J* = 8.5, 5.3 Hz, 2H), 7.23 (dd, *J* = 5.9, 2.8 Hz, 2H'), 7.10 – 7.03 (m, 2H + 2H'), 3.75 (dd, *J* = 6.3, 6.1 Hz, 1H'), 3.62 (m, 2H), 3.16 – 3.07 (m, 1H + 1H'), 2.77 – 2.72 (m, Hz, 1H').

¹³C NMR (101 MHz, CDCl₃) δ 196.9 (CHO'), 195.7 (CHO), 169.1 (Cq), 167.3 (Cq'), 163.79 (Cq'), 163.76 (Cq), 161.33 (Cq'), 161.30 (Cq), 150.1 (Cq'), 150.0 (Cq), 146.6 (Cq), 146.4 (Cq'), 145.5 (Cq'), 145.4 (Cq), 131.74 (Cq'), 131.71 (Cq'), 130.9 (CH), 130.8 (CH), 128.7 (Cq), 128.63 (CH'), 128.61 (Cq), 128.5 (CH'), 121.09 (CH), 121.06 (CH'), 120.0 (CH'), 119.7 (CH), 116.3 (CH'), 116.2 (CH), 116.1 (CH'), 115.9 (CH), 107.3 (CH'), 107.2 (CH), 39.4 (CH'), 38.7 (CH), 34.9 (CH), 31.6 (CH'), 26.7 (CH'), 22.5 (CH).

¹⁹F NMR (376 MHz, CDCl₃) δ -113.43, -113.65'.

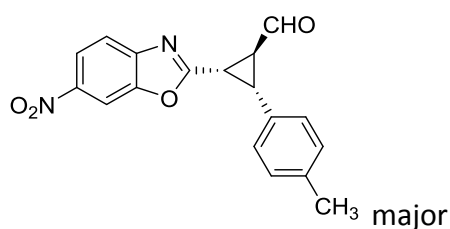
HRMS *m/z* (ESI+) Exact mass calculated for C₁₇H₁₂FN₂O₄ [M+H]⁺: 327.0776, found: 327.0769.

Compound 392g



The reaction was performed following the general procedure adding: 2-(diphenyl((trimethylsilyl)oxy)methyl)pyrrolidine (31 mg, 0.094 mmol, 20 mol% equiv), (*E*)-3-(*p*-tolyl)acrylaldehyde (137 mg, 0.940 mmol, 2 equiv), 2-(chloromethyl)-6-nitrobenzoxazole (100 mg, 0.470 mmol, 1 equiv), Pd(OAc)₂ (5 mg, 0.024 mmol, 5 mol% equiv), CH₃CN (1 mL) and 2,6-lutidine (50 mg, 0.470 mmol, 1 equiv). The crude was purified by flash column chromatography (hexane/EtOAc 5:1) to obtain 100 mg of the desired products as yellow oil. Yield: 66%. The diastereomeric ratio was calculated based on the isolated products after column chromatography. dr: 5.3:1.6:1

(1*S*,2*S*,3*R*)-2-(6-nitrobenzoxazol-2-yl)-3-(*p*-tolyl)cyclopropane-1-carbaldehyde



IR (CHCl₃, liquid film): 3106, 2922, 2853, 1714 (CHO), 1571 (aromatic NO₂), 1522, 1344 (aromatic NO₂), 751, 735 cm⁻¹.

¹H NMR (400 MHz, CDCl₃) δ 9.87 (d, *J* = 2.9 Hz, 1H, CHO), 8.24 (d, *J* = 1.9 Hz, 1H, Het), 8.21 (dd, *J* = 8.7, 2.1 Hz, 1H, Het), 7.65 (d, *J* = 8.7 Hz, 1H, Het), 7.10 (d, *J* = 8.0 Hz, 2H, Ar), 6.99 (d, *J* = 7.9 Hz, 2H, Ar), 3.54 (ddd, *J* = 5.6, 5.5, 2.9 Hz, 1H, CHCHO), 3.42 – 3.31 (m, 2H, CHAr, CHHet), 2.23 (s, 3H, CH₃).

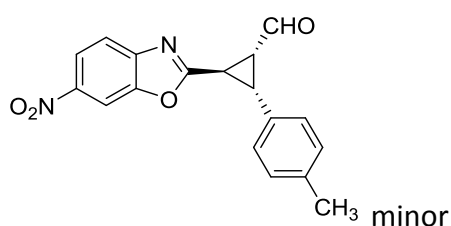
¹³C NMR (101 MHz, CDCl₃) δ 197.5 (CHO), 166.8 (Cq), 150.0 (Cq), 146.3 (Cq), 145.2 (Cq), 137.8 (Cq), 129.9 (Cq), 129.4 (CH), 128.6 (CH), 120.7 (CH), 119.7 (CH), 107.1 (CH), 34.8 (CH), 34.6 (CH), 26.3 (CH), 21.2 (CH₃).

The enantiomeric excess was determined by **HPLC** using a Chiralpak AY-H column (hexane/*i*PrOH = 80:20, flow rate 1.0 mL/min, λ = 210 nm): t_r (S) = 22.7, t_r (R) = 21.3, 99% (R and S) *ee*.

$[\alpha]_D^{22} = +131.3^\circ$ ($c = 0.5$, CHCl_3) (**R catalyst**)

HRMS m/z (ESI+) Exact mass calculated for $\text{C}_{18}\text{H}_{15}\text{N}_2\text{O}_4$ $[\text{M}+\text{H}]^+$: 323.1026, found: 323.1024.

(1*R*,2*R*,3*R*)-2-(6-nitrobenzoxazol-2-yl)-3-(*p*-tolyl)cyclopropane-1-carbaldehyde



Mixture of minor and minor':

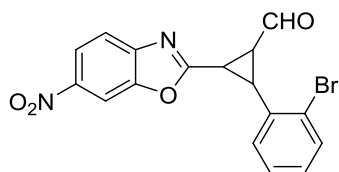
Purity: 62%, the starting benzoxazole was also present in the NMR

^1H NMR (400 MHz, CDCl_3) δ 9.66 (d, $J = 5.8$ Hz, 1H'), 9.14 (d, $J = 5.0$ Hz, 1H), 8.41 (m, 1H + 1H'), 8.31 (m, 1H + 1H'), 7.76 (d, $J = 8.8$ Hz, 1H'), 7.75 (d, $J = 8.8$ Hz, 1H'), 7.26-7.24 (m, 2H), 7.19 – 7.11 (m, 2H + 4H'), 3.72 (dd, $J = 6.3, 6.2$ Hz, 1H'), 3.61 (m, $J = 6.3$ Hz, 2H), 3.13 (dd, $J = 8.9, 6.5$ Hz, 1H'), 3.04 (ddd, $J = 9.3, 9.3, 5.0$ Hz, 1H), 2.77 – 2.72 (m, 1H'), 2.35 (s, 3H'), 2.34 (s, 3H).

^{13}C NMR (101 MHz, CDCl_3) δ 197.3 (CHO'), 196.2 (CHO), 171.9 (Cq), 169.4 (Cq), 152.4 (Cq), 150.0 (Cq), 146.7 (Cq), 138.2 (Cq), 132.9 (Cq), 129.9 (CH'), 129.8 (CH), 129.0 (CH), 126.7 (CH'), 121.1 (CH), 120.9 (CH'), 119.9 (CH'), 119.7 (CH), 107.3 (CH'), 107.2 (CH), 39.6 (CH'), 38.9 (CH), 35.2 (CH), 32.2 (CH'), 26.8 (CH'), 22.3 (CH), 21.30 (CH), 21.29 (CH').

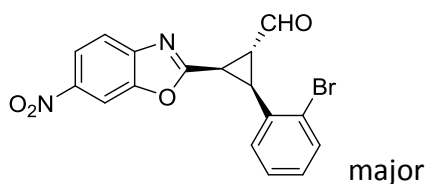
HRMS m/z (ESI+) Exact mass calculated for $\text{C}_{18}\text{H}_{15}\text{N}_2\text{O}_4$ $[\text{M}+\text{H}]^+$: 323.1026, found: 323.1033.

Compound 392h



The reaction was performed following the general procedure adding: 2-(diphenyl((trimethylsilyl)oxy)methyl)pyrrolidine (31 mg, 0.094 mmol, 20 mol% equiv), (*E*)-3-(2-bromophenyl)acrylaldehyde (198 mg, 0.940 mmol, 2 equiv), 2-(chloromethyl)-6-nitrobenzoxazole (100 mg, 0.470 mmol, 1 equiv), Pd(OAc)₂ (5 mg, 0.024 mmol, 5 mol% equiv), CH₃CN (1 mL) and 2,6-lutidine (50 mg, 0.470 mmol, 1 equiv). The crude was purified by flash column chromatography (hexane/EtOAc 4:1) to obtain 147 mg of the desired products as yellow oil. Yield: 81%. The diastereomeric ratio was calculated based on the isolated products after column chromatography. dr: 13.4:2.3:1

(1*R*,2*S*,3*R*)-2-(2-bromophenyl)-3-(6-nitrobenzoxazol-2-yl)cyclopropane-1-carbaldehyde



IR (CHCl₃, liquid film): 3107, 2922, 2850, 1713 (CHO), 1570 (aromatic NO₂), 1513, 1342 (aromatic NO₂), 757 cm⁻¹.

¹H NMR (400 MHz, CDCl₃) δ 9.87 (d, *J* = 2.8 Hz, 1H, CHO), 8.22 (d, *J* = 2.0 Hz, 1H, Het), 8.19 (dd, *J* = 8.7, 2.1 Hz, 1H, Het), 7.59 (d, *J* = 8.7 Hz, 1H, Het), 7.44 (d, *J* = 7.8 Hz, 1H, Ar), 7.24 – 7.20 (m, 2H, Ar), 7.13 – 7.07 (m, 1H, Ar), 3.54 – 3.47 (m, 2H, CH), 3.40 (dd, *J* = 8.9, 6.9 Hz, 1H, CH).

¹³C NMR (101 MHz, CDCl₃) δ 196.9 (CHO), 166.8 (Cq), 149.8 (Cq), 146.3 (Cq), 145.1 (Cq), 133.6 (Cq), 132.9 (CH), 130.7 (CH), 129.7 (CH), 127.4 (CH), 126.0 (Cq), 120.7 (CH), 119.6 (CH), 107.0 (CH), 35.8 (CH), 35.6 (CH), 26.0 (CH).

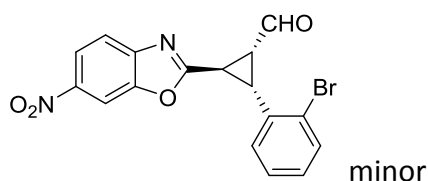
The enantiomeric excess was determined by **HPLC** using a Chiralpak OD-H column (hexane/*i*PrOH = 70:30, flow rate 0.8 mL/min, λ = 210 nm): *t_r* (S) = 52.2, *t_r* (R) = 34.0, >99% (R and S) *ee*.

$[\alpha]_D^{20} = -62.3^\circ$ ($c = 1.0$, CHCl_3) (**S catalyst**)

$[\alpha]_D^{20} = +58.7^\circ$ ($c = 1.3$, CHCl_3) (**R catalyst**)

HRMS m/z (ESI+) Exact mass calculated for $\text{C}_{17}\text{H}_{12}\text{Br}^{79}\text{N}_2\text{O}_4$ $[\text{M}+\text{H}]^+$: 386.9975, found: 386.9964.

(1*R*,2*R*,3*R*)-2-(2-bromophenyl)-3-(6-nitrobenzoxazol-2-yl)cyclopropane-1-carbaldehyde

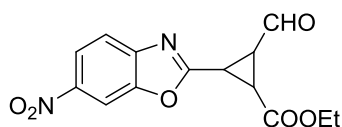


Mainly minor diastereomer present in the NMR with traces of major diastereomer, minor' and starting aldehyde.

^1H NMR (400 MHz, CDCl_3) δ 9.38 (d, $J = 3.7$ Hz, 1H, CHO), 8.44 (d, $J = 2.1$ Hz, 1H, Het), 8.32 (dd, $J = 8.7, 2.1$ Hz, 1H, Het), 7.78 (d, $J = 8.8$ Hz, 1H, Het), 7.60 (dd, $J = 7.9, 0.8$ Hz, 1H, Ar), 7.41 (d, $J = 7.2$ Hz, 1H, Ar), 7.37 – 7.33 (m, 1H, Ar), 7.24 – 7.20 (m, 1H, Ar), 3.61 (dd, $J = 6.5, 4.9$ Hz, 1H, CHHet), 3.55 (dd, $J = 9.4, 6.7$ Hz, 1H, CHAr), 3.30 (ddd, $J = 9.4, 4.6, 3.9$ Hz, 1H, CHCHO).

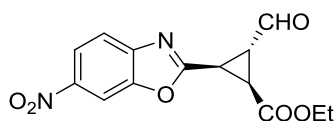
HRMS m/z (ESI+) Exact mass calculated for $\text{C}_{17}\text{H}_{12}\text{Br}^{79}\text{N}_2\text{O}_4$ $[\text{M}+\text{H}]^+$: 386.9975, found: 386.9978.

Compound 392i



The reaction was performed following the general procedure adding: 2-(diphenyl((trimethylsilyl)oxy)methyl)pyrrolidine (31 mg, 0.094 mmol, 20 mol% equiv), ethyl (*E*)-4-oxobut-2-enoate (198 mg, 0.940 mmol, 2 equiv), 2-(chloromethyl)-6-nitrobenzoxazole (100 mg, 0.470 mmol, 1 equiv), Pd(OAc)₂ (5 mg, 0.024 mmol, 5 mol% equiv), CH₃CN (1 mL) and 2,6-lutidine (50 mg, 0.470 mmol, 1 equiv). The crude was purified by flash column chromatography (hexane/EtOAc 4:1) to obtain 147 mg of the desired products as yellow oil. Yield: 81%. The diastereomeric ratio was calculated based on the isolated products after column chromatography. dr: >15

ethyl (1*S*,2*R*,3*R*)-2-formyl-3-(6-nitrobenzoxazol-2-yl)cyclopropane-1-carboxylate



IR (CHCl₃, liquid film): 3019, 2920, 2851, 1730 (CHO), 1577 (aromatic NO₂), 1528, 1346 (aromatic NO₂), 1214 (ester), 746 cm⁻¹.

¹H NMR (400 MHz, CDCl₃) δ 9.87 (d, *J* = 2.0 Hz, 1H, CHO), 8.41 (d, *J* = 2.0 Hz, 1H, Het), 8.29 (dd, *J* = 8.8, 2.1 Hz, 1H, Het), 7.78 (d, *J* = 8.8 Hz, 1H, Het), 4.06 (q, *J* = 7.1 Hz, 2H, OCH₂CH₃), 3.53 (ddd, *J* = 5.9, 5.4, 2.1 Hz, 1H, CHCHO), 3.27 (dd, *J* = 9.5, 5.9 Hz, 1H, CH), 2.82 (dd, *J* = 9.5, 5.4 Hz, 1H, CH), 1.12 (t, *J* = 7.1 Hz, 3H, CH₃).

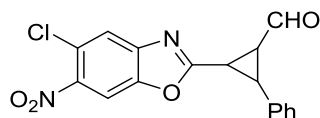
¹³C NMR (101 MHz, CDCl₃) δ 195.9 (CHO), 167.4 (Cq), 165.4 (Cq), 150.1 (Cq), 146.3 (Cq), 145.6 (Cq), 120.9 (CH), 120.2 (CH), 107.4 (CH), 62.1 (CH₂), 33.2 (CH), 29.6 (CH), 24.4 (CH), 14.1 (CH₃).

The enantiomeric excess was determined by **HPLC** using a Chiralpak AY-H column (hexane/*i*PrOH = 50:50, flow rate 1.0 mL/min, λ = 210 nm): *t_r* (S) = 31.8, *t_r* (R) = 35.2, 81% (R) / 87% (S) *ee*.

[α]_D²² = -45.8° (c = 0.4, CHCl₃) (**S catalyst**)

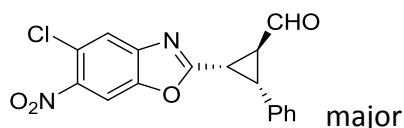
HRMS m/z (ESI+) Exact mass calculated for $C_{14}H_{13}N_2O_6$ $[M+H]^+$: 305.0768, found: 305.0763.

Compound 402a



The reaction was performed following the general procedure adding: 2-(diphenyl((trimethylsilyl)oxy)methyl)pyrrolidine (26 mg, 0.081 mmol, 20 mol% equiv), cinnamaldehyde (107 mg, 0.810 mmol, 2 equiv), 5-chloro-2-(chloromethyl)-6-nitrobenzoxazole (100 mg, 0.405 mmol, 1 equiv), $Pd(OAc)_2$ (4.5 mg, 0.020 mmol, 5 mol% equiv), CH_3CN (1 mL) and 2,6-lutidine (43 mg, 0.405 mmol, 1 equiv). The crude was purified by flash column chromatography (hexane/EtOAc 10:1) to obtain 106 mg of the desired products as yellow oil. Yield: 68%. The diastereomeric ratio was calculated based on the isolated products after column chromatography. dr: 10.5:3.3:1

(1S,2S,3R)-2-(5-chloro-6-nitrobenzoxazol-2-yl)-3-phenylcyclopropane-1-carbaldehyde



IR ($CHCl_3$, liquid film): 3101, 2922, 2849, 1713 (CHO), 1564 (aromatic NO_2), 1531, 1344 (aromatic NO_2), 752 cm^{-1} .

1H NMR (400 MHz, $CDCl_3$) δ 9.89 (d, $J = 2.7$ Hz, 1H, CHO), 7.89 (s, 1H, Het), 7.69 (s, 1H, Het), 7.22 – 7.17 (m, 5H, Ph), 3.56 (ddd, $J = 6.1, 5.1, 2.8$ Hz, 1H, CHCHO), 3.44 – 3.33 (m, 2H, , CHPh, CHHet).

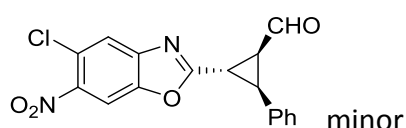
^{13}C NMR (101 MHz, $CDCl_3$) δ 197.2 (CHO), 167.3 (Cq), 148.2 (Cq), 144.71 (Cq), 144.67 (Cq), 132.8 (Cq), 128.8 (CH), 128.7 (CH), 128.1 (CH), 123.8 (Cq), 122.2 (CH), 108.4 (CH), 35.0 (CH), 34.5 (CH), 26.1 (CH).

The enantiomeric excess was determined by **HPLC** using a Chiralpak IC column (hexane/*i*PrOH = 85:15, flow rate 1.0 mL/min, λ = 210 nm): t_r (S) = 30.7, t_r (R) = 33.9, >99% (R and S) *ee*.

$[\alpha]_D^{21} = +99.6^\circ$ ($c = 0.4$, CHCl₃) (**R catalyst**)

HRMS m/z (ESI+) Exact mass calculated for C₁₇H₁₂Cl³⁵N₂O₄ [M+H]⁺: 343.0480, found: 343.0472.

(1*S*,2*S*,3*S*)-2-(5-chloro-6-nitrobenzoxazol-2-yl)-3-phenylcyclopropane-1-carbaldehyde



Mixture of minor and minor':

¹H NMR (400 MHz, CDCl₃) δ 9.57 (d, $J = 5.5$ Hz, 1H'), 9.06 (d, $J = 4.9$ Hz, 1H), 7.99 (s, 1H + 1H'), 7.73 (s, 1H'), 7.71 (s, 1H), 7.29 – 7.13 (m, 5H + 5H'), 3.63 (dd, $J = 6.3, 6.3$ Hz, 1H'), 3.59 – 3.48 (m, 2H), 3.05 (dd, $J = 8.9, 6.5$ Hz, 1H'), 2.97 (dt, $J = 9.7, 4.9$ Hz, 1H), 2.70 (ddd, $J = 8.9, 6.2, 5.7$ Hz, 1H').

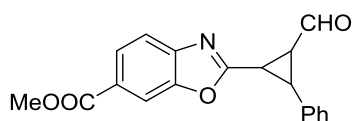
¹³C NMR (101 MHz, CDCl₃) δ 196.9 (CHO'), 195.9 (CHO), 169.9 (Cq), 168.2 (Cq'), 148.4 (Cq'), 148.3 (Cq), 145.2 (Cq), 145.0 (Cq'), 144.97 (Cq'), 144.8 (Cq), 135.8 (CH'), 132.8 (CH), 129.3 (CH'), 129.2 (CH), 129.1 (CH), 128.4 (Cq), 128.3 (Cq'), 126.8 (CH'), 124.2 (Cq), 124.4 (Cq') 122.5 (CH'), 122.3 (CH), 108.8 (CH'), 108.7 (CH), 39.5 (CH'), 38.9 (CH), 35.6 (CH), 32.5 (CH'), 26.7 (CH'), 22.1 (CH).

The enantiomeric excess was determined by **HPLC** using a Chiralpak IC column (hexane/*i*PrOH = 85:15, flow rate 1.0 mL/min, λ = 210 nm): t_r (S) = 37.7, t_r (R) = 40.1, 90% (R) *ee*.

$[\alpha]_D^{21} = -15.4^\circ$ ($c = 0.6$, CHCl₃) (**S catalyst**)

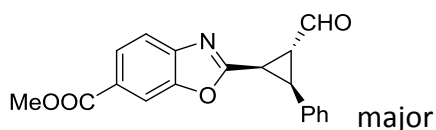
HRMS m/z (ESI+) Exact mass calculated for C₁₇H₁₂Cl³⁵N₂O₄ [M+H]⁺: 343.0480, found: 343.0476.

Compound 402b



The reaction was performed following the general procedure adding: 2-(diphenyl((trimethylsilyl)oxy)methyl)pyrrolidine (29mg, 0.089 mmol, 20 mol% equiv), cinnamaldehyde (117 mg, 0.886 mmol, 2 equiv), methyl 2-(chloromethyl)benzoxazole-6-carboxylate (100 mg, 0.443 mmol, 1 equiv), Pd(OAc)₂ (5 mg, 0.022 mmol, 5 mol% equiv), CH₃CN (1 mL) and 2,6-lutidine (48 mg, 0.443 mmol, 1 equiv). The crude was purified by flash column chromatography (hexane/EtOAc 5:1) to obtain 111 mg of the desired products as yellow oil. Yield: 78%. The diastereomeric ratio was calculated based on the isolated products after column chromatography. dr: 4.5:1.9:1

methyl 2-((1R,2R,3S)-2-formyl-3-phenylcyclopropyl)benzoxazole-6-carboxylate



IR (CHCl₃, liquid film): 3061, 2952, 2847, 1717 (CHO, CO ester), 1434, 1287 (ester), 1269 (ester), 746 cm⁻¹.

¹H NMR (400 MHz, CDCl₃) δ 9.87 (d, J = 2.9 Hz, 1H, CHO), 8.00 (d, J = 0.9 Hz, 1H, Het), 7.98 (dd, J = 8.3, 1.5 Hz, 1H, Het), 7.58 (d, J = 8.3 Hz, 1H, Het), 7.24 – 7.14 (m, 5H, Ph), 3.91 (s, 3H, OCH₃), 3.54 (ddd, J = 5.5, 5.5, 2.9 Hz, 1H, CHCHO), 3.41 – 3.33 (m, 2H, CHPh, CHHet).

¹³C NMR (101 MHz, CDCl₃) δ 197.6 (CHO), 166.5 (Cq), 164.3 (Cq), 150.4 (Cq), 144.8 (Cq), 133.2 (Cq), 128.7 (CH), 128.4 (CH), 127.7 (CH), 126.9 (Cq), 126.1 (CH), 119.2 (CH), 111.9 (CH), 52.4 (CH₃), 34.4 (CH), 34.3 (CH), 26.2 (CH).

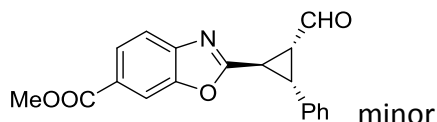
The enantiomeric excess was determined by **HPLC** using a Chiralpak AY-H column (hexane/*i*PrOH = 80:20, flow rate 1.0 mL/min, λ = 230 nm): t_r (S) = 21.1, t_r (R) = 20.0, 98% (R) / 98% (S) *ee*.

[α]_D²² = -104.6° (c = 0.8, CHCl₃) (S catalyst)

$[\alpha]_D^{22} = +105.8^\circ$ ($c = 0.4$, CHCl_3) (**R catalyst**)

HRMS m/z (ESI+) Exact mass calculated for $\text{C}_{19}\text{H}_{16}\text{NO}_4$ $[\text{M}+\text{H}]^+$: 322.1074, found: 322.1079.

methyl 2-((1*R*,2*R*,3*S*)-2-formyl-3-phenylcyclopropyl)benzoxazole-6-carboxylate



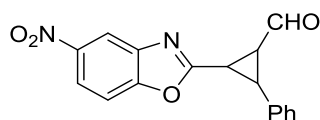
Mixture of minor and minor' (inverted compared to the previous products as in this case the minor' is prevalent):

^1H NMR (400 MHz, CDCl_3) δ 9.64 (d, $J = 6.0$ Hz, 1H'), 9.13 (d, $J = 5.2$ Hz, 1H), 8.22 – 8.18 (m, 1H + 1H'), 8.09 (d, $J = 8.4$ Hz, 1H + d, $J = 8.4$ Hz, 1H'), 7.71 (d, $J = 8.3$ Hz, 1H'), 7.70 (d, $J = 8.3$ Hz, 1H), 7.41 – 7.22 (m, 5H + 5H'), 3.97 (s, 3H + 3H'), 3.76 (dd, $J = 6.3$, 6.3 Hz, 1H'), 3.69 – 3.59 (m, 2H), 3.17 (dd, $J = 8.9$, 6.5 Hz, 1H'), 3.04 (ddd, $J = 9.7$, 5.4, 5.0 Hz, 1H), 2.73 (ddd, $J = 8.9$, 6.0, 6.0 Hz, 1H').

^{13}C NMR (101 MHz, CDCl_3) δ 197.3 (CHO'), 196.3 (CHO), 166.9 (Cq), 166.53 (Cq'), 166.50 (Cq), 165.2 (Cq'), 150.4 (Cq'), 150.3 (Cq), 145.1 (Cq), 144.9 (Cq'), 136.1 (Cq'), 133.1 (Cq), 129.0 (CH'), 129.0 (CH + CH'), 128.9 (CH), 128.0 (CH), 127.9 (CH'), 127.3 (Cq), 127.1 (Cq'), 126.6 (CH'), 126.5 (CH), 119.4 (CH'), 119.1 (CH), 112.14 (CH'), 112.07 (CH), 52.4 (CH_3 + CH_3'), 39.5 (CH'), 38.5 (CH), 34.8 (CH), 31.7 (CH'), 26.6 (CH'), 22.1 (CH).

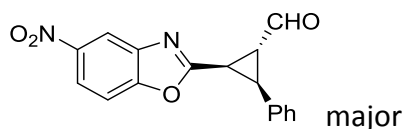
HRMS m/z (ESI+) Exact mass calculated for $\text{C}_{19}\text{H}_{16}\text{NO}_4$ $[\text{M}+\text{H}]^+$: 322.1074, found: 322.1079.

Compound 402c



The reaction was performed following the general procedure adding: 2-(diphenyl((trimethylsilyl)oxy)methyl)pyrrolidine (31mg, 0.094 mmol, 20 mol% equiv), cinnamaldehyde (124 mg, 0.940 mmol, 2 equiv), 2-(chloromethyl)-5-nitrobenzoxazole (100 mg, 0.470 mmol, 1 equiv), Pd(OAc)₂ (5 mg, 0.024 mmol, 5 mol% equiv), CH₃CN (1 mL) and 2,6-lutidine (50 mg, 0.470 mmol, 1 equiv). The crude was purified by flash column chromatography (hexane/EtOAc 3:1) to obtain 80 mg of the desired products as dark yellow oil. Yield: 55%. The diastereomeric ratio was calculated based on the isolated products after column chromatography. dr: 6.2:1.3:1

(1*R*,2*R*,3*S*)-2-(5-nitrobenzoxazol-2-yl)-3-phenylcyclopropane-1-carbaldehyde



IR (CHCl₃, liquid film): 3105, 2923, 2852, 1714 (CHO), 1526, 1347 (aromatic NO₂), 743 cm⁻¹.

¹H NMR (400 MHz, CDCl₃) δ 9.89 (d, *J* = 2.8 Hz, 1H, CHO), 8.44 (d, *J* = 2.3 Hz, 1H, Het), 8.19 (dd, *J* = 8.9, 2.3 Hz, 1H, Het), 7.42 (d, *J* = 9.0 Hz, 1H, Het), 7.23 – 7.14 (m, 5H, Ph), 3.56 (ddd, *J* = 5.5, 5.4, 2.8 Hz, 1H, CHCHO), 3.38 (d, *J* = 5.5 Hz, 2H, CHPh, CHHet).

¹³C NMR (101 MHz, CDCl₃) δ 194.5 (CHO), 162.0 (Cq), 151.3 (Cq), 142.4 (Cq), 138.4 (Cq), 130.1 (Cq), 125.8 (CH), 125.6 (CH), 125.0 (CH), 118.1 (CH), 113.2 (CH), 107.6 (CH), 31.8 (CH), 31.4 (CH), 23.1 (CH).

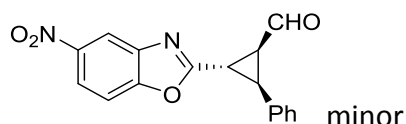
The enantiomeric excess was determined by **HPLC** using a Chiralpak OD-H column (hexane/*i*PrOH = 70:30, flow rate 1.0 mL/min, λ = 210 nm): *t_r* (S) = 20.6, *t_r* (R) = 19.8, 99% (R) / 98% (S) *ee*.

[α]_D²² = -41.6° (*c* = 0.8, CHCl₃) (**S catalyst**)

$[\alpha]_D^{22} = +36.2^\circ$ (c = 0.5, CHCl₃) (**R catalyst**)

HRMS *m/z* (ESI+) Exact mass calculated for C₁₇H₁₃N₂O₄ [M+H]⁺: 309.0870, found: 309.0868.

(1*R*,2*R*,3*R*)-2-(5-nitrobenzoxazol-2-yl)-3-phenylcyclopropane-1-carbaldehyde



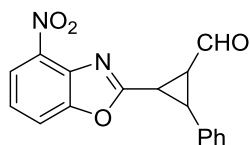
Mixture of minor and minor':

¹H NMR (400 MHz, CDCl₃) δ 9.66 (d, *J* = 5.7 Hz, 1H'), 9.15 (d, *J* = 5.0 Hz, 1H), 8.57 (d, *J* = 2.2 Hz, 1H'), 8.55 (d, *J* = 2.2 Hz, 1H), 8.31 (dd, *J* = 8.9, 2.5 Hz, 1H + dd, *J* = 8.9, 2.5 Hz, 1H'), 7.62 (bd, *J* = 8.9 Hz, 1H + 1H'), 7.41 – 7.24 (m, 10H), 3.75 (dd, *J* = 6.3, 6.3 Hz, 1H'), 3.69 – 3.59 (m, 2H), 3.16 (dd, *J* = 8.9, 6.5 Hz, 1H'), 3.06 (ddd, *J* = 9.7, 5.0, 4.9 Hz, 1H), 2.77 (ddd, *J* = 8.9, 5.9, 5.9 Hz, 1H').

¹³C NMR (101 MHz, CDCl₃) δ 197.2 (CHO), 196.1 (CHO), 167.6 (Cq), 165.9 (Cq), 154.4 (Cq), 154.3 (Cq), 145.7 (2 Cq), 141.9 (Cq), 141.7 (Cq), 136.0 (Cq), 132.9 (Cq), 129.2 (CH), 129.1 (CH), 129.0 (CH), 128.3 (CH), 128.2 (CH), 126.8 (CH), 121.4 (CH), 121.2 (CH), 116.4 (CH), 116.1 (CH), 110.9 (CH), 110.8 (CH), 39.4 (CH), 38.6 (CH), 35.2 (CH), 32.1 (CH), 26.6 (CH), 22.0 (CH).

HRMS *m/z* (ESI+) Exact mass calculated for C₁₇H₁₃N₂O₄ [M+H]⁺: 309.0870, found: 309.0877.

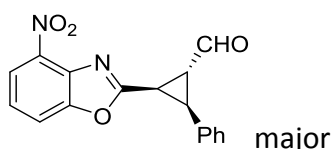
Compound 402d



The reaction was performed following the general procedure adding: 2-(diphenyl((trimethylsilyl)oxy)methyl)pyrrolidine (31mg, 0.094 mmol, 20 mol% equiv),

cinnamaldehyde (124 mg, 0.940 mmol, 2 equiv), 2-(chloromethyl)-4-nitrobenzoxazole (100 mg, 0.470 mmol, 1 equiv), Pd(OAc)₂ (5 mg, 0.024 mmol, 5 mol% equiv), CH₃CN (1 mL) and 2,6-lutidine (50 mg, 0.470 mmol, 1 equiv). The crude was purified by flash column chromatography (hexane/EtOAc 3:1) to obtain 74 mg of the desired products as dark yellow oil. Yield: 51%. The diastereomeric ratio was calculated based on the isolated products after column chromatography. dr: 2.3:1.6:1

(1*R*,2*R*,3*S*)-2-(4-nitrobenzoxazol-2-yl)-3-phenylcyclopropane-1-carbaldehyde



Mixture of major (m) and minor:

IR (CHCl₃, liquid film): 3020, 2852, 1713 (CHO), 1561 (aromatic NO₂), 1526, 1343 (aromatic NO₂), 1214, 747 cm⁻¹.

¹H NMR (400 MHz, CDCl₃) δ 9.88 (d, *J* = 2.8 Hz, 1H^m), 9.14 (d, *J* = 5.0 Hz, 1H), 8.20 (d, *J* = 8.3 Hz, 1H), 8.10 (d, *J* = 8.2 Hz, 1H^m), 7.85 (d, *J* = 8.1 Hz, 1H), 7.61 (d, *J* = 8.1 Hz, 1H^m), 7.49 (dd, *J* = 8.2 Hz, 1H), 7.39 – 7.15 (m, 6H^m + 5H), 3.77 – 3.72 (m, 2H), 3.64 (ddd, *J* = 5.6, 5.6, 2.9 Hz, 1H^m), 3.50 (dd, *J* = 9.8, 5.1 Hz, 1H^m), 3.44 – 3.34 (m, 1H^m), 3.12 (ddd, *J* = 9.2, 5.2, 5.2 Hz, 1H).

¹³C NMR (101 MHz, CDCl₃) δ 197.3 (CHO^m), 195.9 (CHO), 167.9 (Cq), 165.5 (Cq^m), 152.3 (Cq), 152.2 (Cq^m), 138.8 (Cq), 138.7 (Cq^m), 136.1 (Cq), 135.7 (Cq^m), 132.9 (Cq^m), 132.8 (Cq), 129.0 (CH), 128.9 (CH), 128.7 (CH^m), 128.4 (CH^m), 128.1 (CH), 127.8 (CH^m), 124.4 (CH), 124.2 (CH^m), 121.1 (CH), 120.8 (CH^m), 116.4 (CH), 116.2 (CH^m), 38.6 (CH), 35.1 (CH), 34.7 (CH^m), 34.5 (CH^m), 26.2 (CH^m), 22.1 (CH).

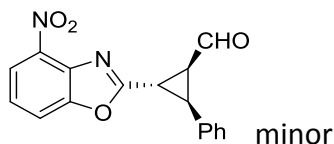
The enantiomeric excess was determined by **HPLC** using a Chiralpak AY-H column (hexane/*i*PrOH = 70:30, flow rate 1.0 mL/min, λ = 210 nm): *t_r* (S) = 37.7, *t_r* (R) = 21.7, >99% (R and S) *ee*.

[α]_D²² = −5.2° (*c* = 0.8, CHCl₃) (**S catalyst**)

[α]_D²² = +6.6° (*c* = 0.7, CHCl₃) (**R catalyst**)

HRMS m/z (ESI+) Exact mass calculated for $C_{17}H_{13}N_2O_4$ $[M+H]^+$: 309.0870, found: 309.0871.

(1*R*,2*R*,3*R*)-2-(4-nitrobenzoxazol-2-yl)-3-phenylcyclopropane-1-carbaldehyde



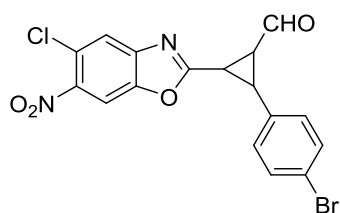
Mixture of major^m, minor, minor' and traces of starting benzoxazole:

1H NMR (400 MHz, $CDCl_3$) δ 9.88 (d, J = 2.8 Hz, 1H^m), 9.73 (d, J = 5.6 Hz, 1H'), 9.14 (d, J = 5.0 Hz, 1H), 8.20 (d, J = 8.3 Hz, 1H), 8.10 (d, J = 8.2 Hz, 4H^m), 7.85 (ddd, J = 8.1, 4.7, 0.8 Hz, 4H + '), 7.64 – 7.57 (m, 4H^m), 7.50 (td, J = 8.2, 3.3 Hz, 5H + '), 7.42 – 7.13 (m, 51H), 3.85 (dd, J = 6.3, 6.3 Hz, 1H'), 3.78 – 3.72 (m, 2H), 3.64 (ddd, J = 6.0, 5.2, 2.9 Hz, 1H^m), 3.51 (dd, J = 9.8, 5.1 Hz, 1H^m), 3.45 – 3.34 (m, 1H^m), 3.29 (dd, J = 8.9, 6.6 Hz, 1H'), 3.12 (ddd, J = 9.2, 5.2, 5.2 Hz, 1H), 2.79 (ddd, J = 8.9, 5.9, 5.9 Hz, 1H').

^{13}C NMR (101 MHz, $CDCl_3$) δ 197.3 (CHO^m), 197.1 (CHO'), 195.9 (CHO), 167.9 (Cq), 166.4 (Cq'), 165.5 (Cq^m), 152.3 (Cq'), 152.3 (Cq), 152.2 (Cq^m), 138.8 (Cq), 138.6 (Cq^m), 136.1 (Cq), 135.9 (Cq'), 135.8 (Cq'), 135.7 (Cq^m), 132.9 (Cq^m), 132.8 (Cq), 129.0 (CH), 128.97 (CH'), 128.90 (CH), 128.7 (CH^m), 128.4 (CH^m), 128.1 (CH), 128.0 (CH'), 127.8 (CH^m), 126.6 (CH'), 125.7 (CH'), 124.6 (CH'), 124.4 (CH), 124.2 (CH^m), 121.1 (CH), 120.8 (CH^m), 117.2 (CH'), 116.5 (CH'), 116.4 (CH), 116.2 (CH^m), 39.7 (CH'), 38.6 (CH), 35.9 (CH'), 35.1 (CH), 34.7 (CH^m), 34.5 (CH^m), 32.1 (CH'), 26.6 (CH'), 26.3 (CH^m), 22.1 (CH).

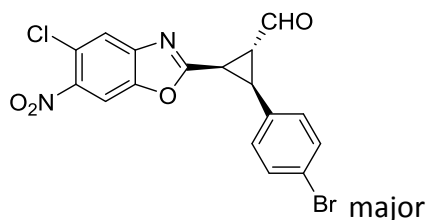
HRMS m/z (ESI+) Exact mass calculated for $C_{17}H_{13}N_2O_4$ $[M+H]^+$: 309.0870, found: 309.0871.

Compound 402e



The reaction was performed following the general procedure adding: 2-(diphenyl((trimethylsilyl)oxy)methyl)pyrrolidine (26 mg, 0.081 mmol, 20 mol% equiv), (*E*)-3-(4-bromophenyl)acrylaldehyde (171 mg, 0.810 mmol, 2 equiv), 5-chloro-2-(chloromethyl)-6-nitrobenzoxazole (100 mg, 0.405 mmol, 1 equiv), Pd(OAc)₂ (4.5 mg, 0.020 mmol, 5 mol% equiv), CH₃CN (1 mL) and 2,6-lutidine (43 mg, 0.405 mmol, 1 equiv). The crude was purified by flash column chromatography (hexane/EtOAc 4:1) to obtain 145 mg of the desired products as yellow oil. Yield: 85%. The diastereomeric ratio was calculated based on the isolated products after column chromatography. dr: 8.1:4.8:1

(1*R*,2*S*,3*R*)-2-(4-bromophenyl)-3-(5-chloro-6-nitrobenzoxazol-2-yl)cyclopropane-1-carbaldehyde



IR (CHCl₃, liquid film): 3101, 2923, 2850, 1713 (CHO), 1565 (aromatic NO₂), 1531, 1446, 1345 (aromatic NO₂), 755 cm⁻¹.

¹H NMR (400 MHz, CDCl₃) δ 9.89 (d, *J* = 2.6 Hz, 1H, CHO), 7.92 (s, 1H, Het), 7.69 (s, 1H, Het), 7.33 (d, *J* = 8.4 Hz, 2H, Ar), 7.09 (d, *J* = 8.4 Hz, 2H, Ar), 3.53 (dd, *J* = 5.6, 5.6, 2.6 Hz, 1H, CHCHO), 3.35 (ddd, *J* = 9.8, 5.7 Hz, 2H, CHAr, CHHet).

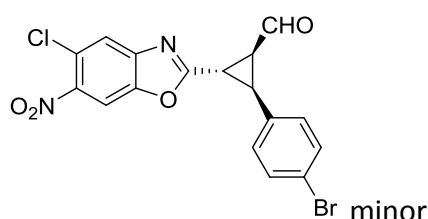
¹³C NMR (101 MHz, CDCl₃) δ 196.8 (CHO), 166.7 (Cq), 148.1 (Cq), 144.6 (Cq), 144.4 (Cq), 131.7 (CH), 130.3 (CH), 123.8 (Cq), 123.8 (Cq), 122.2 (CH), 122.1 (Cq), 108.4 (CH), 34.2 (CH), 34.2 (CH), 25.9 (CH).

The enantiomeric excess was determined by **HPLC** using a Chiralpak OD-H column (hexane/*i*PrOH = 85:15, flow rate 1.0 mL/min, λ = 210 nm): t_r (S) = 39.2, t_r (R) = 30.6, 98% (R) / 97% (S) *ee*.

$[\alpha]_D^{21} = -153.8^\circ$ ($c = 0.6$, CHCl₃) (**S catalyst**)

HRMS m/z (ESI+) Exact mass calculated for C₁₇H₁₁Br⁷⁹Cl³⁵N₂O₄ [M+H]⁺: 420.9585, found: 420.9587.

(1*R*,2*R*,3*R*)-2-(4-bromophenyl)-3-(5-chloro-6-nitrobenzoxazol-2-yl)cyclopropane-1-carbaldehyde



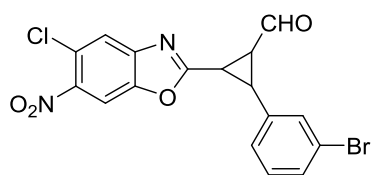
Mixture of minor and minor':

¹H NMR (400 MHz, CDCl₃) δ 9.66 (d, $J = 5.3$ Hz, 1H'), 9.26 (d, $J = 4.2$ Hz, 1H), 8.09 (s, 1H + 1H'), 7.83 (s, 1H'), 7.81 (s, 1H), 7.51 (d, $J = 8.3$ Hz, 2H'), 7.49 (d, $J = 8.3$ Hz, 2H), 7.23 (d, $J = 8.4$ Hz, 2H), 7.13 (d, $J = 8.4$ Hz, 2H'), 3.69 (dd, $J = 6.3, 6.3$ Hz, 1H'), 3.58 (bd, $J = 6.8$ Hz, 2H), 3.15 – 3.08 (m, 1H + 1H'), 2.80 – 2.72 (m, 1H').

¹³C NMR (101 MHz, CDCl₃) δ 196.2 (CHO'), 195.1 (CHO), 169.4 (Cq), 167.6 (Cq'), 148.1 (Cq), 144.9 (Cq), 144.7 (Cq'), 144.7 (Cq'), 134.7 (Cq), 132.2 (CH'), 132.0 (CH), 131.6 (Cq), 130.6 (CH), 128.3 (CH'), 124.1 (Cq), 122.4 (CH'), 122.3 (Cq), 122.1 (CH), 122.0 (Cq'), 108.6 (CH'), 108.5 (CH), 39.0 (CH'), 38.5 (CH), 35.0 (CH), 31.6 (CH'), 26.4 (CH'), 22.0 (CH).

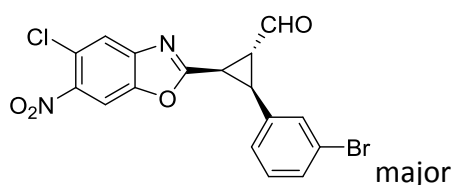
HRMS m/z (ESI+) Exact mass calculated for C₁₇H₁₁Br⁷⁹Cl³⁵N₂O₄ [M+H]⁺: 420.9585, found: 420.9585.

Compound 402f



The reaction was performed following the general procedure adding: 2-(diphenyl((trimethylsilyl)oxy)methyl)pyrrolidine (26 mg, 0.081 mmol, 20 mol% equiv), (*E*)-3-(3-bromophenyl)acrylaldehyde (171 mg, 0.810 mmol, 2 equiv), 5-chloro-2-(chloromethyl)-6-nitrobenzoxazole (100 mg, 0.405 mmol, 1 equiv), Pd(OAc)₂ (4.5 mg, 0.020 mmol, 5 mol% equiv), CH₃CN (1 mL) and 2,6-lutidine (43 mg, 0.405 mmol, 1 equiv). The crude was purified by flash column chromatography (hexane/EtOAc 4:1) to obtain 112 mg of the desired products as yellow oil. Yield: 66%. The diastereomeric ratio was calculated based on the isolated products after column chromatography. dr: 17.4:6.3:1

(1*R*,2*S*,3*R*)-2-(3-bromophenyl)-3-(5-chloro-6-nitrobenzoxazol-2-yl)cyclopropane-1-carbaldehyde



IR (CHCl₃, liquid film): 3101, 2922, 2850, 1714 (CHO), 1564(aromatic NO₂), 1531, 1446, 1344(aromatic NO₂), 754 cm⁻¹.

¹H NMR (400 MHz, CDCl₃) δ 9.92 (d, *J* = 2.5 Hz, 1H, CHO), 7.94 (s, 1H, Het), 7.72 (s, 1H, Het), 7.44 (dd, *J* = 1.7, 1.7 Hz, 1H, Ar), 7.33 (ddd, *J* = 7.7, 1.6, 1.6 Hz, 1H, Ar), 7.14 – 7.05 (m, 2H, Ar), 3.56 (ddd, *J* = 5.6, 5.6, 2.5 Hz, 1H, CHCHO), 3.41 – 3.34 (m, 2H, CHAr, CHHet).

¹³C NMR (101 MHz, CDCl₃) δ 196.7 (CHO), 166.6 (Cq), 148.1 (Cq), 144.7 (Cq), 144.4 (Cq), 134.9 (Cq), 132.0 (CH), 131.2 (CH), 130.0 (CH), 127.2 (CH), 123.8 (Cq), 122.5 (Cq), 122.2 (CH), 108.4 (CH), 34.2 (CH), 34.1 (CH), 26.0 (CH).

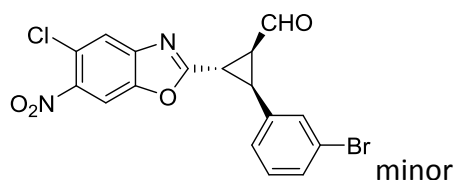
The enantiomeric excess was determined by **HPLC** using a Chiralpak OD-H column (hexane/*i*PrOH = 70:30, flow rate 1.0 mL/min, λ = 210 nm): t_r (S) = 38.2, t_r (R) = 32.9, 91% (R) / 97% (S) *ee*.

$[\alpha]_D^{21} = -107.2^\circ$ ($c = 1.3$, CHCl₃) (**S catalyst**)

$[\alpha]_D^{21} = +97.9^\circ$ ($c = 2.0$, CHCl₃) (**R catalyst**)

HRMS m/z (ESI+) Exact mass calculated for C₁₇H₁₁Br⁷⁹Cl³⁵N₂O₄ [M+H]⁺: 420.9585, found: 420.9581.

(1*R*,2*R*,3*R*)-2-(3-bromophenyl)-3-(5-chloro-6-nitrobenzoxazol-2-yl)cyclopropane-1-carbaldehyde



Mixture of minor and minor':

¹H NMR (400 MHz, CDCl₃) δ 9.67 (d, $J = 5.3$ Hz, 1H'), 9.26 (d, $J = 4.3$ Hz, 1H), 8.10 (s, 1H + 1H'), 7.84 (s, 1H'), 7.82 (s, 1H), 7.54 (bs, 1H), 7.49 – 7.43 (m, 1H + 1H'), 7.41 (t, $J = 1.7$ Hz, 1H'), 7.32 – 7.17 (m, 2H + 2H'), 3.71 (dd, $J = 6.3, 6.3$ Hz, 1H'), 3.64 – 3.60 (m, 2H), 3.19 – 3.08 (m, 1H + 1H'), 2.84 – 2.76 (ddd, $J = 9.0, 6.0, 5.4$ Hz, 1H').

¹³C NMR (101 MHz, CDCl₃) δ 196.2 (CHO'), 195.0 (CHO), 169.3 (Cq), 167.5 (Cq'), 148.1 (Cq'), 148.0 (Cq), 144.9 (Cq), 144.7 (Cq), 138.0 (Cq'), 134.8 (Cq), 132.1 (CH), 131.4 (CH), 131.2 (CH'), 130.6 (CH'), 130.4 (CH), 129.8 (CH'), 127.6 (CH), 125.4 (CH'), 124.1 (Cq), 124.0 (Cq'), 123.1 (Cq'), 122.9 (Cq), 122.4 (CH'), 122.1 (CH), 108.6 (CH+CH'), 38.9 (CH'), 38.5 (CH), 34.8 (CH), 31.5 (CH'), 26.4 (CH'), 21.9 (CH).

HRMS m/z (ESI+) Exact mass calculated for C₁₇H₁₁Br⁷⁹Cl³⁵N₂O₄ [M+H]⁺: 420.9585, found: 420.9589.

6.2.5 Crystallographic data and experimental 392d minor diastereomer obtained with (*R*)-catalyst

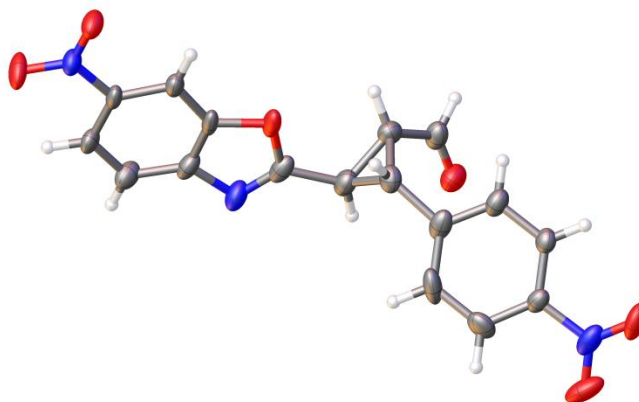


Figure 26. Thermal ellipsoids drawn at the 50% probability level

Experimental. Single clear colourless fragment-shaped crystals of (2014sot0046) were recrystallised from a mixture of TCM and hexane by slow evaporation. A suitable crystal ($0.09 \times 0.08 \times 0.05 \text{ mm}^3$) was selected and mounted on a MITIGEN holder in perfluoroether oil on a Rigaku AFC12 FRE-HF diffractometer. The crystal was kept at $T = 100(2) \text{ K}$ during data collection. Using Olex2,^[201] the structure was solved with the ShelXT (Sheldrick, 2008) structure solution program, using the Direct Methods solution method. The model was refined with version of ShelXL^[202] using Least Squares minimisation.

Crystal Data. $\text{C}_{17}\text{H}_{11}\text{N}_3\text{O}_6$, $M_r = 353.29$, monoclinic, $P2_1/c$ (No. 14), $a = 9.9877(5) \text{ \AA}$, $b = 15.1541(7) \text{ \AA}$, $c = 10.2131(6) \text{ \AA}$, $\beta = 103.161(5)^\circ$, $\alpha = \gamma = 90^\circ$, $V = 1505.20(14) \text{ \AA}^3$, $T = 100(2) \text{ K}$, $Z = 4$, $Z' = 1$, $\mu (\text{MoK}\alpha) = 0.121$, 14536 reflections measured, 3884 unique ($R_{\text{int}} = 0.0709$) which were used in all calculations. The final wR_2 was 0.3428 (all data) and R_1 was 0.1503 ($I > 2(I)$).

Compound	2014sot0046
Formula	C ₁₇ H ₁₁ N ₃ O ₆
$D_{calc.}/\text{g cm}^{-3}$	1.559
μ/mm^{-1}	0.121
Formula Weight	353.29
Colour	clear colourless
Shape	fragment
Max Size/mm	0.09
Mid Size/mm	0.08
Min Size/mm	0.05
T/K	100(2)
Crystal System	monoclinic
Space Group	P2 ₁ /c
$a/\text{\AA}$	9.9877(5)
$b/\text{\AA}$	15.1541(7)
$c/\text{\AA}$	10.2131(6)
$\alpha/^\circ$	90
$\beta/^\circ$	103.161(5)
$\gamma/^\circ$	90
$V/\text{\AA}^3$	1505.20(14)
Z	4
Z'	1
$\theta_{min}/^\circ$	3.380
$\theta_{max}/^\circ$	28.699
Measured Refl.	14536
Independent Refl.	3884
Reflections Used	3045
R_{int}	0.0709
Parameters	235
Restraints	0
Largest Peak	1.092
Deepest Hole	-0.552
GooF	1.080
wR_2 (all data)	0.3428
wR_2	0.3307
R_1 (all data)	0.1725
R_1	0.1503

Experimental Extended.⁶ A clear colourless fragment-shaped crystal with dimensions $0.09 \times 0.08 \times 0.05 \text{ mm}^3$ was mounted on a MITIGEN holder in perfluoroether oil. Data were collected using a Rigaku AFC12 FRE-HF diffractometer equipped with an Oxford Cryostream low-temperature apparatus operating at $T = 100(2) \text{ K}$.

Data were measured using profile data from ω -scans of 1.0° per frame for 15.0 s using MoK_α radiation (Rotating Anode, 45.0 kV, 55.0 mA). The total number of runs and images was based on the strategy calculation from the program CrystalClear (Rigaku). The actually achieve resolution was $\Theta = 28.699$.

Cell parameters were retrieved using the CrysAlisPro (Agilent, V1.171.37.31, 2014) software and refined using CrysAlisPro (Agilent, V1.171.37.31, 2014) on 6234 reflections, 43 of the observed reflections.

Data reduction was performed using the CrysAlisPro (Agilent, V1.171.37.31, 2014) software which corrects for Lorentz polarisation. The final completeness is 99.60 out to 28.699 in Θ . The absorption coefficient (MU) of this material is 0.121 and the minimum and maximum transmissions are 0.56971 and 1.00000.

The structure was solved by Direct Methods using the ShelXT^[202] structure solution program and refined by Least Squares using version of ShelXL.^[202]

The structure was solved in the space group $P2_1/c$ (# 14). All non-hydrogen atoms were refined anisotropically. Hydrogens positions were calculated geometrically and refined using the riding model.

⁶ CrysAlisPro Software System, Agilent Technologies UK Ltd, Yarnton, Oxford, UK (2014). CrystalClear, Rigaku.

6.2.6 Conformational analysis and absolute configuration

All the attempts to obtain good enantiopure crystals of the compounds prepared were not successful. For this reason the relative and absolute configuration was determined by a combination of conformational analysis and theoretical simulations of chiro-optical spectra. Compound **392d** was selected as representative compound because good racemic crystals were obtained for the minor diastereomer (**392d-minor**). X-ray data allowed the determination of the relative configuration of the three stereogenic centres of the cyclopropane ring as R^*,R^*,R^* (**Figure 24**).

Although the rigidity of the cyclopropane core reduces the number of conformations to be considered,^[203] two conformational degrees of freedom due to the rotation of the aldehyde and of the benzoxazole moiety must be considered for the conformational analysis step.

The whole conformational space was explored by means of Monte Carlo searching together with the MMFF94 molecular mechanics force field as implemented in Titan 1.0.5 (Wavefunction inc.)

All the conformations found by MM search within a 10 kcal/mol window were then optimized using DFT at the B3LYP/6-31+G(d,p) level using the Gaussian 09 suite of programs.⁷ The harmonic vibrational frequencies of each optimized conformation were calculated at the same level to confirm their stability (no imaginary frequencies were observed) and to evaluate the ZPE corrected enthalpy and free energy of each conformation. After DFT minimization, four conformations were found to be enclosed in a 1 kcal/mol window as shown in **Figure 27** and marked as **a-d** in **Table 17** and **Table 18**.

⁷ Program Gaussian 09, rev D.01. M. J. Frisch, G. W. Trucks, H. B. Schlegel, G. E. Scuseria, M. A. Robb, J. R. Cheeseman, G. Scalmani, V. Barone, B. Mennucci, G. A. Petersson, H. Nakatsuji, M. Caricato, X. Li, H. P. Hratchian, A. F. Izmaylov, J. Bloino, G. Zheng, J. L. Sonnenberg, M. Hada, M. Ehara, K. Toyota, R. Fukuda, J. Hasegawa, M. Ishida, T. Nakajima, Y. Honda, O. Kitao, H. Nakai, T. Vreven, J. A. Montgomery, Jr., J. E. Peralta, F. Ogliaro, M. Bearpark, J. J. Heyd, E. Brothers, K. N. Kudin, V. N. Staroverov, R. Kobayashi, J. Normand, K. Raghavachari, A. Rendell, J. C. Burant, S. S. Iyengar, J. Tomasi, M. Cossi, N. Rega, J. M. Millam, M. Klene, J. E. Knox, J. B. Cross, V. Bakken, C. Adamo, J. Jaramillo, R. Gomperts, R. E. Stratmann, O. Yazyev, A. J. Austin, R. Cammi, C. Pomelli, J. W. Ochterski, R. L. Martin, K. Morokuma, V. G. Zakrzewski, G. A. Voth, P. Salvador, J. J. Dannenberg, S. Dapprich, A. D. Daniels, Ö. Farkas, J. B. Foresman, J. V. Ortiz, J. Cioslowski, and D. J. Fox, Gaussian, Inc., Wallingford CT, 2009.

Table 17. Relative energies of the four conformations of **392d-minor**

The relative energies have been evaluated using ZPE-corrected enthalpies and different optimization levels: B3LYP/6-31+G(d,p) and M06-2X/6-31+G(d,p). Populations are calculated using Boltzmann distribution at 298°K.

Conformation	H° (B3LYP)	H° (M06-2X)	Pop. (B3LYP)	Pop. (M06-2X)
a	0.74	1.25	14	8
b	0.48	0.88	21	14
c	0.63	0.89	17	14
d	0.00	0.00	48	64

Table 18. Relative energies of the four conformations of **392d-minor**

The relative energies have been evaluated using ZPE-corrected Gibbs free energies and different optimization levels: B3LYP/6-31+G(d,p) and M06-2X/6-31+G(d,p). Populations are calculated using Boltzmann distribution at 298°K.

Conformation	G° (B3LYP)	G° (M06-2X)	Pop. (B3LYP)	Pop. (M06-2X)
a	0.47	0.61	18	16
b	0.08	0.28	35	29
c	0.94	1.00	8	9
d	0.00	0.00	39	46

As predictable, the four conformations correspond to the four different relative dispositions of the CHO and benzoxazole group, and the relative energies (both as ZPE-corrected enthalpies or Gibbs free energies) suggested that all these conformations should be appreciably populated. To check whether a different theoretical level provided different results, the four ground states were optimised again at the M06-2X/6-31+G(d,p) level with similar results in terms of relative energies. Conformation **d** was always the most stable, albeit it does not correspond to that observed in the solid

state, that is conformation **c**. In addition to that, the dihedral angle between the plane of the *p*-nitrophenyl ring and the cyclopropane plane calculated for conformations **c** and **d** is rather different with respect to that observed in the solid state. However, both the calculation levels yield the same results and the different dihedral angle observed in the X-ray structure could be the result of crystal lattice stabilisation. Indeed, when the geometry read from X-ray data was used as input to DFT optimization, the *p*-nitrophenyl ring was rotated to provide again conformation **c**.

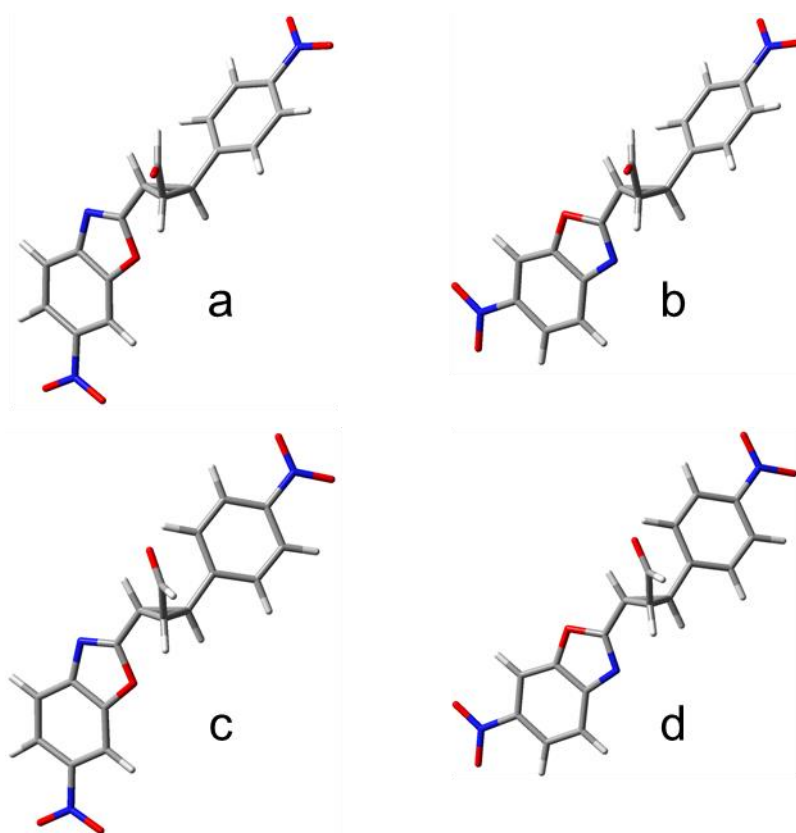


Figure 27. 3D view of the four conformations of the model compound **392d-minor**

6.2.6.1 Absolute configuration

The determination of the absolute configuration (AC) of chiral molecules using chiroptical techniques like optical rotation (OR), electronic circular dichroism (ECD), and vibrational circular dichroism (VCD) has gained feasibility and reliability because of the development of methods for the prediction of these properties based on density

functional theory (DFT) and on its Time-Dependent formalism (TD-DFT).^[204–207] In the present case the theoretical calculation of the electronic circular dichroism spectra (ECD) was selected for the absolute configuration assignment because of the presence of good UV chromophores. The ECD spectrum of **392d-minor (obtained with (R)-catalyst)** was acquired in HPLC-grade acetonitrile solution ($6 \cdot 10^{-5}$ M) with a cell path of 0.5 cm in the 190–400 nm region by the sum of 16 scans at 50 nm/min scan rate (**Figure 28**). Albeit rather weak, the experimental ECD spectrum exhibits three negative Cotton effects at 321, 238 and 206 nm, a broad positive branch at 265–290 nm, as well as two weak positive branches at 222 and 194 nm.

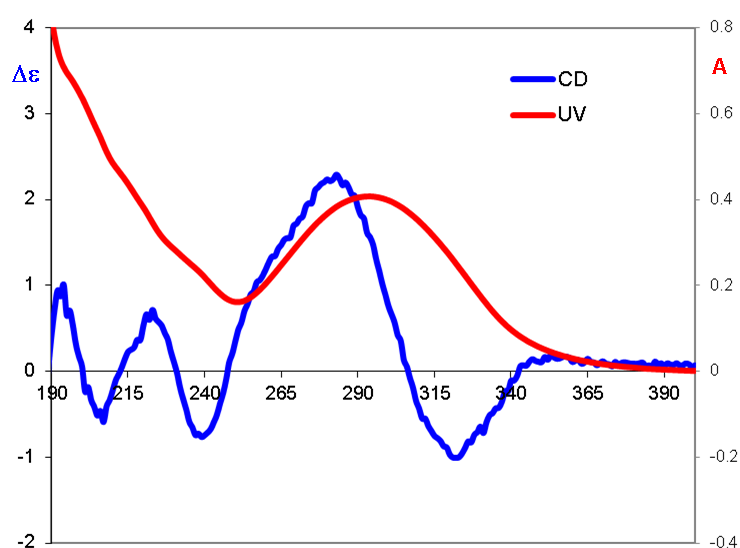


Figure 28. ECD (blue trace) and UV (red trace) spectra of **392d-minor (R)-catalyst**. Spectra were recorded in acetonitrile, $6 \cdot 10^{-5}$ M, 0.5 cm cell path

The electronic excitation energies and rotational strengths have been calculated for the isolated molecule in the gas phase for the four conformations **a-d** using TD-DFT. In a preliminary test, two different basis sets (6-311++G(2d,p) and def2-TZVPP) were employed to calculate the ECD spectrum of conformation **d** using the CAM-B3LYP functional^[208] and the two geometries provided by the B3LYP and M06-2X optimisation steps. The results are reported in **Figure 29**, showing that the basis sets and input geometries did not influence the calculated ECD spectrum at a great extent.

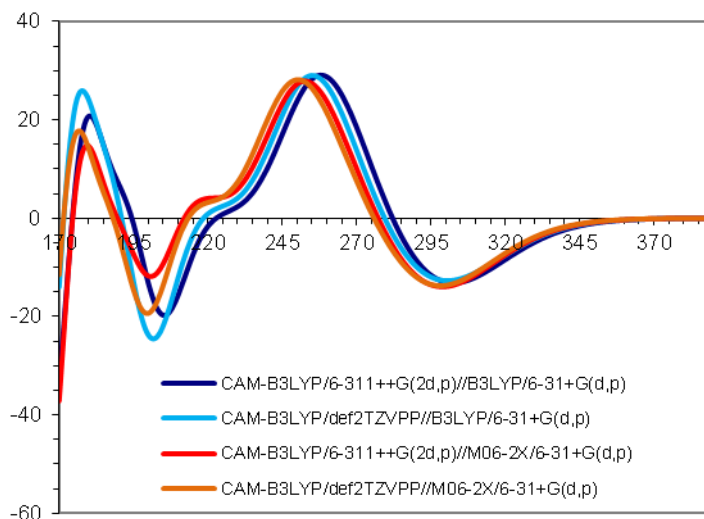


Figure 29. TD-DFT simulated spectra calculated for conformation **d** of **392d-minor**

The spectra were calculated using the same CAM-B3LYP functional, two different basis sets (6-311++G(2d,p) and def2TZVPP) and two different input geometries from B3LYP/6-31+G(d,p) and M06-2X/6-31+G(d,p) optimization. For each calculation the first 60 excited states were calculated, and the spectrum was obtained using a 0.30 eV line width at half height

The ECD spectra of the four conformations were calculated with four different methods (functionals), to ascertain if different computational approaches provide different shapes of the simulated spectra (**Figure 30**).^[209]

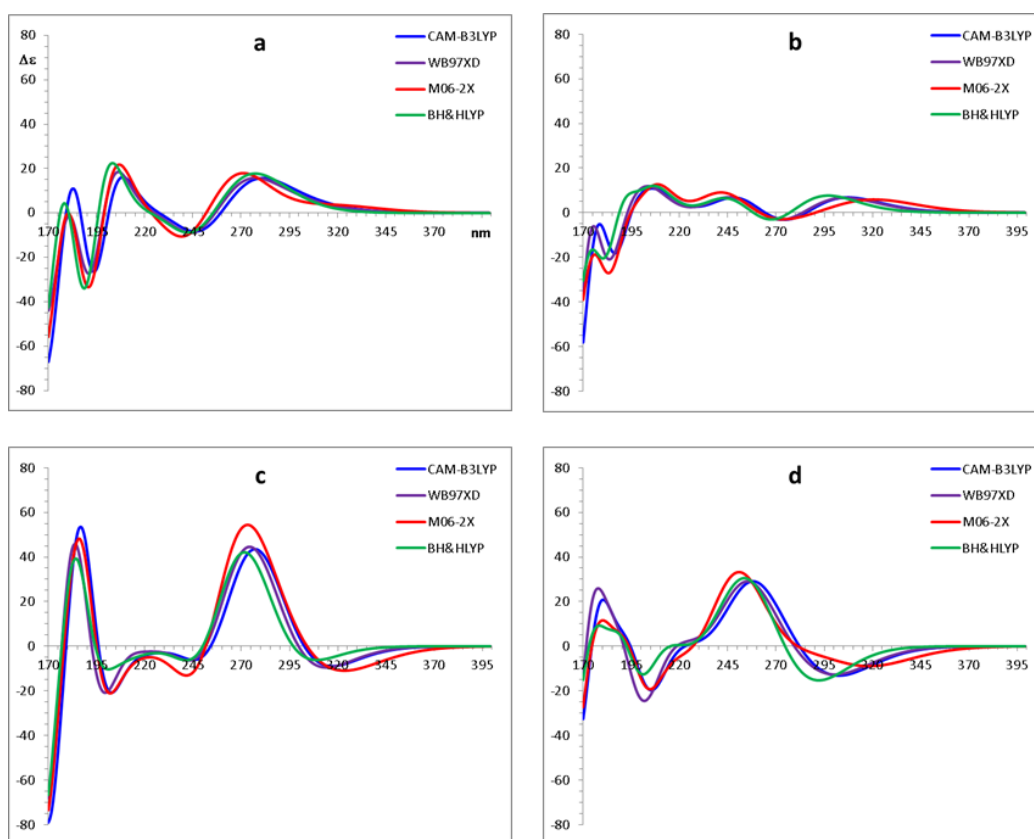


Figure 30. TD-DFT simulated spectra calculated for the four conformations of **392d-minor**

The spectra were calculated using four different functionals (CAM-B3LYP, BH&HLYP, M06-2X, ω B97-XD) and the same 6-311++G(2d,p) basis set. For each conformation the first 60 excited states were calculated, and the spectrum was obtained using a 0.30 eV line width at half height

Simulations were performed using the B3LYP-optimised geometries with the hybrid functionals BH&HLYP⁸ and M06-2X,^[210] ω B97XD that include empirical dispersion^[211] and CAM-B3LYP that includes long range correction using the Coulomb Attenuating Method. Given the result of the preliminary tests, the calculations employed the B3LYP-optimised geometries and the 6-311++G(2d,p) basis set, that is computationally cheaper than def2TZVPP, still providing good accuracy.^[212–217] The rotational strengths were calculated in both length and velocity representation, the resulting values being

⁸ In Gaussian 09 the BH&HLYP functional has the form: $0.5 \cdot E_X^{\text{HF}} + 0.5 \cdot E_X^{\text{LSDA}} + 0.5 \cdot \Delta E_X^{\text{Becke88}} + E_C^{\text{LYP}}$

very similar (RMS difference < 5 %). Errors due to basis set incompleteness should be therefore very small.^[218]

Although the spectra simulated within the same functional for the four conformation are quite different, they are nevertheless consistent with the simulation of the positive Cotton effect in the 245-270 nm region (**Figure 30**). This part of the UV spectrum is dominated by the two UV transitions of the *p*-nitrophenyl moiety (oriented on the long axis) and of the 5-nitrobenzoxazole moiety. The almost coincidence of the simulated spectra for the same conformation on varying the functional, represent a good proof of the simulations consistency.

The population-weighted spectra to be compared with the experimental spectrum were obtained using the percentages derived from ZPE corrected enthalpies (**Table 17**). As shown in **Figure 31**, the spectra simulated assuming 1*R*,2*R*,3*R* absolute configuration match well the Cotton effects at 321, 283 nm. The best simulation was obtained by the ω B97-XD functional, but all the simulated spectra show a good agreement with the experimental one.

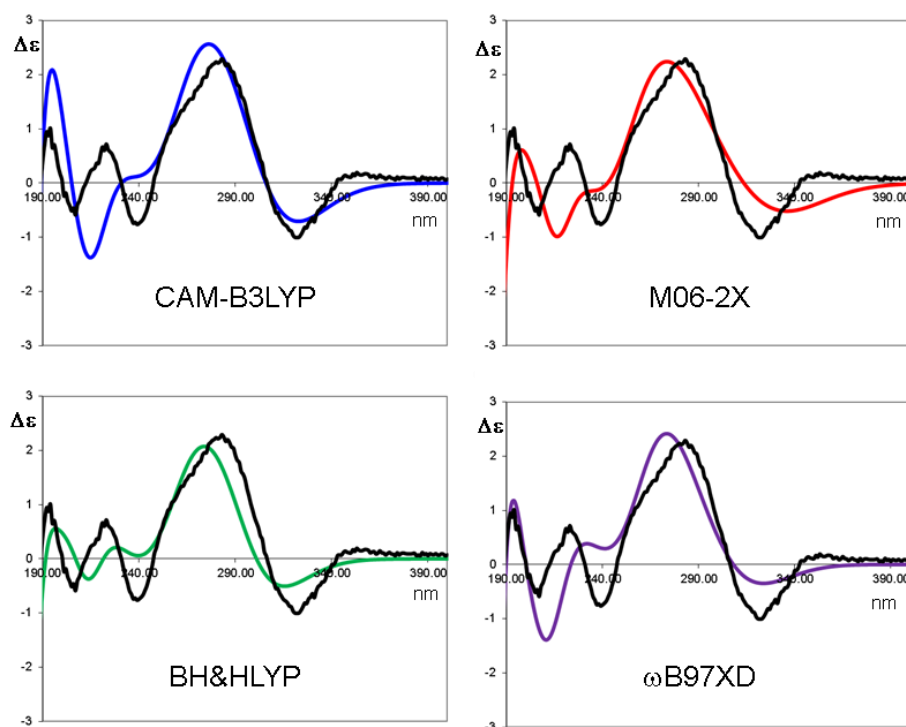


Figure 31. Simulations of the experimental ECD spectrum of **392d-minor** (obtained with (*R*)-catalyst).

For each quadrant, the black line correspond to the experimental spectrum. The colored lines correspond to the simulations obtained using the populations derived from B3LYP/6-31+G(d,p) optimisation. The simulated spectra were vertically scaled and red-shifted by 7-14 nm to get the best match with the experimental spectrum. All the simulations are for the 1*R*,2*R*,3*R* absolute configuration.

6.2.6.2 Major diastereomer

Good single crystals of the major diastereomer could not be obtained and the assignment of the relative configuration was determined by NMR. The ¹H and ¹³C signals were assigned by means of 2D-NMR experiments (COSY, HSQC and HMBC), and NOE spectra were acquired using the DPFGE sequence.^[219] In the case of the major isomer of **392d** (**obtained with (S)-catalyst**) (**392d-major**), the ¹H signals of the hydrogens of cyclopropane were heavily overlapped in a variety of solvent (CDCl₃, DMSO, CD₃CN), and the compound was not chemically stable in CD₃OD. More resolved spectra were obtained for the parent compound **392a** that exhibited a resolved ¹H spectrum in CD₃CN (**Figure 32**). A close inspection of the ¹H spectrum provided useful information about the relative disposition of the three hydrogens of the cyclopropane ring (named as H1, H2 and H3 in **Figure 32**).

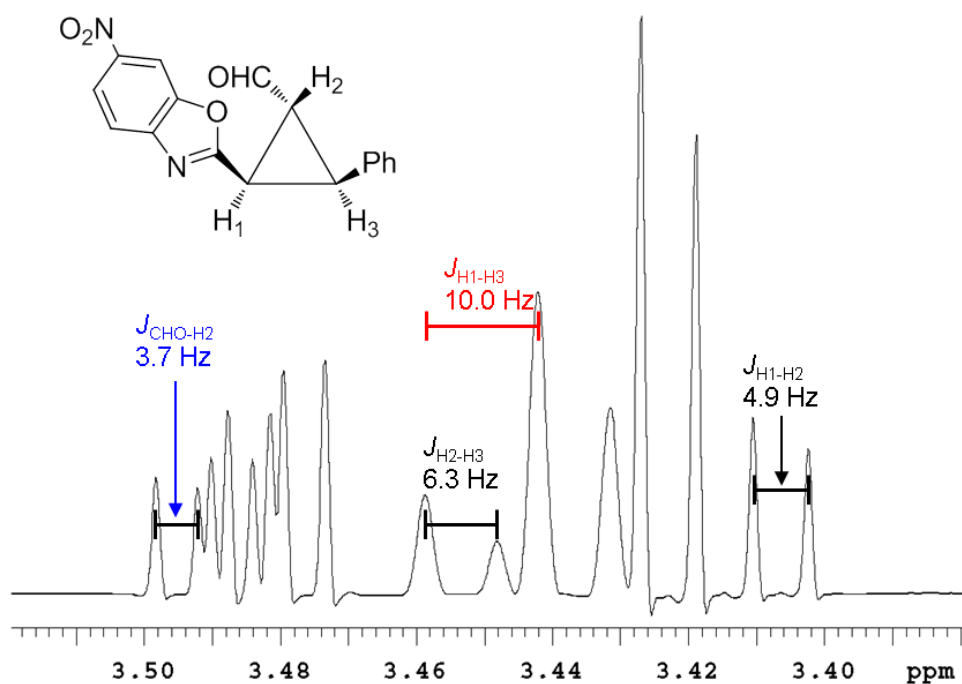


Figure 32. ^1H spectrum of the aliphatic region of **392a-major** (600 MHz, CD_3CN)

The two vicinal 3J coupling constants H2-H1 and H2-H3 have similar values (4.9 and 6.3 Hz, respectively), while the H1-H3 coupling constant between the two CH bearing the aromatic rings is rather large (10.0 Hz). The large value of the latter suggests that the dihedral angle between the two hydrogens is close to 0° (thus a *syn* relationship of the aromatic rings), while the smaller coupling constants of H1 and H3 with H2 are a clear indication of a *gauche* disposition of H2 with respect to H1 and H3 (thus a *trans* relationship of the hydrogens).

As a confirmation, the ^1H spectrum of **392d-minor** showed a similar set of rate constants, but the large one (9.9 Hz) took place between H2 and H3 (see **Table 19**).

To have further support to the assignment based on coupling constant, DFT calculations were run to calculate the coupling constants values of the major isomer supposing the $1R^*, 2R^*, 3S^*$ relative configuration. Due to the rigidity of cyclopropane, the relative disposition of the key hydrogens of the stereogenic centers are fixed independently from the different conformations of the CHO and benzoxazole, and the values of the coupling constants can elucidate the relative stereochemistry.^[220] Before running the NMR simulations, a conformational search was run by means of Monte

Carlo searching together with the MMFF94 molecular mechanics force field. All the conformations found by MM search were then optimised using DFT at the B3LYP/6-31+G(d,p) level and their stability was checked by vibrational analysis. As for **392d-minor**, four conformations were found to be enclosed in a 2 kcal/mol window as shown in **Figure 33** and marked as **a-d** in **Table 19**. Again, the four conformations correspond to the four different relative dispositions of the CHO and benzoxazole group.

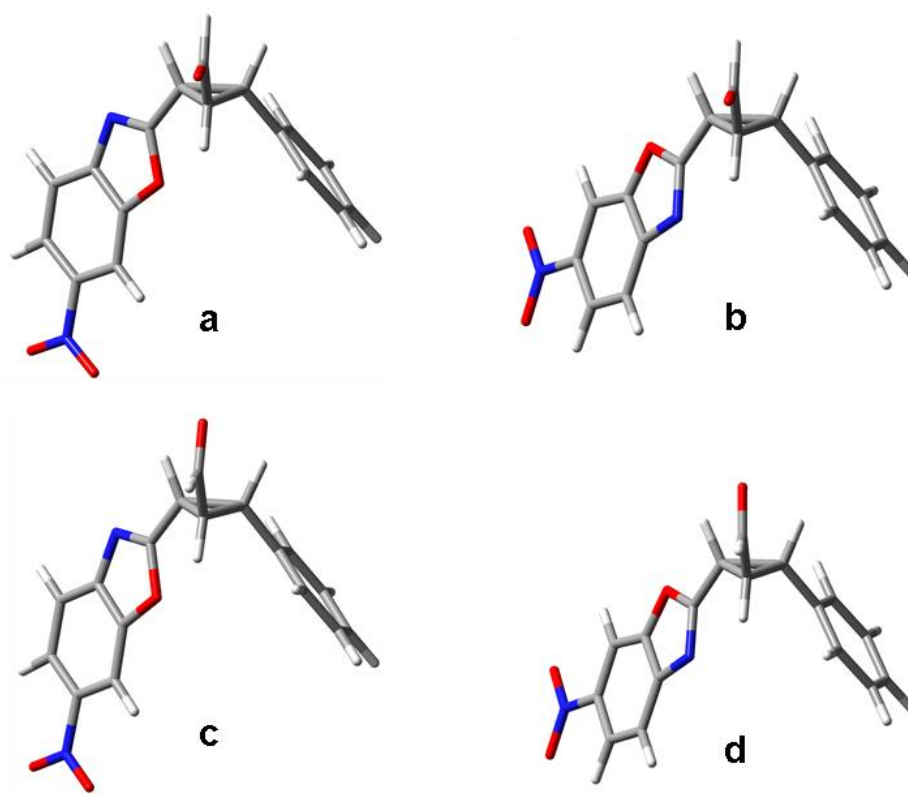


Figure 33. Geometries of the four conformations of **392a-major**

Table 19. Relative energies of the four conformations of **392a-major**

The relative energies were evaluated using ZPE-corrected enthalpies and different optimisation levels: B3LYP/6-31+G(d,p) and M06-2X/6-31+G(d,p). Populations are calculated using Boltzmann distribution at 298°K.

Conformation	H° (B3LYP)	H° (M06-2X)	Pop. (B3LYP)	Pop. (M06-2X)
a	0.58	0.97	15	9
b	0.73	1.37	12	4
c	0.00	0.00	41	44
d	0.17	0.01	31	43

The simulations of the coupling constants were run at the at the B3LYP/6-311++G(2d,p) level using the GIAO method and including the Fermi contact term (Gaussian 09 keyword: spinspin, mixed). The calculated coupling constants for the $1R^*, 2R^*, 3S^*$ relative configuration (**Table 20**) are in a very good agreement with the experimental values of **392a-major**.

Table 20. Calculated and experimental coupling constants for the four diastereomers of **392d**.

Calculations were run at the GIAO-B3LYP/6-311++G(2d,p)//B3LYP/6-31+G(d,p) level. In parenthesis are reported the calculated J-couplings of the conformations in which the H2-C(CO)-H dihedral is close to 180°. In italics are reported the calculated values for those conformations in which the H1-C1-Cq-O \approx 180°. Plain text values are relative to values for those conformations in which the H1-C1-Cq-O \approx 0°

3J	Calcd. for ($1R^*, 2S^*, 3S^*$)	Calcd. for ($1R^*, 2S^*, 3R^*$)	Calcd. for ($1R^*, 2R^*, 3S^*$)	Calcd. for 392d-minor ^a ($1R^*, 2R^*, 3R^*$)	Expl. 392a- major	Expl. 392a- minor
H2-CHO	2.0 (6.9) 1.9 (6.5)	1.8 (6.7) 1.7 (6.9)	1.7 (6.9) 1.7 (6.9)	1.5 (7.6) 1.5 (7.3)	3.7	3.9
H2-H1	9.5 (10.0) 9.0 (9.6)	9.7 (10.1) 9.9 (10.4)	4.9 (5.1) 4.7 (5.1)	5.5 (4.2) 5.7 (4.8)	4.9	4.9
H2-H3	10.8 (10.4) 10.1 (10.4)	5.4 (7.2) 5.5 (6.8)	6.4 (6.9) 6.2 (6.6)	11.3 (11.2) 11.1 (11.2)	6.3	9.9

H1-H3	10.3(10.5) 10.7 (10.7)	7.2 (6.7) 7.6 (7.2)	11.2 (11.3) 11.2 (11.3)	7.4 (6.7) 7.9 (6.9)	10.0	6.6
--------------	---------------------------	------------------------	----------------------------	------------------------	------	-----

^a relative configuration from X-ray data

As a check of the calculation reliability, the coupling constants were calculated also for **392d-minor**, which relative configuration was known from X-ray data. Also in this case the calculated values fully matched the experimental values. It should be noted that in both compounds the experimental value of the H2-CHO coupling constant clearly results from the weighted average of two conformations where the dihedral angle H2-C-(CO)-H is close to 0° or 180° (see below). The resulting experimental value seems to suggest that both of the two conformations are populated roughly at the same extent. The full set of coupling constants were calculated also for the remaining two diastereomers due to the inversion at C2 carbon (**Table 20**, columns 2 and 3). In both cases the set of calculated couplings does not match the experimental data, thus confirming the previous assignment of the (1*R**,2*R**,3*S**) relative configuration to **392a-major**.

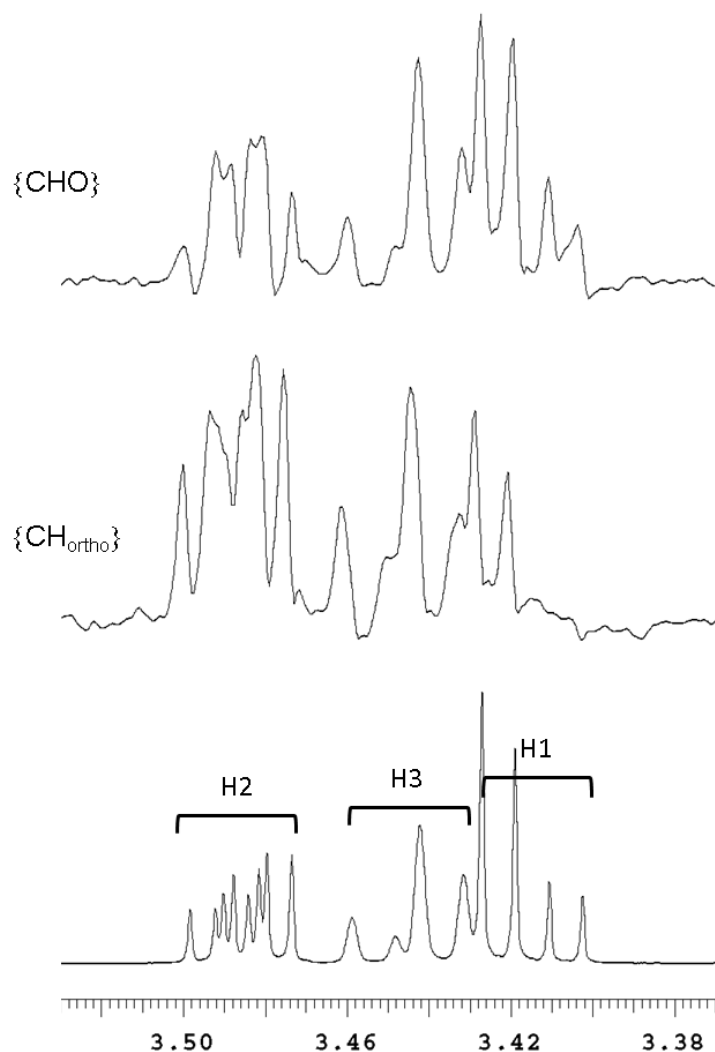


Figure 34. DPGSE NOE spectra of **392a-major** (600 MHz in CD₃CN).

Bottom: control spectrum. Middle trace: NOE obtained on saturation of the *ortho*-phenyl signal. Top trace: NOE obtained on saturation of the CHO signal.

NOE spectra were recorded to further confirm the relative configuration of the major diastereomer of **392a**. These spectra, however, were thwarted by the distance constraints imposed by the cyclopropanic ring and by the partial overlapping of the key signals (H1, H2 and H3). On saturation of the CHO signal (**Figure 34**), comparable NOEs were observed for H1 and H3, while on saturation of the *ortho* hydrogens of the phenyl ring the NOE on H2 is larger than that on H3 and H1. These results again confirm the relative configuration previously assigned by the coupling constants analysis.

6.2.6.3 Absolute configuration of 392d-major

For coherence with the first assignment, the absolute configuration of the major diastereomer was performed on compound **392d-major** (obtained with (S)-catalyst). The ECD spectrum was acquired in HPLC-grade acetonitrile solution ($1 \cdot 10^{-4}$ M) with a cell path of 0.2 cm in the 195-400 nm region by the sum of 16 scans at 50 nm/min scan rate (**Figure 35**). The spectrum of **392d-major** is similar to the of the minor isomer, but the relative intensities of the Cotton effects are different. In this case the two branches at 310 and 270 nm seem to generate a weak exciton coupling and that at 245 nm is much more weaker that the corresponding one of the minor isomer.

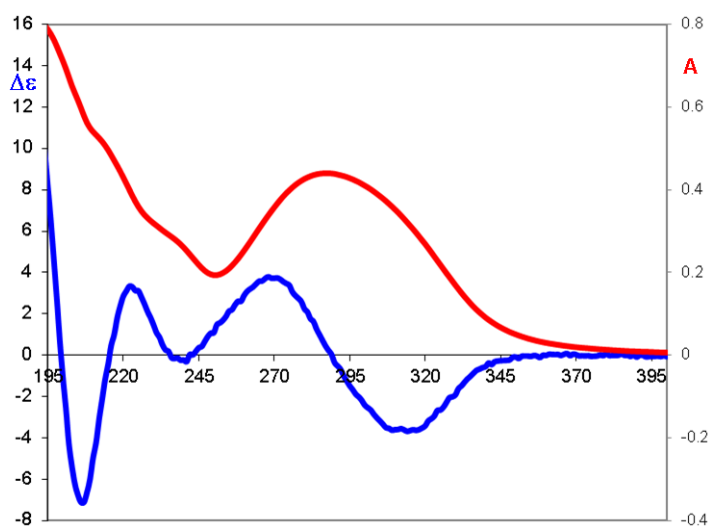


Figure 35. ECD (blue trace) and UV (red trace) spectra of **392d-major** (obtained with (S)-catalyst). Spectra were recorded in acetonitrile, $1 \cdot 10^{-4}$ M, 0.2 cm cell path.

The four stable conformations of **392d-major** were again optimised at the B3LYP/6-31+G(d,p) level starting from the geometries obtained for **392a-major**. Calculations were run in the gas-phase and including two different solvents (chloroform and acetonitrile) using the PCM method.^[221] The relative energies and corresponding populations derived from Boltzmann statistics are reported in **Table 21**.

The electronic excitation energies and rotational strengths have been calculated for the isolated molecule in the gas phase with the four different methods (functionals)

already employed for the simulation of the ECD spectrum of the minor diastereomer (CAM-B3LYP, BH&HLYP, M06-2X, and ω B97XD). In analogy with **392d-minor**, TD-DFT calculations employed the 6-311++G(2d,p) basis set, yielding the results reported in **Figure 36**.

Table 21. Relative energies of the four conformations of **392d-major**

They were evaluated using ZPE-corrected enthalpies obtained from B3LYP/6-31+G(d,p) optimizations in gas phase and including two different solvents (CHCl₃ and CH₃CN) with the PCM method. Populations are calculated using Boltzmann distribution at 298 °K.

Conf.	gas phase	PCM(CHCl ₃)	PCM(CH ₃ CN)	Pop%	Pop%	Pop%
a	1.46	0.20	0.00	5	23	33
b	1.12	0.18	0.08	11	22	28
c	0.79	0.21	0.25	17	23	22
d	0.00	0.00	0.37	67	32	17

Within the same conformation, the four kind of calculations provide very similar traces. However, at a variance with the minor isomer, the simulated spectra for conformations **a** and **d** are nearly opposite to that simulated for **b** and **c**. The two pairs of conformations showing opposite spectra are different because of the $\approx 180^\circ$ rotation of the benzoxazole ring. A rationale of the opposite calculated traces can be found in a close analysis of the different disposition of the *p*-nitrophenyl ring and benzoxazole in the two conformations. (**Figure 37**).

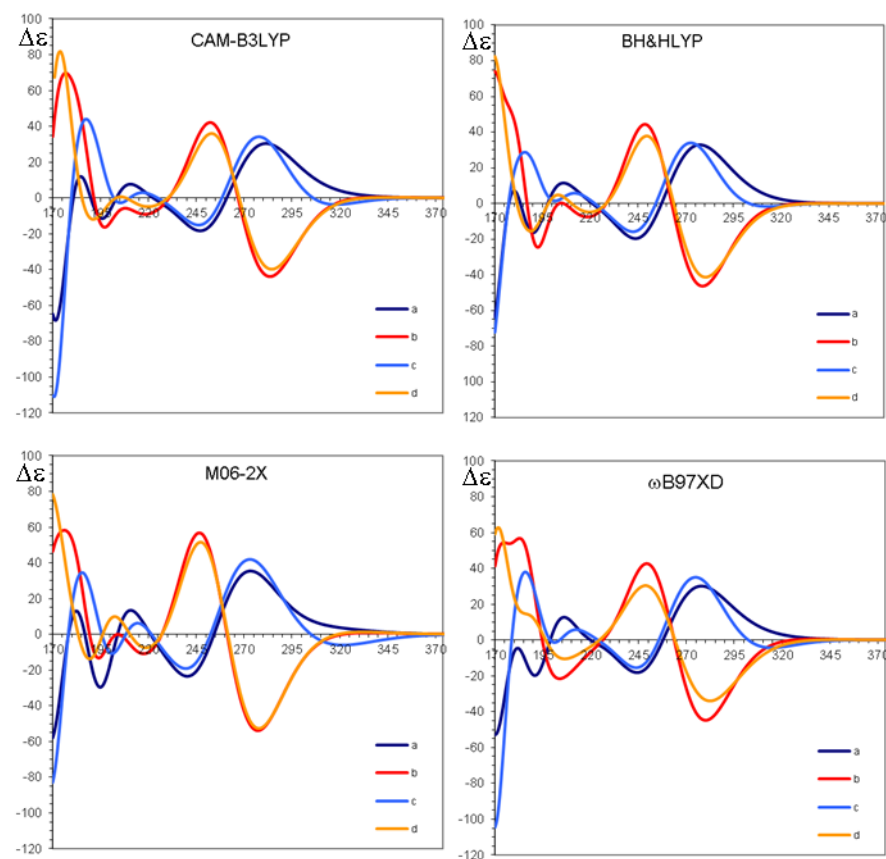


Figure 36. Calculated ECD for each conformation of **392d-major** with different functionals and the same 6-311++G(2d,p) basis set

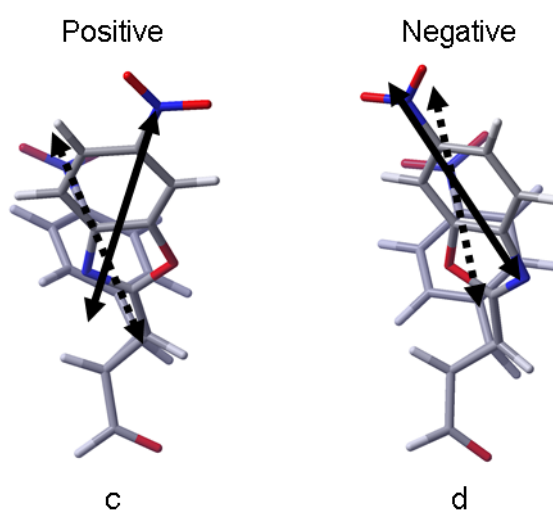


Figure 37. View of the dipoles of **392d-major** acting in the generation of the UV spectrum in the 250-350 nm region.

In both conformations the *p*-nitrophenyl ring is far away from the observer and the benzoxazole is close. The dotted arrows correspond to the UV transition of the *p*-nitrophenyl ring oriented along the long axis, while the full arrow are that of benzoxazole.

The dihedral angles generated by the two dipoles of along the long axes of *p*-nitrophenyl and benzoxazole in the two conformations yield opposite sign, thus explaining the opposite exciton coupling in the simulations.

Being the ECD spectrum the weighted average of the spectra of the four conformations, the correct ratio to be used is crucial for the success of the ECD simulation (in the following discussion only conformations **c** and **d** will be considered since the spectrum of the second conformation of each pair due to CHO rotation is identical). In similar cases^[215,222] the conformational ratio could be evaluated by Dynamic NMR or NOE experiments, but in the present situation this approach is thwarted by the absence of any benzoxazole hydrogen in the closeness of the cyclopropanic ring. To overcome this difficulties, a carefully degassed CDCl₃ NMR sample was prepared in order to extend the effective radius of the NOE effect. CDCl₃ was selected as solvent because of its low viscosity that allows longer T1 relaxation times. In CDCl₃ the two signals of the two CH of cyclopropane bearing the aromatic rings (H1 and H3) are exactly overlapped and yield a doublet, whereas the CH(CHO) signal is a triplet of doublets due to the coupling with the two isochronous CH of cyclopropane and with the CHO. DPGFSE NOE spectra were acquired using long mixing times (4-6 s) corresponding to the T1 relaxation time of the cyclopropanic hydrogens measured at ambient temperature by the inversion-recovery sequence (**Figure 38**).

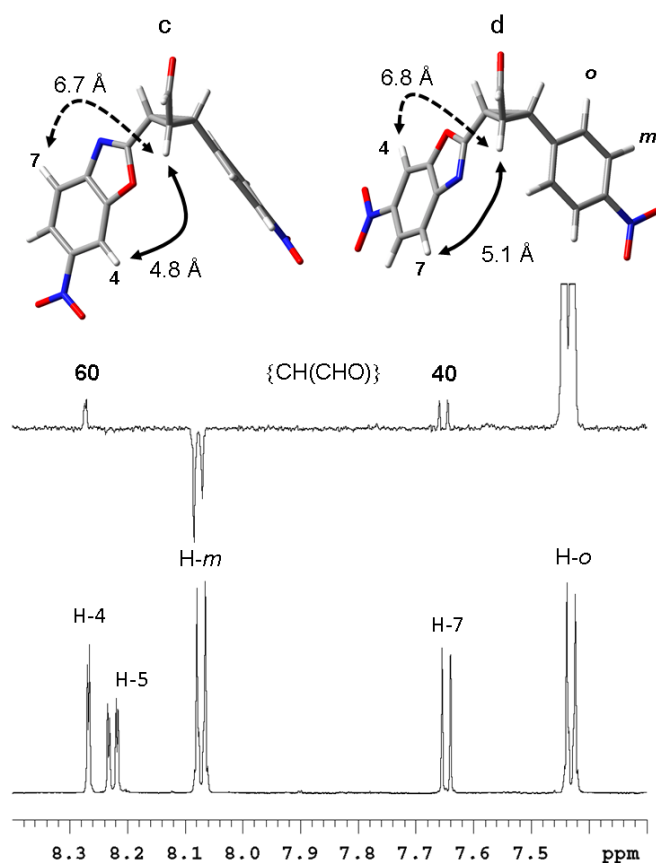


Figure 38. DPGSE-NOE of **392d-major** recorded on saturation of the CH(CHO) signal and using 4 s mixing time.

The negative NOE at 8.08 ppm is due to transferred NOE from the NOE signal at 7.44 ppm.

On saturating the CH(CHO) signal, weak but comparable NOEs were observed on the two aromatic signals in position 4 (*ortho* to the oxygen of benzoxazole) and in position 7 (*ortho* to the nitrogen) of benzoxazole. If only one conformation were populated, NOE should be visible mainly on one signal of the benzoxazole. Taking into account only conformation **c**, the theoretical NOE ratio should be 88:12 in favour of the NOE on H-4. If only conformation **d** were populated, the observed NOE ratio should be reversed to 14:86 (ratio were calculated using the distances of the optimized structures, and using the r^{-6} rule). The experimental evidence of a 60:40 H-4:H-7 ratio suggests that both conformations are appreciably populated. When considering the distances extracted from calculations, the experimental NOE ratio corresponds to a 56:44 ratio in favour of the **c** conformation. Unfortunately the same NOE spectrum

taken in acetonitrile did not allow to see any long-range enhancement, most probably because of faster relaxation times that did not allow to develop measurable NOEs for H-4 and H-7. As from **Table 21**, conformation **d** was calculated to be the most stable in the gas phase and in chloroform, whereas conformation **a** is the most stable in acetonitrile. Nevertheless, the energy differences are very small and well support the NOE results obtained in chloroform. To evaluate the variations caused by the different conformational ratios, the simulations of the experimental ECD spectrum were obtained using the three different sets of relative energies reported in **Table 21**. From the simulations reported in **Figure 39** it is evident that the simulations obtained using the relative ratio suggested by PCM calculations provide better results than that obtained using the gas-phase conformational ratio. Nevertheless, each simulation well reproduces the experimental trace, and the 1*R*, 2*R*, 3*S* absolute configuration can be reliably assigned to the major isomer of **392d**.

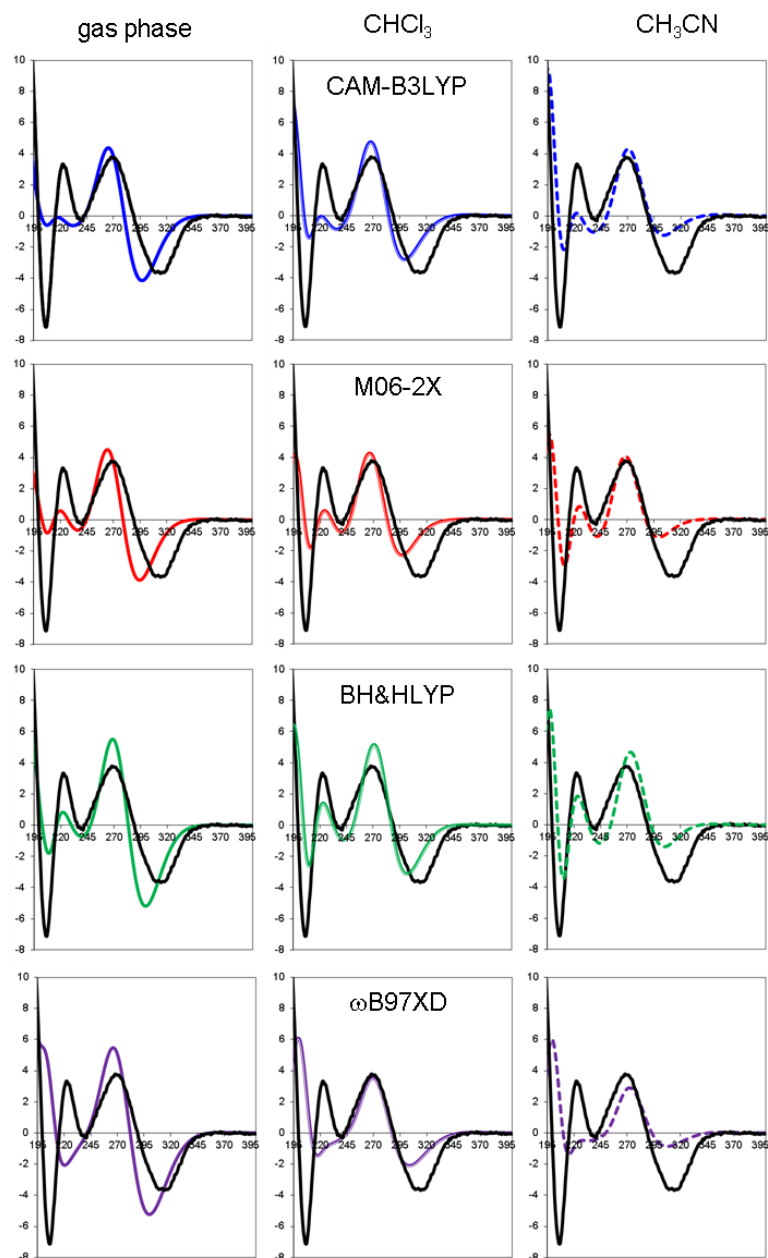


Figure 39. Simulations of the experimental ECD spectrum of **392d-major**.

For each graph, the black line correspond to the experimental spectrum. The colored lines correspond to the simulations obtained using the populations derived from B3LYP/6-31+G(d,p) geometry optimizations. Left column: gas-phase optimization; middle column: PCM optimization with chloroform; right column: PCM optimization with acetonitrile. The simulated spectra were vertically scaled and red-shifted by 12-18 nm to get the best match with the experimental spectrum. All the simulations are for the *1R,2R,3S* absolute configuration.

List of References

- [1] W. Len, *Teratology* **1988**, 38, 203–215.
- [2] G. W. Mellin, M. Katzenstein, *New Eng. J. Med.* **1962**, 267, 1238–1244.
- [3] S. Wnendt, M. Finkam, W. Winter, J. Ossig, G. Raabe, *Chirality* **1996**, 8, 390–396.
- [4] Y. Takeuchi, T. Shiragami, K. Kimura, E. Suzuki, N. Shibata, *Org. Lett.* **1999**, 1, 1571–1573.
- [5] G. Lindeberg, *J. Chem. Educ.* **1987**, 64, 1062–1064.
- [6] A. Datta, S. R. Kumar, S. Roy, *Tetrahedron* **2001**, 57, 1169–1173.
- [7] V. S. Martin, S. S. Woodard, T. Katsuki, Y. Yamada, M. Ikeda, K. B. Sharpless, *J. Am. Chem. Soc.* **1981**, 103, 6237–6240.
- [8] Y. Gao, J. M. Klunder, R. M. Hanson, H. Masamune, S. Y. Ko, K. B. Sharpless, *J. Am. Chem. Soc.* **1987**, 109, 5765–5780.
- [9] Y. Fujima, M. Ikunaka, T. Inoue, J. Matsumoto, *Org. Process Res. Dev.* **2006**, 10, 905–913.
- [10] H. Pellissier, *Tetrahedron* **2008**, 64, 1563–1601.
- [11] V. Jurkauskas, S. L. Buchwald, *J. Am. Chem. Soc.* **2002**, 124, 2892–2893.
- [12] D. A. Evans, J. Bartroli, T. L. Shih, *J. Am. Chem. Soc.* **1981**, 103, 2127–2129.
- [13] D. A. Evans, M. D. Ennis, D. J. Mathre, *J. Am. Chem. Soc.* **1982**, 104, 1737–1739.
- [14] D. A. Evans, K. T. Chapman, J. Bisaha, *J. Am. Chem. Soc.* **1984**, 106, 4261–4263.
- [15] J. A. Ellman, T. D. Owens, T. P. Tang, *Acc. Chem. Res.* **2002**, 35, 984–995.
- [16] A. Job, F. C. Janeck, W. Bettray, R. Peters, D. Enders, *Tetrahedron* **2002**, 58, 2253–2329.
- [17] W. Oppolzer, C. Chapuis, G. Bernardinelli, *Helv. Chim. Acta* **1984**, 67, 1397–1401.
- [18] K. Kiegiel, J. Jurczak, *Tetrahedron Lett.* **1999**, 40, 1009–1012.
- [19] W. S. Knowles, M. J. Sabacky, *Chem. Commun.* **1968**, 1445–1446.
- [20] W. S. Knowles, *Acc. Chem. Res.* **1983**, 16, 106–112.

- [21] A. Miyashita, A. Yasuda, H. Takaya, K. Toriumi, T. Ito, T. Souchi, R. Noyori, *J. Am. Chem. Soc.* **1980**, *102*, 7932–7934.
- [22] T. Ohta, H. Takaya, R. Noyori, *Inorg. Chem.* **1988**, *27*, 566–569.
- [23] V. From, S. M. Available, *J. Am. Chem. Soc.* **1988**, *110*, 629–631.
- [24] T. Katsuki, K. B. Sharpless, *J. Am. Chem. Soc.* **1980**, *102*, 5974–5976.
- [25] E. N. Jacobsen, I. Markò, W. S. Mungall, G. Schroder, K. B. Sharpless, *J. Am. Chem. Soc.* **1988**, *110*, 1968–1970.
- [26] W. S. Knowles, *Angew. Chem. Int. Ed.* **2002**, *41*, 1998–2007.
- [27] R. Noyori, *Angew. Chem. Int. Ed.* **2002**, *41*, 2008–2022.
- [28] K. B. Sharpless, *Angew. Chem. Int. Ed.* **2002**, *41*, 2024–2032.
- [29] M. T. Reetz, *J. Am. Chem. Soc.* **2013**, *135*, 12480–12496.
- [30] L. Rosenthaler, *Biochem. Z.* **1908**, *14*, 238–253.
- [31] S. Pizzarello, A. L. Weber, *Science* **2004**, *303*, 1151.
- [32] J. Casas, M. Engqvist, I. Ibrahim, B. Kaynak, A. Córdova, *Angew. Chem. Int. Ed. Engl.* **2005**, *44*, 1343–1345.
- [33] B. A. Northrup, D. W. C. MacMillan, *Science* **2004**, *305*, 1752–1755.
- [34] G. Bredig, K. Fajans, *Ber. Dtsh. Chem. Ges.* **1908**, *41*, 752–763.
- [35] G. Bredig, P. S. Fiske, *Biochem. Z.* **1913**, *46*, 7–23.
- [36] H. Pracejus, *Justus Liebigs Ann. Chem.* **1960**, *634*, 9–22.
- [37] Z. G. Hajos, D. R. Parrish, *J. Org. Chem.* **1974**, *39*, 1615–1621.
- [38] U. Eder, G. Sauer, R. Wiechert, *Angew. Chem. Int. Ed.* **1971**, *10*, 496–497.
- [39] S. Julia, J. Guixer, J. Masana, J. Rocas, S. Colonna, R. Annunziata, H. Molinari, *J. Chem. Soc. Perkin Trans.* **1982**, *22*, 1317–1324.
- [40] S. Julia, J. Masana, J. C. Vega, *Angew. Chem.* **1980**, *337*, 968–969.
- [41] B. List, R. A. Lerner, C. F. Barbas III, *J. Am. Chem. Soc.* **2000**, *122*, 2395–2396.
- [42] K. A. Ahrendt, C. J. Borths, D. W. C. Macmillan, *J. Am. Chem. Soc.* **2000**, *122*, 4243–4244.

- [43] J. Seayad, B. List, *Org. Biomol. Chem.* **2005**, *3*, 719–724.
- [44] B. List, *Synlett* **2001**, *11*, 1675–1686.
- [45] P. Melchiorre, M. Marigo, A. Carlone, G. Bartoli, *Angew. Chem. Int. Ed.* **2008**, *47*, 6138–6171.
- [46] P. I. Dalko, L. Moisan, *Angew. Chem. Int. Ed.* **2001**, *40*, 3726–3748.
- [47] A. Dondoni, A. Massi, *Angew. Chem. Int. Ed.* **2008**, *47*, 4638–4660.
- [48] B. List, *J. Am. Chem. Soc.* **2002**, *124*, 5656–5657.
- [49] S. E. Denmark, B. M. Eklov, P. J. Yao, M. D. Eastgate, *J. Am. Chem. Soc.* **2009**, *131*, 11770–11787.
- [50] K. Tanaka, A. Mori, S. Inoue, *J. Org. Chem.* **1990**, 181–185.
- [51] T. Okino, Y. Hoashi, Y. Takemoto, *J. Am. Chem. Soc.* **2003**, *125*, 12672–12673.
- [52] S. Brandau, A. Landa, J. Franzén, M. Marigo, K. A. Jørgensen, *Angew. Chem. Int. Ed.* **2006**, *45*, 4305–4309.
- [53] A.-N. Alba, X. Companyó, A. Moyano, R. Rios, *Chem. Eur. J.* **2009**, *15*, 7035–7038.
- [54] F. Ullah, G.-L. Zhao, L. Deiana, M. Zhu, P. Dziedzic, I. Ibrahem, P. Hammar, J. Sun, A. Córdova, *Chem. Eur. J.* **2009**, *15*, 10013–10017.
- [55] S. Zhang, Y. Zhang, Y. Ji, H. Li, W. Wang, *Chem. Commun.* **2009**, *32*, 4886–4888.
- [56] C. Cassani, X. Tian, E. C. Escudero-Adan, P. Melchiorre, *Chem. Commun.* **2011**, *47*, 233–235.
- [57] X. Companyo, A. Zea, A.-N. R. Alba, A. Mazzanti, A. Moyano, R. Rios, *Chem. Commun.* **2010**, *46*, 6953–6955.
- [58] S. Vera, Y. Liu, M. Marigo, E. Escudero-Adán, P. Melchiorre, *Synlett* **2011**, *4*, 489–494.
- [59] M. B. Cid, S. Duce, S. Morales, E. Rodrigo, J. L. G. Ruano, *Org. Lett.* **2010**, *12*, 3586–3589.
- [60] S. Mukherjee, J. W. Yang, S. Hoffmann, B. List, *Chem. Rev.* **2007**, *107*, 5471–5569.
- [61] D. Seebach, A. K. Beck, D. M. Badine, M. Limbach, A. Eschenmoser, A. M. Treasurywala, R. Hobi, *Helv. Chim. Acta* **2007**, *90*, 425–471.

- [62] J. W. Yang, M. T. H. Fonseca, B. List, *J. Am. Chem. Soc.* **2005**, 15036–15037.
- [63] Y. Huang, A. M. Walji, C. H. Larsen, D. W. C. Macmillan, *J. Am. Chem. Soc.* **2005**, 127, 15051–15053.
- [64] M. Marigo, T. Schulte, J. Franze, K. A. Jørgensen, *J. Am. Chem. Soc.* **2005**, 127, 15710–15711.
- [65] R. K. Kunz, D. W. C. MacMillan, *J. Am. Chem. Soc.* **2005**, 127, 3240–3241.
- [66] C. Zhong, X. Shi, *Eur. J. Org. Chem.* **2010**, 16, 2999–3025.
- [67] Z. Du, Z. Shao, *Chem. Soc. Rev.* **2013**, 42, 1337–1378.
- [68] A. E. Allen, D. W. C. Macmillan, *Chem. Sci.* **2012**, 3, 633–658.
- [69] I. Ibrahim, S. Santoro, F. Himo, A. Córdova, *Adv. Synth. Catal.* **2011**, 353, 245–252.
- [70] V. Ceban, P. Putaj, M. Meazza, M. B. Pitak, S. J. Coles, J. Vesely, R. Rios, *Chem. Commun.* **2014**, 50, 7447–7450.
- [71] G.-L. Zhao, F. Ullah, L. Deiana, S. Lin, Q. Zhang, J. Sun, I. Ibrahim, P. Dziedzic, A. Córdova, *Chem. Eur. J.* **2010**, 16, 1585–1591.
- [72] G. Valero, J. Schimer, I. Cisarova, J. Vesely, A. Moyano, R. Rios, *Tetrahedron Lett.* **2009**, 50, 1943–1946.
- [73] X. Companyó, A. Mazzanti, A. Moyano, A. Janecka, R. Rios, *Chem. Commun.* **2013**, 49, 1184–1186.
- [74] A. Mazzanti, T. Calbet, M. Font-Bardia, A. Moyano, R. Rios, *Org. Biomol. Chem.* **2012**, 10, 1645–1652.
- [75] M. Boehringer, H. Fischer, M. Hennig, D. Hunziker, J. Huwyler, B. Kuhn, B. M. Loeffler, T. Luebbers, P. Mattei, R. Narquizian, et al., *Bioorg. Med. Chem. Lett.* **2010**, 20, 1106–1108.
- [76] S. Kolczewski, R. Marty, Hans-Peter Narquizian, E. Pinard, H. Stalder, *U.S. Pat. Appl. Publ.* **2010**, US 2010021.
- [77] H. Graf, L. Franz, H. Sauter, E. Ammermann, E. H. Pommer, *Ger. Offen.* **1988**, DE 3644825.
- [78] D. Heber, M. Verborg, K. Mohr, *Arzneimittelforschung.* **1994**, 44, 809–814.
- [79] J. P. Michael, *Nat. Prod. Rep.* **2000**, 17, 603–620.

- [80] D. Best, H. W. Lam, *J. Org. Chem.* **2014**, *79*, 831–845.
- [81] J.-Y. Liu, H.-Y. Niu, S. Wu, G.-R. Qu, H.-M. Guo, *Chem. Commun.* **2012**, *48*, 9723–9725.
- [82] B. Qian, S. Guo, J. Shao, Q. Zhu, L. Yang, C. Xia, H. Huang, *J. Am. Chem. Soc.* **2010**, *132*, 3650–3651.
- [83] M. Rueping, N. Tolstoluzhsky, *Org. Lett.* **2011**, *13*, 1090–1097.
- [84] R. Niu, J. Xiao, T. Liang, X. Li, *Org. Lett.* **2012**, *14*, 676–679.
- [85] J.-J. Jin, H.-Y. Niu, G.-R. Qu, H.-M. Guo, J. S. Fossey, *RSC Adv.* **2012**, *2*, 5968–5971.
- [86] B. Qian, D. Shi, L. Yang, H. Huang, *Adv. Synth. Catal.* **2012**, *354*, 2146–2150.
- [87] H. Komai, T. Yoshino, S. Matsunaga, M. Kanai, *Org. Lett.* **2011**, *13*, 1706–1709.
- [88] D. Best, S. Kujawa, H. W. Lam, *J. Am. Chem. Soc.* **2012**, *134*, 18193–18196.
- [89] A. J. Simpson, H. W. Lam, *Org. Lett.* **2013**, *15*, 2586–2589.
- [90] T. Li, J. Zhu, D. Wu, X. Li, S. Wang, H. Li, J. Li, W. Wang, *Chem. Eur. J.* **2013**, *19*, 9147–9150.
- [91] S. Mangelinckx, N. Giubellina, N. De Kimpe, S. Ring, *Chem. Rev.* **2004**, *104*, 2353–2399.
- [92] T. Komnenos, *Liebigs Ann. Chem.* **1883**, *218*, 145.169.
- [93] A. Michael, *J. Prakt. Chem.* **1887**, *35*, 349.
- [94] A. Michael, *Am. Chem. J.* **1887**, *9*, 115.
- [95] A. Michael, *J. Prakt. Chem.* **1894**, *49*, 20.
- [96] M.-J. Wu, C.-C. Wu, P.-C. Lee, *Tetrahedron Lett.* **1992**, *33*, 2547–2548.
- [97] L. Falborg, K. A. Jorgensen, *J. Chem. Soc. Perkin Trans. 1* **1996**, *1*, 2823–2826.
- [98] S. B. Tsogoeva, *Eur. J. Org. Chem.* **2007**, *2007*, 1701–1716.
- [99] J. D'Angelo, D. Desmaele, F. Dumas, A. Guignant, *Tetrahedron: Asymmetry* **1992**, *3*, 459–505.
- [100] Y. Zhang, W. Wang, *Catal. Sci. Technol.* **2012**, *2*, 42–53.

- [101] R. Dalpozzo, G. Bartoli, G. Bencivenni, *Symmetry* **2011**, *3*, 84–125.
- [102] S. P. Brown, N. C. Goodwin, D. W. C. Macmillan, *J. Am. Chem. Soc.* **2003**, *125*, 1192–1194.
- [103] H. Gotoh, H. Ishikawa, Y. Hayashi, *Org. Lett.* **2007**, *9*, 5307–5309.
- [104] L. Zu, H. Xie, H. Li, J. Wang, W. Wang, *Adv. Synth. Catal.* **2007**, *349*, 2660–2664.
- [105] Y. Wang, P. Li, X. Liang, T. Y. Zhang, J. Ye, *Chem. Commun.* **2008**, 1232–1234.
- [106] S. Brandau, A. Landa, J. Franzén, M. Marigo, K. A. Jørgensen, *Angew. Chem. Int. Ed.* **2006**, *45*, 4305–4309.
- [107] Y. Wang, P. Li, X. Liang, J. Ye, *Adv. Synth. Catal.* **2008**, *350*, 1383–1389.
- [108] P. Galzerano, G. Bencivenni, F. Pesciaioli, A. Mazzanti, B. Giannichi, L. Sambri, G. Bartoli, P. Melchiorre, *Chem. Eur. J.* **2009**, *15*, 7846–7849.
- [109] S. Cabrera, E. Reyes, A. Milelli, S. Kobbelgaard, K. A. Jørgensen, V. Uni, D.-A. C, *J. Am. Chem. Soc.* **2008**, *130*, 12031–12037.
- [110] M. Nielsen, C. B. Jacobsen, N. Holub, K. A. Jørgensen, D.-A. C, *J. Am. Chem. Soc.* **2009**, *131*, 10581–10586.
- [111] A. D. Fotiadou, A. L. Zografos, *Org. Lett.* **2012**, *14*, 5664–5667.
- [112] Y. Hayashi, H. Gotoh, T. Hayashi, M. Shoji, *Angew. Chem. Int. Ed.* **2005**, *44*, 4212–4215.
- [113] P. T. Anastas, M. M. Kirchhoff, *Acc. Chem. Res.* **2002**, *35*, 686–694.
- [114] R. A. Sheldon, *Chem. Commun.* **2008**, 3352–3365.
- [115] A. Bruggink, R. Schoevaart, T. Kieboom, *Org. Process Res. Dev.* **2003**, *7*, 622–640.
- [116] M. Cameron, R. S. Hoerrner, J. M. Mcnamara, M. Figus, S. Thomas, *Org. Process Res. Dev.* **2006**, *10*, 149–152.
- [117] A. Hantzsch, *Chem. Ber.* **1881**, *14*, 1637–1638.
- [118] B. Gruppen, T. Zerfall, Z. Kennzeichnung, E. Siedepunktsgleichung, E. Verbindung, D. Chloroform-lösungen, D. Absorptionsmaxima, E. Ekmment, *Angew. Chem.* **1959**, *71*, 386.
- [119] C. Mannich, W. Krosche, *Arch. Pharm.* **1912**, *250*, 647–667.
- [120] M. Passerini, *Gazz. Chim. Ital.* **1921**, *51*, 126–129.

- [121] P. Biginelli, *Chem. Ber.* **1891**, *24*, 1317.
- [122] A. Alba, X. Companyó, M. Viciano, R. Rios, *Curr. Org. Chem.* **2009**, 1432–1474.
- [123] L. F. Tietze, *Chem. Rev.* **1996**, *96*, 115–136.
- [124] K. C. Nicolaou, D. J. Edmonds, P. G. Bulger, *Angew. Chem. Int. Ed.* **2006**, *45*, 7134–7186.
- [125] H. Pellissier, *Chem. Rev.* **2013**, *113*, 442–524.
- [126] J. R. Scheerer, J. F. Lawrence, G. C. Wang, D. A. Evans, *J. Am. Chem. Soc.* **2007**, *38*, 8968–8969.
- [127] D. R. Ijzendoorn, P. N. M. Botman, R. H. Blaauw, B. V Chiralix, P. O. Box, C. B. Nijmegen, *Org. Lett.* **2006**, *8*, 239–242.
- [128] T. Takahashi, W. Katouda, Y. Sakamoto, S. Tomida, H. Yamada, *Tetrahedron Lett.* **1995**, *36*, 2273–2276.
- [129] J. Poulin, C. M. Grisé-Bard, L. Barriault, *Chem. Soc. Rev.* **2009**, *38*, 3092–3101.
- [130] J. D. Winkler, H. S. Kim, S. Kim, *Tetrahedron Lett.* **1995**, *36*, 687–690.
- [131] Y. Zhang, G. Wu, G. Agnel, E. Negishi, *J. Am. Chem. Soc.* **1990**, *112*, 8590–8592.
- [132] W. Oppolzer, R. J. Devita, *J. Org. Chem.* **1991**, *56*, 6256–6257.
- [133] D. L. Priebbenow, S. G. Stewart, F. M. Pfeffer, *Tetrahedron Lett.* **2012**, *53*, 1468–1471.
- [134] A. I. Scott, *Synlett* **1994**, *11*, 871–883.
- [135] B. List, *Synlett* **2001**, *11*, 1675–1686.
- [136] J. P. Vigneron, M. Dhaenens, A. Horeau, *Tetrahedron* **1973**, *29*, 1055–1059.
- [137] D. Enders, M. R. M. Hüttl, C. Grondal, G. Raabe, *Nature* **2006**, *441*, 861–863.
- [138] V. Ceban, T. O. Olomola, M. Meazza, R. Rios, *Molecules* **2015**, *20*, 8574–8582.
- [139] G. Bartoli, G. Bencivenni, R. Dalpozzo, *Synthesis* **2014**, *46*, 979–1029.
- [140] H. Pellissier, *Tetrahedron* **2008**, *64*, 7041–7095.
- [141] F. Gnad, O. Reiser, *Chem. Rev.* **2003**, *103*, 1603–1623.
- [142] J. Petruszka, *Chem. Rev.* **2003**, *103*, 1057–1070.

- [143] J. Salaun, *Top. Curr. Chem.* **2000**, 207, 1–67.
- [144] R. Faust, *Angew. Chem. Int. Ed.* **2001**, 40, 2251–2253.
- [145] J. Pietruszka, *Chem. Rev.* **2003**, 103, 1051–1070.
- [146] Y. Nishii, N. Maruyama, K. Wakasugi, Y. Tanabe, *Bioorg. Med. Chem.* **2001**, 9, 33–39.
- [147] W. A. Donaldson, *Tetrahedron* **2001**, 57, 8589–8627.
- [148] R. Csuk, J. Schabel, Y. von Scholz, *Tetrahedron: Asymmetry* **1996**, 7, 3505–3512.
- [149] M. Hogberg, P. Engelhardt, L. Vrang, H. Zhang, *Bioorg. Med. Chem. Lett.* **2000**, 10, 265–268.
- [150] D. K. Mohapatra, A. Datta, *J. Org. Chem.* **1998**, 63, 642–646.
- [151] Y. Katsuda, *Pestic. Sci.* **1999**, 55, 775–782.
- [152] D. Agrawal, V. K. Yadav, *Chem. Commun.* **2008**, 6471–6488.
- [153] R. P. Wurz, A. B. Charette, *Org. Lett.* **2005**, 7, 2313–2316.
- [154] A. C. Carson, A. M. Kerr, *Chem. Soc. Rev.* **2009**, 38, 2969–3276.
- [155] F. De Simone, J. Waser, *Synthesis* **2009**, 20, 3353–3354.
- [156] Z. Zhang, Q. Zhang, S. Sun, T. Xiong, Q. Liu, *Angew. Chem. Int. Ed.* **2007**, 46, 1726–1729.
- [157] H. N. C. Wong, M. Hon, C. Tse, Y. Yip, J. Tank, T. Hudlicky, *Chem. Rev.* **1989**, 89, 165–198.
- [158] H. Reissig, R. Zimmer, C. Ring, *Chem. Rev.* **2003**, 103, 1151–1196.
- [159] E. H. Simmons, D. R. Smith, *J. Am. Chem. Soc.* **1958**, 1556, 5323–5324.
- [160] E. H. Simmons, D. R. Smith, *J. Am. Chem. Soc.* **1959**, 81, 4256–4264.
- [161] J. Furukawa, N. Kawabata, J. Nishimura, *Tetrahedron Lett.* **1966**, 28, 3353–3354.
- [162] J. Furukawa, N. Kawabata, J. Nishimura, *Tetrahedron* **1967**, 24, 53–58.
- [163] M. Cheeseman, F. J. P. Feuillet, A. L. Johnson, S. D. Bull, *Chem. Commun.* **2005**, 2372–2374.
- [164] B. Charette, C. Molinaro, C. Hc, *J. Am. Chem. Soc.* **1998**, 120, 11943–11952.

- [165] M. Lacasse, C. Poulard, B. Charette, *J. Am. Chem. Soc.* **2005**, *127*, 12440–12441.
- [166] E. Muray, O. Illa, J. a Castillo, A. Alvarez-Larena, J. L. Bourdelande, V. Branchadell, R. M. Ortuño, *J. Org. Chem.* **2003**, *68*, 4906–4911.
- [167] J. Crawford, A. Mishra, *J. Am. Chem. Soc.* **1966**, *88*, 3963–3969.
- [168] I. Nozaki, S. Moriuti, H. Takaya, R. Noyori, *Tetrahedron Lett.* **1966**, *43*, 5239–5244.
- [169] R. Rios, J. Liang, M. M.-C. Lo, G. C. Fu, *Chem. Commun.* **2000**, *2*, 377–378.
- [170] E. J. Corey, M. Chaykovsky, *J. Am. Chem. Soc.* **1962**, *84*, 866–867.
- [171] V. K. Aggarwal, H. W. Smith, V. H. Jones, R. Fieldhouse, *Chem. Commun.* **1997**, *1*, 1785–1786.
- [172] C. D. Papageorgiou, M. A. Cubillo de Dios, S. V Ley, M. J. Gaunt, *Angew. Chem. Int. Ed.* **2004**, *43*, 4641–4644.
- [173] J. Vesely, G.-L. Zhao, A. Bartoszewicz, A. Córdova, *Tetrahedron Lett.* **2008**, *49*, 4209–4212.
- [174] J. Zhang, Z. Hu, L. Dong, Y. Xuan, C.-L. Lou, M. Yan, *Tetrahedron: Asymmetry* **2009**, *20*, 355–361.
- [175] I. Ibrahim, G.-L. Zhao, R. Rios, J. Vesely, H. Sundén, P. Dziedzic, A. Córdova, *Chem. Eur. J.* **2008**, *14*, 7867–7879.
- [176] R. Rios, H. Sundén, J. Vesely, G.-L. Zhao, P. Dziedzic, A. Córdova, *Adv. Synth. Catal.* **2007**, *349*, 1028–1032.
- [177] H. Xie, L. Zu, H. Li, J. Wang, W. Wang, *J. Am. Chem. Soc.* **2007**, *129*, 10886–10894.
- [178] X. Companyó, A.-N. Alba, F. Cárdenas, A. Moyano, R. Rios, *Eur. J. Org. Chem.* **2009**, 3075–3080.
- [179] A. Russo, S. Meninno, C. Tedesco, A. Lattanzi, *Eur. J. Org. Chem.* **2011**, 5096–5103.
- [180] F. Pesciaoli, P. Righi, A. Mazzanti, G. Bartoli, G. Bencivenni, *Chem. Eur. J.* **2011**, *17*, 2842–2845.
- [181] L. S. Aitken, L. E. Hammond, R. Sundaram, K. Shankland, G. D. Brown, A. J. A. Cobb, *Chem. Commun.* **2015**, *51*, 13558–13561.
- [182] H. Gotoh, T. Uchimar, Y. Hayashi, *Chem. Eur. J.* **2015**, *21*, 12337–12346.

- [183] S. Kanchiku, H. Suematsu, K. Matsumoto, T. Uchida, T. Katsuki, *Angew. Chem. Int. Ed.* **2007**, *46*, 3889–3891.
- [184] S. Bachmann, M. Furler, A. Mezzetti, *Organometallics* **2001**, *20*, 2102–2108.
- [185] A. Nordqvist, C. Björkelid, M. Andaloussi, A. M. Jansson, S. L. Mowbray, A. Karlén, M. Larhed, *J. Org. Chem.* **2011**, *76*, 8986–8998.
- [186] T.-S. Jiang, J.-H. Li, *Chem. Commun.* **2009**, 7236–7238.
- [187] H. Chen, H. Jiang, C. Cai, J. Dong, W. Fu, *Org. Lett.* **2011**, *13*, 992–994.
- [188] M. Andaloussi, L. M. Henriksson, A. Wie, M. Lindh, C. Bj, A. M. Larsson, S. Suresh, H. Iyer, B. R. Srinivasa, T. Bergfors, et al., *J. Med. Chem.* **2011**, *2*, 4964–4976.
- [189] C. Skeleton, E. Kim, M. Koh, B. J. Lim, S. B. Park, *J. Am. Chem. Soc.* **2011**, *133*, 6642–6649.
- [190] C.-X. Wei, L.-P. Guan, J.-H. Jia, K.-Y. Chai, Z.-S. Quan, *Arch. Pharm. Res.* **2009**, *32*, 23–31.
- [191] R.-G. Xing, Y.-N. Li, Q. Liu, Q.-Y. Meng, J. Li, X.-X. Shen, Z. Liu, B. Zhou, X. Yao, Z.-L. Liu, *Eur. J. Org. Chem.* **2010**, 6627–6632.
- [192] P. D. Davis, D. F. C. Moffat, M. J. Batchelor, *Substituted 2-Pyrimidineamines, Their Preparation and Their Use as Proteine Kinase Inhibitors*, **2000**, US6093716.
- [193] S. J. Coles, P. A. Gale, *Chem. Sci.* **2012**, *3*, 683–689.
- [194] L. Palatinus, G. Chapuis, *J. Appl. Crystallogr.* **2007**, *40*, 786–790.
- [195] G. M. Sheldrick, *Acta Crystallogr. A* **2008**, *A64*, 112–122.
- [196] W. S. Saari, J. J. S. Wai, T. E. Fisher, C. M. Thomas, J. M. Hoffman, C. S. Rooney, A. M. Smith, J. H. Jones, D. L. Bamberger, M. E. Goldman, et al., *J. Med. Chem* **1992**, *2*, 232–233.
- [197] Y. Xie, L. Li, *Tetrahedron Lett.* **2014**, *55*, 3892–3895.
- [198] J. Zhu, J. Liu, R. Ma, H. Xie, J. Li, H. Jiang, W. Wang, *Adv. Synth. Catal.* **2009**, *351*, 1229–1232.
- [199] F. Cermola, *J. Chem. Res.* **2005**, *2005*, 677–681.
- [200] E. Kolehmainen, K. Laihia, P. Manttari, *Magn. Reson. Chem.* **1991**, *29*, 1109–1113.

- [201] O. V. Dolomanov, L. J. Bourhis, R. J. Gildea, J. a. K. Howard, H. Puschmann, *J. Appl. Crystallogr.* **2009**, *42*, 339–341.
- [202] G. M. Sheldrick, *Acta Crystallogr. A* **2008**, *A64*, 112–122.
- [203] P. L. Polavarapu, E. A. Donahue, G. Shanmugam, G. Scalmani, E. K. Hawkins, C. Rizzo, I. Ibnusaud, G. Thomas, D. Habel, D. Sebastian, *J. Phys. Chem. A* **2011**, *115*, 5665–5673.
- [204] G. Pescitelli, L. Di Bari, N. Berova, *Chem. Soc. Rev.* **2011**, *40*, 4603–4625.
- [205] T. D. Crawford, M. C. Tam, M. L. Abrams, *J. Phys. Chem. A* **2007**, *111*, 12057–12068.
- [206] G. Bringmann, T. Bruhn, K. Maksimenka, Y. Hemberger, *Eur. J. Org. Chem.* **2009**, *2009*, 2717–2727.
- [207] A. Mazzanti, D. Casarini, *WIREs Comput. Mol. Sci.* **2011**, *2*, 613–641.
- [208] T. Yanai, D. P. Tew, N. C. Handy, *Chem. Phys. Lett.* **2004**, *393*, 51–57.
- [209] C. E. Check, T. M. Gilbert, *J. Org. Chem.* **2005**, *70*, 9828–9834.
- [210] Y. Zhao, D. G. Truhlar, *Theor. Chem. Acc.* **2007**, *120*, 215–241.
- [211] J.-D. Chai, M. Head-Gordon, *Phys. Chem. Chem. Phys.* **2008**, *10*, 6615–6620.
- [212] G. Cera, M. Chiarucci, A. Mazzanti, M. Mancinelli, M. Bandini, *Org. Biomol. Chem.* **2012**, *14*, 1350–1353.
- [213] X. Companyó, A. Mazzanti, A. Moyano, A. Janecka, R. Rios, *Chem. Commun.* **2013**, *49*, 1184–1186.
- [214] L. Caruana, M. Fochi, S. Ranieri, A. Mazzanti, L. Bernardi, *Chem. Commun.* **2013**, *49*, 880–882.
- [215] M. Ambroggi, A. Ciogli, M. Mancinelli, S. Ranieri, A. Mazzanti, *J. Org. Chem.* **2013**, *78*, 3709–3719.
- [216] L. Caruana, M. Fochi, M. C. Franchini, S. Ranieri, A. Mazzanti, L. Bernardi, *Chem. Commun.* **2014**, *50*, 445–447.
- [217] P. Gunasekaran, S. Perumal, J. C. Mene, M. Mancinelli, S. Ranieri, A. Mazzanti, *J. Org. Chem.* **2014**, *79*, 11039–11050.
- [218] P. J. Stephens, D. M. Mccann, F. J. Devlin, J. R. Cheeseman, M. J. Frisch, *J. Am. Chem. Soc.* **2004**, *126*, 7514–7521.

- [219] J. Stonehouse, P. Adell, J. Keeler, A. J. Shaka, *J. Am. Chem. Soc.* **1994**, *116*, 6037–6038.
- [220] J. D. Graham, M. T. Rogers, *J. Am. Chem. Soc.* **1962**, *84*, 2249–2252.
- [221] J. Tomasi, B. Mennucci, R. Cammi, *Chem. Rev.* **2005**, *105*, 2999–3093.
- [222] E. Paradisi, P. Righi, A. Mazzanti, S. Ranieri, G. Bencivenni, *Chem. Commun.* **2012**, *48*, 11178–11180.

UNIVERSITY OF SOUTHAMPTON

FACULTY OF CHEMISTRY

Department of Chemistry - Faculty of Organic Chemistry: Synthesis, Catalysis
and Flow

Volume 1 of 1

Section 2

**“Green chemistry: first organophotocatalytic approach to the synthesis
of phosphoramidates”**

by

Marta Meazza

Thesis for the degree of Doctor of Philosophy

February 2016

UNIVERSITY OF SOUTHAMPTON

ABSTRACT

FACULTY OF NATURAL AND ENVIRONMENTAL SCIENCES

Organic Chemistry

Thesis for the degree of Doctor of Philosophy

**DEPARTMENT OF CHEMISTRY - FACULTY OF ORGANIC CHEMISTRY: SYNTHESIS,
CATALYSIS AND FLOW**

Marta Meazza

Photocatalysis has become lately a common strategy for the synthesis of new atom-atom bond. Light is a renewable source that should be witnessed as the future for industrial processes.

Our research group started a quest of new green procedures and, for this reason, we turned our attention to photocatalysis. The use of light as the initiator of a chemical reaction presents several advantages in terms of renewable source of energy, cost and generation of waste.

On the other hand, atom economy should be one of the main driving force in the design of new strategies for the synthesis of organic compounds. In this area, Cross Dehydrogenative Couplings have emerged as an useful approach. Formally, in CDC reactions two unfunctionalised molecules react together generating a new atom-atom bond and obtaining hydrogen as the only by-product. In this part of my thesis are described our last efforts in the green chemistry area joining the two concepts of photocatalysis and CDC reactions to generate new green protocols for the formation of atom-atom bonds.

Fascinated by the widely use of phosphoramidates as catalysts, flame retardants or even in biological applications, we focused the attention on their synthesis. All the methodologies previously reported in the literature are based on the use of halogens, phosphoryl chlorides, stoichiometric oxidants or transition metal catalysts. We studied the reaction between phosphites and amines to generate phosphoramidates in a CDC process using a photocatalytic oxidation with oxygen acting as a stoichiometric oxidant.

The reaction was catalysed by an organic dye (Rose Bengal), and the phosphoramidates were obtained in excellent yields in reasonable reaction times when irradiated with green LED light. Importantly, we developed a protocol to isolated the final products without the use of any chromatographic technique making all the process a clear example of green methodology. Moreover we designed a homemade photoreactor that improved reaction times.

Contents

Contents.....	i
List of tables	iii
List of figures	v
List of Schemes	vii
DECLARATION OF AUTHORSHIP	ix
Definitions and Abbreviations.....	xi
1. Introduction	1
1.1 Green chemistry	1
1.2 Photochemistry	3
1.2.1 Photocatalysis	4
1.2.2 Photocatalysts	5
1.2.2.1 Iridium or Ruthenium complexes	6
1.2.2.2 Organic dyes	8
1.2.2.3 Semiconductors	9
1.3 Cross-Dehydrogenative Couplings	10
1.3.1 CDC with metal organic dyes as catalysts	13
2. Objectives	17
3. Phosphoramidates	19
3.1 Synthesis of phosphoramidates	20
4. Organophotocatalytic synthesis of phosphoramidates	25
4.1 Research hypothesis and proposed reaction mechanism	25
4.2 Photoreactor.....	27
4.3 Results and discussions	28
4.3.1 Optimization of the reaction conditions.....	28
4.3.1.1 Screening of organic dyes.....	28
4.3.1.2 Screening of solvents.....	28
4.3.1.3 Screening of LEDs	30
4.3.1.4 Screening of Rose Bengal	30
4.3.1.5 Conversions with different aniline's loading.....	31
4.3.1.6 Screening of solvents for aliphatic amines.....	32

4.3.2	Scope of the reaction with anilines.....	33
4.3.3	Scope of the reaction with aliphatic amines.....	36
4.3.4	Scope of the reaction with different phosphites	38
4.3.5	Studies on the mechanism	38
4.3.5.1	Competition experiment	38
4.3.5.2	Recyclability test.....	39
4.3.5.3	Reaction with radical scavenger.....	39
4.3.5.4	Scale-up of the reaction	40
5.	Conclusions.....	41
6.	Experimental section	43
6.1	General procedure for the synthesis of phosphoramidates	44
6.2	Final products characterisation	45
	List of References	59

List of tables

Table 1. Initial tests	25
Table 2. Screening of solvents	29
Table 3. Screening of LEDs	30
Table 4. Screening of loading of Rose Bengal	31
Table 5. Study of the conversion with different aniline's loading	32
Table 6. Screening of solvents with aliphatic amines	33
Table 7. Scope of the reaction with aromatic amines	34
Table 8. Scope of the reaction with aliphatic amines	36

List of figures

Figure 1. $\text{Ru}(\text{bpy})_3\text{X}_n$ and $\text{Ir}(\text{ppy})_3$	6
Figure 2. Most commonly used organic dyes	9
Figure 3. SET process of semiconductors activated by visible light.....	10
Figure 4. Examples of phosphoramidates' derivatives used in medicinal chemistry.....	19
Figure 5. Applications of phosphoramidates' derivatives	20
Figure 6. Photo and scheme of the photoreactor used in this project	27

List of Schemes

Scheme 1. Photoinduced energy transfer	5
Scheme 2. Photoinduced electron transfer	5
Scheme 3. General mechanism of a reaction photocatalysed by Ru(bpy) ₃ ²⁺	6
Scheme 4. Yoon's [2+2] cycloaddition of a bis(enone)	7
Scheme 5. Proposed reaction mechanism of merging aminocatalysis and photocatalysis	8
Scheme 6. Pd catalysed couplings	10
Scheme 7. Scheme of a CDC reaction	11
Scheme 8. Examples of CDC reactions using stoichiometric oxidants: peroxides (a), DDQ (b), hypervalent iodines (c) and transition metals activating oxygen (d)	12
Scheme 9. Possible ways of decomposition of amine radical cation	13
Scheme 10. Tan's CDC between an <i>N</i> -aryl-tetrahydroisoquinoline and nitroalkanes catalysed by Rose Bengal and green LEDs	13
Scheme 11. Proposed mechanism of the CDC reactions activated by organic dyes and visible light	14
Scheme 12. Rueping's CDC reaction of tetrahydroisoquinoline as electrophile and a range of different nucleophiles	14
Scheme 13. König's CDC reactions between <i>N</i> -aryl-tetrahydroisoquinoline and different nucleophiles catalysed by Eosin Y and green light	15
Scheme 14. General mechanism of the Atherton-Todd reaction	20
Scheme 15. Nucleophilic substitutions of phosphate diesters by alkylamines using POCl ₃	21
Scheme 16. Breifuss' synthesis of phosphoramidates starting from nitroarenes	21

Scheme 17. Mechanism of the Staudinger-phosphite synthesis of phosphoramidates	22
Scheme 18. Chang's synthesis of phosphoramidates with phosphoryl azides catalysed by Ir complex.....	22
Scheme 19. CDC catalysed by Cu salts and O ₂ and proposed mechanism.....	23
Scheme 20. Proposed mechanism of Prabhu's CDC reaction catalysed by I ₂ and H ₂ O ₂	24
Scheme 21. General scheme of the CDC reaction between dialkylphosphite and amines	25
Scheme 22. Proposed mechanism.....	26
Scheme 23. Conditions for the screening of organic dyes	28
Scheme 24. Scope of the reaction with anilines.....	34
Scheme 25. Reaction with tetrahydroisoquinoline for the competition between Kabachnik-Fields product and the phosphoramidation one	36
Scheme 26. Kabachnik-Fields reaction with tetrahydroisoquinoline.....	37
Scheme 27. Rationalisation of the N-P bond formation instead of the C-P.....	37
Scheme 28. Substrate scope with different phosphites.....	38
Scheme 29. Competition experiment between an aniline with an EWG and an EDG ...	38
Scheme 30. Recyclability of Rose Bengal.....	39
Scheme 31. Reaction with radical scavenger	39
Scheme 32. Multigram reaction	40

DECLARATION OF AUTHORSHIP

I, Marta Meazza

declare that the thesis entitled

“Green chemistry: first organophotocatalytic approach to the synthesis of phosphoramidates”

and the work presented in the thesis are both my own, and have been generated by me as the result of my own original research. I confirm that:

- this work was done wholly or mainly while in candidature for a research degree at this University;
- where any part of this thesis has previously been submitted for a degree or any other qualification at this University or any other institution, this has been clearly stated;
- where I have consulted the published work of others, this is always clearly attributed;
- where I have quoted from the work of others, the source is always given. With the exception of such quotations, this thesis is entirely my own work;
- I have acknowledged all main sources of help;
- where the thesis is based on work done by myself jointly with others, I have made clear exactly what was done by others and what I have contributed myself;
- parts of this work have been published as:

“First pure organophotocatalytic synthesis of phosphoramidates” Marta Meazza, Agnieszka Kowalczyk, Luke Shirley, Jung Woon Yang, Hao Gao and Ramon Rios, *Adv. Synth. Catal.*, **2015**, *in press*, DOI 10.1002/adsc.201501068

Signed:

Date:.....

Definitions and Abbreviations

A	Electron acceptor
Ac	Acetyl
Ar	Aryl
bd	broad doublet
bpy	2,2'-bipyridine
br	broad
<i>n</i> -Bu	normal Butyl
<i>t</i> -Bu	tertiary Butyl
°C	degrees centigrade
CB	Conductance Band
CDC	Cross-Dehydrogenative Coupling
Cq	quaternary carbon
δ	chemical shift
D	electron donor
d	doublet
DCM	Dichloromethane
dd	doublet of doublets
DDQ	2,3-Dichloro-5,6-Dicyanobenzoquinone
DG	Directing Group
DMF	N,N-Dimethylformamide
dtd	doublet of triplets of doublets

E, E ⁺	Electrophile
EDG	Electron Donating Group
equiv	equivalents
ESI+	Electrospray Ionization (positive mode)
Et	Ethyl
EtOAc	Ethyl Acetate
EWG	Electron Withdrawing Group
g	gram
h	hour
HRMS	High Resolution Mass Spectrometry
Hz	Hertz
IR	Infra Red
[IrCp*Cl ₂] ₂	(Pentamethylcyclopentadienyl)Iridium Dichloride Dimer
<i>J</i>	coupling constant
m	multiplet
Me	Methyl
mg	milligram
MHz	Mega Hertz
mL	millilitre
mmol	millimoles
m.p.	melting point
Mw	Microwave

<i>m/z</i>	mass / charge ratio
μl	microliter
NMR	Nuclear Magnetic Resonance
NOE	Nuclear Overhauser Effect
NSAID	Nonsteroidal Anti-Inflammatory Drug
Nu	Nucleophile
PC	Photocatalyst
Ph	Phenyl
ppm	parts per million
<i>i</i> -Pr	Isopropyl
<i>n</i> -Pr	Normal Propyl
ProTide	PROdrug + nucleoTIDE
RB	Rose Bengal
rt	room temperature
s	singlet
SOMO	Singly Occupied Molecular Orbital
SET	Single Electron Transfer
t	triplet
td	triplet of doublets
TEMPO	(2,2,6,6-Tetramethylpiperidin-1-yl)oxyl
Tf	Trifluoromethanesulfonyl
TFA	Trifluoroacetic Acid

TLC	Thin Layer Chromatography
TOF	Time of Flight
VB	Valence Band

1. Introduction

1.1 Green chemistry

The area of green chemistry, or sustainable chemistry, is based on the development of chemical processes minimising the production of hazardous substances.^[1,2] Green chemistry was developed since the early 1990s and is based on 12 principles,^[3] developed by Anastas and Warner:^[4]

1. Prevention: it is better to prevent waste than to treat or clean up waste after it has been created.

Regarding the first principle, Sheldon developed the concept of E-factor^[5] that is the calculation of the total amount of waste in a process, considering the amount of reagents, solvents, yields and fuel used. The ideal E factor is zero and is a useful tool to compare chemical processes.

2. Atom Economy: synthetic methods should be designed to maximise the incorporation of all materials used in the process into the final product.

This concept, also called atom efficiency, was introduced by Trost.^[6] It is used to evaluate the amount of waste in a process and it does not take into account the substances that do not appear in the stoichiometric equation.

3. Less Hazardous Chemical Syntheses: wherever practicable, synthetic methods should be designed to use and generate substances that possess little or no toxicity to human health and the environment.
4. Designing Safer Chemicals: chemical products should be designed to affect their desired function while minimising their toxicity.
5. Safer Solvents and Auxiliaries: the use of auxiliary substances (e.g., solvents, separation agents, *etc.*) should be made unnecessary wherever possible and innocuous when used.

6. Design for Energy Efficiency: energy requirements of chemical processes should be recognised for their environmental and economic impacts and should be minimised. If possible, synthetic methods should be conducted at ambient temperature and pressure.
7. Use of Renewable Feedstocks: a raw material or feedstock should be renewable rather than depleting whenever technically and economically practicable.
8. Reduce Derivatives: unnecessary derivatisation (use of blocking groups, protection/deprotection, temporary modification of physical/chemical processes) should be minimised or avoided if possible, because such steps require additional reagents and can generate waste.
9. Catalysis: catalytic reagents (as selective as possible) are superior to stoichiometric reagents.
10. Design for Degradation: chemical products should be designed so that at the end of their function they break down into innocuous degradation products and do not persist in the environment.
11. Real-time analysis for Pollution Prevention: analytical methodologies need to be further developed to allow for real-time, in-process monitoring and control prior to the formation of hazardous substances.
12. Inherently Safer Chemistry for Accident Prevention: substances and the form of a substance used in a chemical process should be chosen to minimise the potential for chemical accidents, including releases, explosions, and fires.

As stated in the principle 9, catalysis is important for green chemistry as it allows the production of less waste and reduces the energy requirements. The works of the Nobel Prize winners in 2001, Sharpless, Noyori and Knowles^[7-9] met some of the requirement for green chemistry processes.

They were still using transition metal catalysts that produce toxic wastes, so the development of organocatalysis and biocatalysis respond even more to the request of

using less toxic catalysts. (These type of catalysis are discussed in Volume 1, Chapter 1 of this thesis)

Photocatalysis, as sub-category of photochemistry, is another step in the search for the development of greener procedures. It uses a light source (a renewable source of energy) to activate the reagents toward a chemical transformations, especially with the use of visible light sources.

For the purpose of this thesis only the visible light photochemistry and photocatalysis will be described in the next sections.

1.2 Photochemistry

Photochemistry is the study of the chemical reactions that happen under the influence of a source of light. Few reactions are reported in the 19th century using the sun as the light source.^[10] Giacomo Ciamician, an Italian chemist that worked at the beginning of the 20th century, is considered the “father of photochemistry”.^[11] In particular, as the fuel was a limited source of energy, he promoted the use of the sun as an unlimited source of energy in an article called “The photochemistry of the future”.

There are two fundamental laws governing photochemistry:

- The first law of photochemistry (Grotthuss-Draper law) states that a compound must absorb the light to have sufficient energy to break or reorganise a covalent bond;
- The second law of photochemistry (Stark-Einstein law) states that only one molecule is activated for each photon absorbed by the system.

The energy supplied by each wavelength is calculated by the Planck-Einstein relation:

$$E = \frac{hc}{\lambda}$$

Where h is the constant of proportionality or Planck constant, c is the speed of light and λ is the wavelength. From the equation is possible to notice that when considering the visible light ($\lambda = 400\text{-}800\text{ nm}$) the E will be lower than using shorter wavelengths

near the ultraviolet ($\lambda = 200\text{-}400\text{ nm}$). Consequently UV light can more easily promote a photochemical reaction compared to visible light. A major drawback in the use of visible light is that most organic molecules are not able to absorb light at longer wavelengths. The solution is to use photosensitizers or photocatalysts.^[12]

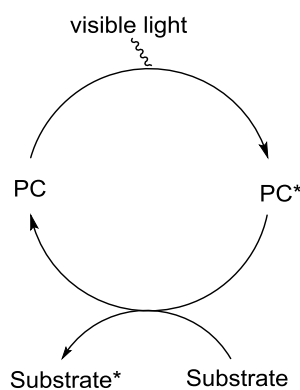
1.2.1 Photocatalysis

The photocatalysis is based on the use of a catalyst that can absorb the visible light and activate in this way the reaction. The idea came from observing plants performing the photosynthesis in which chlorophyll acts as a catalyst. Chlorophyll absorbs energy from sunlight and excites an electron from a lower to a higher state making possible the transfer of the electron to another molecule and its concurrent return to the ground state. A chain of such electron-transfer processes allows at the end the reduction of carbon dioxide and its fixation into sugars. The initial donors are water molecules that will be converted in oxygen.^[13]

The photocatalytic reactions often occur at room temperature and the light source is usually a commercial light bulb: these are clear advantages towards greener procedures, compared to the use of high or low temperatures or UV lamp as source of light. Another advantage is that, as most organic molecules do not absorb the visible light, it is unlikely that side-reactions will happen.^[14]

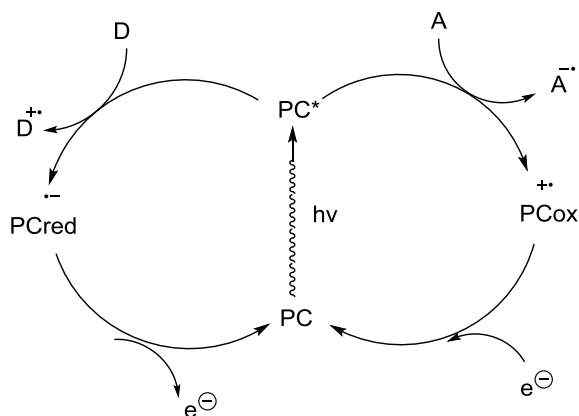
When a molecule absorbs a photon becomes excited and one electron is promoted to an unoccupied molecular orbital and if the spin does not change the two unpaired electrons have opposite spin and the molecule is in a singlet state. If the spin changes, then the two electrons have the same spin and the molecule is in a triplet state. Any of these photoexcited states is more reactive than the starting one.

In a photocatalysed reaction, a photocatalyst (PC) absorbs the light and triggers an energy transfer process or an electron transfer process.^[15] In **Scheme 1** is presented the scheme of a photoinduced energy transfer that can occur from a PC in either a singlet or triplet state.



Scheme 1. Photoinduced energy transfer

The most common pathway is the photoredox catalysis, based on a single electron transfer process (SET) from the photoexcited catalyst that can act as an electron donor or electron acceptor. As shown in **Scheme 2**, the excited photocatalyst (PC^*) can oxidise an electron donor (D) becoming an electron negative radical or it can reduce an electron acceptor (A) becoming an electron positive radical species, both happening through a single electron transfer process. This is followed by a second SET process, reacting with another electron donor or acceptor.



Scheme 2. Photoinduced electron transfer

1.2.2 Photocatalysts

The most common type of catalysts that are activated by visible light can be classified as:

- Iridium or Ruthenium complexes

- Porphyrins or organic dyes
- Semiconductors

1.2.2.1 Iridium or Ruthenium complexes

This type of catalysts are currently the most commonly used, in particular $\text{Ru}(\text{bpy})_3\text{X}_n$ **1** and $\text{Ir}(\text{ppy})_3$ **2** shown in **Figure 1**.^[16,17]

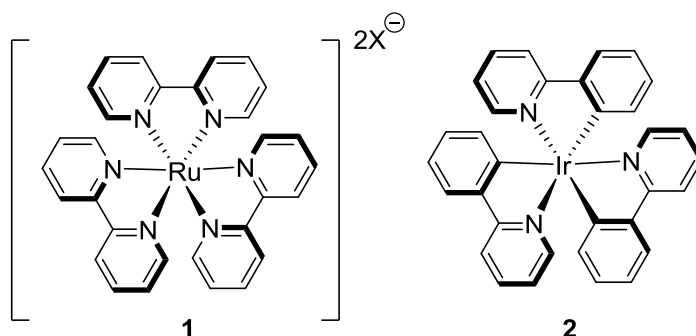
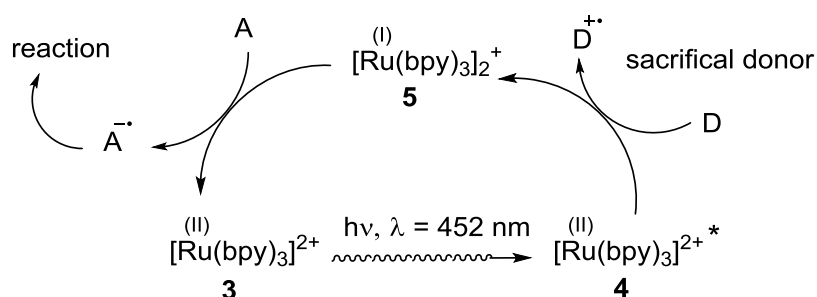


Figure 1. $\text{Ru}(\text{bpy})_3\text{X}_n$ and $\text{Ir}(\text{ppy})_3$

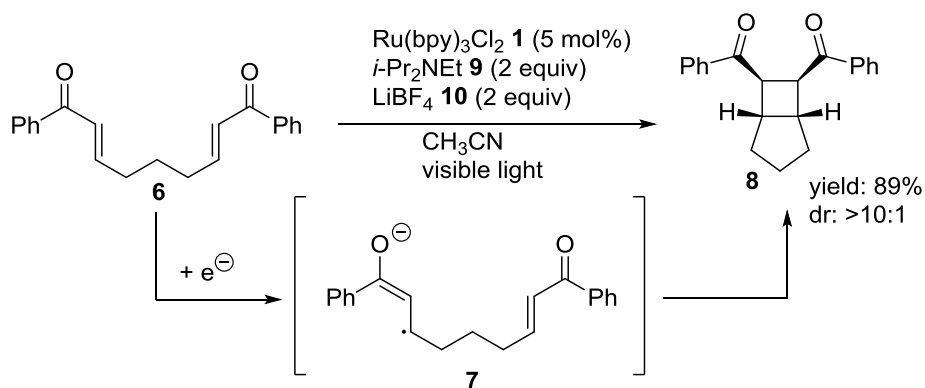
$\text{Ru}(\text{bpy})_3\text{X}_n$ **1** was the first to be developed and is still the most used, in particular for its reductive properties. In **Scheme 3** the general mechanism of a reaction photocatalysed by $\text{Ru}(\text{bpy})_3^{2+}$ **3** is presented. The complex absorbs a photon from the light source and becomes the excited form $\text{Ru}(\text{bpy})_3^{2+*}$ **4** that is subsequently reduced to the $\text{Ru}(\text{I})$ species **5** in the presence of an electron donor (D). In the subsequent step the $\text{Ru}(\text{bpy})_3^+$ **5** acts as electron donor for different kind of substrates (A).



Scheme 3. General mechanism of a reaction photocatalysed by $\text{Ru}(\text{bpy})_3^{2+}$

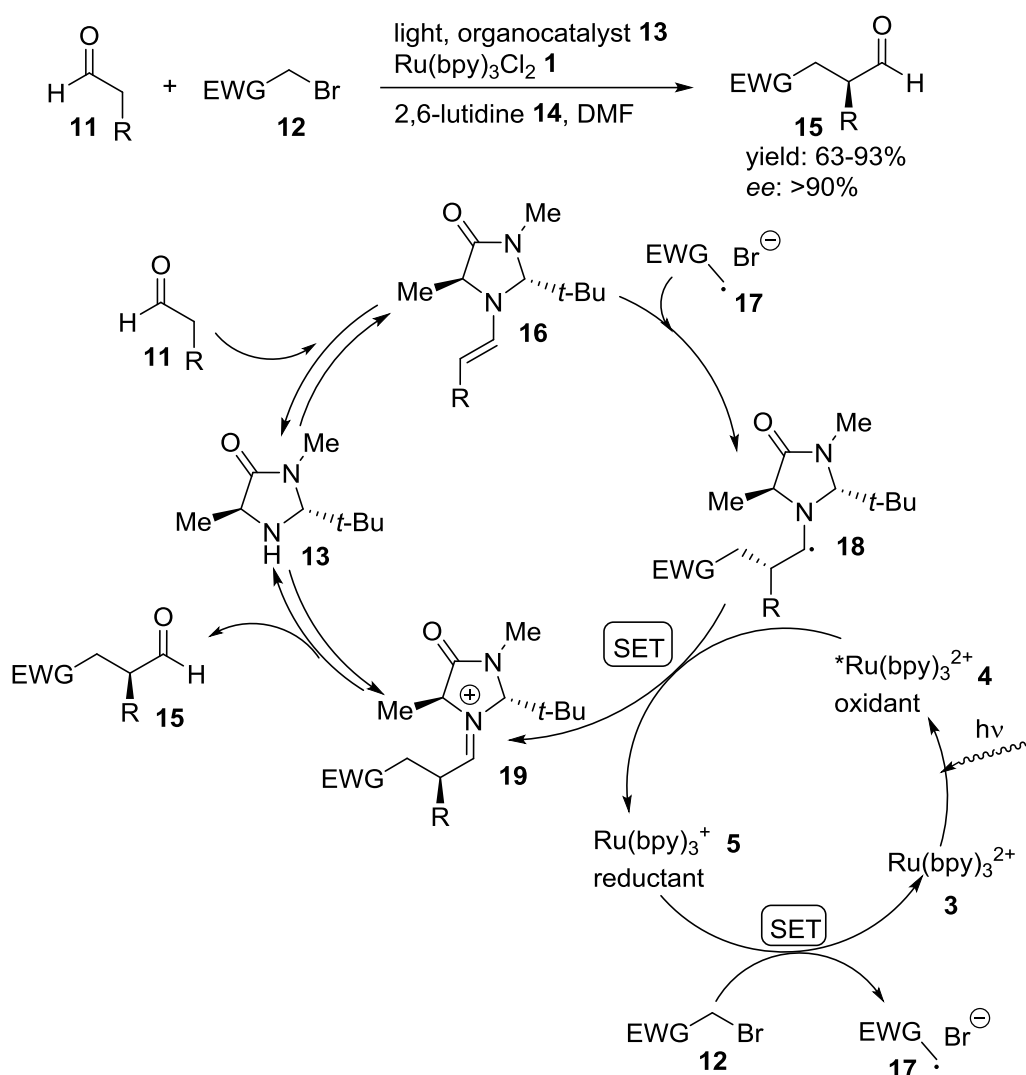
The advantages of this catalyst are the long lifetime of the photoexcited state and the chemical stability of the ground-state form.

In 2008 Yoon *et al.* reported one of the first examples using $\text{Ru}(\text{bpy})_3\text{Cl}_2$ **1** in a synthetically useful transformation.^[18] They reported the use of this complex as catalyst for the [2+2] cycloaddition of a bis(enone) **6** obtaining the final product **8** in good yield and stereoselectivity (**Scheme 4**).



Scheme 4. Yoon's [2+2] cycloaddition of a bis(enone)

In the same year MacMillan *et al.* reported the first example of merging photoredox catalysis and asymmetric organocatalysis in the α -alkylation of aldehydes.^[19] The reaction mechanism proposed by MacMillan is presented in **Scheme 5**. In one catalytic cycle the metal complex **1** is activated by the light and acts, at first, as an oxidant with the intermediate **18** to render the iminium intermediate **19** and then as a reductant to form an electron-deficient alkyl radical **17**. This radical will react with the SOMO of the enamine intermediate **16** formed in the organocatalytic cycle by the reaction of the aldehyde **11** with the secondary amine catalyst **13**. This will lead to the formation of the radical **18** that will undergo a SET process to render the iminium intermediate **19**. The hydrolysis of the iminium ion releases the final aldehyde **15** and the starting catalyst **13** that will re-enter in the catalytic cycle.



Scheme 5. Proposed reaction mechanism of merging aminocatalysis and photocatalysis

1.2.2.2 Organic dyes

Looking for more green reactions, organic chemists studied the use of organic dyes as photocatalysts. Some of the most commonly employed photocatalysts are shown in **Figure 2**. They are all highly conjugated molecules that can absorb a photon from visible light and have an excited state life long enough to be able to act as oxidants or reductants. Organic dyes have the advantage to be less toxic, less expensive and more stable than the corresponding metal complex photocatalysts. More details of the mechanism of activation of organic dyes will be discussed in the section relative to cross-dehydrogenative coupling reactions.

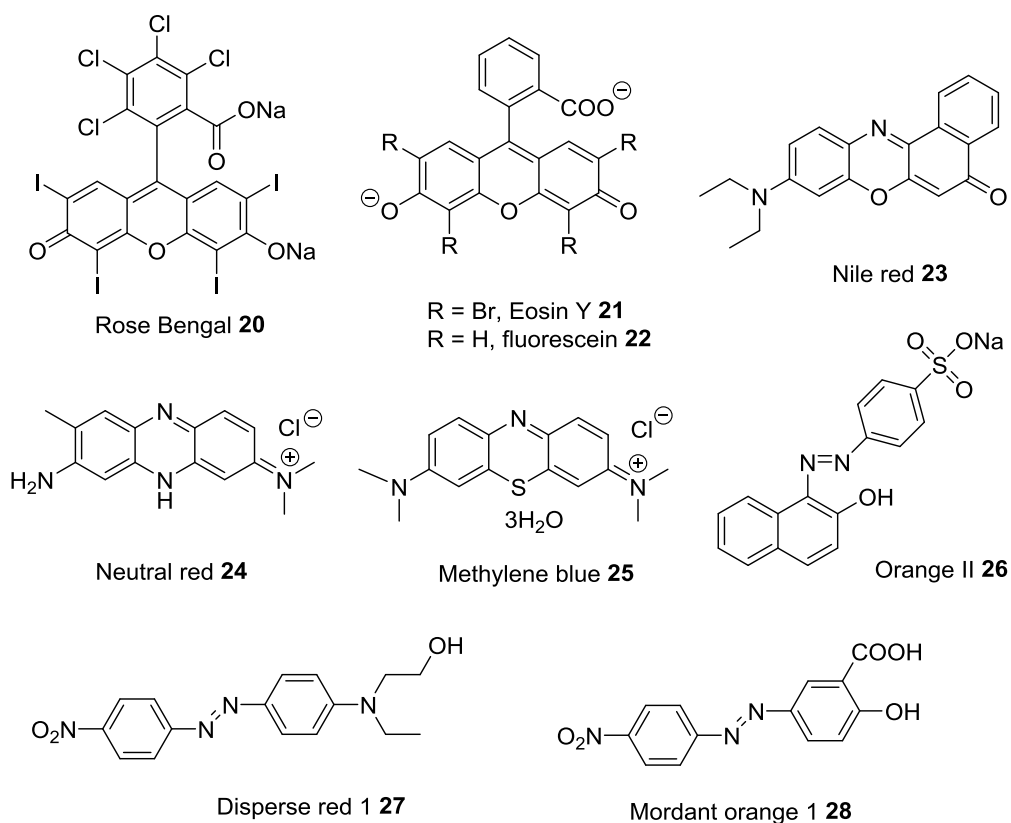


Figure 2. Most commonly used organic dyes

1.2.2.3 Semiconductors

Semiconductors are easily available, cheap and non-toxic; the most used one is TiO₂.

After excitation by a light source of the valence band (VB) of the semiconductor, the electrons are excited in the conductance band (CB) as an electron-hole pair. After their migration to the surface of the semiconductor, a SET can take place with an electron acceptor (A) or an electron donor (D) as shown in **Figure 3**.

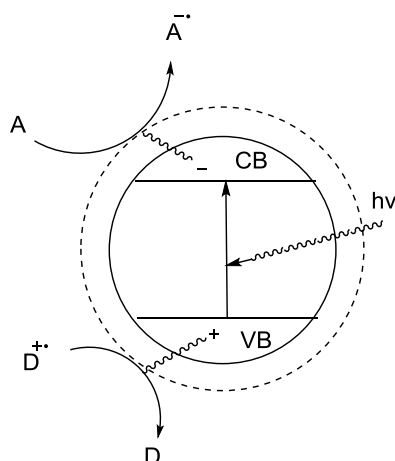
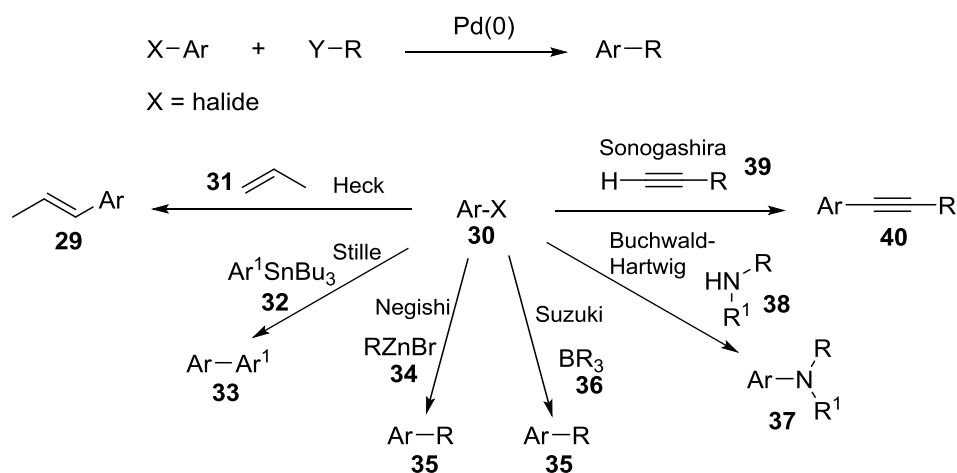


Figure 3. SET process of semiconductors activated by visible light

1.3 Cross-Dehydrogenative Couplings

Carbon-carbon bond formations are among the most important synthetic chemistry processes. The most common methods to form C-C bonds are the transition-metal catalysed cross-coupling reactions, in particular those catalysed by Pd (**Scheme 6**).^[20] The disadvantage of these reactions is the need for a prefunctionalised starting material (Y), thus adding an extra step to the synthesis.



Scheme 6. Pd catalysed couplings

Inspired by the search for greener and more sustainable procedure, Cross-Dehydrogenative Coupling (CDC) reactions were developed.^[21] This chemistry overcomes the drawbacks of the functional group chemistry, developing

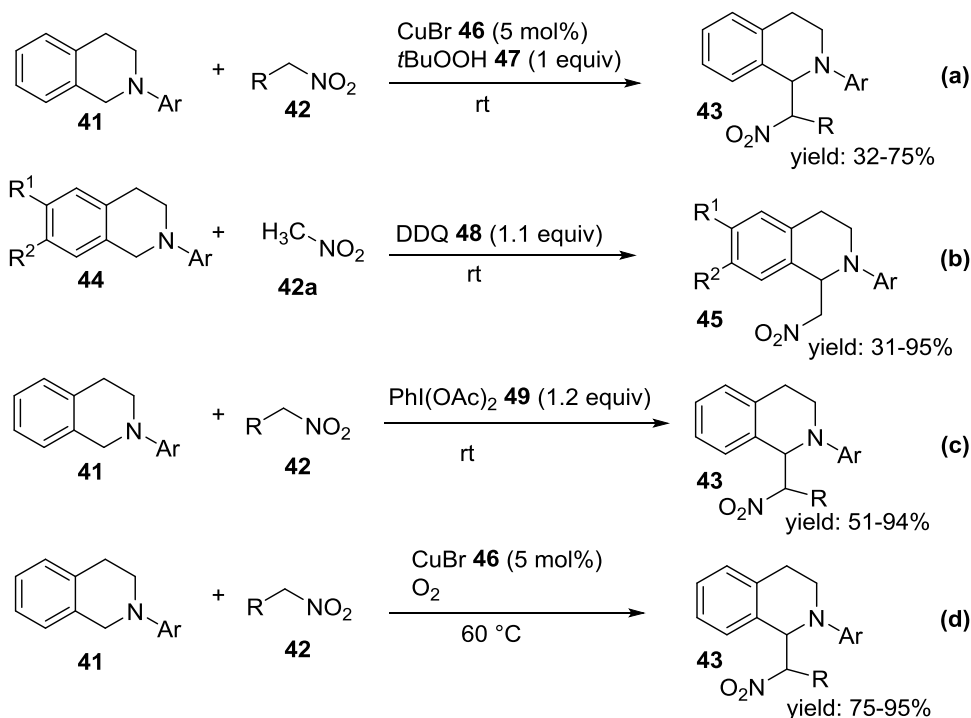
methodologies that directly activate the C-H bond (**Scheme 7**), creating the new bond whilst eliminating a hydrogen atom from each reagent. The benefits are the production of less waste, the lower costs and the minor number of synthetic steps required. Challenges include the selective activation of one C-H over the others present in the molecule and the low reactivity of the C-H bond.



Scheme 7. Scheme of a CDC reaction

Even if examples are present in literature since 1960s, the CDC reactions have seen a huge development in the last fifteen years. This methodology has been used not only for the formation of carbon-carbon bond,^[22,23] but also carbon-heteroatom bond^[24] and more recently, heteroatom-heteroatom bond.^{[25][26]}

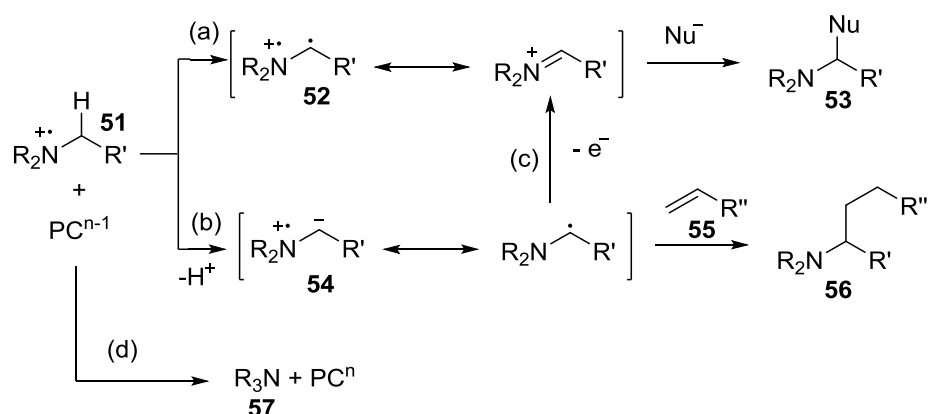
However, CDC reactions often require the use of oxidants to generate the reactive species. In the literature, amines can go through CDC processes due to their oxidation to imines. For example tetrahydroisoquinolines **41** and **44** can react with nitromethane **42a** through a CDC reaction using different oxidation approaches (**Scheme 8**): stoichiometric oxidants such as peroxides **47**,^[27] 2,3-dichloro-5,6-dicyanobenzoquinone (DDQ, **48**)^[28] or hypervalent iodines **49**,^[29] transition metals **46** or photocatalysts to activate oxygen.^[30]



Scheme 8. Examples of CDC reactions using stoichiometric oxidants: peroxides (a), DDQ (b), hypervalent iodines (c) and transition metals activating oxygen (d)

In recent years, light activated CDC reactions have been developed, most of them catalysed by transition metal complexes^[31] and, more recently, by organic dyes. Precisely the use of oxygen as stoichiometric oxidant, activated by photocatalysts, is the greener procedure.

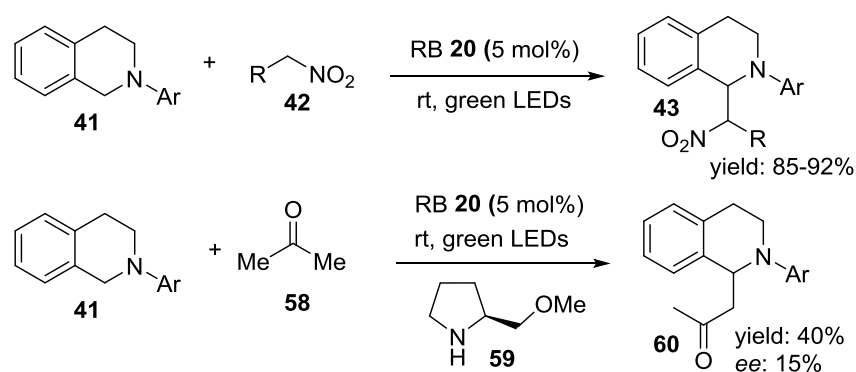
Electron-rich alkylamines are the most common electrophiles used in photocatalytic CDC reactions. After the oxidation of the amines thanks to the excited photocatalyst, a radical cation **51** is formed on the amine. This intermediate can decompose in different ways (**Scheme 9**): (a) abstraction of the proton in α -position of the amine with the formation of an iminium ion **52** that can be attacked by a nucleophile; (b) deprotonation with the formation of a carbon radical intermediate **54**; these species can react with olefins or arenes or (c) can generate an iminium ion through oxidation *via* a SET; (d) regeneration of the neutral amine **57** via a SET with the reduced photocatalyst.



Scheme 9. Possible ways of decomposition of amine radical cation

1.3.1 CDC with metal organic dyes as catalysts

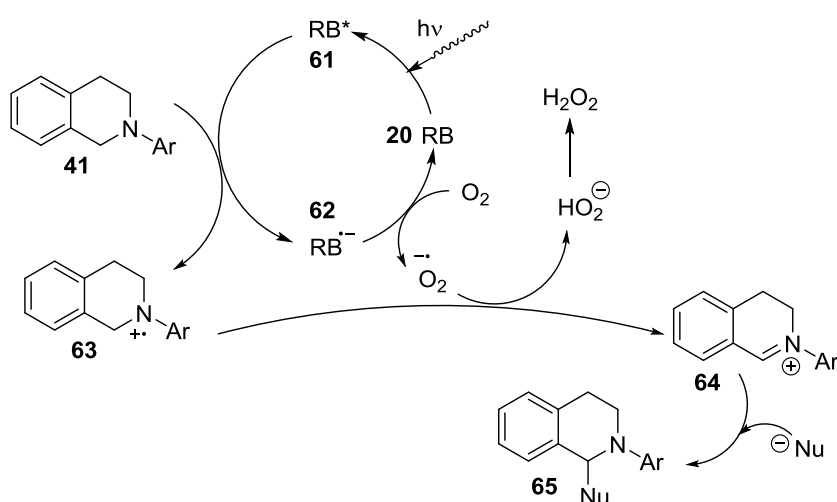
In the last years several photochemical reactions catalysed by organic dyes have been developed as the dyes are less toxic, cheaper and more stable than the metal catalysts. Tan *et al.* reported a CDC between a *N*-aryl-tetrahydroisoquinoline **41** and nitroalkanes **42** catalysed by Rose Bengal **20** and green LEDs as the source of light. They also reported the same reaction using acetone **58**, activated by pyrrolidine/trifluoroacetic acid (TFA) as nucleophiles or a chiral version using *L*-proline or its derivatives **59**, obtaining all the products **60** in good yields but with low enantioselectivities (**Scheme 10**).^[32]



Scheme 10. Tan's CDC between an *N*-aryl-tetrahydroisoquinoline and nitroalkanes catalysed by Rose Bengal and green LEDs

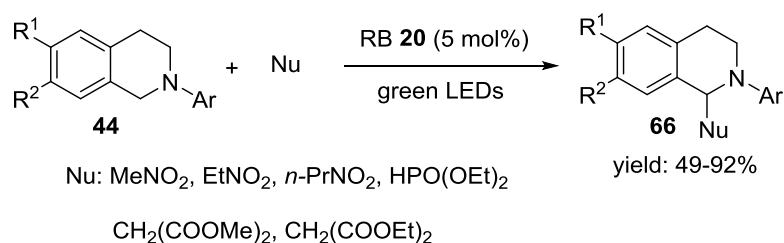
The proposed mechanism is presented in **Scheme 11**: the Rose Bengal (RB, **20**) is excited by the light to form RB* **61**, this form abstracts an electron from the *N*-aryl-

tetrahydroisoquinoline **41** through a SET process, forming a radical anion on the RB **62** and a radical cation on the amine **63**. Then the RB radical anion **62** is re-oxidised to the starting RB by oxygen with the formation of an oxygen radical anion. This last radical anion reacts with the amine radical cation **63** with the formation of hydroperoxide anion and an iminium cation **64** that can be trapped by different nucleophiles.



Scheme 11. Proposed mechanism of the CDC reactions activated by organic dyes and visible light

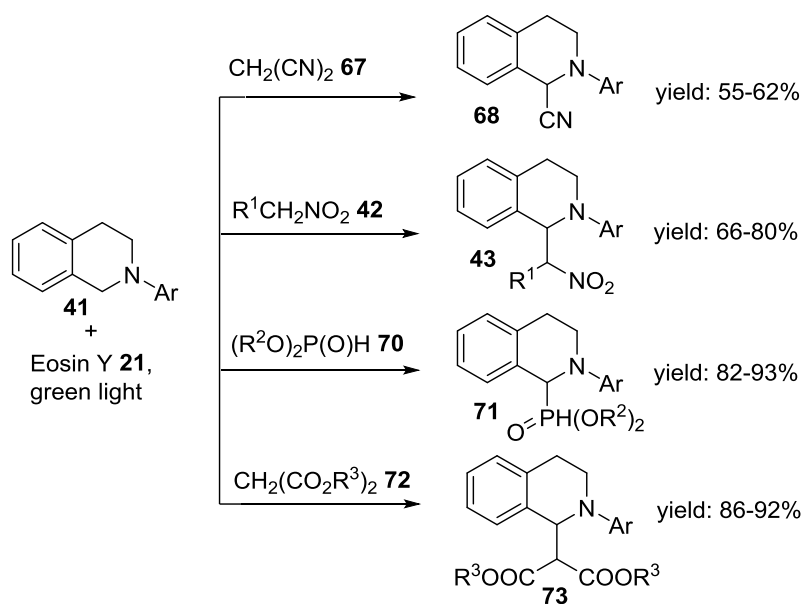
Rueping and co-workers developed a similar CDC reaction, catalysed by green light and Rose Bengal **20** as dye, using a tetrahydroisoquinoline **44** as electrophile and a range of different nucleophiles (**Scheme 12**).^[33] They performed these reactions with a flow reactor, allowing for a more efficient, uniform and reproducible reaction.



Scheme 12. Rueping's CDC reaction of tetrahydroisoquinoline as electrophile and a range of different nucleophiles

König *et al.* reported similar reactions but catalysed by Eosin Y **21** and green light to oxidise *N*-aryl-tetrahydroisoquinoline **41**.^[34] The nucleophiles that attack the

intermediate iminium ion are malononitrile **67**, nitroalkanes **42**, dialkylphosphonates **70** and malonates **72** as shown in **Scheme 13**.



Scheme 13. König's CDC reactions between *N*-aryl-tetrahydroisoquinoline and different nucleophiles catalysed by Eosin Y and green light

2. Objectives

Fascinated by the use of organic dyes as photocatalysts for visible light CDC atom-atom forming reactions, we planned their use in the formation of phosphorous-nitrogen bonds. The objectives of this project are the development of CDC reaction catalysed by visible light and an organic dye in the formation of a P-N bond, in particular between phosphites and amines in order to synthesise phosphoramidates in a safer and greener way, avoiding the use of toxic reagents.

Phosphoramidates attracted our interest as they are important scaffolds. To cite just a few examples, they are used as scaffolds of biological active molecules, as chiral ligands, as organocatalysts and in the ProTide technology. Despite their importance, the synthesis of phosphoramidates requires the use of harsh conditions or halides or transition metals (more information on phosphoramidates' synthesis and their use will be presented in Chapter 3).

3. Phosphoramidates

Phosphoramidates are important structures in biologically active molecules (**Figure 4**) for example as constituents of antibiotics as the antifungal antibiotic phosphomidosine **74**^[35] or the microcin C7 **75**,^[36,37] an antibiotic that inhibits the protein synthesis in vivo. Phosphoramidates' derivatives are also used as nonsteroidal anti-inflammatory drugs (NSAID) **76**, for the treatment of osteoarthritis^[38] and phosphoramidate ProTide technology^[39] has been used to bypass the rate-limiting step of the initial phosphorylation of nucleosides.

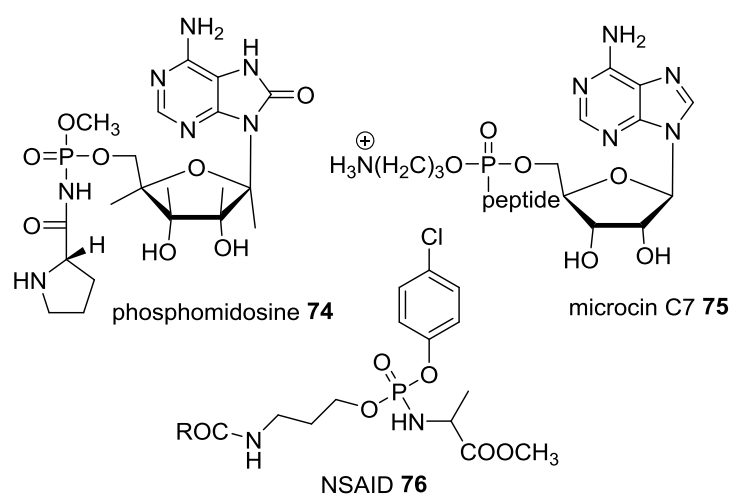


Figure 4. Examples of phosphoramidates' derivatives used in medicinal chemistry

Phosphoramidates **77** have been used as flame retardants **79**^[40] and in Mass Spectrometry **82**^[41,42] improving the ionisation efficiency in the electrospray ionisation. Moreover, in the last years has been reported the use of phosphoramidates' derivatives as ligands **78** in hydroaminoalkylation reactions^[43] and, by Zhou and co-workers, as catalysts (**80** and **81**) for the addition of oxindoles to nitrostyrenes^[44] and for the Michael addition of fluorinated silyl enol ethers^[45] (**Figure 5**).

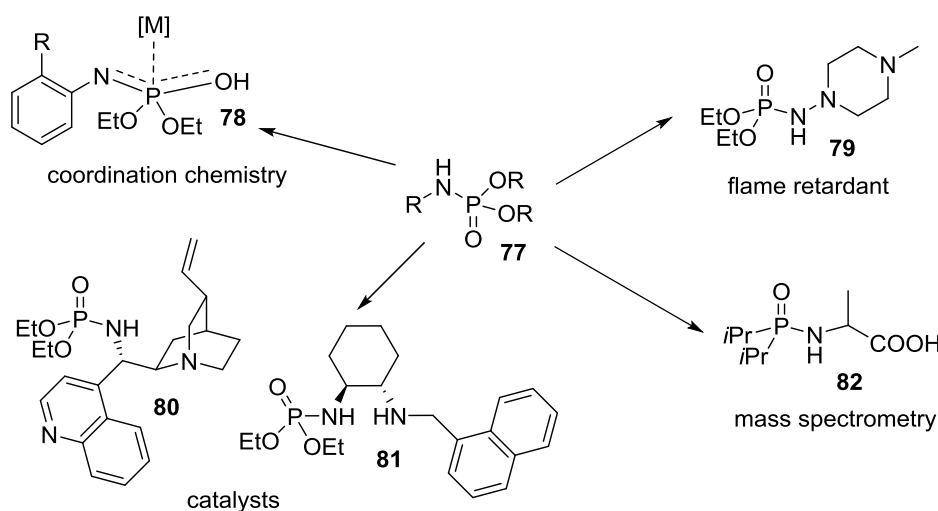
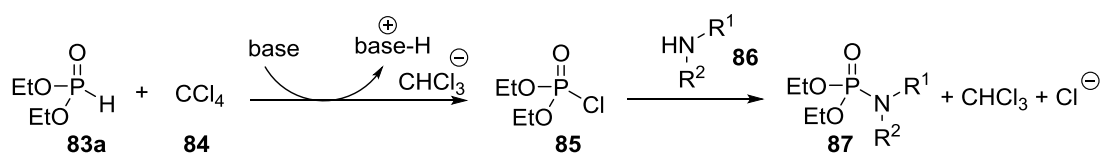


Figure 5. Applications of phosphoramidates' derivatives

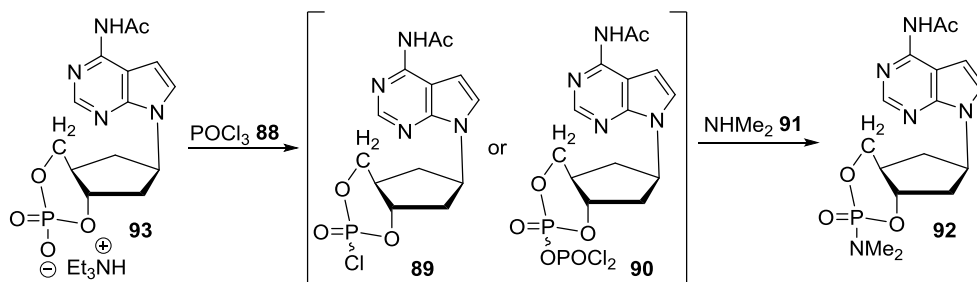
3.1 Synthesis of phosphoramidates

The most common way to synthesise phosphoramidates is through the use of phosphorous halides *via* the Atherton-Todd reaction between a dialkylphosphite and a primary or secondary amine in the presence of a base and carbon tetrachloride. The reaction was first reported by Atherton and Todd in 1945;^[46] the proposed mechanism is based on the reaction of the dialkylphosphite **83a** with CCl_4 **84** and a base with the formation of a chlorophosphate **85** as intermediate that will then react with the amine **86**, rendering the final phosphoramidate **87** (**Scheme 14**).^[47]



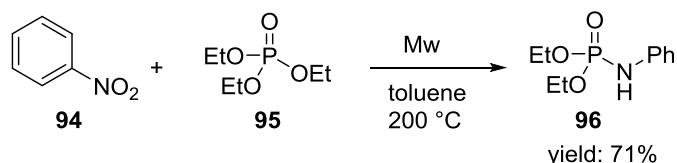
Scheme 14. General mechanism of the Atherton-Todd reaction

Other methods to synthesise phosphoramidates involve the reaction between phosphate diesters with PPh_3 and CCl_4 ^[48] or the nucleophilic substitutions of phosphate diesters **93** by alkylamines **91** using POCl_3 **88**.^[49] As shown in **Scheme 15**, the activated intermediate is probably a phosphorochloridate **89** or a dichlorophosphoric anhydride **90**.



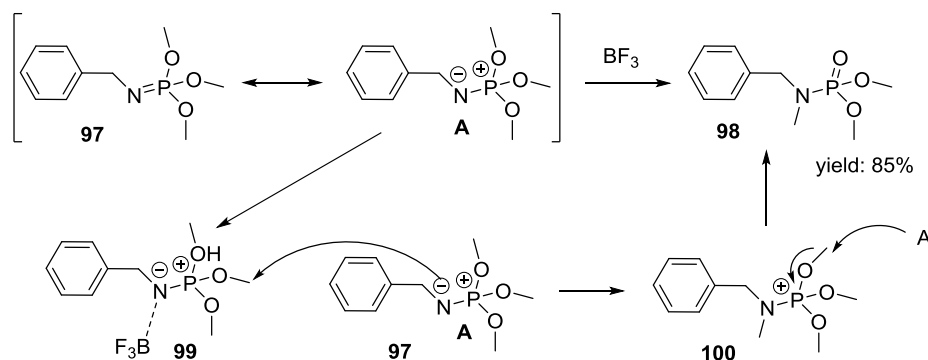
Scheme 15. Nucleophilic substitutions of phosphate diesters by alkylamines using POCl_3

The drawback of all these methodologies is the formation and handling of toxic and unstable reagents such as the carcinogenic carbon tetrachloride and the intermediate halogenated halides. To solve this problem Breifuss *et al.* developed a reaction between nitroarenes **94** and phosphorous reagents **95** for the synthesis of *N*-arylphosphoramidates **96**.^[50] In this case toxic and dangerous reagents are not used, but the phosphite has to be used in excess (6 equivalents) along with temperature of 200 °C in a microwave reactor (**Scheme 16**).



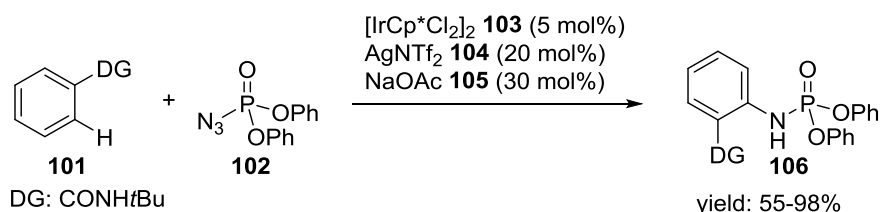
Scheme 16. Breifuss' synthesis of phosphoramidates starting from nitroarenes

Other methods involve the use of organic azides or phosphoryl azides, called the Staudinger-phosphite method.^[51] Hackenber *et al.* reported in 2008^[52] a reaction between azides and phosphites to give a phosphoramidate intermediate **97** that, after a rearrangement catalysed by BF_3 in benzene, renders the phosphoramidates **98** in good yields (**Scheme 17**).



Scheme 17. Mechanism of the Staudinger-phosphite synthesis of phosphoramidates

In 2014 Chang *et al.* reported a synthesis of phosphoramidates **106** through the reaction of phosphoryl azides **102** and aromatic systems containing directing groups **101** catalysed by an Ir(III) complex **103**, as shown in **Scheme 18**.^[53]

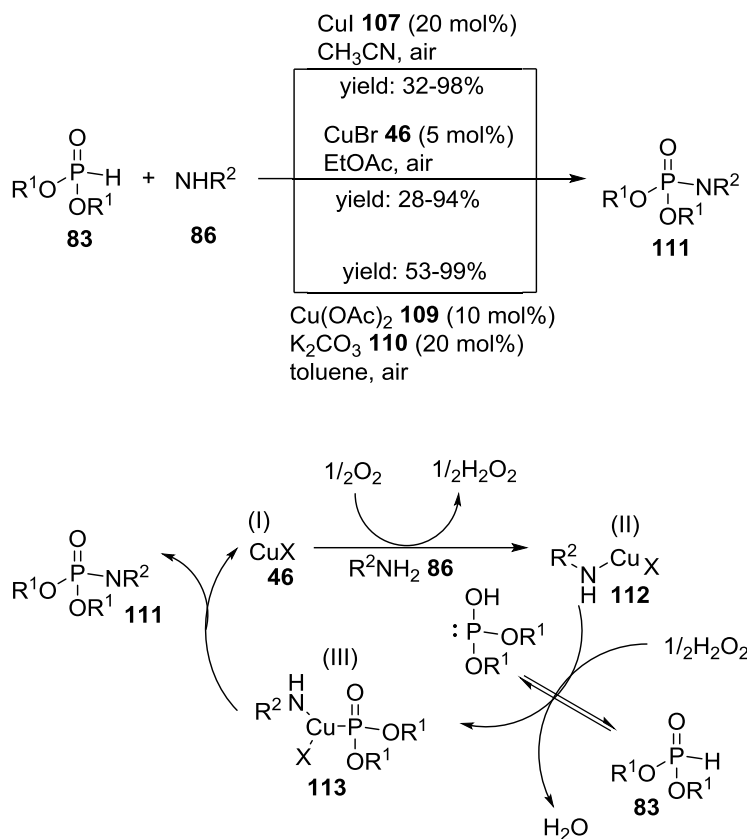


Scheme 18. Chang's synthesis of phosphoramidates with phosphoryl azides catalysed by Ir complex

The methodologies reported until now are based on the prefunctionalisation of the starting material before performing the actual reaction that will render the final phosphoramidate, leading to longer and more expensive procedures in terms of money and resources. In the last years, looking for more green procedures for the synthesis of phosphoramidates, cross-dehydrogenative couplings have been developed, also called oxidative couplings. In these cases there is no need for prefunctionalised starting materials leading to more atom economical processes.

In 2013 three different research groups published CDC reactions catalysed by copper salts. In particular Hayes *et al.* reported the oxidative coupling of amines **86** and phosphonates **83** using CuI **107** as catalyst and the air oxygen as the sole oxidant.^[26] Chen, Yu and co-workers^[54] reported a CDC reaction between arylamines and dialkylphosphites catalysed by CuBr **46** and O_2 and Mizuno *et al.*^[55] reported a CDC

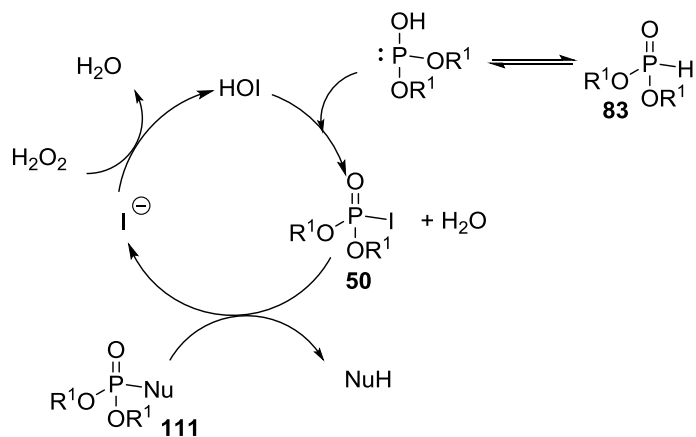
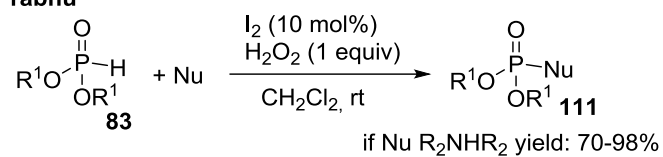
reaction between amides and dialkylphosphites catalysed by $\text{Cu}(\text{OAc})_2$ **109** and O_2 (**Scheme 19**). As shown in the proposed mechanism, these reactions use air oxygen as the sole oxidant and produce water as waste.



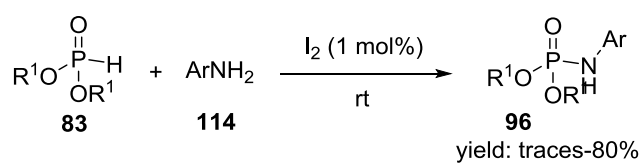
Scheme 19. CDC catalysed by Cu salts and O_2 and proposed mechanism

In the last years Prabhu *et al.* and Vishwakarma and Singh *et al.* reported the use of molecular iodine to catalyse the phosphoramidation reaction. Prabhu^[25] used H_2O_2 as stoichiometric oxidant: iodine reacts with H_2O_2 forming the hypoiodous acid (HIO) that reacts with dialkylphosphite **83** to give phosphoryl iodide **50**. This intermediate is attacked by different nucleophiles to render the final products **111** in good yields using mild conditions. Singh^[56] used I_2 to perform the reaction between dialkylphosphites **83** and anilines **114**.

Prabhu



Singh

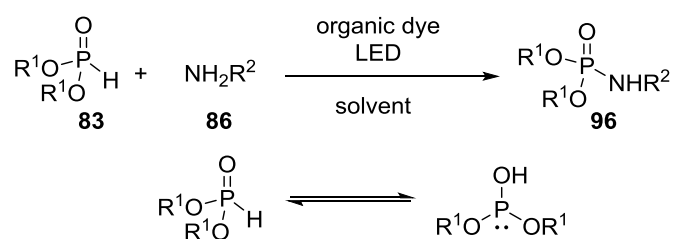


Scheme 20. Proposed mechanism of Prabhu's CDC reaction catalysed by I₂ and H₂O₂

4. Organophotocatalytic synthesis of phosphoramidates

4.1 Research hypothesis and proposed reaction mechanism

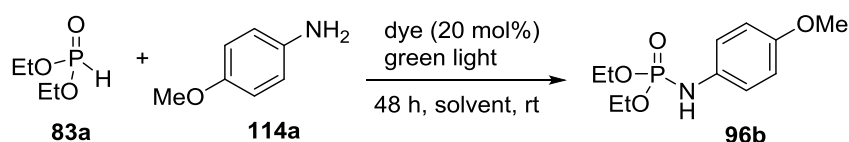
Due to the importance of the phosphoramidates scaffolds (Chapter 3) and based on the increasing development of CDC reactions (Chapter 1), we planned to develop a CDC reaction for the synthesis of phosphoramidates. We envisioned that a dialkylphosphite **83** would react with an amine **86** through a SET photoredox process catalysed by an organic dye, activated by visible light (**Scheme 21**).



Scheme 21. General scheme of the CDC reaction between dialkylphosphite and amines

First we tested the reaction between 2 equivalents of *p*-anisidine **114a** and 1 equivalent of diethylphosphite **83a** as the final product **96b** had already been synthesised by Hayes and co-workers.^[26] The reaction was performed at room temperature and checked by TLC after 48 hours, then the product was isolated (**Table 1**).

Table 1. Initial tests



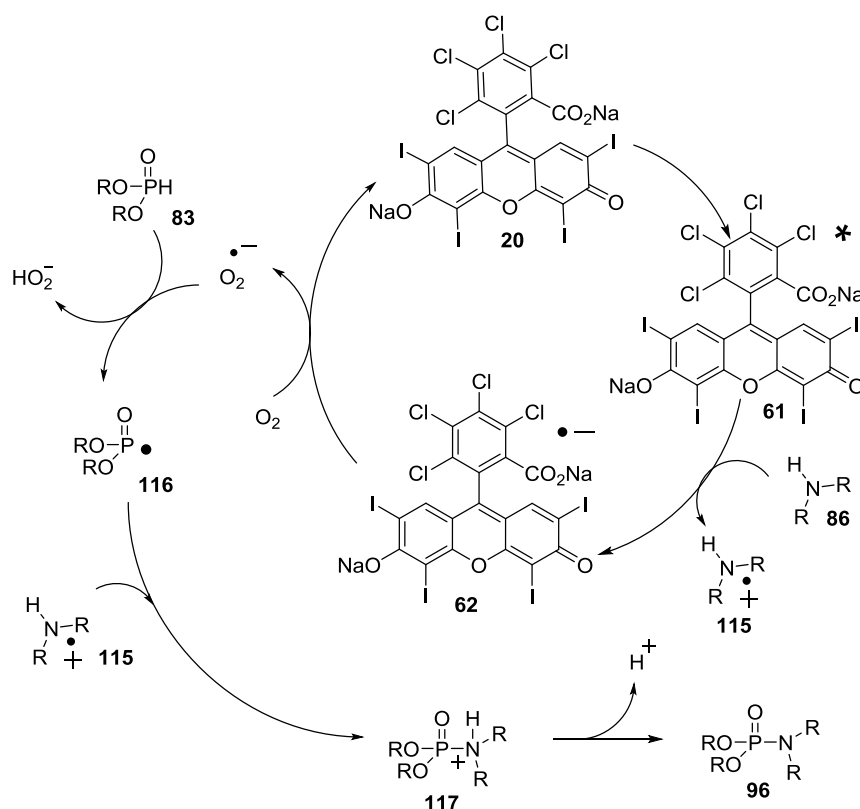
Entry	Dye	Solvent	Yield ^[a]
1	Eosin Y 21	CH ₃ CN	0
2	Methylene blue 25	CH ₃ CN	0

Entry	Dye	Solvent	Yield ^[a]
3	Rose Bengal 20	CH ₃ CN	36
4	Rose Bengal 20	toluene	40

[a] Yields are of the isolated products

From these preliminary results it was clear that only Rose Bengal **20** works in this reaction whilst the other two dyes tested did not give any product (**Table 1**, entries 1 and 2). The conversion obtained with CH₃CN and toluene is comparable (**Table 1**, entries 3 and 4). Green light (wavelength: 495–570 nm) is the best wavelength able to activate Rose Bengal as reported in literature and in Chapter 1 and 3.

The proposed reaction mechanism, catalysed by Rose Bengal, is outlined in **Scheme 22**.



Scheme 22. Proposed mechanism

Rose Bengal **20** accepts a photon from the green light to form the excited triplet state **61**. The activated Rose Bengal (RB) removes one electron from the amine **86** through a

single electron transfer (SET) process, forming the amine radical cation **115** and the RB radical anion **62**. The RB radical anion is re-oxidised to the ground state **20** by molecular oxygen present in the air with the formation of the anion superoxide that reacts with the dialkylphosphite **83** to form the phosphorous radical **116** and hydroperoxide anion. The phosphite radical **116** reacts with the amine radical cation **115** to render intermediate **117** that, after deprotonation, gives the final phosphoramidate **96**.

4.2 Photoreactor

To perform these reactions, we have assembled the photoreactor shown in **Figure 6**. The photoreactor consists of a glass cylinder wrapped with a row of green LEDs and placed on a heater-stirrer apparatus. The reactions are carried out in closed vials placed inside the cylinder and put on the metal heated plate.

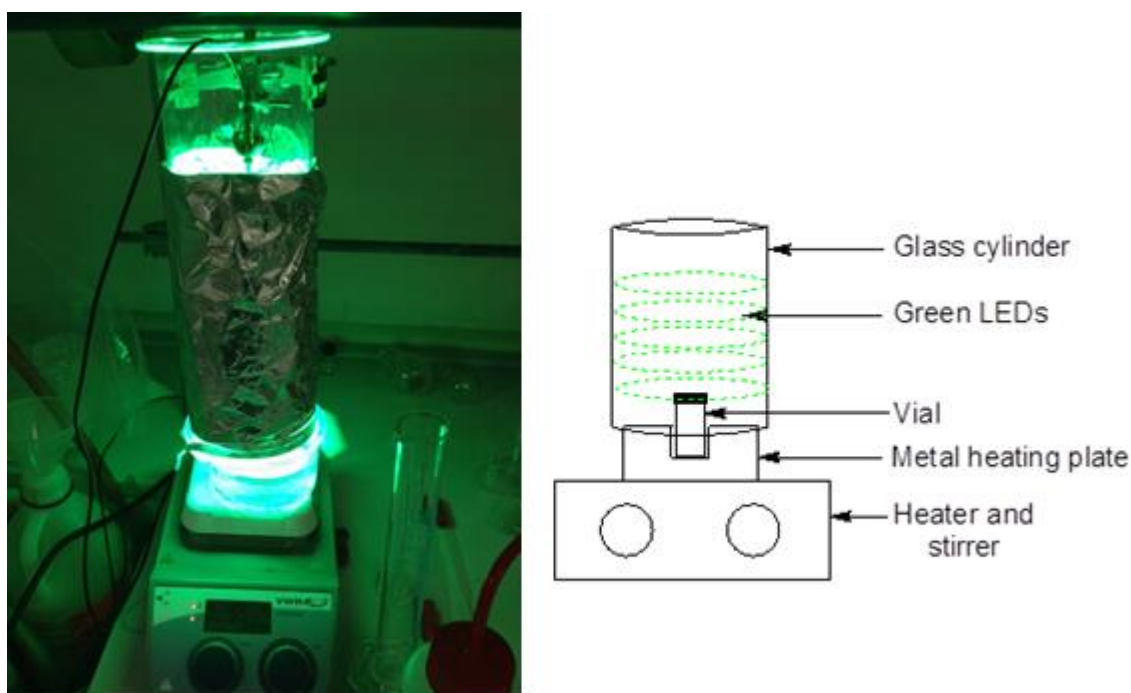


Figure 6. Photo and scheme of the photoreactor used in this project

4.3 Results and discussions

After obtaining the first positive results we proceeded on the optimisation of the reaction conditions and the study of the scope of the reaction. To control when the full conversion was reached, the reactions have been checked by ^{31}P -NMR (the starting material resonates at δ 7.31 and the final product at δ 2.38).

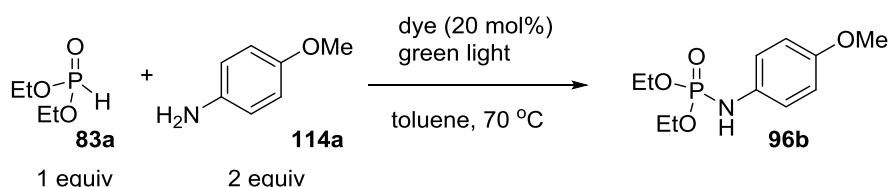
It has to be noted that there is no need for a column chromatography to purify the final products as we optimised an effective acid/base work up by diluting the crude in CHCl_3 and washing at first with 0.5 M HCl and then with saturated NaHCO_3 aqueous solution.

This adds considerable importance to this work as it does not require expensive, time consuming and waste generating purification, making it a greener procedure easier to up-scale in an industrial setting.

4.3.1 Optimization of the reaction conditions

4.3.1.1 Screening of organic dyes

First we tested different dyes in the conditions reported in **Scheme 23**.



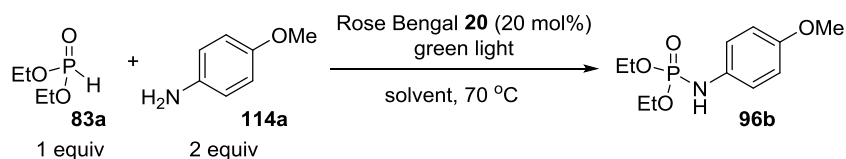
Scheme 23. Conditions for the screening of organic dyes

The dyes tested are: Rose Bengal **20**, Eosin Y **21**, Nile red **23**, Neutral red **24**, Methylene blue **25**, Orange II sodium salt **26**, Disperse red 1 **27**, Mordant orange 1 **28**.

No conversion was observed in the NMR of the crude except with Rose Bengal.

4.3.1.2 Screening of solvents

Then we tested different solvents with and without molecular sieves, using Rose Bengal **20** as the dye and the results are presented in **Table 2**.

Table 2. Screening of solvents

Entry	Solvent	Molecular Sieves	Conversion ^[a] 24 h (%)	Conversion ^[a] 2 days (%)	Conversion ^[a] 3 days (%)	Yield ^[b] (%)
1	toluene	no	17	51	full	54
2	DMF	yes	0	0	0	---
3	EtOH	yes	0	0	0	---
4	EtOAc	yes	31	86	full	not clean
5	CH ₃ CN	yes	10	27	69 (4 days)	59
6	CH ₃ CN	no	11	---	66 (4 days)	95
7	DMF	no	degradation	---	---	---
8	EtOH	no	product + impurities	---	---	---
9	EtOAc	no	82	full	---	not clean

[a] Conversions are calculated from ³¹P-NMR of the crude

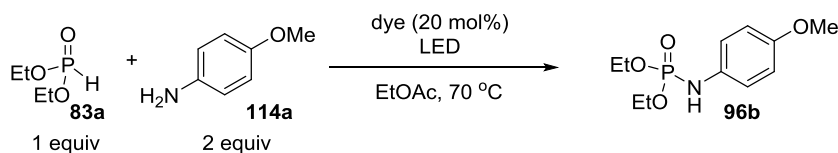
[b] Yields are of pure isolated product

The results show that the reaction does not work with DMF and EtOH as solvents independently from the presence of molecular sieves (**Table 2**, entries 2, 3, 7 and 8) giving no conversion or side products. Both toluene, CH₃CN and EtOAc showed full conversion from the NMR of the crude. The fastest reaction was with EtOAc, especially without the molecular sieves, but in both cases the product isolated after the extraction was not clean (**Table 2**, entries 4 and 9). Toluene gave full conversion after 3 days (**Table 2**, entry 1) while CH₃CN required more than 4 days to achieve full conversion. In the end, the solvent chosen was CH₃CN without molecular sieves as the isolated yield was quantitative (95%, **Table 2**, entry 6), compared with the use of molecular sieves (59%, **Table 2**, entry 5) or the use of toluene (54%, **Table 2**, entry 1).

4.3.1.3 Screening of LEDs

A screening of different LEDs and organic dyes was done as presented in **Table 3**.

Table 3. Screening of LEDs



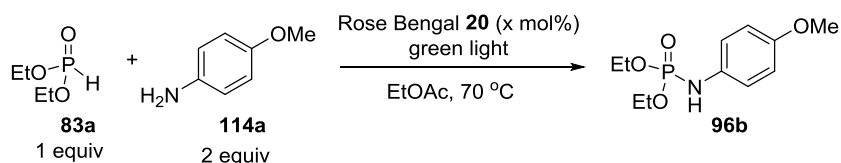
Entry	Dye	LED Colour	Conversion ^[a] 48 h (%)
1	Rose Bengal 20	Blue	42
2	Rose Bengal 20	--- (tin foil wrapped)	0
3	Rose Bengal 20	White	35
4	Eosin Y 21	Blue	0
5	Methylene blue 25	Blue	0

[a] Conversions are calculated from ³¹P-NMR of the crude

The reaction works with Rose Bengal **20** with blue and white light (**Table 3**, entries 1 and 3) but, in both cases, the conversions after 2 days are lower than that achieved using Rose Bengal and green light (**Table 4**, entry 1). The reaction does not work with Eosin Y **21** with blue light as well as with Methylene blue **25** and blue light (**Table 3**, entries 4 and 5). A test reaction was done without the presence of any sort of light and with the vial wrapped with tin foil (**Table 3**, entry 2). As expected, no conversion was seen in the crude NMR as a source of light is needed to activate the organic dyes.

4.3.1.4 Screening of Rose Bengal

Then a screening of different loadings of Rose Bengal **20** was performed and the results are shown in **Table 4**.

Table 4. Screening of loading of Rose Bengal

Entry	Rose Bengal (equiv %)	Conversion ^[a] 24 h (%)	Conversion ^[a] 2 days (%)	Conversion ^[a] 4 days (%)
1	20	8	56	86
2	10	7	37	55
3	5	3	22	35
4	0	---	---	---

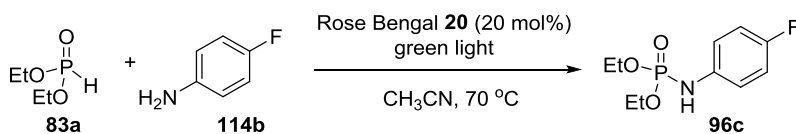
[a] Conversions are calculated from ³¹P-NMR of the crude

The reaction works even with 5 mol% of Rose Bengal **20**. As the reaction is too slow with 10 and 5 mol% (**Table 4**, entries 2 and 3), 20 mol% (**Table 4**, entry 1) was chosen as the best amount of the dye. As a control, the reaction was tested without the organic dye (**Table 4**, entry 4). No conversion was observed in the NMR of the crude, proving the need of the dye as explained in the proposed mechanism.

4.3.1.5 Conversions with different aniline's loading

Up until this point the screenings were performed using 2 equivalents of the aniline **114b** and we wanted to check if there would be any difference using different ratios of the two starting materials (**Table 5**).

Table 5. Study of the conversion with different aniline's loading



Entry	Equiv aniline	Conversion ^[a] 1 day (%)	Conversion ^[a] 2 days (%)	Conversion ^[a] 3 days (%)	Conversion ^[a] 4 days (%)	Conversion ^[a] 5 days (%)
1	0.5	0	0	14	product + acid + SM	product + acid + SM
2	1	0	9	35	product + acid + SM	product + acid
3	2	6	10	40	75	full

[a] Conversions are calculated from ³¹P-NMR of the crude

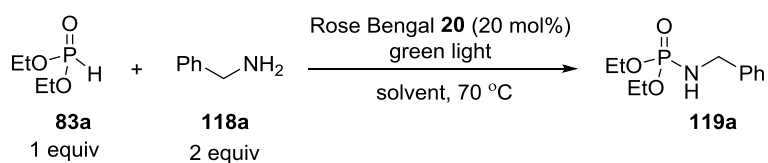
A clean NMR of the crude was seen only using 2 equivalents of aniline **114b** (**Table 5**, entry 3), while using 1:1 ratio (**Table 5**, entry 2) or 2 equivalents of diethylphosphite **83a** (**Table 5**, entry 1) the NMR showed a slower formation of the product for the first 3 days and then the formation of the phosphoric acid as a side product without any improvement on the conversion.

The best conditions for the reaction between diethylphosphite **83** and anilines **114** are: 1 equivalent of diethylphosphite, 2 equivalents of aniline, 20 mol% of Rose Bengal and CH₃CN as the solvent.

4.3.1.6 Screening of solvents for aliphatic amines

When the reaction was tested with aliphatic amines **118**, in the best conditions found, the reaction did not give full conversion and only traces of products **119** were obtained after the workup. For this reason, a screening of solvents was done using diethylphosphite **83a** and benzylamine **118a**.

Table 6. Screening of solvents with aliphatic amines

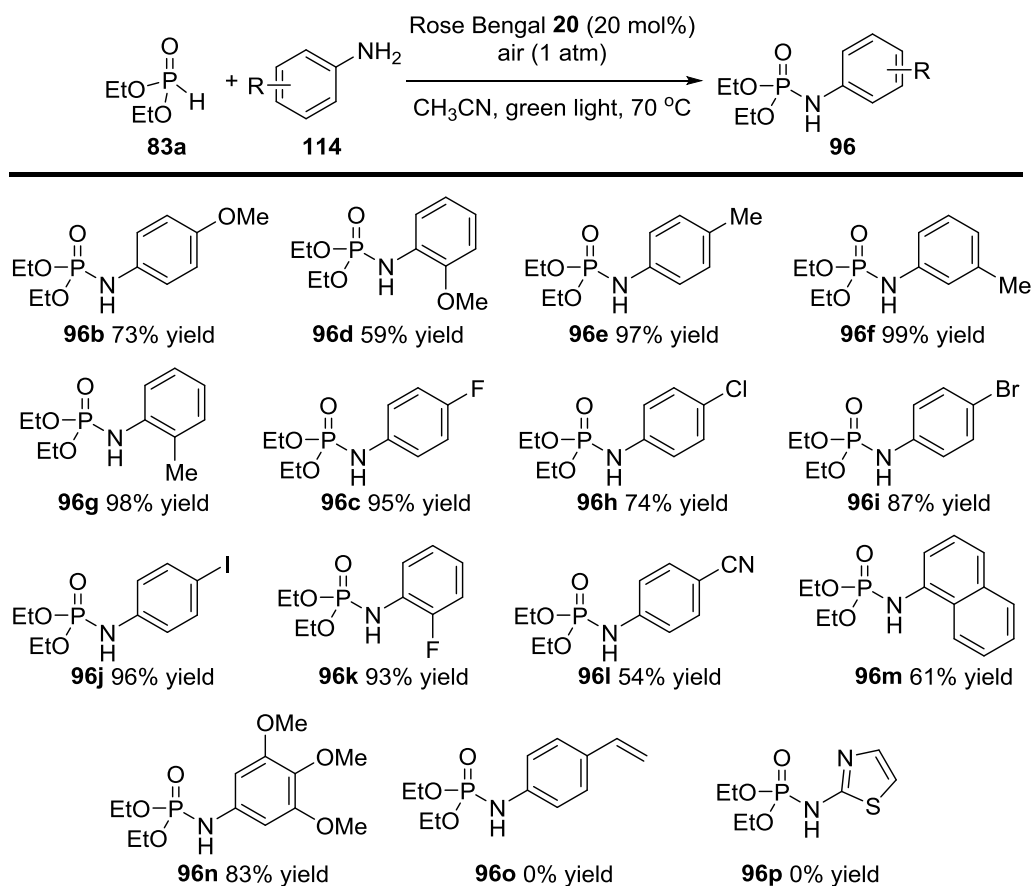


Solvent	toluene	CHCl ₃	CH ₃ CN (molecular sieves)	CH ₃ CN/H ₂ O 9:1	EtOAc
Result 24 h	27% conv. clean	no conv	no conv + 2 side products	product + 2 side product	product + side product

As shown in **Table 6**, the reaction did not work in CHCl₃ and, when using CH₃CN or EtOAc, the NMR of the crude showed the formation of side products. The best solvent, in the case of aliphatic amines, was found to be toluene that, after 24 hours, gave 27% conversion without the formation of any by-product.

4.3.2 Scope of the reaction with anilines

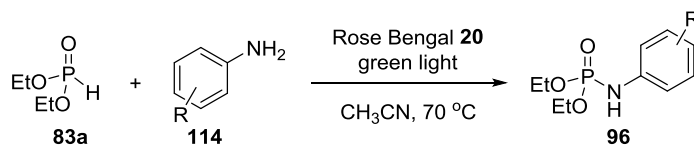
Having the optimal conditions in hand, we studied the scope of the reaction as regards the anilines **114** and the results are presented in **Scheme 24**.



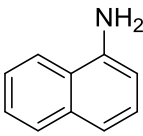
Scheme 24. Scope of the reaction with anilines

More information about the time needed to reach full conversion are presented in **Table 7**.

Table 7. Scope of the reaction with aromatic amines



Product	R	Time full conversion ^[a] (days)	Yield (%)
96b	4-OMe 114a	10	95
96d	2-OMe 114c	7	59
96e	4-CH ₃ 114d	5	97
96f	3-CH ₃ 114e	7	99

Product	R	Time full conversion ^[a] (days)	Yield (%)
96g	2-CH ₃ 114f	6	98
96c	4-F 114b	7	73
96h	4-Cl 114g	8	74
96i	4-Br 114h	7	87
96j	4-I 114i	2	96
96k	2-F 114j	6	93
96l	4-CN 114k	7	54
96m	 114l	6	61
96n	3,4,5-OMe 114m	6	83

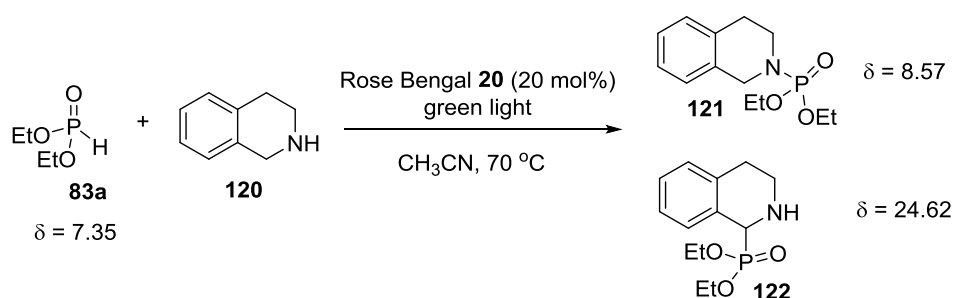
[a] Conversions are calculated from ³¹P-NMR of the crude

The reaction works well when an electron donating group is present on the aniline such as OMe or Me. In the case of the Me substituted anilines the products were obtained in almost quantitative yields with the substituent in *ortho*, *meta* or *para* position (**96g**, **96f** and **96e**). When the aniline was substituted with 4-OMe or with the 3,4,5-OMe, the final products **96b** and **96n** were obtained in quantitative yields, instead lower yields were obtained with the 2-OMe substituted aniline **96d**. High yields were obtained also with all the halogenated anilines: 4-F, 4-Cl, 4-Br, 4-I, 2-F (**96c**, **96h**, **96i**, **96j** and **96k**). When an electron-withdrawing substituent (4-CN) or a sterically congested aniline were used, lower yields were achieved (**96l** and **96m**).

The limitations of this methodology are the use of heteroaromatic amines and vinyl anilines. The 2-aminothiazole **96p** decomposes in the reaction conditions and the 4-vinyl aniline **96o** rendered complex mixtures due to its sensitive radical nature which may give oligo- or polymerisation.

4.3.3 Scope of the reaction with aliphatic amines

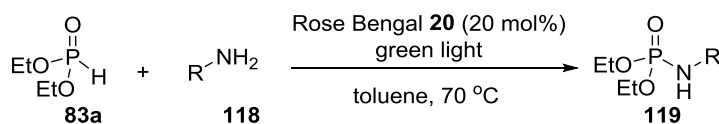
Then we studied the scope of the reaction with aliphatic amines **118**, more challenging substrates. Rueping *et al.* reported a reaction between the tetrahydroisoquinoline **120** and diethylphosphite **83a**, catalysed by a Ruthenium photocatalyst **1** and light.^[24] They obtained the Kabachnik-Fields product **122** with a C-P bond formation. When our reaction conditions were tested, a mixture of the Kabachnik-Fields product **122** and the phosphoramidate **121** was obtained in 14:1 ratio, with a clear preference towards the K-F one (**Scheme 25**).



Scheme 25. Reaction with tetrahydroisoquinoline for the competition between Kabachnik-Fields product and the phosphoramidation one

When other primary aliphatic amines **118** were tested with Rose Bengal **20** as the organic dye and toluene as the solvent, the phosphoramidate products **119** were obtained with moderate yields and the results are shown in **Table 8**. Unfortunately, the reaction did not work with secondary amines like morpholine **123**, pyrrolidine **124** and piperidine **125**.

Table 8. Scope of the reaction with aliphatic amines



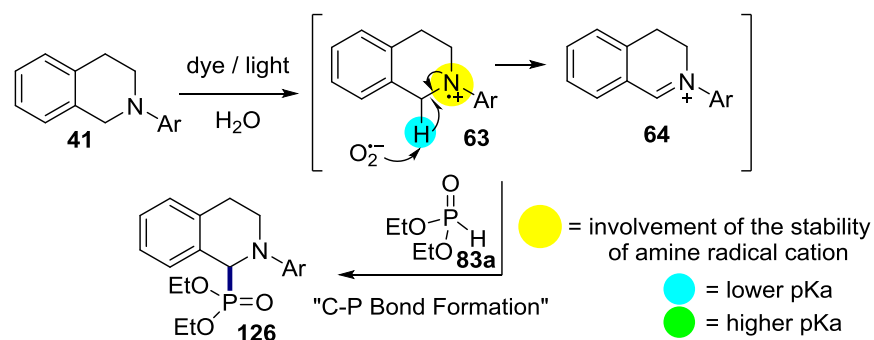
Product	Amine	Time full conversion ^[a] (days)	Yield ^[b] (%)
119a	benzylamine 118a	6	59
119b	isopropylamine 118b	4	42

Product	Amine	Time full conversion ^[a] (days)	Yield ^[b] (%)
119c	<i>tert</i> -butylamine 118c	4	53

[a] Conversions are calculated from ³¹P-NMR of the crude

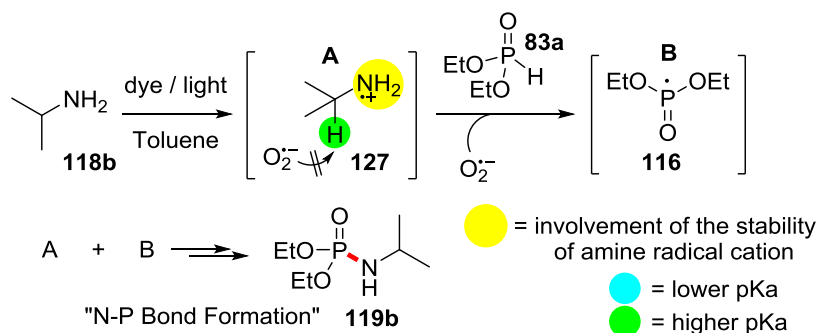
[b] Yields are of pure isolated products

The different reactivity of the amines **118a**, **b** and **c** and the tetrahydroisoquinoline **41** depends on the stabilisation of tertiary **63** or primary **127** amine radical cations. In the case of the tetrahydroisoquinoline **63** there is a subsequent deprotonation at the α -position of amine radical cations by a base (e.g. superoxide anion) due to the lower pKa value of the relevant acidic protons (**Scheme 26**).



Scheme 26. Kabachnik-Fields reaction with tetrahydroisoquinoline

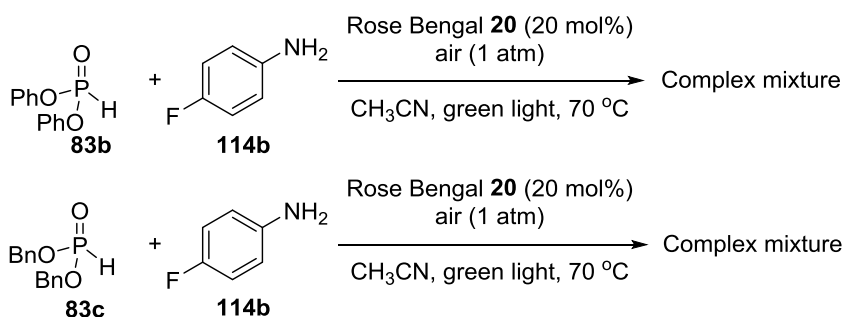
In the case of the other amines, the pKa value of the α -protons is higher so there is no deprotonation and the NH_2 radical cation **127** can react with the phosphorous radical **116** (**Scheme 27**).



Scheme 27. Rationalisation of the N-P bond formation instead of the C-P

4.3.4 Scope of the reaction with different phosphites

Then we studied the scope of the reaction with different phosphorous sources. 4-F aniline **114b** was chosen as it gave one of the fastest reactions with diethylphosphite **83a**. As it is shown in **Scheme 28**, the reaction with diphenylphosphite **83b** or dibenzylphosphite **83c** rendered a mixture of products.

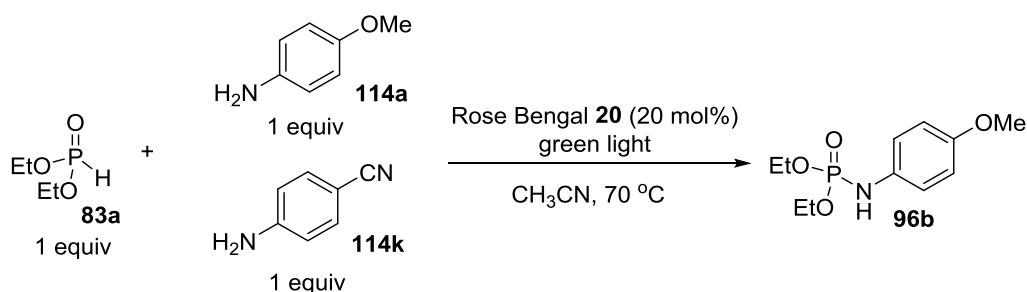


Scheme 28. Substrate scope with different phosphites

4.3.5 Studies on the mechanism

4.3.5.1 Competition experiment

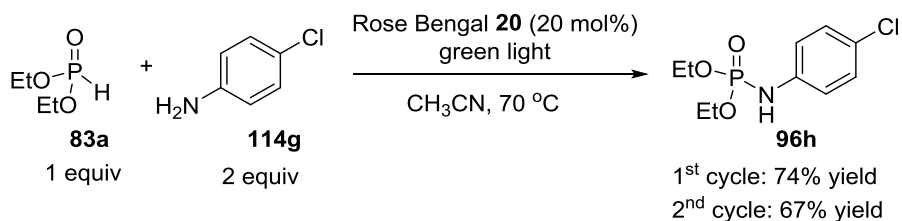
To verify the formation and stabilisation of the amine radical cation intermediate **115** (page 26), a reaction was performed with equal molar ratio of 4-anisidine **114a** and 4-cyanoaniline **114k** in the same vial under the optimal reaction conditions found (**Scheme 29**). As expected from the mechanism, the only product formed was the phosphoramidate **96b** derived from 4-anisidine **114a**, indicating that an electron-donating group such as OMe stabilises the amine radical cation **115**.



Scheme 29. Competition experiment between an aniline with an EWG and an EDG

4.3.5.2 Recyclability test

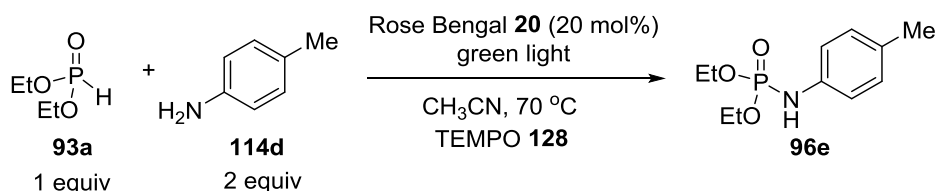
After washing and extracting the product diethyl (4-chlorophenyl)phosphoramidate **96h**, the Rose Bengal **20** was extracted from the aqueous basic phase and used again to perform the same reaction. The recycled Rose Bengal showed a similar reactivity, in fact in the first cycle the product **96h** was obtained with 74% yields and with 67% yield in the second cycle (**Scheme 30**).



Scheme 30. Recyclability of Rose Bengal

4.3.5.3 Reaction with radical scavenger

To prove that a radical intermediate is involved in the key step, the reaction was tested adding a radical scavenger. The reaction was performed, following the general procedure, using the 4-Me aniline **114d** and adding 1 equivalent of TEMPO ((2,2,6,6-tetramethylpiperidin-1-yl)oxyl, **128**) (**Scheme 31**).

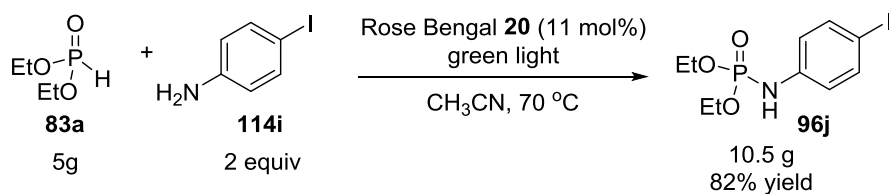


Scheme 31. Reaction with radical scavenger

After 24 hours no conversion was seen in the crude NMR and after 4 days only 13% conversion while, in the normal conditions, full conversion should be reached after 5 days. If no radical intermediate would have been involved in the reaction mechanism, the rate of the reaction should have remained the same.

4.3.5.4 Scale-up of the reaction

Finally, in order to show the suitability of this methodology in a multigram synthesis, and a possible industrial scale-up, we tested the reaction on a five gram scale of diethylphosphite **83a** (Scheme 32). The product **96j** was obtained in high yield without the need of a column chromatography.



Scheme 32. Multigram reaction

5. Conclusions

In summary, we developed a new methodology for the synthesis of phosphoramidates starting from diethylphosphites and primary amines, catalysed by an organic dye and green light. The products were obtained with excellent yields. As the light is a renewable energy and Rose Bengal is a cheap and non-toxic chemical, this methodology improves the existing methodologies eliminating the use of metals or halide reagents and, in particular, the requirement of column chromatography as a purification step. For these reasons, this new reaction fulfils the requirements of the green chemistry.

6. Experimental section

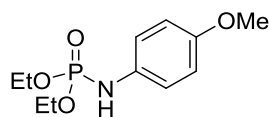
Thin layer chromatography (TLC) was performed on Merck TLC Silicagel 60 F₂₅₄. Product spots were visualized by UV-light at 254 nm. Column chromatography was effectuated using silica gel (Geduran Si60, 40-63 μm). Melting points were measured with a Gallenkamp Electrothermal apparatus and are uncorrected. Infra-red spectra were recorded on a Nicolet 380 FT-IR; the IR analysis were performed with the compounds dissolved in CHCl_3 . ^1H -NMR, ^{13}C -NMR, ^{19}F -NMR, 2D-NMR were recorded with a Bruker DPX400 NMR. High resolution mass spectra were recorded using a MaXis (Bruker Daltonics, Bremen, Germany) mass spectrometer equipped with a Time of Flight (TOF) analyser.

6.1 General procedure for the synthesis of phosphoramidates

In a closed vial were added in this sequence: the organic dye Rose Bengal (73 mg, 0.072 mmol, 20 mol% equiv), the amine (0.724 mmol, 2 equiv), the solvent (1.5 mL) and diethyl phosphate (47 μ l, 0.362 mmol, 1 equiv). The reaction mixture was stirred at 70 °C in the photoreactor under green light (see table of results for reaction times). CHCl_3 was added to the crude mixture and the organic phase was washed with 0.5 M HCl (3 x 20 ml), then with saturated NaHCO_3 aqueous solution (3 x 20 ml). The organic phases were dried over MgSO_4 , filtered and the solvent was evaporated under *vacuo* to afford the desired phosphoramidate.

6.2 Final products characterisation

diethyl (4-methoxyphenyl)phosphoramidate (96b)



The reaction was performed following the general procedure using (89 mg, 0.724 mmol) of 4-methoxyaniline and CH_3CN as a solvent. 80 mg of black solid were obtained. Yield: 95%.

mp: 55-57 °C.

IR (CHCl_3 , liquid film): 3175 (N-H stretch), 2982, 2905 (aliphatic C-H stretch), 1512, 1481 (aromatic C=C stretch), 1220 (P=O stretch), 1028, 974 (P-OR ester stretch) cm^{-1} .

^1H NMR (400 MHz, CDCl_3) δ 6.94 (d, J = 8.9 Hz, 2H, Ar), 6.82 (d, J = 8.9 Hz, 2H, Ar), 5.01 (d, J = 8.5 Hz, 1H, NH), 4.25 – 4.02 (m, 4H, CH_2), 3.78 (s, 3H, OCH_3), 1.32 (t, J = 7.1 Hz, 6H, CH_3).

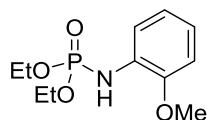
^{13}C NMR (101 MHz, CDCl_3) δ 155.0 (Cq), 132.5 (Cq), 119.3 (d, J = 6.6 Hz, CH), 114.7 (CH), 62.8 (d, J = 5.0 Hz, CH_2), 55.6 (CH_3), 16.1 (d, J = 7.2 Hz, CH_3).

^{31}P NMR (162 MHz, CDCl_3) δ 2.42.

HRMS m/z (ESI+) Exact mass calculated for $\text{C}_{11}\text{H}_{19}\text{NO}_4\text{P}$ $[\text{M}+\text{H}]^+$: 260.1046, found: 260.1045.

The experimental data obtained is in accordance with the data reported in literature.^[26]

diethyl (2-methoxyphenyl)phosphoramidate (96d)



The reaction was performed following the general procedure using (89 mg, 0.724 mmol) of 2-methoxyaniline and CH₃CN as a solvent. 55 mg of brown oil were obtained. Yield: 59%.

IR (CHCl₃, liquid film): 3409 (N-H stretch), 2981, 2930 (aliphatic C-H stretch), 1600, 1508 (aromatic C=C stretch), 1245 (P=O stretch), 1024, 972 (P-OR ester stretch) cm⁻¹.

¹H NMR (400 MHz, CDCl₃) δ 7.20 (dd, *J* = 7.5, 1.8 Hz, 1H, Ar), 6.94 – 6.83 (m, 3H, Ar), 5.74 (d, *J* = 10.2 Hz, 1H, NH), 4.26 – 4.01 (m, 4H, CH₂), 3.86 (s, 3H, OCH₃), 1.32 (t, *J* = 7.1 Hz, 6H, CH₃).

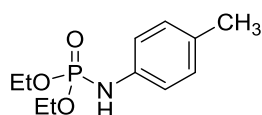
¹³C NMR (101 MHz, CDCl₃) δ 147.5 (d, *J* = 10.1 Hz, Cq), 129.2 (d, *J* = 2.0 Hz, Cq), 121.4 (CH), 121.1 (CH), 116.1 (d, *J* = 1.2 Hz, CH), 110.2 (CH), 62.8 (d, *J* = 4.9 Hz, CH₂), 55.6 (CH₃), 16.1 (d, *J* = 7.2 Hz, CH₃).

³¹P NMR (162 MHz, CDCl₃) δ 2.30.

HRMS *m/z* (ESI+) Exact mass calculated for C₁₁H₁₉NO₄P [M+H]⁺: 260.1046, found: 260.1047.

The experimental data obtained is in accordance with the data reported in literature.^[56]

diethyl *p*-tolylphosphoramidate (96e)



The reaction was performed following the general procedure using (80 μl, 0.724 mmol) of *p*-toluidine and CH₃CN as a solvent. 85 mg of red solid were obtained. Yield: 97%.

mp: 89-91 °C.

IR (CHCl₃, liquid film): 3191, 3163 (N-H stretch), 2981, 2929, 2868 (aliphatic C-H stretch), 1514, 1480 (aromatic C=C stretch), 1221 (P=O stretch), 1020, 969 (P-OR ester stretch) cm⁻¹.

¹H NMR (400 MHz, CDCl₃) δ 7.06 (d, *J* = 8.3 Hz, 2H, Ar), 6.90 (d, *J* = 7.8 Hz, 2H, Ar), 5.68 (bs, 1H, NH), 4.24 – 3.99 (m, 4H, CH₂), 2.28 (s, 3H, CH₃), 1.32 (t, *J* = 7.1 Hz, 6H, CH₂CH₃).

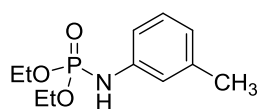
¹³C NMR (101 MHz, CDCl₃) δ 136.9 (d, *J* = 4.2 Hz, Cq), 131.1 (d, *J* = 3.7 Hz, Cq), 129.8 (CH), 117.4 (d, *J* = 7.1 Hz, CH), 62.7 (d, *J* = 4.8 Hz, CH₂), 20.6 (CH₃), 16.1 (d, *J* = 7.2 Hz, CH₃).

³¹P NMR (162 MHz, CDCl₃) δ 2.29.

HRMS *m/z* (ESI+) Exact mass calculated for C₁₁H₁₉NO₃P [M+H]⁺: 244.1097, found: 244.1098.

The experimental data obtained is in accordance with the data reported in literature.^[54]

diethyl *m*-tolylphosphoramidate (96f)



The reaction was performed following the general procedure using (80 µl, 0.724 mmol) of *m*-toluidine and CH₃CN as a solvent. 88 mg of brown solid were obtained. Yield: 99%.

mp: 65-68 °C.

IR (CHCl₃, liquid film): 3173 (N-H stretch), 2982, 2907 (aliphatic C-H stretch), 1509, 1486 (aromatic C=C stretch), 1229 (P=O stretch), 1023, 974 (P-OR ester stretch) cm⁻¹.

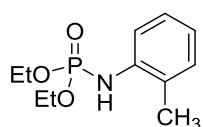
¹H NMR (400 MHz, CDCl₃) δ 7.13 (dd, *J* = 8.1, 8.1 Hz, 1H, Ar), 6.84 – 6.82 (m, 2H, Ar), 6.77 (d, *J* = 7.6 Hz, 1H, NH), 6.29 – 6.27 (m, 1H, Ar), 4.25 – 4.03 (m, 4H, CH₂), 2.31 (s, 3H, CH₃), 1.32 (t, *J* = 7.1 Hz, 6H, CH₂CH₃).

¹³C NMR (101 MHz, CDCl₃) δ 139.7 (Cq), 139.2 (Cq), 129.1 (CH), 122.4 (CH), 118.0 (d, *J* = 7.7 Hz, CH), 114.3 (d, *J* = 6.9 Hz, CH), 62.7 (d, *J* = 4.8 Hz, CH₂), 21.5 (CH₃), 16.1 (d, *J* = 7.2 Hz, CH₃).

³¹P NMR (162 MHz, CDCl₃) δ 2.55.

HRMS *m/z* (ESI+) Exact mass calculated for C₁₁H₁₉NO₃P [M+H]⁺: 244.1097, found: 244.1099.

diethyl *o*-tolylphosphoramidate (96g)



The reaction was performed following the general procedure using (80 μl, 0.724 mmol) of *o*-toluidine and CH₃CN as a solvent. 86 mg of brown oil were obtained. Yield: 98%.

IR (CHCl₃, liquid film): 3210 (N-H stretch), 2981, 2908 (aliphatic C-H stretch), 1501, 1415 (aromatic C=C stretch), 1238 (P=O stretch), 1024, 974 (P-OR ester stretch) cm⁻¹.

¹H NMR (400 MHz, CDCl₃) δ 7.21 (d, *J* = 7.9 Hz, 1H, Ar), 7.14 (t, *J* = 8.0 Hz, 2H, Ar), 6.91 (t, *J* = 7.2 Hz, 1H, Ar), 4.95 (d, *J* = 8.1 Hz, 1H, NH), 4.25 – 4.02 (m, 4H, CH₂), 2.24 (s, 3H, CH₃), 1.32 (t, *J* = 7.1 Hz, 6H, CH₂CH₃).

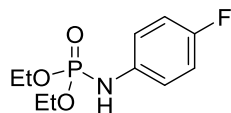
¹³C NMR (101 MHz, CDCl₃) δ 137.7 (Cq), 130.6 (CH), 127.1 (CH), 125.1 (d, *J* = 10.9 Hz, Cq), 121.9 (CH), 117.0 (d, *J* = 1.4 Hz, CH), 62.9 (d, *J* = 5.0 Hz, CH₂), 17.7 (CH₃), 16.1 (d, *J* = 7.2 Hz, CH₃).

³¹P NMR (162 MHz, CDCl₃) δ 2.22.

HRMS *m/z* (ESI+) Exact mass calculated for C₁₁H₁₉NO₃P [M+H]⁺: 244.1097, found: 244.1097.

The experimental data obtained is in accordance with the data reported in literature.^[56]

diethyl (4-fluorophenyl)phosphoramidate (96c)



The reaction was performed following the general procedure using (62 μ l, 0.724 mmol) of 4-fluoroaniline and CH_3CN as a solvent. 65 mg of black solid were obtained. Yield: 73%.

mp: 50-51 $^{\circ}\text{C}$.

IR (CHCl_3 , liquid film): 3176 (N-H stretch), 3090 (aromatic C-H stretch), 2982, 2906 (aliphatic C-H stretch), 1509 (aromatic C=C stretch), 1214 (P=O stretch), 1025, 975 (P-OR ester stretch) cm^{-1} .

^1H NMR (400 MHz, CDCl_3) δ 7.03 – 6.89 (m, 4H, Ar), 6.21 (s, 1H, NH), 4.33 – 3.88 (m, 4H, CH_2), 1.32 (t, $J = 7.1$ Hz, 6H, CH_3).

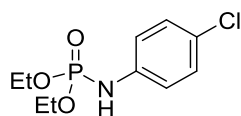
^{19}F NMR (376 MHz, CDCl_3) δ -122.68 (d, $J = 12.7$ Hz).

^{31}P NMR (162 MHz, CDCl_3) δ 2.35.

HRMS m/z (ESI+) Exact mass calculated for $\text{C}_{10}\text{H}_{16}\text{FNO}_3\text{P}$ $[\text{M}+\text{H}]^+$: 248.0846, found: 248.0848.

The experimental data obtained is in accordance with the data reported in literature.^[56] CAS Registry Number: 50672-18-9

diethyl (4-chlorophenyl)phosphoramidate (96h)



The reaction was performed following the general procedure using (92 mg, 0.724 mmol) of 4-chloroaniline and CH₃CN as a solvent. 71 mg of brown solid were obtained. Yield: 74%.

mp: 69.8-71.5 °C.

IR (CHCl₃, liquid film): 3161 (N-H stretch), 3063 (aromatic C-H stretch), 2981 (aliphatic C-H stretch), 1598, 1494 (aromatic C=C stretch), 1224 (P=O stretch), 1025, 977 (P-OR ester stretch) cm⁻¹.

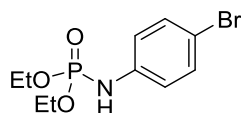
¹H NMR (400 MHz, CDCl₃) δ 7.21 (bd, *J* = 8.7 Hz, 2H, Ar), 6.94 (bd, *J* = 8.8 Hz, 2H, Ar), 5.87 (d, *J* = 8.7 Hz, 1H, NH), 4.26 – 4.01 (m, 4H, CH₂), 1.32 (t, *J* = 7.1 Hz, 6H, CH₃).

¹³C NMR (101 MHz, CDCl₃) δ 138.5 (Cq), 129.2 (CH), 126.6 (Cq), 118.6 (d, *J* = 7.4 Hz, CH), 62.9 (d, *J* = 4.9 Hz, CH₂), 16.1 (d, *J* = 7.1 Hz, CH₃).

³¹P NMR (162 MHz, CDCl₃) δ 1.68.

HRMS *m/z* (ESI+) Exact mass calculated for C₁₀H₁₆Cl³⁵NO₃P [M+H]⁺: 264.0551, found: 264.0549.

diethyl (4-bromophenyl)phosphoramidate (96i)



The reaction was performed following the general procedure using (124 mg, 0.724 mmol) of 4-bromoaniline and CH₃CN as a solvent. 97 mg of brown oil were obtained. Yield: 87%.

IR (CHCl₃, liquid film): 3185, 3153 (N-H stretch), 3056 (aromatic C-H stretch), 2981 (aliphatic C-H stretch), 1595, 1492 (aromatic C=C stretch), 1224 (P=O stretch), 1024, 976 (P-OR ester stretch) cm⁻¹.

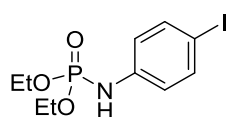
¹H NMR (400 MHz, CDCl₃) δ 7.34 (bd, J = 8.7 Hz, 2H, Ar), 6.92 (bd, J = 8.8 Hz, 2H, Ar), 6.85 (d, J = 9.3 Hz, 1H, NH), 4.23 – 4.01 (m, 4H, CH₂), 1.31 (t, J = 7.1 Hz, 6H, CH₃).

¹³C NMR (101 MHz, CDCl₃) δ 139.1 (Cq), 132.1 (CH), 119.0 (d, J = 7.5 Hz, CH), 113.9 (Cq), 62.9 (d, J = 4.9 Hz, CH₂), 16.1 (d, J = 7.1 Hz, CH₃).

³¹P NMR (162 MHz, CDCl₃) δ 2.11.

HRMS m/z (ESI+) Exact mass calculated for C₁₀H₁₆Br⁷⁹NO₃P [M+H]⁺: 308.0046, found: 308.0049.

diethyl (4-iodophenyl)phosphoramidate (96j)



The reaction was performed following the general procedure using (159 mg, 0.724 mmol) of 4-iodoaniline and CH₃CN as a solvent. 120 mg of brown solid were obtained. Yield: 96%.

mp: 66-68 °C.

IR (CHCl₃, liquid film): 3180, 3146 (N-H stretch), 2981, 2939 (aliphatic C-H stretch), 1591, 1489 (aromatic C=C stretch), 1223 (P=O stretch), 1024, 976 (P-OR ester stretch) cm⁻¹.

¹H NMR (400 MHz, CDCl₃) δ 7.53 (d, J = 8.6 Hz, 2H, Ar), 6.78 (d, J = 8.8 Hz, 2H, Ar), 5.74 (d, J = 8.8 Hz, 1H, NH), 4.25 – 4.00 (m, 4H, CH₂), 1.32 (t, J = 7.1 Hz, 6H, CH₃).

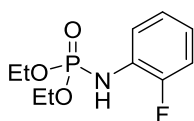
^{13}C NMR (101 MHz, CDCl_3) δ 139.5 (Cq), 138.1 (CH), 119.4 (d, J = 7.2 Hz, CH), 84.1 (Cq), 63.0 (d, J = 4.9 Hz, CH_2), 16.1 (d, J = 7.1 Hz, CH_3).

^{31}P NMR (162 MHz, CDCl_3) δ 1.41.

HRMS m/z (ESI+) Exact mass calculated for $\text{C}_{10}\text{H}_{16}\text{INO}_3\text{P}$ $[\text{M}+\text{H}]^+$: 355.9907, found: 355.9914.

The same reaction was performed on **5 g scale**. In a round bottom flask were added in this sequence: the organic dye Rose Bengal (5 g, 3.9 mmol, 11 mol% equiv), 4-iodoaniline (15.9 g, 72 mmol, 2 equiv), the solvent (75 mL) and diethyl phosphate (5 g, 36 mmol, 1 equiv). After the work-up, 10.5 g of brown solid were obtained. Yield: 82%.

diethyl (2-fluorophenyl)phosphoramidate (96k)



The reaction was performed following the general procedure using (62 μL , 0.724 mmol) of 2-fluoroaniline and CH_3CN as a solvent. 83 mg of black foam were obtained. Yield: 93%.

IR (CHCl_3 , liquid film): 3182 (N-H stretch), 2983, 1619, 1243, 1214 (P=O stretch), 1025, 977 (P-OR ester stretch), 750 cm^{-1} .

^1H NMR (400 MHz, CDCl_3) δ 7.31 – 7.27 (m, 1H, Ar), 7.06 (dd, J = 13.2, 5.6 Hz, 2H, Ar), 6.96 – 6.87 (m, 1H, Ar), 5.35 (d, J = 5.2 Hz, 1H, NH), 4.28 – 4.07 (m, 4H, CH_2), 1.34 (td, J = 7.1, 0.6 Hz, 6H, CH_3).

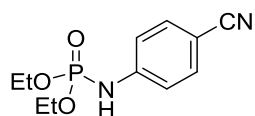
^{13}C NMR (101 MHz, CDCl_3) δ 155.2 (Cq), 127.9 (Cq), 124.6 (d, J = 3.8 Hz, CH), 122.0 (d, J = 7.2 Hz, CH), 118.2 (CH), 115.2 (d, J = 19.2 Hz, CH), 63.2 (d, J = 5.1 Hz, CH_2), 16.1 (d, J = 7.0 Hz, CH_3).

^{19}F NMR (376 MHz, CDCl_3) δ -133.29 (d, J = 13.3 Hz).

^{31}P NMR (162 MHz, CDCl_3) δ 1.28.

HRMS m/z (ESI+) Exact mass calculated for $\text{C}_{10}\text{H}_{16}\text{FNO}_3\text{P}$ $[\text{M}+\text{H}]^+$: 248.0846, found: 248.0848.

diethyl (4-cyanophenyl)phosphoramidate (96l)



The reaction was performed following the general procedure using (85 mg, 0.724 mmol) of 4-aminobenzonitrile and CH_3CN as a solvent. 50 mg of red oil were obtained. Yield: 54%.

IR (CHCl_3 , liquid film): 3363 (N-H stretch), 3052 (aromatic C-H stretch), 2982 (aliphatic C-H stretch), 2220 ($\text{C}\equiv\text{N}$ stretch) 1514, 1477 (aromatic C=C stretch), 1228 (P=O stretch), 1024, 974 (P-OR ester stretch) cm^{-1} .

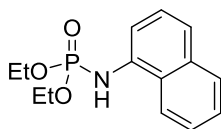
^1H NMR (400 MHz, CDCl_3) δ 7.54 (d, J = 8.6 Hz, 2H, Ar), 7.07 (d, J = 8.7 Hz, 2H, Ar), 4.26 – 4.04 (m, 4H, CH_2), 1.34 (t, J = 7.0 Hz, 6H, CH_3).

^{31}P NMR (162 MHz, CDCl_3) δ 0.61.

HRMS m/z (ESI+) Exact mass calculated for $\text{C}_{11}\text{H}_{16}\text{N}_2\text{O}_3\text{P}$ $[\text{M}+\text{H}]^+$: 255.0893, found: 255.0892.

The experimental data obtained is in accordance with the data reported in literature.^[56]

diethyl naphthalen-1-ylphosphoramidate (96m)



The reaction was performed following the general procedure using (104 mg, 0.724 mmol) of naphthalen-1-amine and CH₃CN as a solvent. 62 mg of black solid were obtained. Yield: 61%.

mp: 103-105 °C.

IR (CHCl₃, liquid film): 3202 (N-H stretch), 2981, 2918, 2849 (aliphatic C-H stretch), 1597, 1579, 1519, 1469 (aromatic C=C stretch), 1239 (P=O stretch), 1022, 972 (P-OR ester stretch) cm⁻¹.

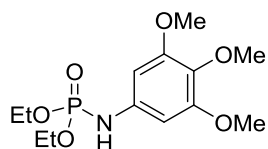
¹H NMR (400 MHz, CDCl₃) δ 7.97 – 7.94 (m, 1H, Ar), 7.90 – 7.80 (m, 1H, Ar), 7.53 (dtd, *J* = 8.1, 6.7, 1.2 Hz, 3H, Ar), 7.44 – 7.35 (m, 2H, Ar), 5.93 – 5.67 (m, 1H, NH), 4.30 – 4.05 (m, 4H, CH₂), 1.31 (t, *J* = 7.1 Hz, 6H, CH₃).

¹³C NMR (101 MHz, CDCl₃) δ 134.6 (Cq), 134.3 (Cq), 128.8 (CH), 126.1 (CH), 126.0 (CH), 125.3 (d, *J* = 2.2 Hz, Cq), 122.8 (CH), 120.2 (m, 2CH), 114.2 (CH), 63.0 (d, *J* = 5.0 Hz, CH₂), 16.1 (d, *J* = 7.1 Hz, CH₃).

³¹P NMR (162 MHz, CDCl₃) δ 2.65.

HRMS *m/z* (ESI+) Exact mass calculated for C₁₄H₁₉NO₃P [M+H]⁺: 280.1097, found: 280.1100.

diethyl (3,4,5-trimethoxyphenyl)phosphoramidate (96n)



The reaction was performed following the general procedure using (133 mg, 0.724 mmol) of 3,4,5-trimethoxyaniline and CH₃CN as a solvent. 96 mg of black foam were obtained. Yield: 83%.

IR (CHCl₃, liquid film): 3233, 2983, 2937 (aliphatic C-H stretch), 1601, 1507 (aromatic C=C stretch), 1452, 1231 (P=O stretch), 1126, 975 (P-OR ester stretch) cm⁻¹.

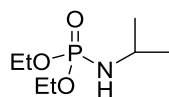
¹H NMR (400 MHz, CDCl₃) δ 6.26 (bs, 2H, Ar), 5.68 (bs, 1H, NH), 4.26 – 4.04 (m, 4H, CH₂), 3.82 (s, 6H, OCH₃), 3.79 (s, 3H, OCH₃), 1.34 (t, *J* = 7.1 Hz, 6H CH₂CH₃).

¹³C NMR (101 MHz, CDCl₃) δ 153.7 (Cq), 135.8 (d, *J* = 3.5 Hz, Cq), 133.0 (d, *J* = 2.2 Hz, Cq), 95.19 (d, *J* = 7.4 Hz, 2CH), 62.9 (d, *J* = 4.8 Hz, CH₂), 61.0 (CH₃), 56.0 (CH₃), 16.2 (d, *J* = 7.1 Hz, CH₃).

³¹P NMR (162 MHz, CDCl₃) δ 2.01, 1.96.

HRMS *m/z* (ESI+) Exact mass calculated for C₁₃H₂₃NO₆P [M+H]⁺: 320.1258, found: 320.1263.

diethyl isopropylphosphoramidate (119b)



The reaction was performed following the general procedure using (106 μl, 0.724 mmol) of propan-2-amine and toluene as a solvent. 30 mg of red oil were obtained. Yield: 42%.

IR (CHCl₃, liquid film): 3020, 2182, 2042, 1214 (P=O stretch), 907 (P-OR ester stretch), 748 cm⁻¹.

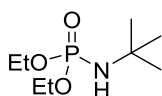
¹H NMR (400 MHz, CDCl₃) δ 4.15 – 4.00 (m, 4H, OCH₂), 3.46 – 3.28 (m, 1H, CH), 2.36 (bs, 1H, NH), 1.34 (td, J = 7.1, 0.6 Hz, 6H, OCH₂CH₃), 1.17 (dd, J = 6.4, 0.6 Hz, 6H, CH₃).

¹³C NMR (101 MHz, CDCl₃) δ 62.2 (CH), 43.8 (CH), 25.3 (d, J = 5.6 Hz, CH₃), 16.2 (d, J = 7.2 Hz, CH₃).

³¹P NMR (162 MHz, CDCl₃) δ 8.09.

HRMS m/z (ESI+) Exact mass calculated for C₇H₁₉NO₃P [M+H]⁺: 196.1097, found: 196.1095.

diethyl *tert*-butylphosphoramidate (119c)



The reaction was performed following the general procedure using (76 μ l, 0.724 mmol) of 2-methylpropan-2-amine and toluene as a solvent. 40 mg of red oil were obtained. Yield: 53%.

IR (CHCl₃, liquid film): 2917, 2848, 2153, 2052, 1558 (P=O stretch), 905 (P-OR ester stretch), 803 cm⁻¹.

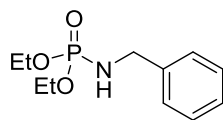
¹H NMR (400 MHz, CDCl₃) δ 4.13 – 4.01 (m, 4H, OCH₂), 2.54 (d, J = 6.0 Hz, 1H, NH), 1.34 (td, J = 7.1, 0.7 Hz, 6H, OCH₂CH₃), 1.28 (d, J = 0.6 Hz, 9H, CH₃).

³¹P NMR (162 MHz, CDCl₃) δ 7.01.

HRMS m/z (ESI+) Exact mass calculated for C₈H₂₁NO₃P [M+H]⁺: 210.1254, found: 210.1248.

The experimental data obtained is in accordance with the data reported in literature.^[26]

diethyl benzylphosphoramidate (119a)



The reaction was performed following the general procedure using (79 μ l, 0.724 mmol) of benzylamine and toluene as a solvent. 52 mg of red oil were obtained. Yield: 59%.

IR (CHCl₃, liquid film): 3235 (N-H stretch), 3022, 2983 (aliphatic C-H stretch), 1644, 1453 (aromatic C=C stretch), 1214 (P=O stretch), 1026, 907 (P-OR ester stretch), 750 cm⁻¹.

¹H NMR (400 MHz, CDCl₃) δ 7.38 – 7.28 (m, 5H, Ph), 4.16 – 3.98 (m, 6H, CH₂ and OCH₂CH₃), 2.96 (bs, 1H, NH), 1.31 (t, J = 7.1 Hz, 6H, CH₃).

³¹P NMR (162 MHz, CDCl₃) δ 8.45.

HRMS m/z (ESI+) Exact mass calculated for C₁₁H₁₉NO₃P [M+H]⁺: 244.1097, found: 244.1103.

The experimental data obtained is in accordance with the data reported in literature.^[26]

List of References

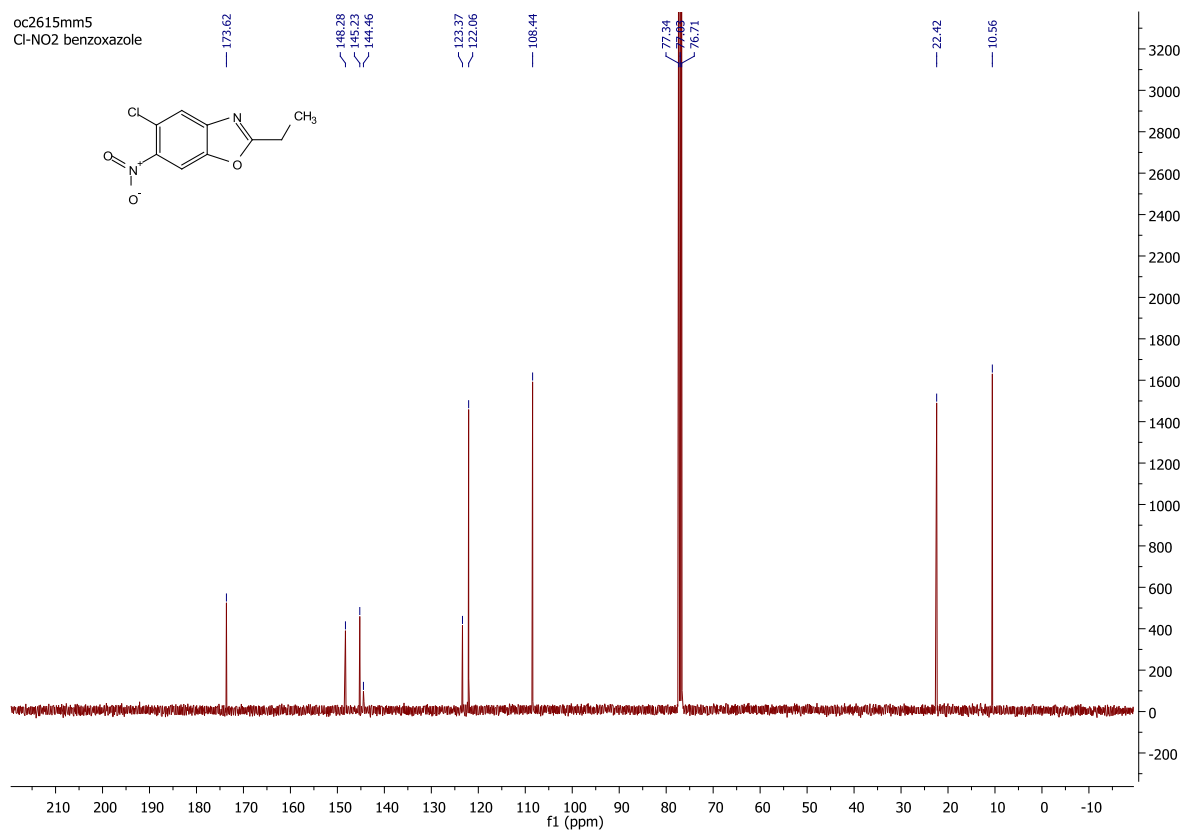
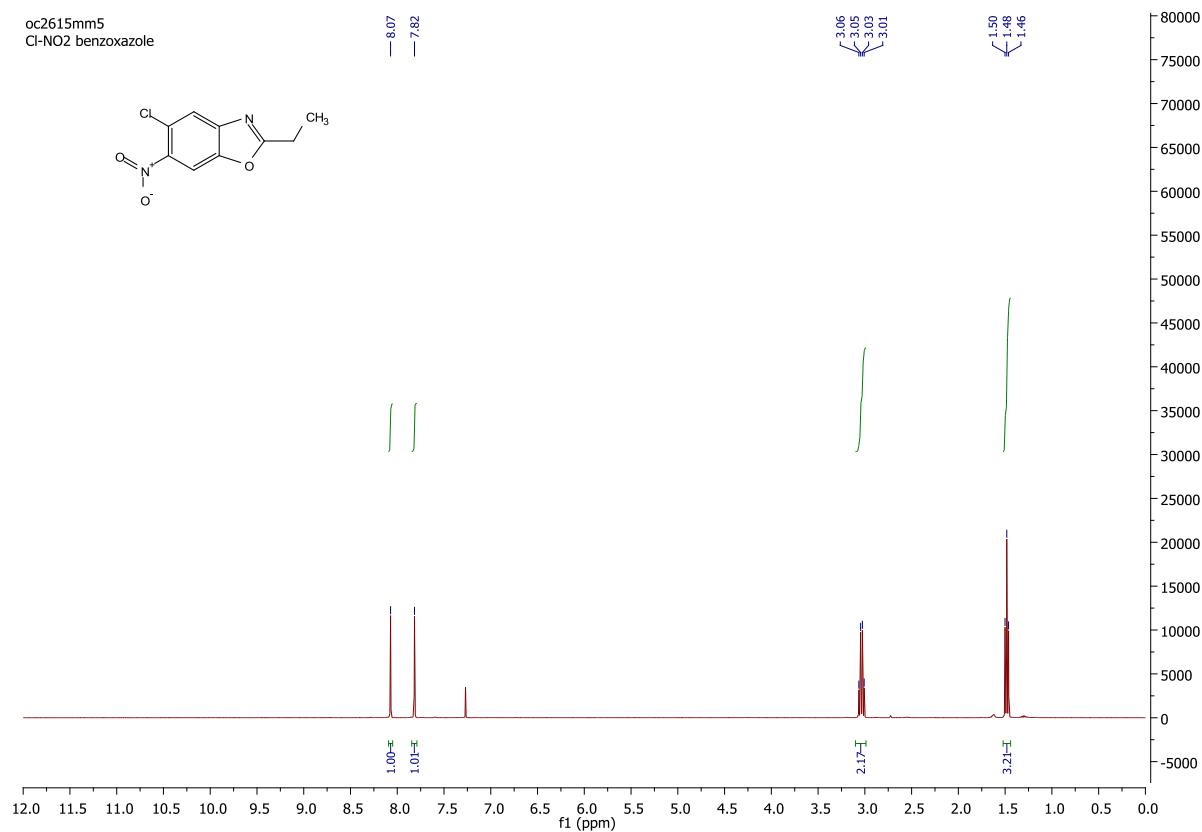
- [1] R. A. Sheldon, *Chem. Commun.* **2008**, 3352–3365.
- [2] P. T. Anastas, M. M. Kirchhoff, *Acc. Chem. Res.* **2002**, *35*, 686–694.
- [3] “<http://www.acs.org/content/acs/en/greenchemistry/what-is-green-chemistry/principles/12-principles-of-green-chemistry.html>”
- [4] P. T. Anastas, J. C. Warner, in *Oxford Univ. Press New York*, **1998**, p. 30.
- [5] R. A. Sheldon, *Green Chem.* **2007**, *9*, 1273–1283.
- [6] B. M. Trost, *Angew. Chem. Int. Ed.* **1995**, *34*, 259–281.
- [7] W. S. Knowles, *Angew. Chem. Int. Ed.* **2002**, *41*, 1998–2007.
- [8] R. Noyori, *Angew. Chem. Int. Ed.* **2002**, *41*, 2008–2022.
- [9] K. B. Sharpless, *Angew. Chem. Int. Ed.* **2002**, *41*, 2024–2032.
- [10] V. H. D. Roth, *Angew. Chem.* **1989**, *101*, 1220–1234.
- [11] G. Ciamician, *Science* **1912**, *36*, 385–394.
- [12] K. Zeitler, *Angew. Chem. Int. Ed.* **2009**, *48*, 9785–9789.
- [13] J. E. Bidlack, K. R. Stern, S. Jansky, *Introductory Plant Biology*, McGraw-Hill, New York, **2003**.
- [14] C. K. Prier, D. a. Rankic, D. W. C. MacMillan, *Chem. Rev.* **2013**, *113*, 5322–5363.
- [15] E. Meggers, *Chem. Commun.* **2015**, *51*, 3290–3301.
- [16] J. M. R. Narayanam, C. R. J. Stephenson, *Chem. Soc. Rev.* **2011**, *40*, 102–113.
- [17] J. W. Tucker, C. R. J. Stephenson, *J. Org. Chem.* **2012**, *77*, 1617–1622.
- [18] M. a Ischay, M. E. Anzovino, J. Du, T. P. Yoon, *J. Am. Chem. Soc.* **2008**, *130*, 12886–12887.
- [19] D. A. Nicewicz, D. W. C. Macmillan, *Science* **2008**, *105*.
- [20] C. C. C. Johansson Seechurn, M. O. Kitching, T. J. Colacot, V. Snieckus, *Angew. Chem. Int. Ed.* **2012**, *51*, 5062–5085.

- [21] C. S. Yeung, V. M. Dong, *Chem. Rev.* **2011**, *111*, 1215–1292.
- [22] C.-J. Li, Z. Li, *Pure Appl. Chem.* **2006**, *78*, 935–945.
- [23] C. Li, *Acc. Chem. Res.* **2009**, *42*, 335–344.
- [24] M. Rueping, S. Zhu, R. M. Koenigs, *Chem. Commun.* **2011**, *47*, 8679–8681.
- [25] J. Dhineshkumar, K. R. Prabhu, *Org. Lett.* **2013**, *15*, 6062–6065.
- [26] J. Fraser, L. J. Wilson, R. K. Blundell, C. J. Hayes, *Chem. Commun.* **2013**, *49*, 8919–8921.
- [27] Z. Li, C. Li, M. U. V, S. S. West, Q. Ha, *J. Am. Chem. Soc.* **2005**, *4*, 3672–3673.
- [28] A. S.-K. Tsang, M. H. Todd, *Tetrahedron Lett.* **2009**, *50*, 1199–1202.
- [29] X.-Z. Shu, X.-F. Xia, Y.-F. Yang, K.-G. Ji, X.-Y. Liu, Y.-M. Liang, *J. Org. Chem.* **2009**, *74*, 7464–7469.
- [30] O. Baslé, C.-J. Li, *Green Chem.* **2007**, *9*, 1047–1050.
- [31] S. A. Girard, T. Knauber, C.-J. Li, *Angew. Chem. Int. Ed.* **2014**, *53*, 74–100.
- [32] Y. Pan, C. W. Kee, L. Chen, C.-H. Tan, *Green Chem.* **2011**, *13*, 2682–2685.
- [33] M. Rueping, C. Vila, T. Bootwicha, *ACS Catal.* **2013**, *3*, 1676–1680.
- [34] D. P. Hari, B. Konig, *Org. Lett.* **2011**, *13*, 3852–3855.
- [35] D. R. Phillips, M. Uramoto, K. Isono, J. A. McCloskey, *J. Org. Chem.* **1993**, *58*, 854–859.
- [36] R. F. Roush, E. M. Nolan, F. Lohr, C. T. Walsh, *J. Am. Chem. Soc.* **2008**, *130*, 8361–8365.
- [37] J. I. Guijarro, J. E. Gonza, F. Baleux, J. L. San Millan, M. A. Castilla, M. Rico, F. Moreno, M. Delepierre, *J. Biol. Chem.* **1995**, *270*, 23520–23532.
- [38] M. Serpi, R. Bibbo, S. Rat, H. Roberts, C. Hughes, B. Caterson, A. T. Gibert, C. Raul, A. Verson, C. McGuigan, *J. Med. Chem* **2012**, *55*, 4629–4639.
- [39] C. McGuigan, A. Gilles, K. Madela, M. Aljarah, S. Holl, S. Jones, J. Vernachio, J. Hutchins, B. Ames, K. D. Bryant, *et al.*, *J. Med. Chem.* **2010**, *53*, 4949–4957.
- [40] T. Nguyen, S. Chang, B. Condon, R. Slopek, E. Graves, *Ind. Eng. Chem. Res.* **2013**, *52*, 4715–4724.

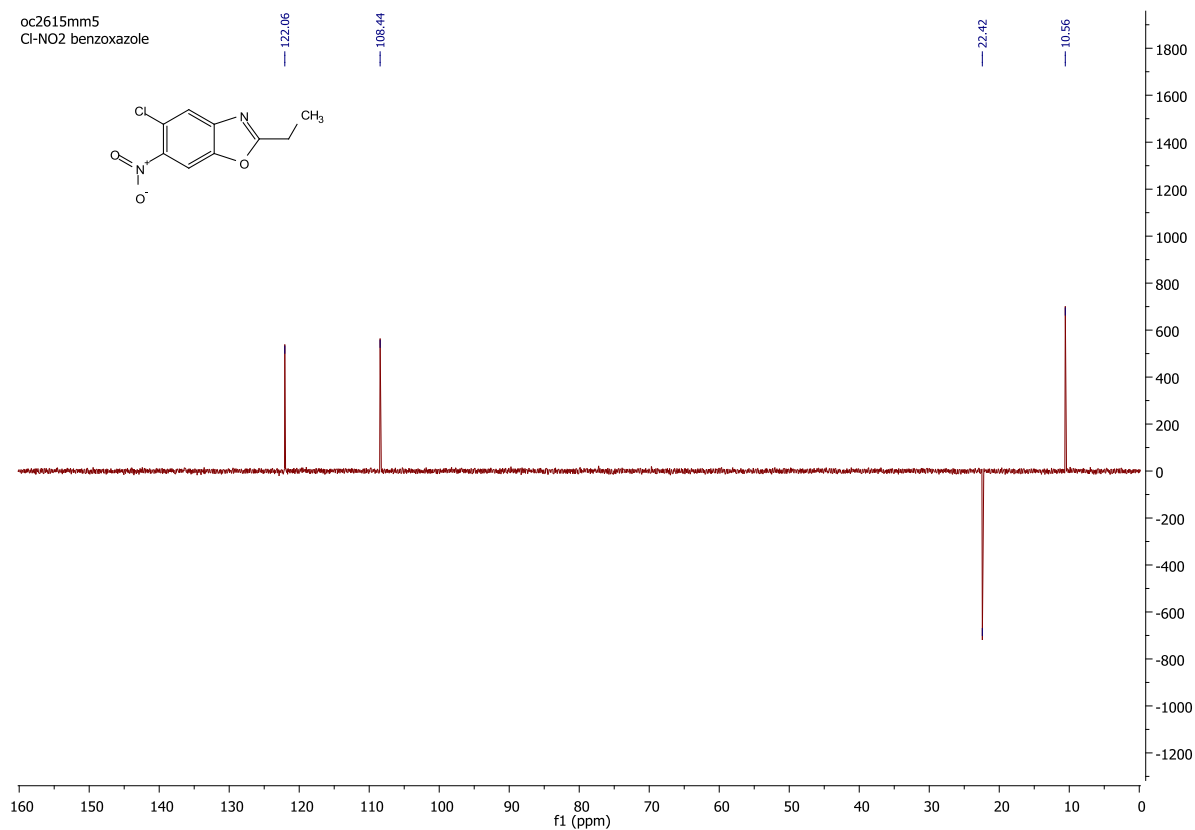
- [41] X. Gao, Z. Tang, M. Lu, H. Liu, Y. Jiang, Y. Zhao, Z. Cai, *Chem. Commun.* **2012**, 48, 10198–10200.
- [42] Y. Chen, J. Zhang, J. Chen, X.-Y. Cao, J. Wang, Y.-F. Zhao, *Rapid Commun. Mass Spectrom.* **2004**, 18, 469–473.
- [43] P. Garcia, Y. Y. Lau, M. R. Perry, L. L. Schafer, *Angew. Chem. Int. Ed.* **2013**, 52, 9144–9148.
- [44] M. Ding, F. Zhou, Y.-L. Liu, C.-H. Wang, X.-L. Zhao, J. Zhou, *Chem. Sci.* **2011**, 2, 2035–2039.
- [45] J.-S. Yu, F.-M. Liao, W.-M. Gao, K. Liao, R.-L. Zuo, J. Zhou, *Angew. Chem. Int. Ed.* **2015**, 54, 7381–7385.
- [46] F. R. Atherton, H. T. Openshaw, A. R. Todd, *J. Chem. Soc.* **1945**, 660–663.
- [47] S. S. Le Corre, M. Berchel, H. Couthon-Gourvès, J.-P. Haelters, P.-A. Jaffrès, *Beilstein J. Org. Chem.* **2014**, 10, 1166–1196.
- [48] R. Appel, H. Einig, *Zeitschrift für Anorg. und Allg. Chemie* **2004**, 414, 236–240.
- [49] R. B. Meyer, D. A. Shuman, R. K. Robins, *Tetrahedron Lett.* **1973**, 4, 269–272.
- [50] R. Haggam, J. Conrad, U. Beifuss, *Tetrahedron Lett.* **2009**, 50, 6627–6630.
- [51] R. Serwa, I. Wilkening, G. Del Signore, M. Mühlberg, I. Claußnitzer, C. Weise, M. Gerrits, C. P. R. Hackenberger, *Angew. Chem. Int. Ed.* **2009**, 48, 8234–8239.
- [52] I. Wilkening, G. del Signore, C. P. R. Hackenberger, *Chem. Commun.* **2008**, 2932–2934.
- [53] H. Kim, J. Park, J. G. Kim, S. Chang, *Org. Lett.* **2014**, 16, 5466–5469.
- [54] G. Wang, Q.-Y. Yu, S.-Y. Chen, X.-Q. Yu, *Tetrahedron Lett.* **2013**, 54, 6230–6232.
- [55] X. Jin, K. Yamaguchi, N. Mizuno, *Org. Lett.* **2013**, 15, 418–421.
- [56] B. A. Dar, N. A. Dangroo, A. Gupta, A. Wali, M. A. Khuroo, R. A. Vishwakarma, B. Singh, *Tetrahedron Lett.* **2014**, 55, 1544–1548.

Synergistic catalysis: enantioselective addition of alkylbenzoxazoles to enals

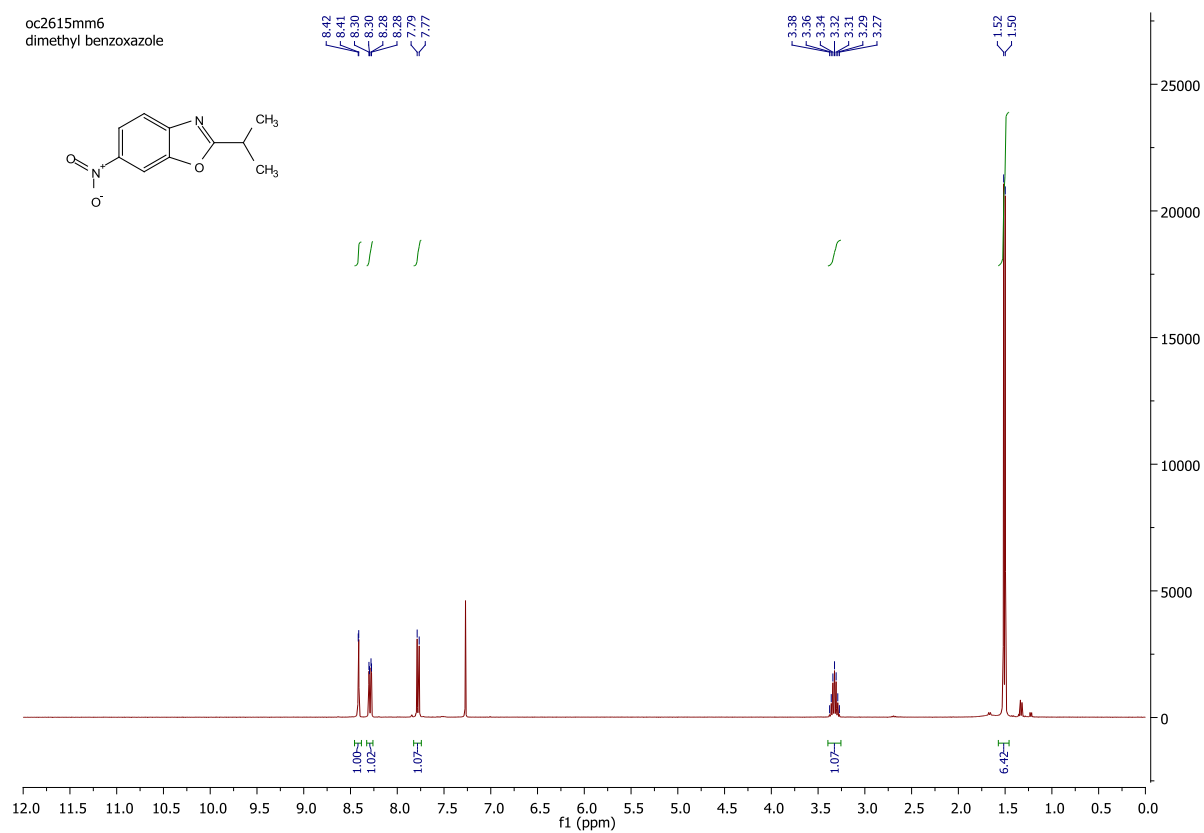
NMR benzoxazoles



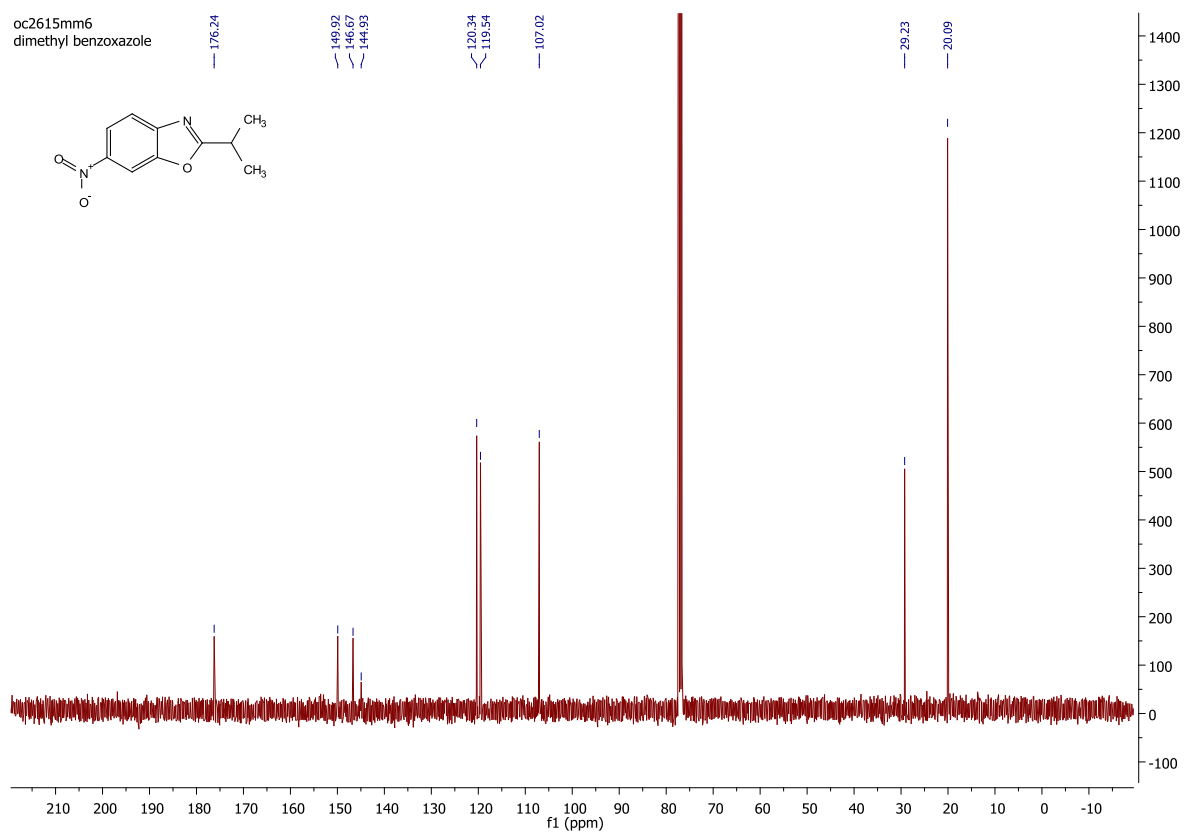
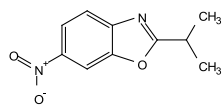
oc2615mm5
Cl-NO2 benzoxazole



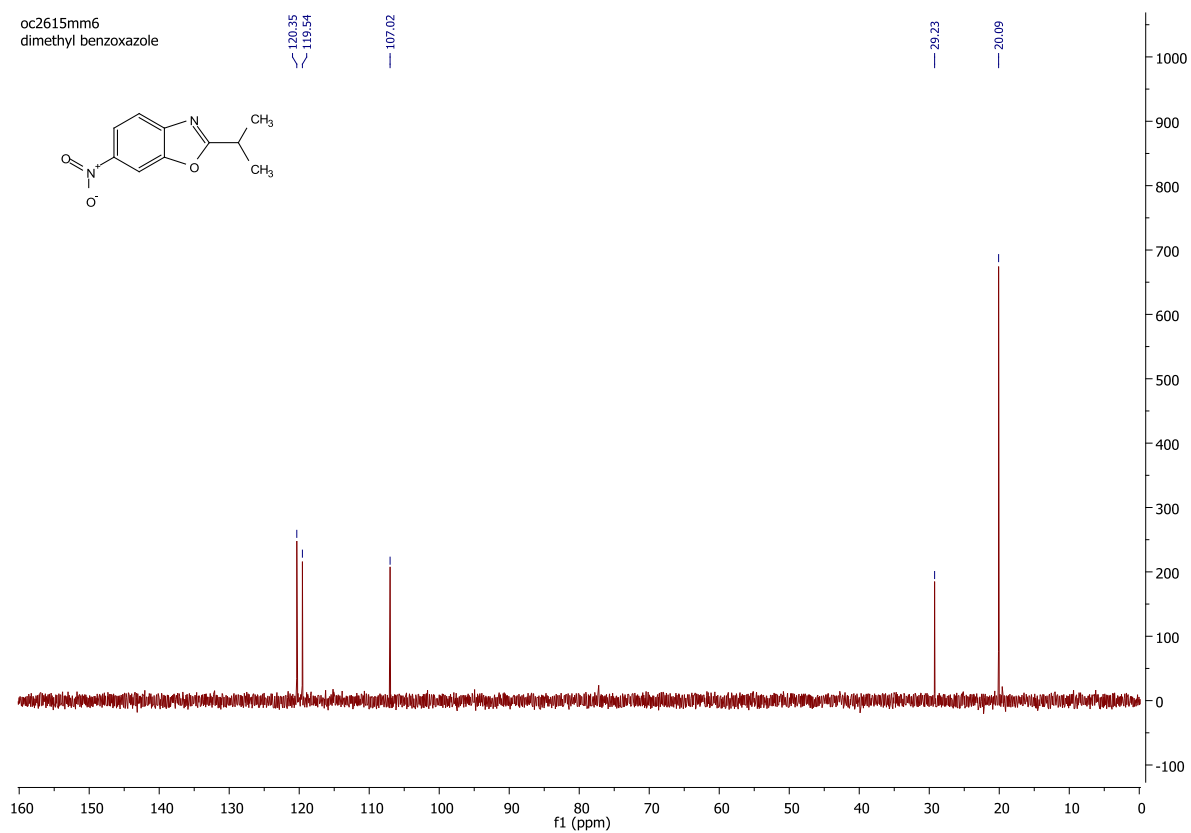
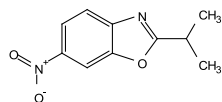
oc2615mm6
dimethyl benzoxazole



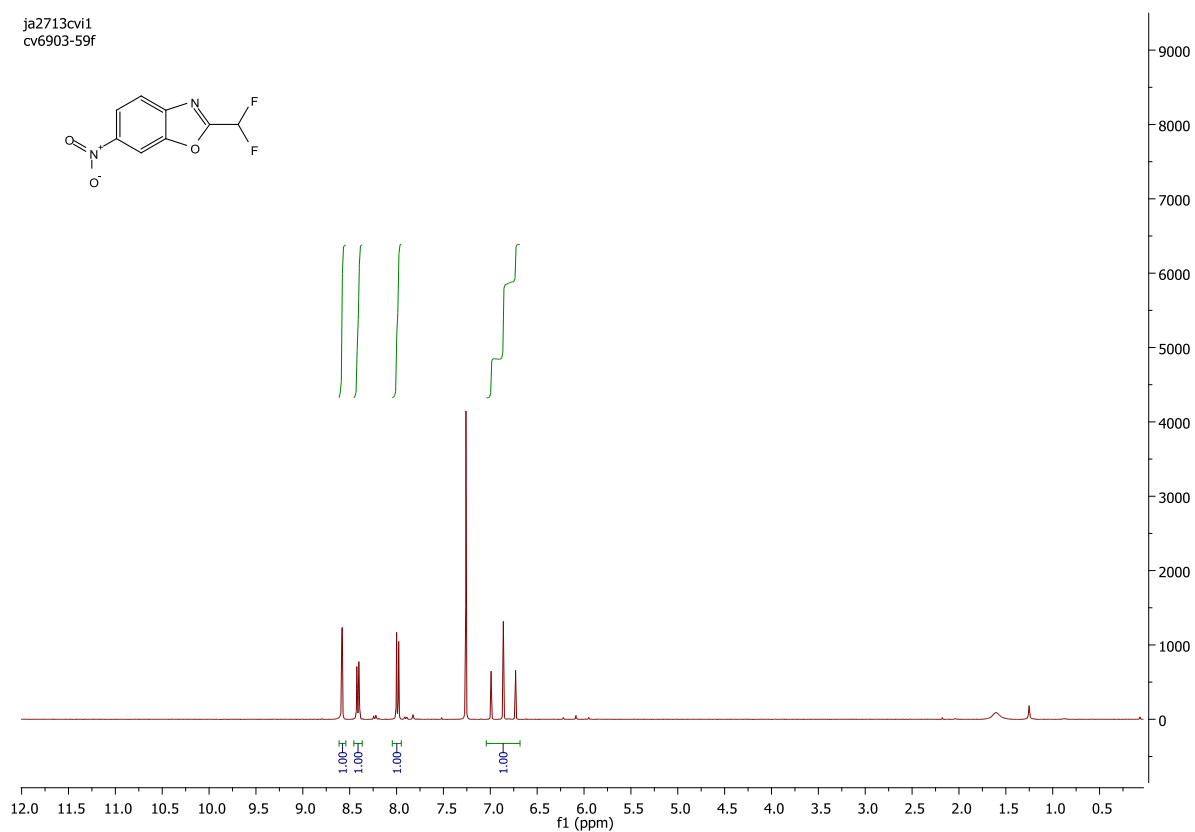
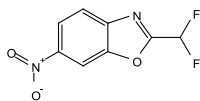
oc2615mm6
dimethyl benzoxazole



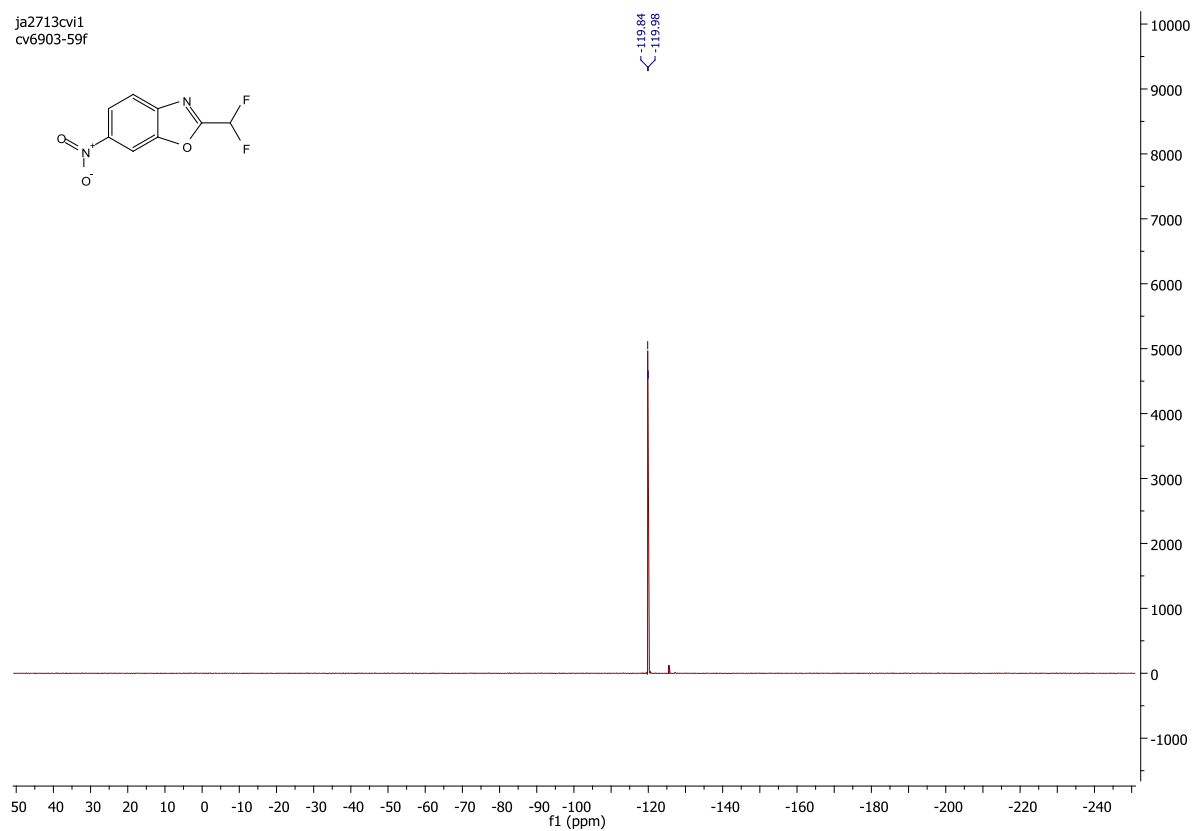
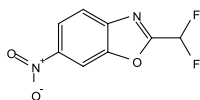
oc2615mm6
dimethyl benzoxazole



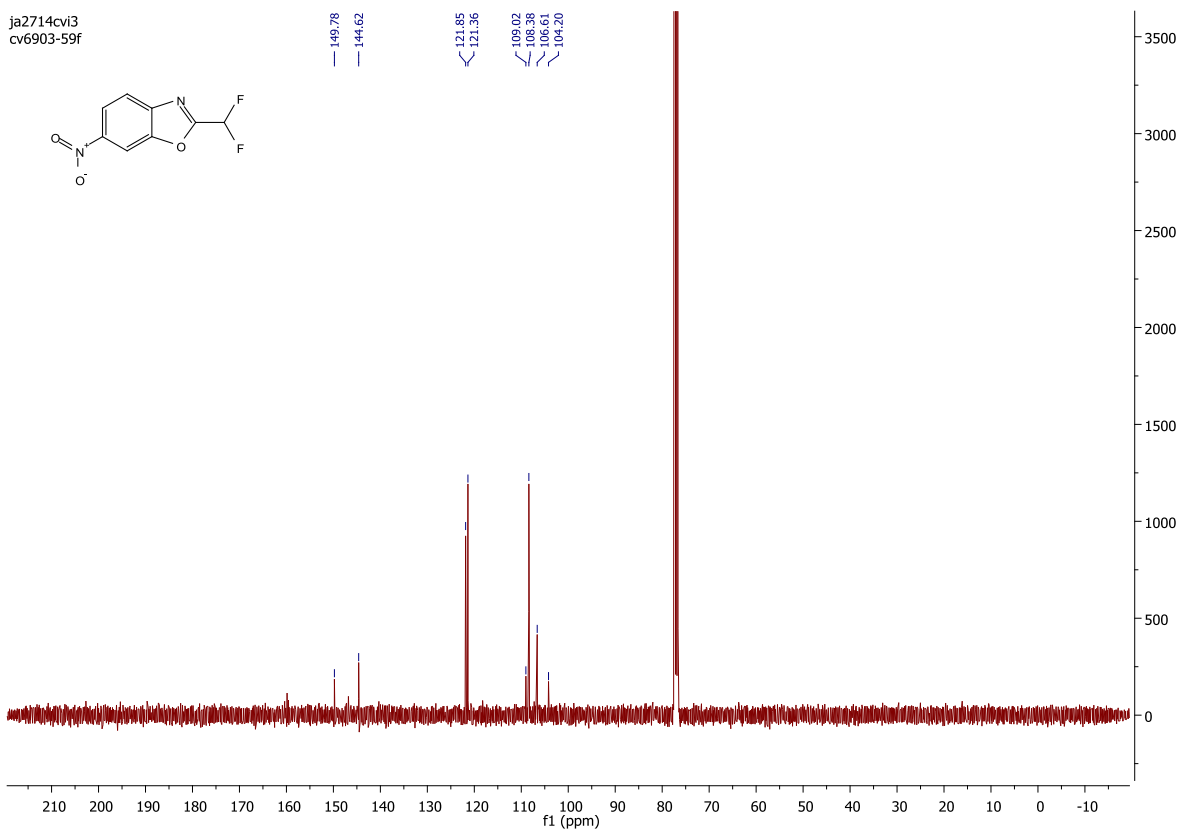
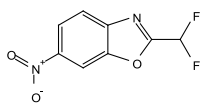
ja2713cvi1
cv6903-59f



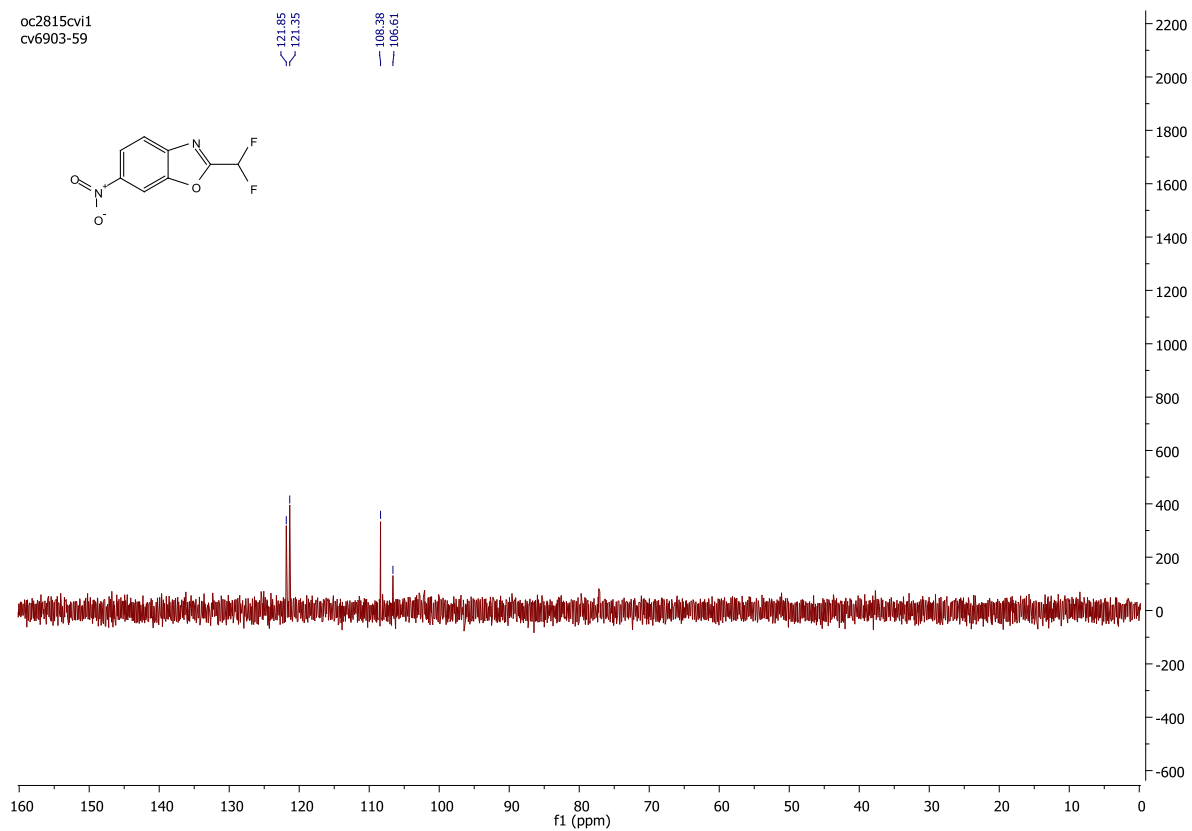
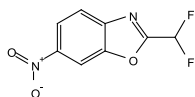
ja2713cvi1
cv6903-59f



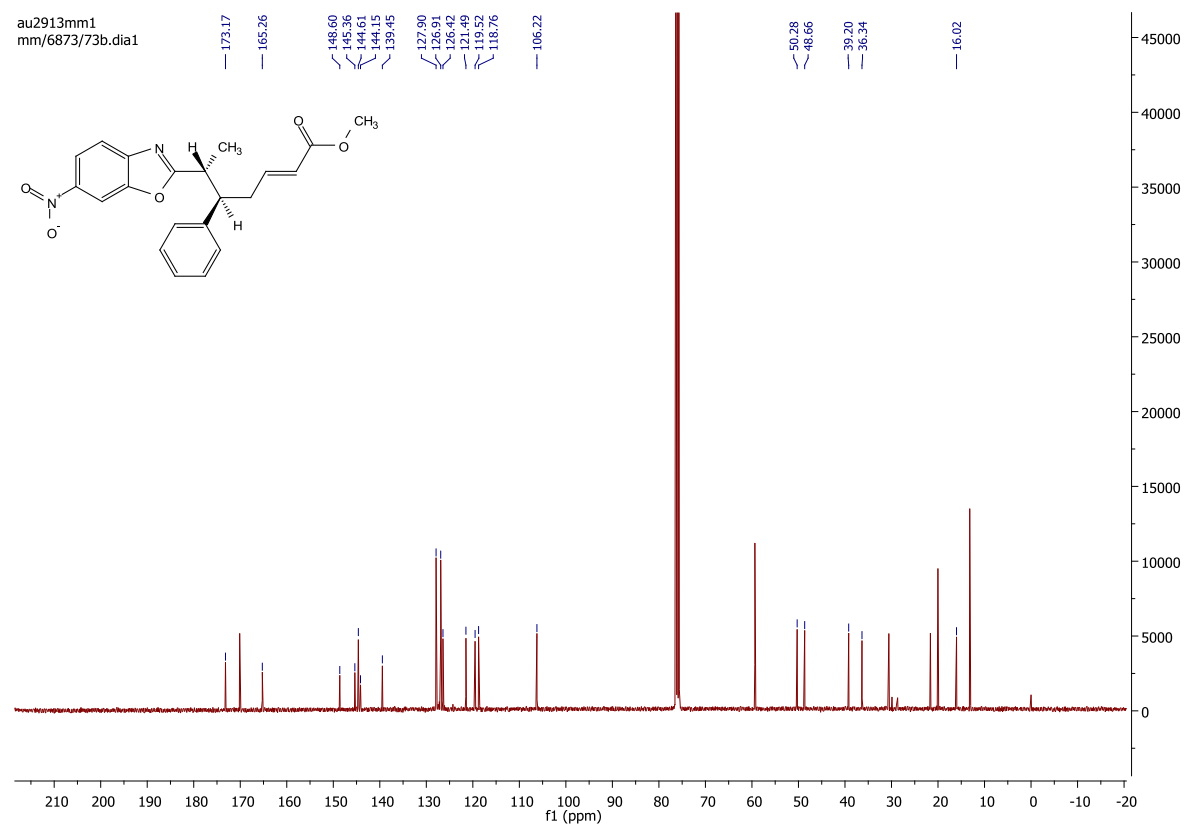
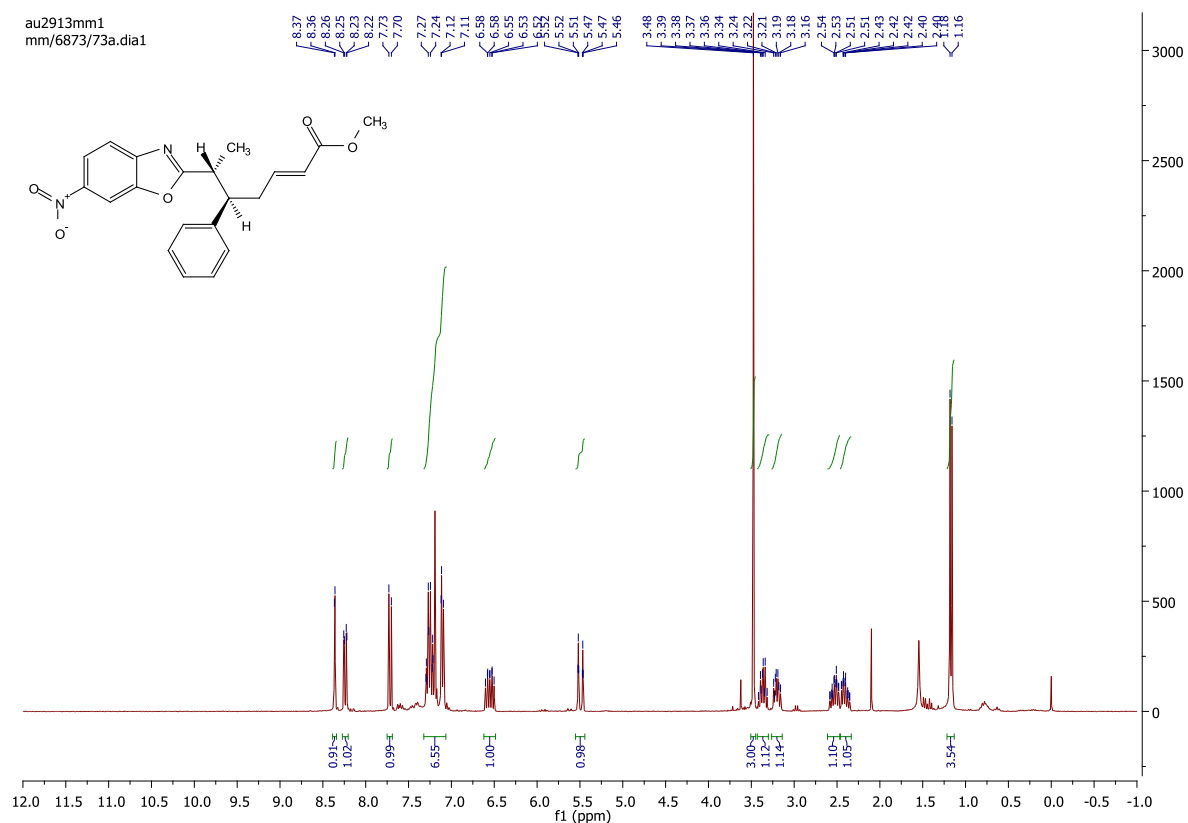
ja2714cvi3
cv6903-59f



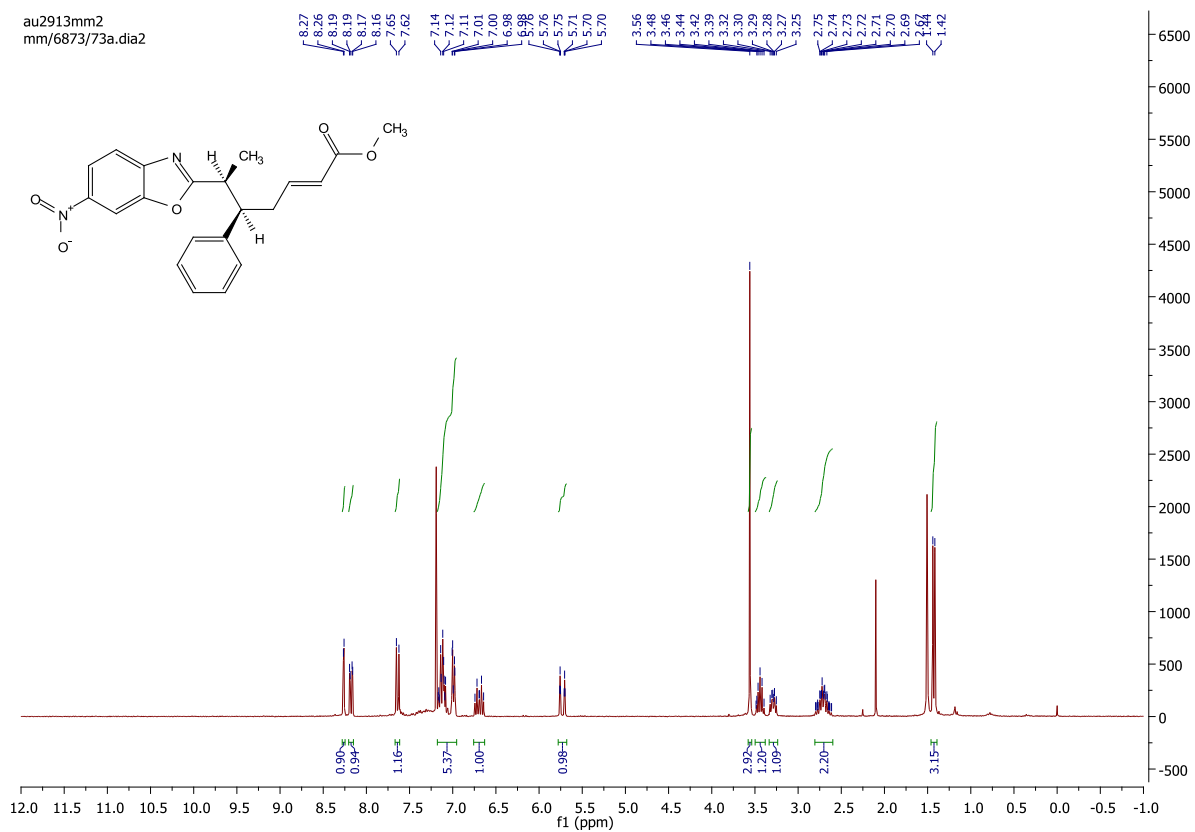
oc2815cvi1
cv6903-59



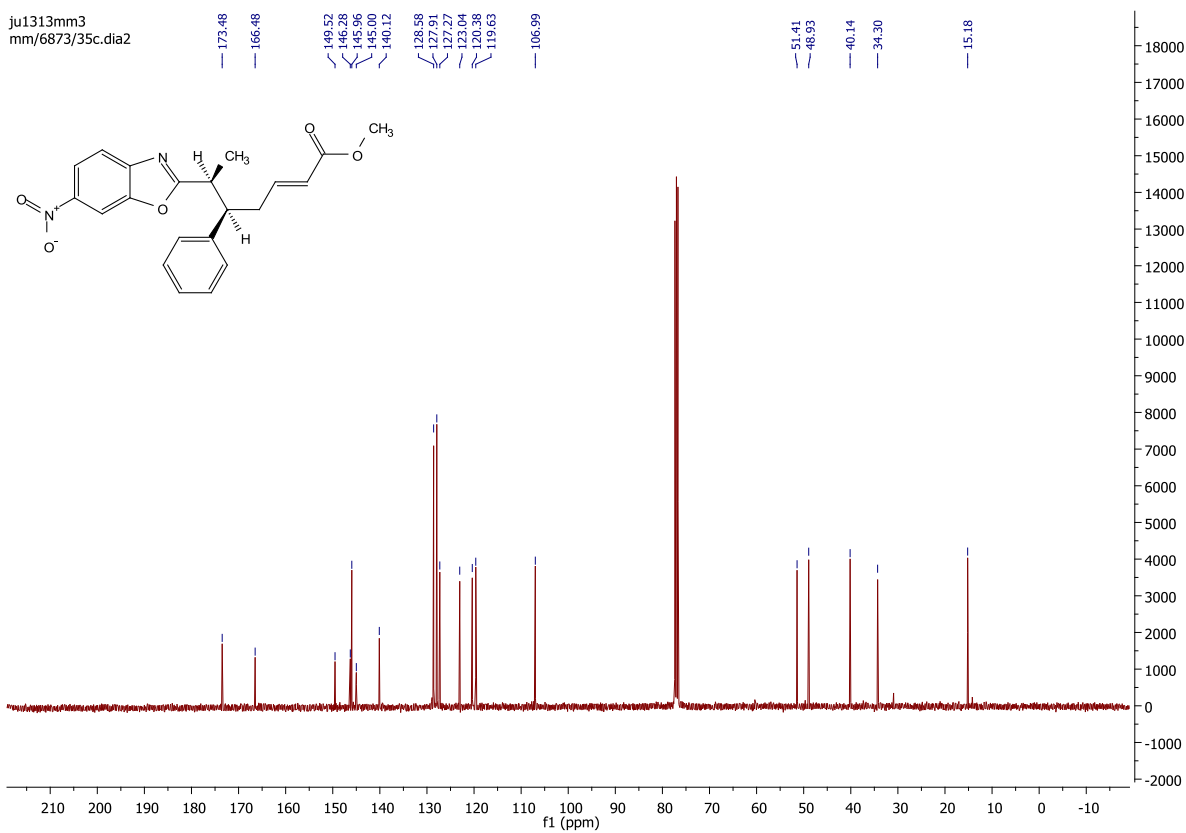
NMR and HPLC final products



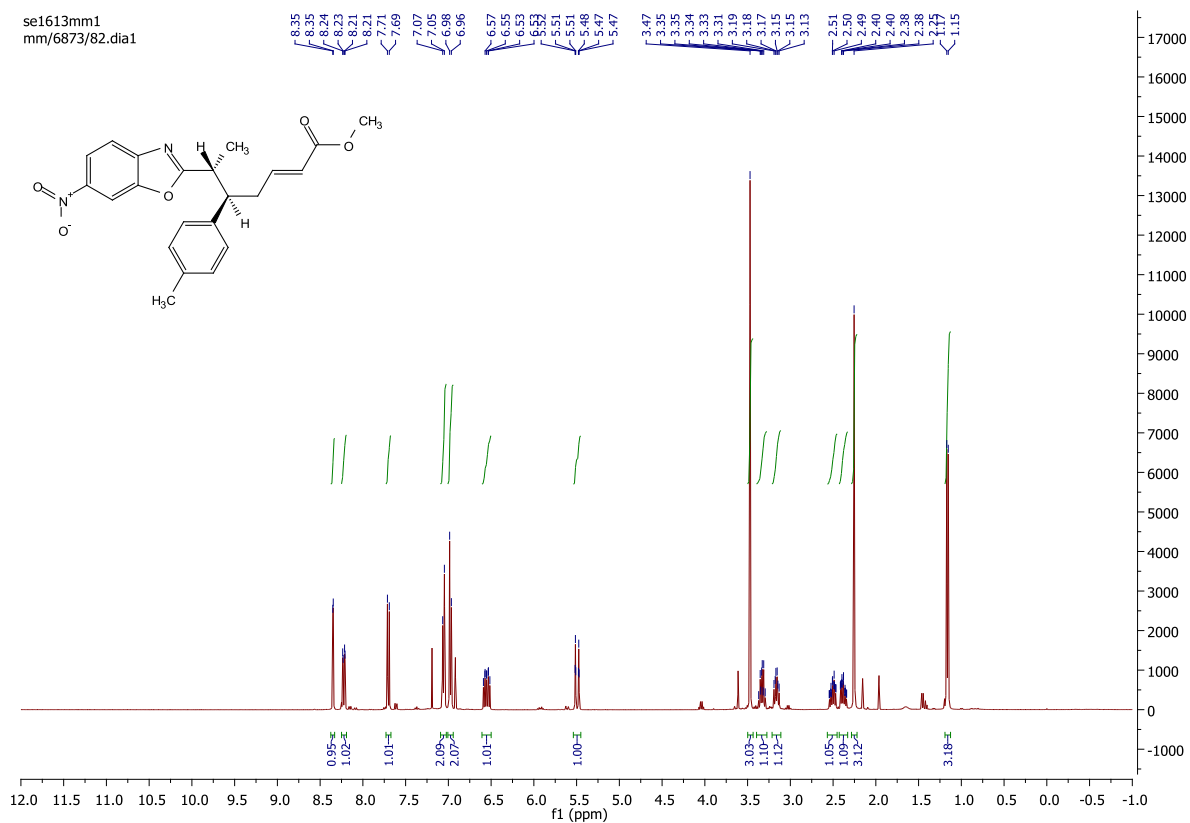
au2913mm2
mm/6873/73a.dia2



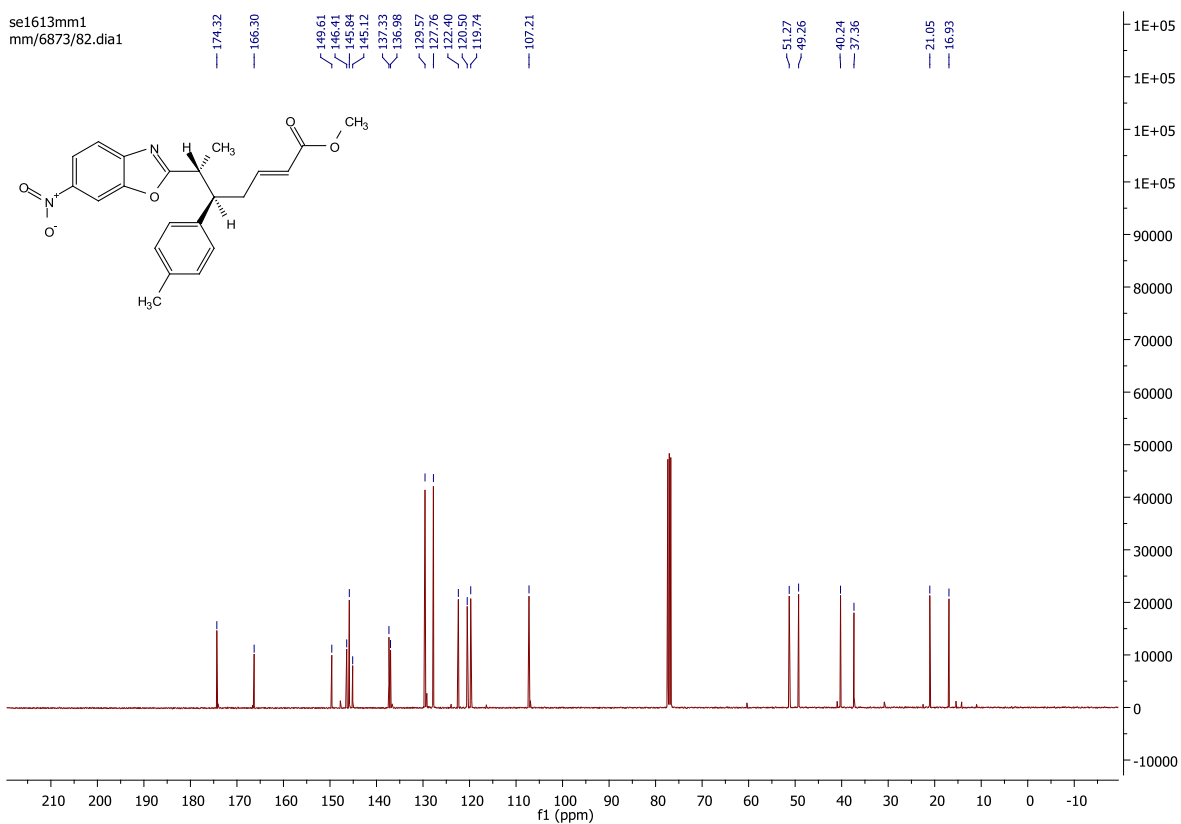
ju1313mm3
mm/6873/35c.dia2

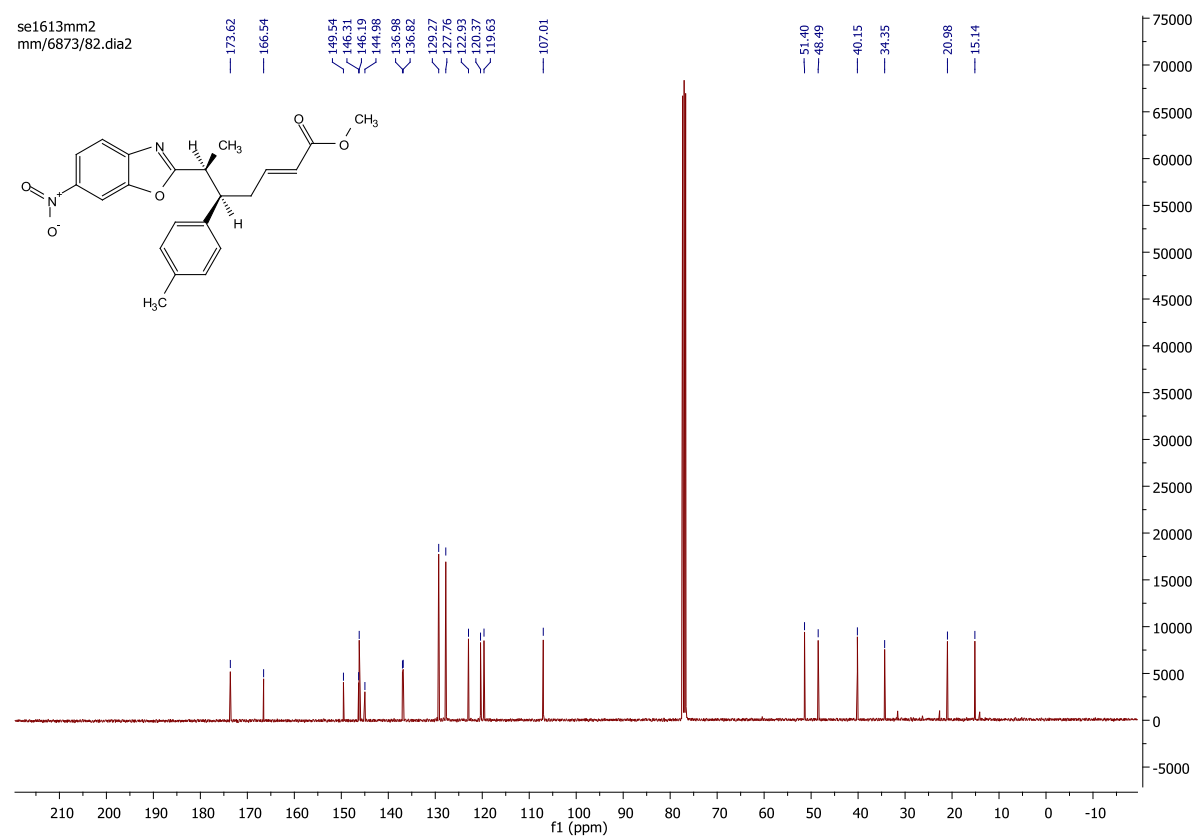
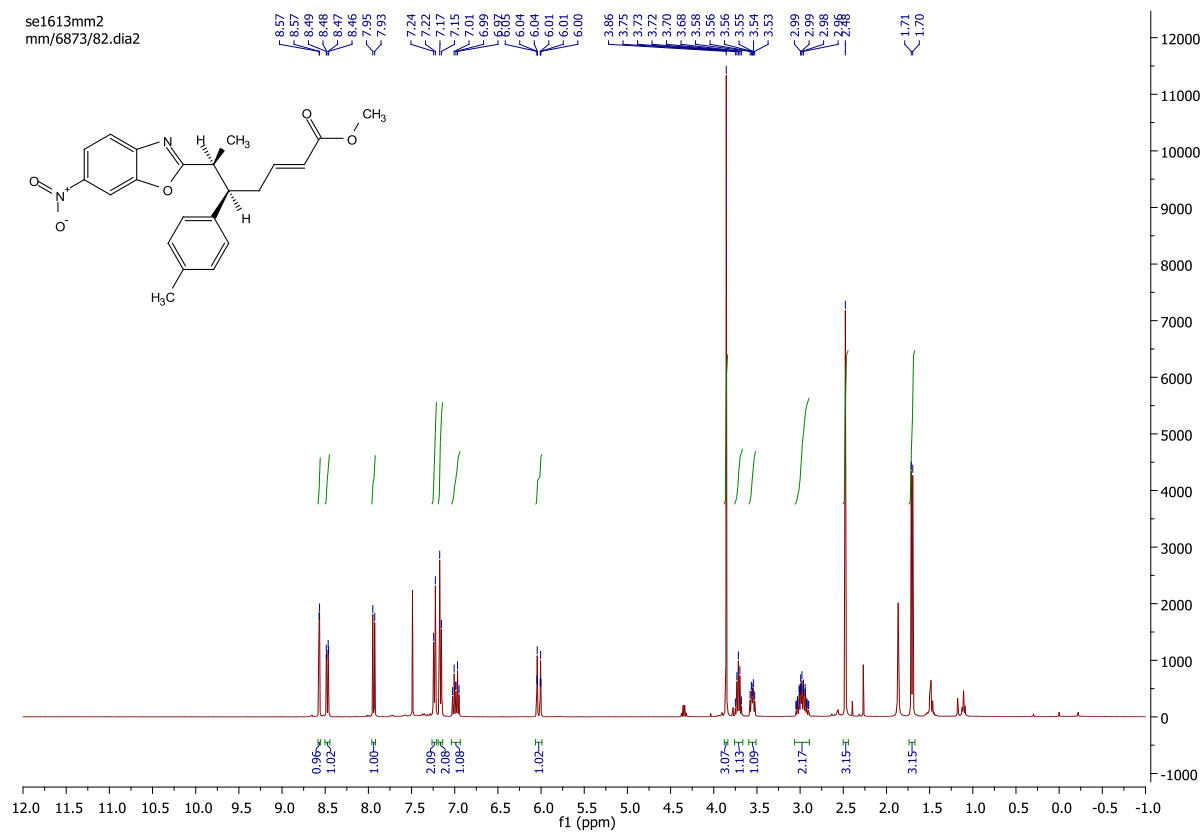


se1613mm1
mm/6873/82.dia1

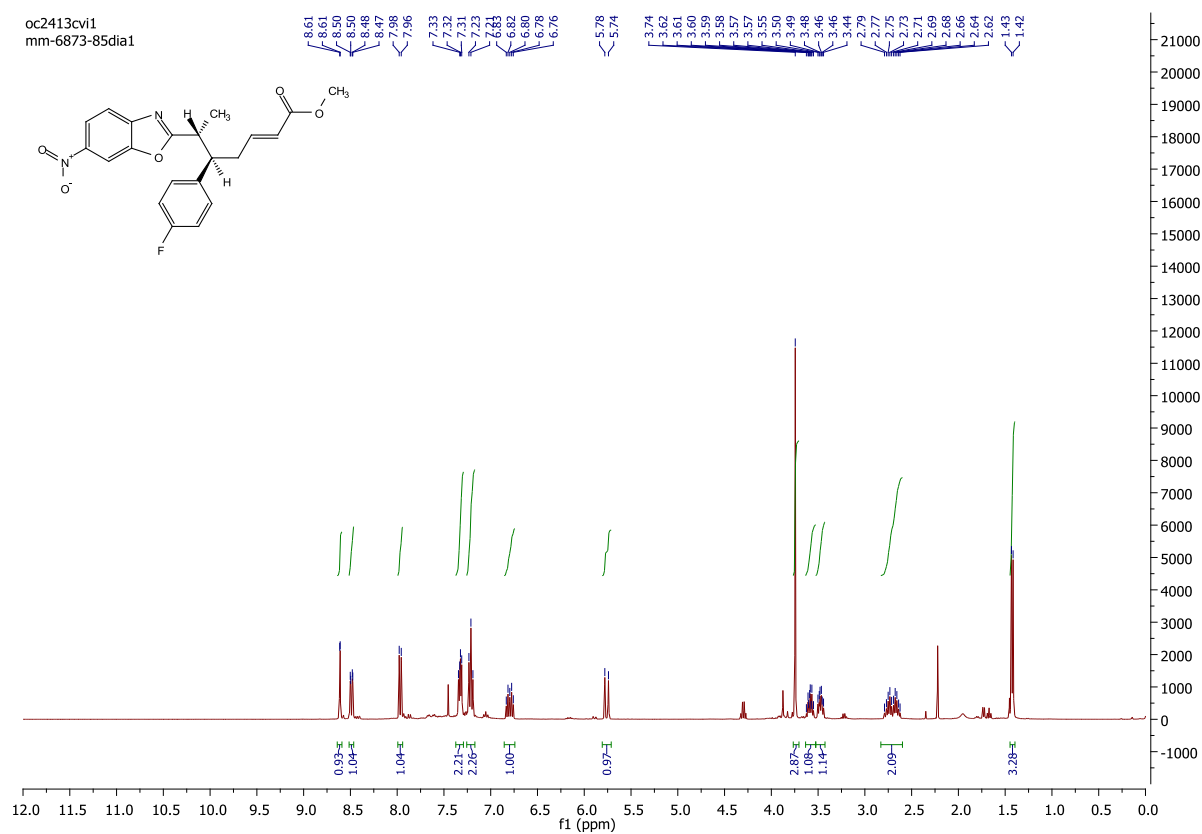


se1613mm1
mm/6873/82.dia1

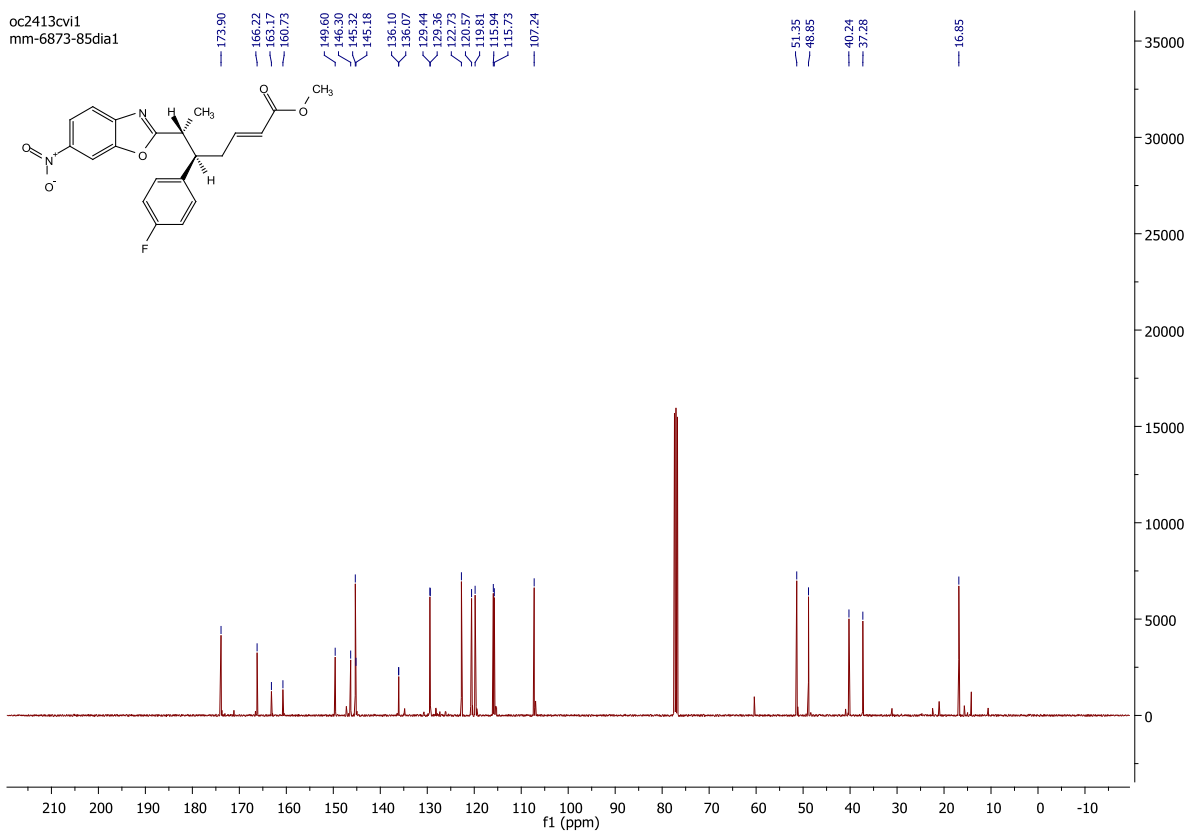


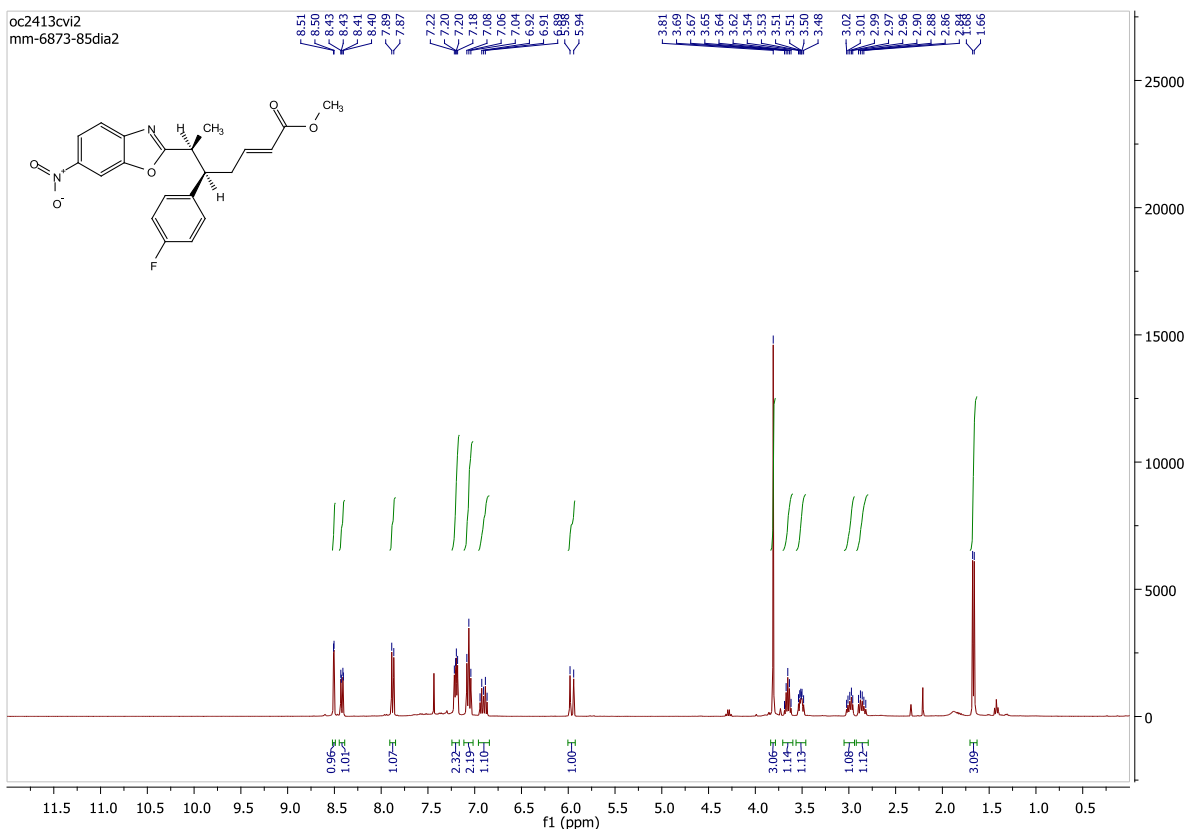
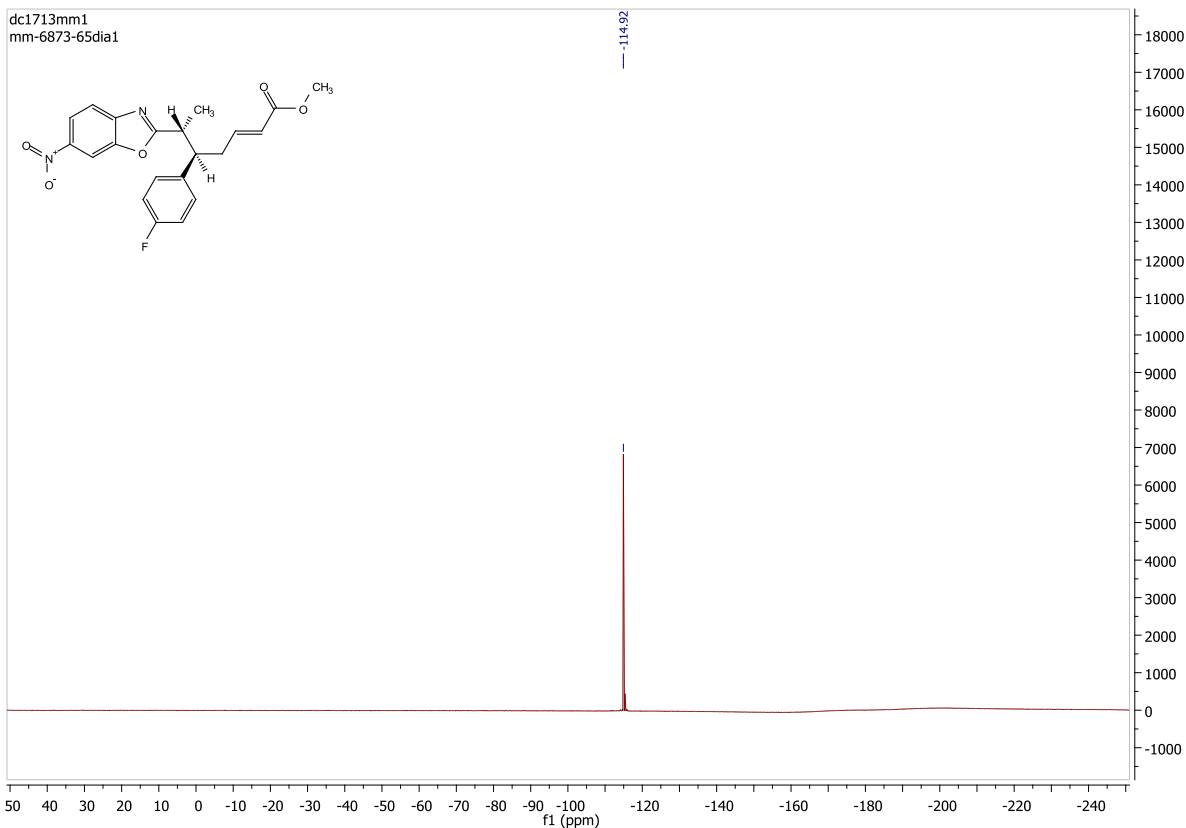


oc2413cvi1
mm-6873-85dia1

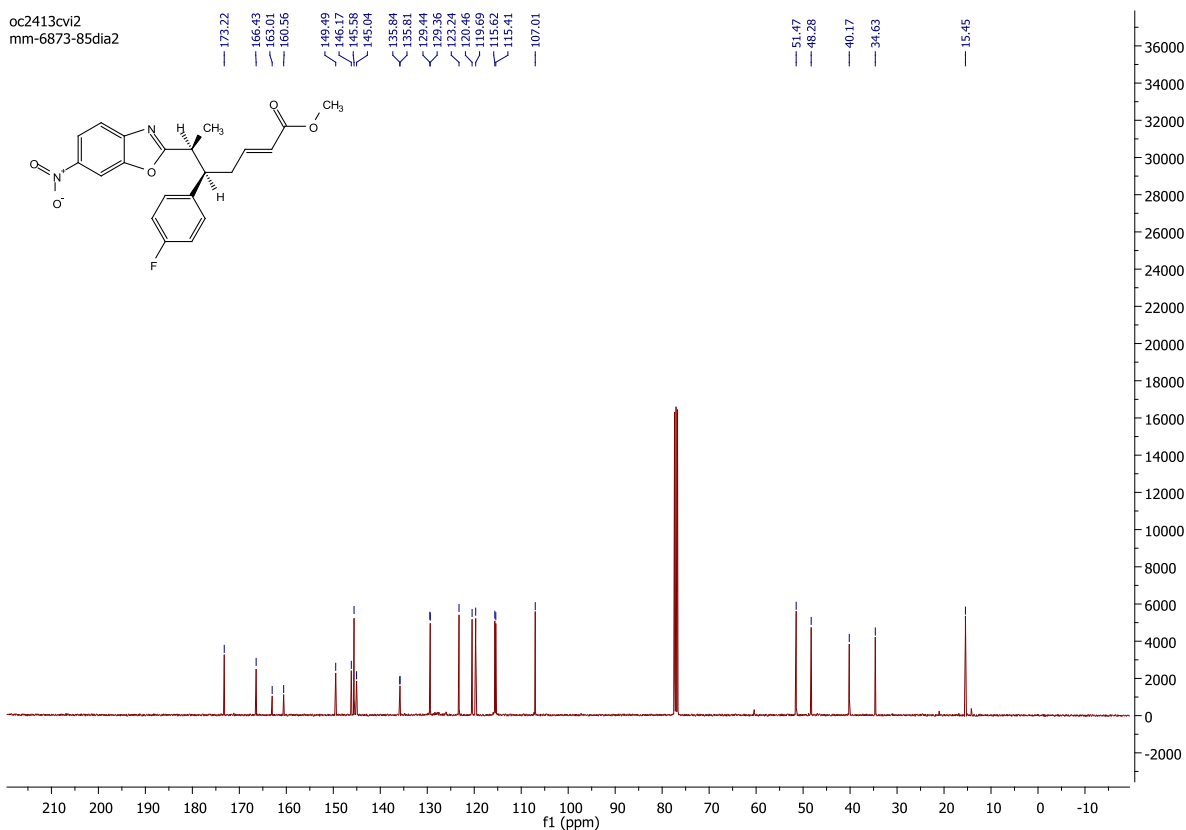


oc2413cvi1
mm-6873-85dia1

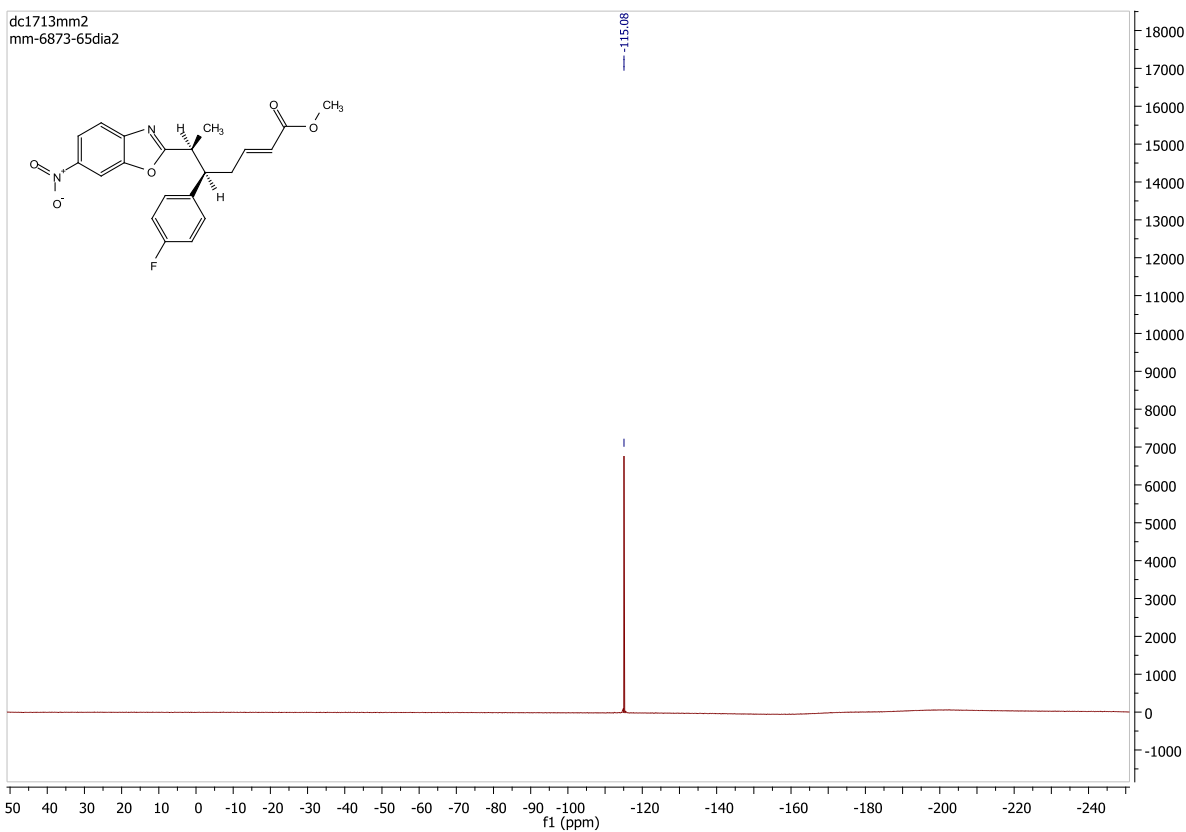


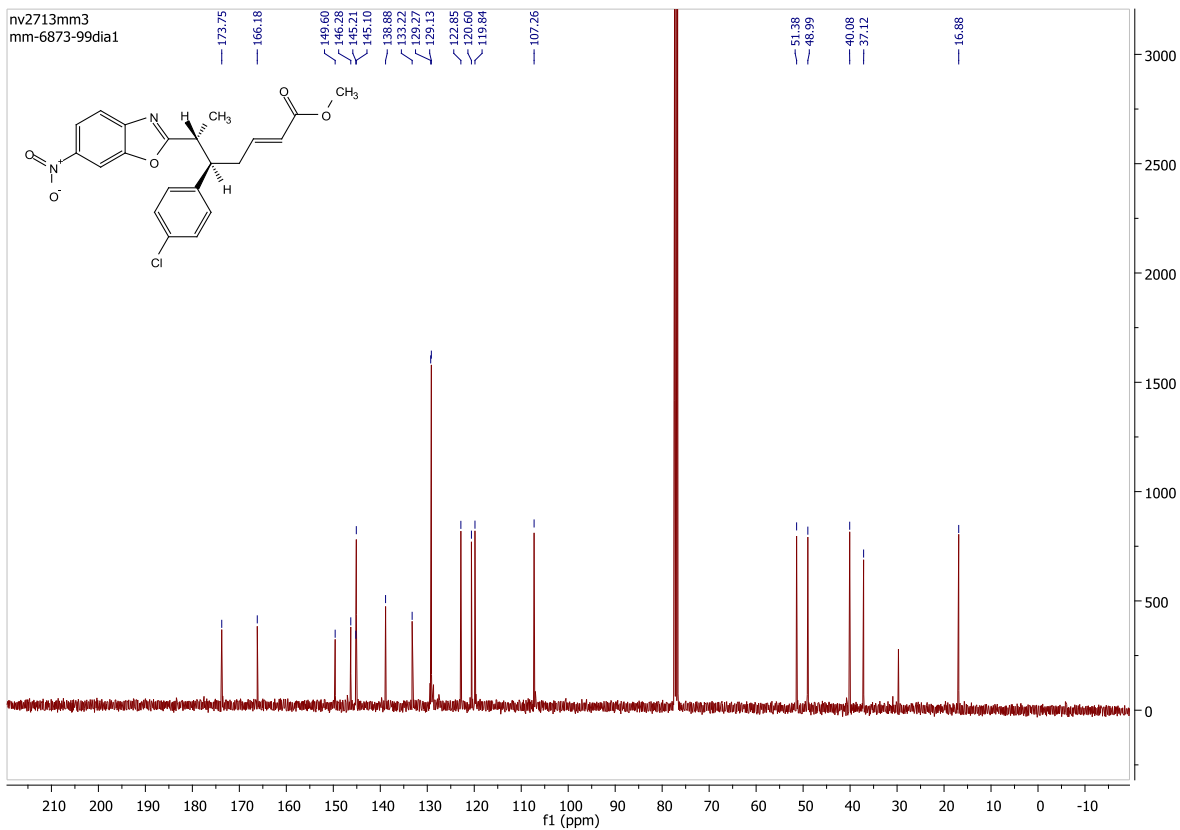
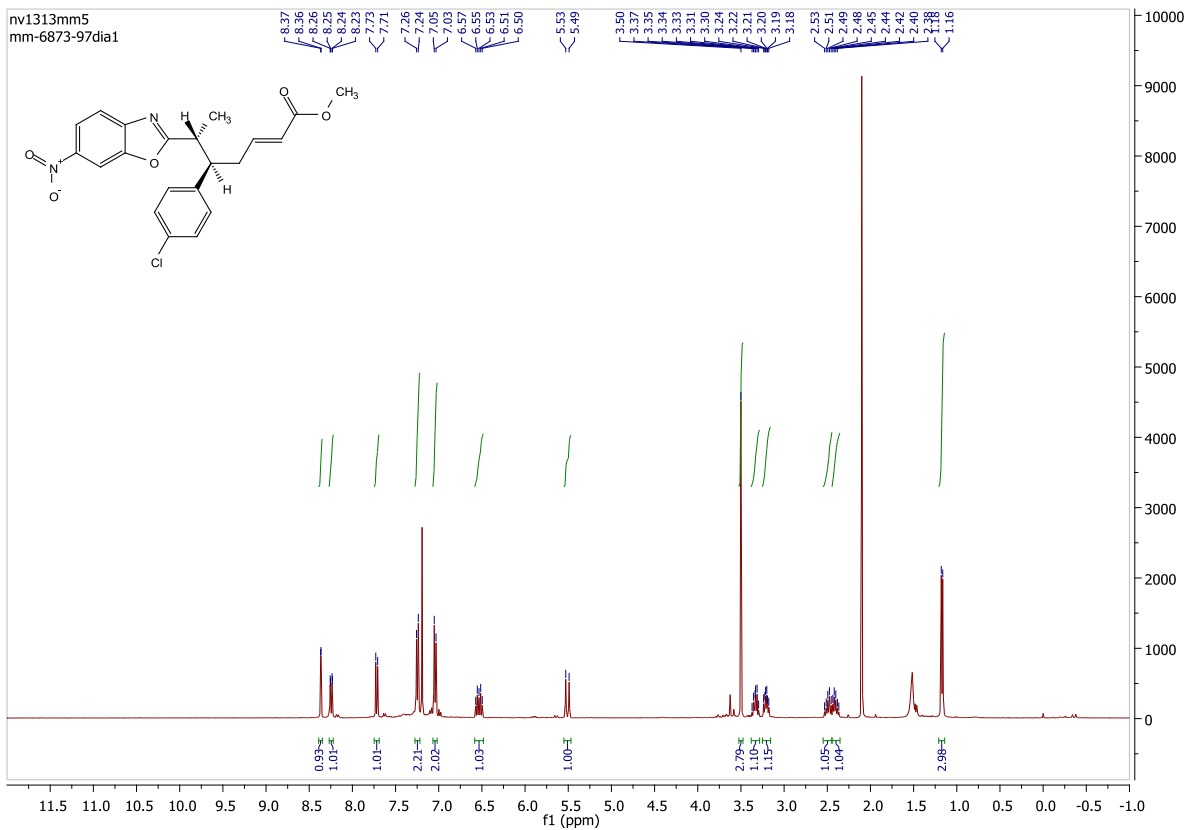


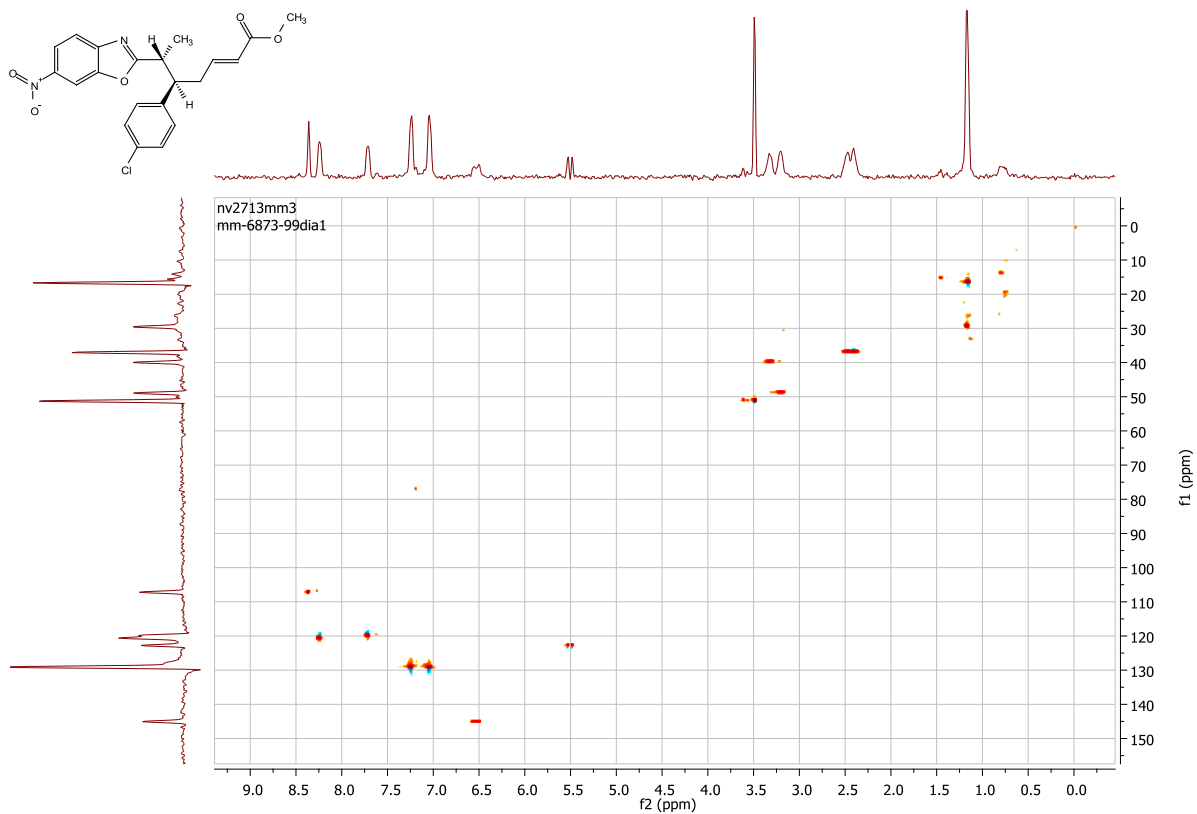
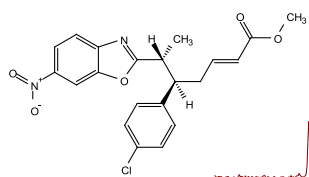
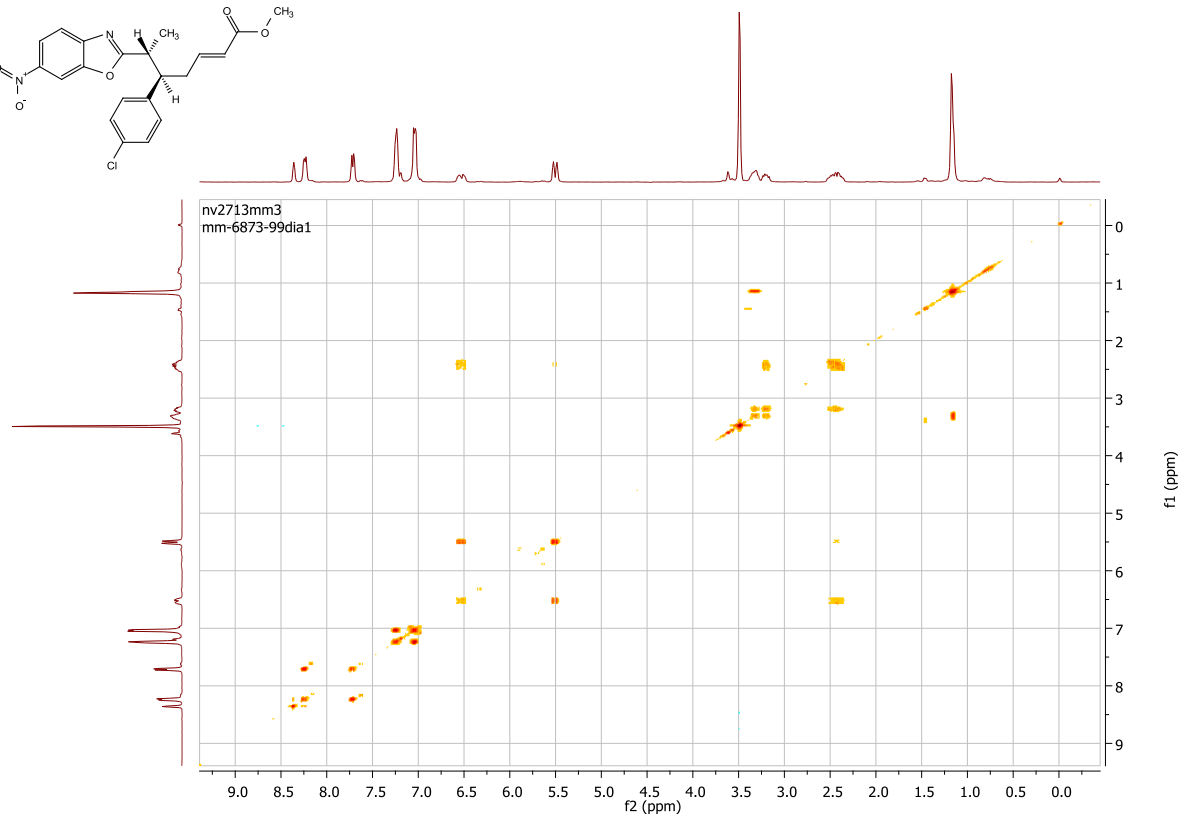
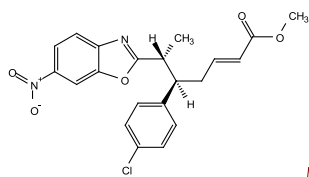
oc2413cv12
mm-6873-85dia2

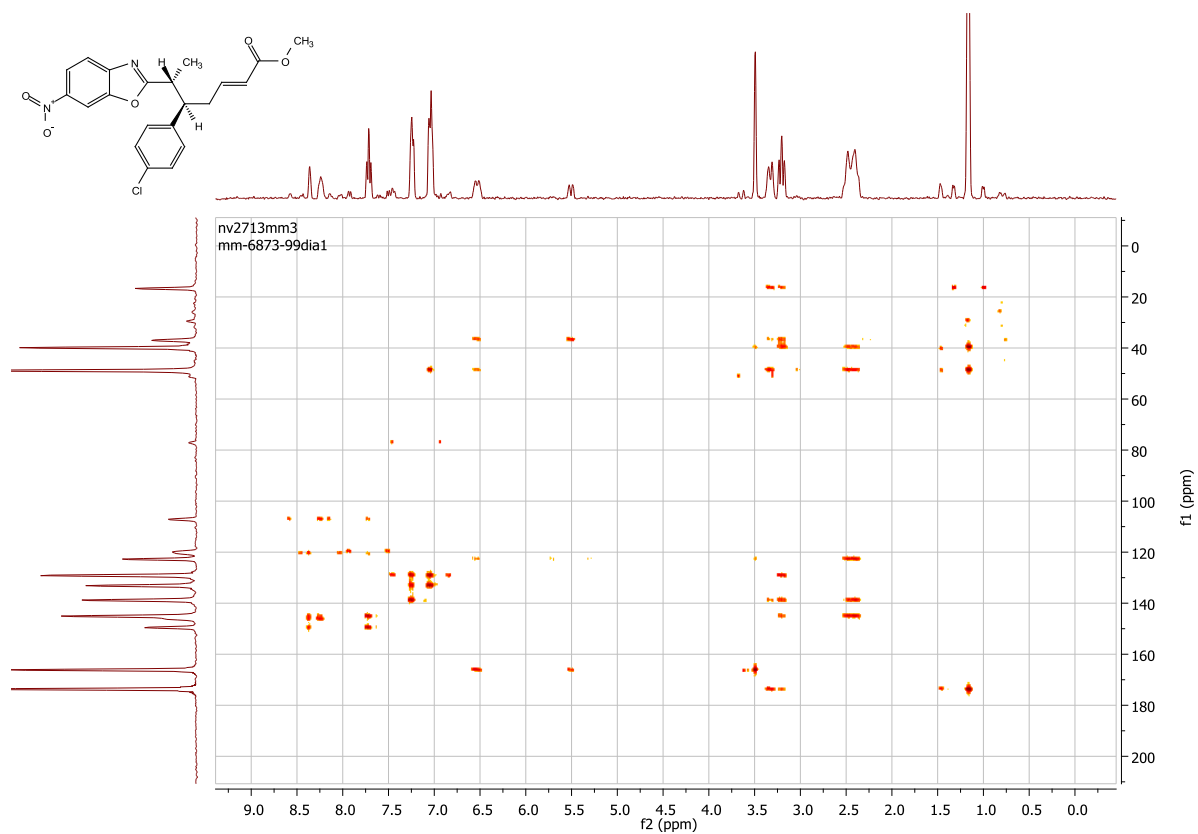
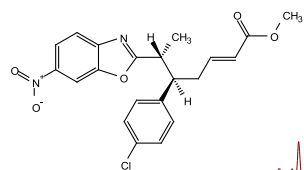


dc1713mm2
mm-6873-65dia2

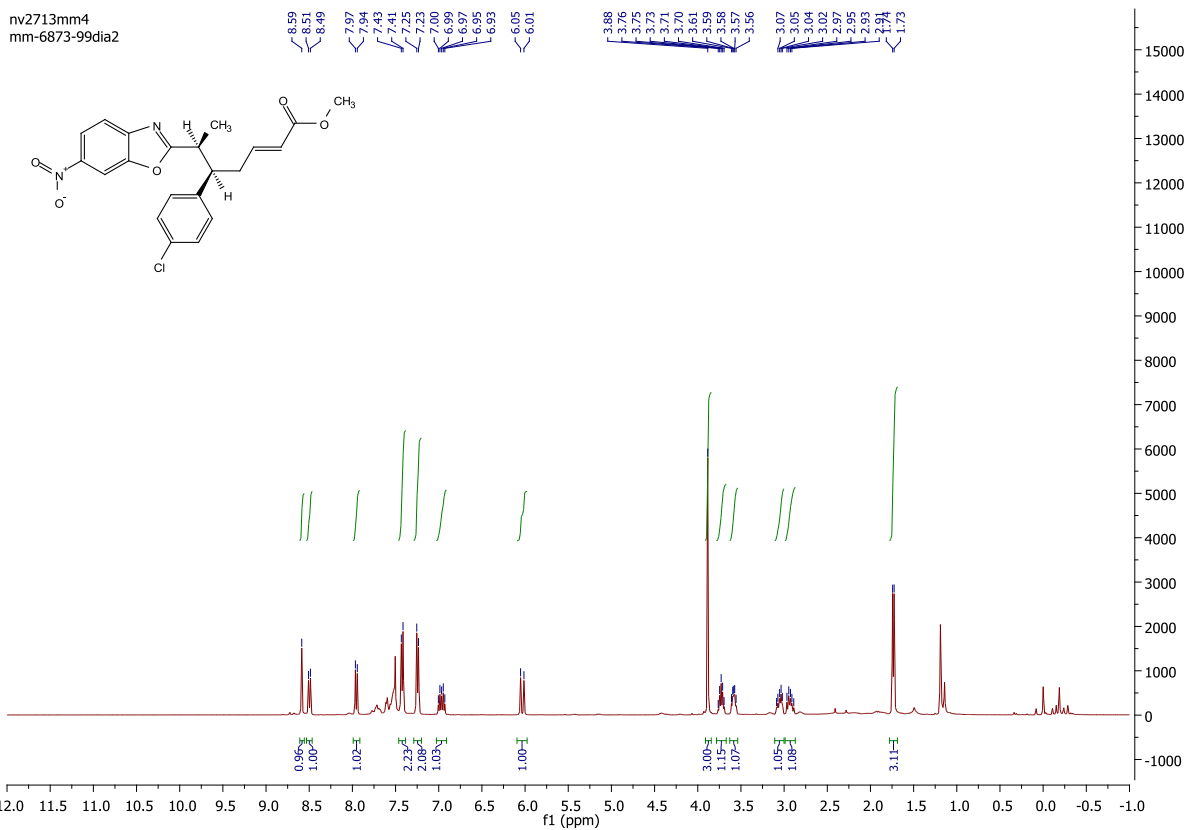




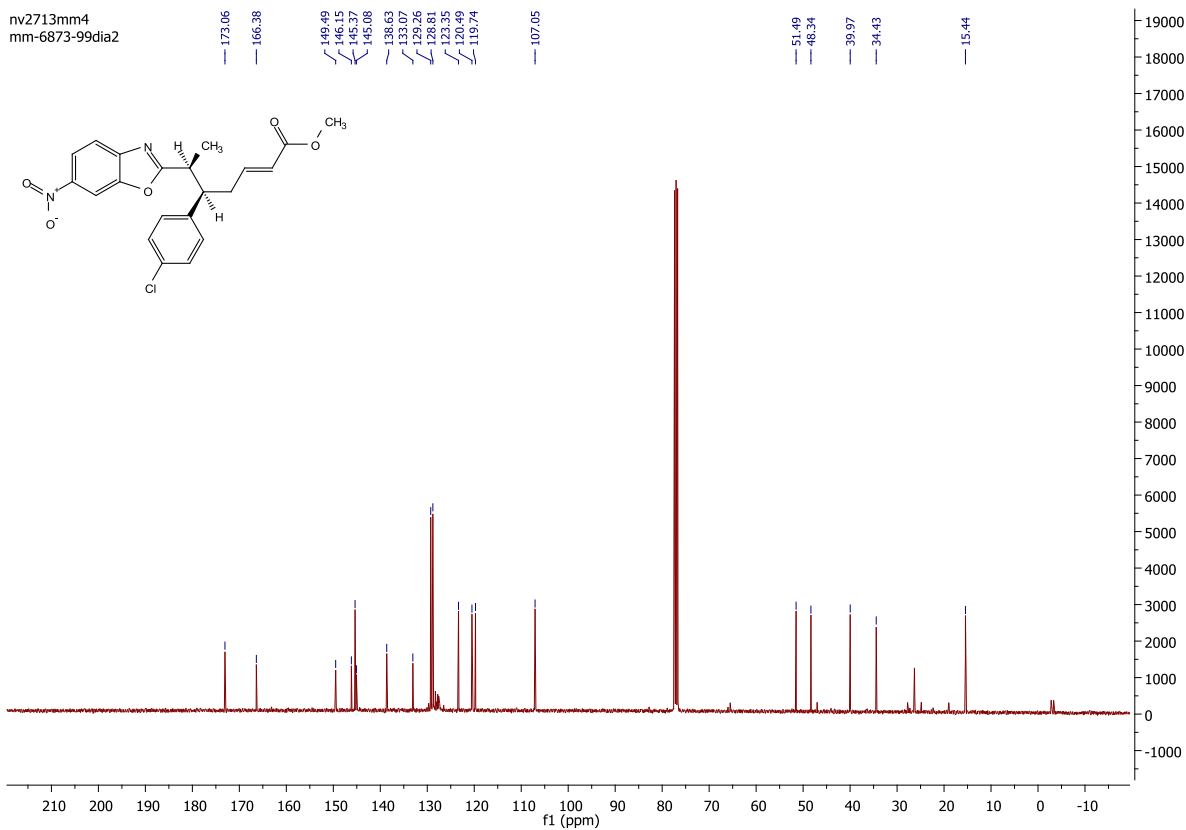


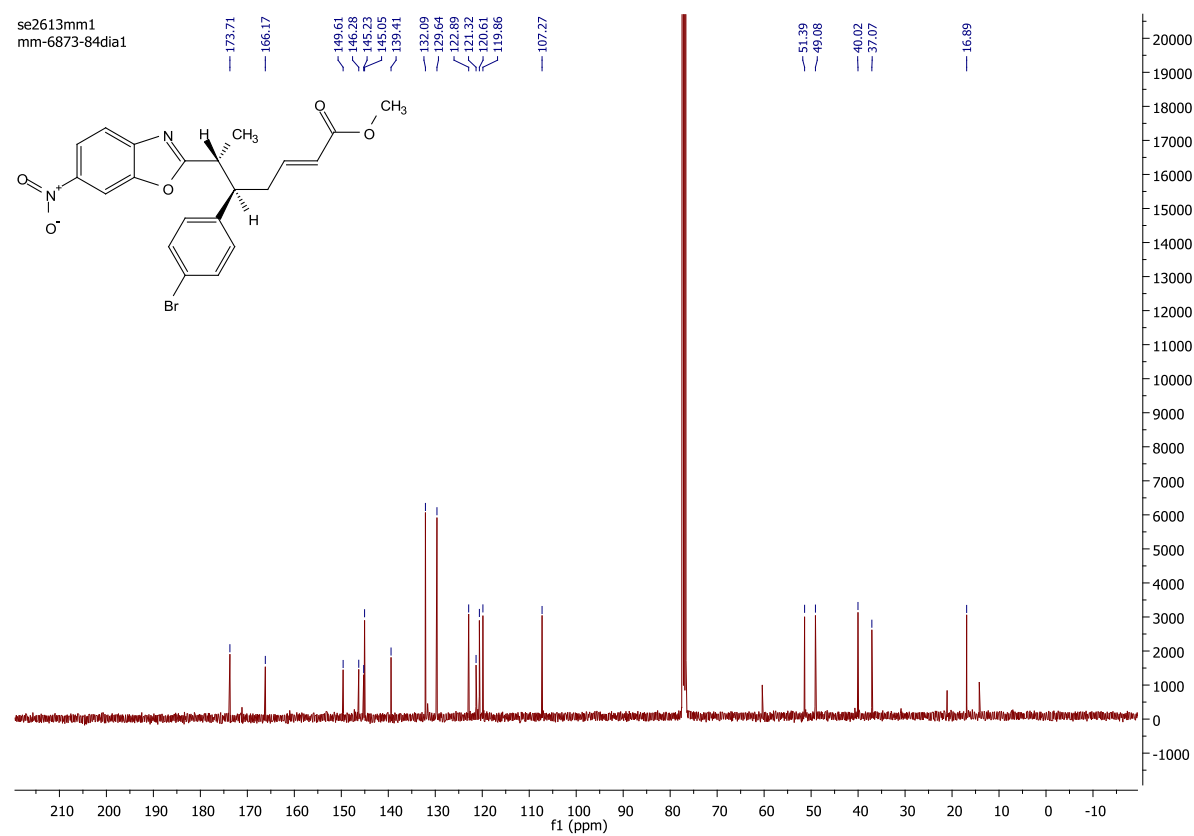
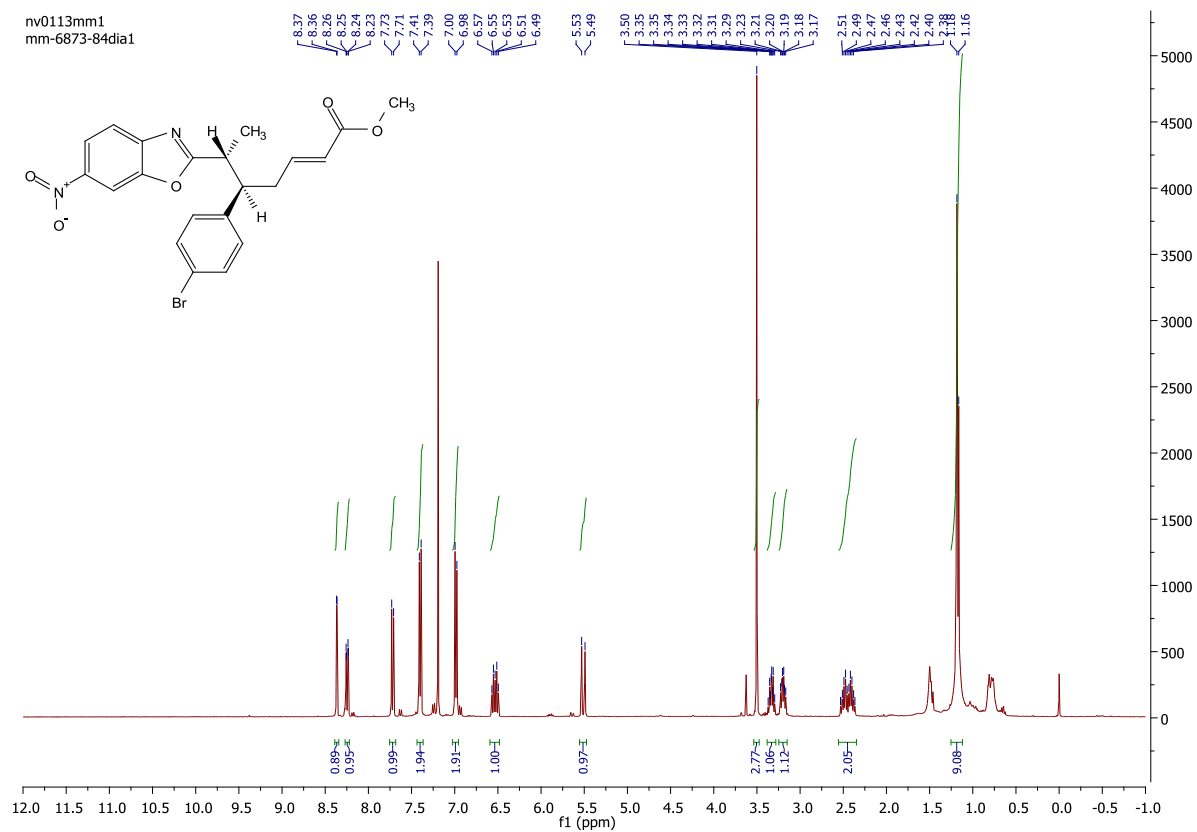


nv2713mm4
mm-6873-99dia2

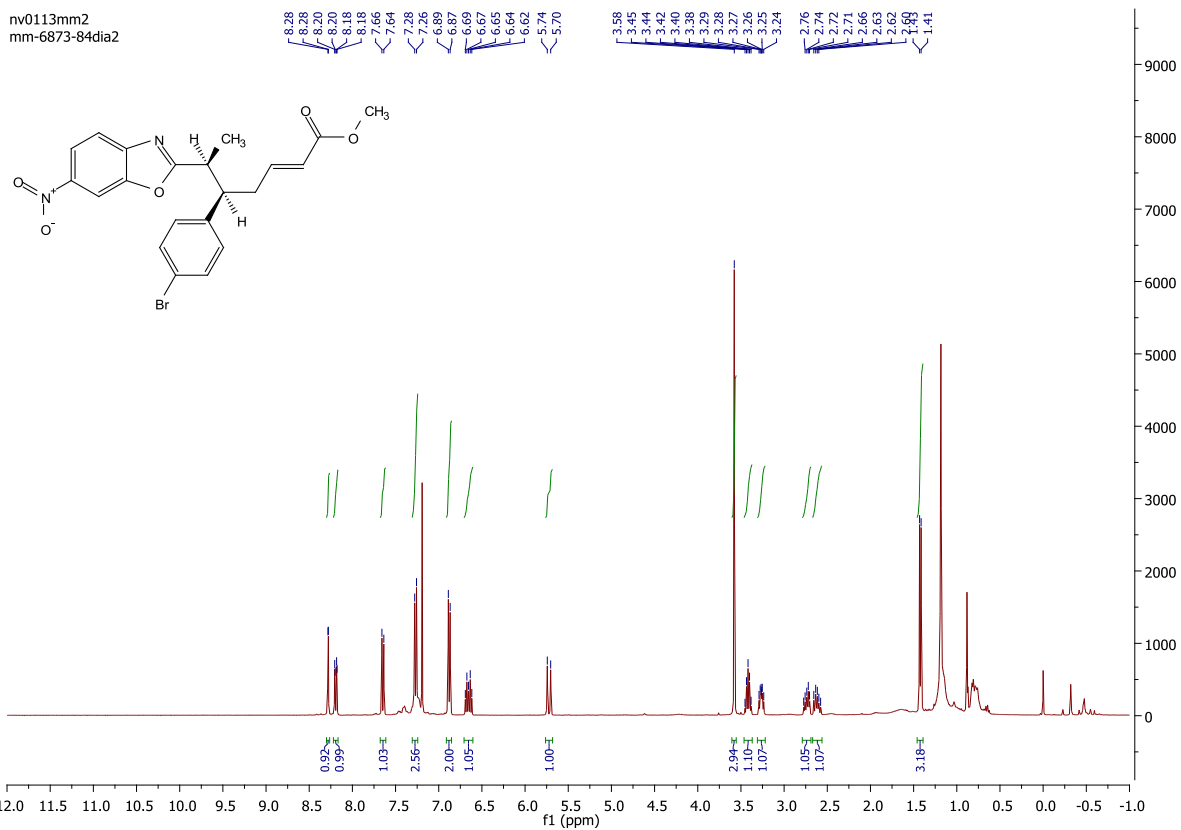


nv2713mm4
mm-6873-99dia2

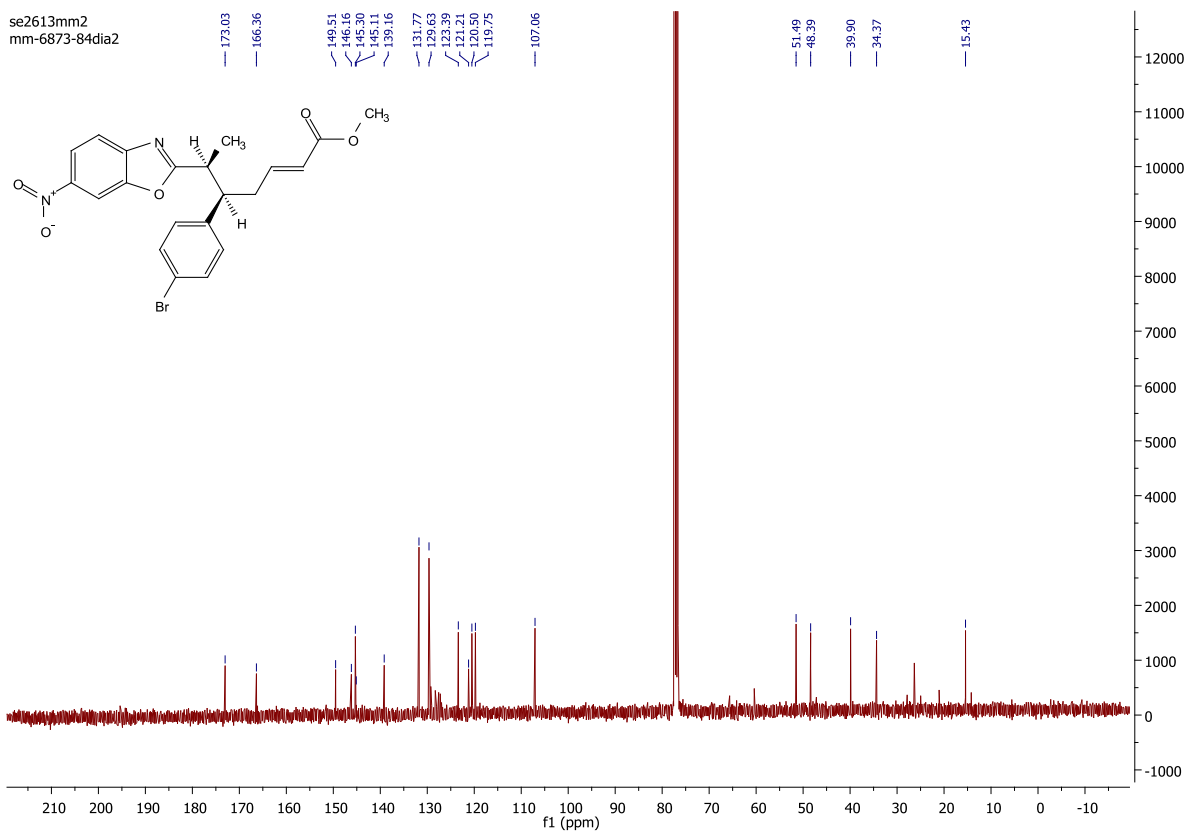


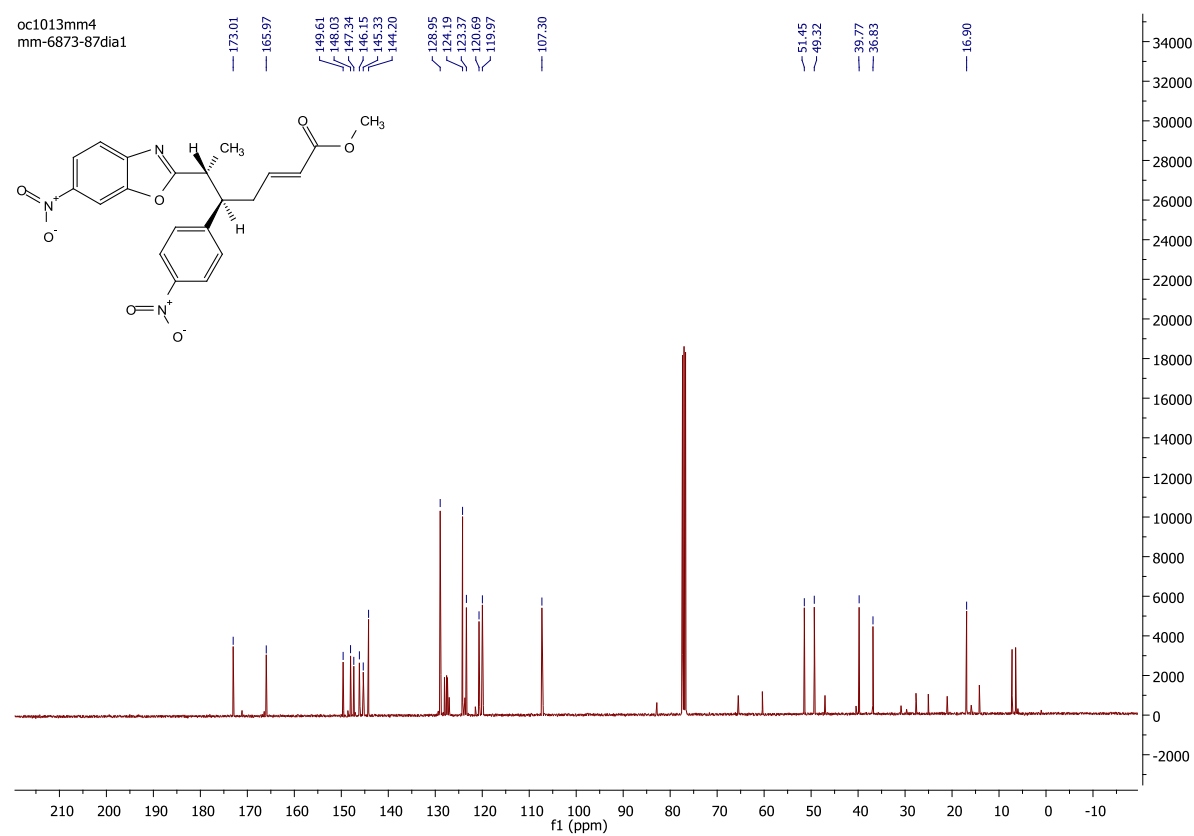
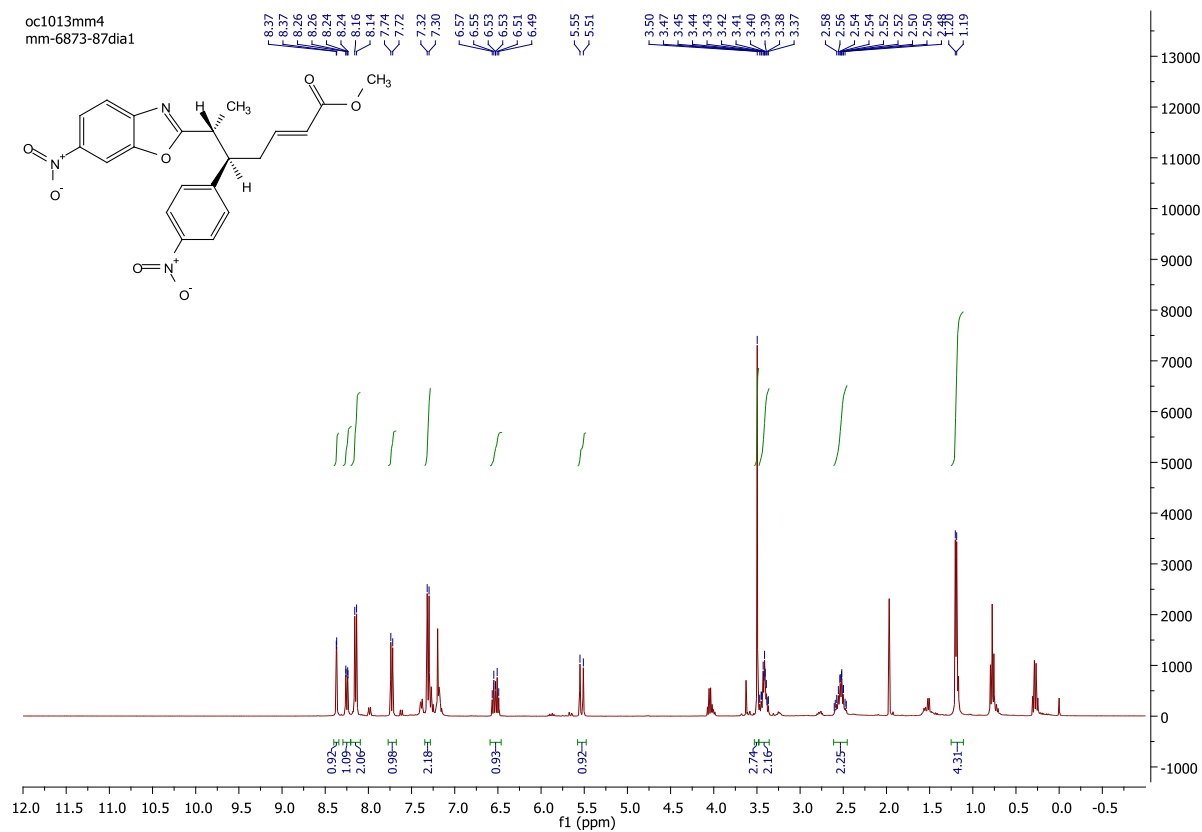


nv0113mm2
mm-6873-84dia2

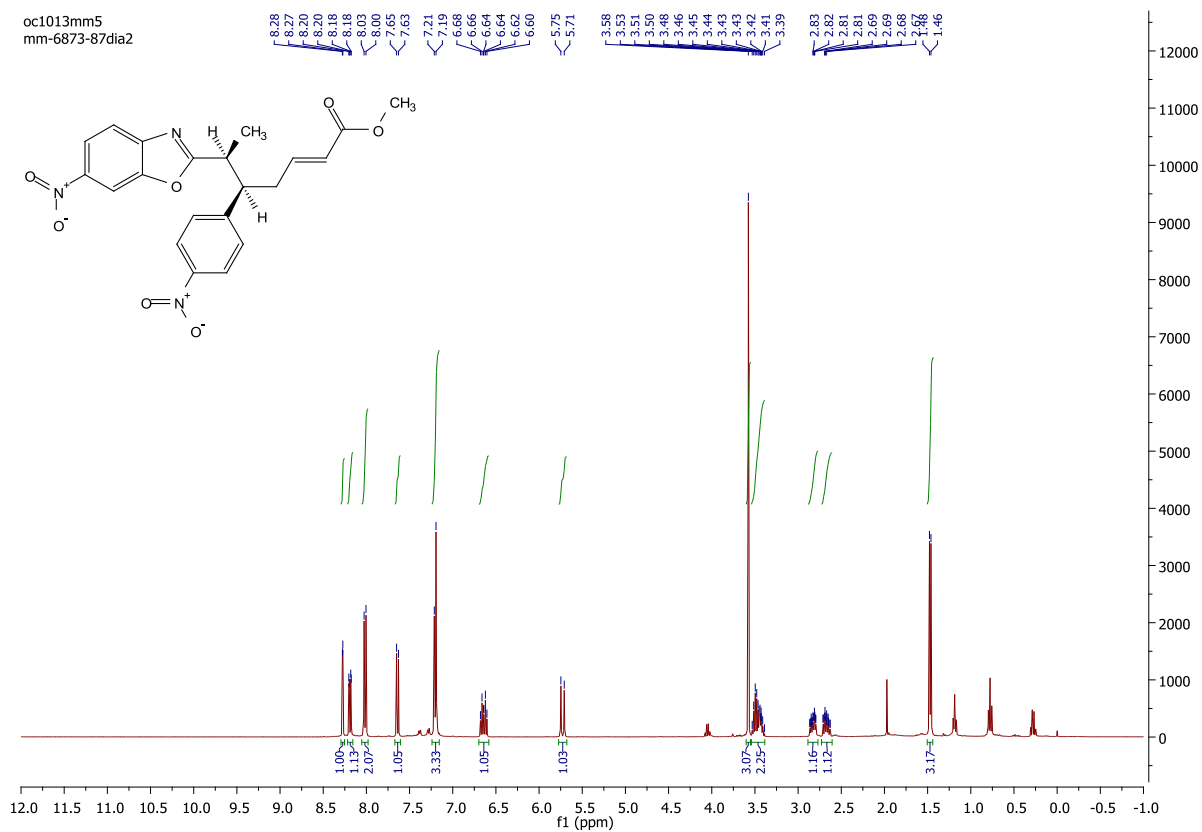


se2613mm2
mm-6873-84dia2

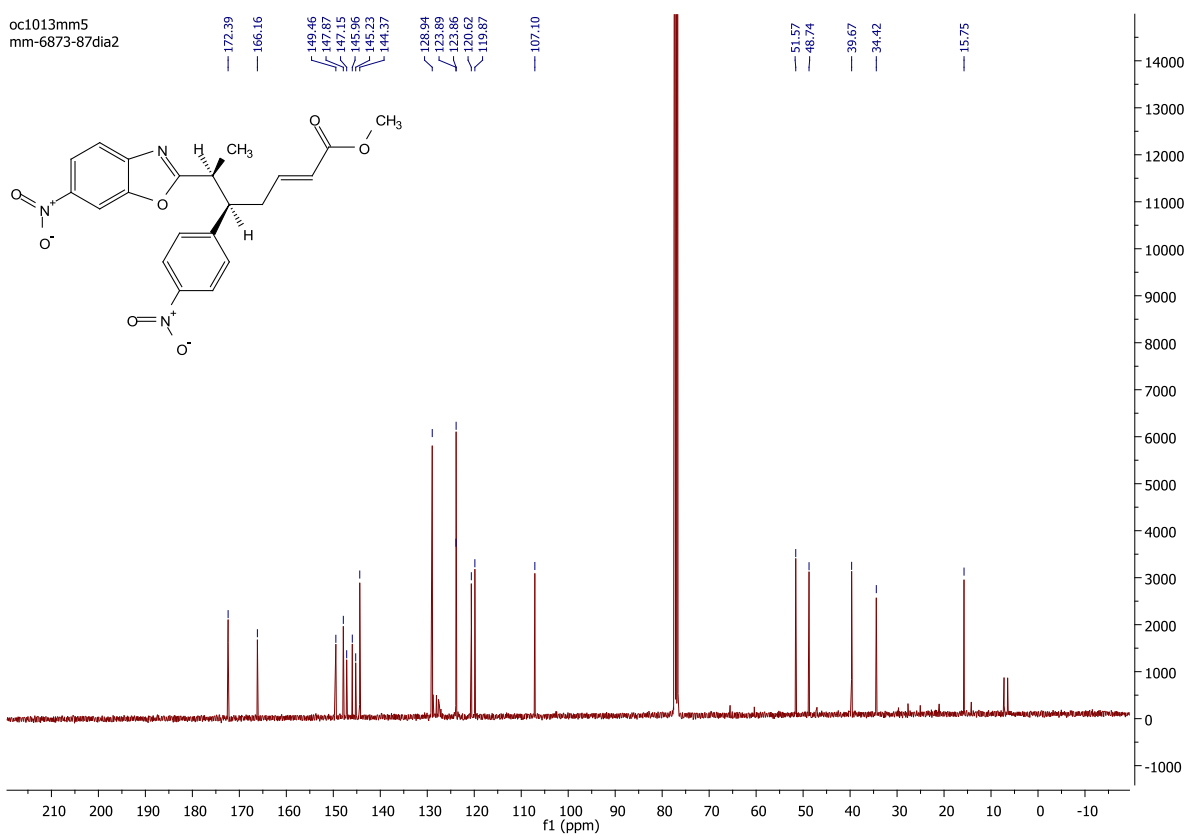


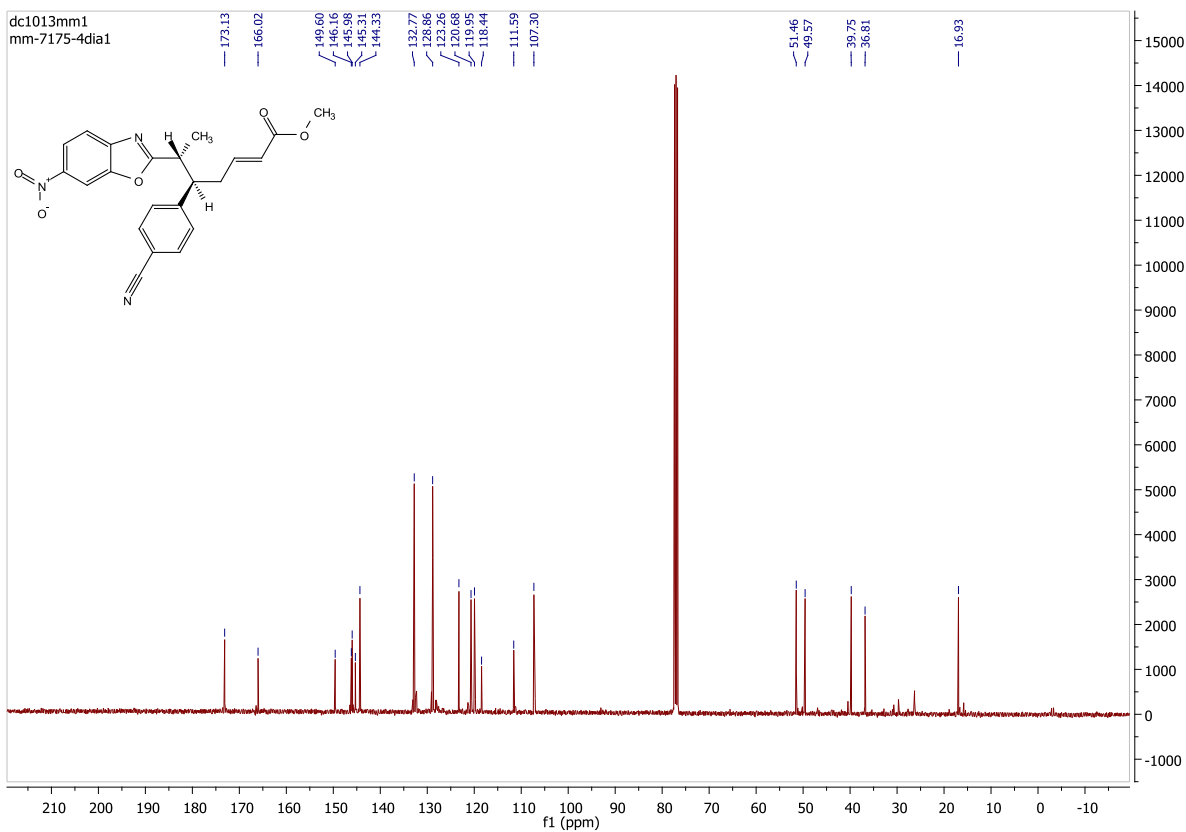
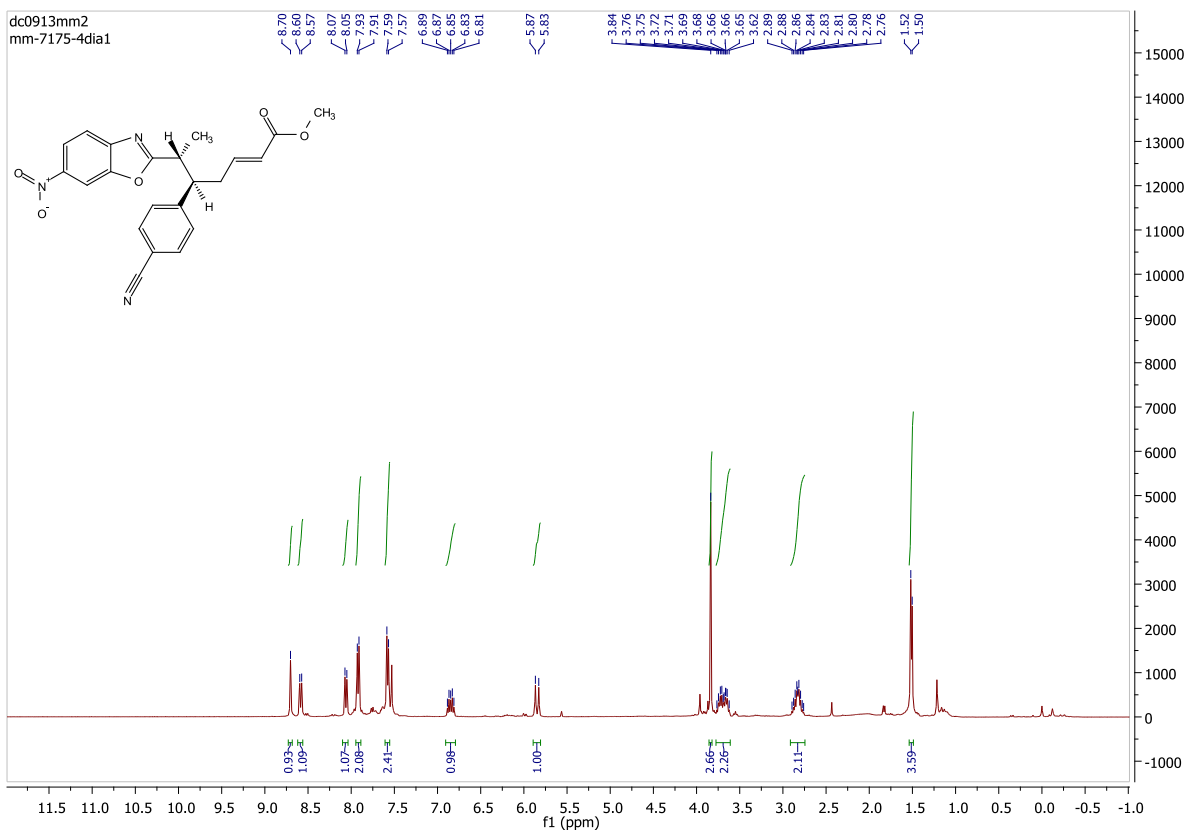


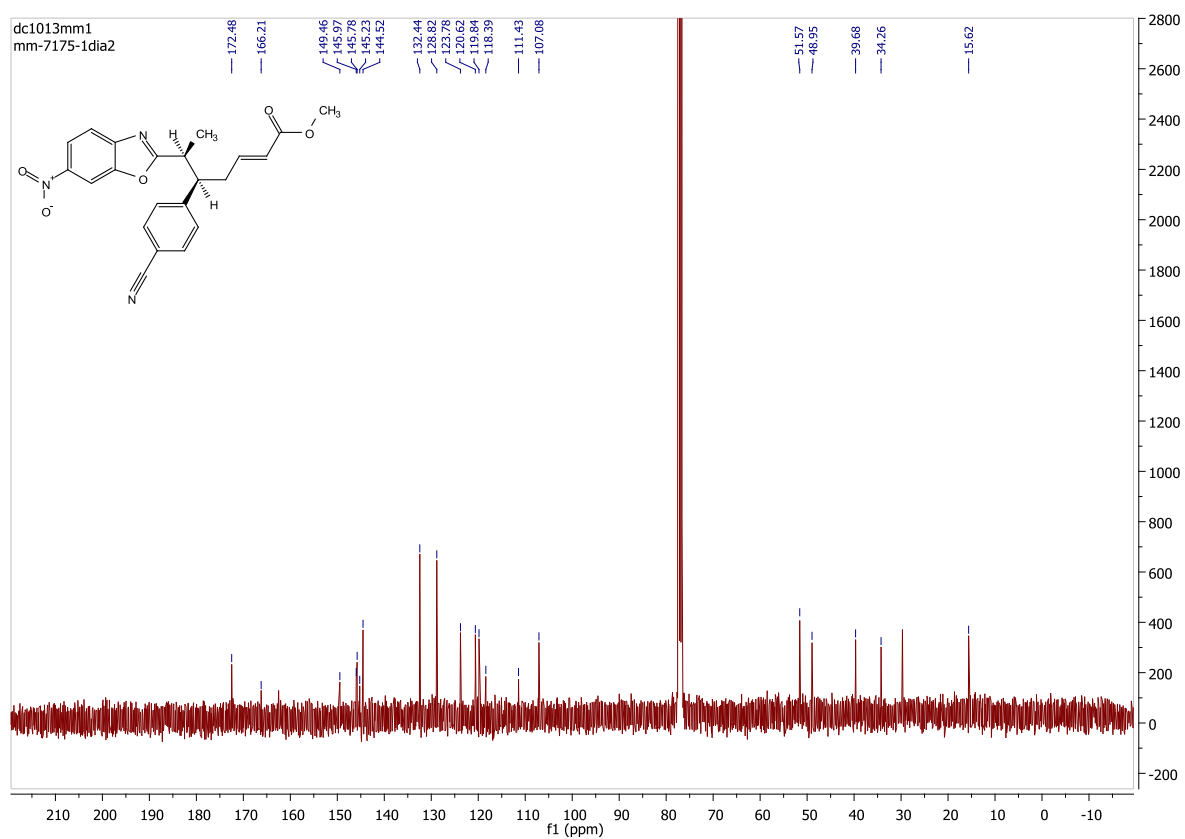
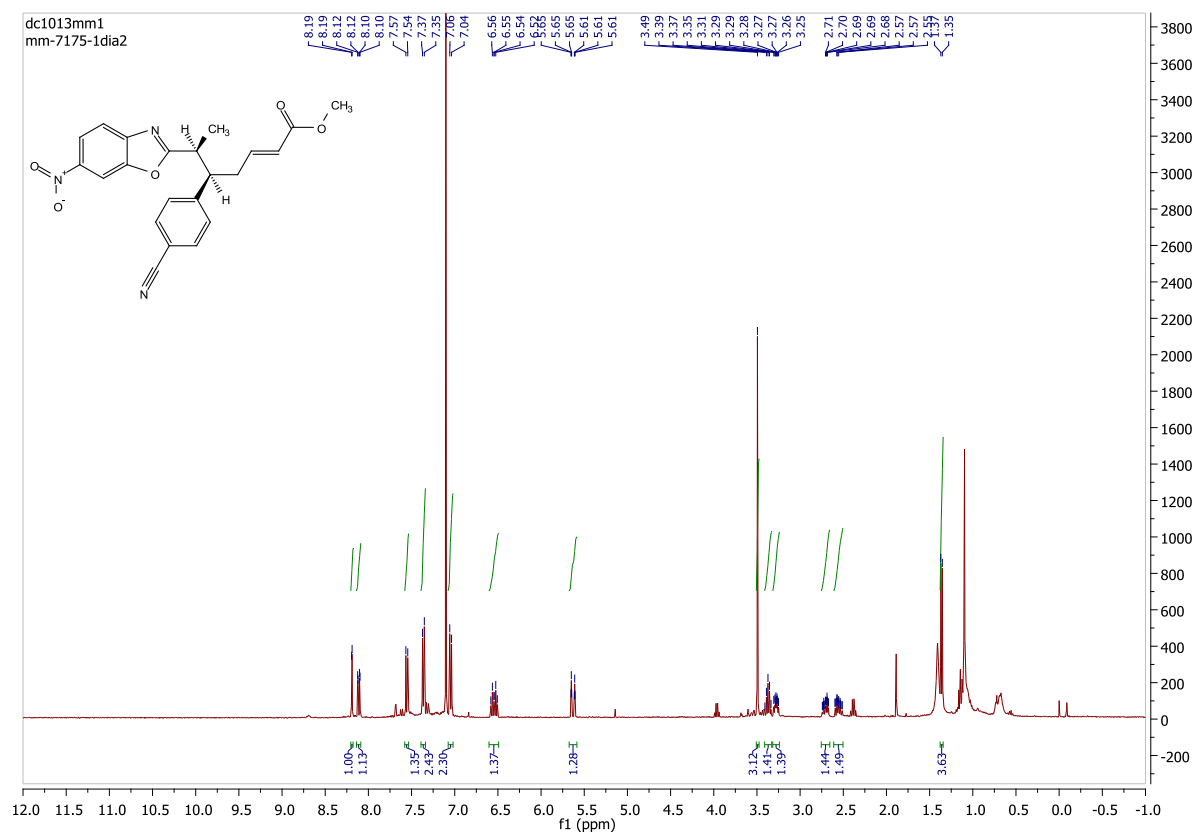
oc1013mm5
mm-6873-87dia2

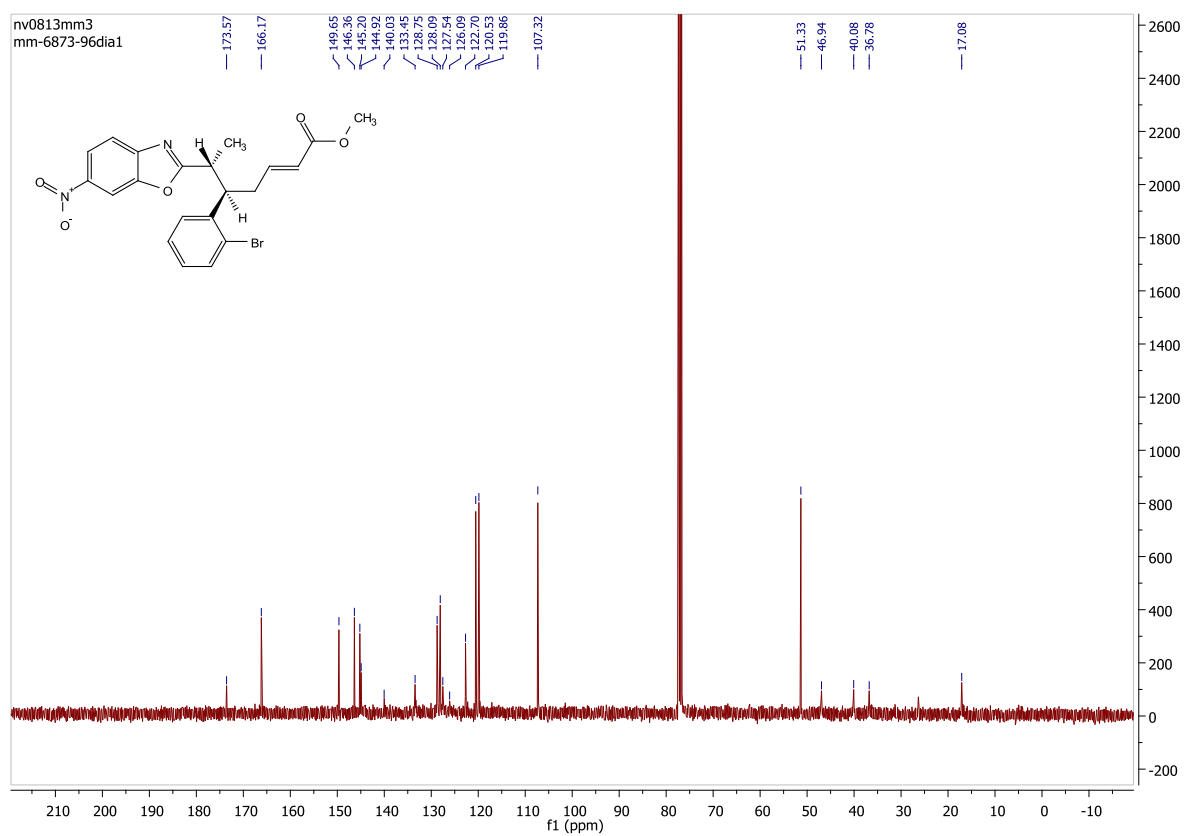
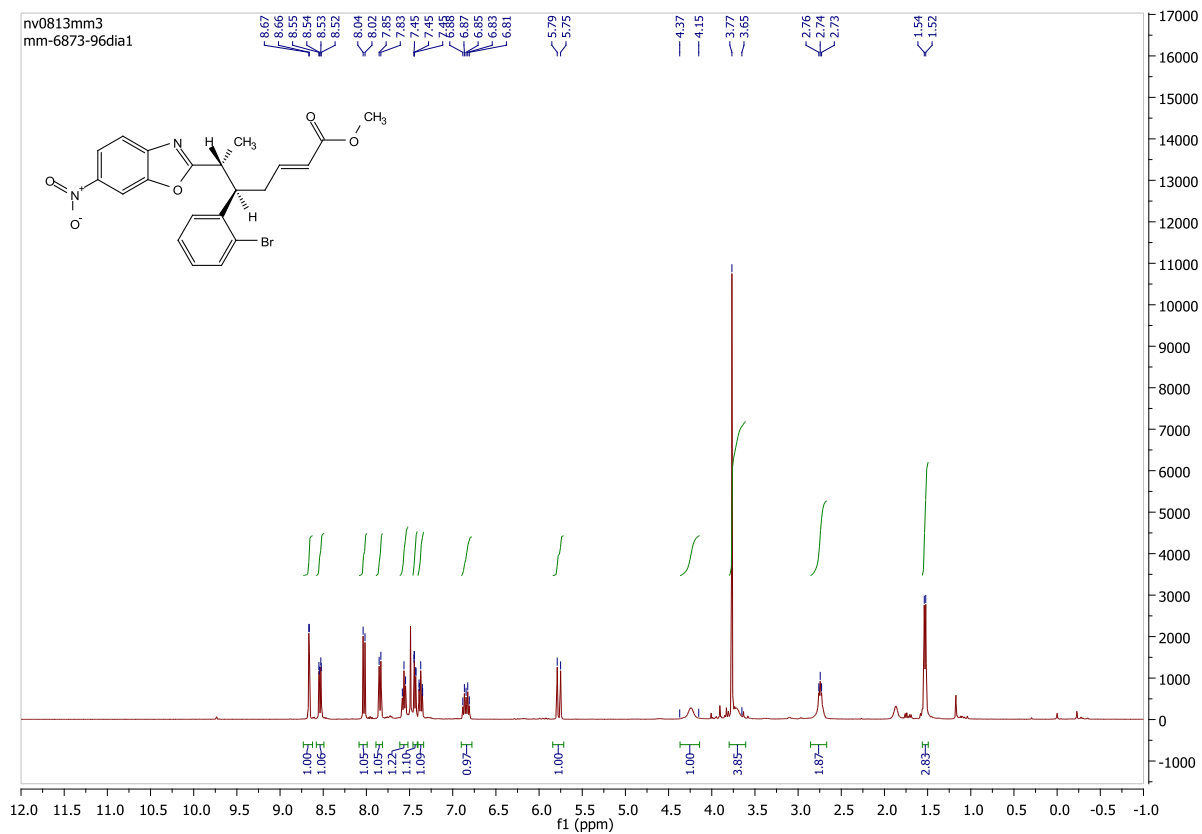


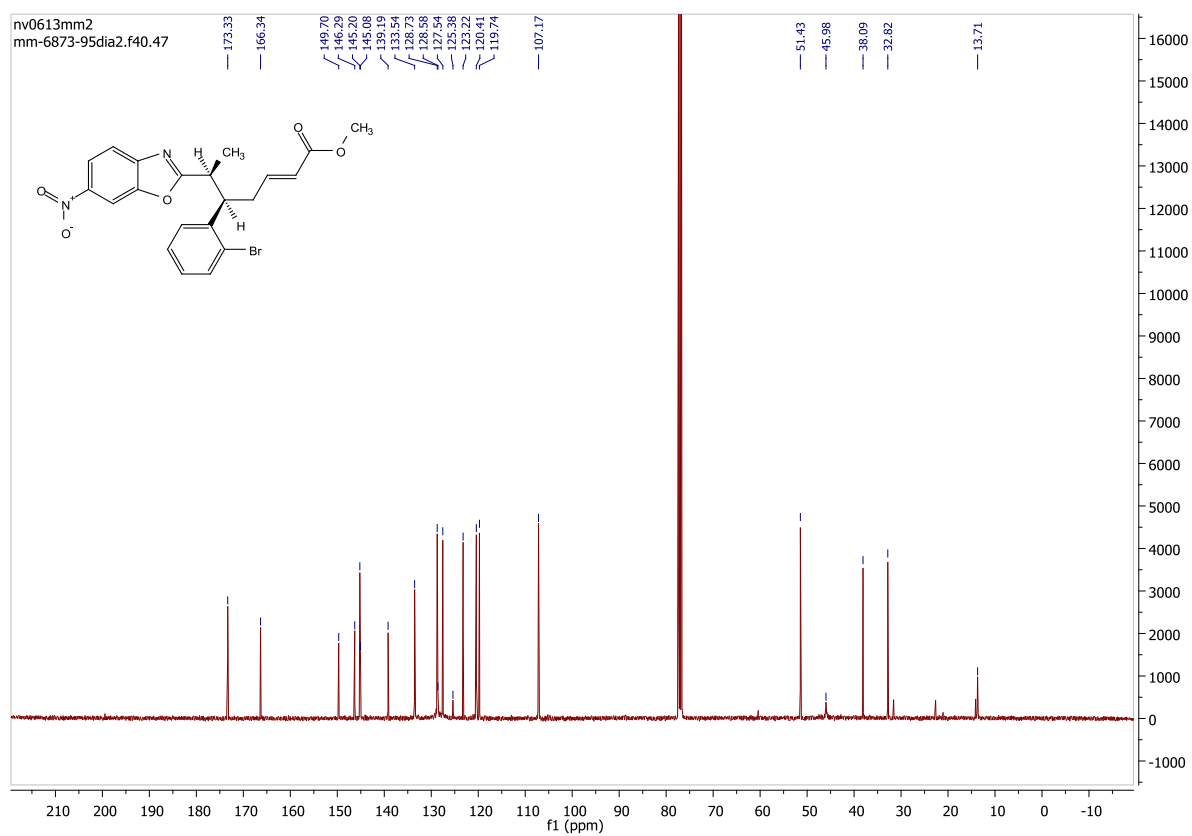
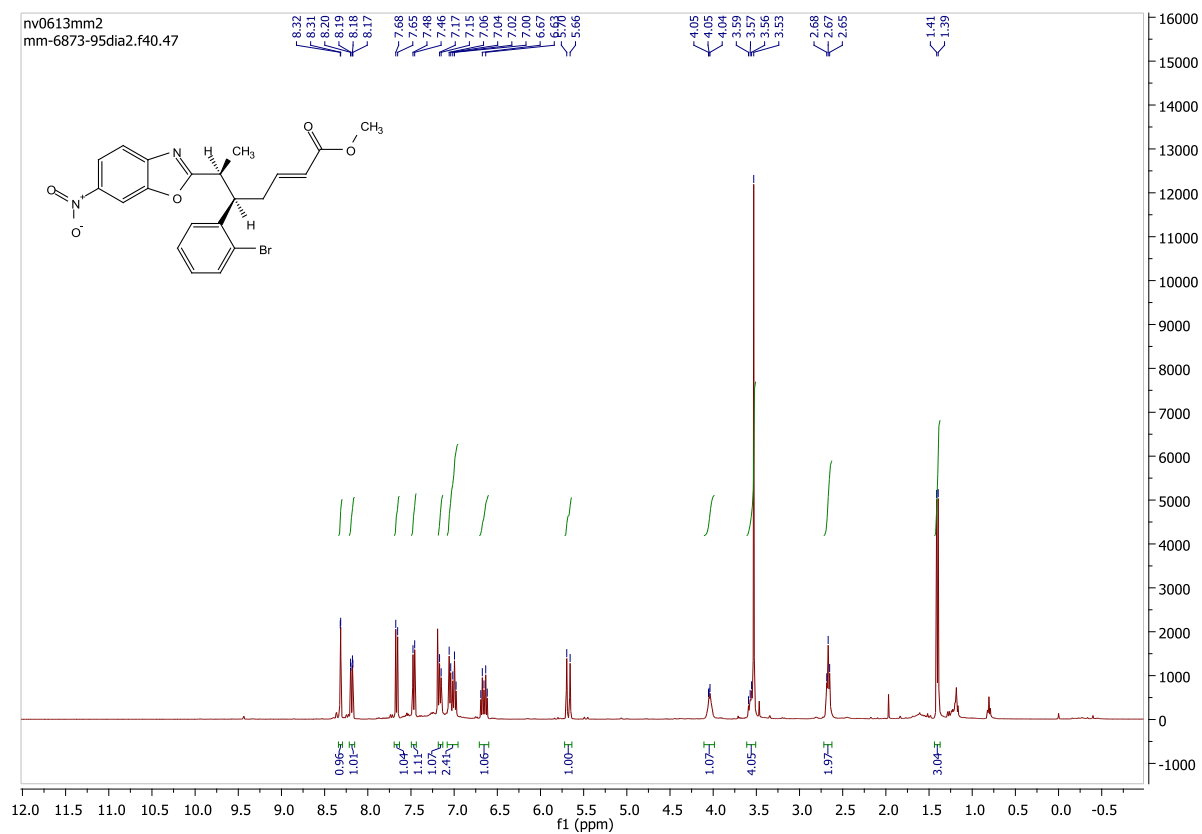
oc1013mm5
mm-6873-87dia2

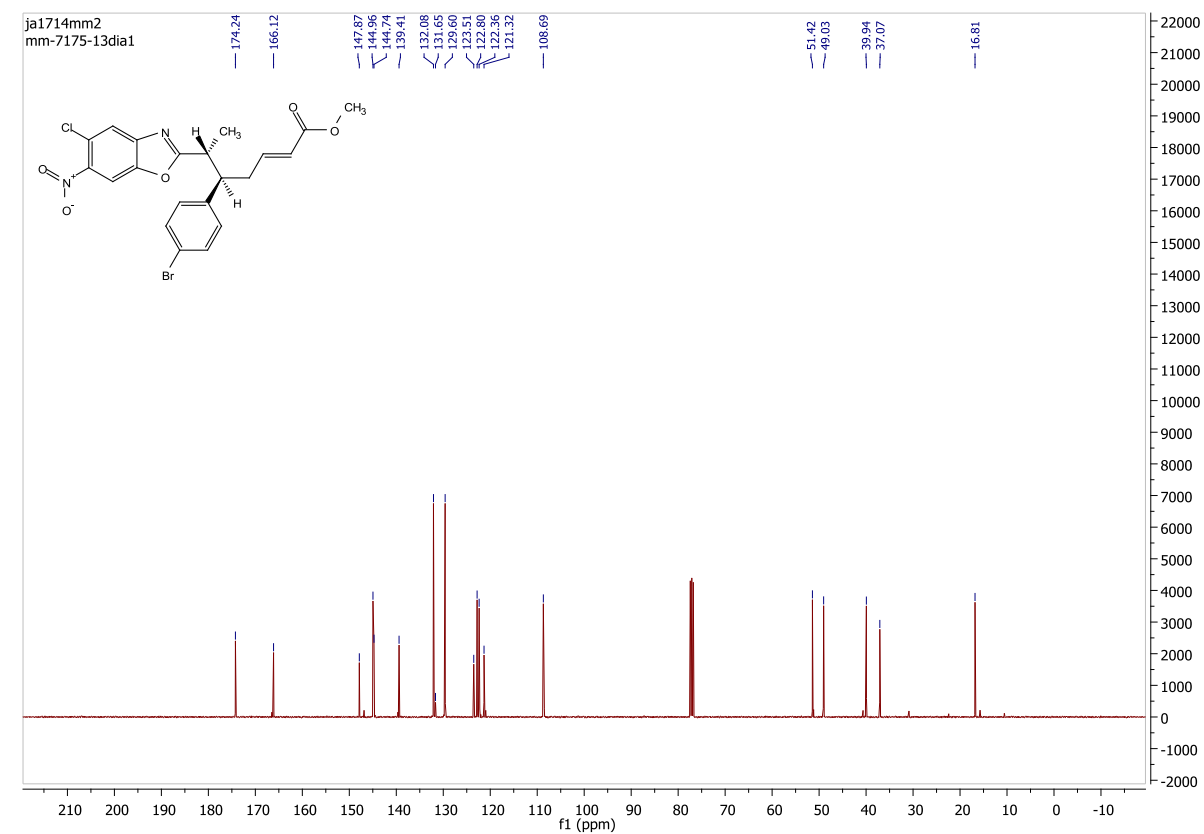
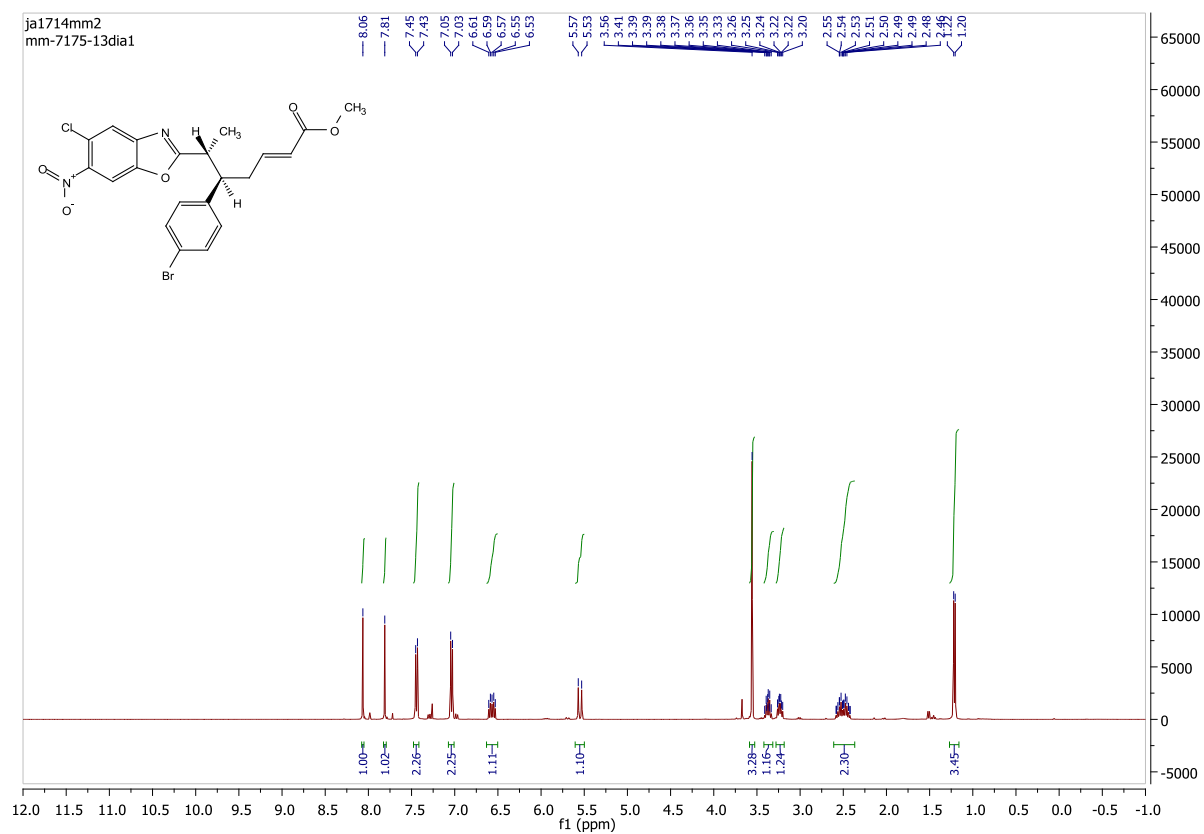


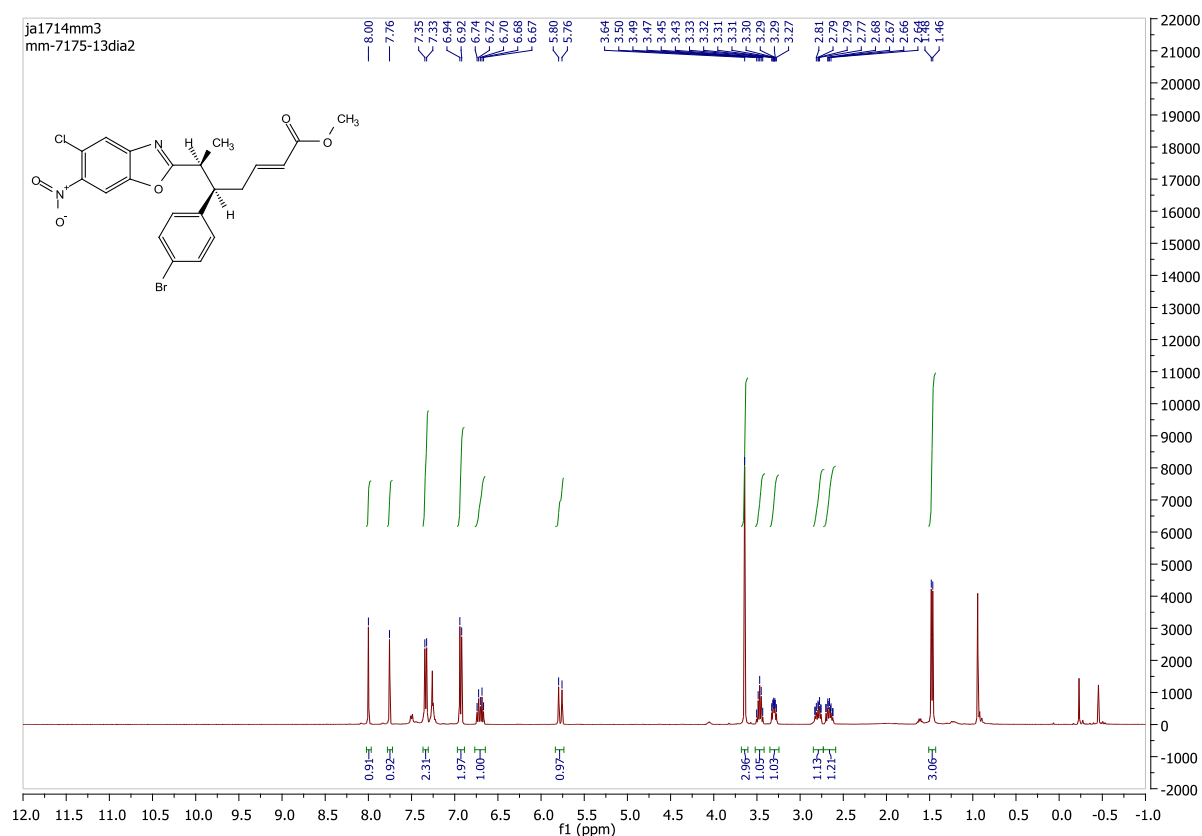
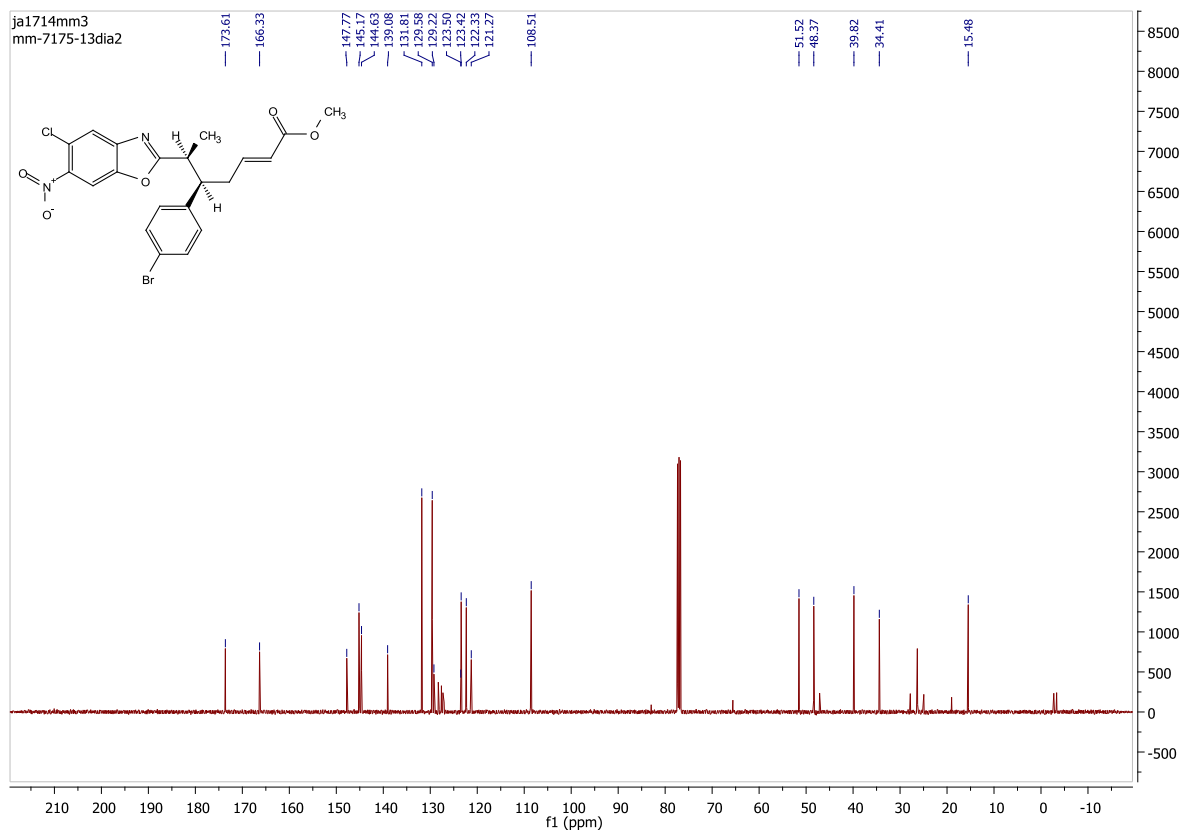




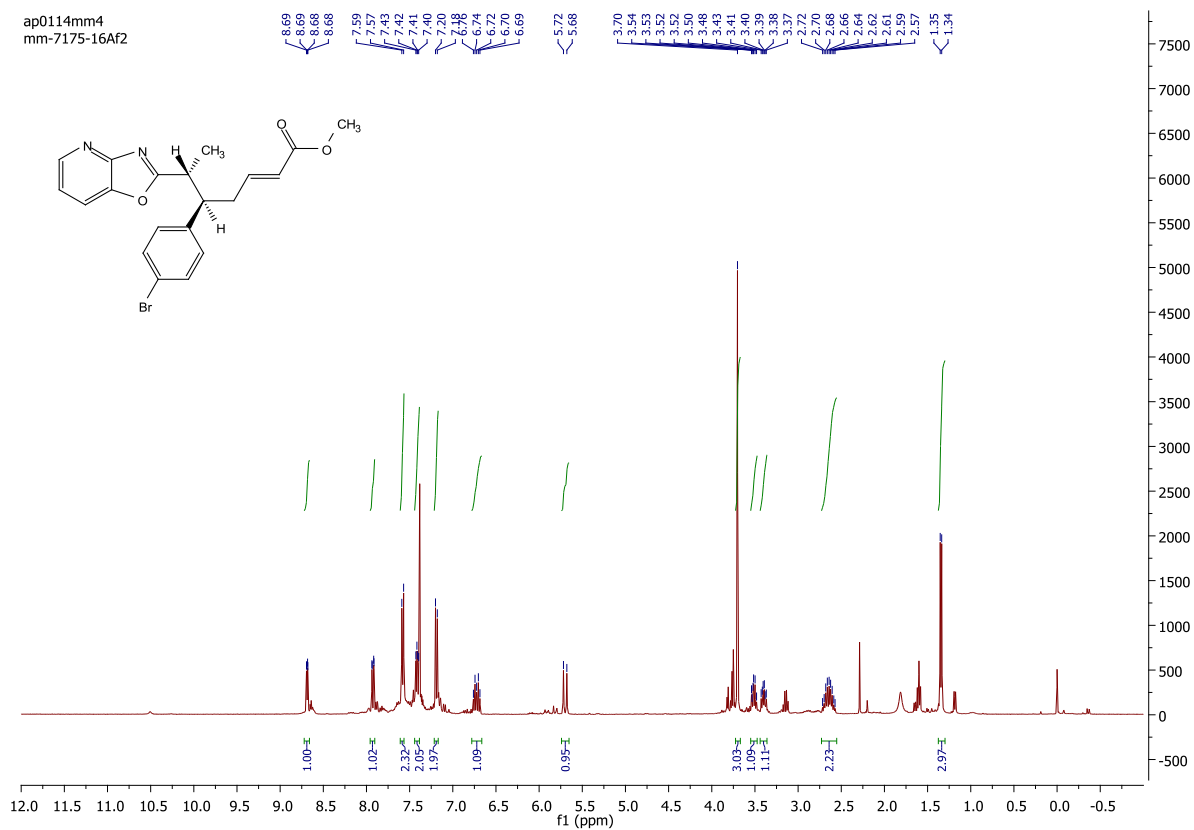




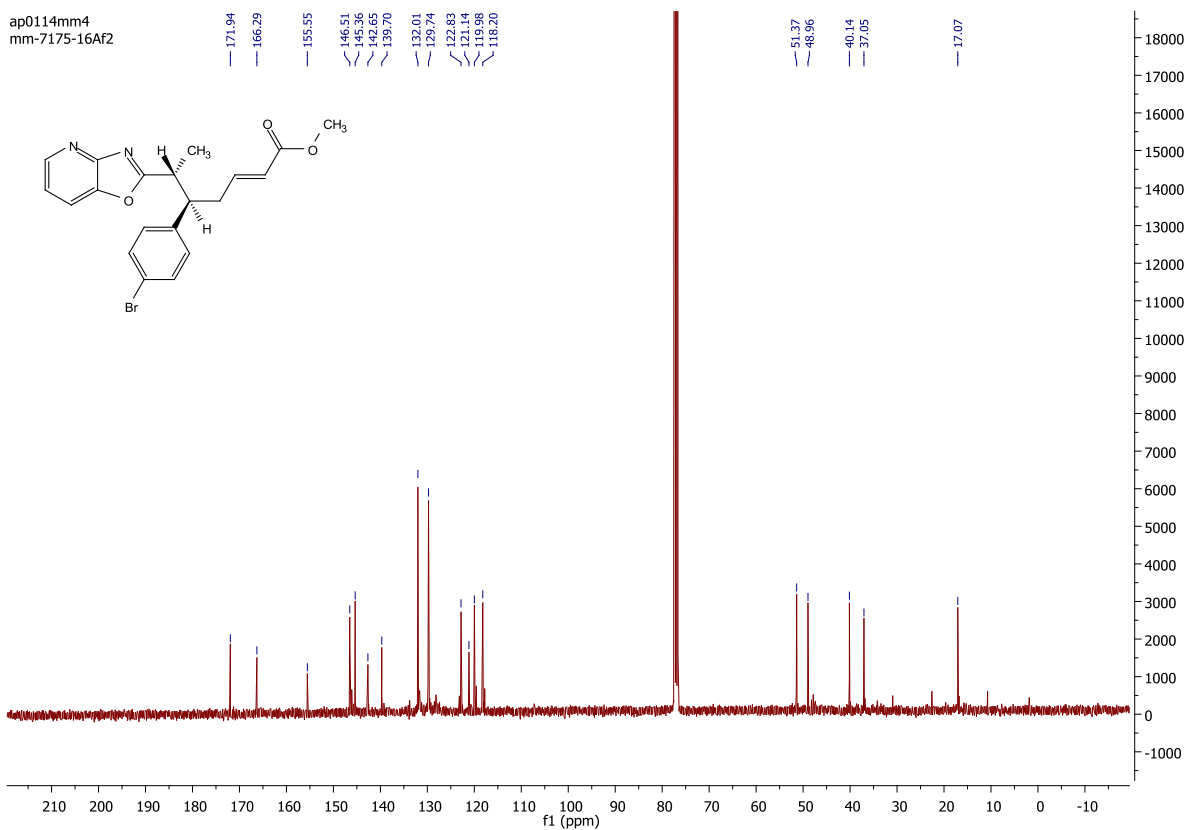




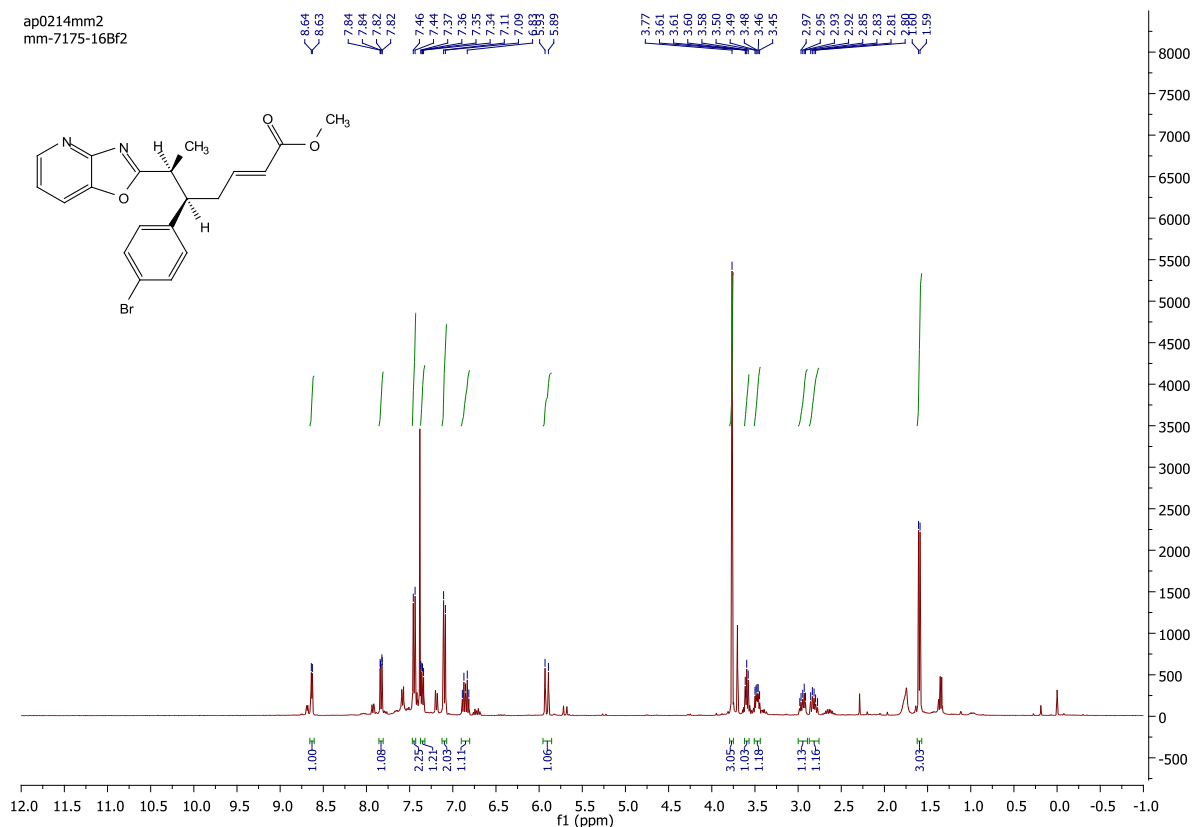
ap0114mm4
mm-7175-16Af2



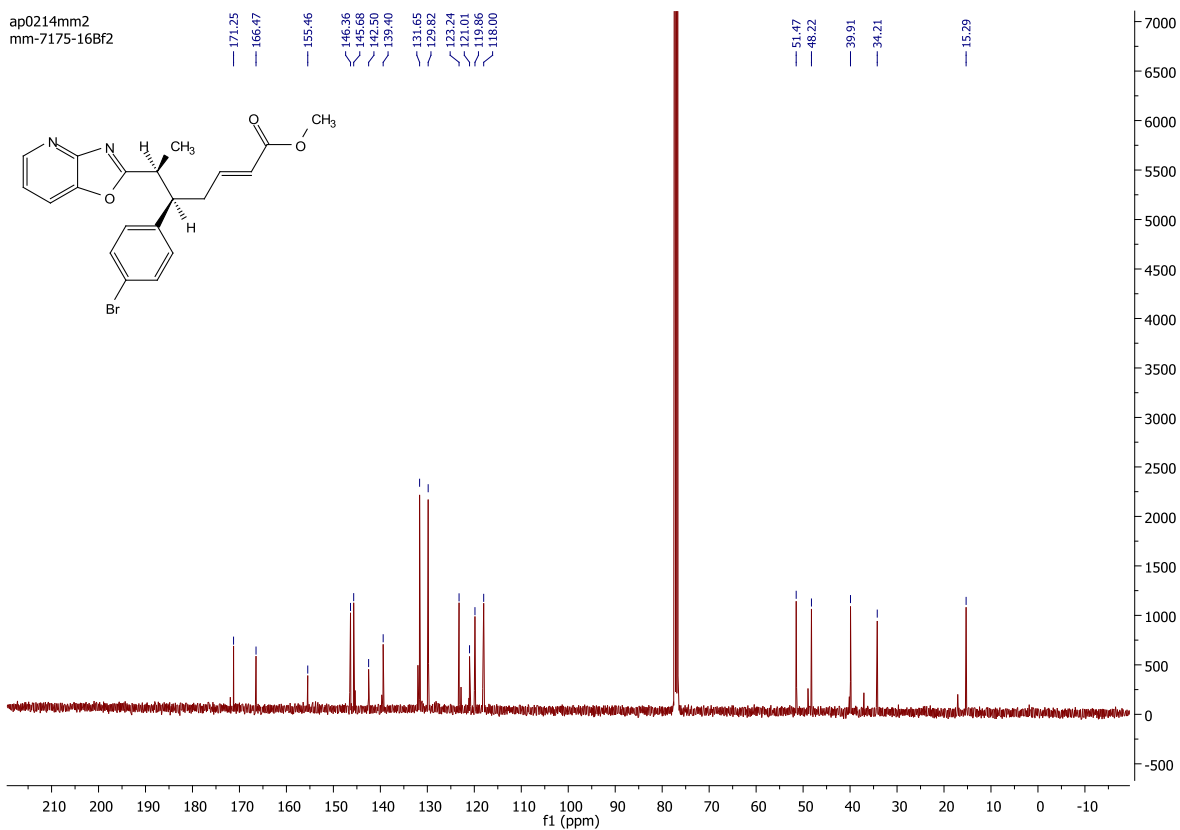
ap0114mm4
mm-7175-16Af2

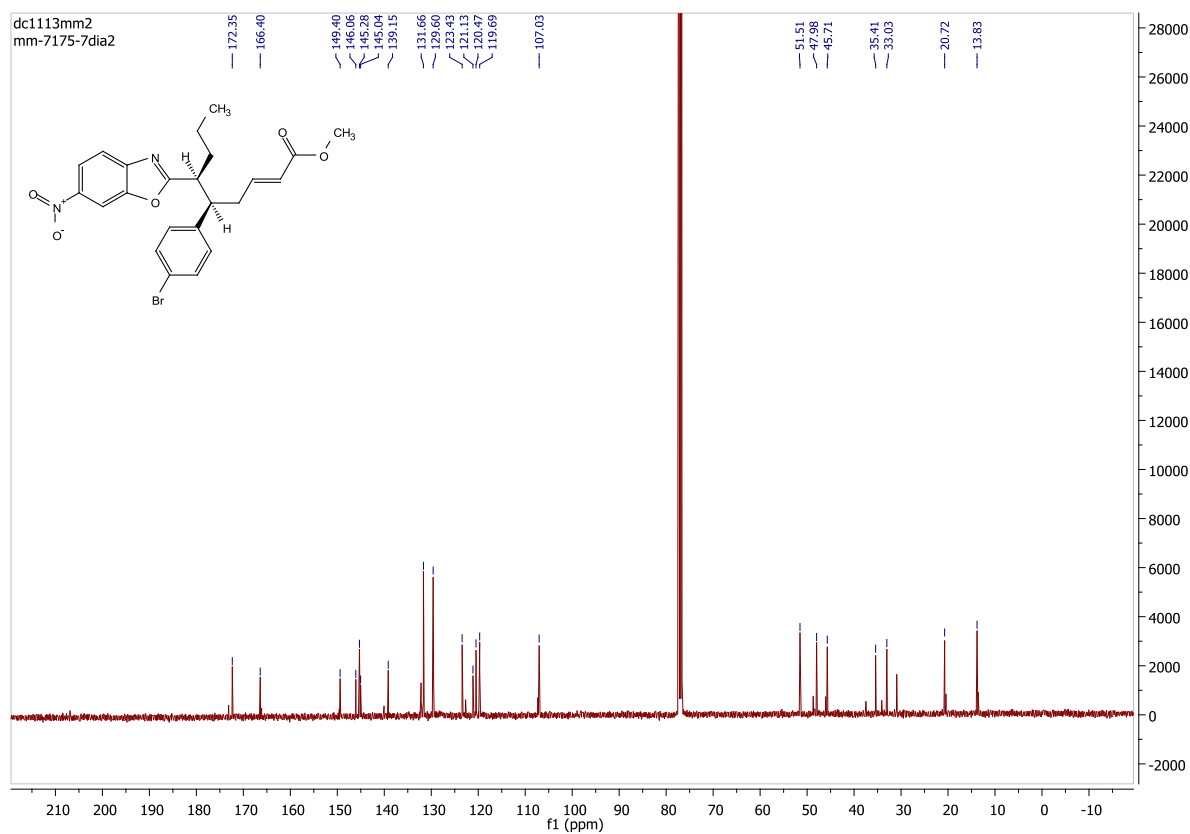
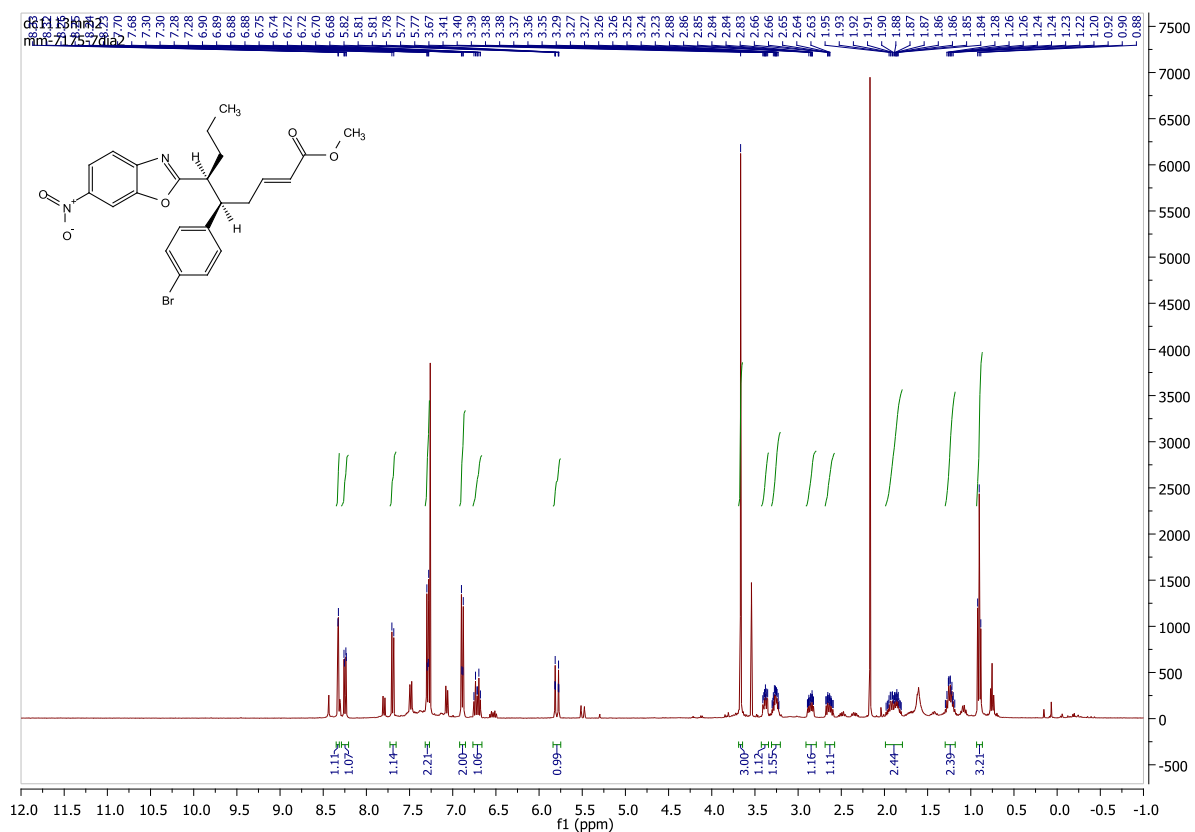


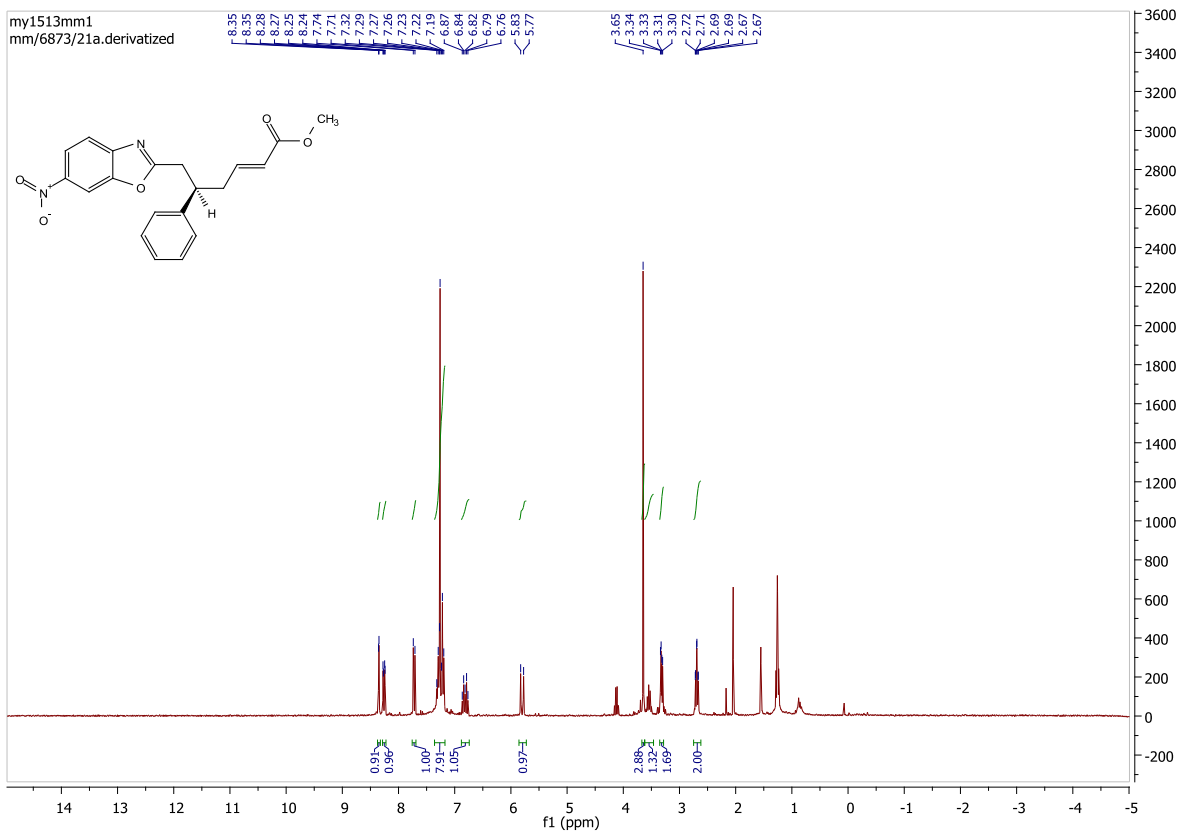
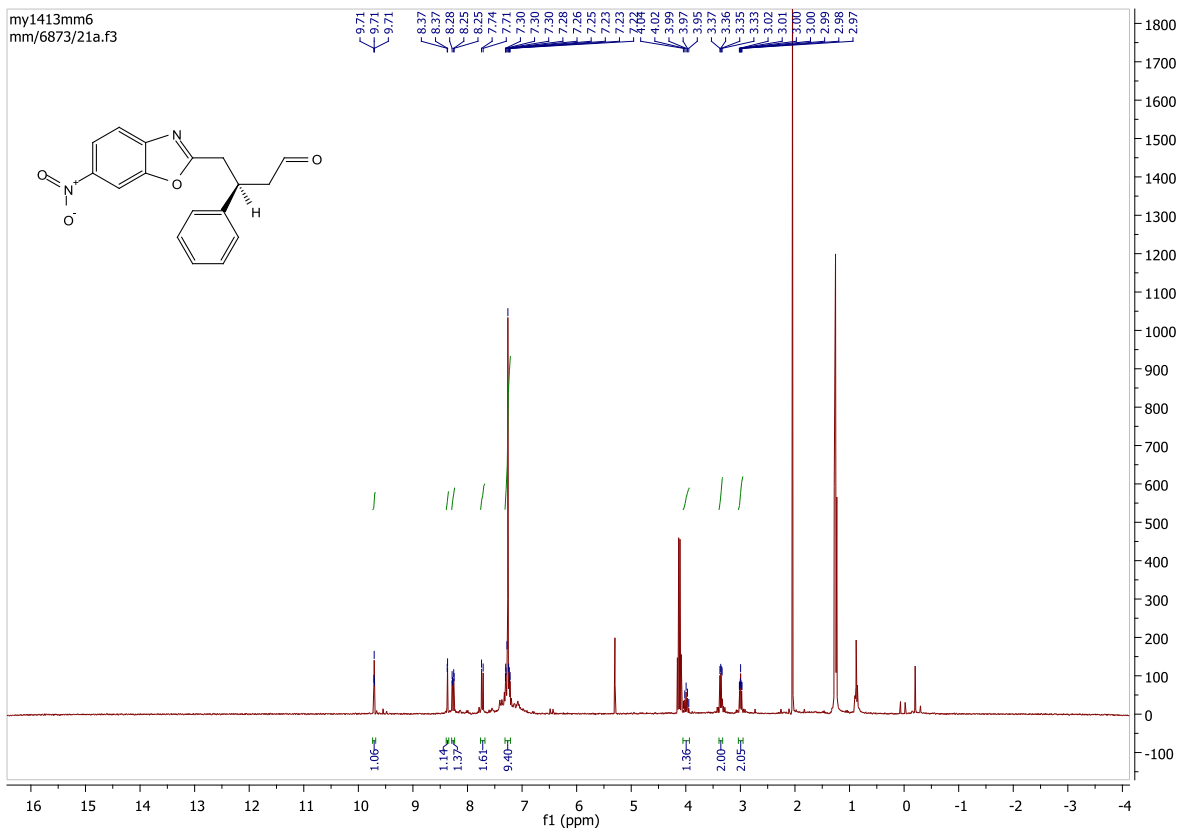
ap0214mm2
mm-7175-16Bf2



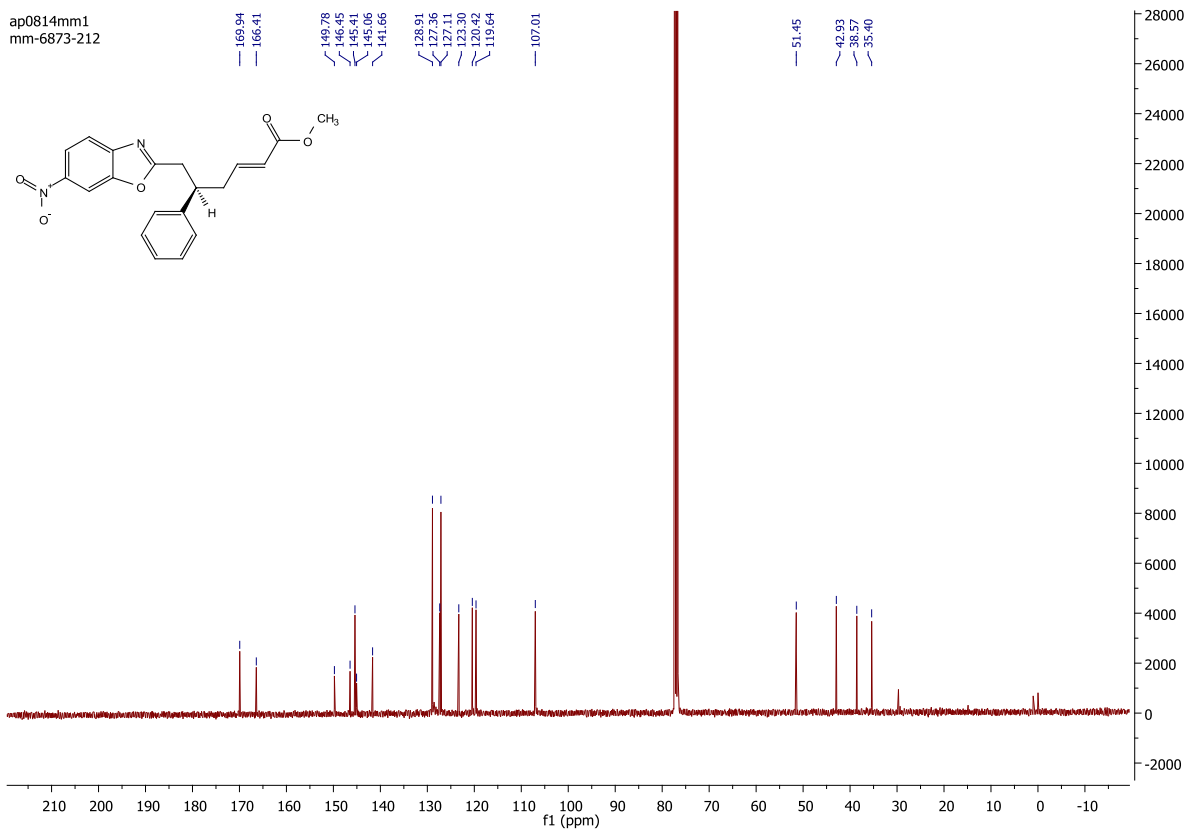
ap0214mm2
mm-7175-16Bf2



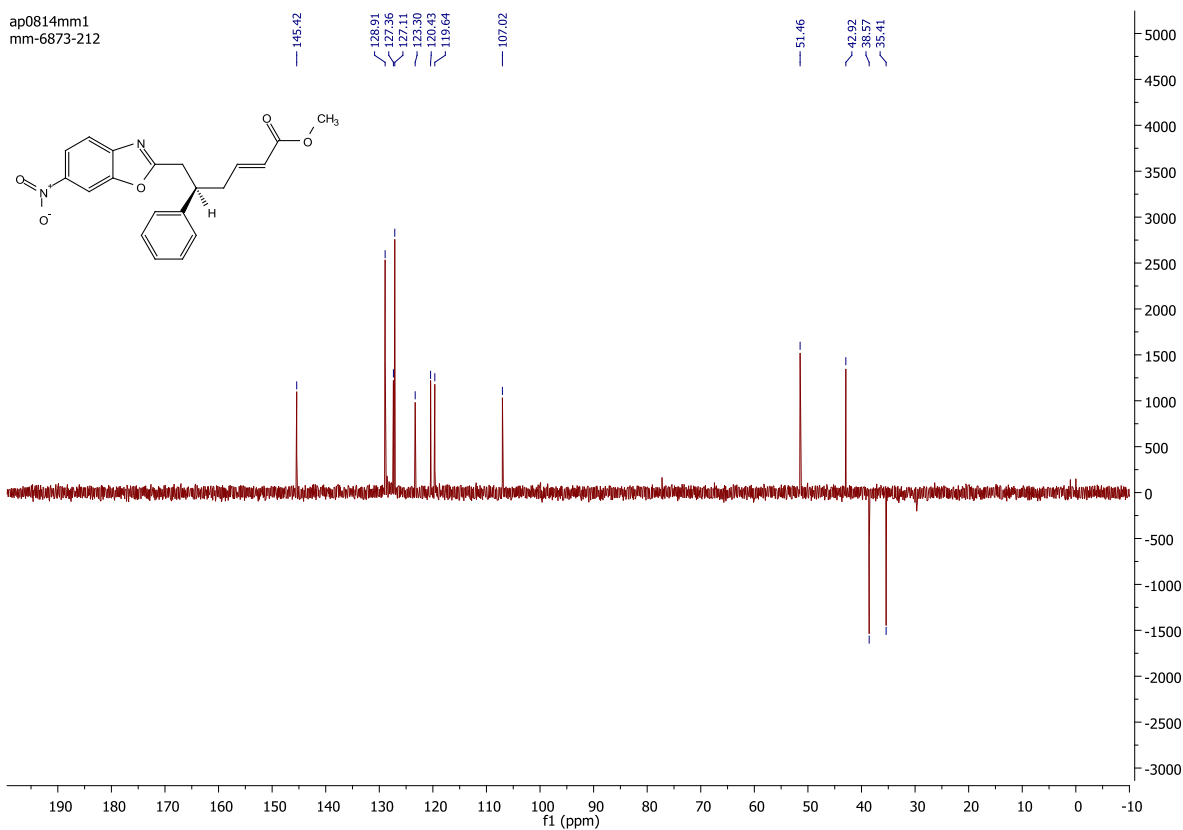


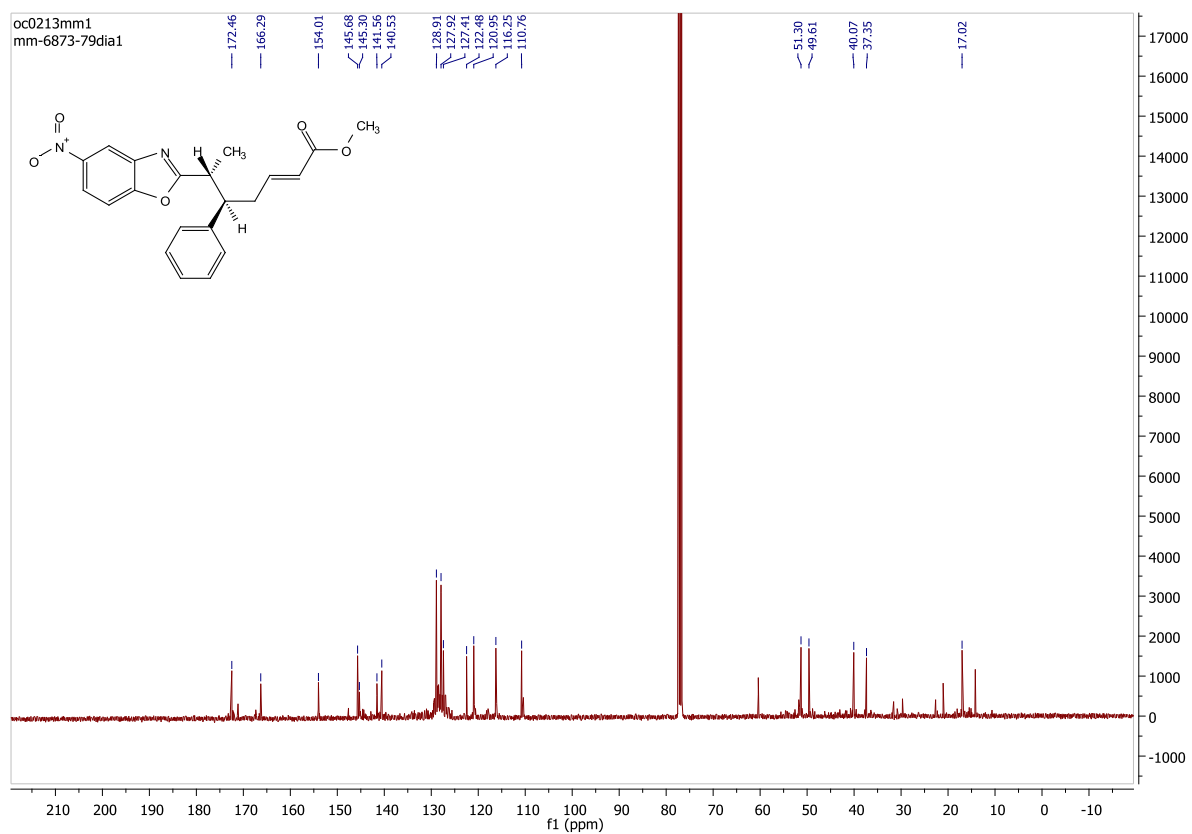
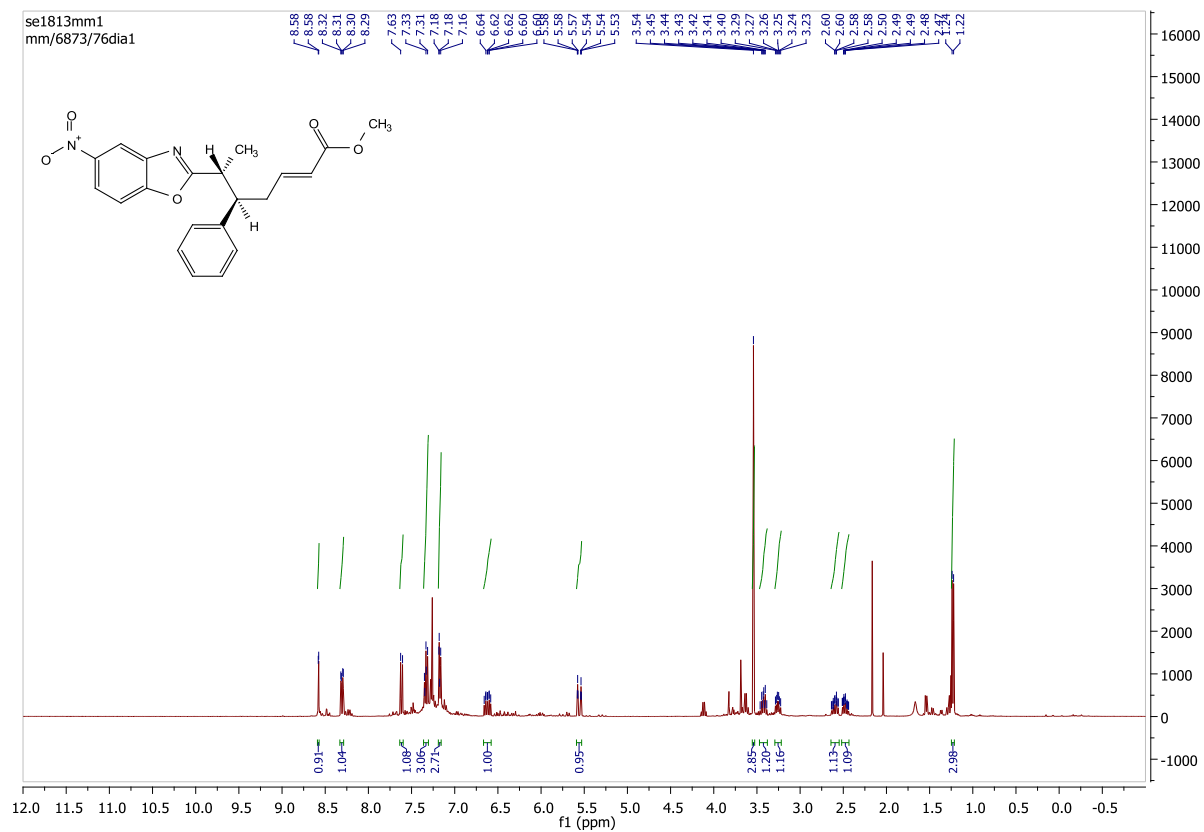


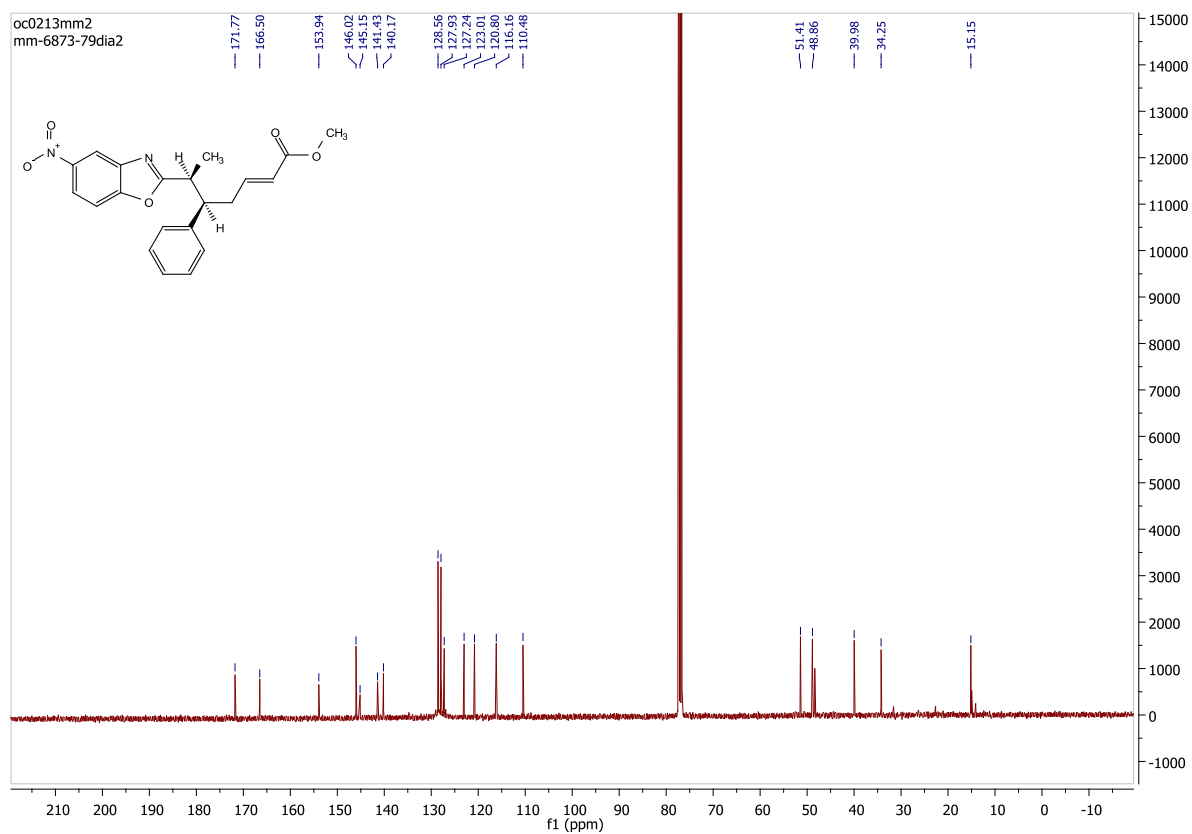
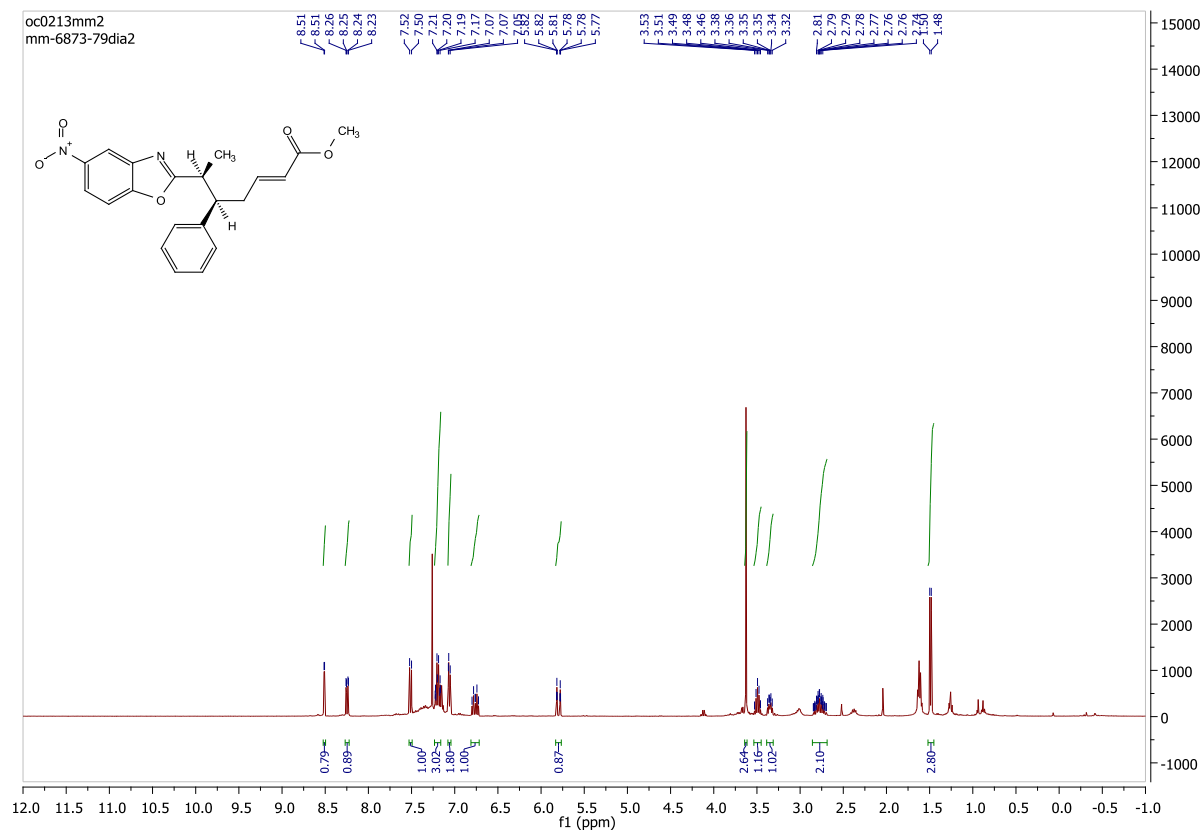
ap0814mm1
mm-6873-212



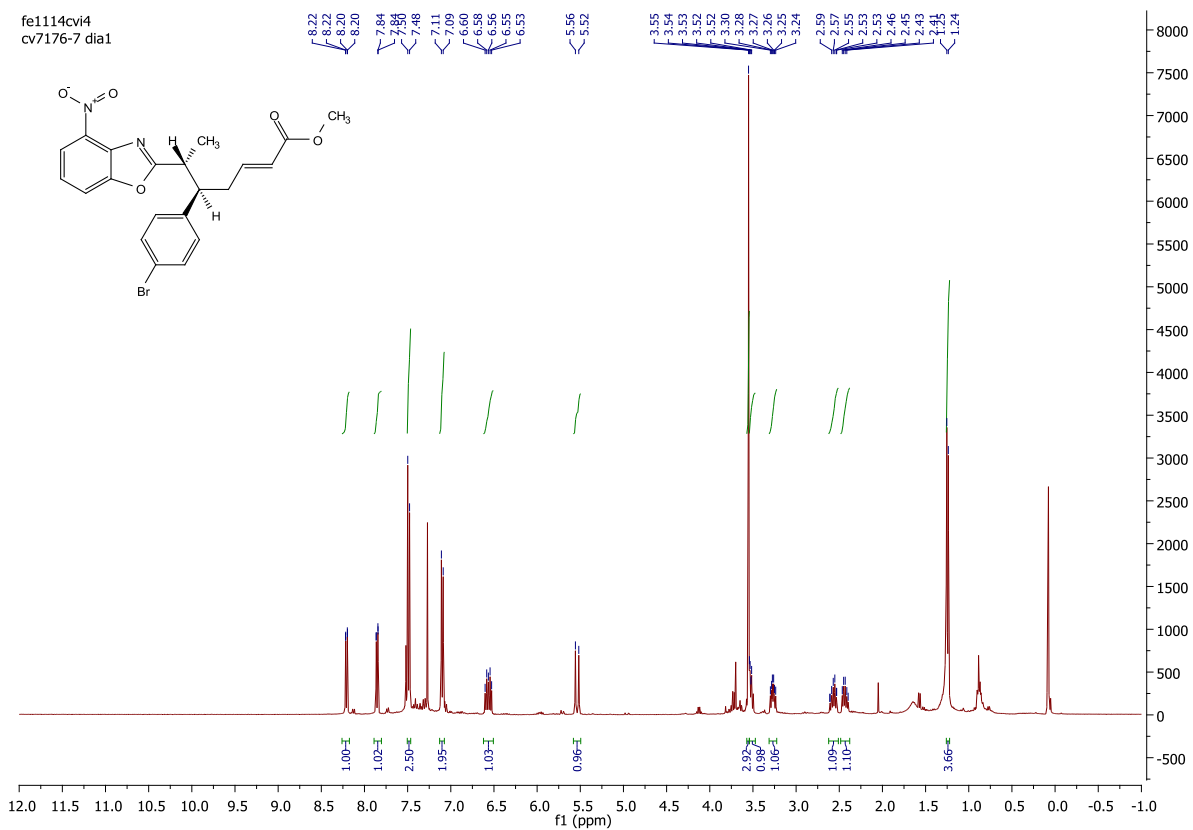
ap0814mm1
mm-6873-212



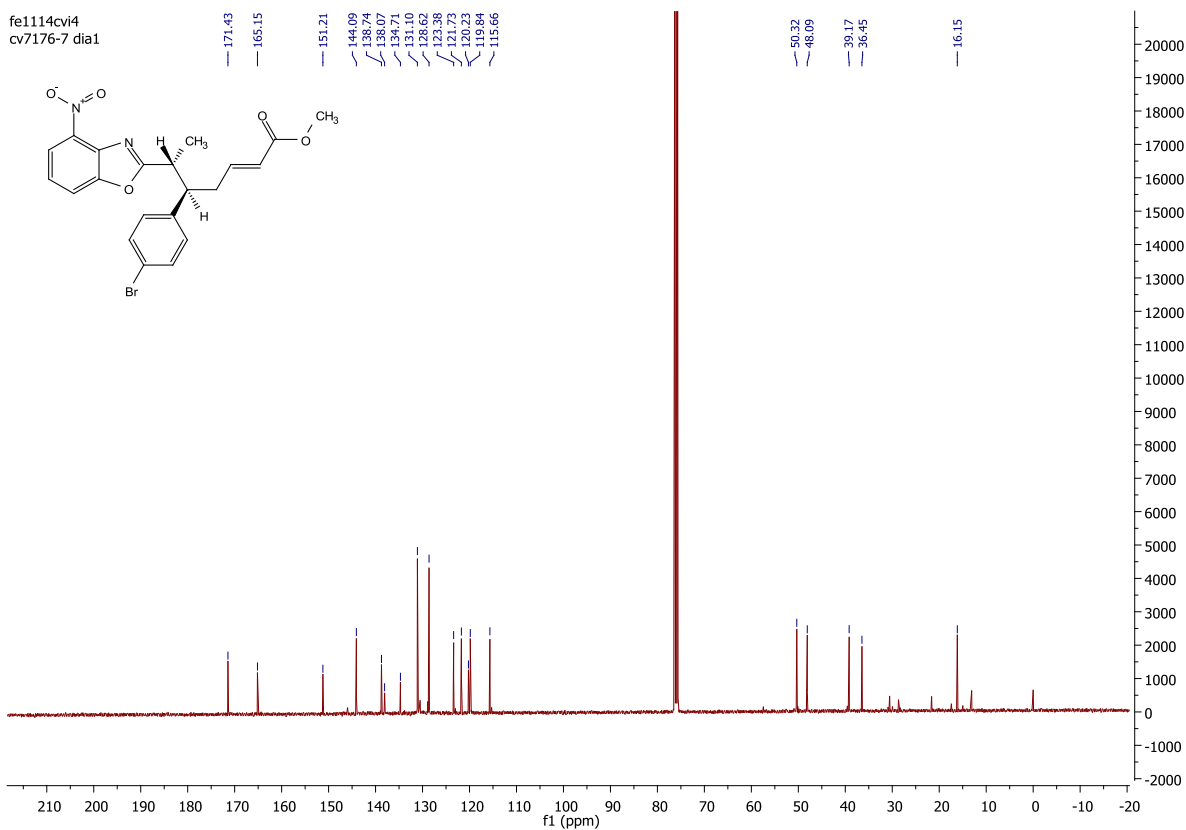




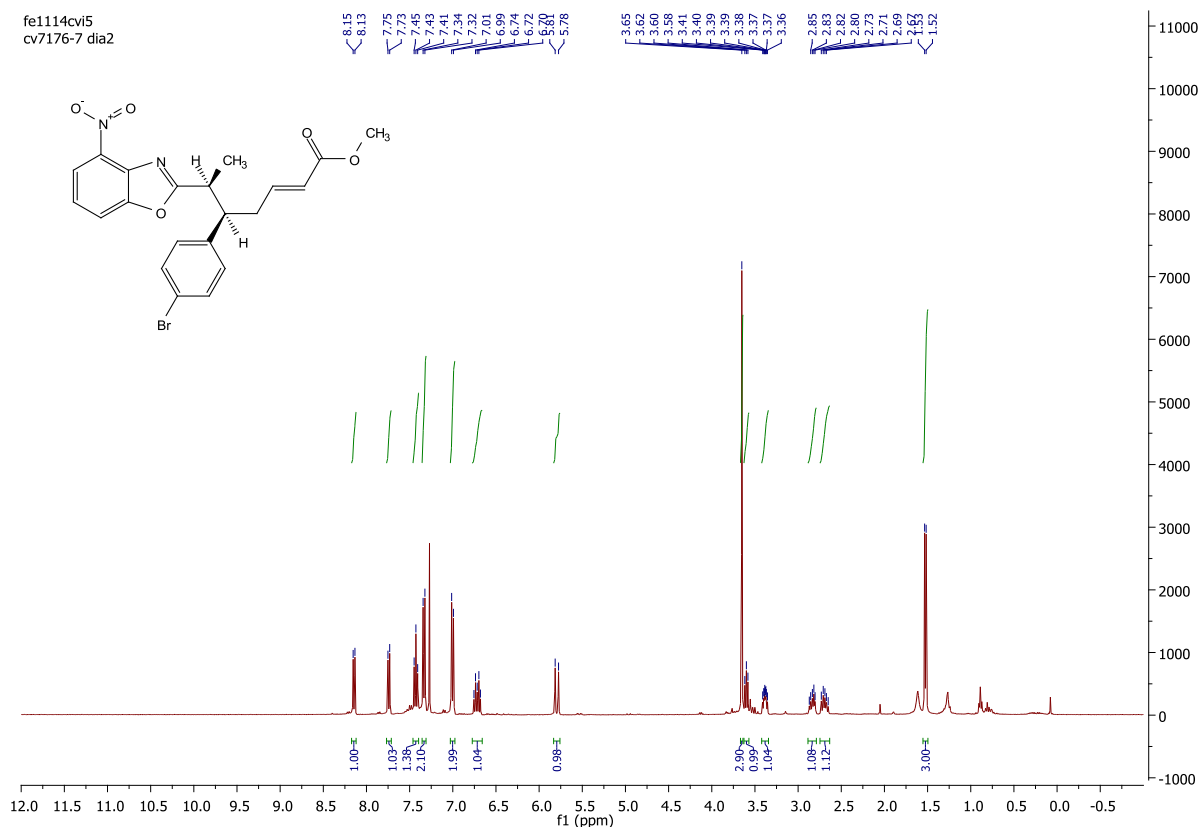
fe1114cv4
cv7176-7 dia1



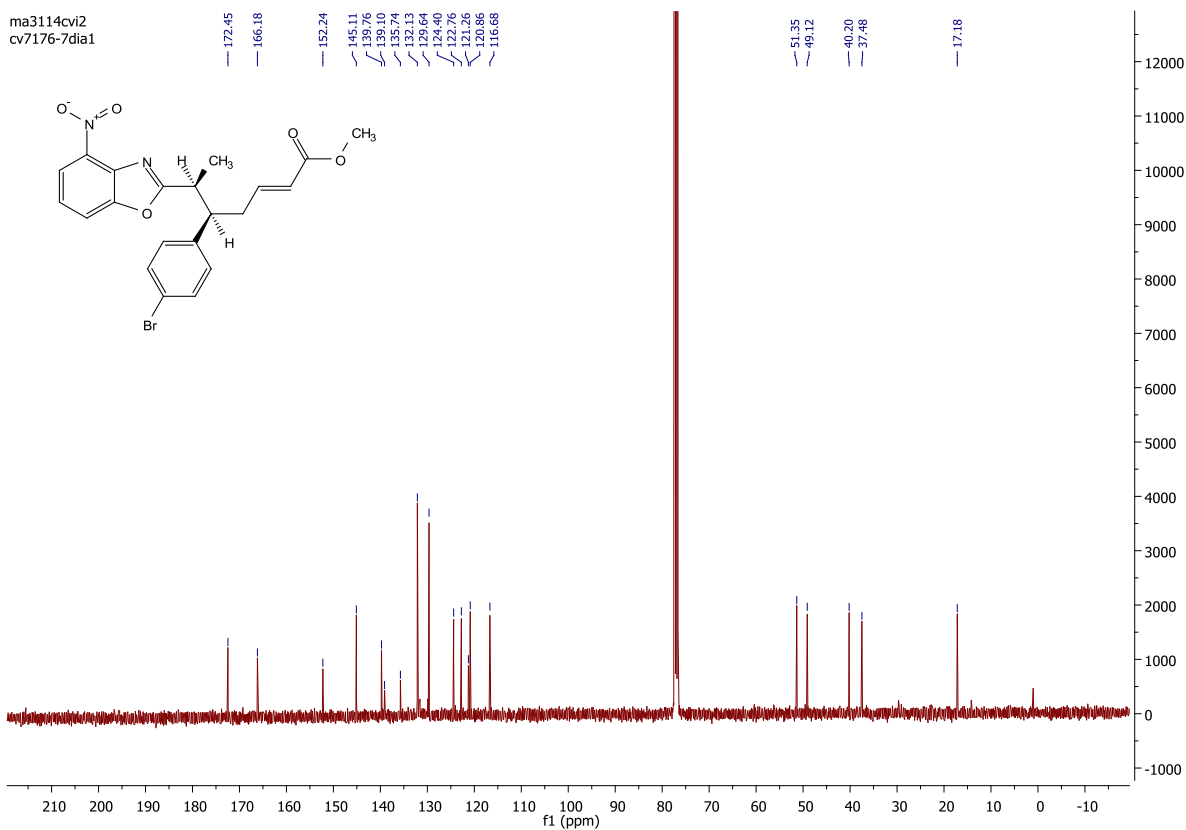
fe1114cv4
cv7176-7 dia1



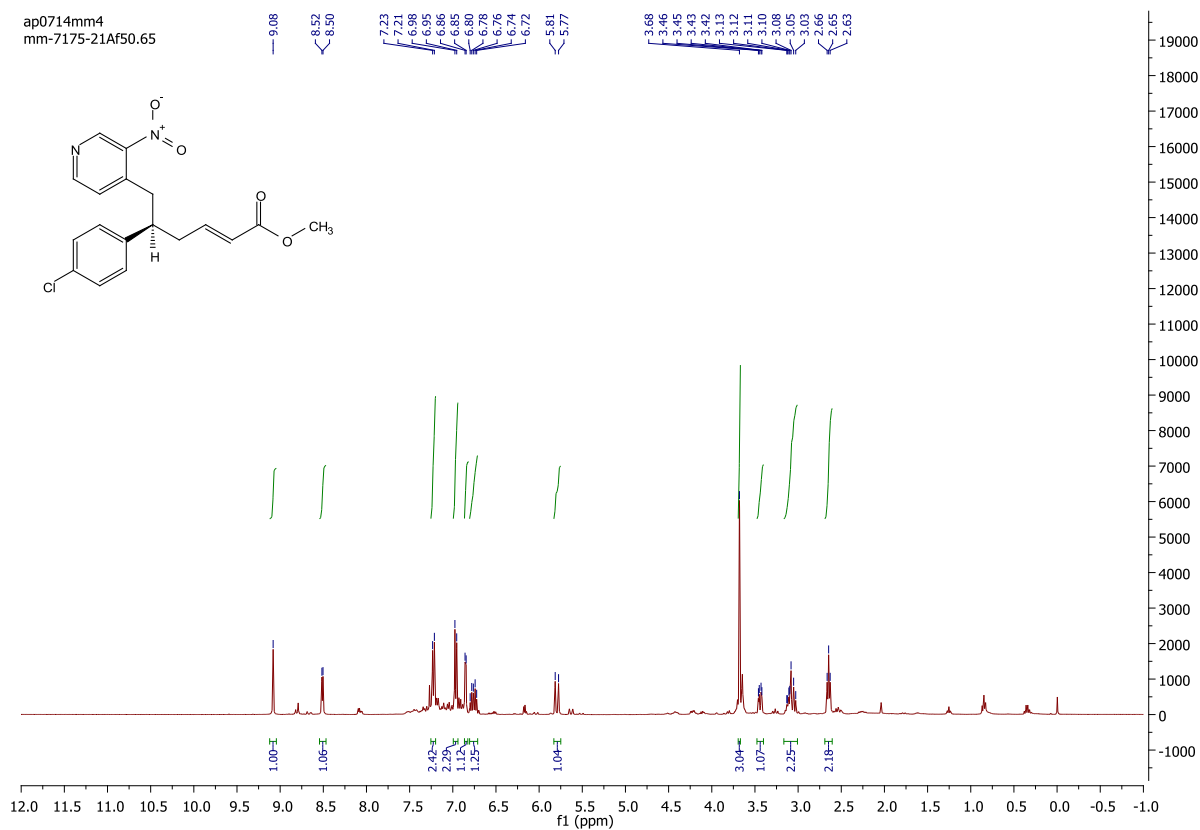
fe1114cv15
cv7176-7 dia2



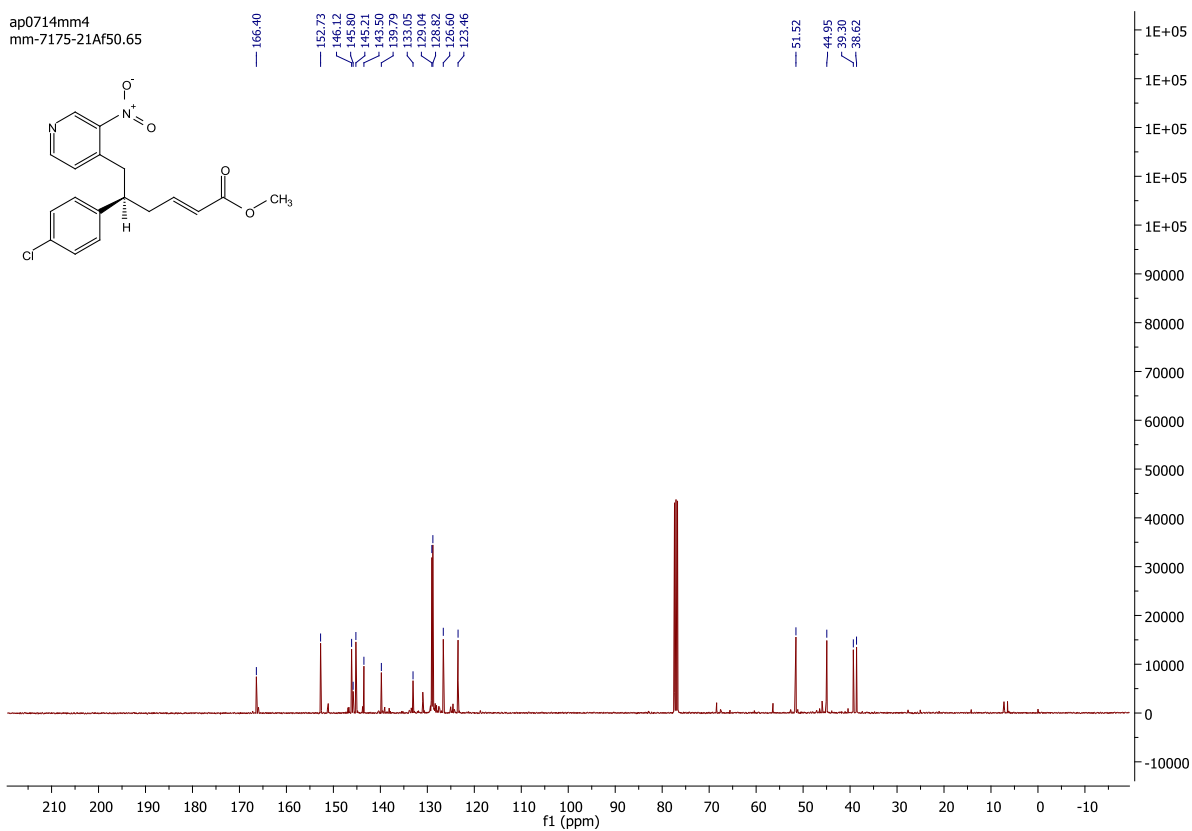
ma3114cv12
cv7176-7dia1

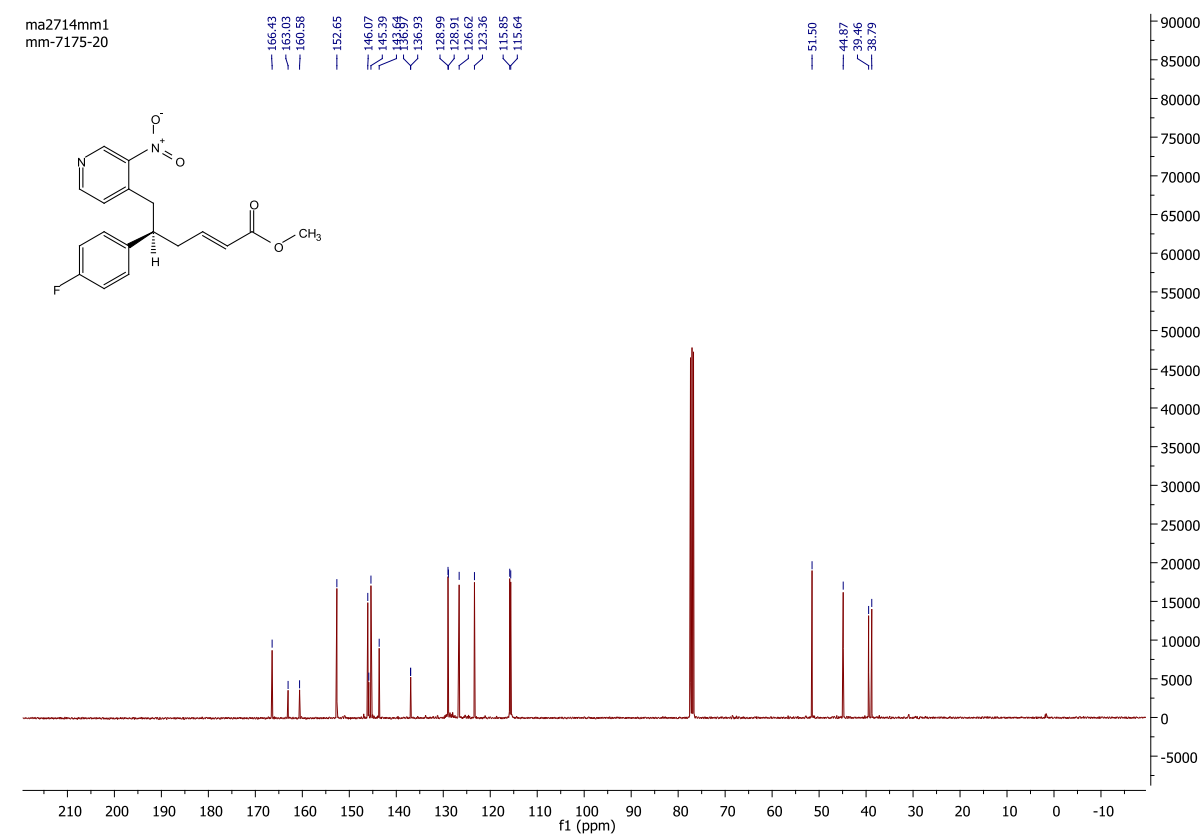
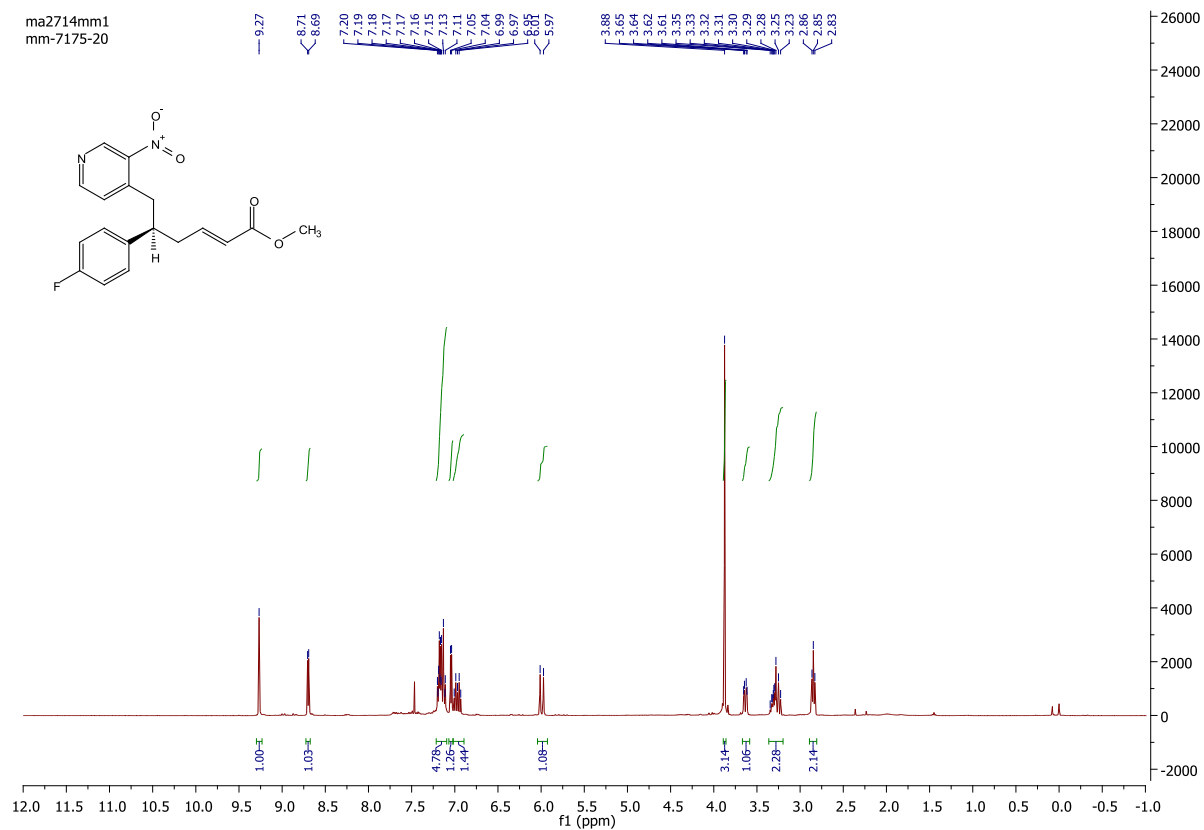


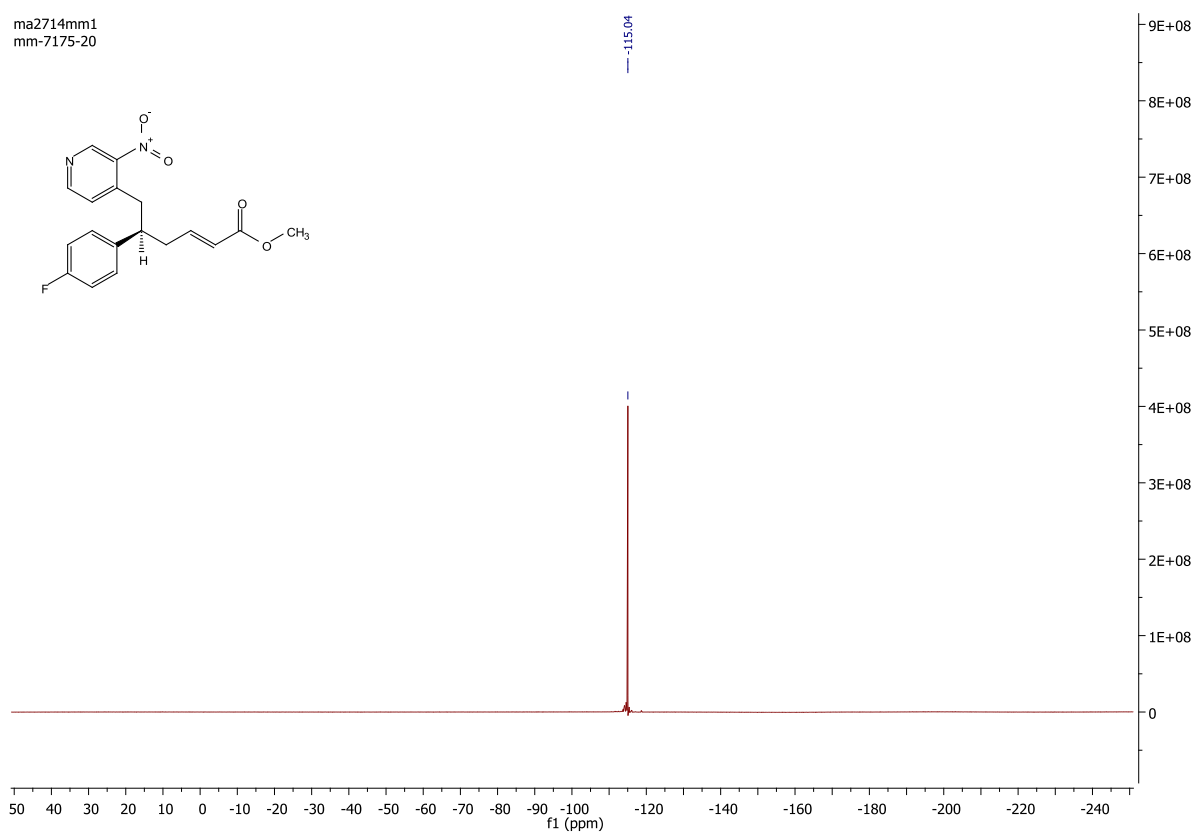
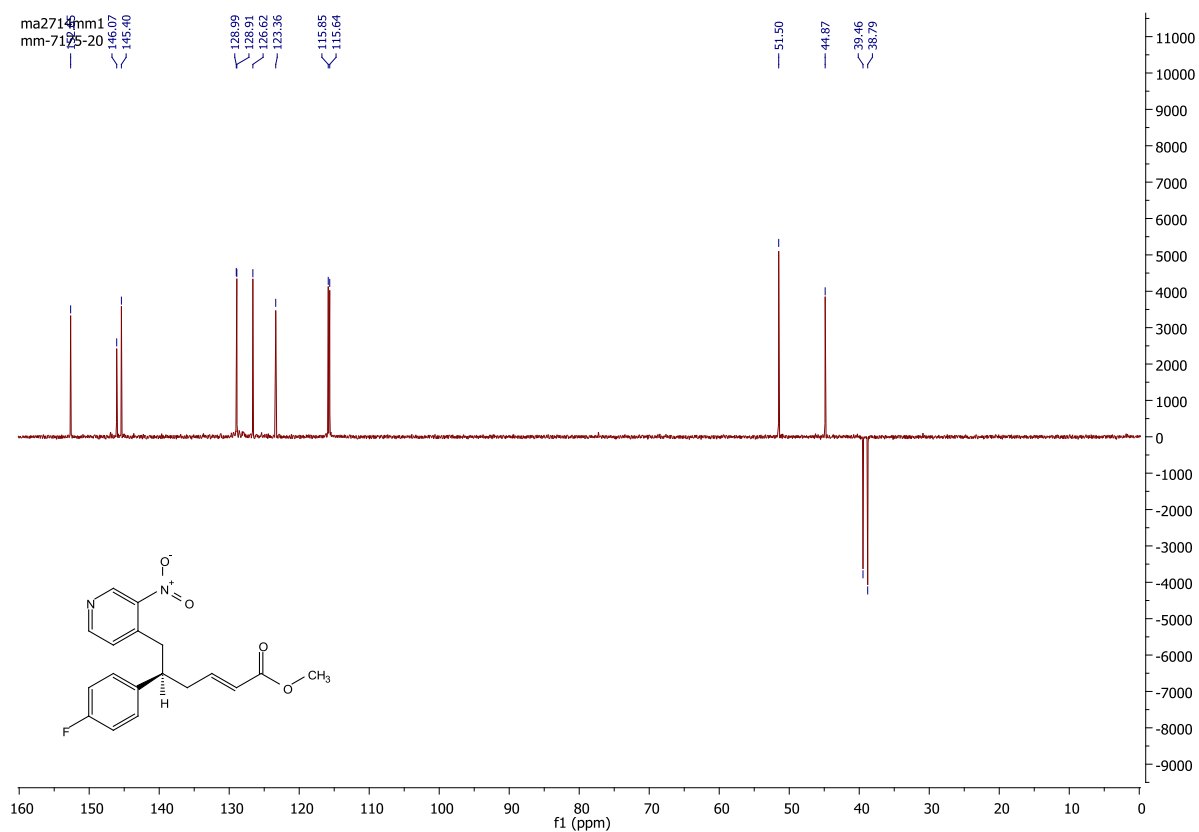
ap0714mm4
mm-7175-21Af50.65



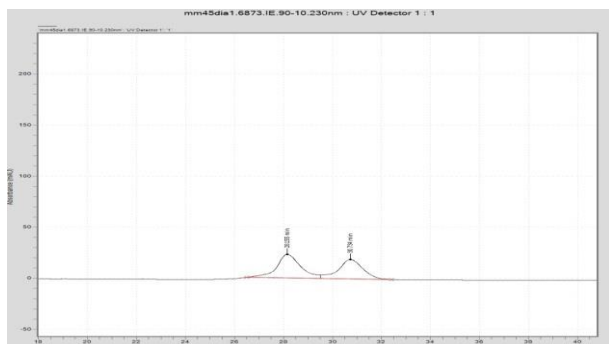
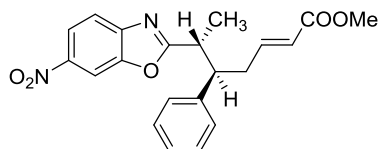
ap0714mm4
mm-7175-21Af50.65



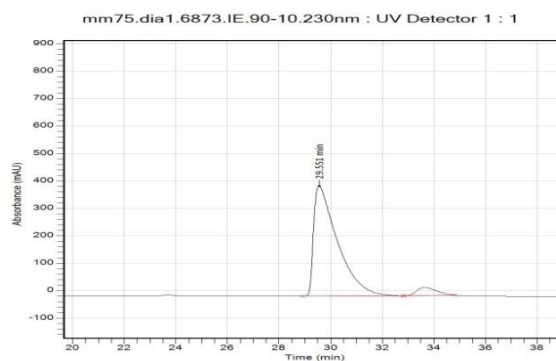




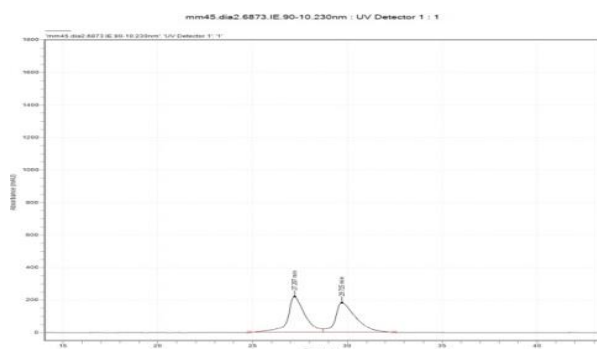
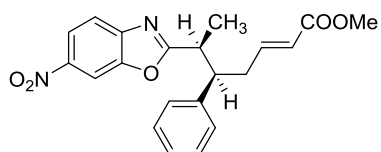
HPLC Traces



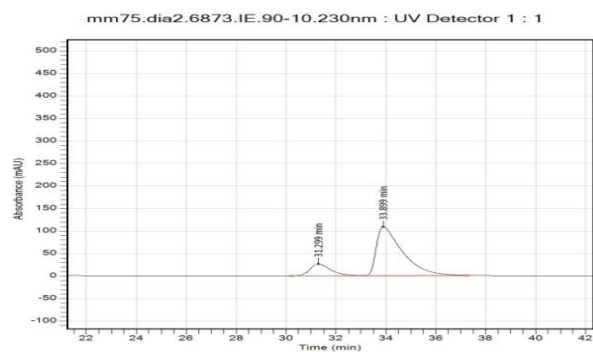
Time	Area	Area %
28.155	1,577,934.1	54.38
30.734	1,323,922.0	45.62
Total	2,901,856.1	100.00



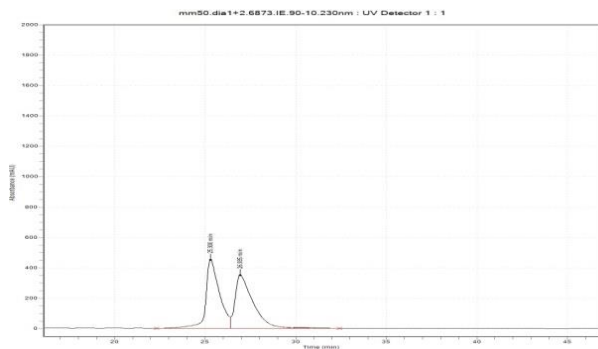
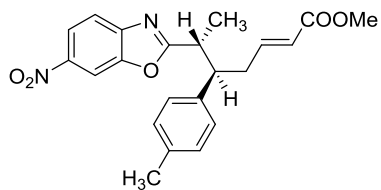
Time	Area	Area %
29.551	25,730,495.9	94.26
33.643	1,565,676.6	5.74
Total	27,296,172.5	100.00



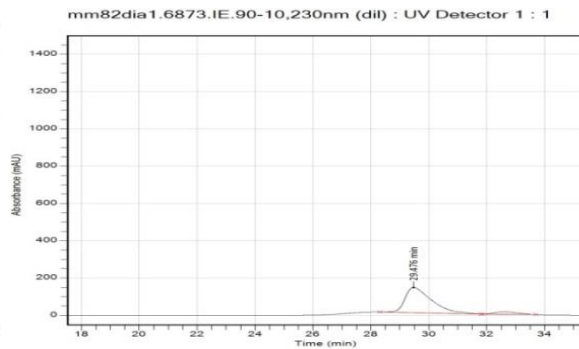
Time	Area	Area %
27.207	13,865,275.8	50.74
29.715	13,462,311.0	49.26
Total	27,327,586.8	100.00



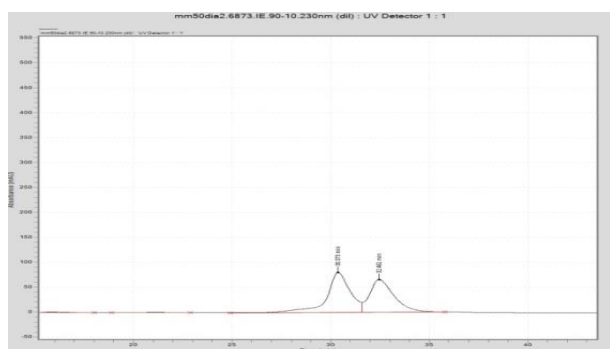
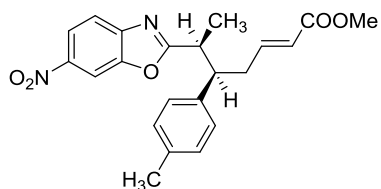
Time	Area	Area %
31.299	1,482,234.5	15.90
33.899	7,842,522.9	84.10
Total	9,324,757.4	100.00



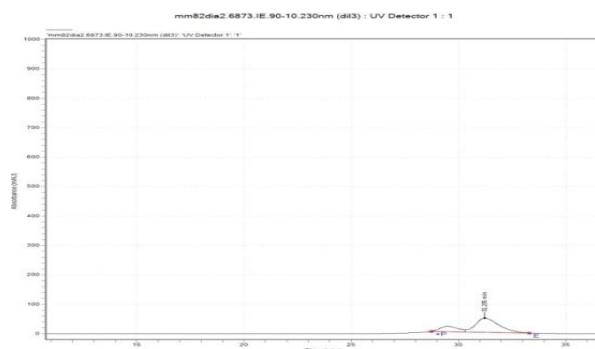
Time	Area	Area %
25.300	23,503,464.1	49.24
26.935	23,844,549.7	49.95
30.296	387,324.1	0.81
Total	47,735,337.8	100.00



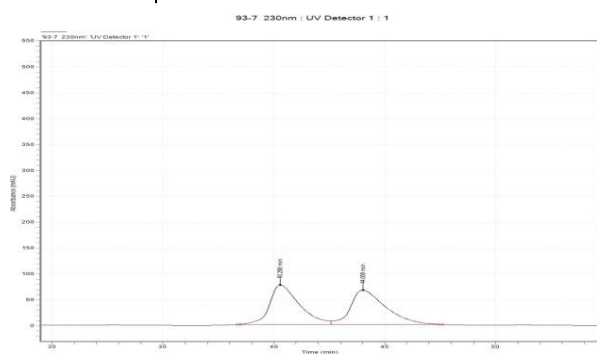
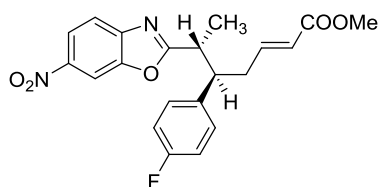
Time	Area	Area %
29.476	8,640,185.2	92.32
32.603	718,949.0	7.68
Total	9,359,134.2	100.00



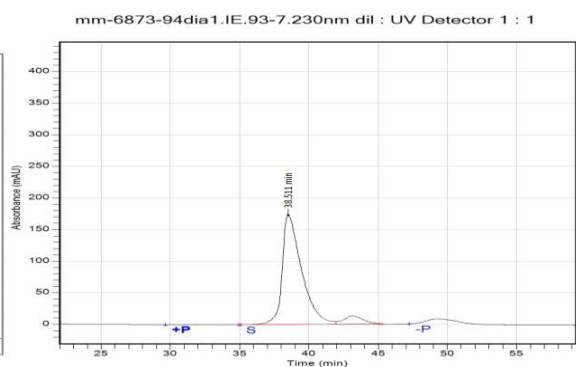
Reference Peak	Area %	Time
	54.10	30.373
	45.90	32.461
Total	100.00	



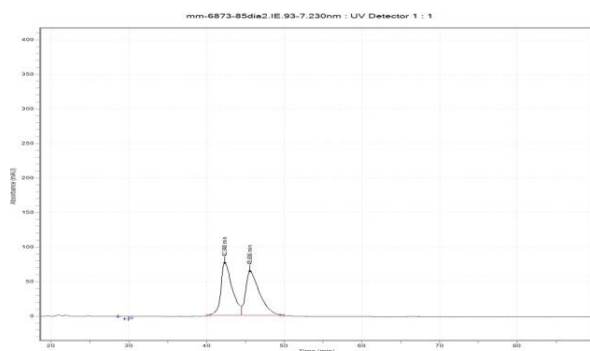
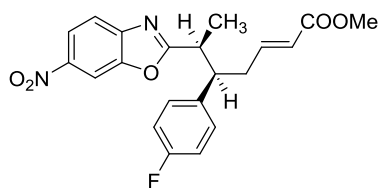
Time	Area	Area %
29.500	1,069,235.8	22.88
31.235	3,603,771.8	77.12
Total	4,673,007.6	100.00



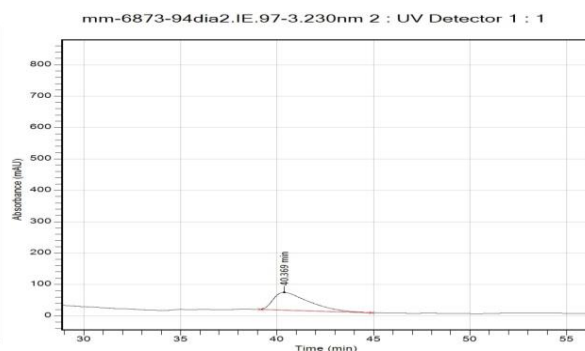
Time	Area	Area %
40.298	7,104,719.9	49.40
44.009	7,276,173.2	50.60
Total	14,380,893.2	100.00



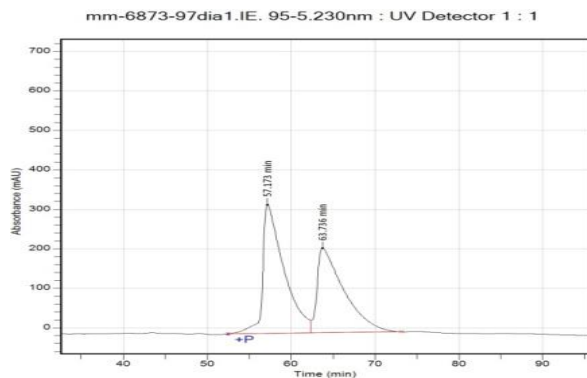
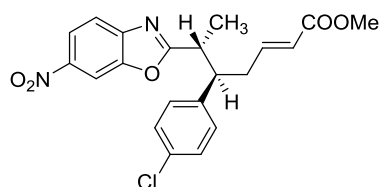
Time	Area	Area %
38.511	16,556,646.4	93.23
43.137	1,202,628.7	6.77
Total	17,759,275.1	100.00



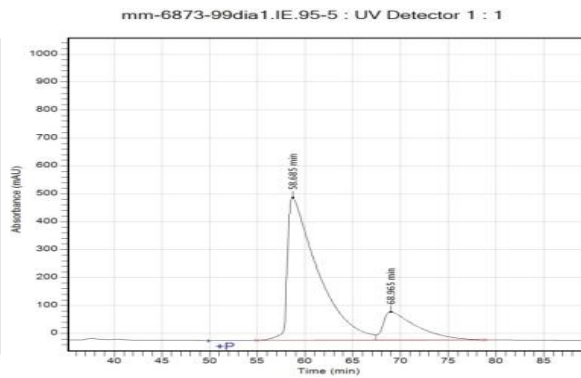
Time	Area	Area %
42.348	7,677,613.5	49.40
45.606	7,862,929.5	50.60
Total	15,540,543.1	100.00



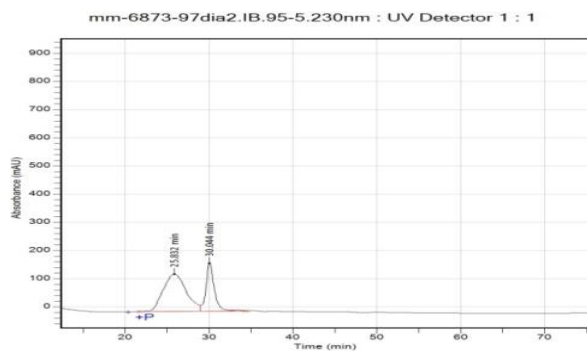
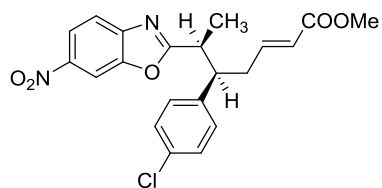
Time	Area	Area %
40.369	7,101,458.6	100.00
Total	7,101,458.6	100.00



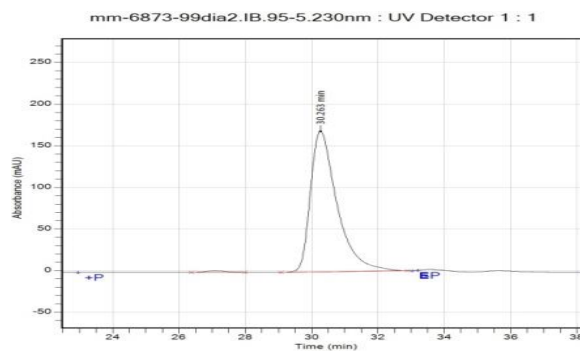
Time	Area	Area %
57.173	57,692,471.5	54.91
63.736	47,370,666.9	45.09
Total	105,063,138.3	100.00



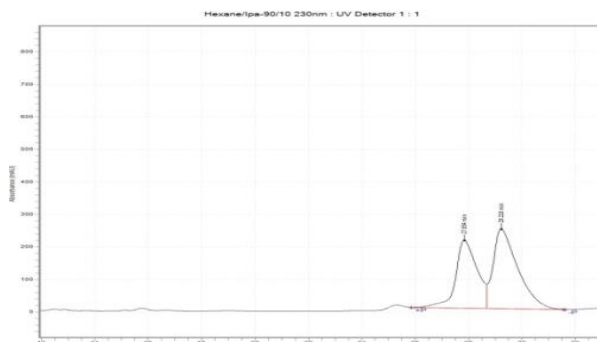
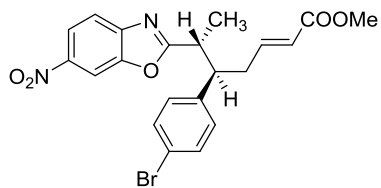
Time	Area	Area %
58.685	113,264,283.1	82.18
68.965	24,557,309.5	17.82
Total	137,821,592.5	100.00



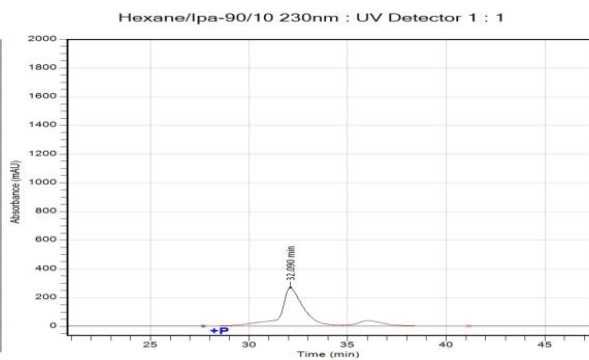
Time	Area	Area %
25.832	25,305,738.3	68.31
30.044	11,741,932.5	31.69
33.364	0.0	0.00
Total	37,047,670.8	100.00



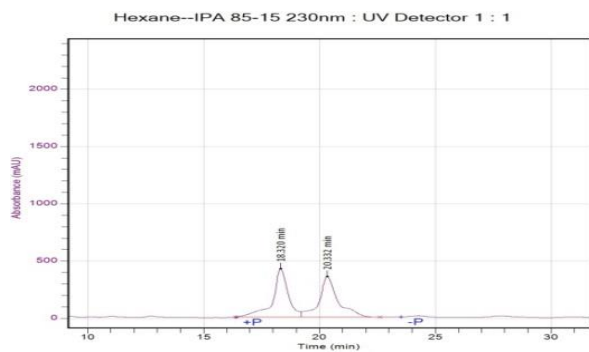
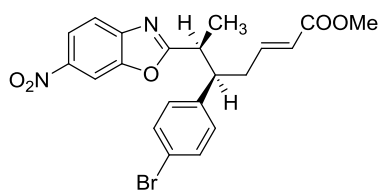
Time	Area	Area %
27.085	78,830.3	0.83
30.263	9,418,231.1	99.17
Total	9,497,061.4	100.00



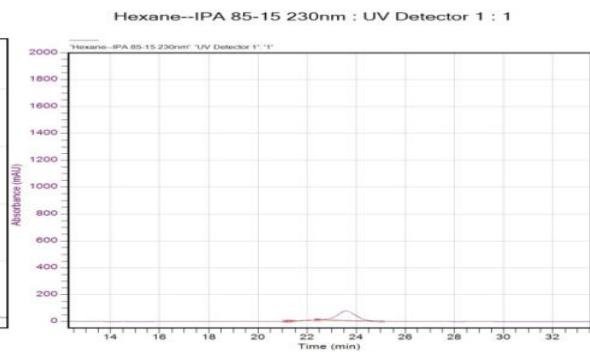
RT (min)	Component Name	Area
27.834		11,724,060.5
29.218		15,731,856.6
		27,455,917.1



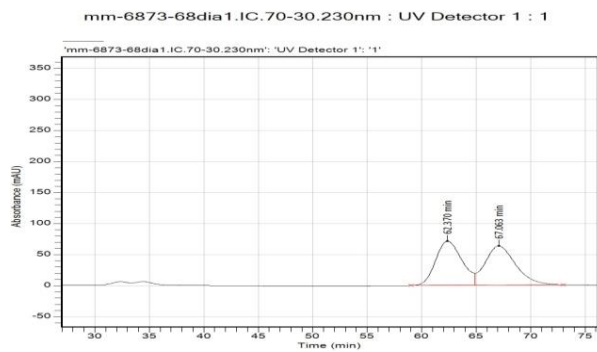
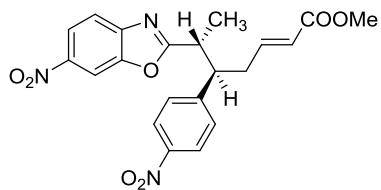
RT (min)	Component Name	Area
32.090		21,340,265.3
36.030		3,391,975.2
		24,732,240.5



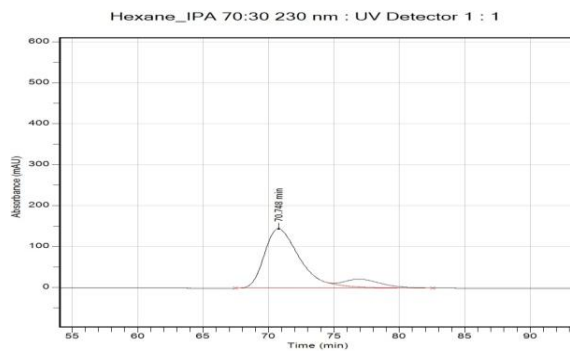
RT (min)	Component Name	Area
18.320		19,361,815.9
20.332		19,823,531.8
		39,185,347.7



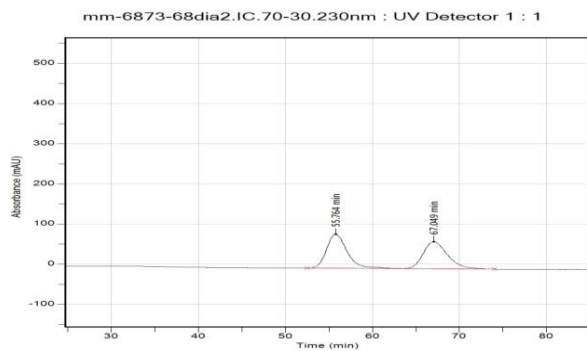
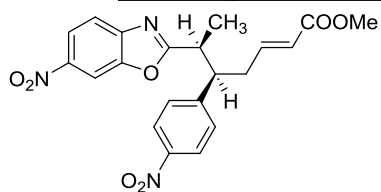
RT (min)	Component Name	Area
21.242		0.0
21.300		0.0
22.458		1.1
23.583		3,700,115.4



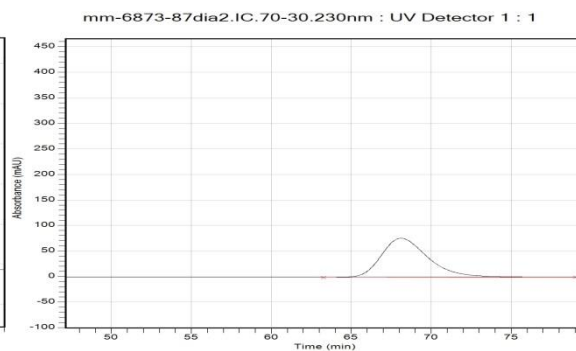
Time	Area	Area %
62.370	11,945,530.6	49.27
67.063	12,301,002.3	50.73
Total	24,246,532.8	100.00



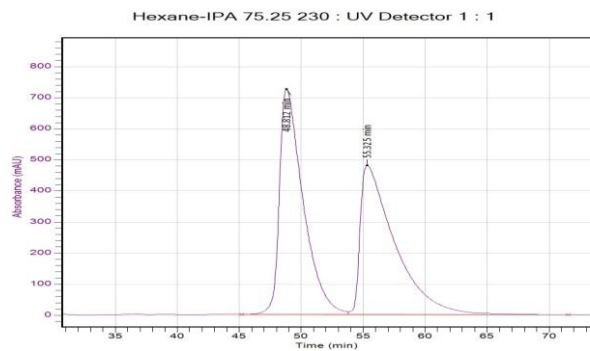
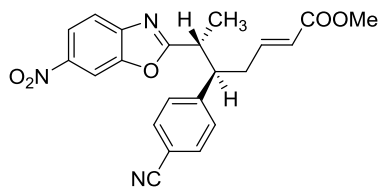
RT (min)	Component Name	Area
70.748		27,844,030.2
76.915		3,467,956.6
		31,311,986.8



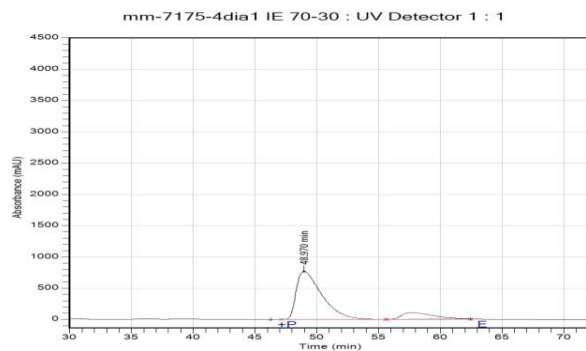
Time	Area	Area %
55.764	13,996,184.1	51.52
67.049	13,169,287.7	48.48
Total	27,165,471.8	100.00



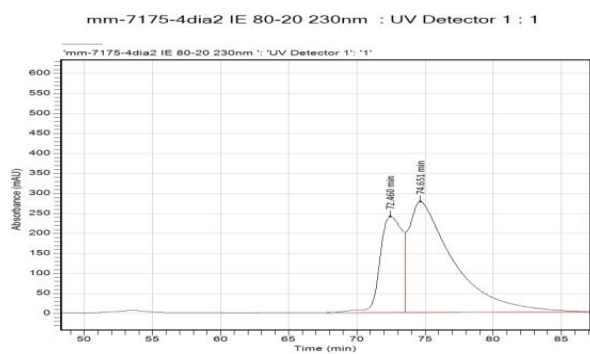
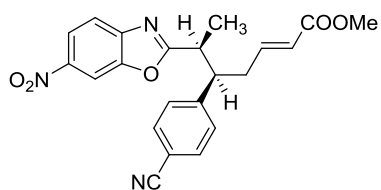
Time	Area	Area %
68.118	15,587,843.3	100.00
Total	15,587,843.3	100.00



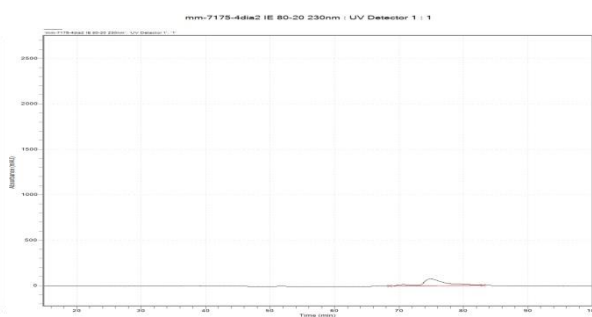
RT (min)	Component Name	Area
48.812		96,413,551.0
55.325		93,195,547.1
		189,609,098.0



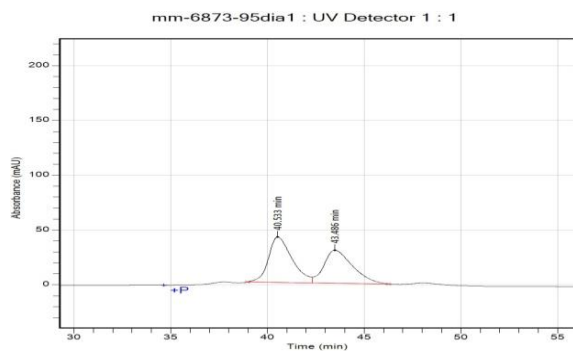
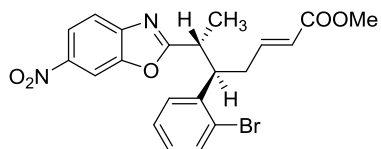
Time	Area	Area %
48.970	110,736,637.0	85.66
57.682	18,533,433.8	14.34
Total	129,270,070.7	100.00



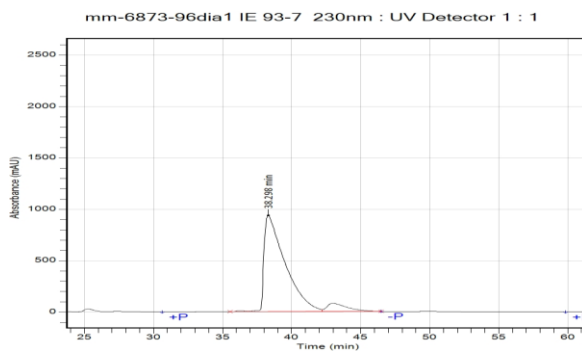
Time	Area	Area %
72.460	27,283,761.1	30.05
74.651	63,518,825.8	69.95
Total	90,802,587.0	100.00



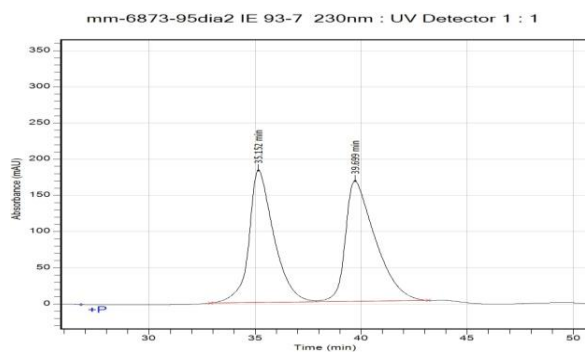
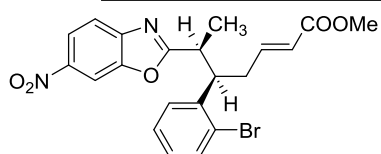
Time	Area	Area %
70.646	2,248,626.3	11.92
74.853	16,618,311.8	88.08
Total	18,866,938.1	100.00



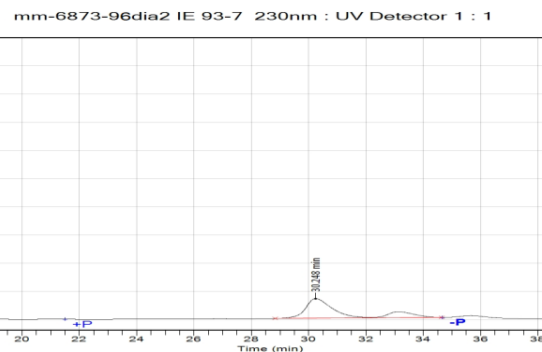
Time	Area	Area %
40.533	3,523,765.6	53.25
43.486	3,093,168.1	46.75
Total	6,616,933.7	100.00



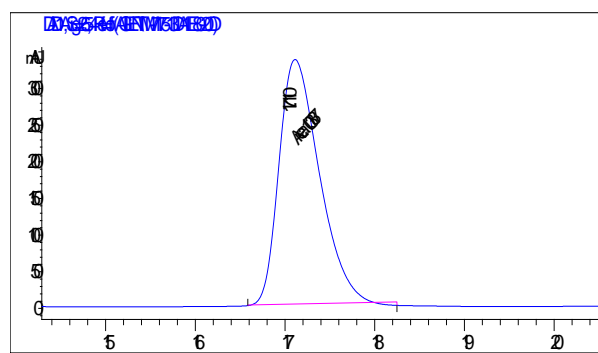
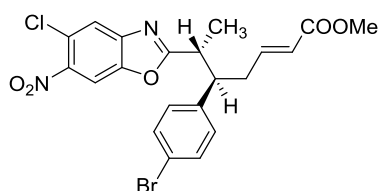
Time	Area	Area %
36.274	372,592.4	0.35
38.298	99,211,178.2	92.09
42.988	8,152,473.4	7.57
Total	107,736,244.0	100.00

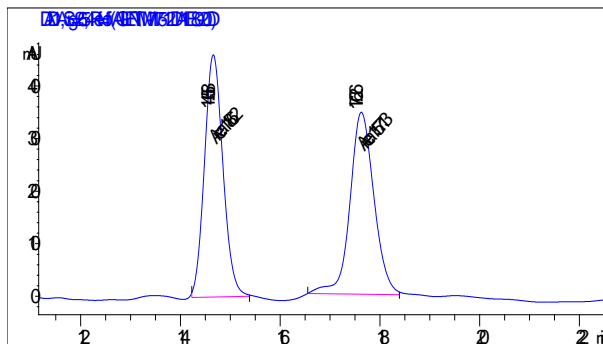


Time	Area	Area %
35.152	14,903,385.9	47.78
39.699	16,285,409.0	52.22
Total	31,188,794.9	100.00

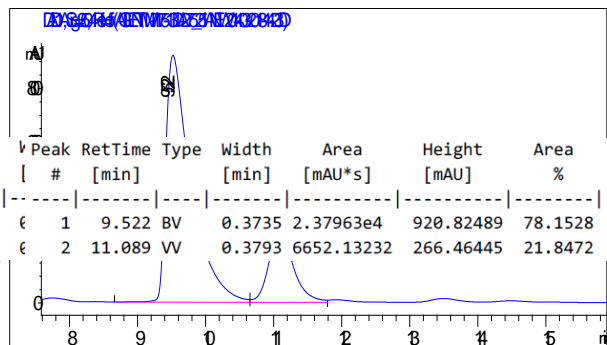
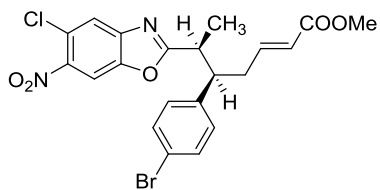


Time	Area	Area %
30.248	4,509,821.7	76.65
33.133	1,374,209.4	23.35
Total	5,884,031.1	100.00

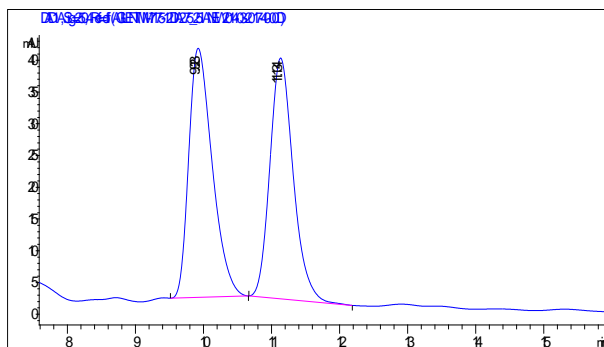


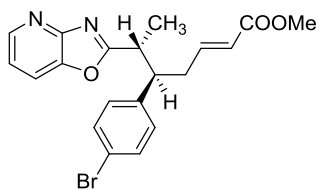


Peak #	RetTime [min]	Type	Width [min]	Area [mAU*s]	Height [mAU]	Area %
1	14.658	MM	0.4291	1186.20056	46.07603	50.6203
2	17.626	MM	0.5572	1157.13062	34.61367	49.3797

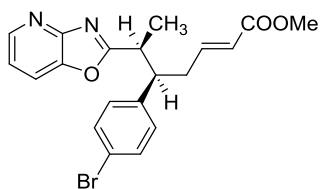


Peak #	RetTime [min]	Type	Width [min]	Area [mAU*s]	Height [mAU]	Area %
1	9.522	BV	0.3735	2.37963e4	920.82489	78.1528
2	11.089	VV	0.3793	6652.13232	266.46445	21.8472

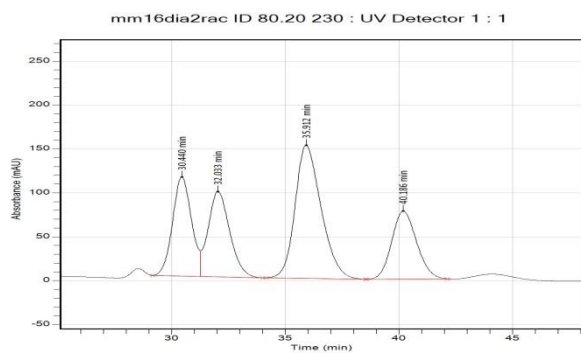




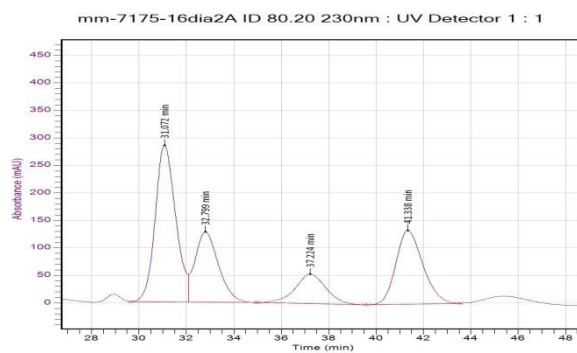
diastereomer 1: peak 2 and peak 3



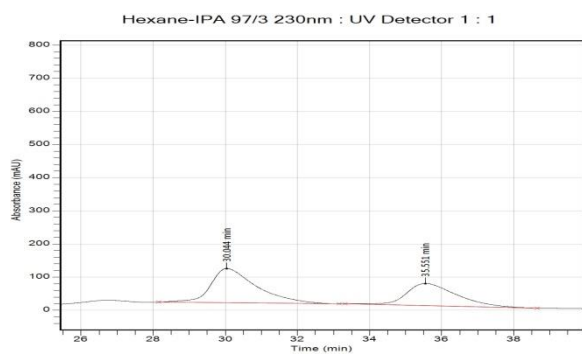
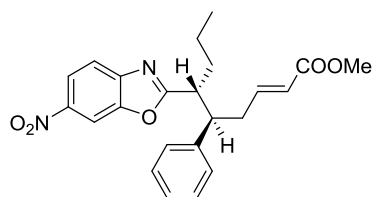
diastereomer 2: peak 1 and peak 4



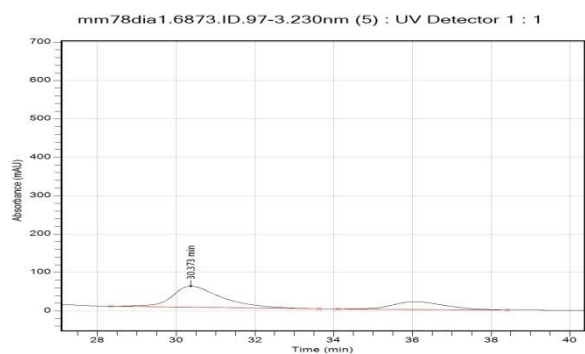
Time	Area	Area %
30.440	6,597,449.8	21.30
32.033	6,428,118.8	20.75
35.912	12,067,542.2	38.96
40.186	5,881,408.9	18.99
Total	30,974,519.7	100.00



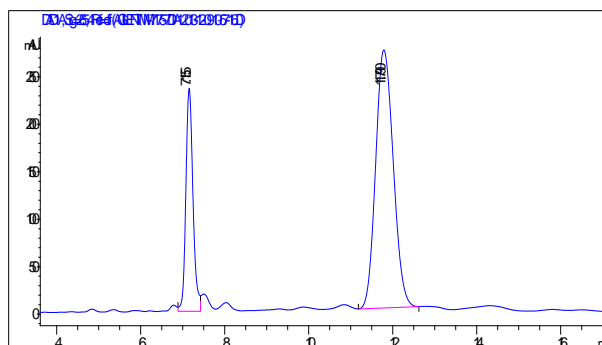
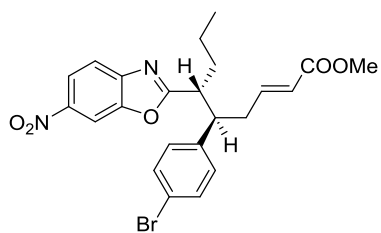
Time	Area	Area %
31.072	17,130,784.8	41.43
32.799	8,821,741.5	21.34
37.224	4,833,034.9	11.69
41.338	10,558,407.6	25.54
Total	41,343,968.8	100.00



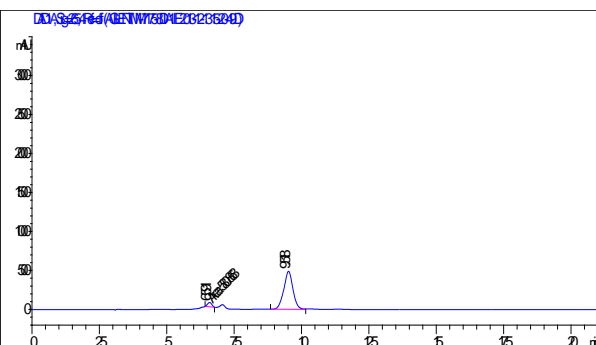
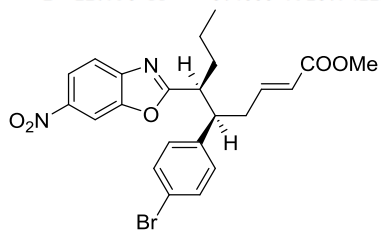
RT (min)	Component Name	Area
30.044		9,173,478.7
33.500		3,141.0
35.551		6,485,547.3
		15,662,167.1



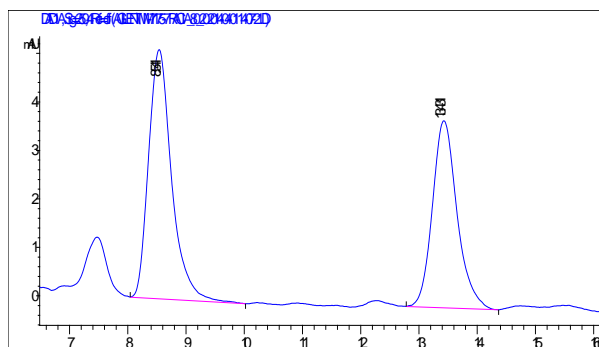
Time	Area	Area %
30.373	4,853,769.2	72.42
36.055	1,848,175.3	27.58
Total	6,701,944.5	100.00



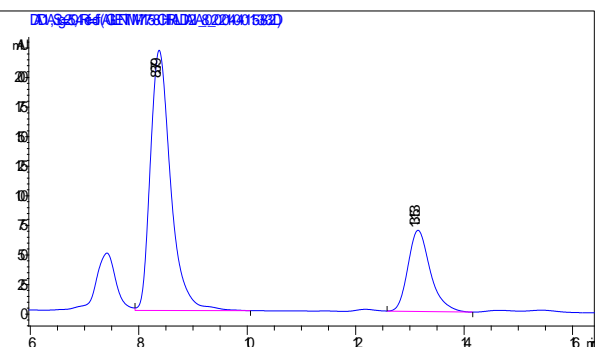
Peak #	RetTime [min]	Type	Width [min]	Area [mAU*s]	Height [mAU]	Area %
1	7.155	VW	0.1816	2767.11060	234.64130	25.8999
2	11.790	BB	0.4600	7916.74219	271.66791	74.1001



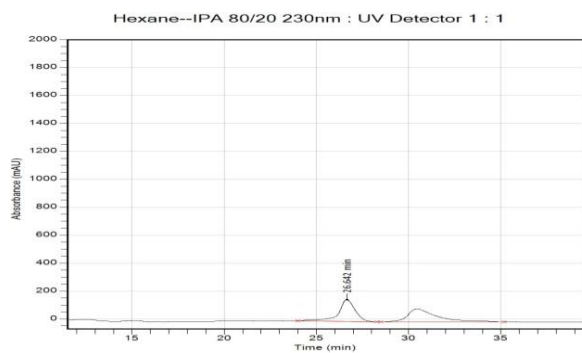
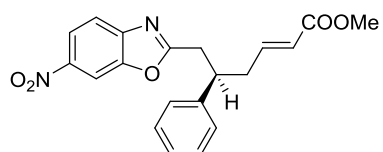
Peak #	RetTime [min]	Type	Width [min]	Area [mAU*s]	Height [mAU]	Area %
1	6.591	PP	0.1790	580.86761	54.09163	4.7920
2	9.518	BV	0.3499	1.15406e4	488.03561	95.2080



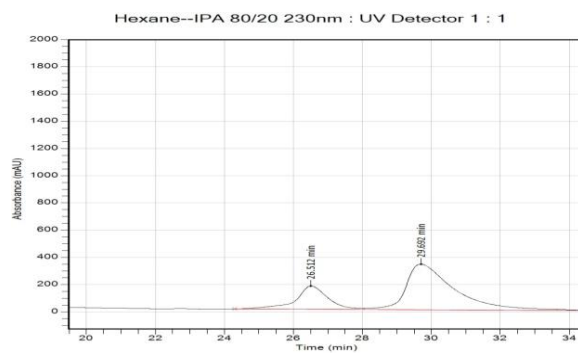
Peak #	RetTime [min]	Type	Width [min]	Area [mAU*s]	Height [mAU]	Area %
1	8.541	BB	0.4188	141.31070	5.13911	55.4663
2	13.431	BB	0.4391	113.45778	3.85745	44.5337



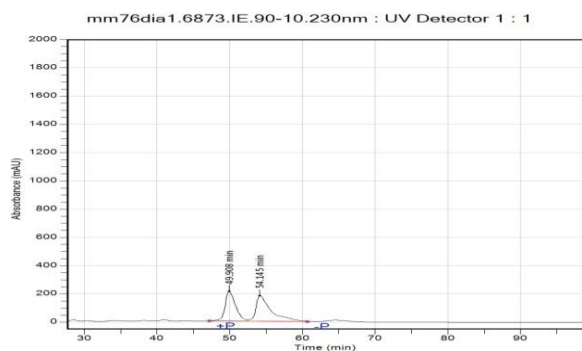
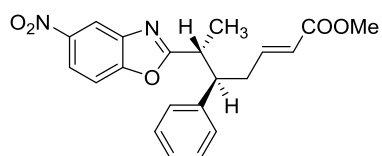
Peak #	RetTime [min]	Type	Width [min]	Area [mAU*s]	Height [mAU]	Area %
1	8.379	VB	0.4037	5727.57861	220.04338	74.4991
2	13.153	BB	0.4354	1960.53845	68.60152	25.5009



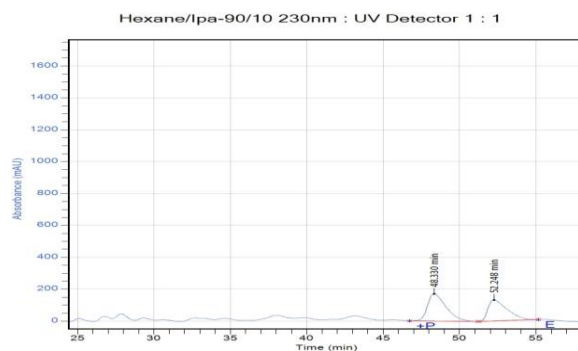
Time	Area	Area %
26.642	9,868,819.0	49.86
30.449	9,925,778.7	50.14
Total	19,794,597.7	100.00



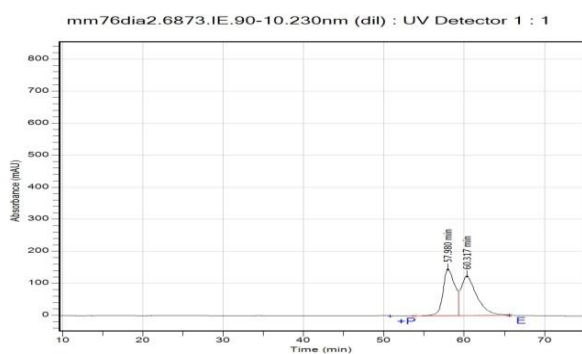
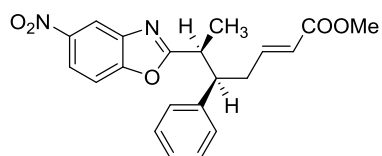
RT (min)	Component Name	Area
26.512		11,222,993.3
29.692		32,866,315.3
		44,089,308.5



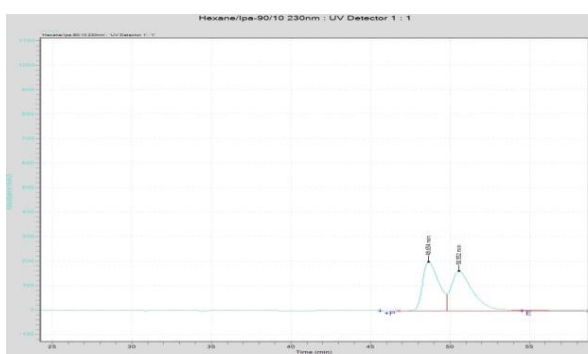
Time	Area	Area %
49.908	20,810,350.0	44.78
54.145	25,659,890.0	55.22
Total	46,470,239.9	100.00

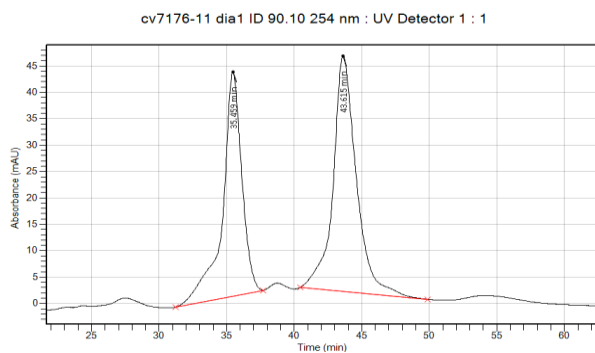
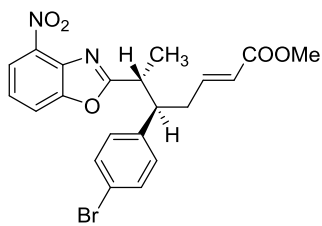


RT (min)	Component Name	Area
48.330		14,412,452.0
52.248		11,373,318.3
		25,785,770.3

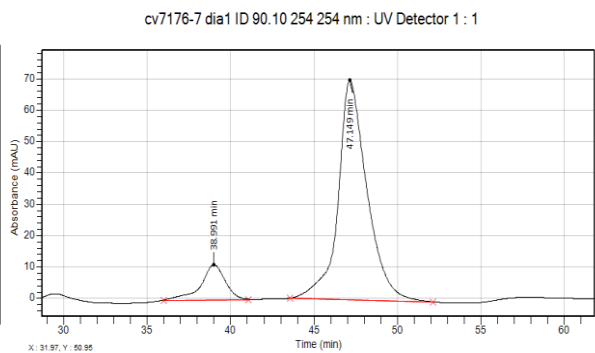


Time	Area	Area %
57.980	15,015,760.1	47.10
60.317	16,863,109.5	52.90
Total	31,878,869.6	100.00

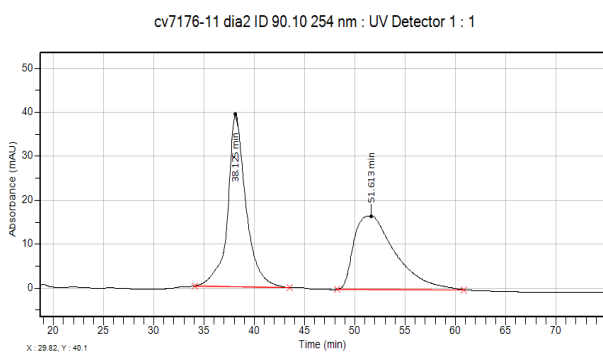
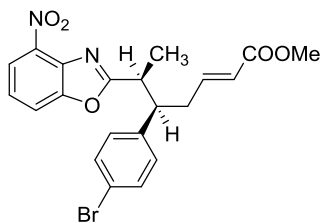




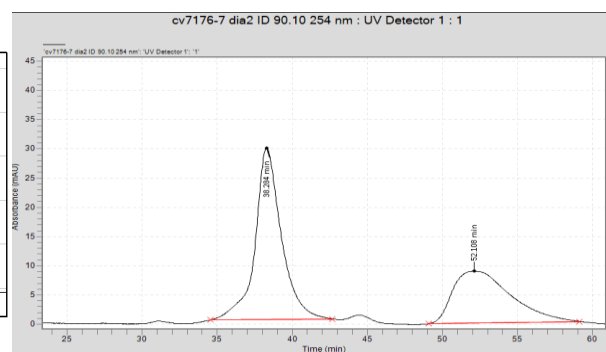
Time	Area	Area %
35.459	4,237,406.9	44.11
43.615	5,368,427.7	55.89
Total	9,605,834.6	100.00



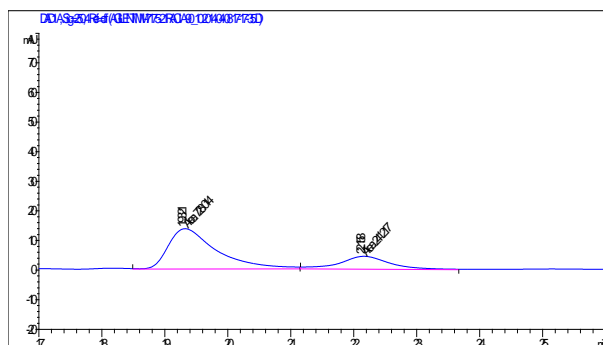
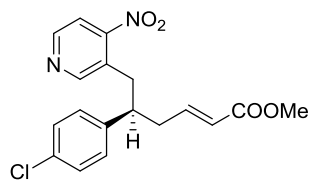
Time	Area	Area %
38.991	1,119,249.3	11.70
47.149	8,444,089.8	88.30
Total	9,563,339.1	100.00



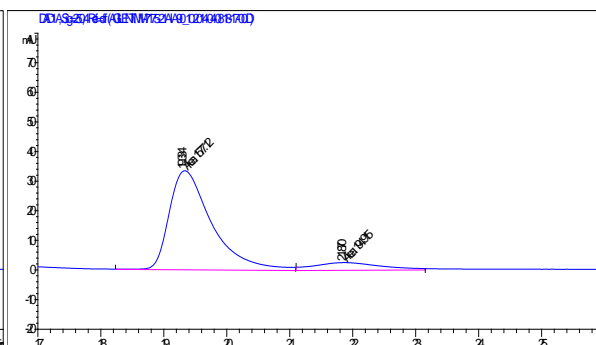
Time	Area	Area %
38.125	4,950,916.4	50.77
51.613	4,800,525.3	49.23
Total	9,751,441.6	100.00



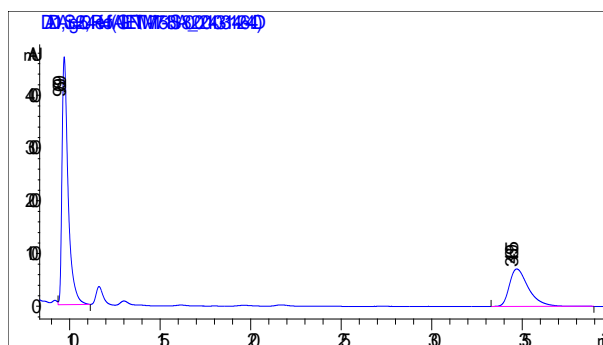
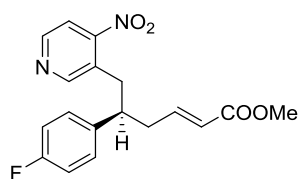
Time	Area	Area %
38.284	3,573,784.3	60.08
52.108	2,374,163.3	39.92
Total	5,947,947.6	100.00



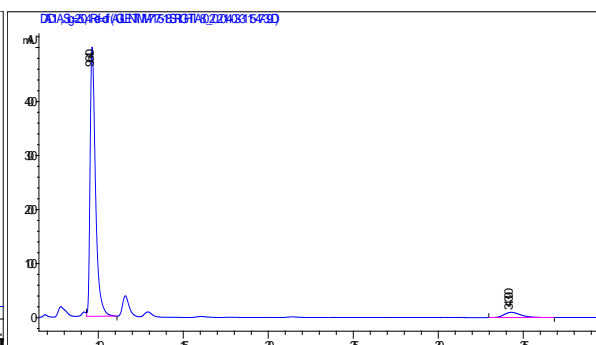
Peak #	RetTime [min]	Type	Width [min]	Area [mAU*s]	Height [mAU]	Area %
1	19.321	MM	0.8907	728.01398	13.62255	75.1126
2	22.158	MM	0.9260	241.21671	4.34142	24.8874



Peak #	RetTime [min]	Type	Width [min]	Area [mAU*s]	Height [mAU]	Area %
1	19.334	MM	0.7853	1577.11682	33.47267	89.0005
2	21.870	MM	1.2381	194.91499	2.62380	10.9995



Peak #	RetTime [min]	Type	Width [min]	Area [mAU*s]	Height [mAU]	Area %
1	9.699	VB	0.3518	1.10190e4	469.52493	68.1249
2	34.695	BB	1.0922	5155.69336	70.91628	31.8751

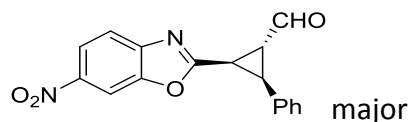


Peak #	RetTime [min]	Type	Width [min]	Area [mAU*s]	Height [mAU]	Area %
1	9.640	VB	0.3357	1.10045e4	498.29498	94.3172
2	34.300	BB	0.9807	663.03918	9.68516	5.6828

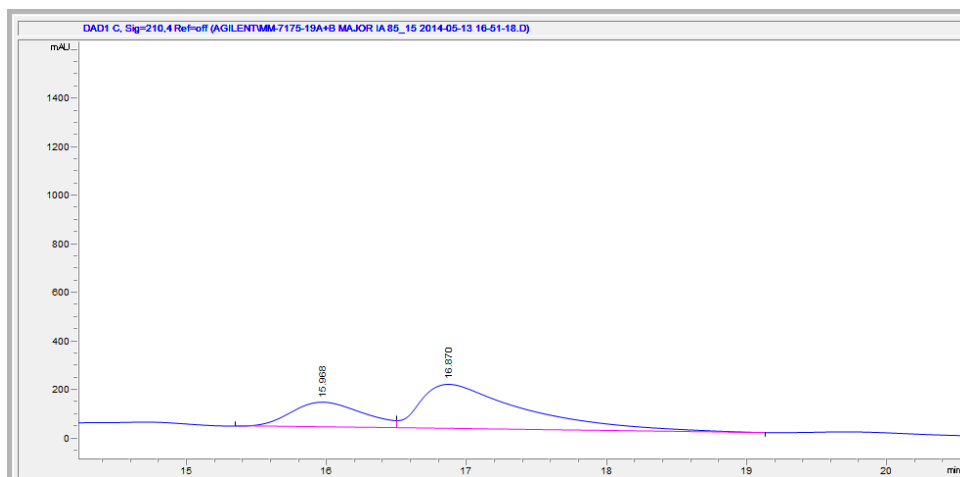
Synergistic catalysis: syn-cyclopropanation of benzoxazoles

HPLC traces

The racemic mixtures used in the HPLC traces were prepared by mixing the product obtained using the organic catalyst with the R configuration and the product obtained using the organic catalyst with the S configuration.

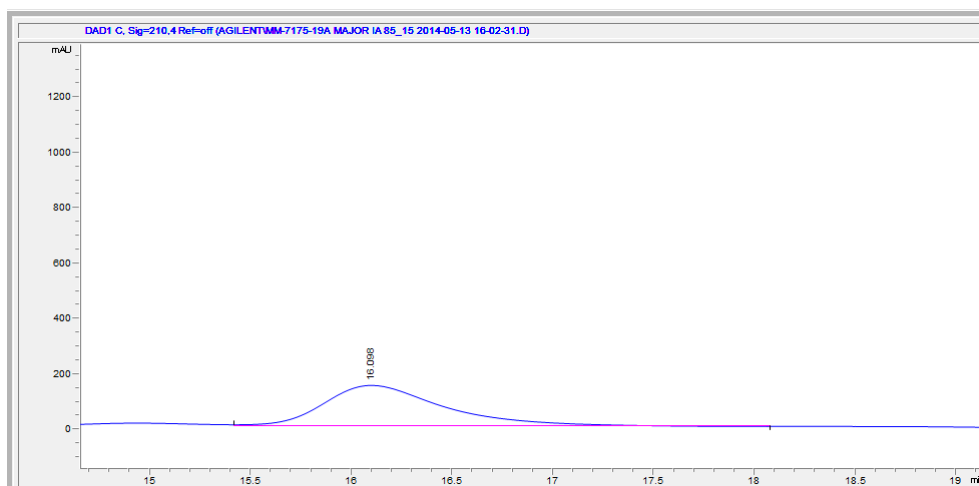


Mixture of S and R: (IA, 85.15, 210, 1ml/min)



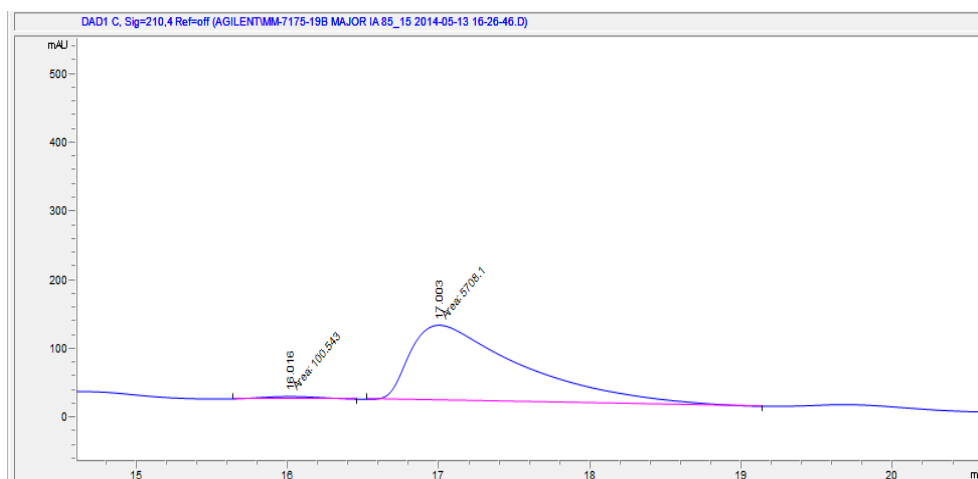
Peak #	RetTime [min]	Type	Width [min]	Area [mAU*s]	Height [mAU]	Area %
1	15.968	BV	0.5569	3712.38623	102.91290	28.3069
2	16.870	VB	0.7268	9402.38672	182.58131	71.6931

Chiral S:

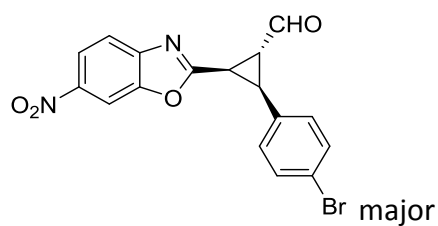


Peak #	RetTime [min]	Type	Width [min]	Area [mAU*s]	Height [mAU]	Area %
1	16.098	VB	0.6283	6266.22656	147.88811	100.0000

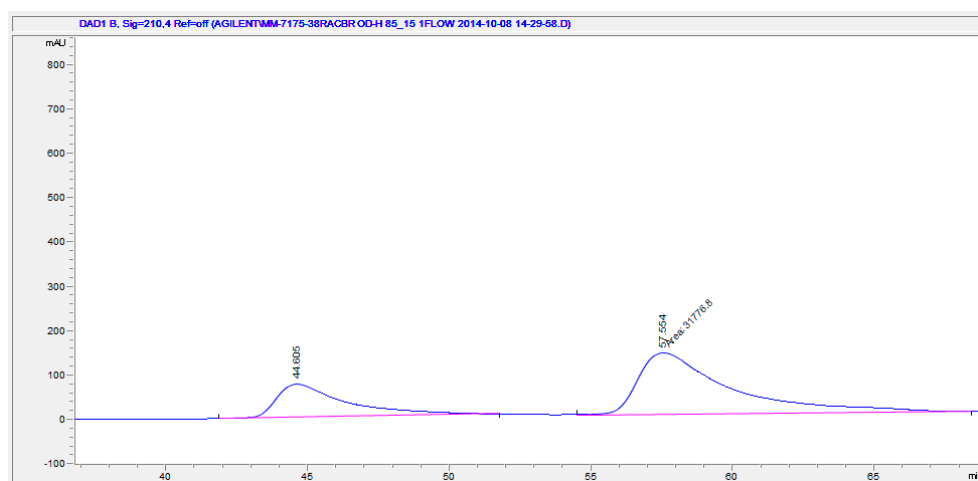
Chiral R:



Peak #	RetTime [min]	Type	Width [min]	Area [mAU*s]	Height [mAU]	Area %
1	16.016	MM	0.4590	100.54274	3.65084	1.7309
2	17.003	MM	0.8683	5708.09961	109.55972	98.2691

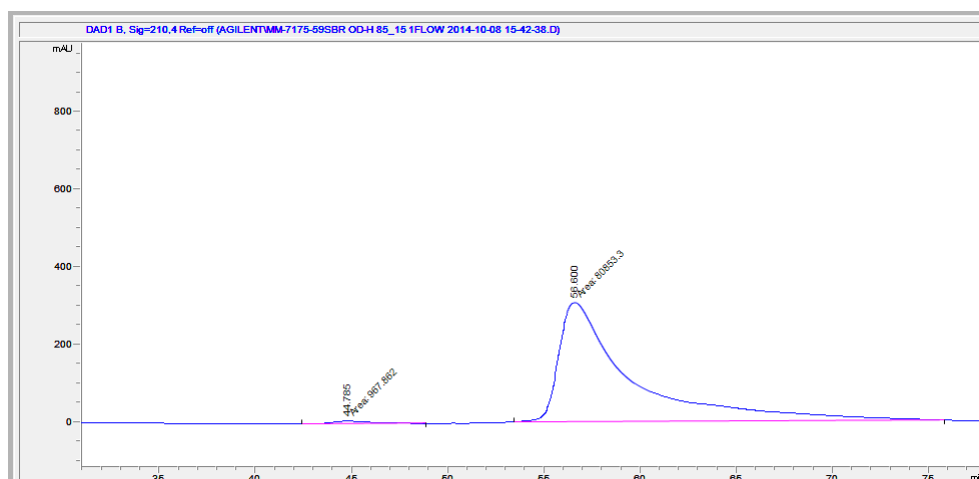


Mixture of S and R: (OD-H, 85.15, 210 nm, 1ml/min)



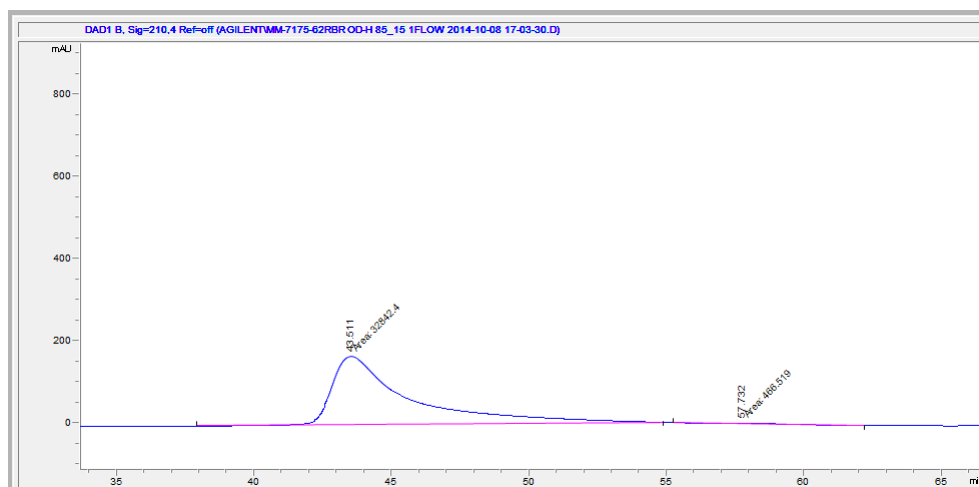
Peak #	RetTime [min]	Type	Width [min]	Area [mAU*s]	Height [mAU]	Area %
1	44.605	BB	2.2703	1.28171e4	75.13073	28.7418
2	57.554	MM	3.7924	3.17768e4	139.64941	71.2582

Chiral S:

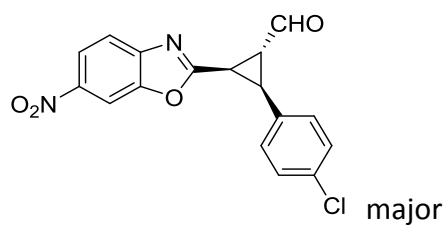


Peak #	RetTime [min]	Type	Width [min]	Area [mAU*s]	Height [mAU]	Area %
1	44.785	MM	2.3673	967.86176	6.81401	1.1829
2	56.600	MM	4.3933	8.08533e4	306.72745	98.8171

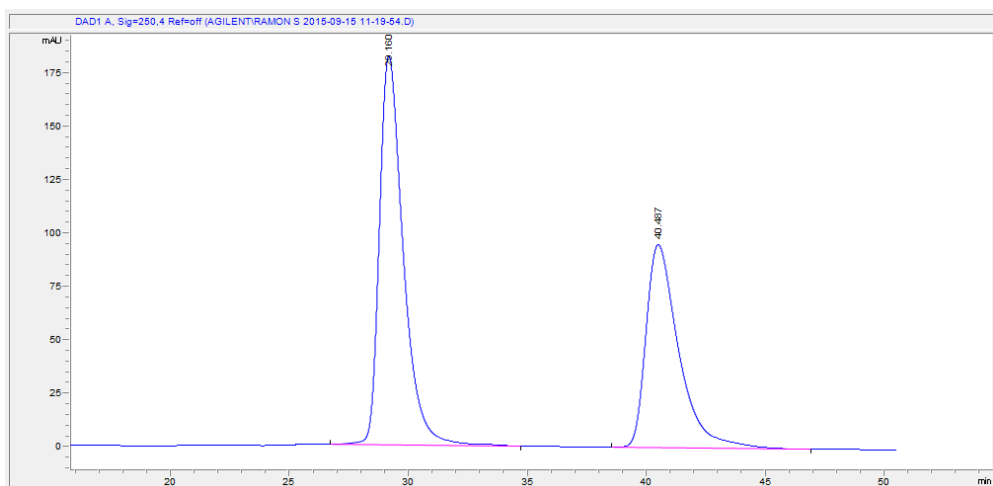
Chiral R:



Peak #	RetTime [min]	Type	Width [min]	Area [mAU*s]	Height [mAU]	Area %
1	43.511	MM	3.2714	3.28424e4	167.31866	98.5994
2	57.732	MM	3.1711	466.51904	2.45191	1.4006

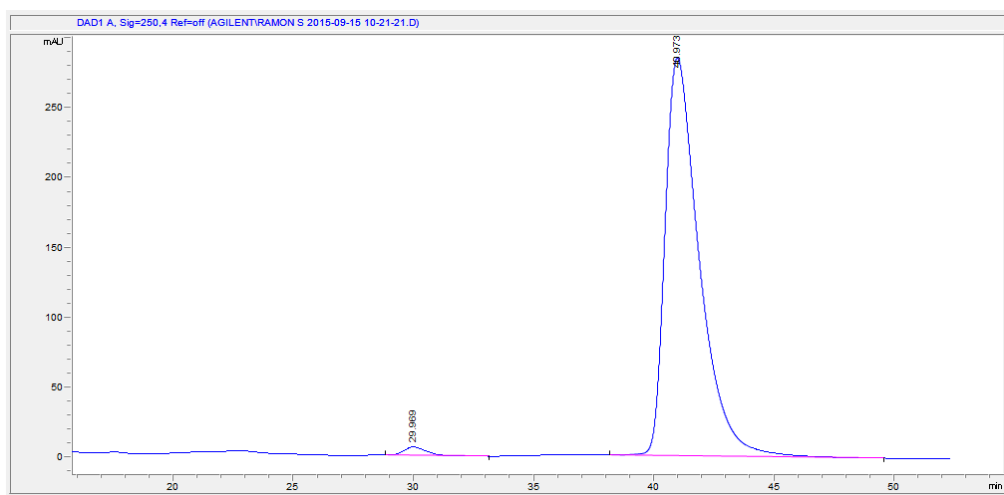


Mixture of S and R: (OD-H, 80.20, 250 nm, 1ml/min)



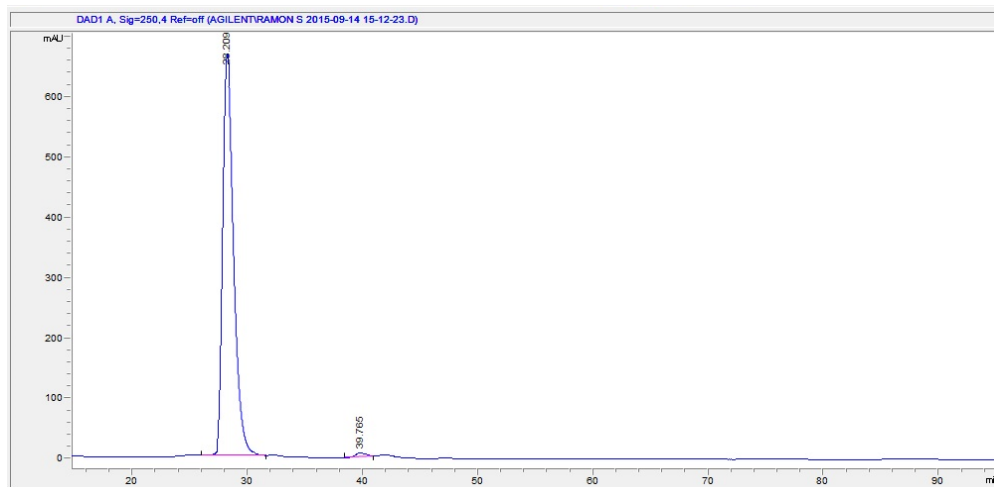
Peak #	RetTime [min]	Type	Width [min]	Area [mAU*s]	Height [mAU]	Area %
1	29.160	BB	1.0484	1.27333e4	182.41916	58.2436
2	40.487	BB	1.4318	9128.81836	95.27521	41.7564

Chiral S:

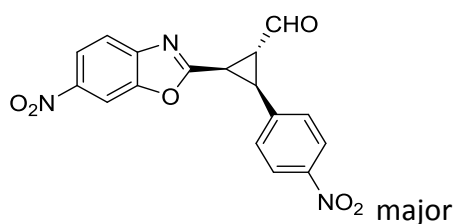


Peak #	RetTime [min]	Type	Width [min]	Area [mAU*s]	Height [mAU]	Area %
1	29.969	BB	0.8179	392.81580	6.01512	1.3698
2	40.973	BB	1.4759	2.82844e4	285.48447	98.6302

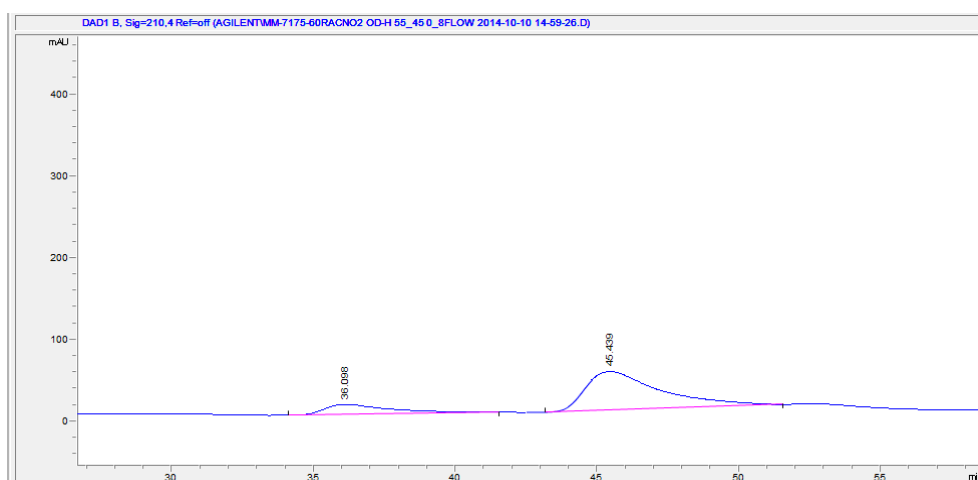
Chiral R:



Peak #	RetTime [min]	Type	Width [min]	Area [mAU*s]	Height [mAU]	Area %
1	28.209	BB	1.0039	4.38354e4	665.96399	99.0009
2	39.765	BB	0.8426	442.39969	6.32062	0.9991

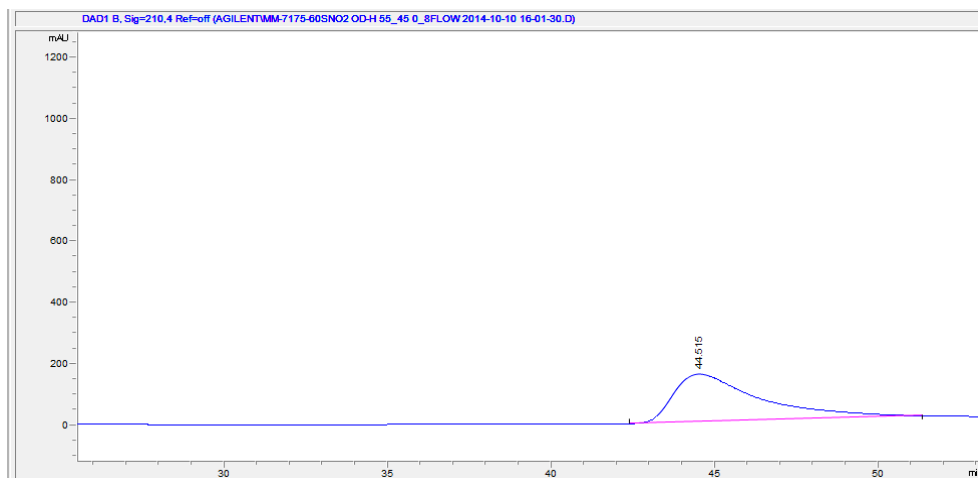


Mixture of S and R: (OD-H, 55.45, 210 nm, 0.8 ml/min)



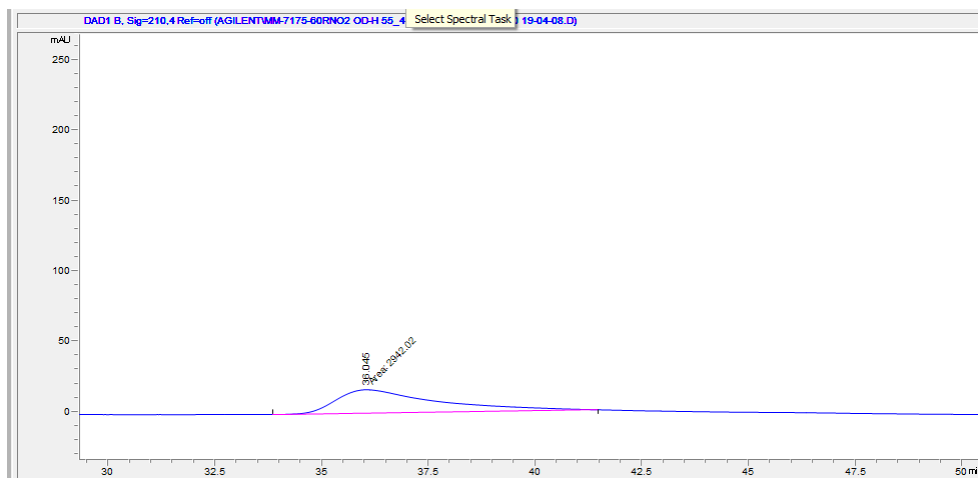
Peak #	RetTime [min]	Type	Width [min]	Area [mAU*s]	Height [mAU]	Area %
1	36.098	BB	1.9035	2012.17493	12.43705	18.9008
2	45.439	BB	2.1550	8633.78027	47.31137	81.0992

Chiral S:

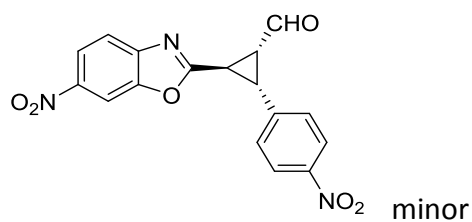


Peak #	RetTime [min]	Type	Width [min]	Area [mAU*s]	Height [mAU]	Area %
1	44.515	BB	2.5273	2.83576e4	155.96089	100.0000

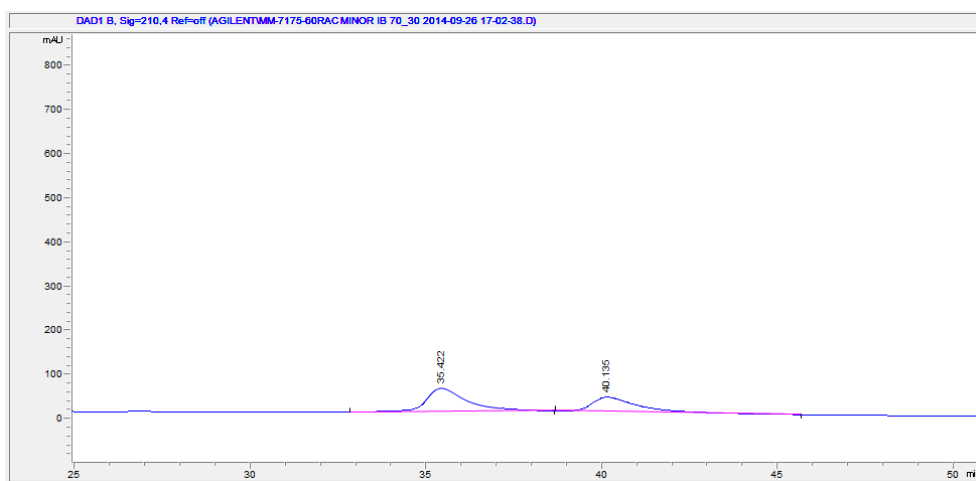
Chiral R:



Peak #	RetTime [min]	Type	Width [min]	Area [mAU*s]	Height [mAU]	Area %
1	36.045	MM	2.8547	2942.01685	17.17661	100.0000

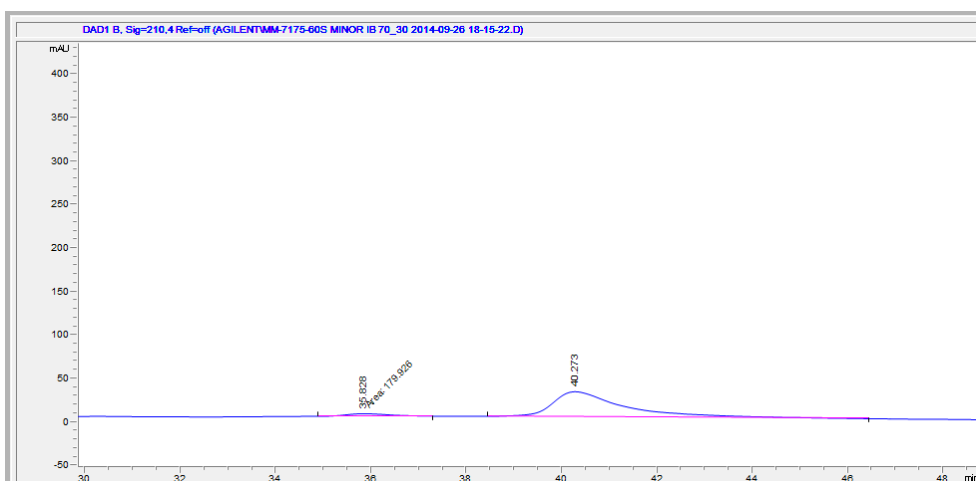


Mixture of S and R: (IB, 70.30, 210 nm, 1 ml/min)



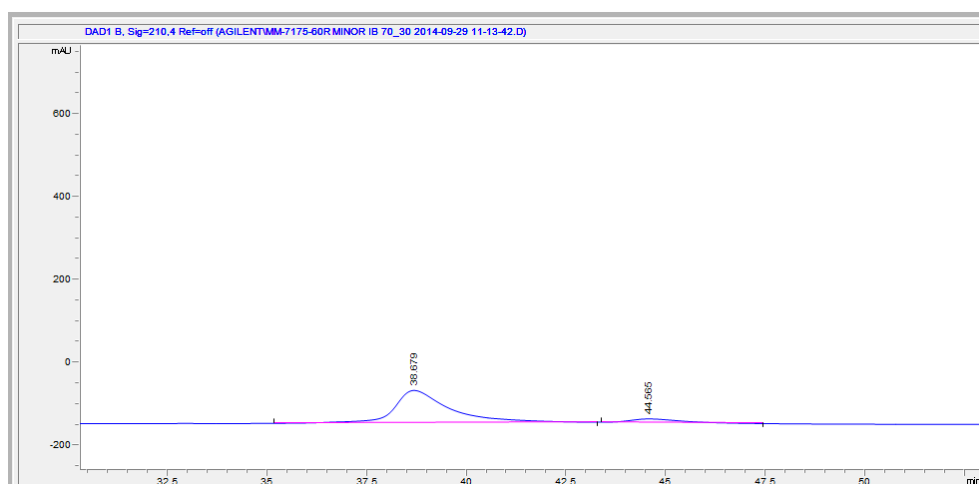
Peak #	RetTime [min]	Type	Width [min]	Area [mAU*s]	Height [mAU]	Area %
1	35.422	BB	1.1864	4404.99756	53.17717	59.1106
2	40.135	BB	1.2752	3047.12915	32.75777	40.8894

Chiral S:

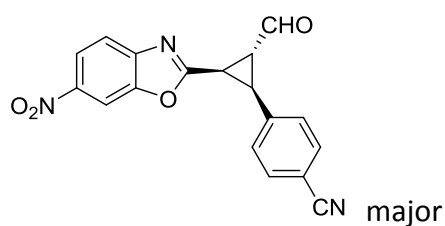


Peak #	RetTime [min]	Type	Width [min]	Area [mAU*s]	Height [mAU]	Area %
1	35.828	MM	1.0256	179.92630	2.92397	5.4440
2	40.273	BB	1.4220	3125.11719	28.93576	94.5560

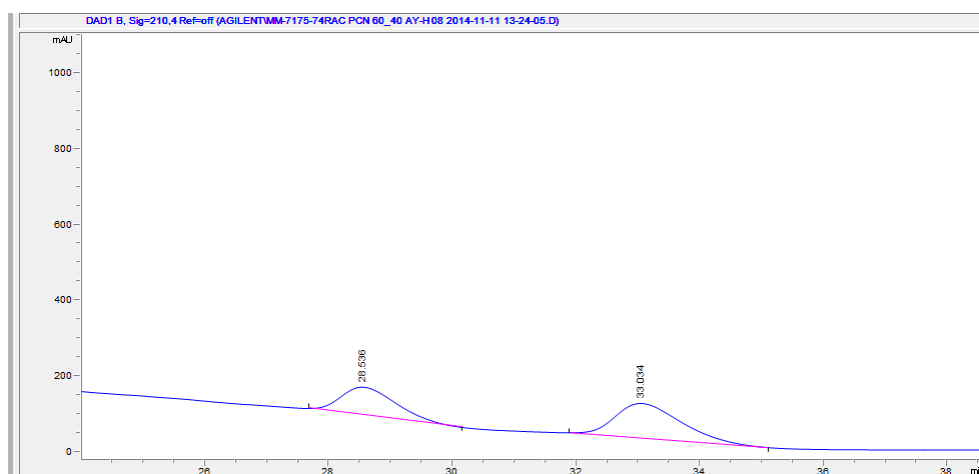
Chiral R:



Peak #	RetTime [min]	Type	Width [min]	Area [mAU*s]	Height [mAU]	Area %
1	38.679	BB	1.3699	7624.45313	78.03210	90.6252
2	44.565	BB	1.1033	788.72156	8.85343	9.3748

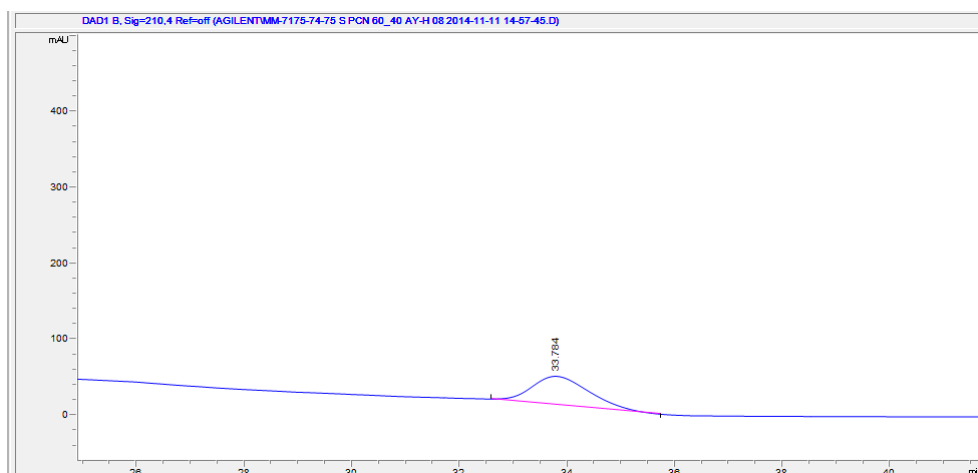


Mixture of S and R: (AY-H, 60.40, 210 nm, 0.8 ml/min)



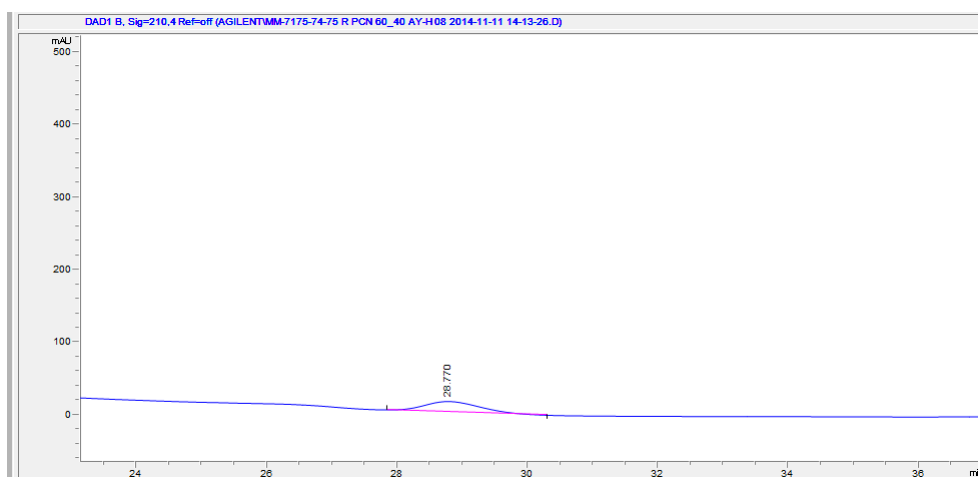
Peak #	RetTime [min]	Type	Width [min]	Area [mAU*s]	Height [mAU]	Area %
1	28.536	BB	0.9626	4597.28223	73.81712	40.1968
2	33.034	BB	1.1206	6839.66553	91.66003	59.8032

Chiral S:

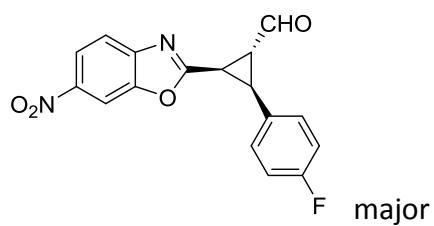


Peak #	RetTime [min]	Type	Width [min]	Area [mAU*s]	Height [mAU]	Area %
1	33.784	BB	1.1124	2820.95850	37.55339	100.0000

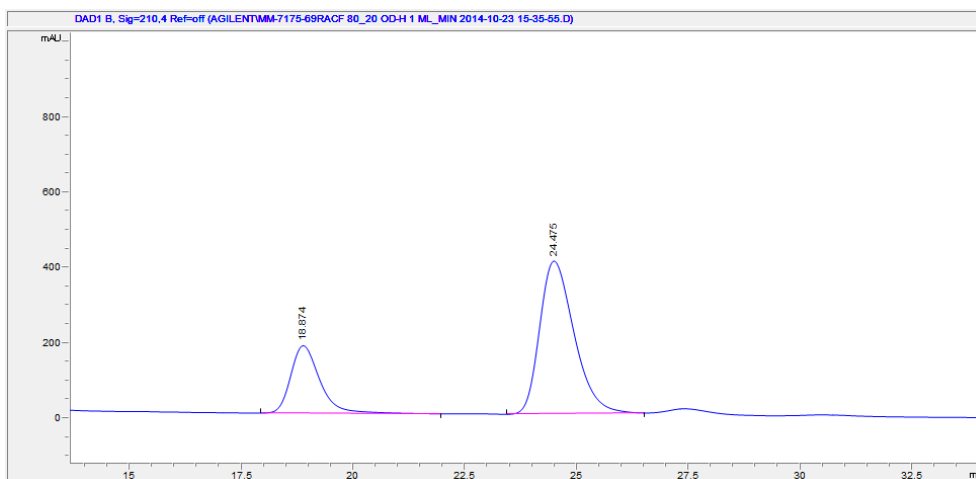
Chiral R:



Peak #	RetTime [min]	Type	Width [min]	Area [mAU*s]	Height [mAU]	Area %
1	28.770	BB	0.8675	854.49066	14.33286	100.0000

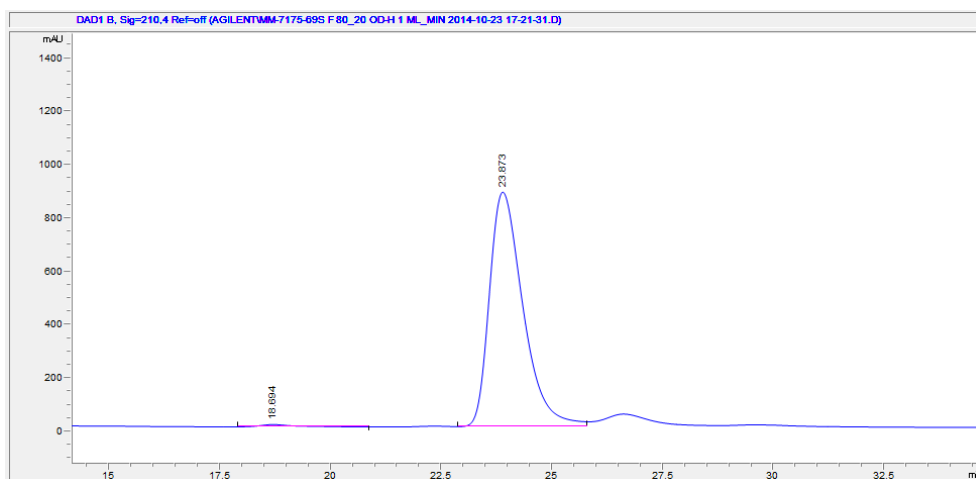


Mixture of S and R: (OD-H, 80.20, 210 nm, 1 ml/min)



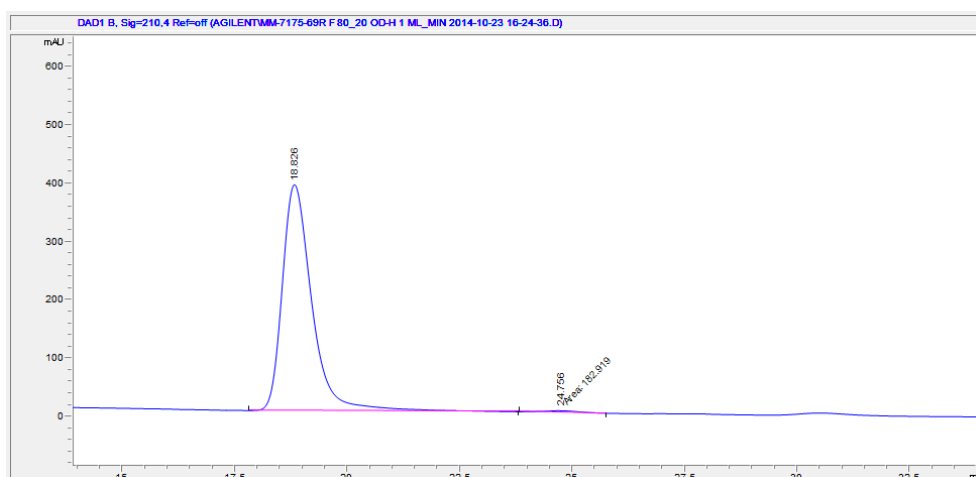
Peak #	RetTime [min]	Type	Width [min]	Area [mAU*s]	Height [mAU]	Area %
1	18.874	BB	0.6916	8130.86133	179.11133	27.3120
2	24.475	BB	0.8246	2.16394e4	405.50552	72.6880

Chiral S:

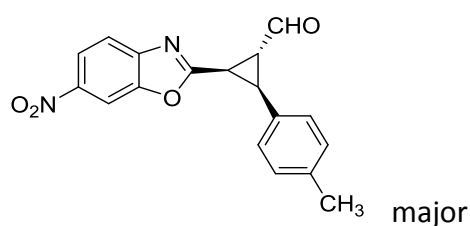


Peak #	RetTime [min]	Type	Width [min]	Area [mAU*s]	Height [mAU]	Area %
1	18.826	BB	0.6974	1.77314e4	386.41232	98.9789
2	24.756	MM	0.9648	182.91948	3.15982	1.0211

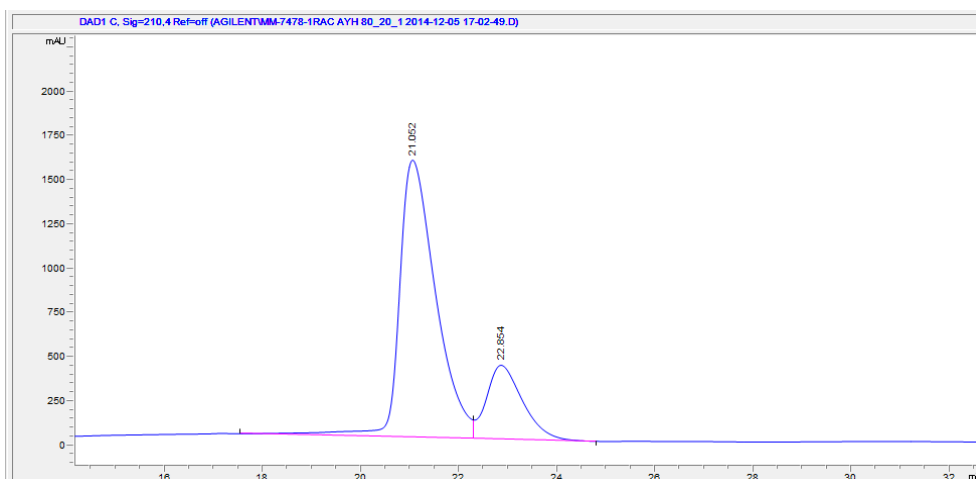
Chiral R:



Peak #	RetTime [min]	Type	Width [min]	Area [mAU*s]	Height [mAU]	Area %
1	18.694	BB	0.7854	476.68951	8.53718	1.0226
2	23.873	BV	0.8031	4.61405e4	878.01160	98.9774

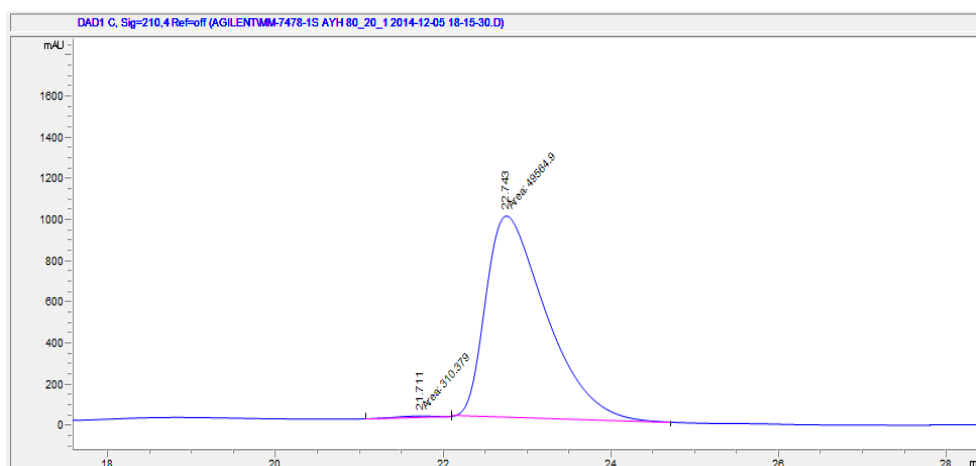


Mixture of S and R: (AY-H, 80.20, 210 nm, 1 ml/min)



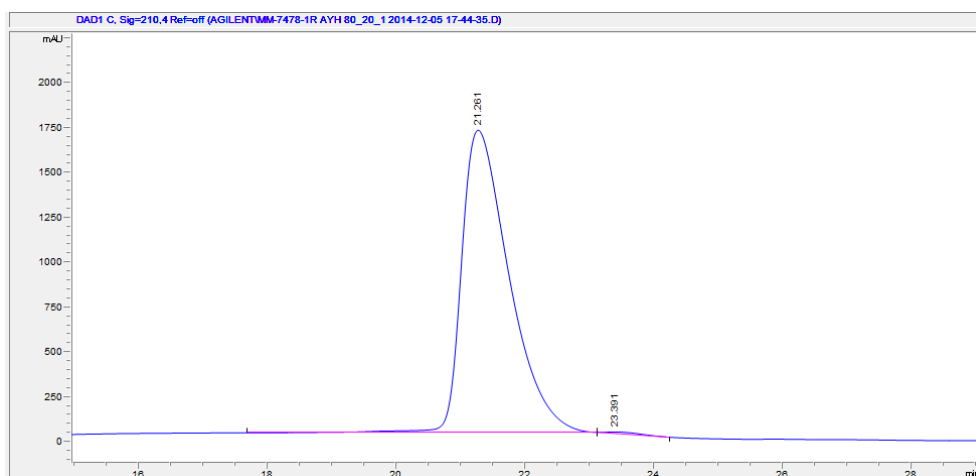
Peak #	RetTime [min]	Type	Width [min]	Area [mAU*s]	Height [mAU]	Area %
1	21.052	BV	0.7827	8.09678e4	1567.39832	79.1073
2	22.854	VB	0.7699	2.13840e4	418.67255	20.8927

Chiral S:

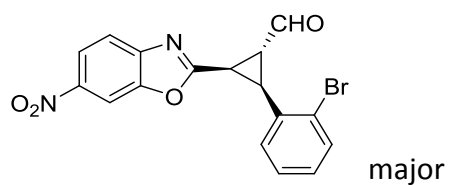


Peak #	RetTime [min]	Type	Width [min]	Area [mAU*s]	Height [mAU]	Area %
1	21.711	MM	0.6588	310.37949	7.85263	0.6223
2	22.743	MM	0.8401	4.95649e4	983.27905	99.3777

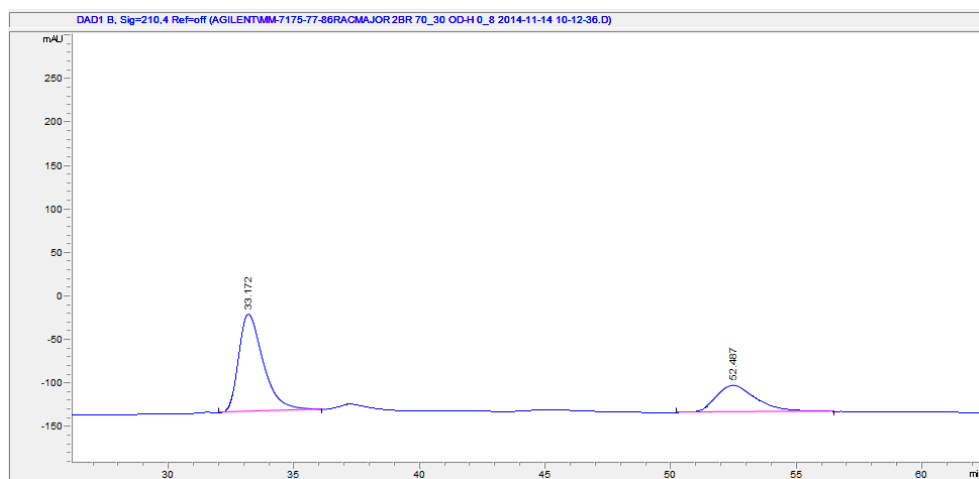
Chiral R:



Peak #	RetTime [min]	Type	Width [min]	Area [mAU*s]	Height [mAU]	Area %
1	21.261	BB	0.7802	8.60503e4	1683.88342	99.5977
2	23.391	BB	0.6158	347.60397	8.45234	0.4023

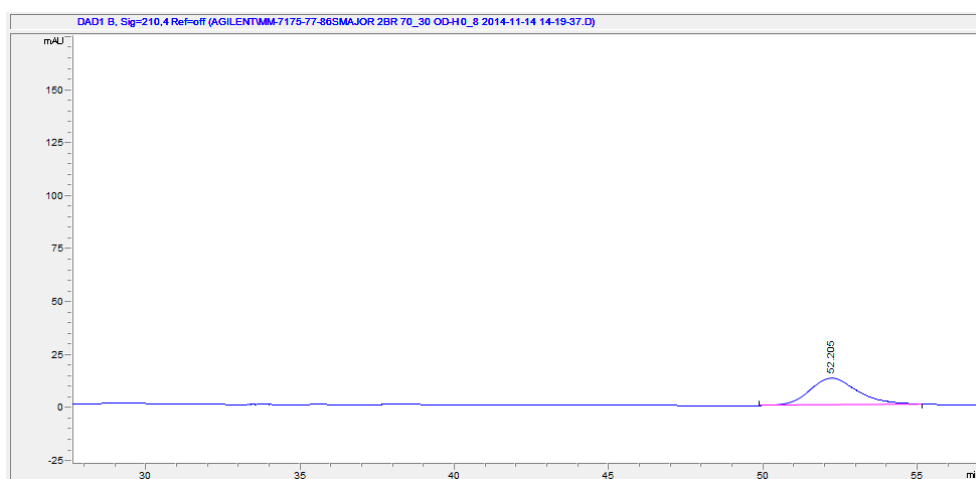


Mixture of S and R: (OD-H, 70.30, 210 nm, 0.8 ml/min)



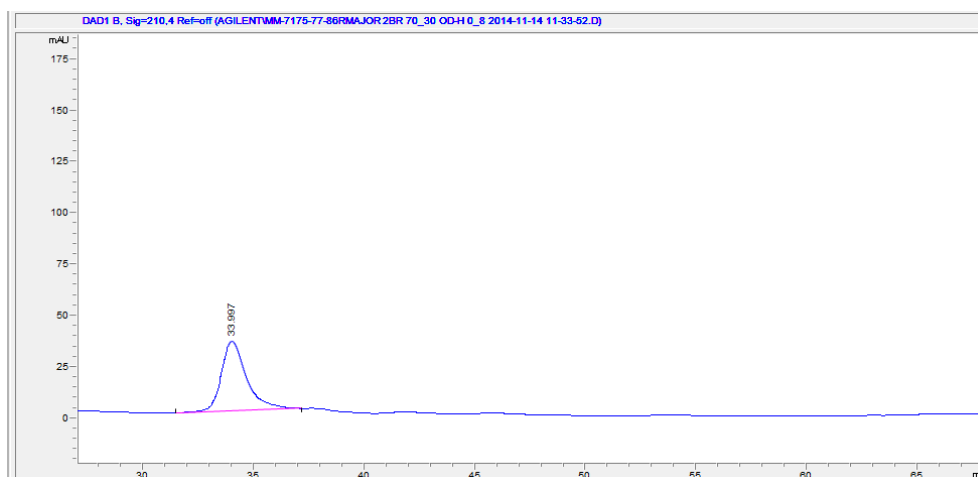
Peak #	RetTime [min]	Type	Width [min]	Area [mAU*s]	Height [mAU]	Area %
1	33.172	BB	1.0412	7677.73486	112.07510	69.1795
2	52.487	BB	1.4034	3420.53955	30.66447	30.8205

Chiral S:

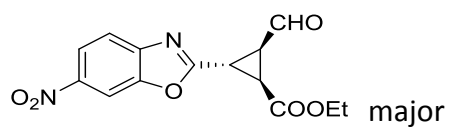


Peak #	RetTime [min]	Type	Width [min]	Area [mAU*s]	Height [mAU]	Area %
1	52.205	BB	1.2947	1362.70691	12.59043	100.0000

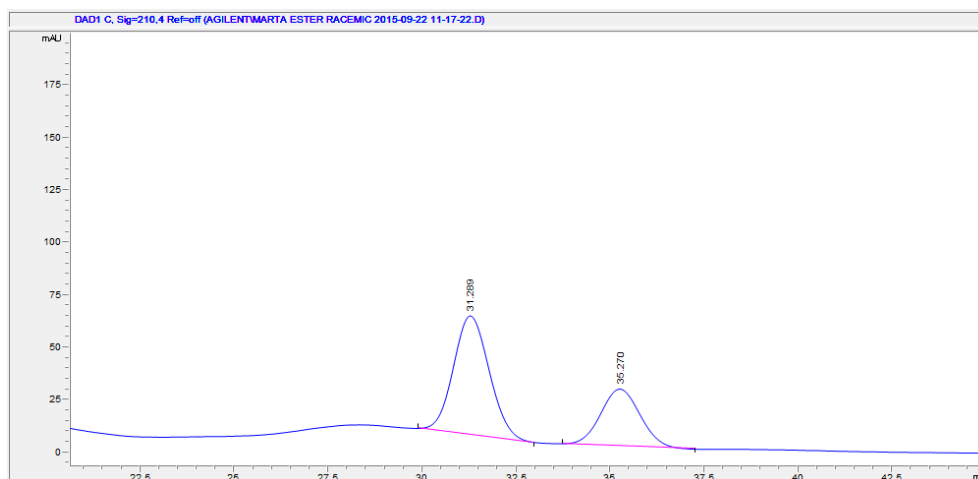
Chiral R:



Peak #	RetTime [min]	Type	Width [min]	Area [mAU*s]	Height [mAU]	Area %
1	33.997	BB	1.1382	2712.94531	34.09796	100.0000

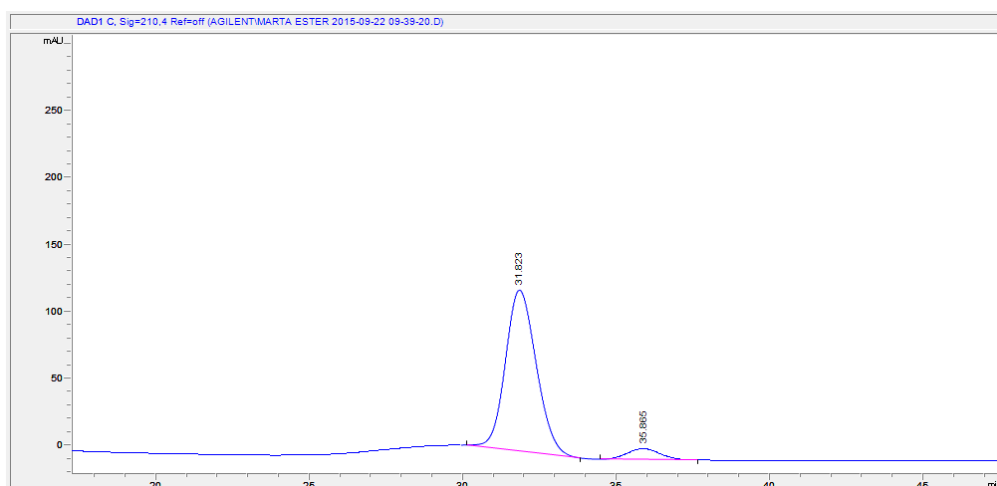


Mixture of S and R: (AY-H, 50.50, 210 nm, 1 ml/min)



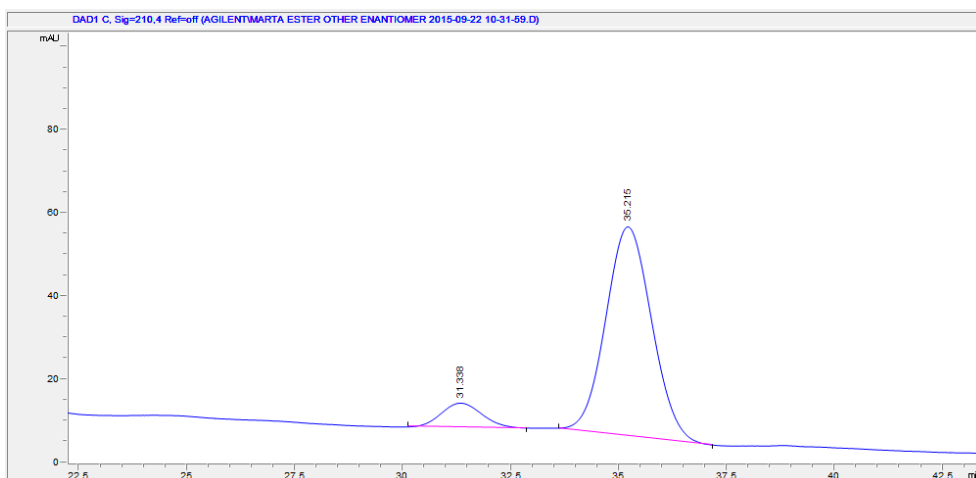
Peak #	RetTime [min]	Type	Width [min]	Area [mAU*s]	Height [mAU]	Area %
1	31.289	BB	1.0116	3765.18457	56.78594	65.3319
2	35.270	BB	1.0351	1997.97766	27.26040	34.6681

Chiral S:

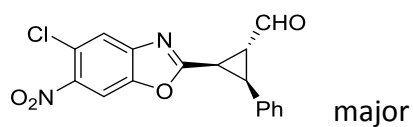


Peak #	RetTime [min]	Type	Width [min]	Area [mAU*s]	Height [mAU]	Area %
1	31.823	BB	1.0799	8389.00195	120.24745	93.3400
2	35.865	BB	0.8745	598.56952	8.11550	6.6600

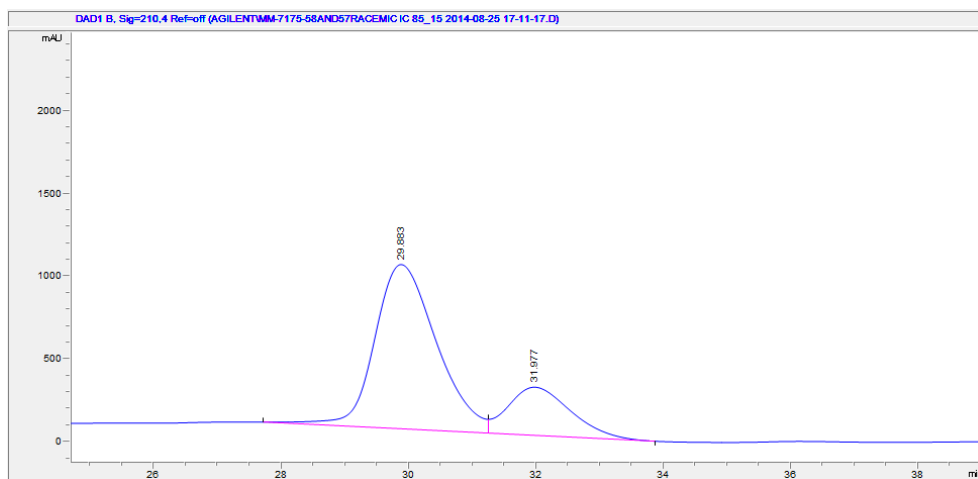
Chiral R:



Peak #	RetTime [min]	Type	Width [min]	Area [mAU*s]	Height [mAU]	Area %
1	31.338	BB	0.7819	385.97067	5.87918	9.3632
2	35.215	BB	1.1297	3736.24438	50.46899	90.6368

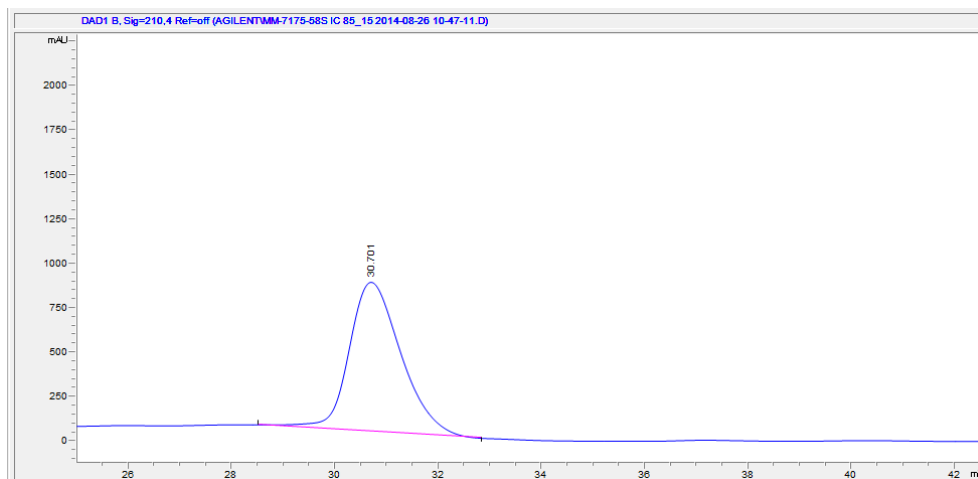


Mixture of S and R: (IC, 85.15, 210 nm, 1 ml/min)



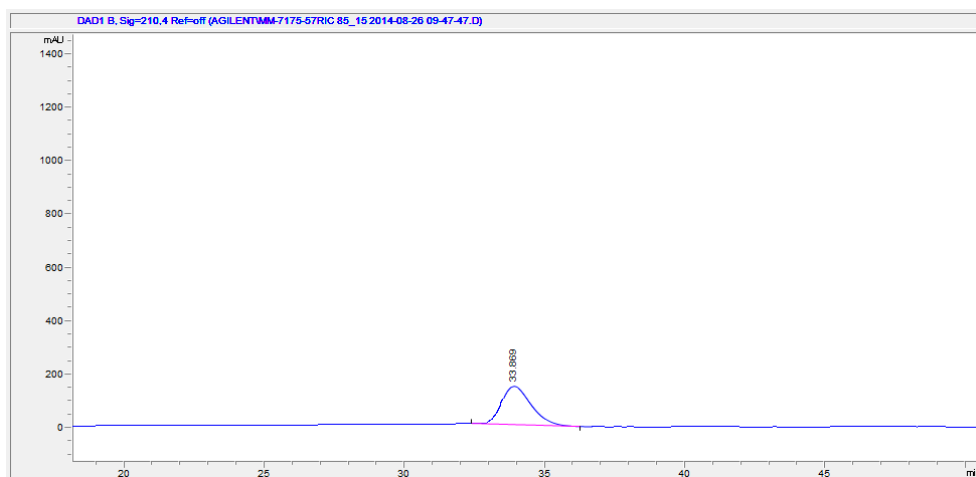
Peak #	RetTime [min]	Type	Width [min]	Area [mAU*s]	Height [mAU]	Area %
1	29.883	BV	1.0365	6.70024e4	991.41626	77.1635
2	31.977	VB	1.0480	1.98293e4	290.62515	22.8365

Chiral S:

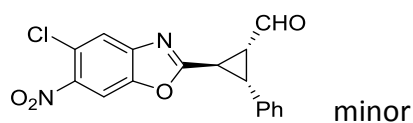


Peak #	RetTime [min]	Type	Width [min]	Area [mAU*s]	Height [mAU]	Area %
1	30.701	BB	1.0580	5.91403e4	843.49738	100.0000

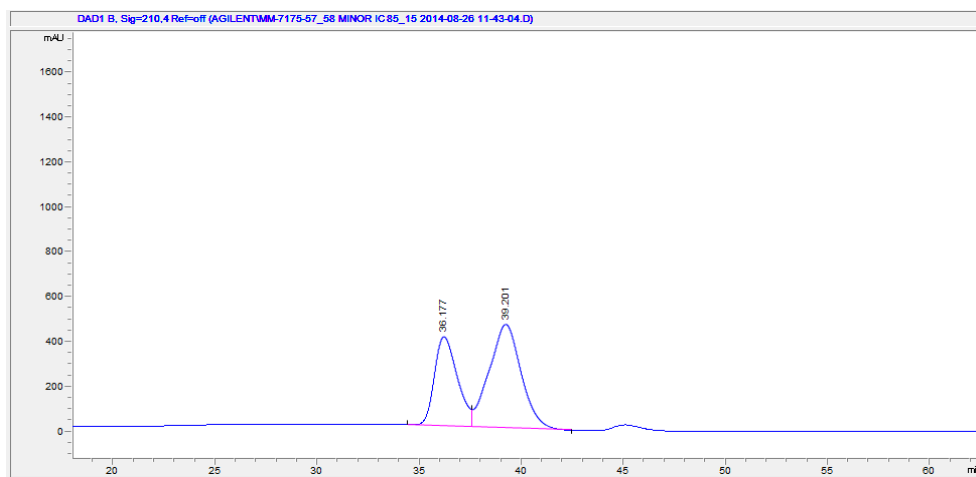
Chiral R:



Peak #	RetTime [min]	Type	Width [min]	Area [mAU*s]	Height [mAU]	Area %
1	33.869	BB	1.1023	1.04667e4	143.95297	100.0000

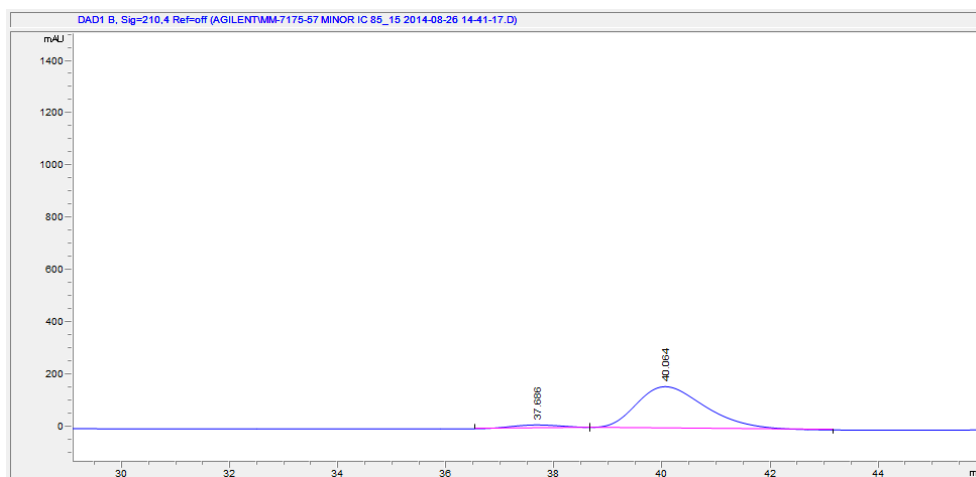


Mixture of S and R: (IC, 85.15, 210 nm, 1 ml/min)

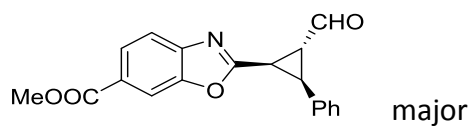


Peak #	RetTime [min]	Type	Width [min]	Area [mAU*s]	Height [mAU]	Area %
1	36.177	BV	1.1856	3.10209e4	396.98383	38.1902
2	39.201	VB	1.5418	5.02063e4	462.02722	61.8098

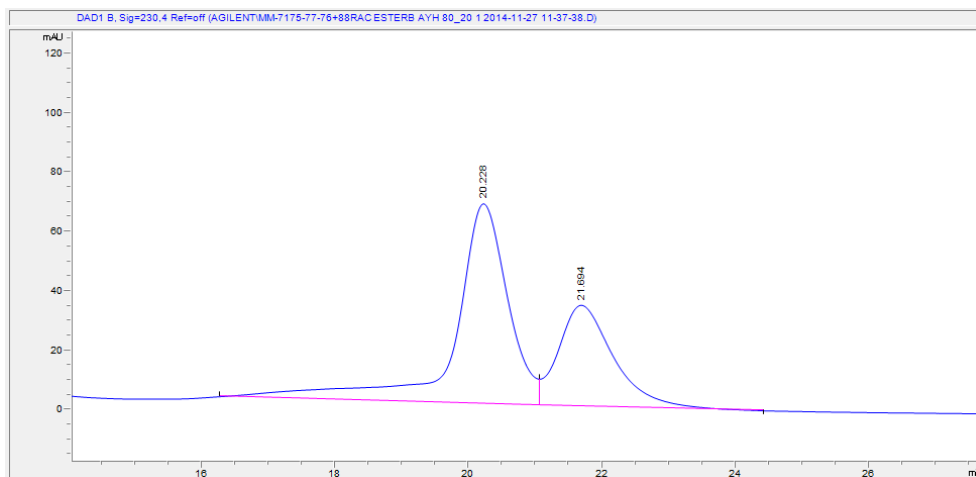
Chiral R:



Peak #	RetTime [min]	Type	Width [min]	Area [mAU*s]	Height [mAU]	Area %
1	37.686	BB	0.8948	733.99097	11.75006	4.9646
2	40.064	BB	1.3182	1.40506e4	158.49655	95.0354

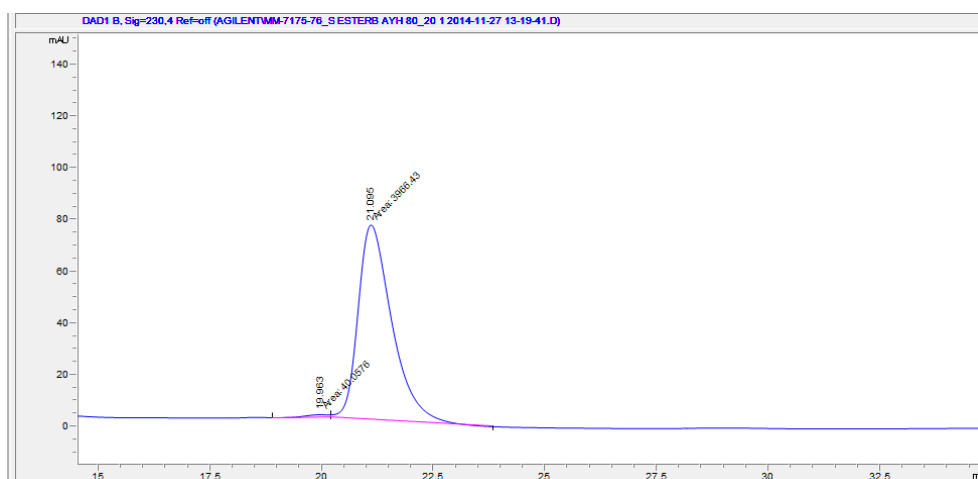


Mixture of S and R: (AY-H, 80.20, 230 nm, 1ml/min)



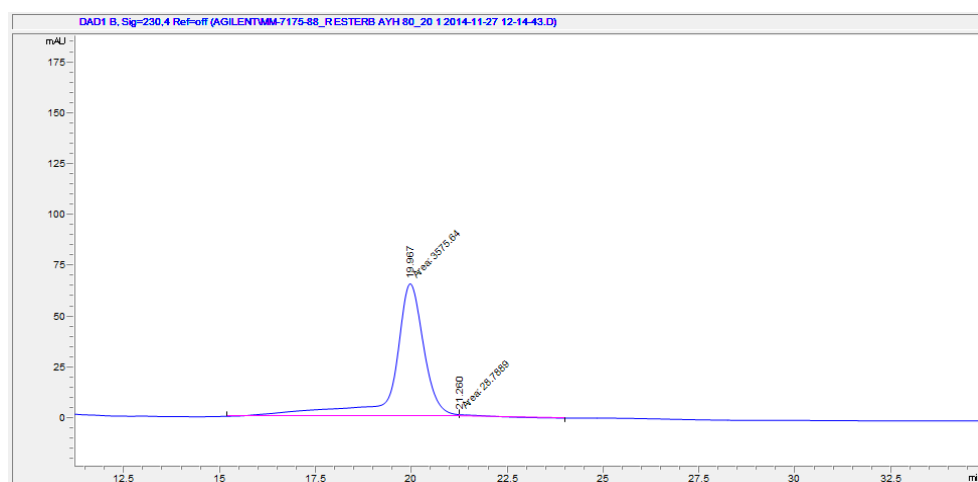
Peak #	RetTime [min]	Type	Width [min]	Area [mAU*s]	Height [mAU]	Area %
1	20.228	BV	0.8164	3785.40845	67.48930	65.8862
2	21.694	VB	0.8453	1959.96216	34.06174	34.1138

Chiral S:

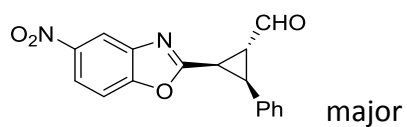


Peak #	RetTime [min]	Type	Width [min]	Area [mAU*s]	Height [mAU]	Area %
1	19.963	MM	0.6765	40.05763	9.86947e-1	0.9998
2	21.095	MM	0.8796	3966.42554	75.15952	99.0002

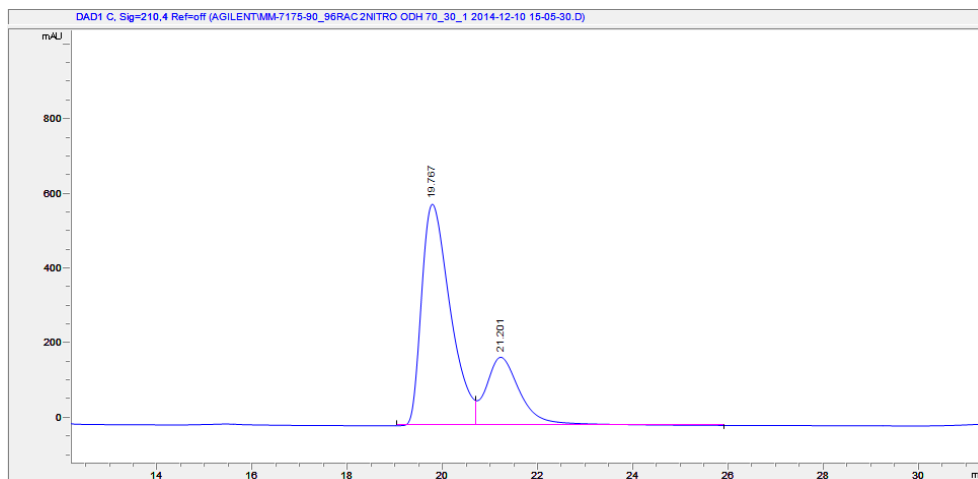
Chiral R:



Peak #	RetTime [min]	Type	Width [min]	Area [mAU*s]	Height [mAU]	Area %
1	19.967	MM	0.9136	3575.64111	65.23161	99.2013
2	21.260	MM	0.5517	28.78887	6.16726e-1	0.7987

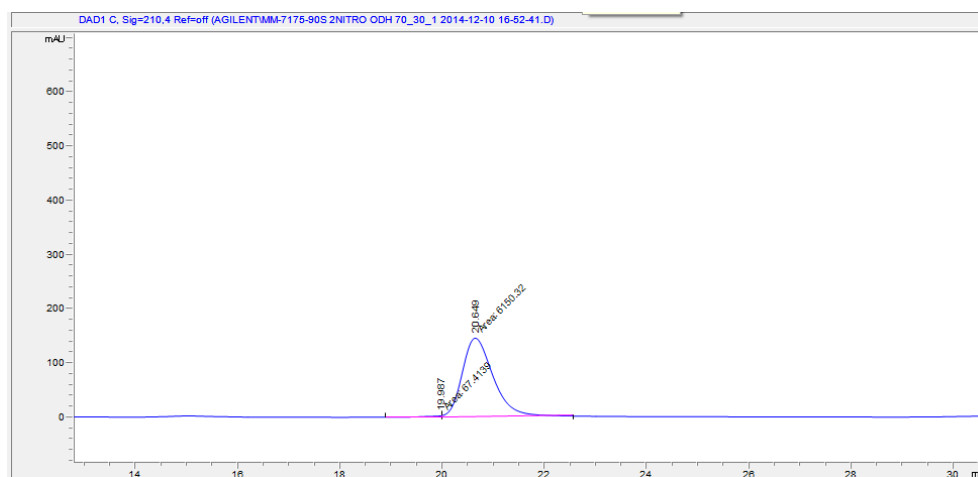


Mixture of S and R: (OD-H, 70.30, 210 nm, 1 ml/min)



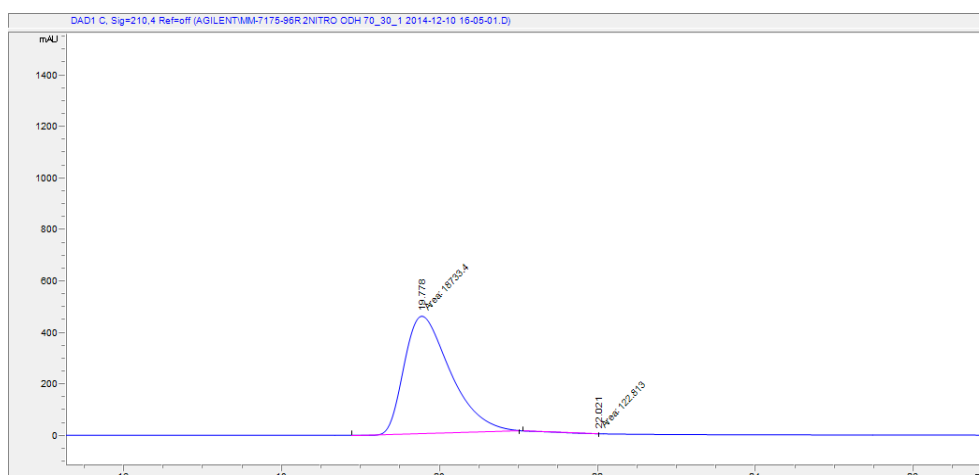
Peak #	RetTime [min]	Type	Width [min]	Area [mAU*s]	Height [mAU]	Area %
1	19.767	BV	0.6455	2.49488e4	594.60162	72.7906
2	21.201	VB	0.7510	9325.92969	183.46526	27.2094

Chiral S:

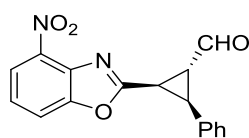


Peak #	RetTime [min]	Type	Width [min]	Area [mAU*s]	Height [mAU]	Area %
1	19.987	MM	0.3926	67.41388	2.86209	1.0842
2	20.649	MM	0.7032	6150.31982	145.77878	98.9158

Chiral R:

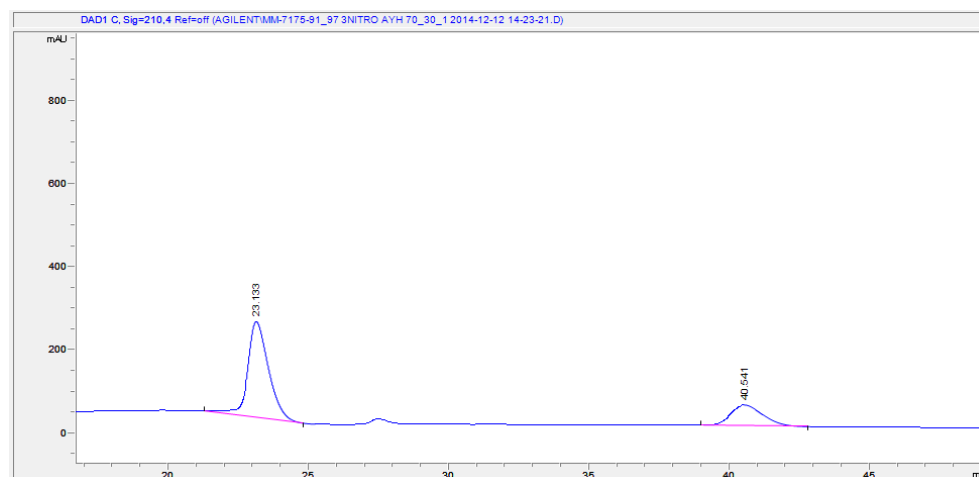


Peak #	RetTime [min]	Type	Width [min]	Area [mAU*s]	Height [mAU]	Area %
1	19.778	MM	0.6811	1.87334e4	458.38950	99.3487
2	22.021	MM	0.5521	122.81274	3.70713	0.6513



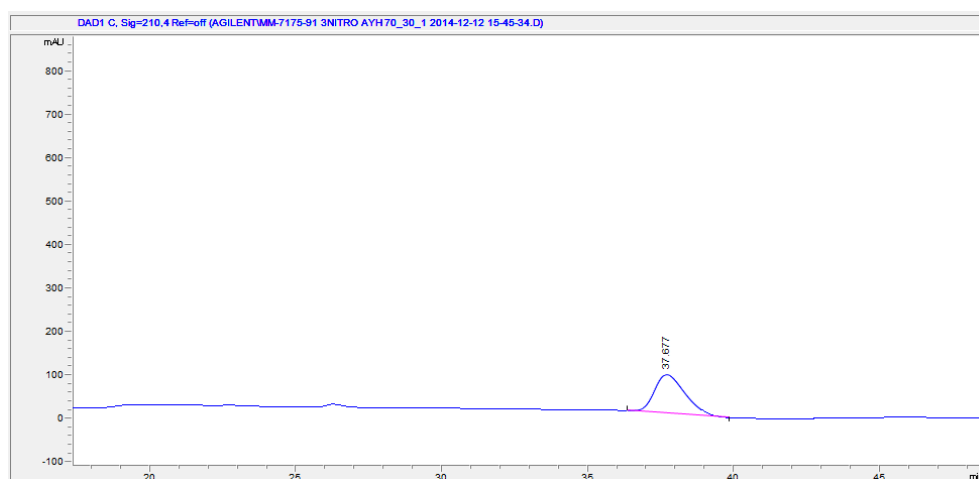
major

Mixture of S and R: (AY-H, 70.30, 210 nm, 1 ml/min)



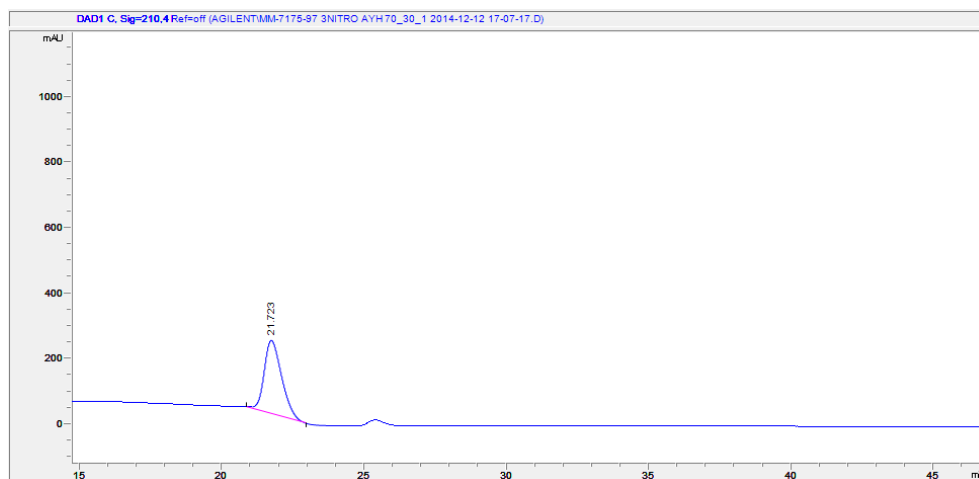
Peak #	RetTime [min]	Type	Width [min]	Area [mAU*s]	Height [mAU]	Area %
1	23.132	BB	0.7765	9084.07031	176.49504	74.9754
2	40.541	BB	1.1741	3031.99414	38.19610	25.0246

Chiral S:

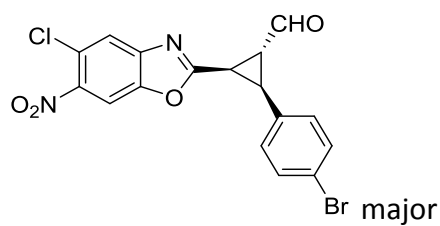


Peak #	RetTime [min]	Type	Width [min]	Area [mAU*s]	Height [mAU]	Area %
1	37.677	BB	1.1013	6581.40137	89.35355	100.0000

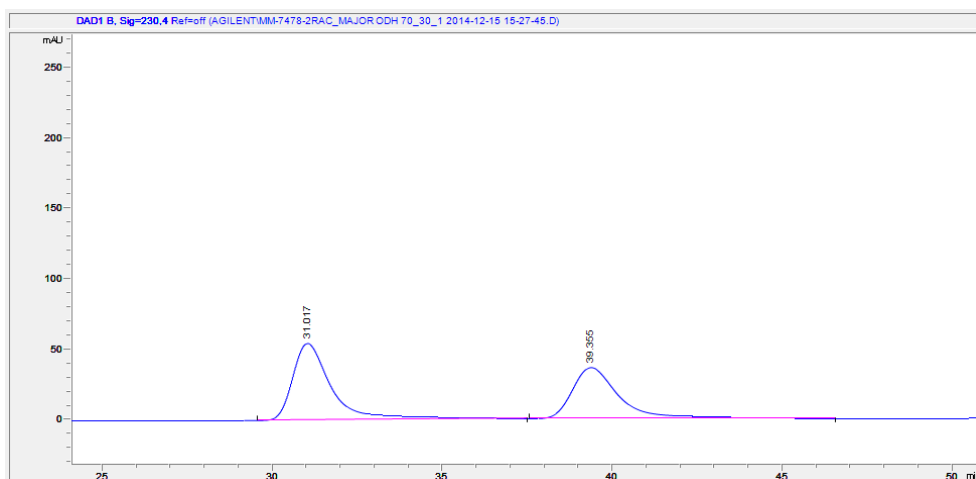
Chiral R:



Peak #	RetTime [min]	Type	Width [min]	Area [mAU*s]	Height [mAU]	Area %
1	21.723	BB	0.6580	9639.62207	224.94237	100.0000

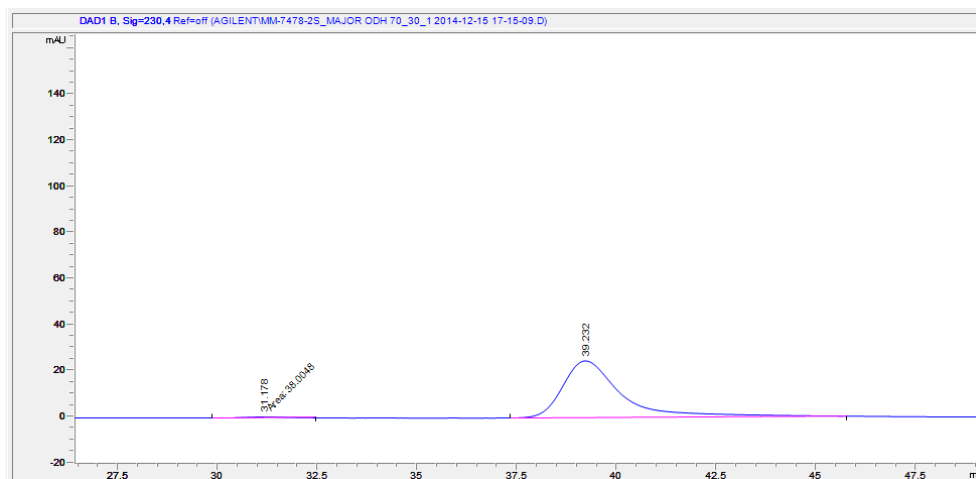


Mixture of S and R: (OD-H, 70.30, 230 nm, 1 ml/min)



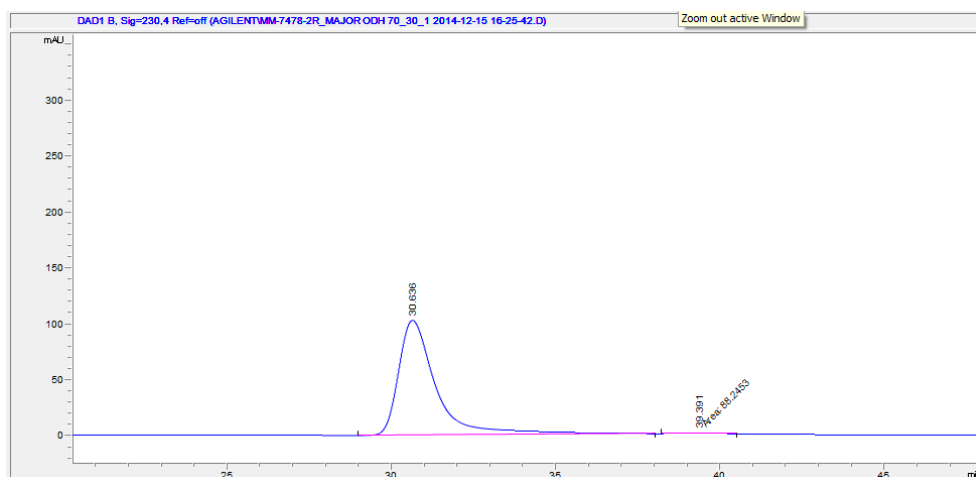
Peak #	RetTime [min]	Type	Width [min]	Area [mAU*s]	Height [mAU]	Area %
1	31.017	BB	1.1881	4379.56885	54.58246	55.2011
2	39.355	BB	1.3760	3554.28076	36.43872	44.7989

Chiral S:

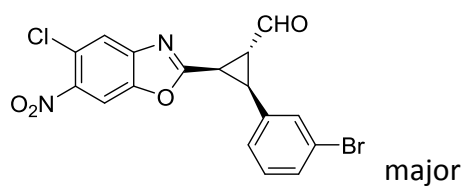


Peak #	RetTime [min]	Type	Width [min]	Area [mAU*s]	Height [mAU]	Area %
1	31.178	MM	1.2502	38.00478	5.06661e-1	1.4972
2	39.232	BB	1.4477	2500.42114	24.56225	98.5028

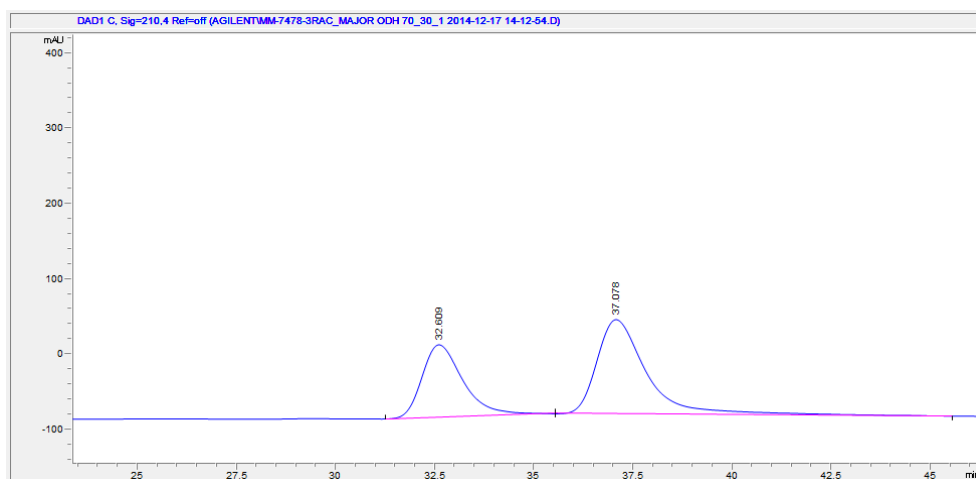
Chiral R:



Peak #	RetTime [min]	Type	Width [min]	Area [mAU*s]	Height [mAU]	Area %
1	30.636	BB	1.1803	8144.36621	102.36057	98.9281
2	39.391	MM	1.3601	88.24529	1.08140	1.0719

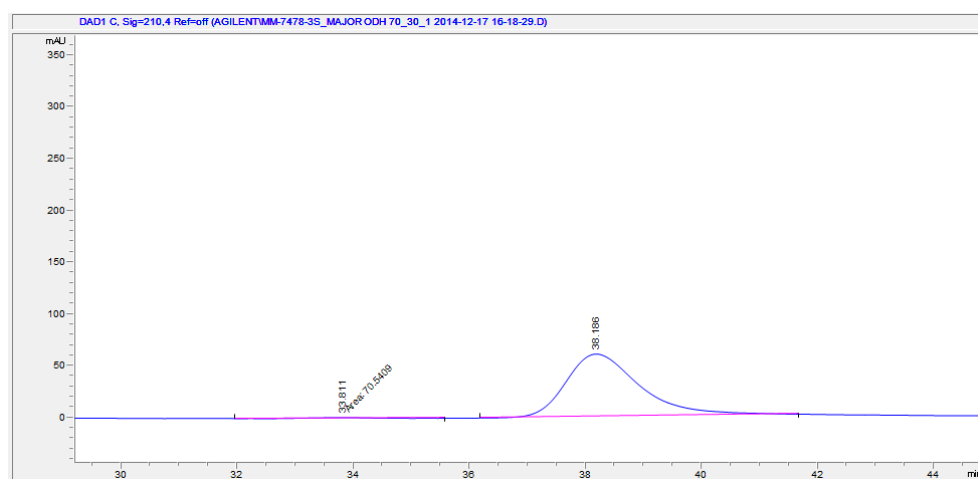


Mixture of S and R: (OD-H, 70.30, 210 nm, 1 ml/min)



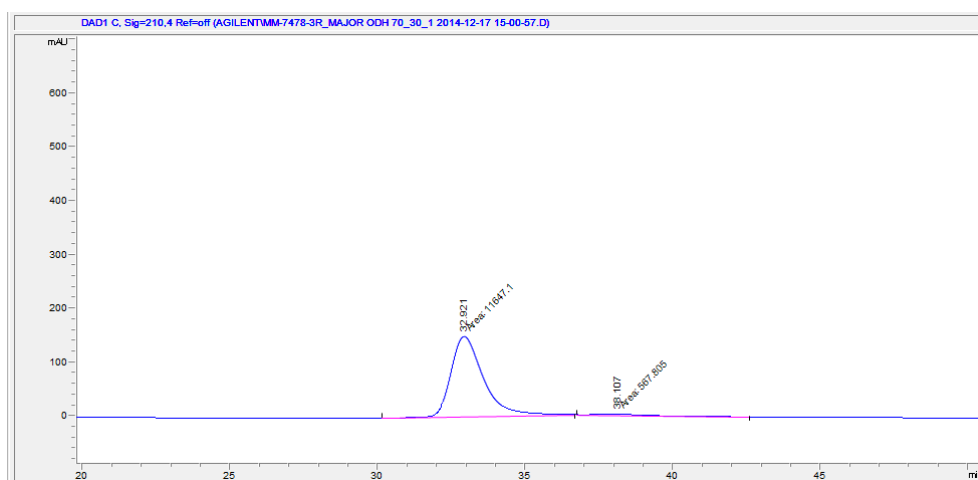
Peak #	RetTime [min]	Type	Width [min]	Area [mAU*s]	Height [mAU]	Area %
1	32.609	BB	1.0866	6947.40869	96.18931	38.4527
2	37.078	BB	1.3132	1.11200e4	125.31839	61.5473

Chiral S:



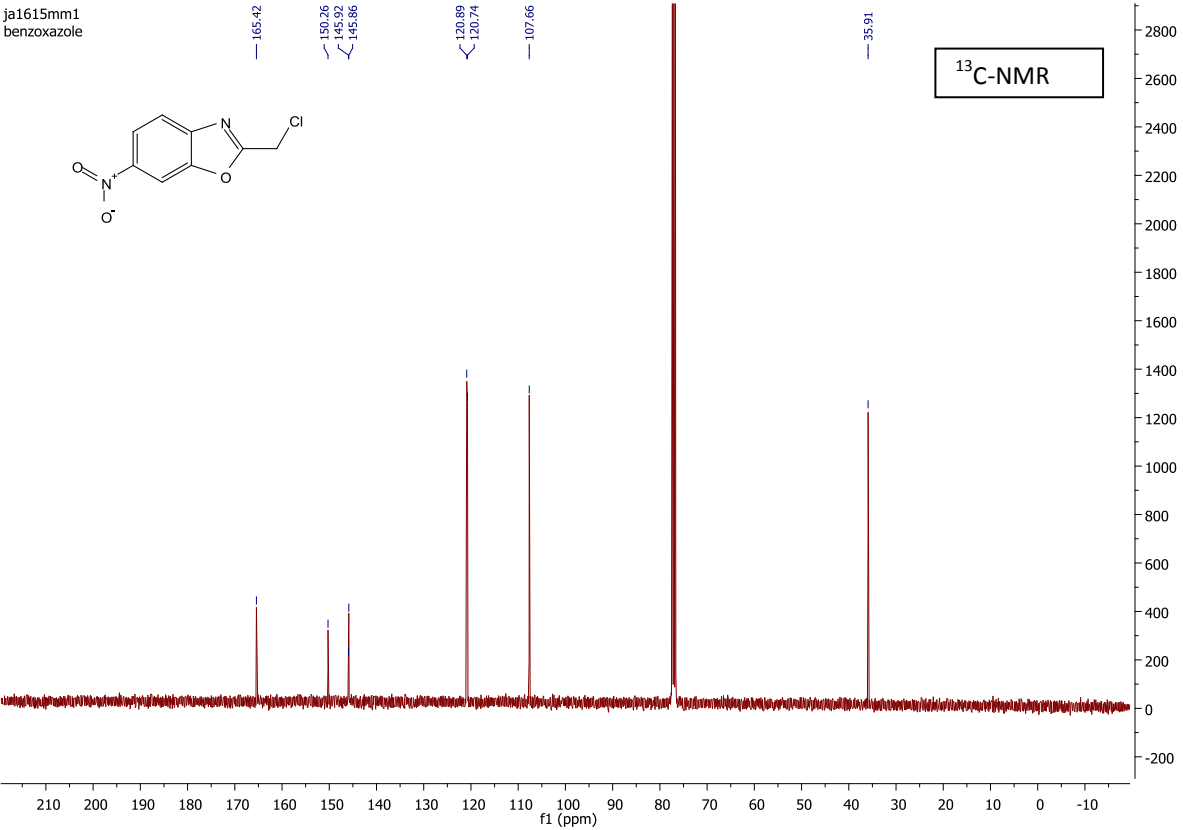
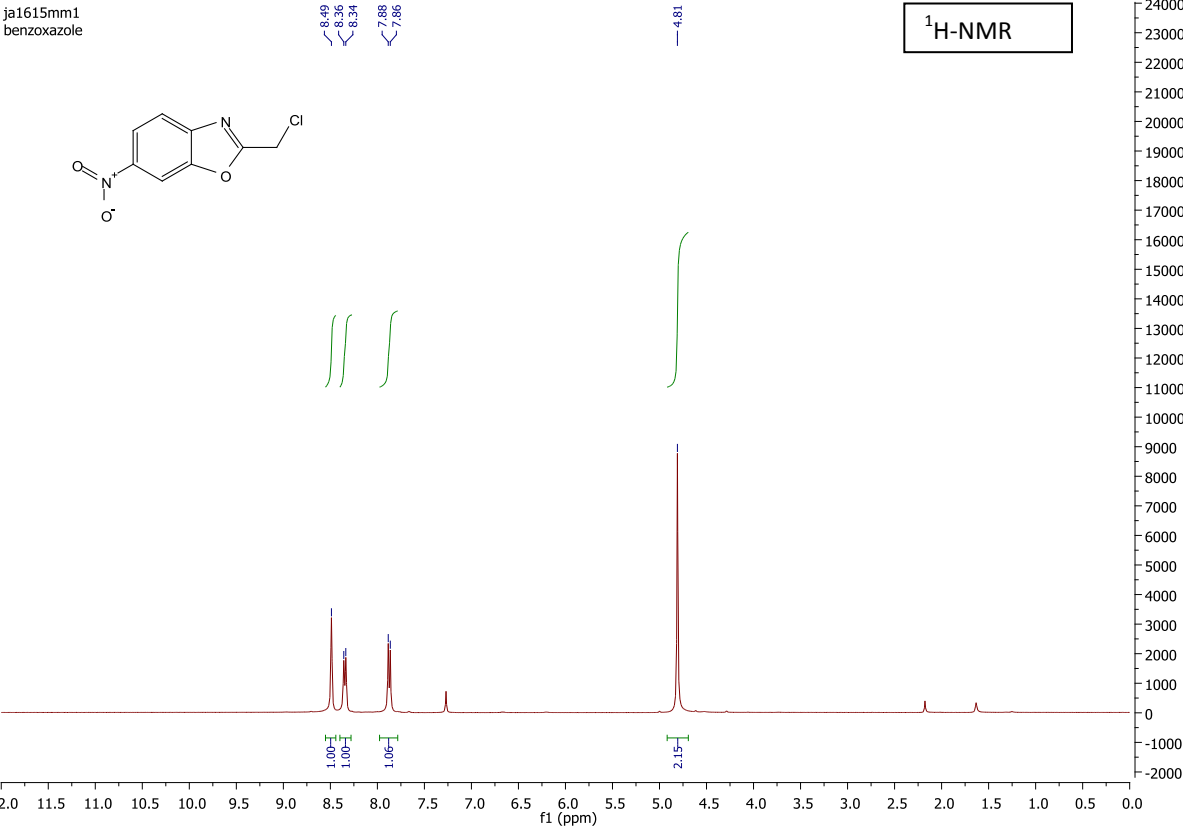
Peak #	RetTime [min]	Type	Width [min]	Area [mAU*s]	Height [mAU]	Area %
1	33.811	MM	1.4206	70.54089	8.27576e-1	1.3019
2	38.186	BB	1.2748	5347.89258	60.40890	98.6981

Chiral R:

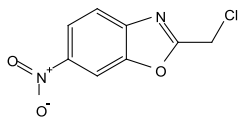


Peak #	RetTime [min]	Type	Width [min]	Area [mAU*s]	Height [mAU]	Area %
1	32.921	MM	1.2967	1.16471e4	149.70476	95.3515
2	38.107	MM	2.9513	567.80548	3.20654	4.6485

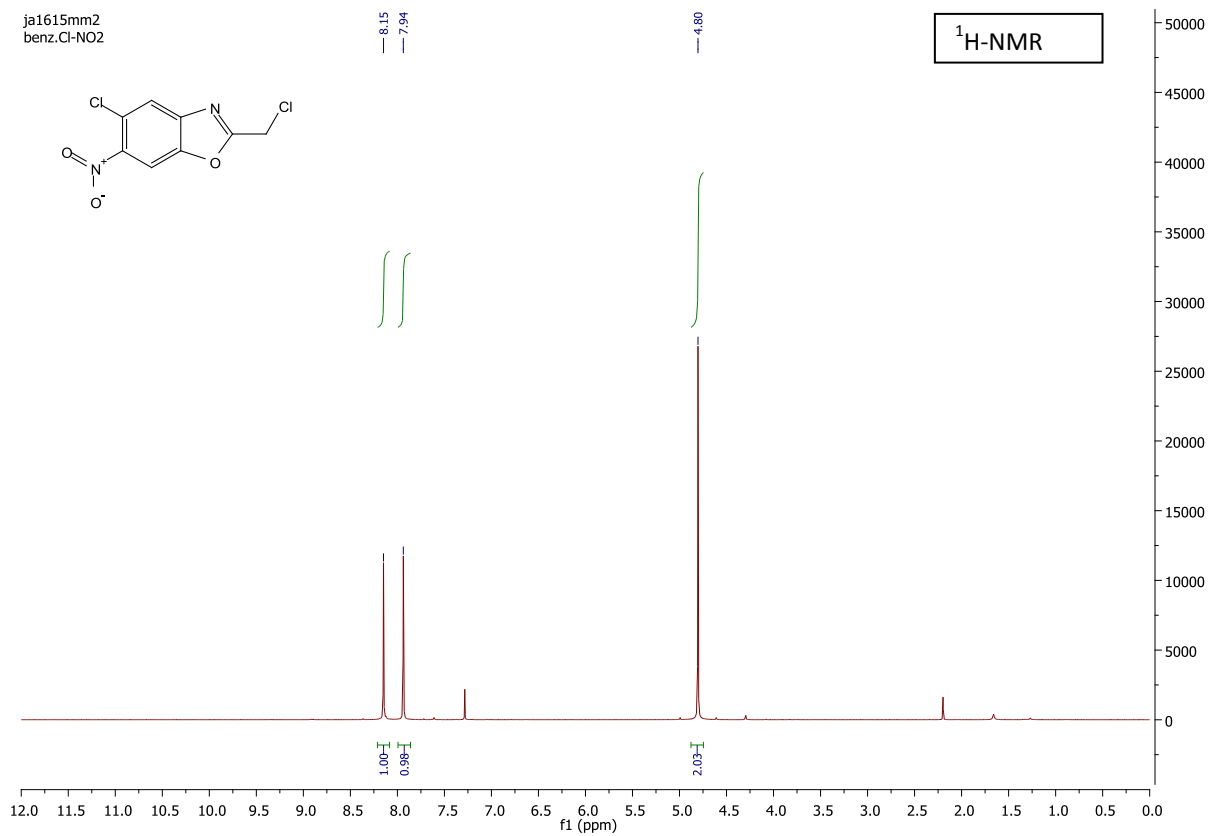
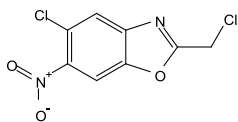
NMR starting materials



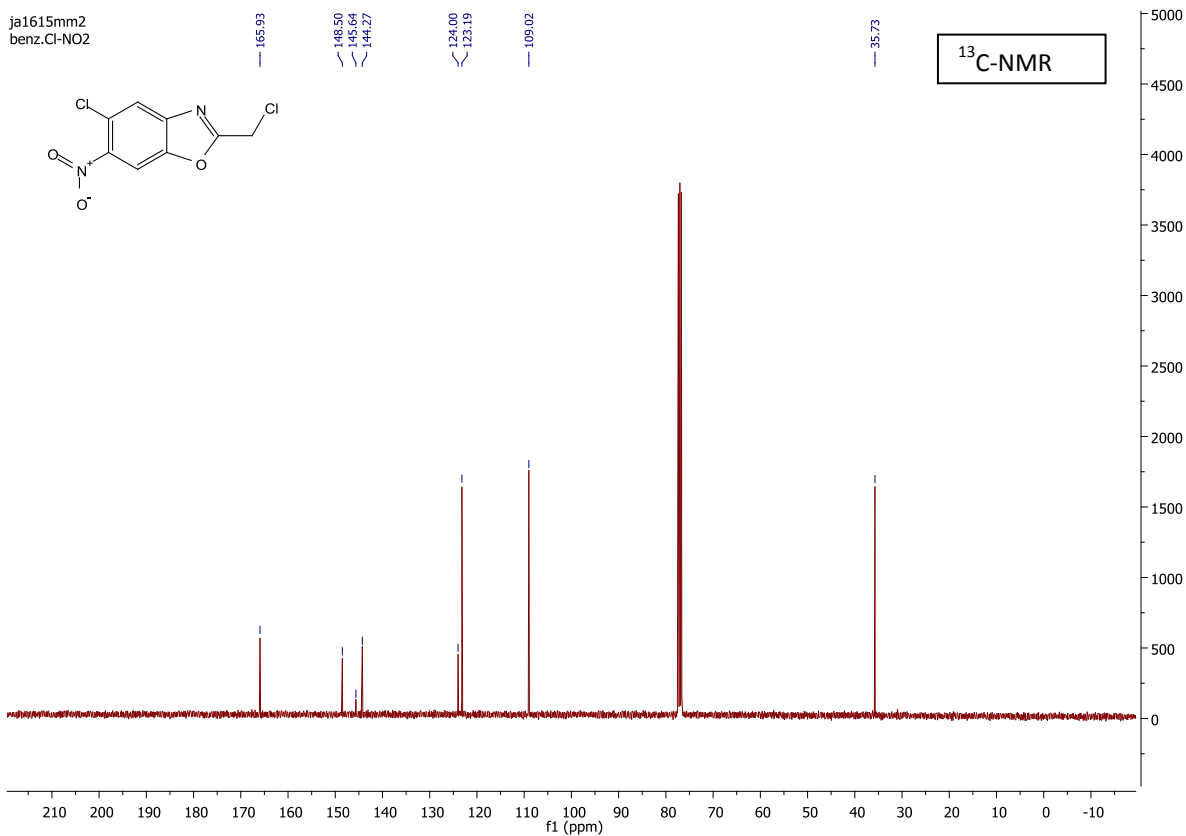
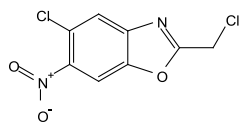
ja1615mm1
benzoxazole



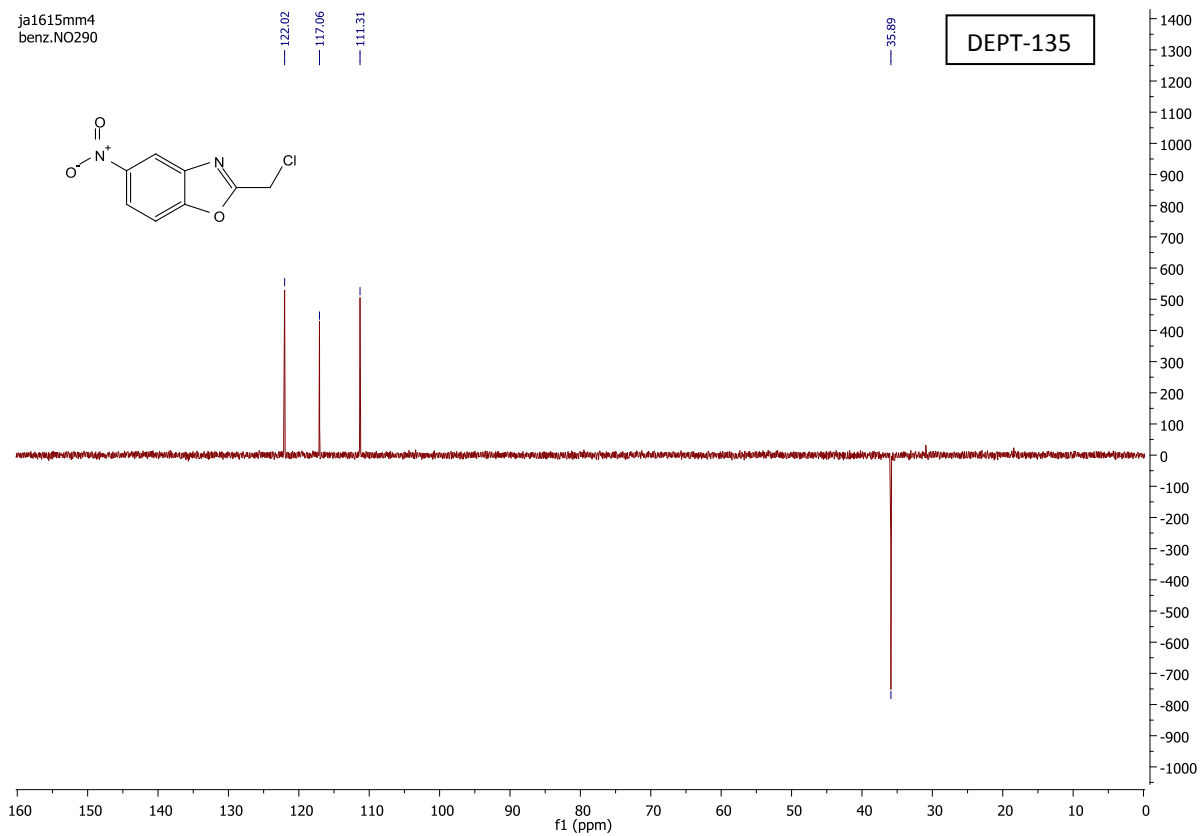
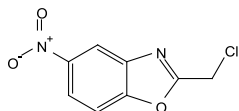
ja1615mm2
benz.Cl-NO2



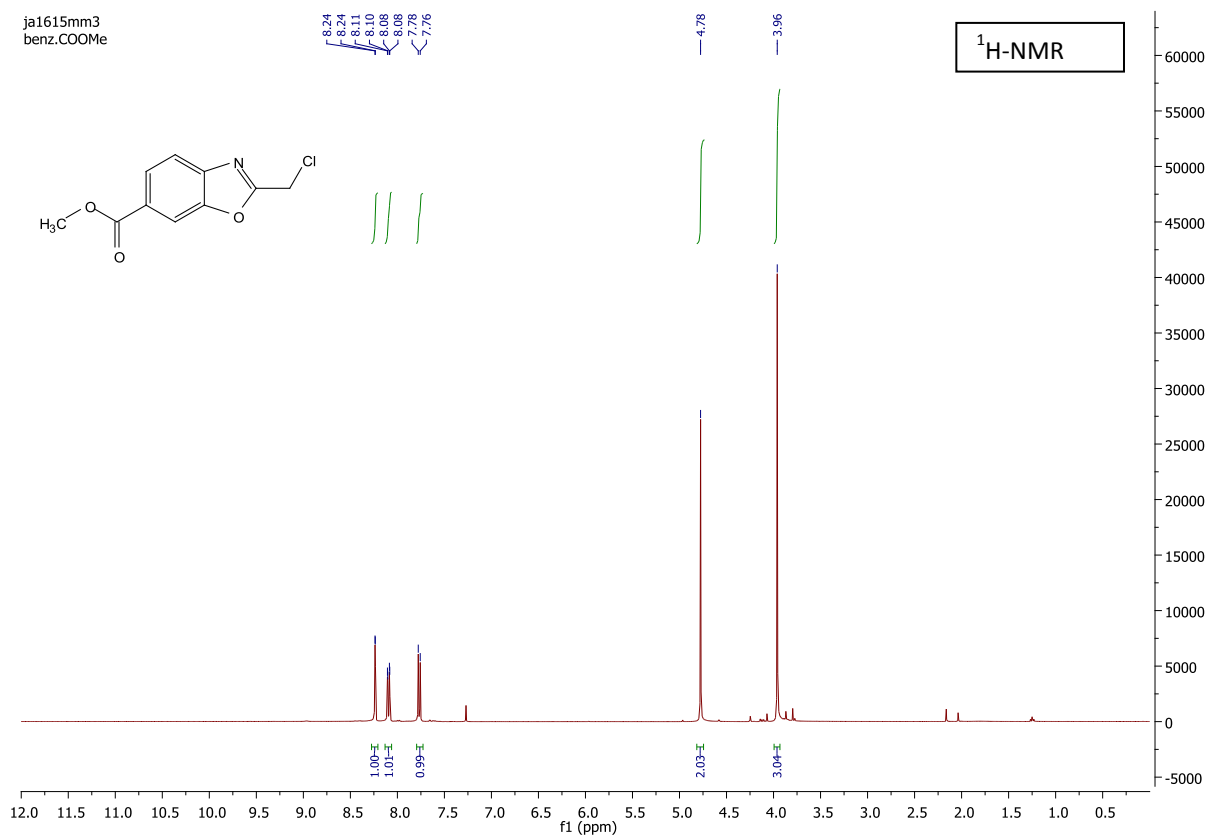
ja1615mm2
benz.Cl-NO2



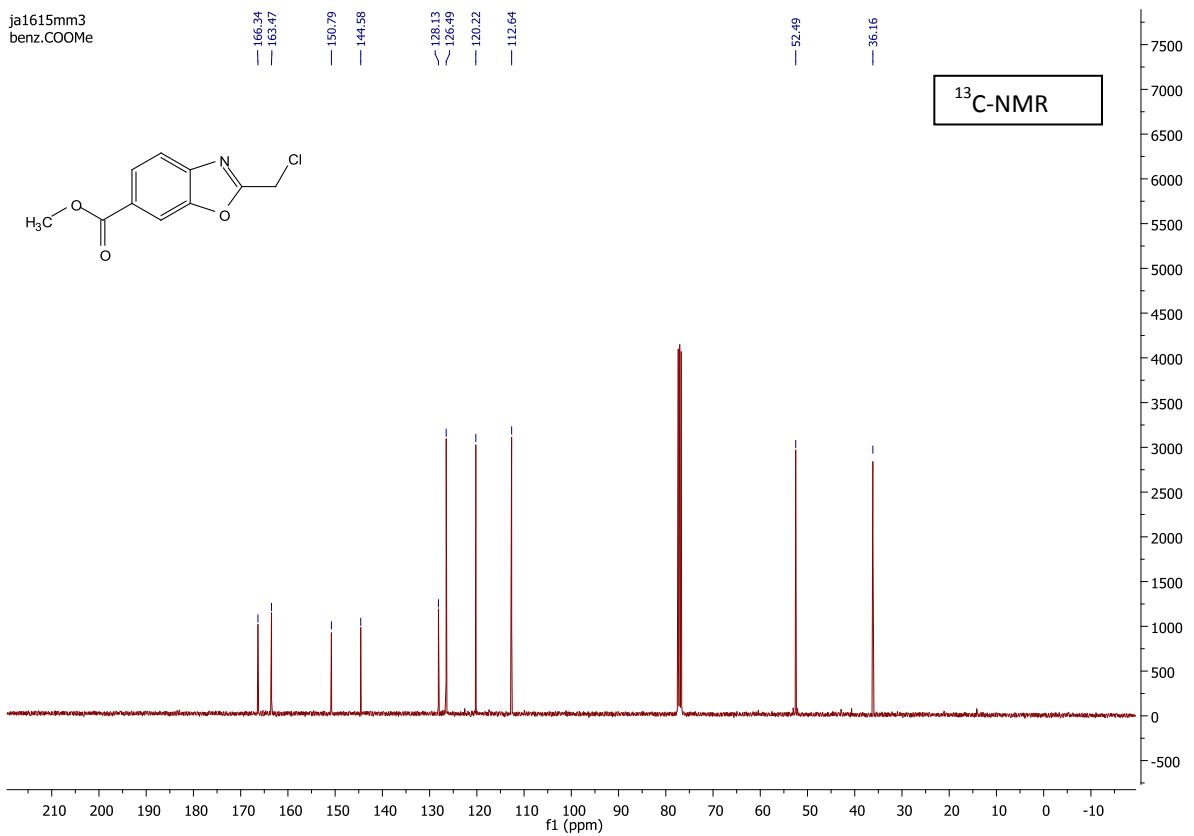
ja1615mm4
benz.NO290



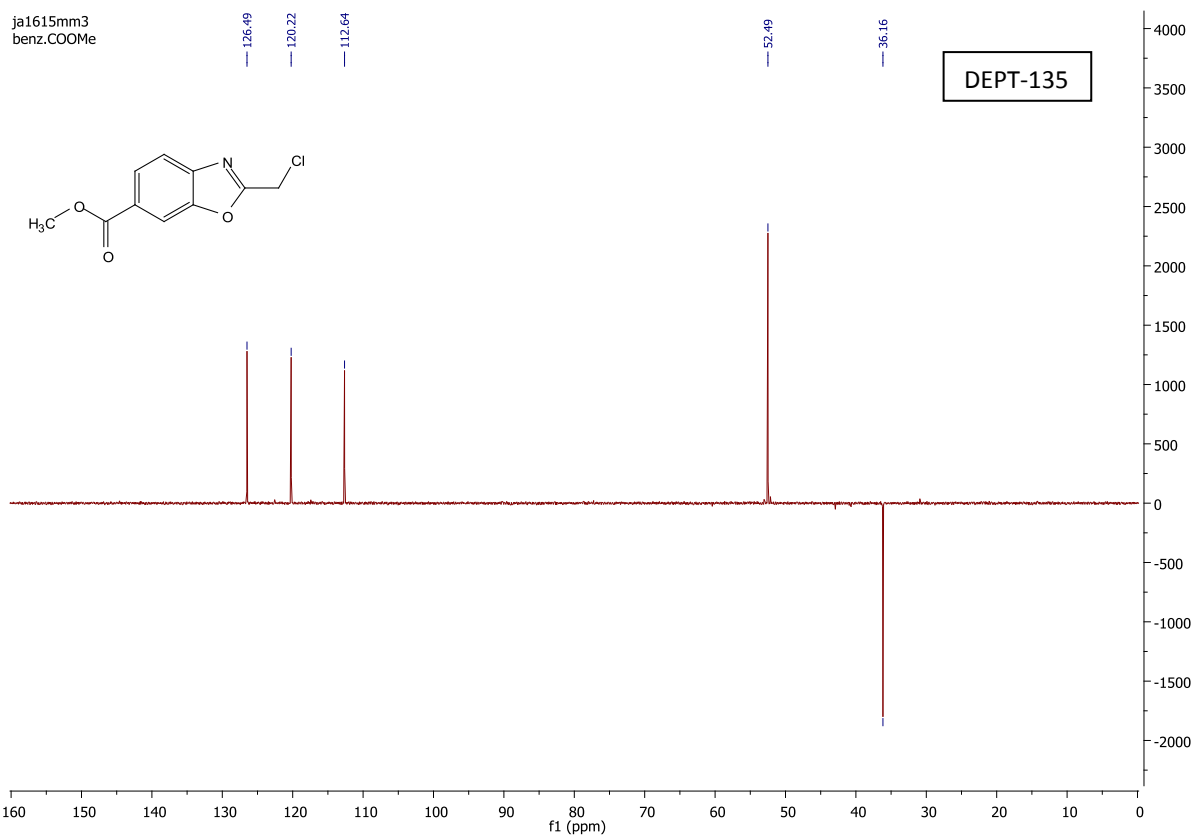
ja1615mm3
benz.COOMe



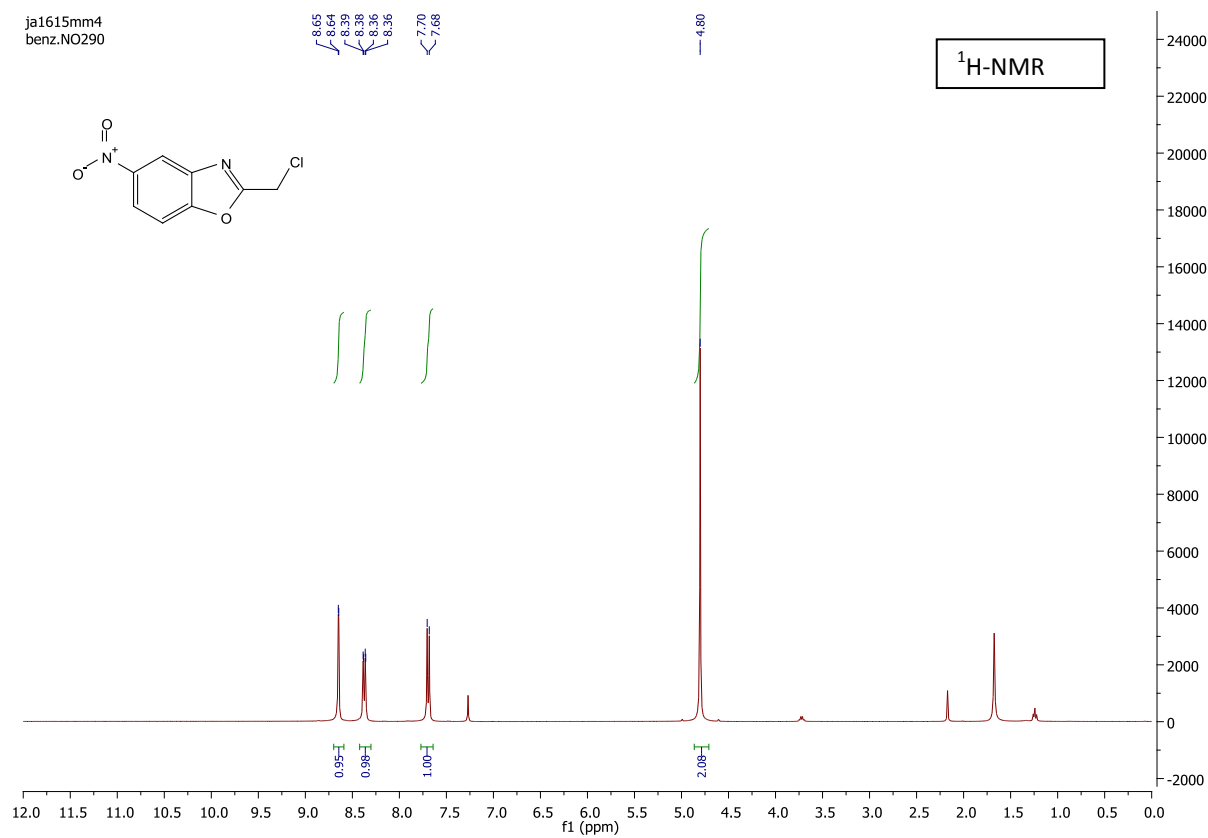
ja1615mm3
benz.COOMe



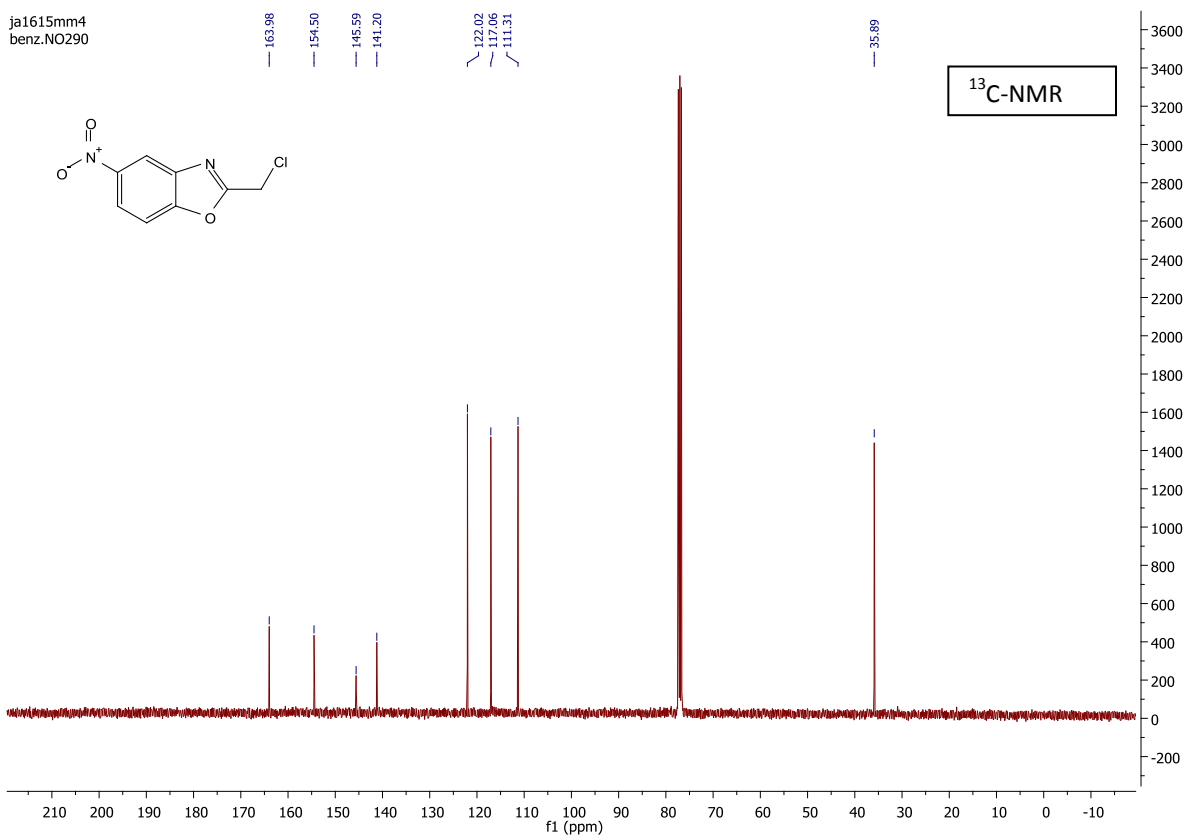
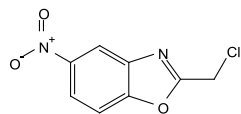
ja1615mm3
benz.COOMe



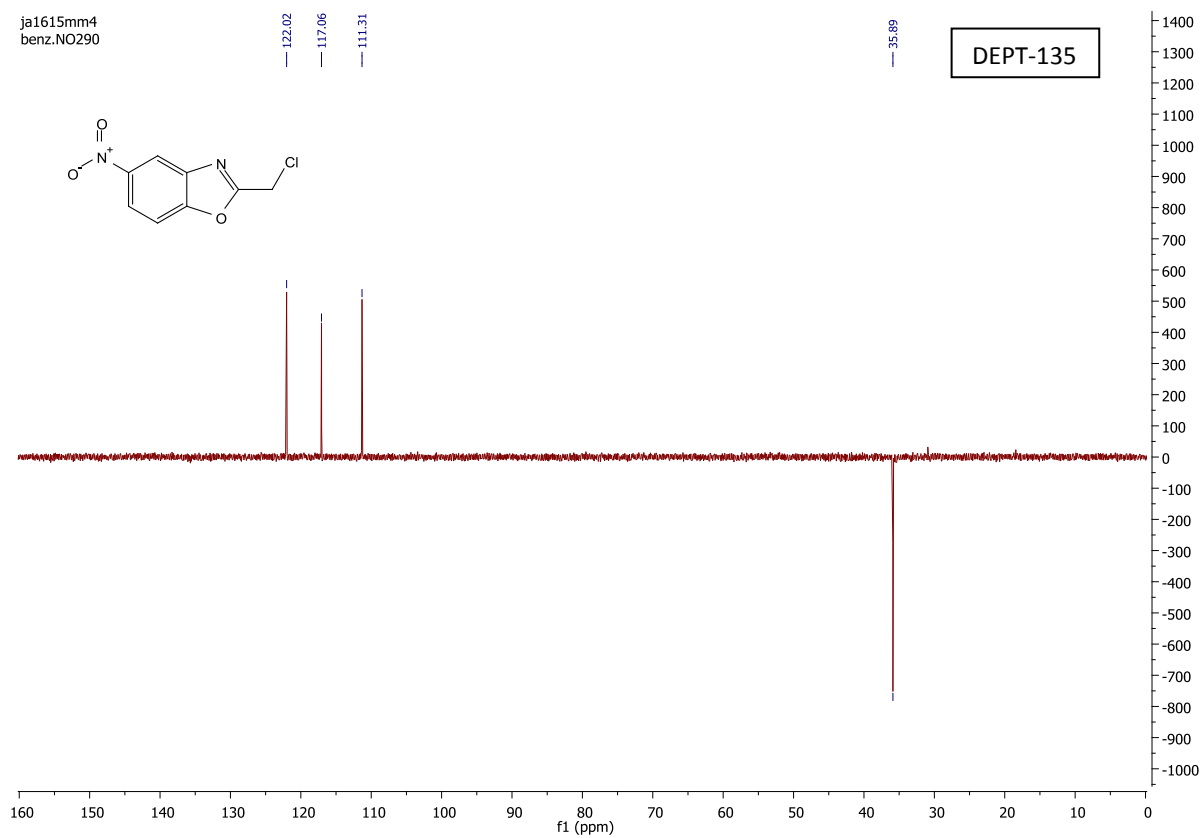
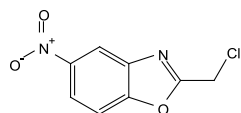
ja1615mm4
benz.NO290



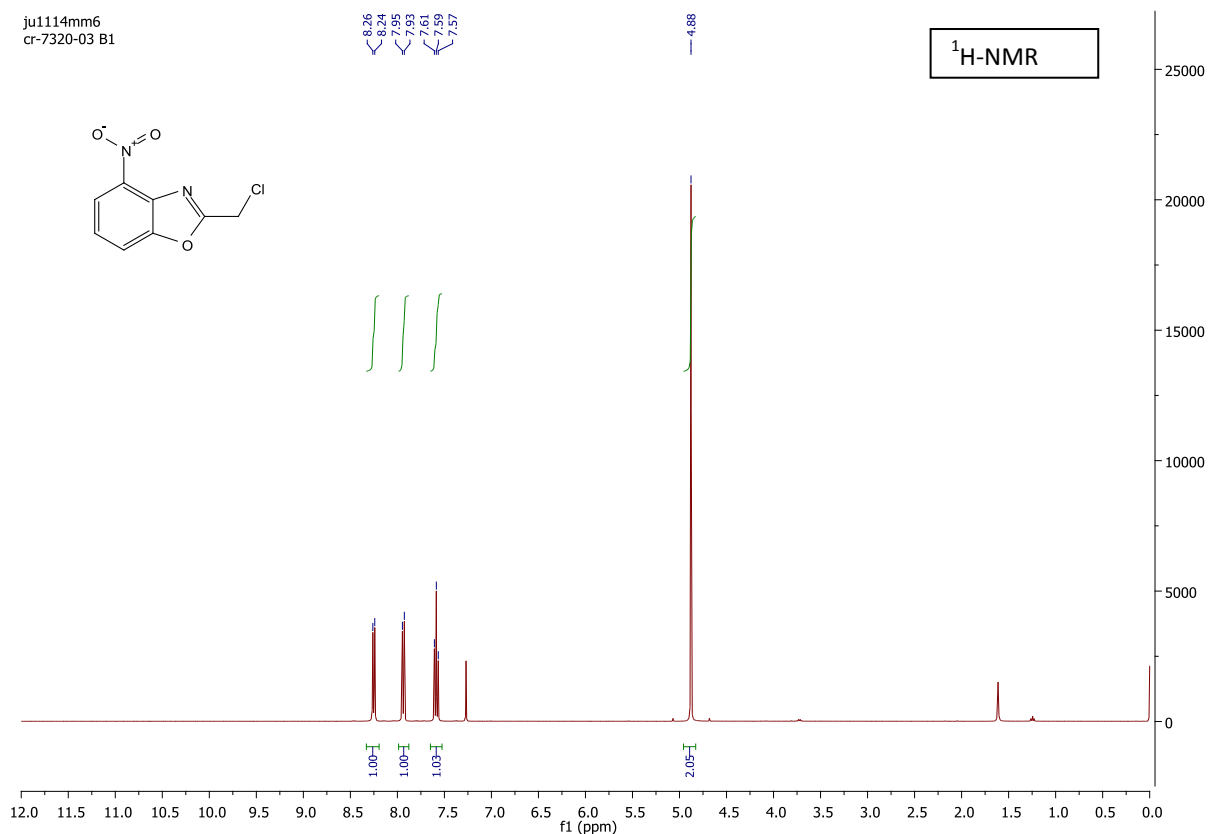
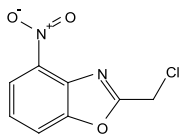
ja1615mm4
benz.NO290



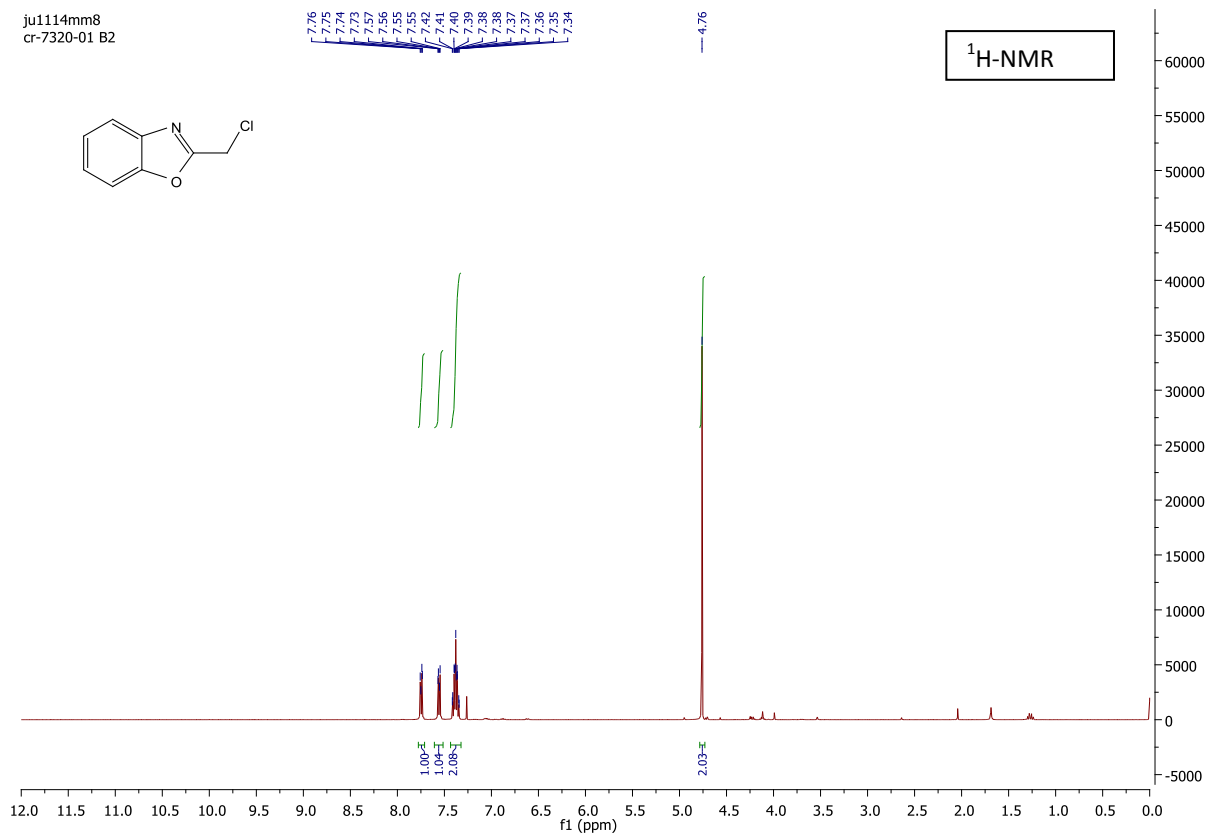
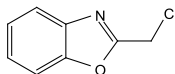
ja1615mm4
benz.NO290



ju1114mm6
cr-7320-03 B1

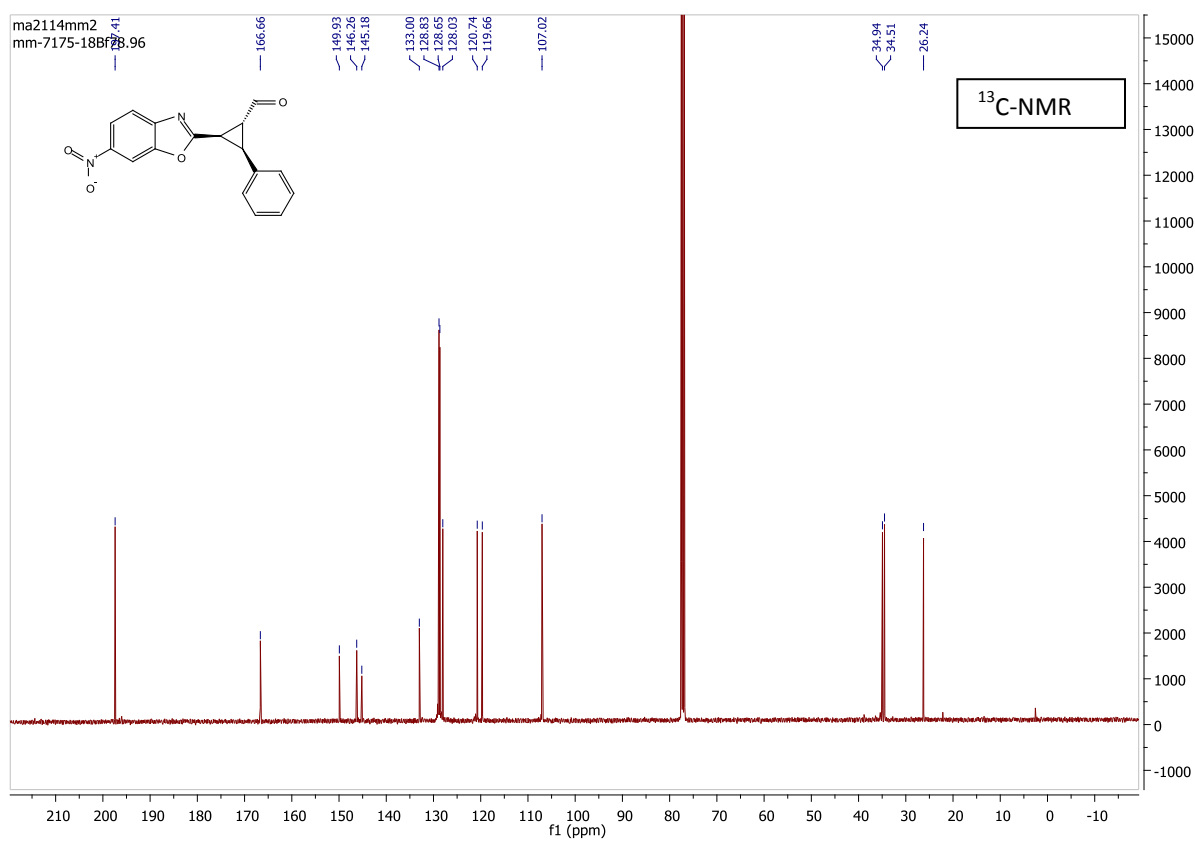
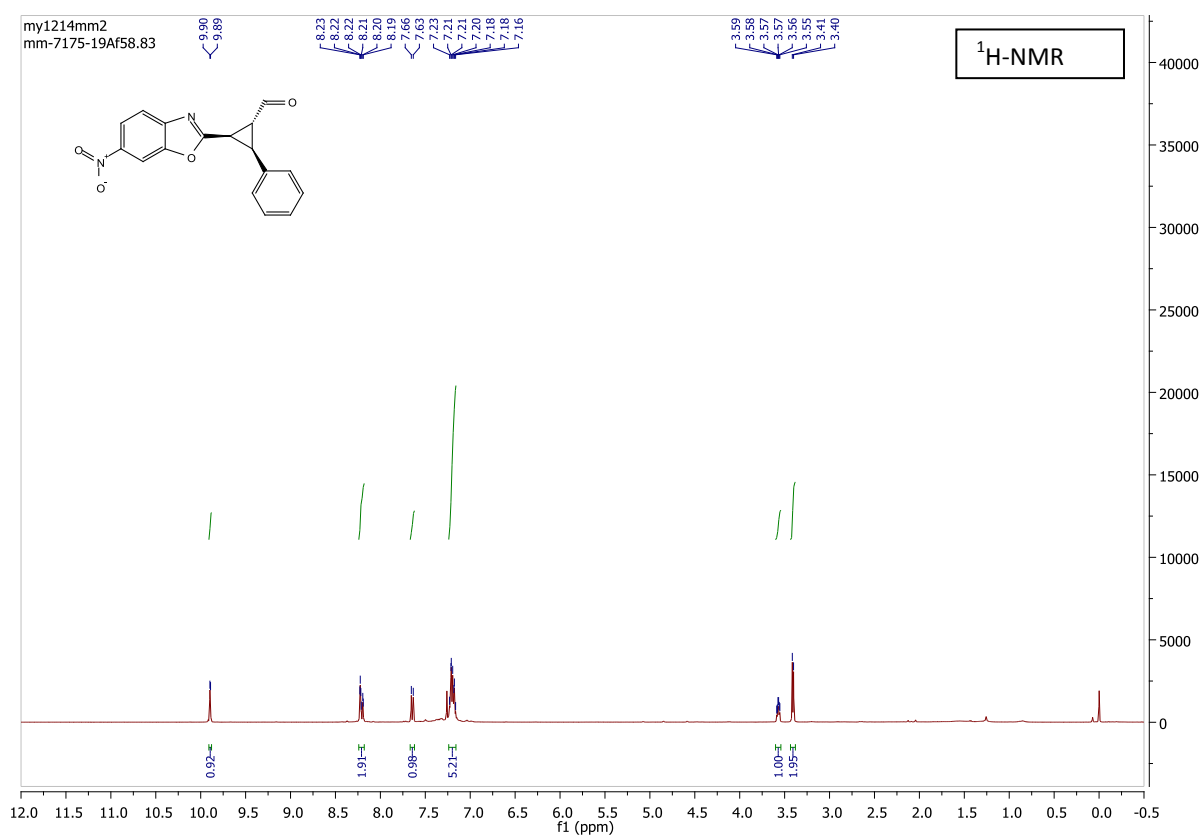


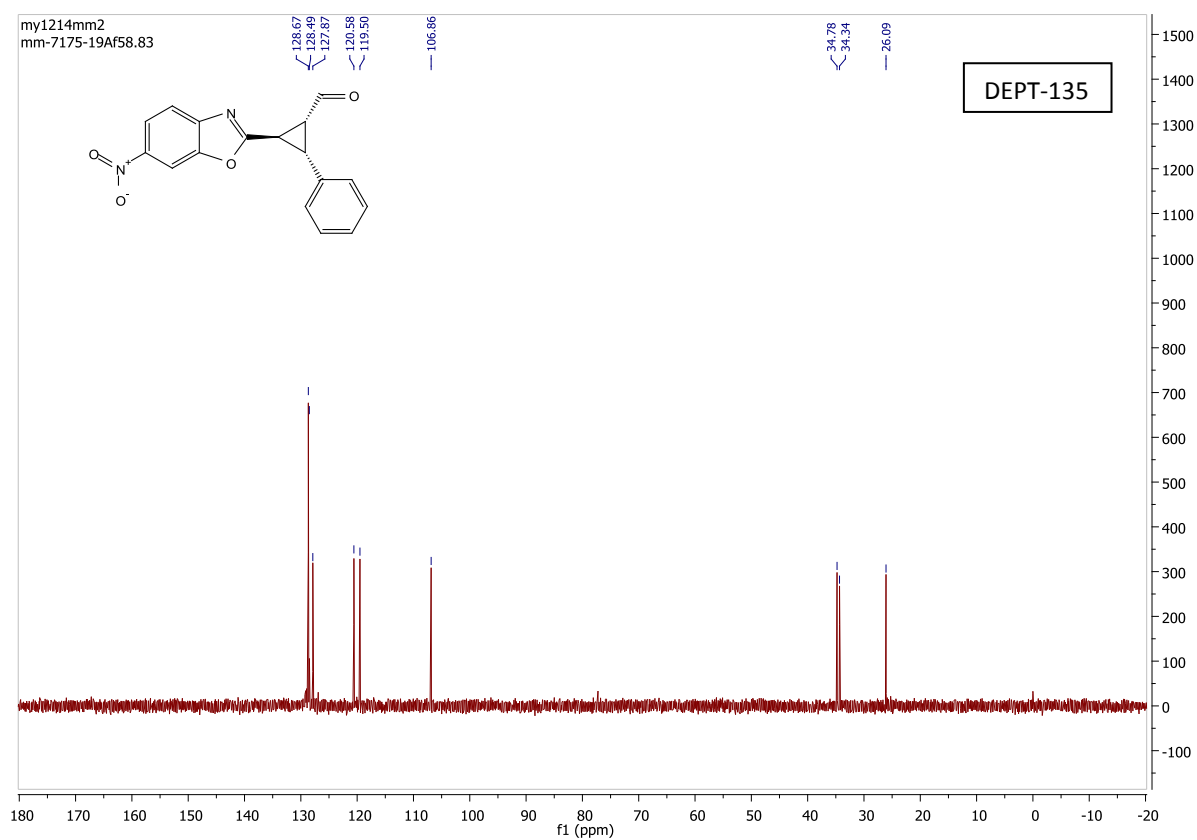
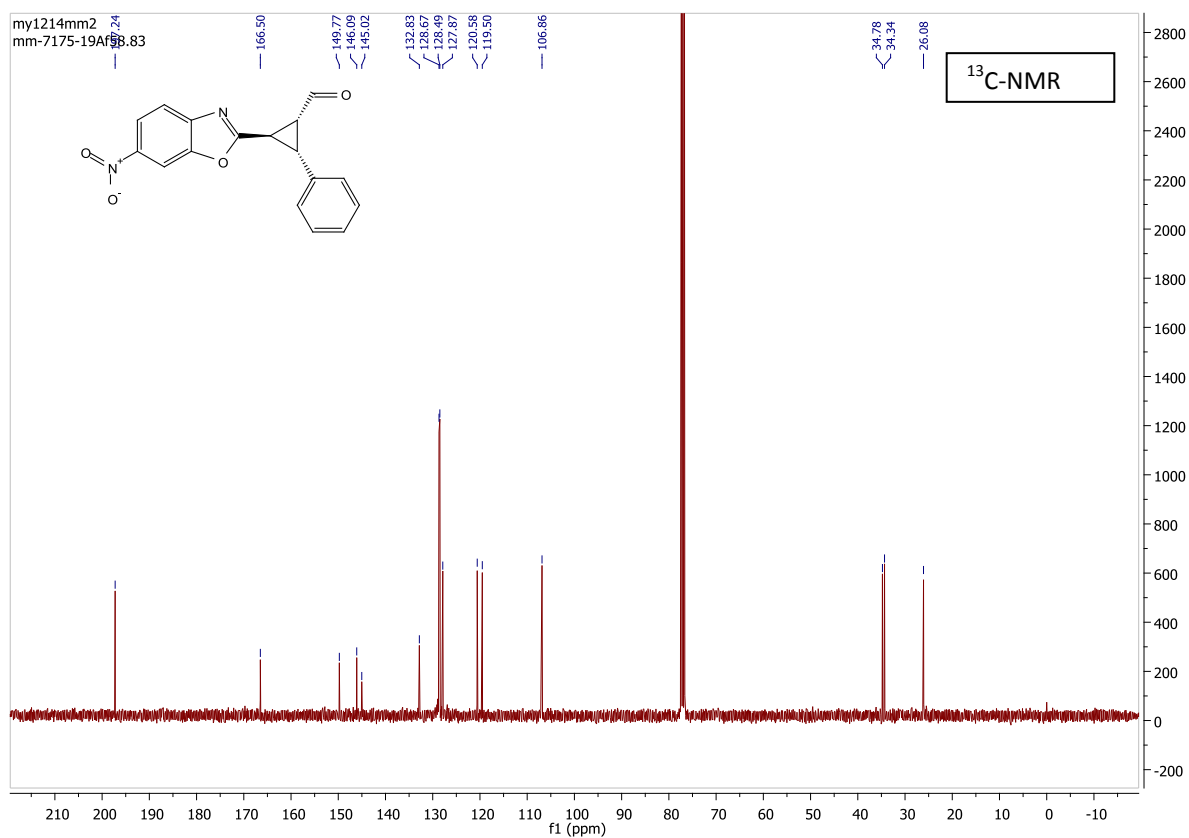
ju1114mm8
cr-7320-01 B2

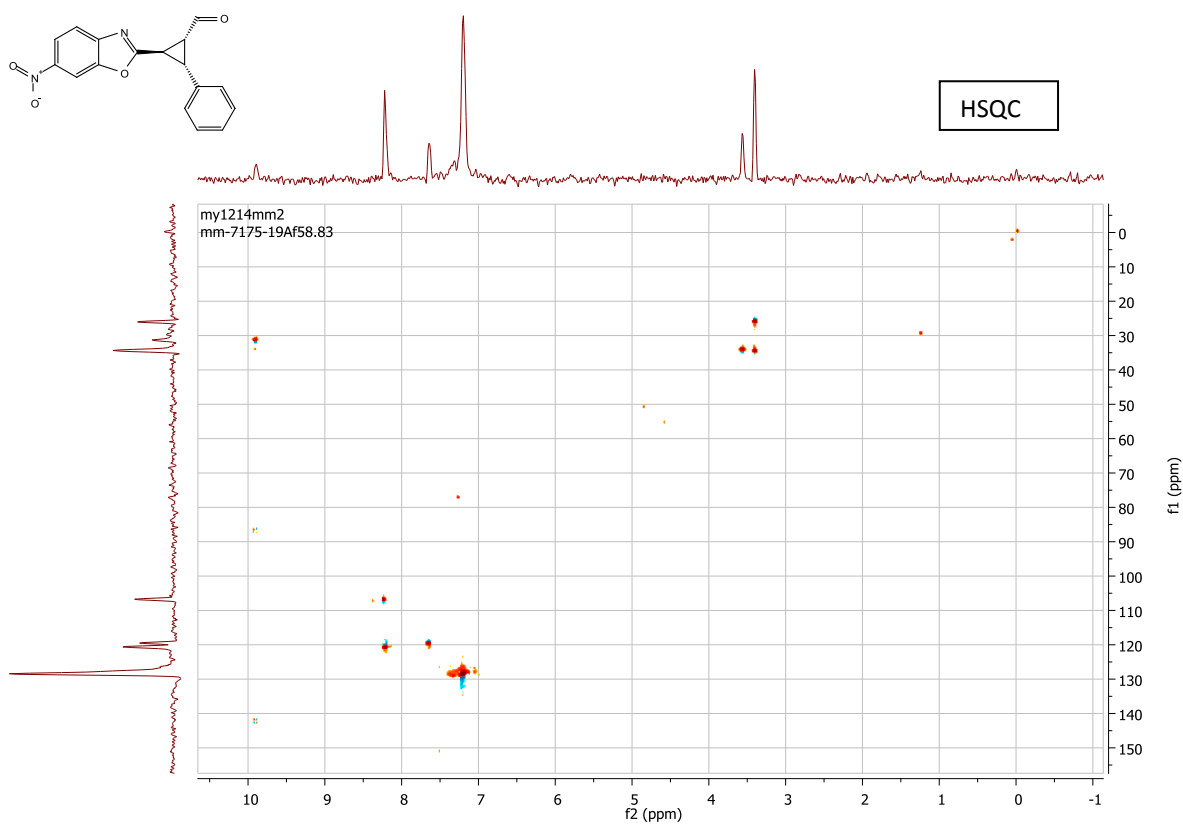
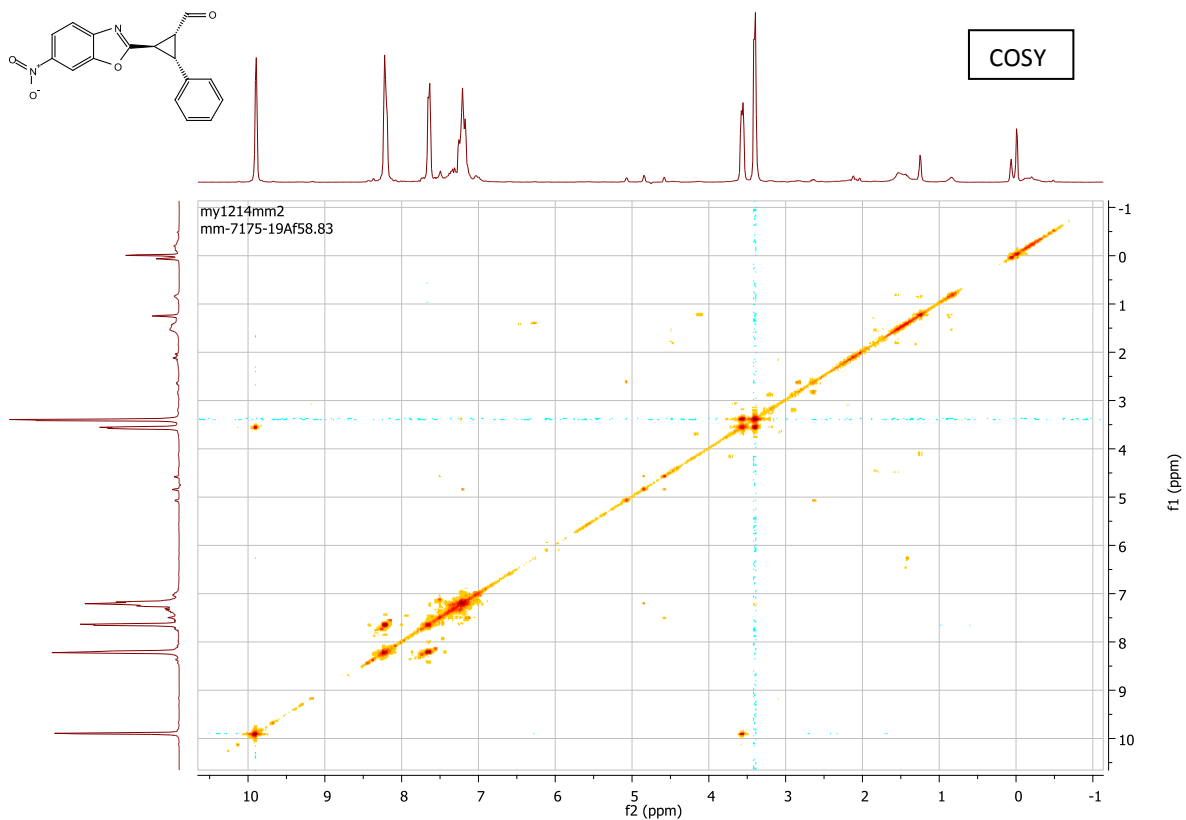


NMR cyclopropanes

major diastereomer:



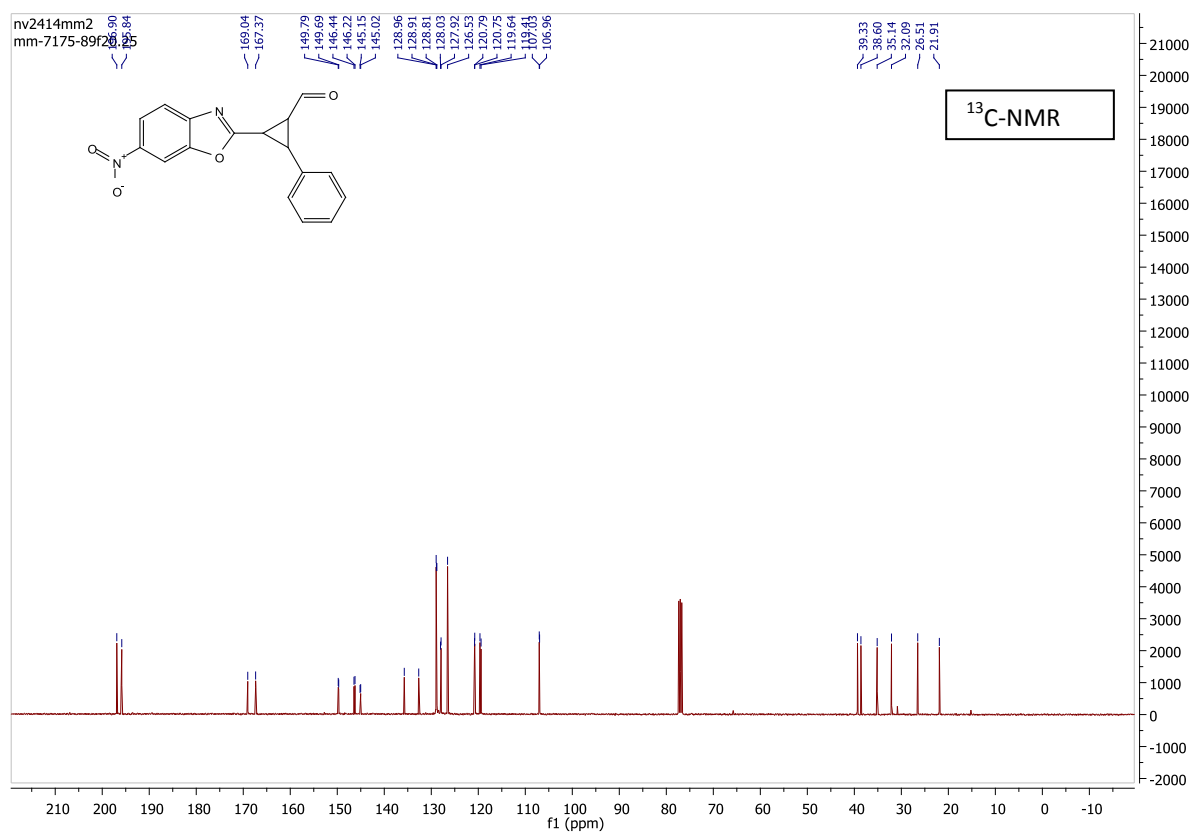


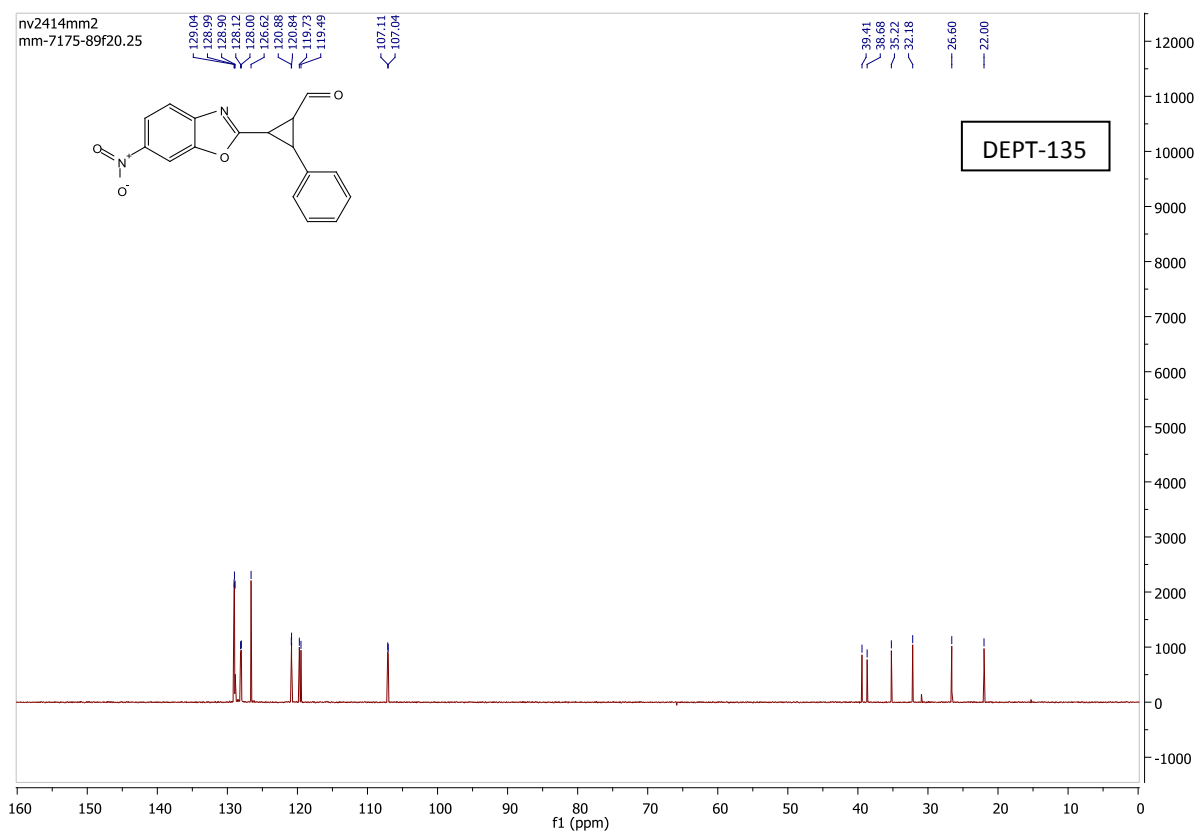


Chemical structure: O=C1C(c2ccccc2)C1c3nc4ccc(cc4o3)C5=CC=C(C=C5)[N+](=O)[O-]

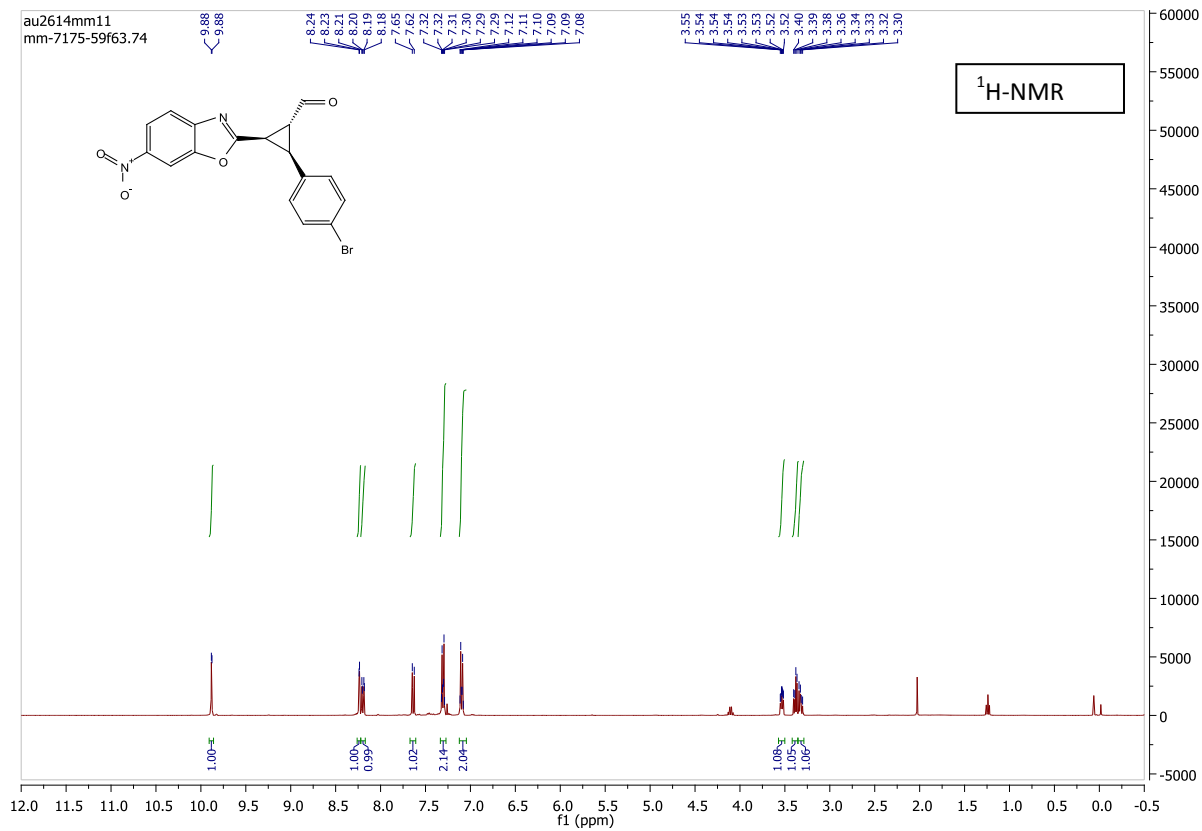
¹H-NMR spectrum (ppm):

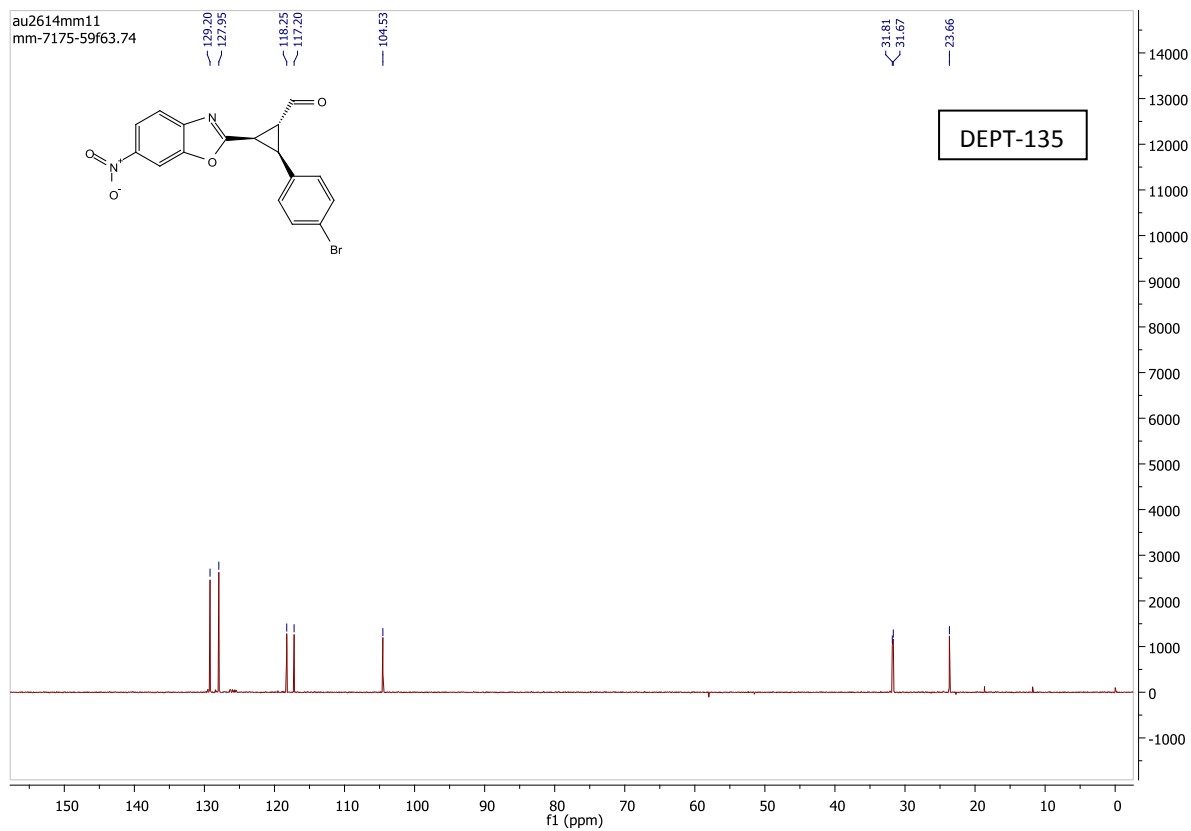
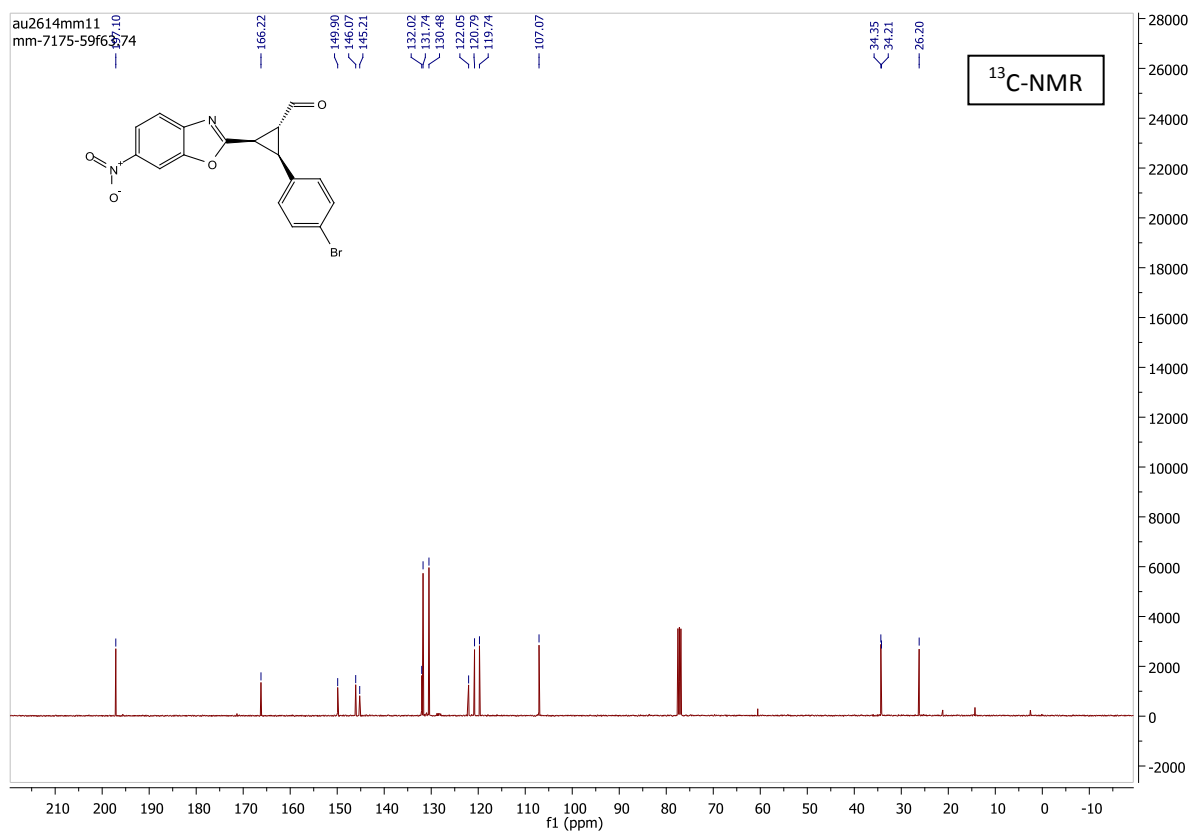
- 10.00 (s, 1H, integration 1.00)
- 9.17 (s, 1H, integration 0.96)
- 8.31 (s, 1H, integration 1.87)
- 8.29 (s, 1H, integration 2.09)
- 7.78 (s, 1H, integration 2.07)
- 7.41 (s, 1H, integration 11.68)
- 7.39 (s, 1H, integration 1.05)
- 7.37 (s, 1H, integration 2.08)
- 7.33 (s, 1H, integration 1.08)
- 7.28 (s, 1H, integration 1.07)
- 7.26 (s, 1H, integration 1.11)
- 3.79 (s, 1H, integration 1.05)
- 3.77 (s, 1H, integration 2.08)
- 3.76 (s, 1H, integration 1.08)
- 3.71 (s, 1H, integration 1.07)
- 3.69 (s, 1H, integration 1.11)
- 3.67 (s, 1H, integration 1.05)
- 3.66 (s, 1H, integration 2.08)
- 3.64 (s, 1H, integration 1.08)
- 3.22 (s, 1H, integration 1.07)
- 3.20 (s, 1H, integration 1.11)
- 3.18 (s, 1H, integration 1.05)
- 3.11 (s, 1H, integration 2.08)
- 3.09 (s, 1H, integration 1.08)
- 3.08 (s, 1H, integration 1.07)
- 3.06 (s, 1H, integration 1.11)
- 2.83 (s, 1H, integration 1.05)
- 2.81 (s, 1H, integration 2.08)
- 2.80 (s, 1H, integration 1.08)
- 2.79 (s, 1H, integration 1.07)
- 2.78 (s, 1H, integration 1.11)



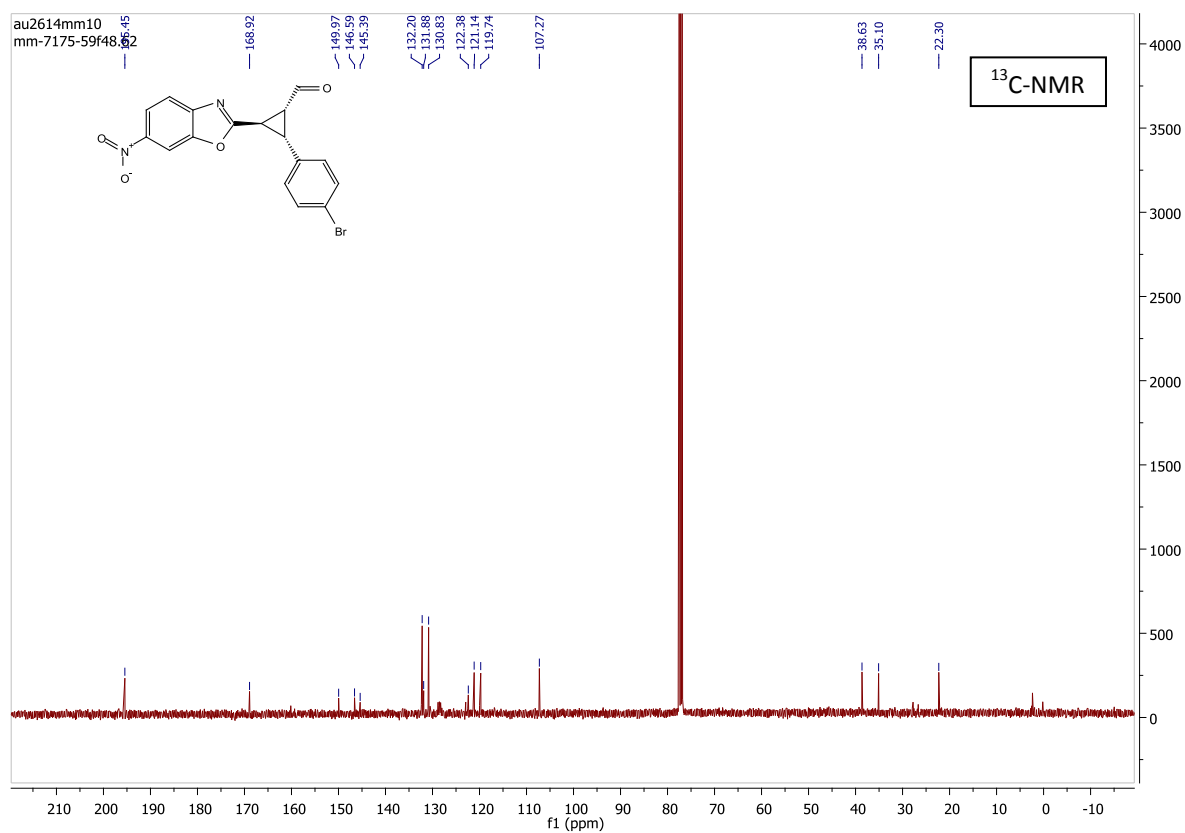
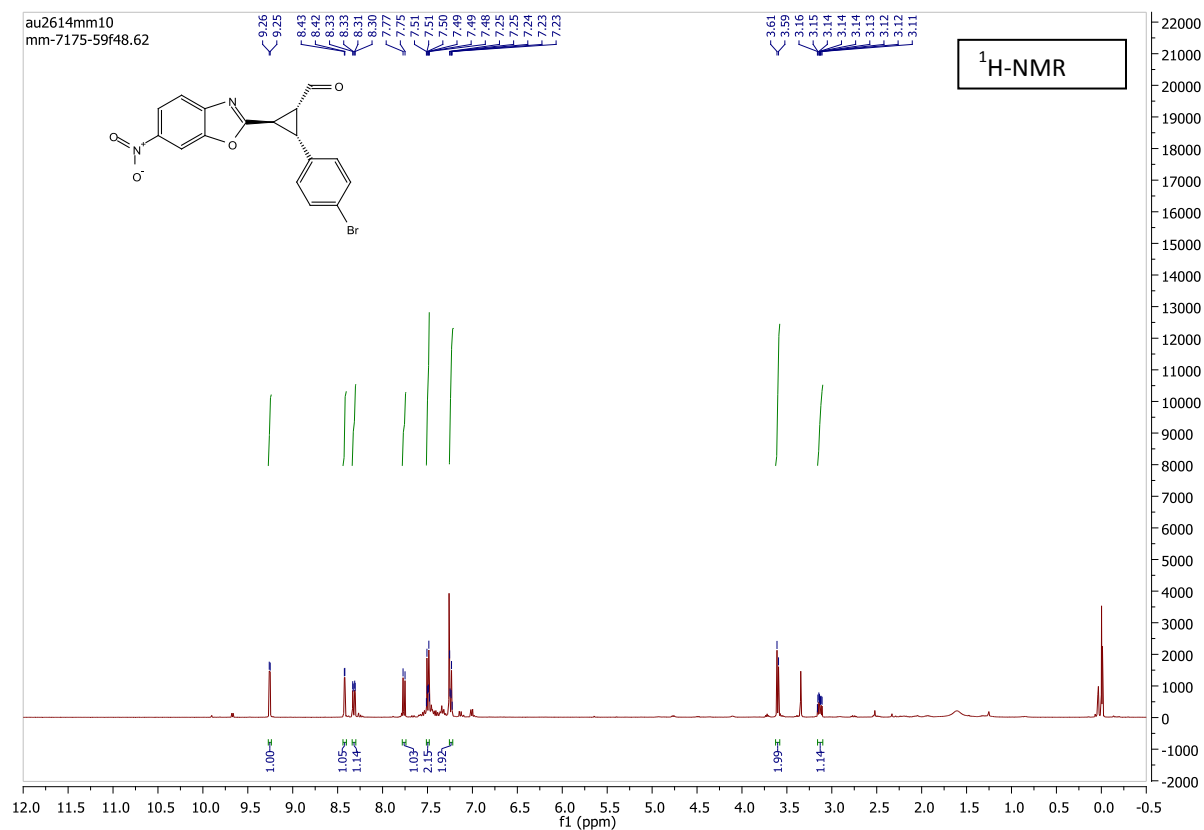


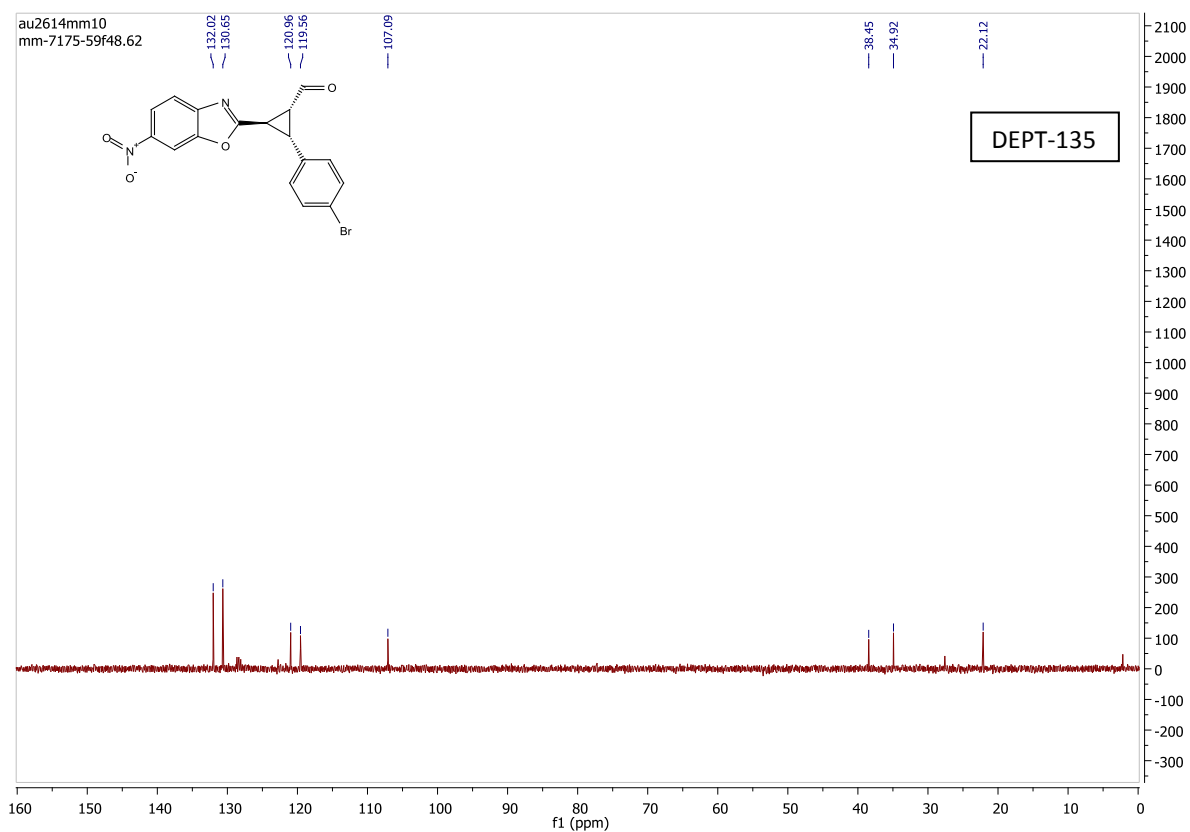
major diastereomer:



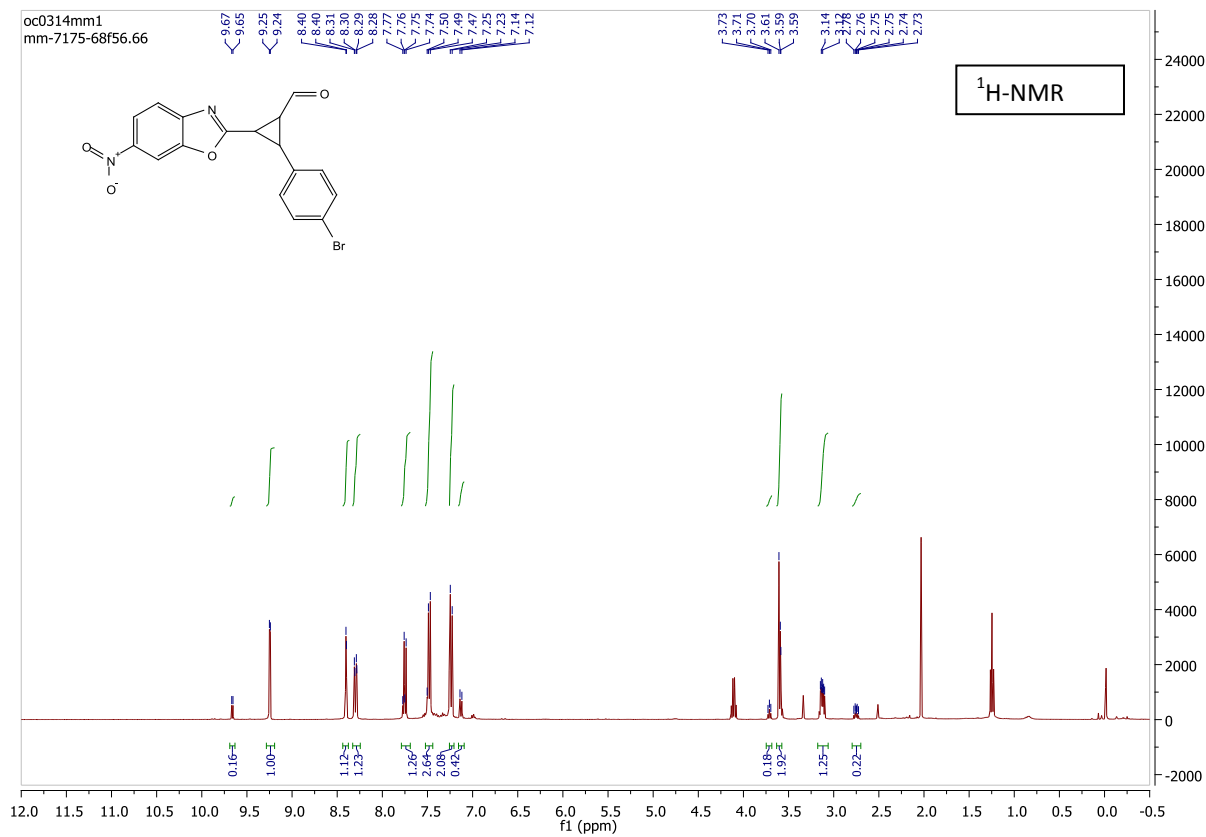


minor diastereomer:

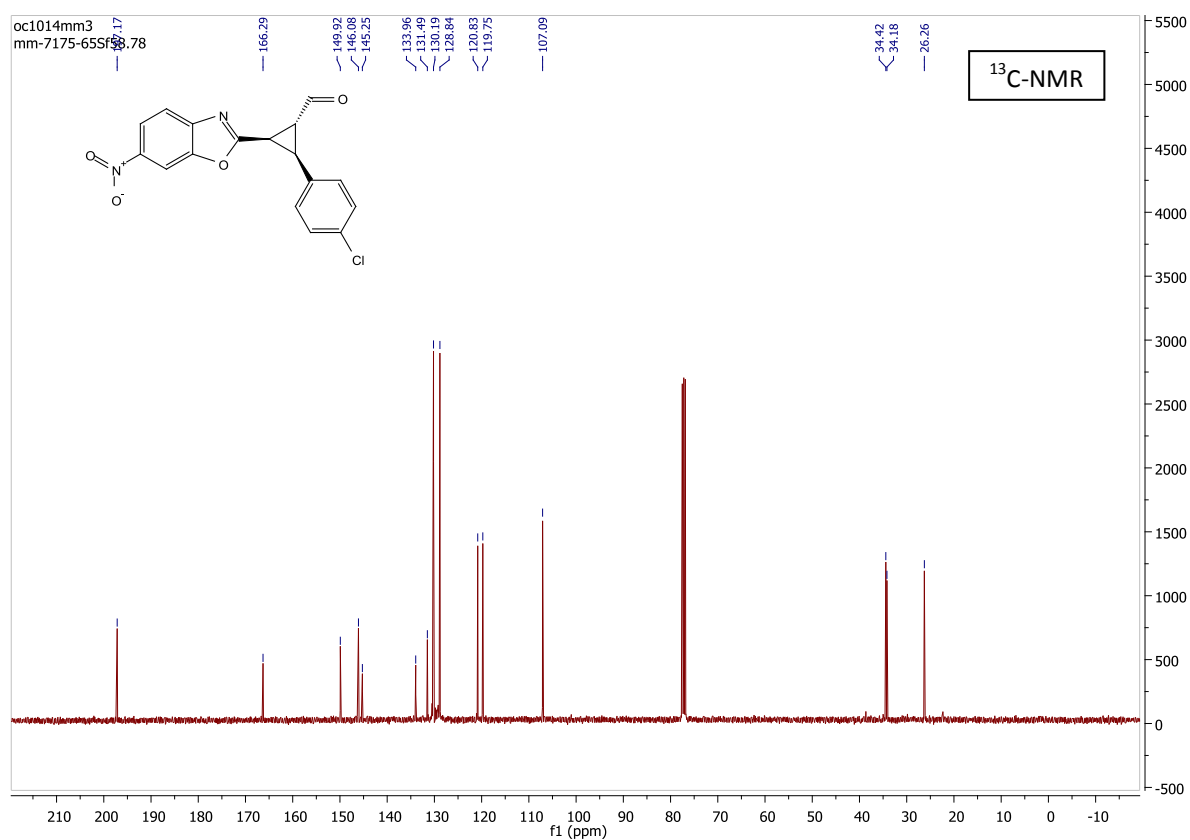
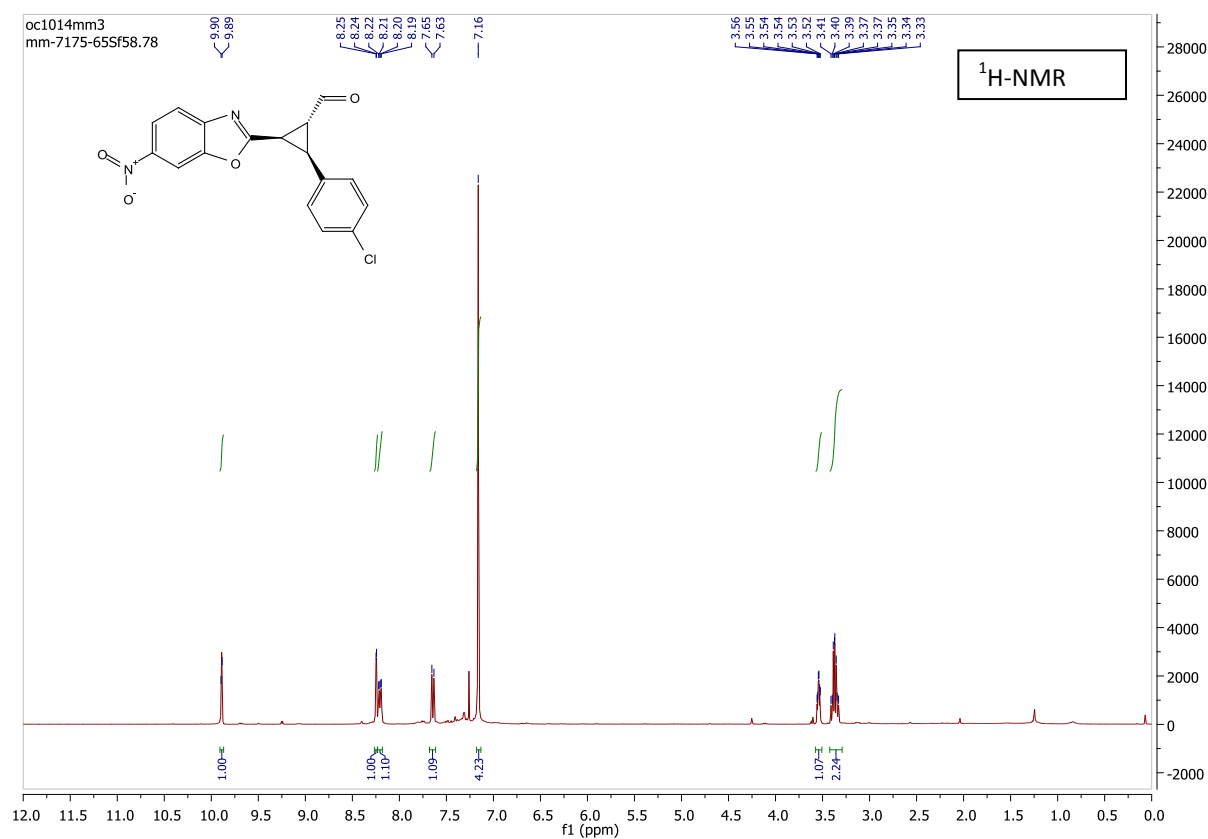


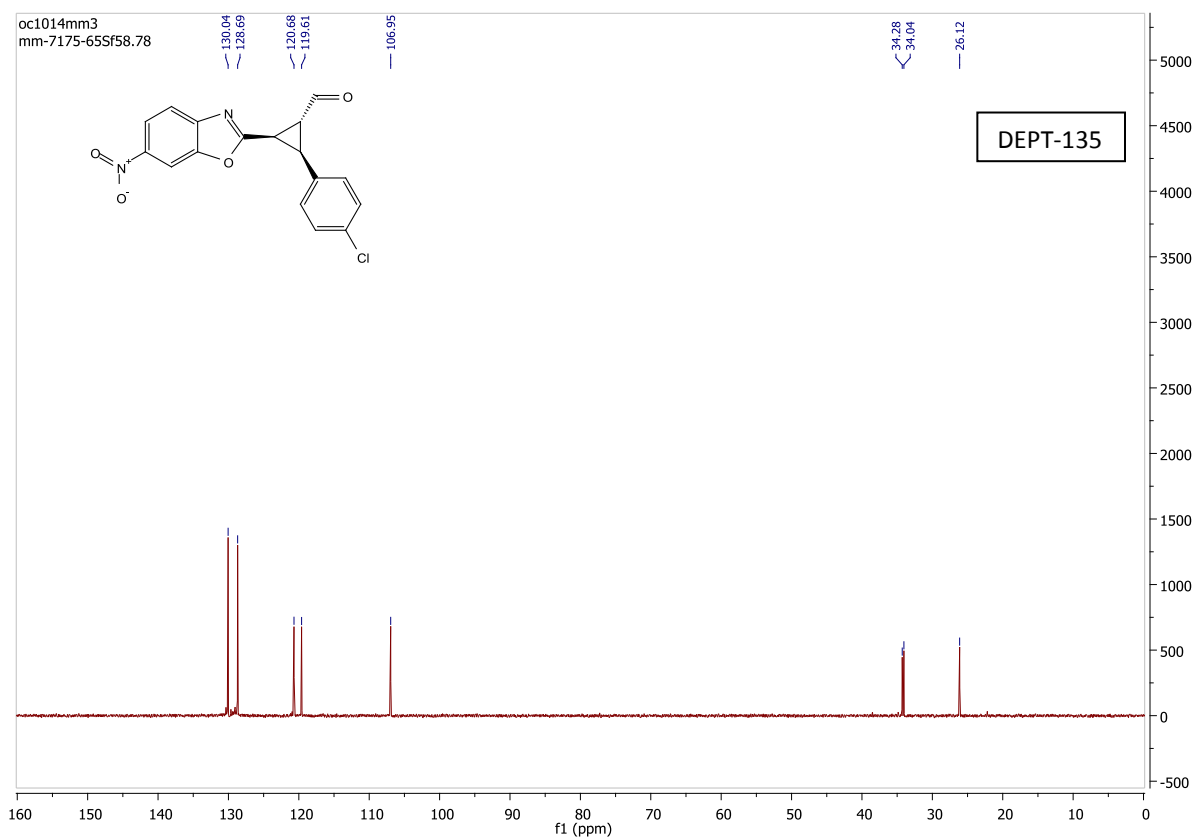


mixture of minor and minor' diastereomers:

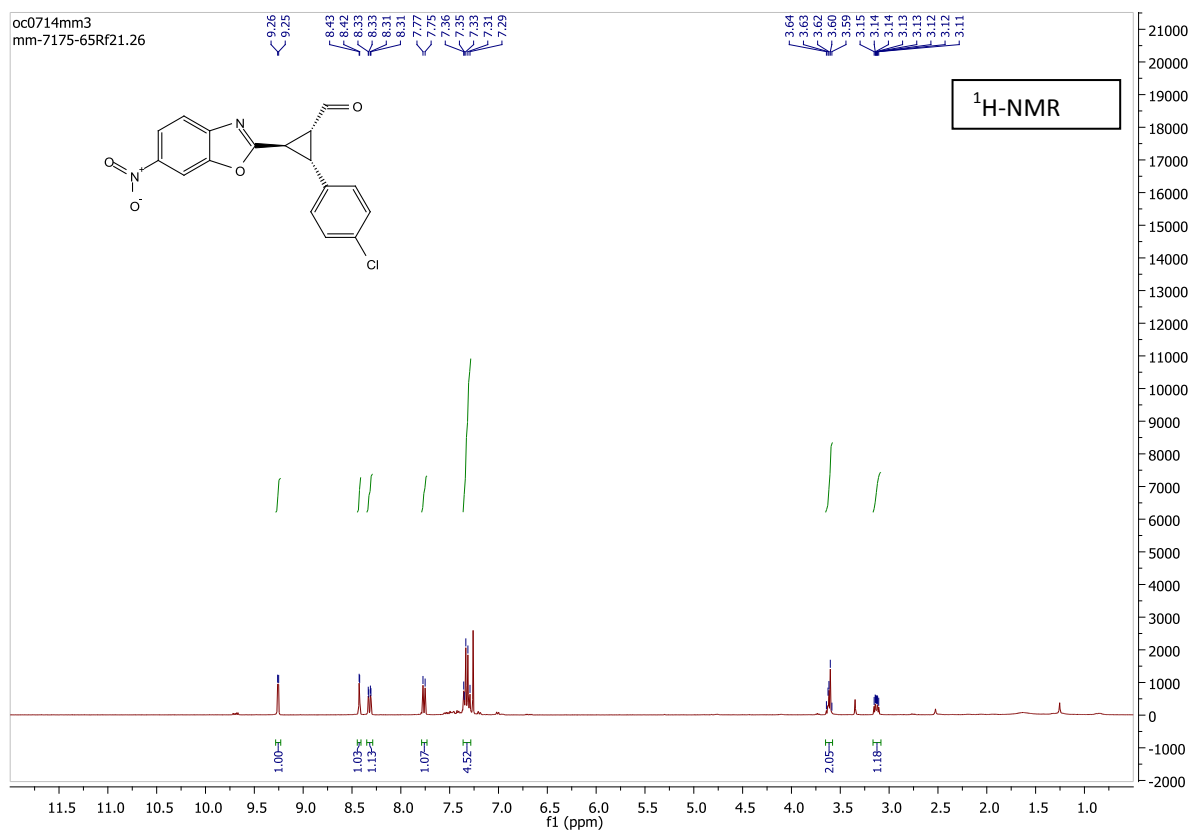


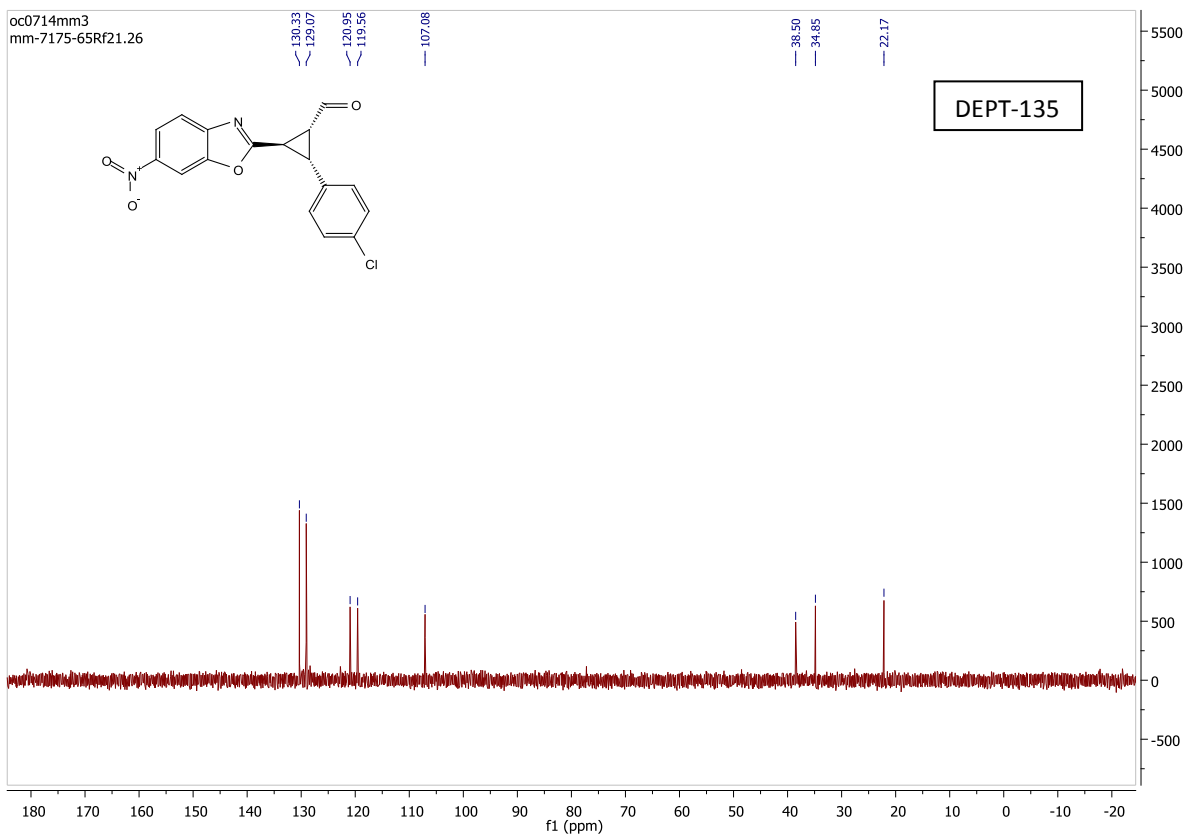
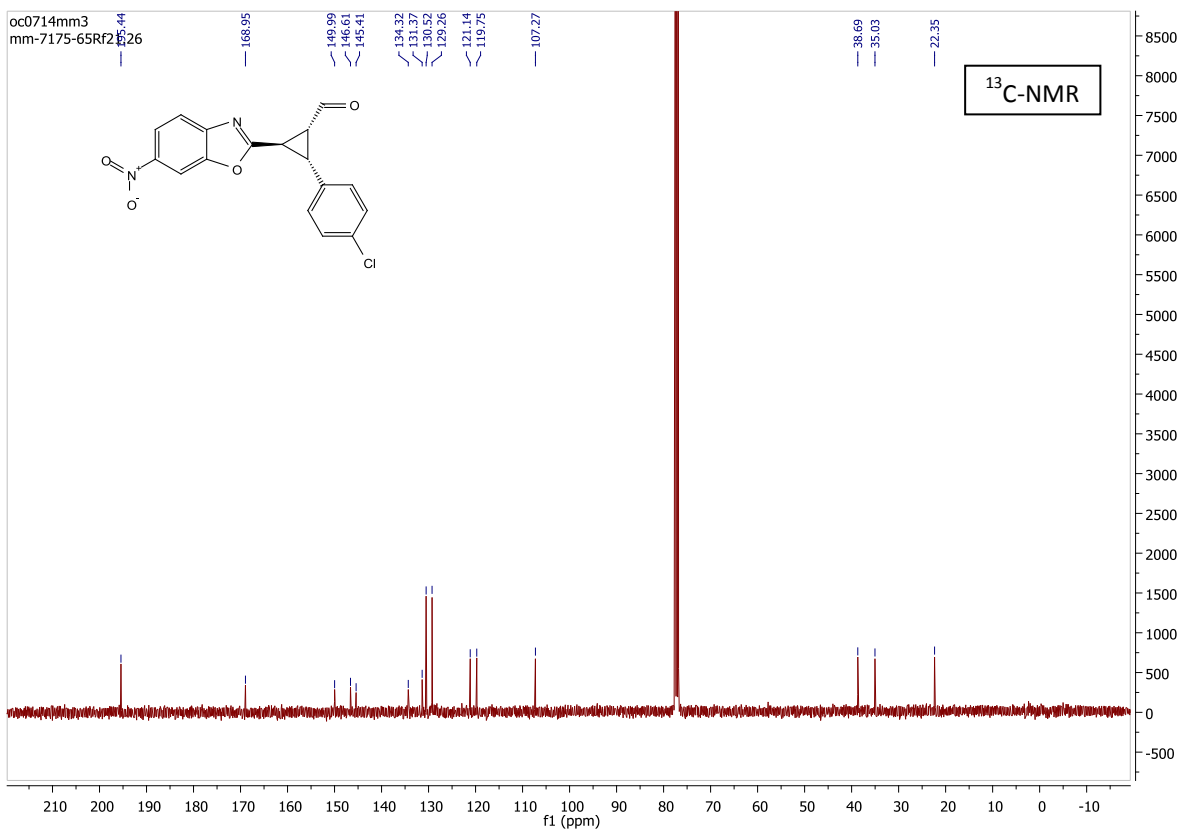
major diastereomer:



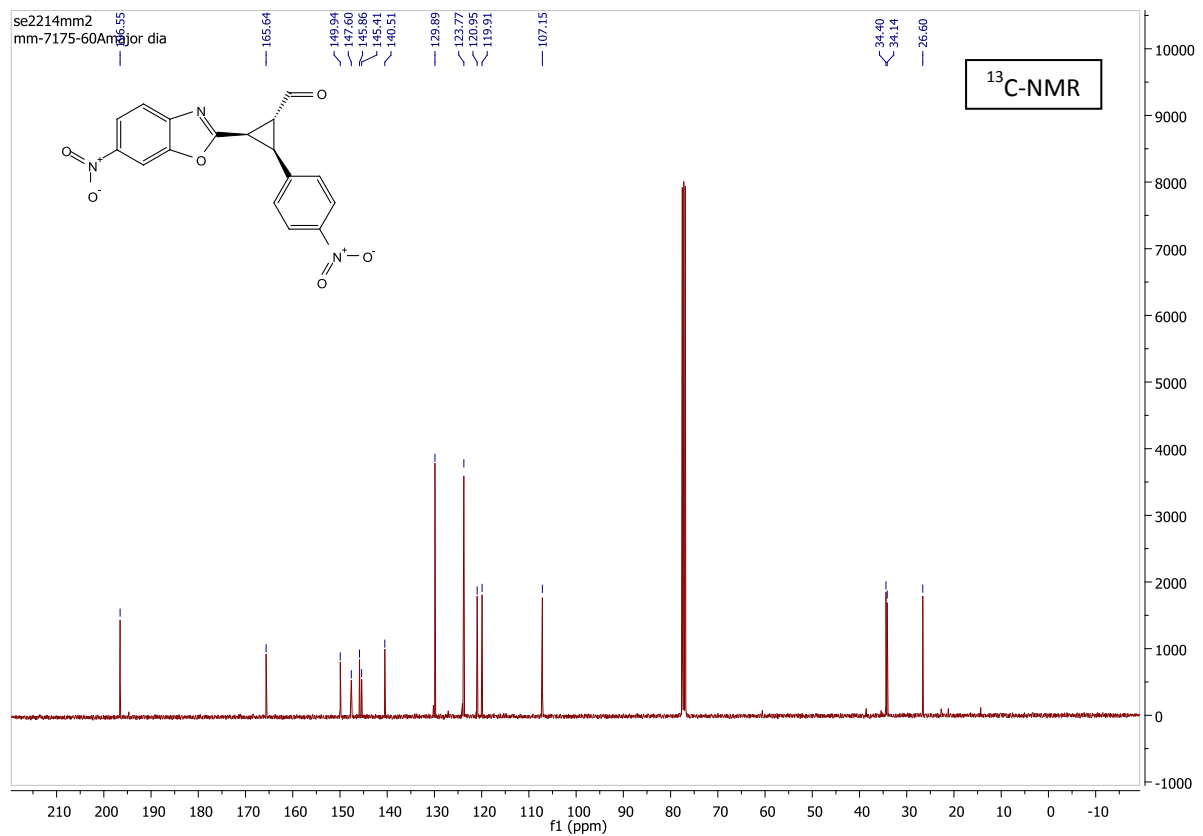
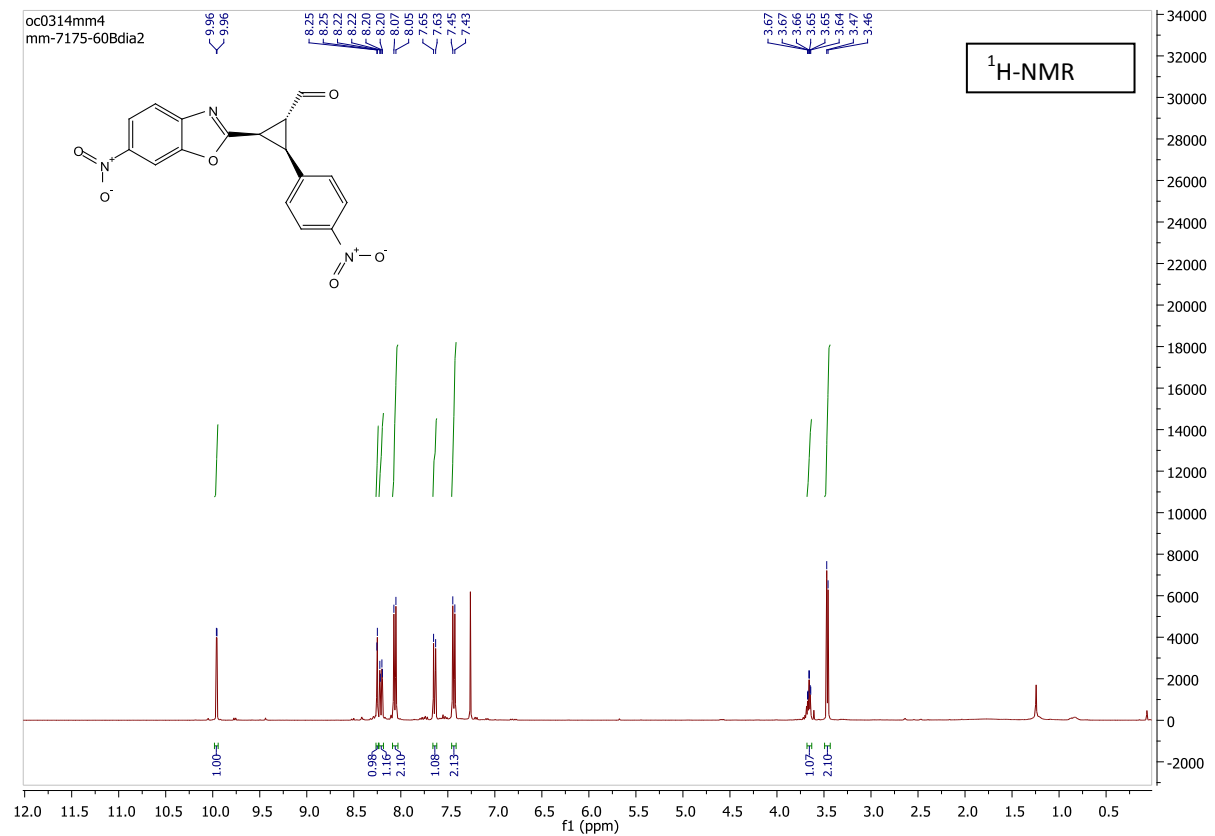


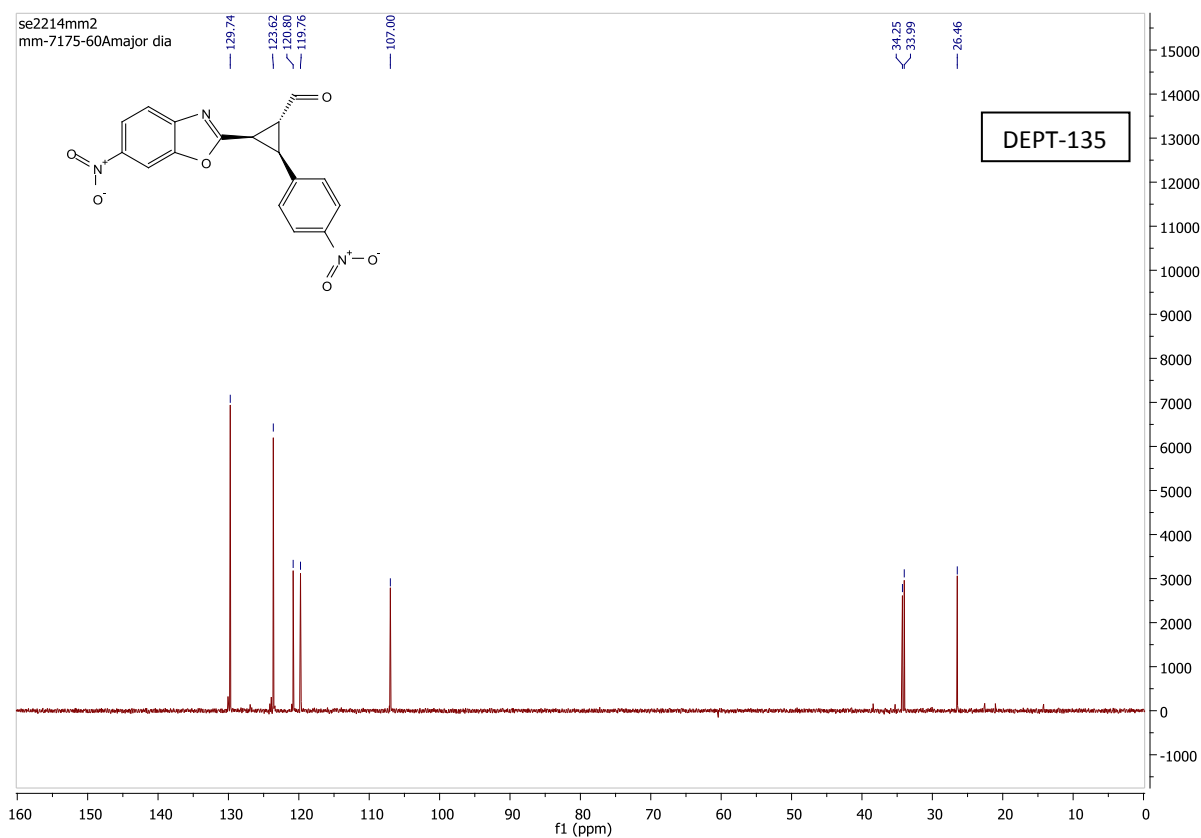
minor diastereomer with traces of minor':



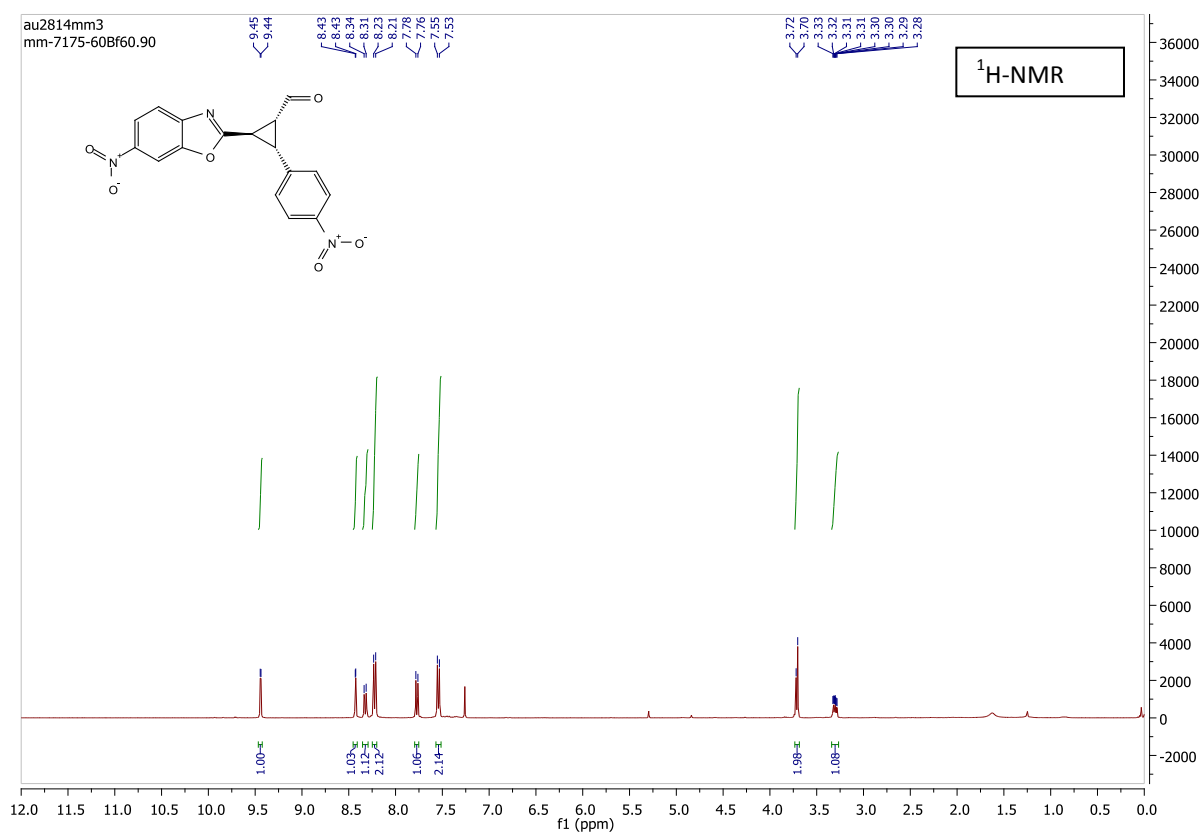


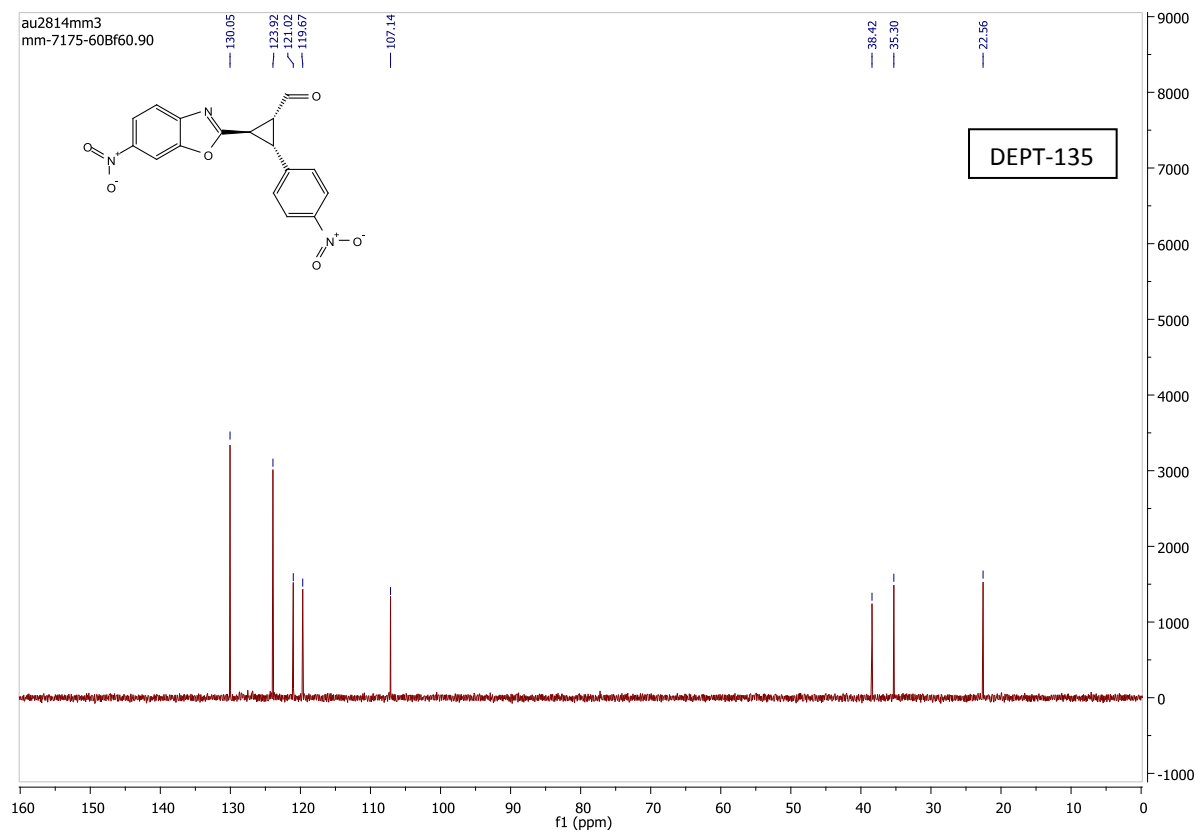
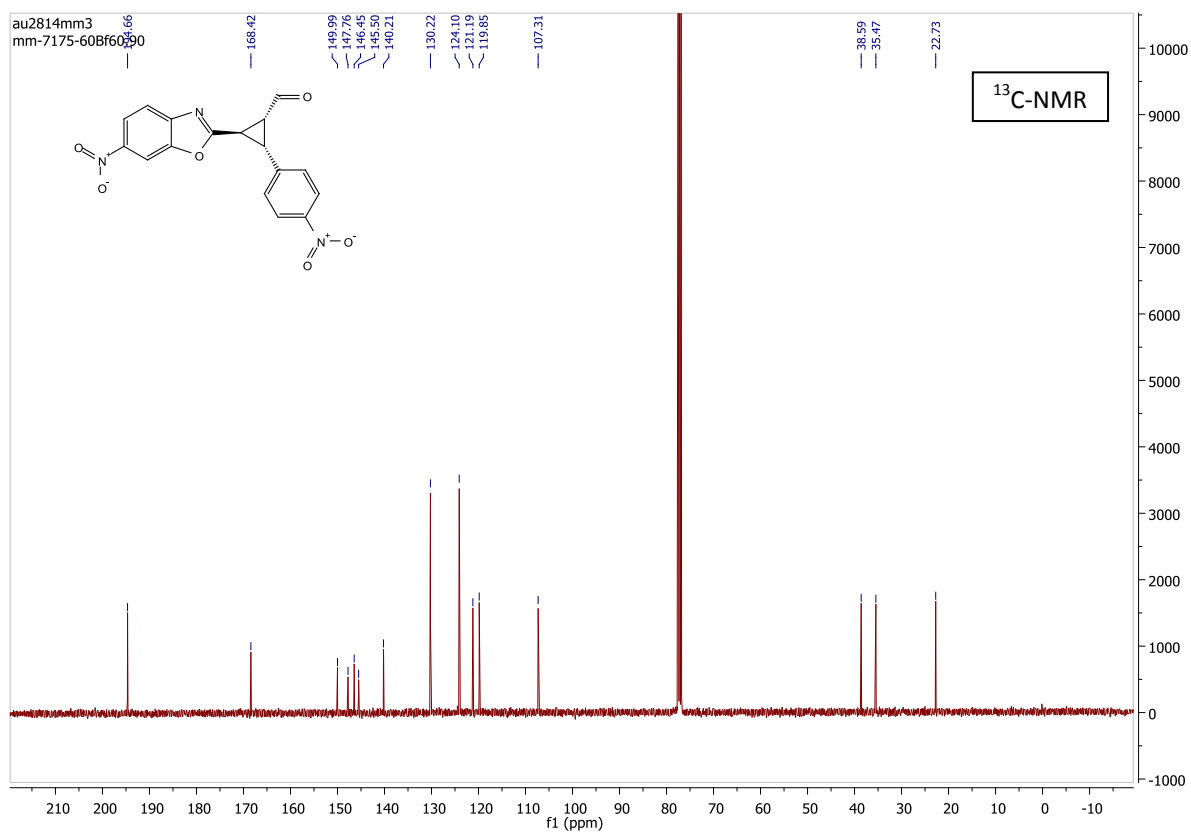
major diastereomer:



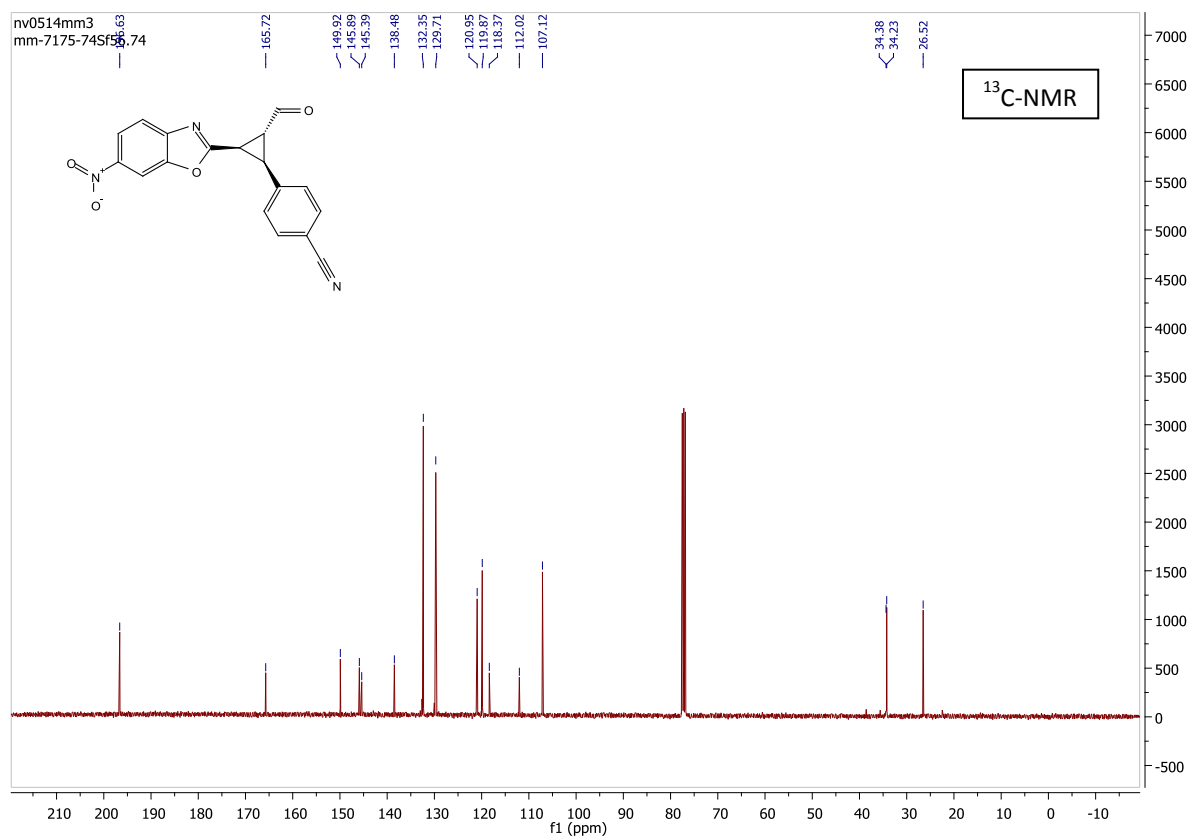
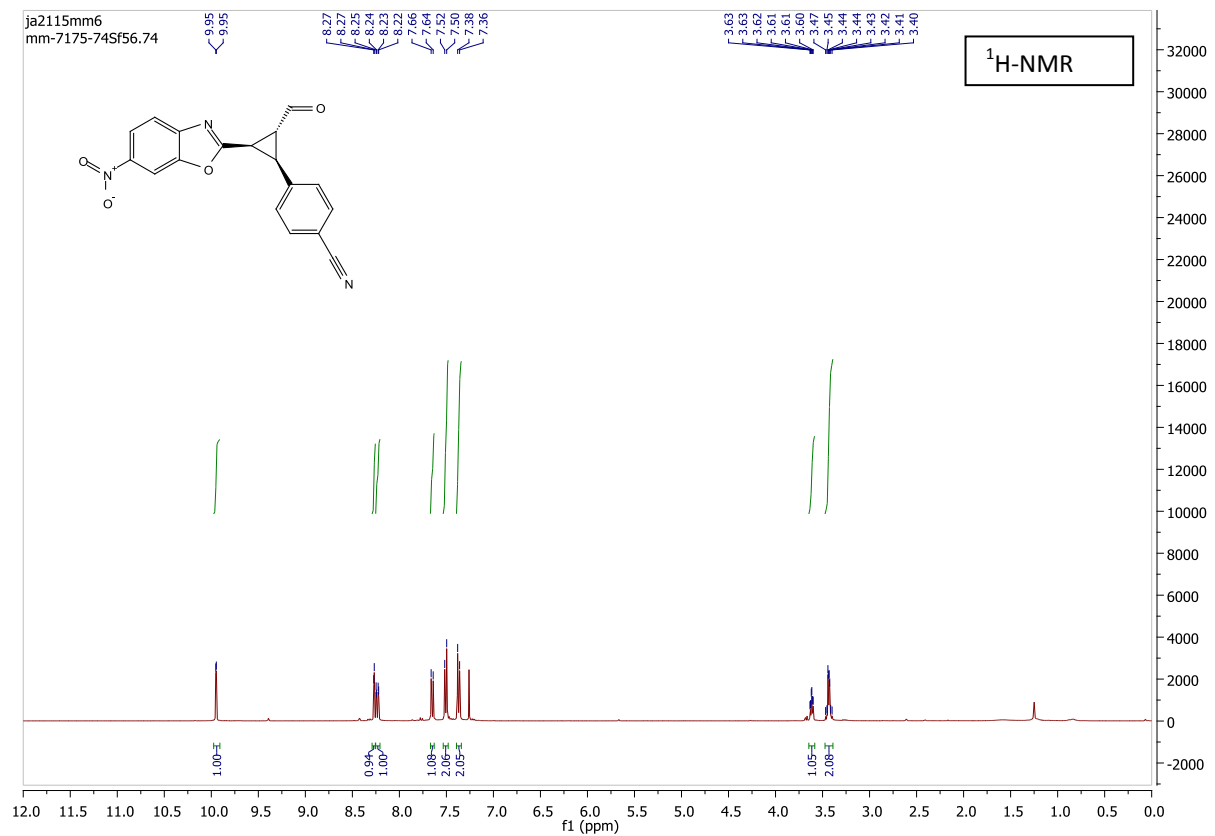


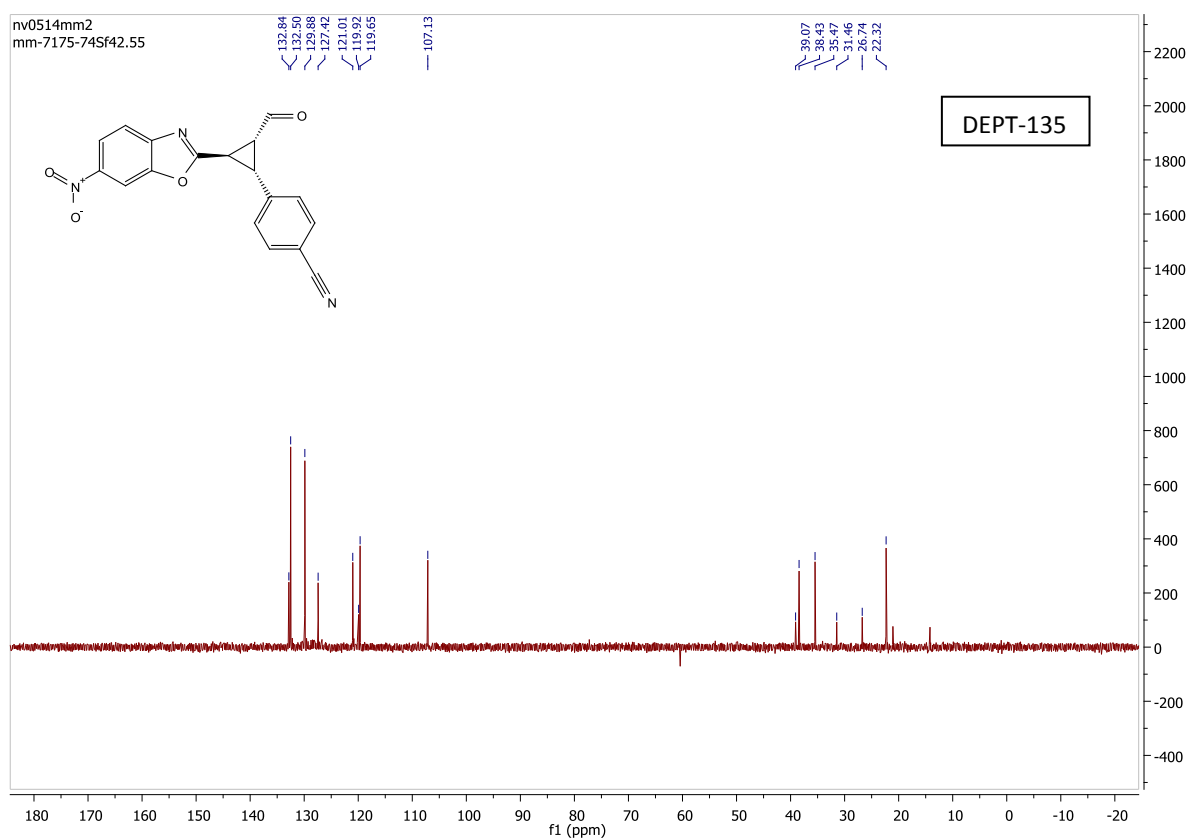
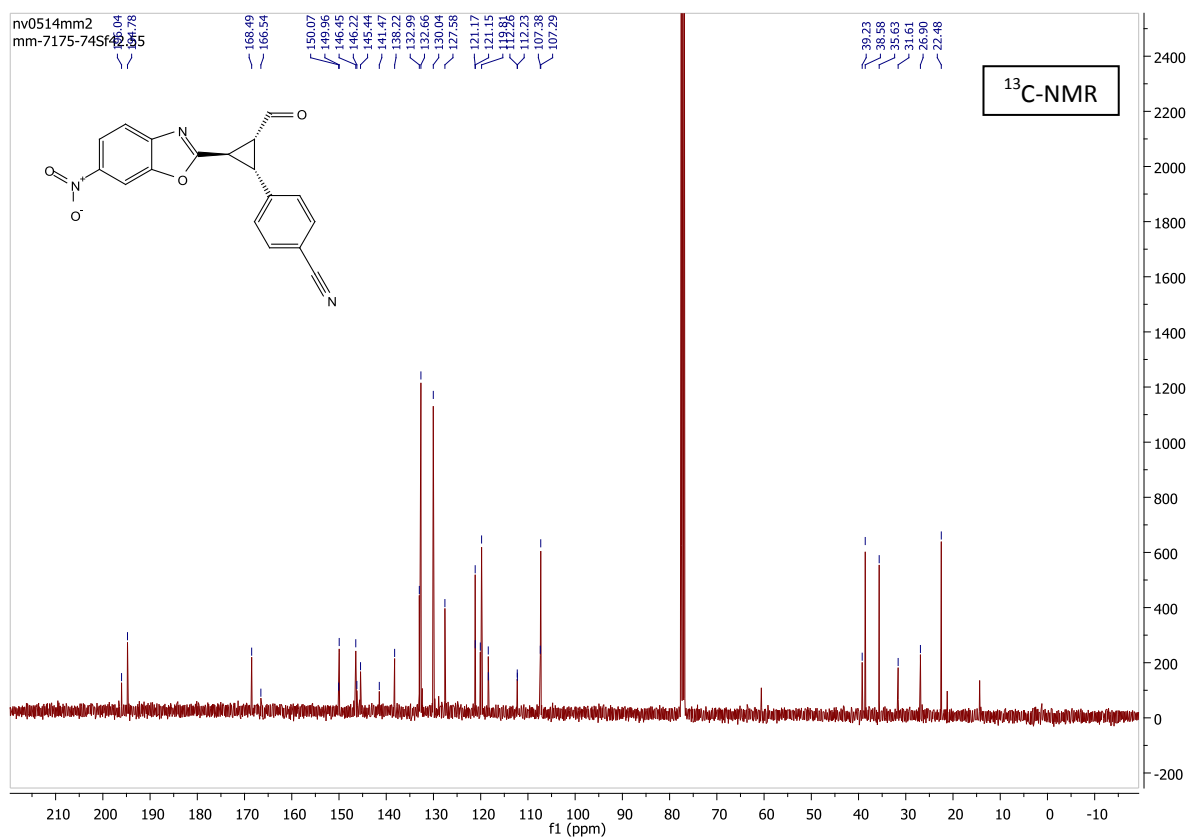
minor diastereomer:



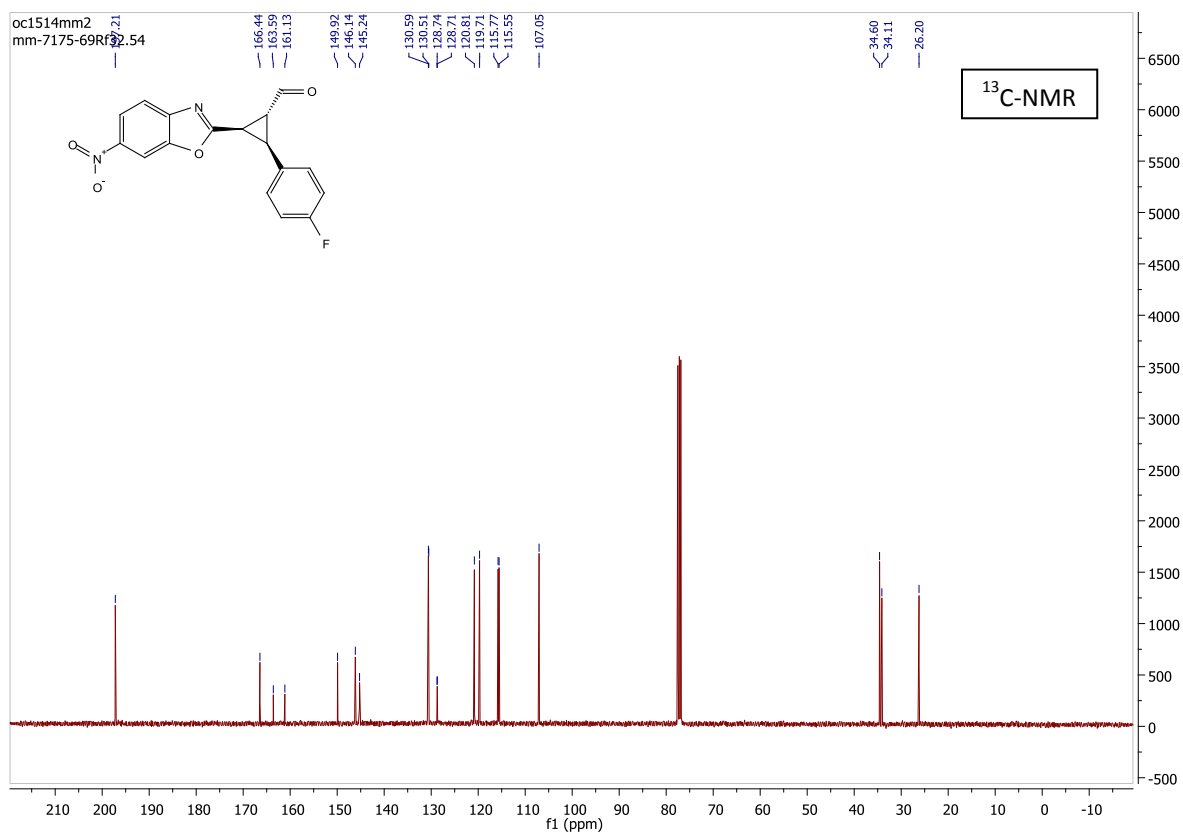
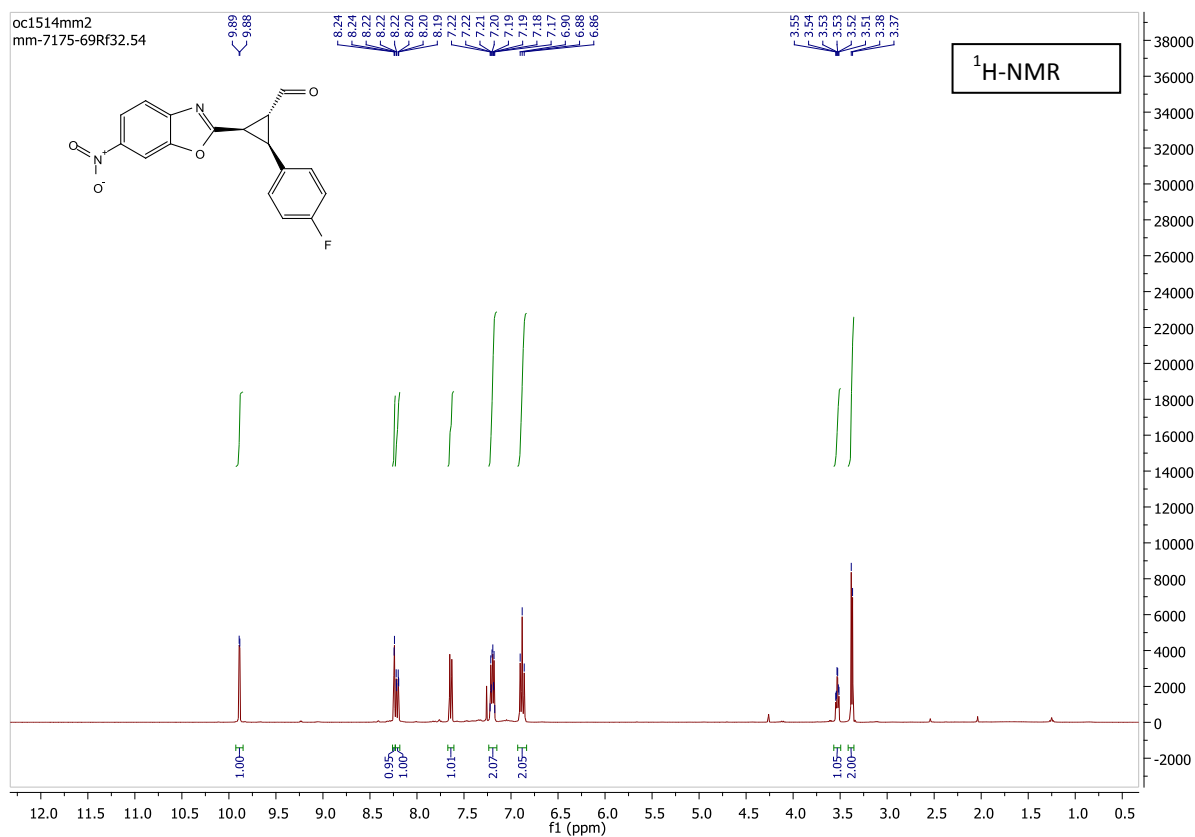


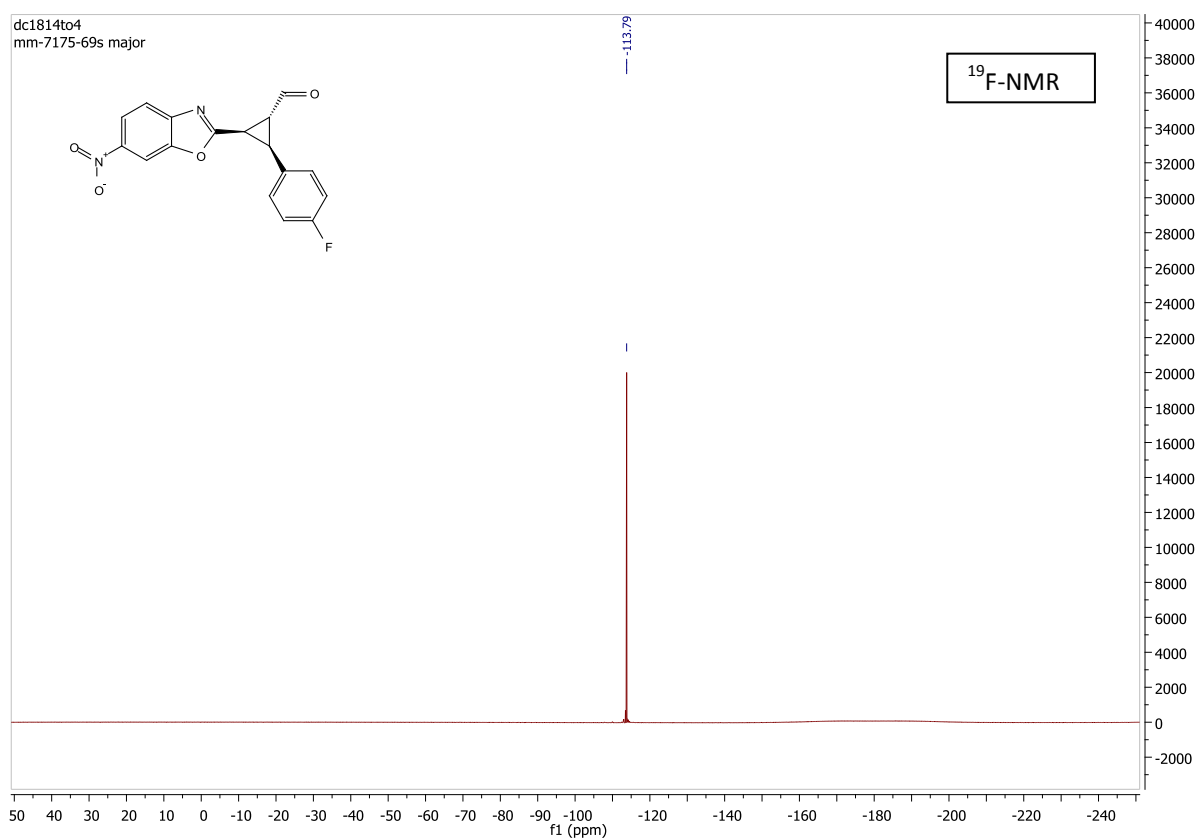
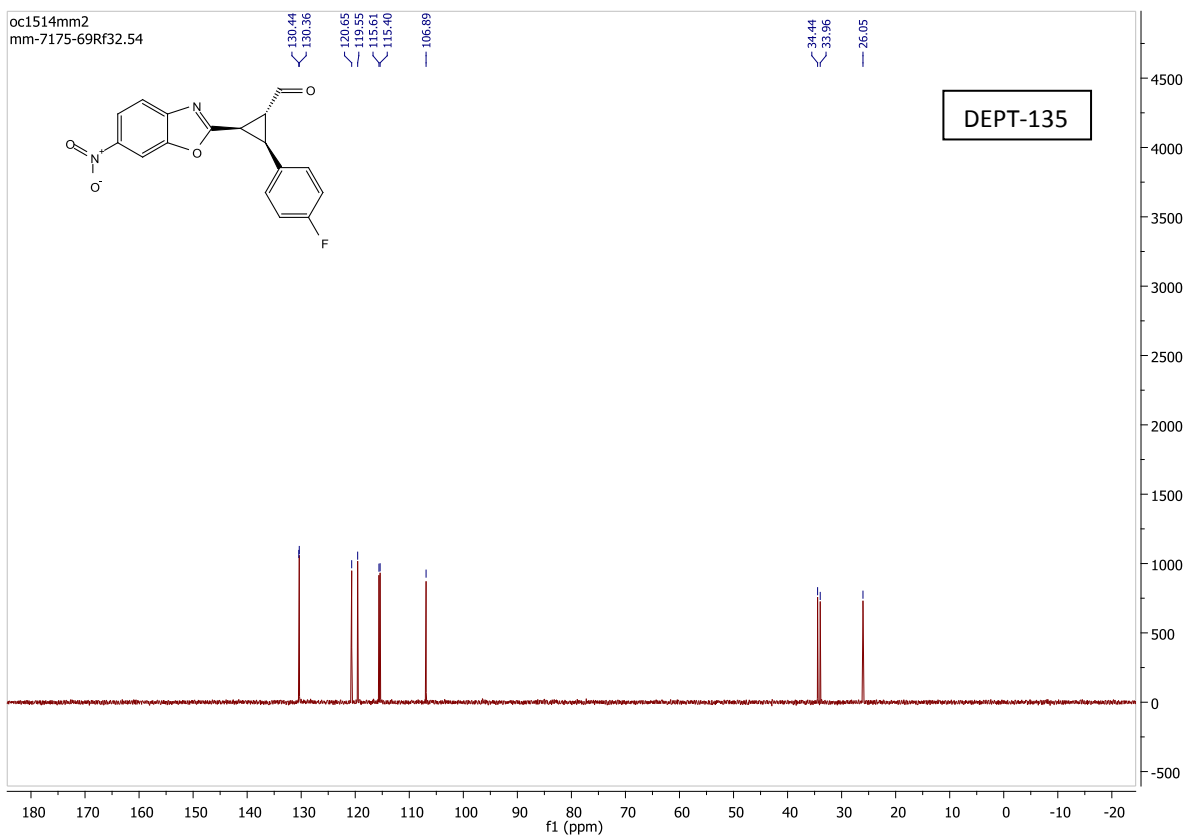
major diastereomer:



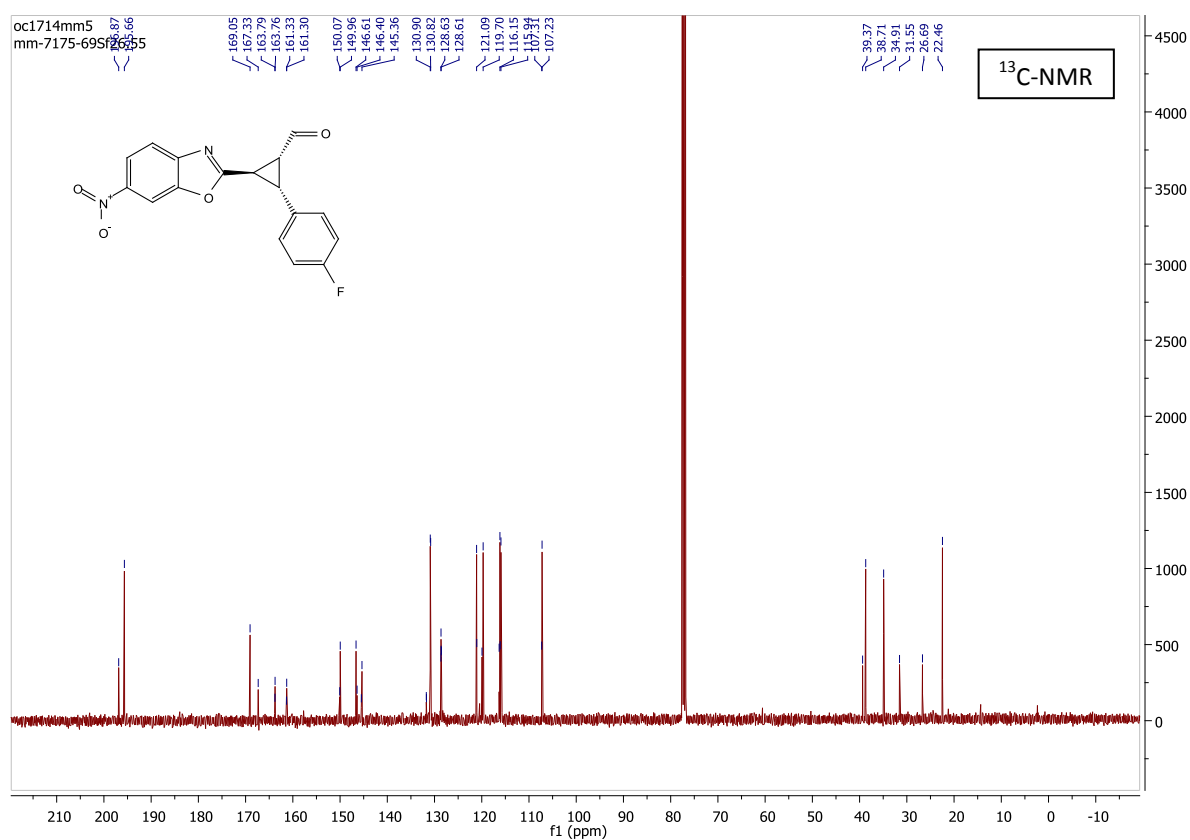
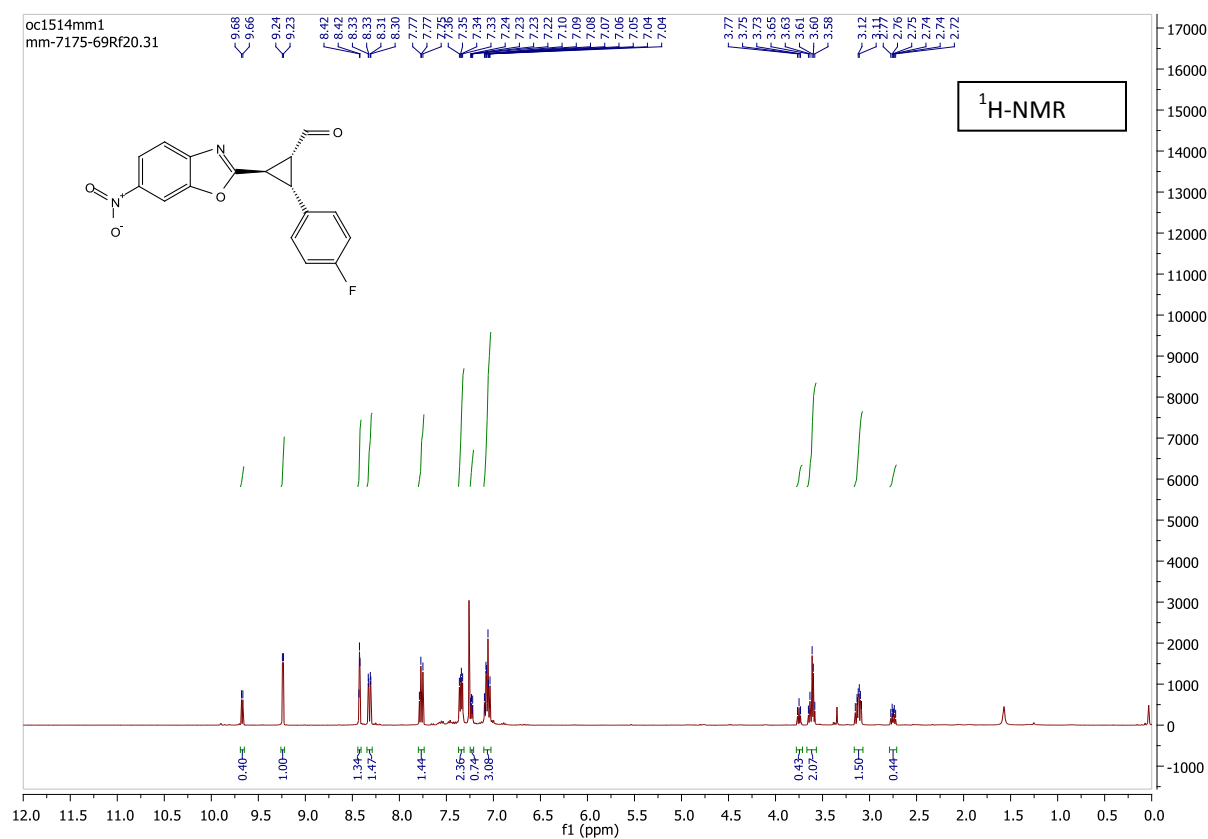


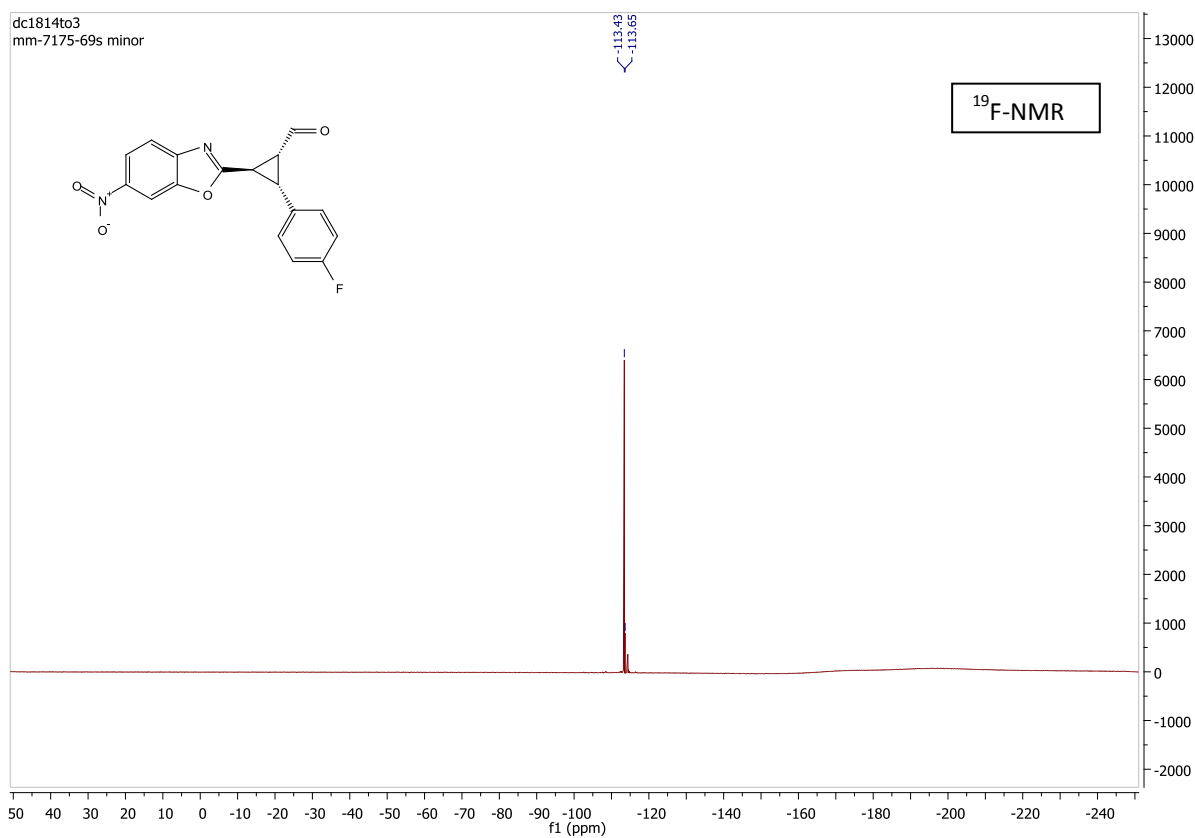
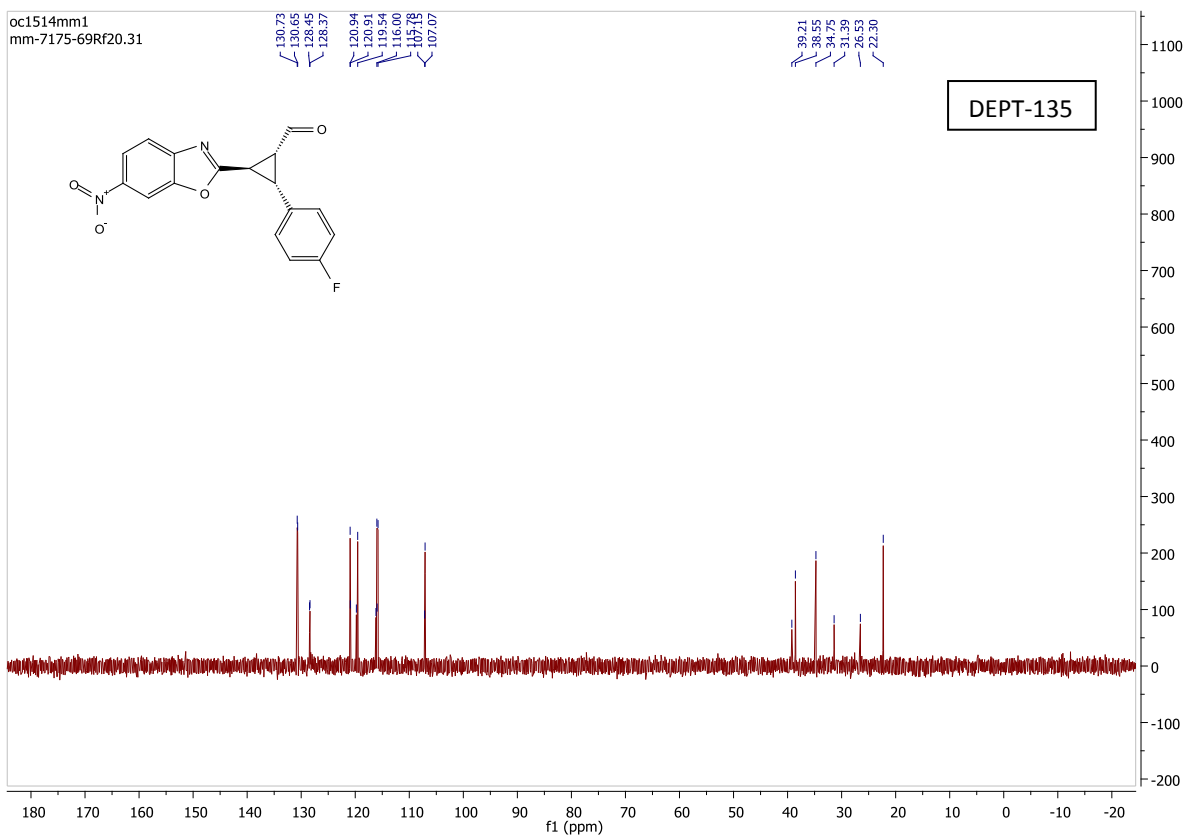
major diastereomer:



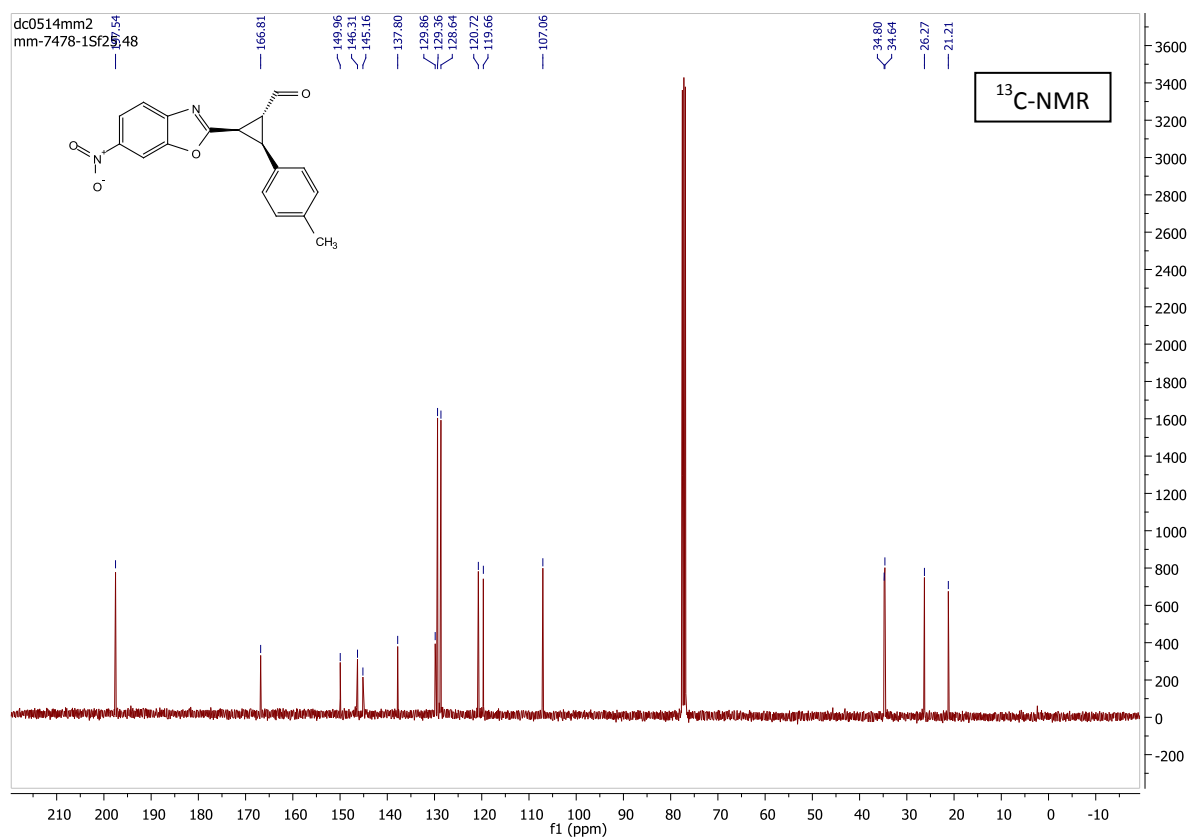
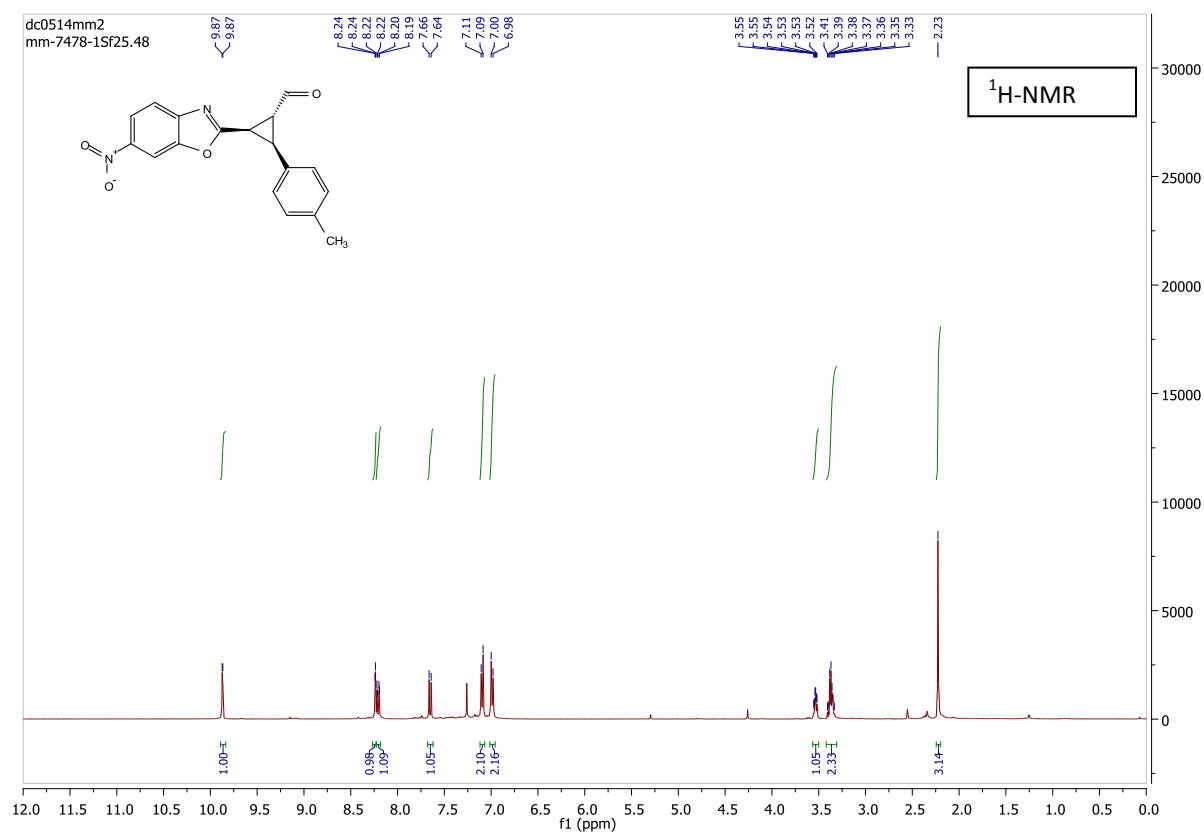


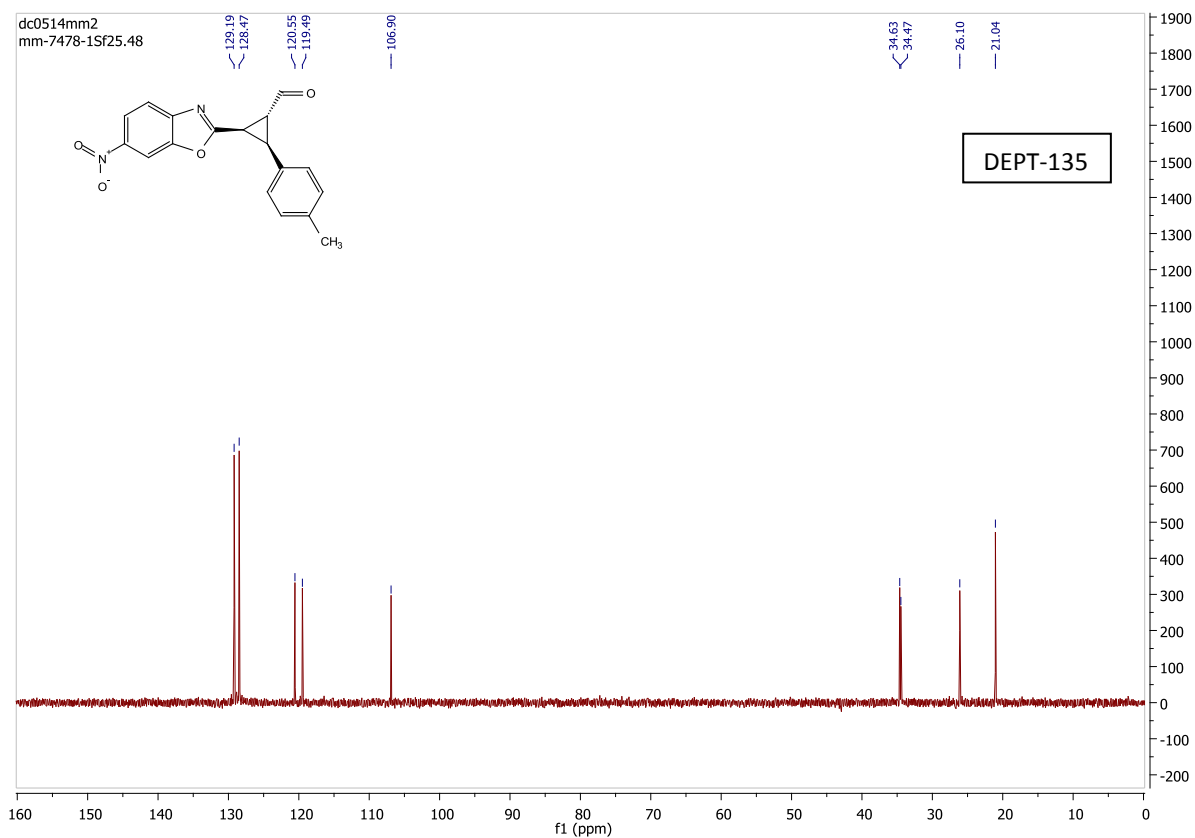
mixture of minor and minor' diastereomers:



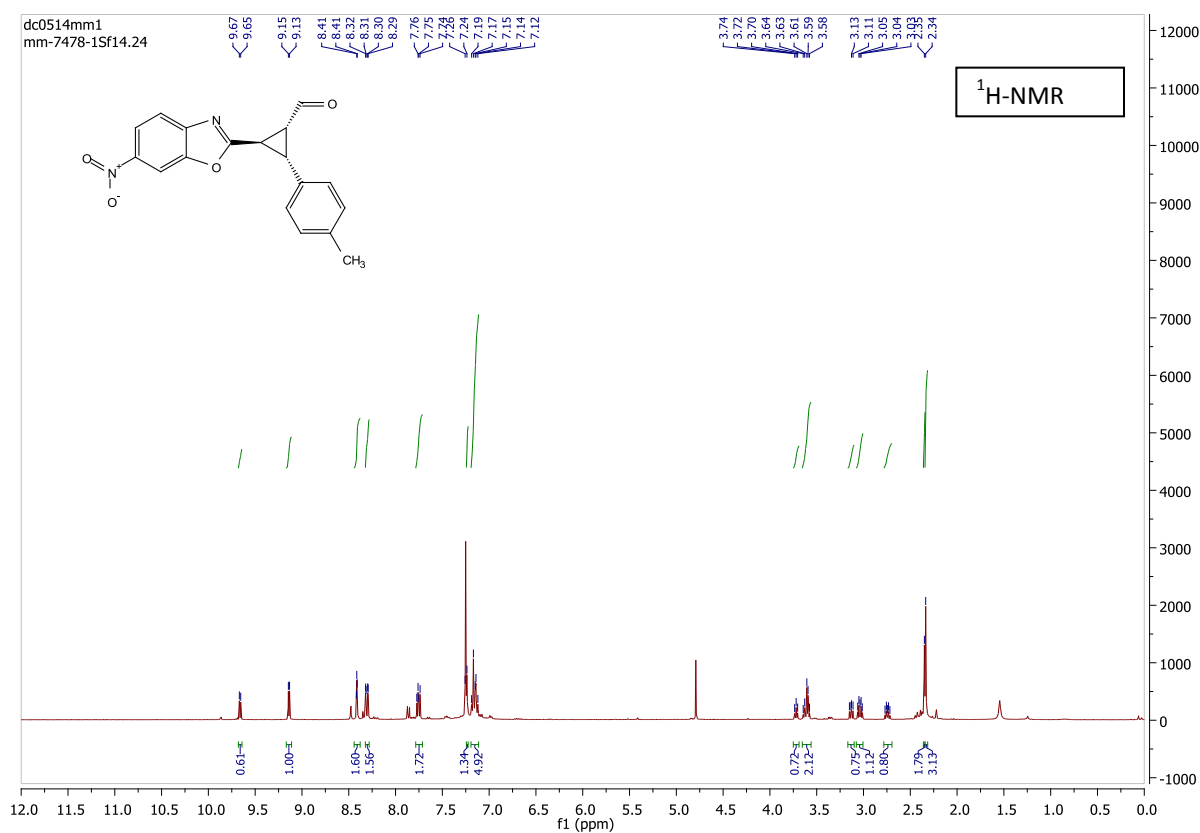


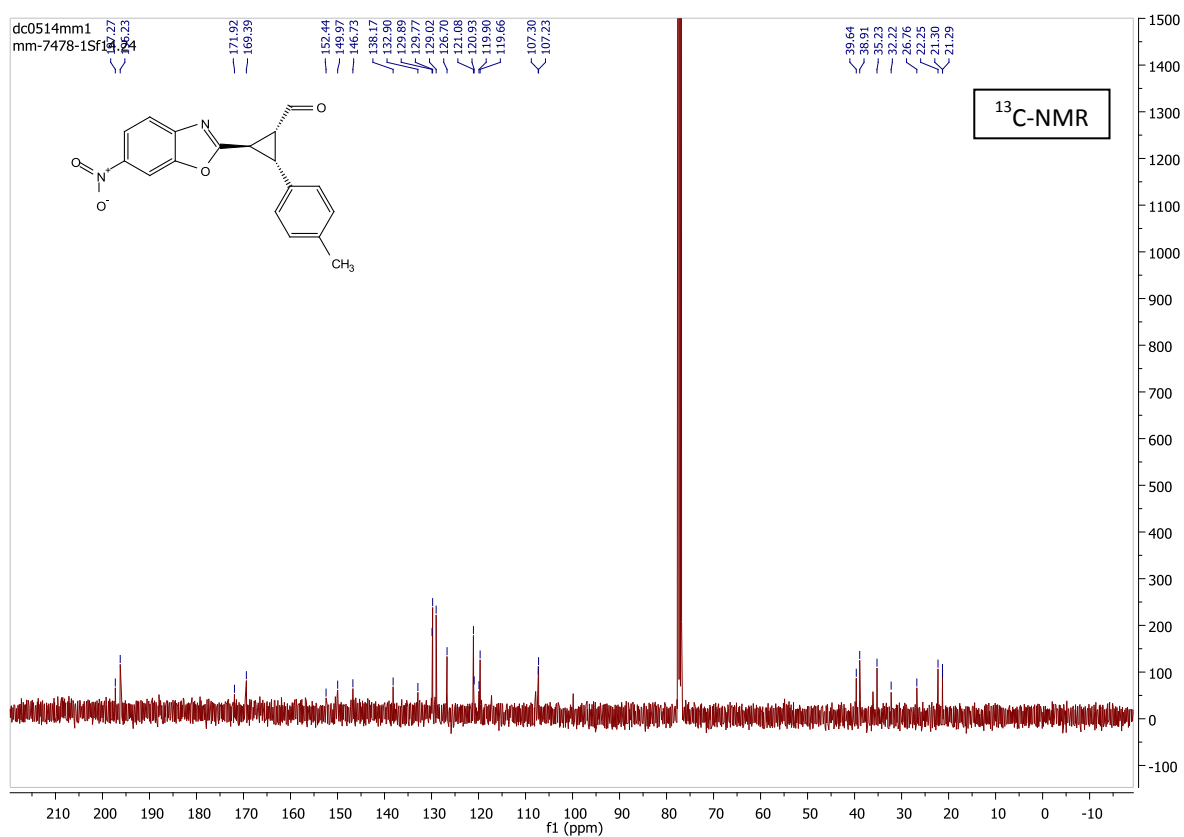
major diastereomer:



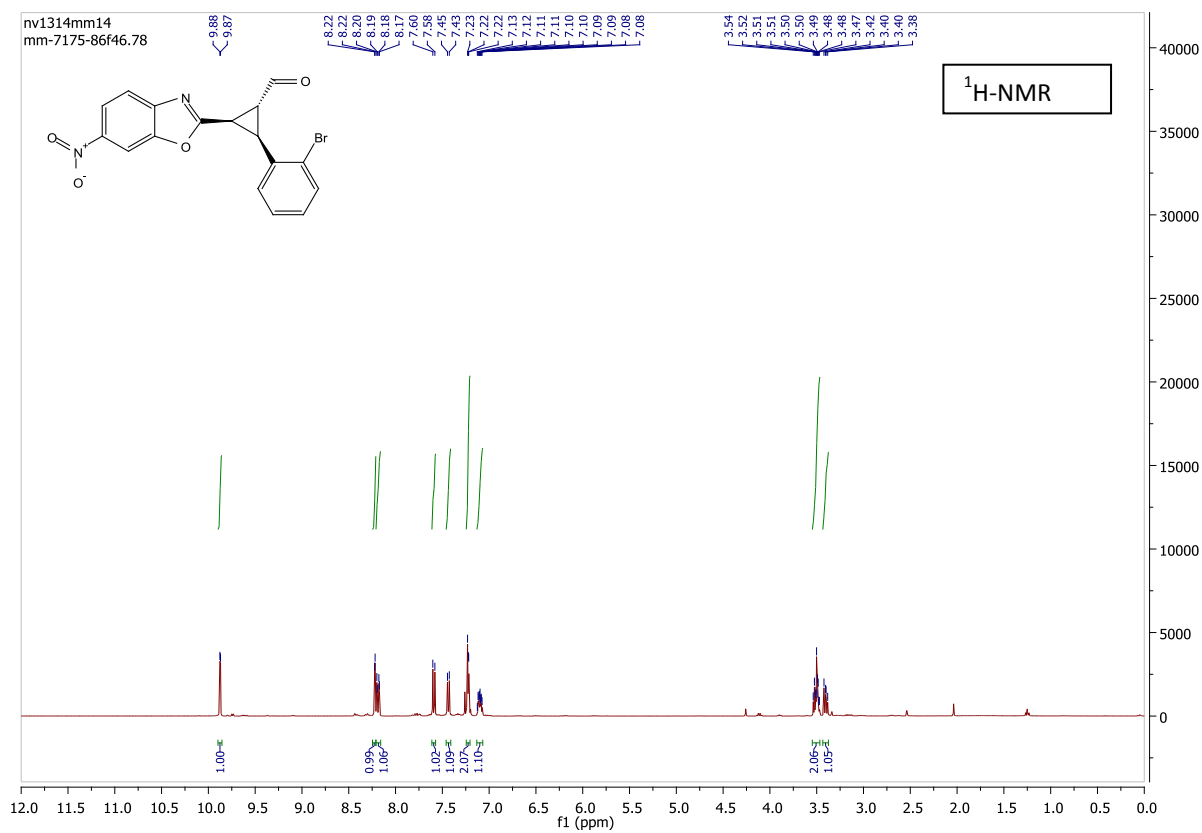


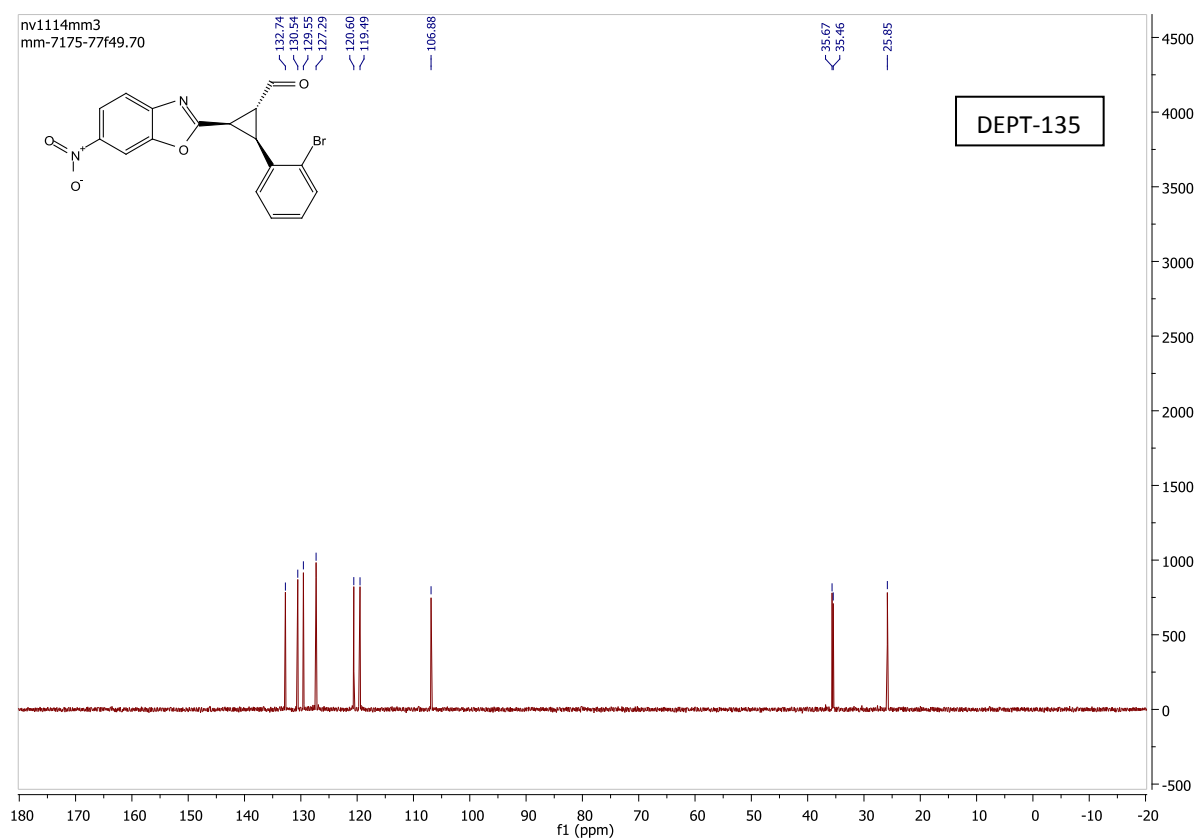
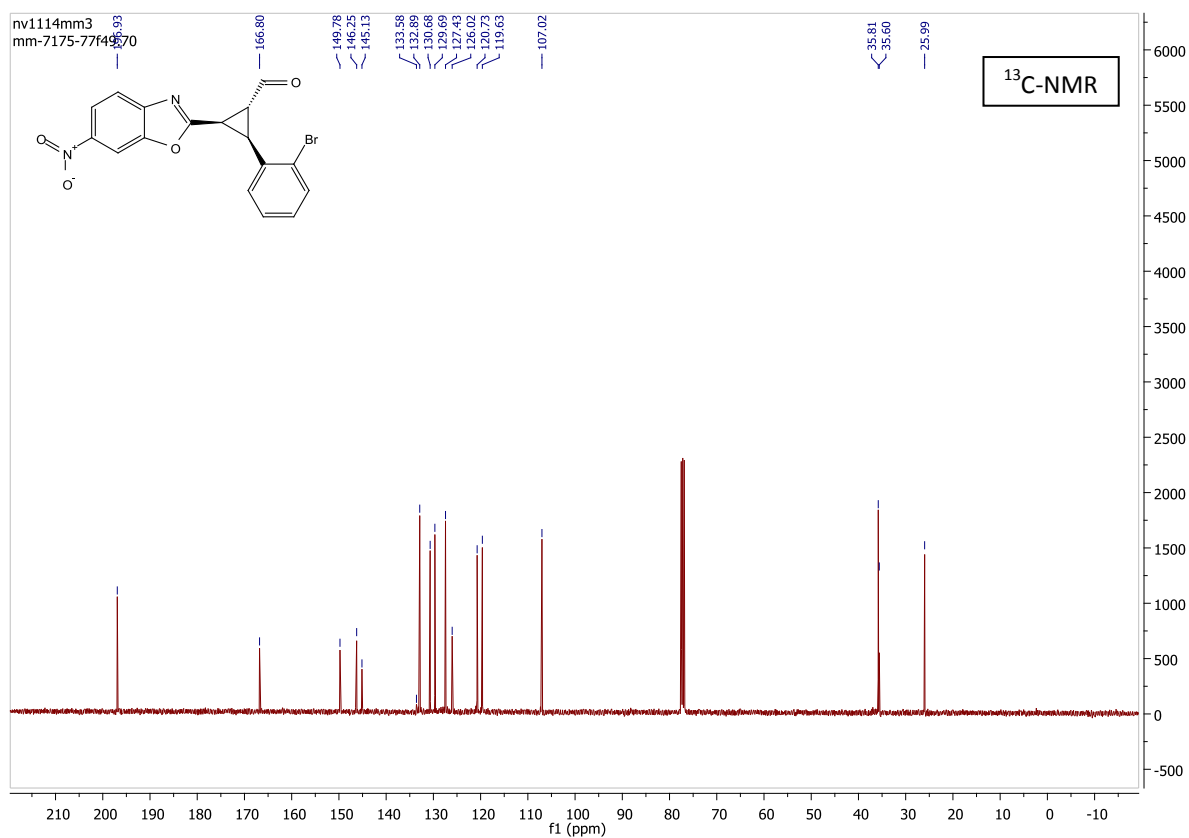
mixture of minor and minor' diastereomers:



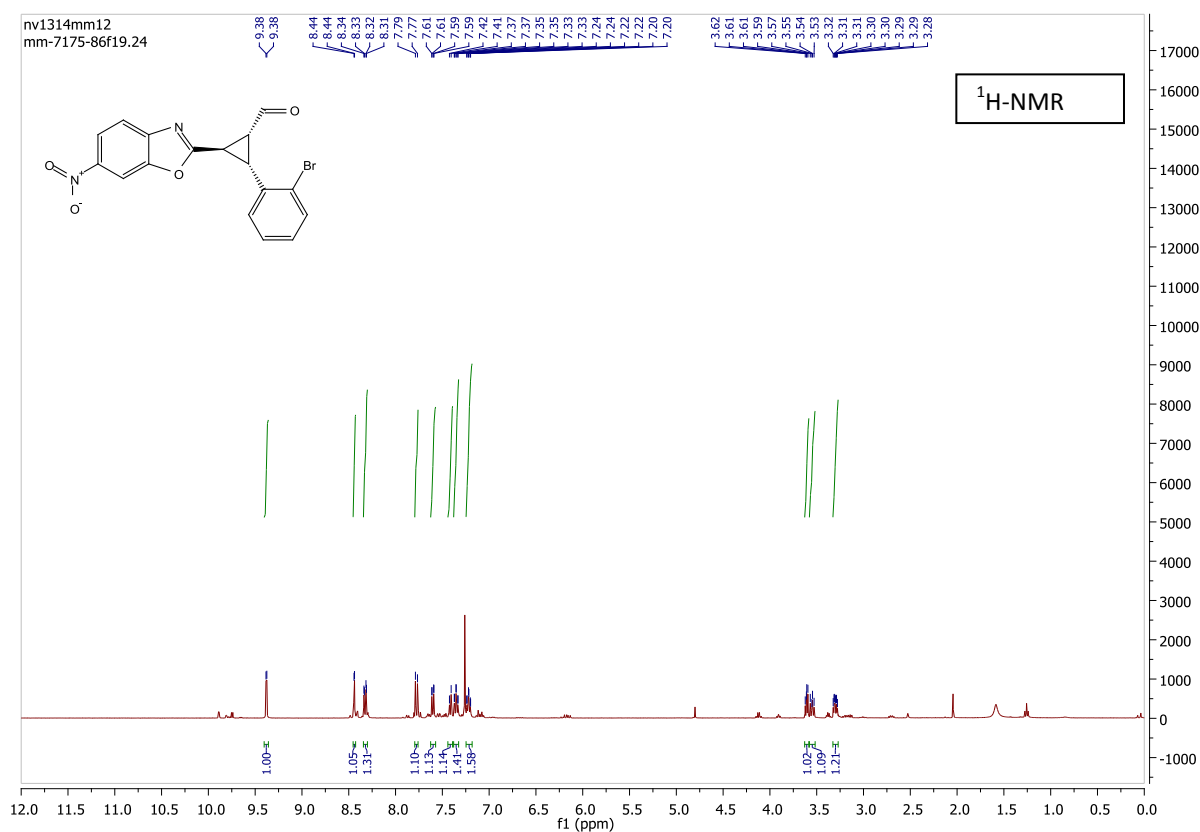


major diastereomer:

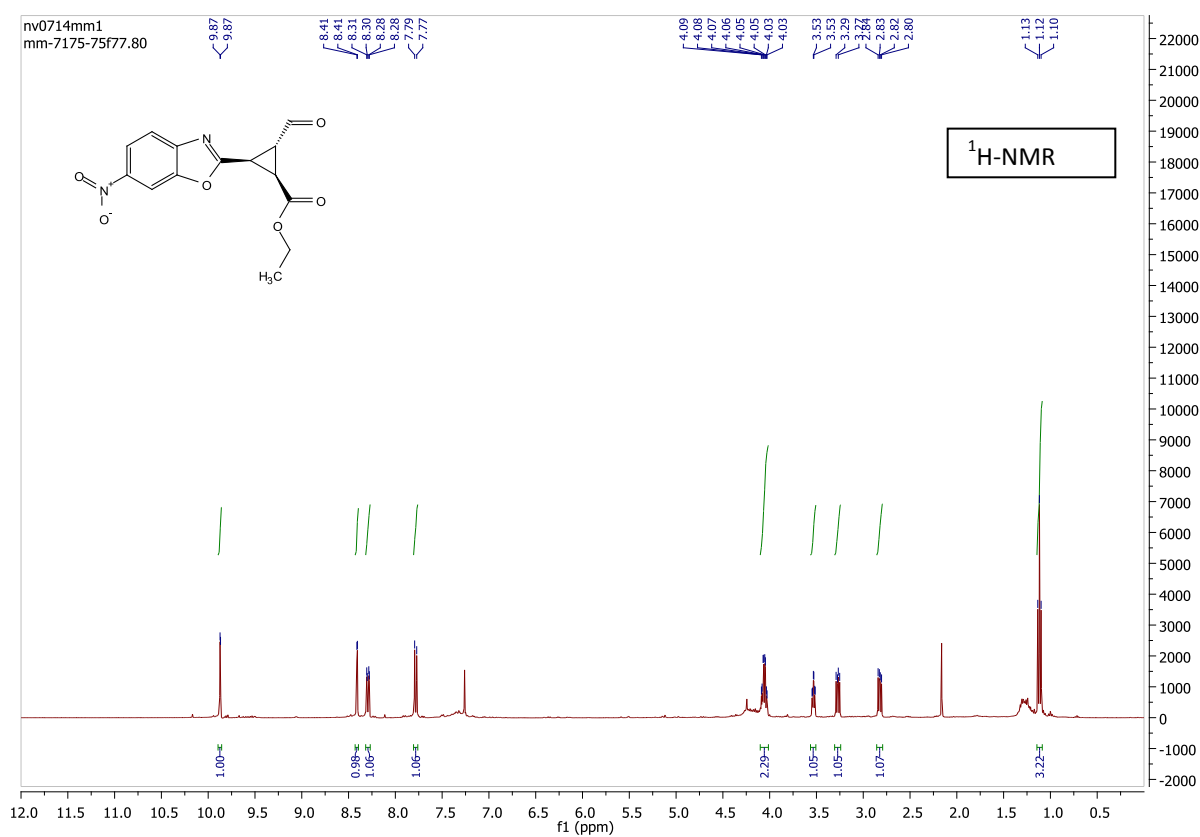


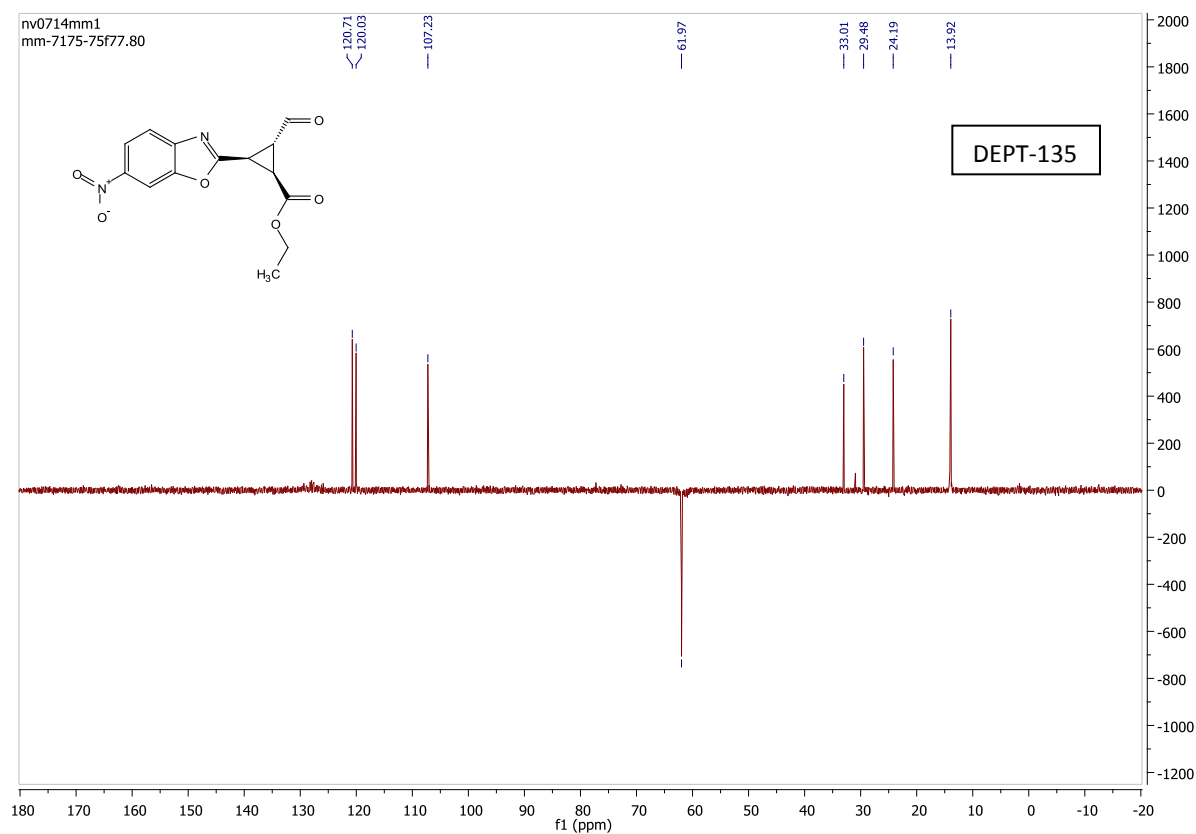
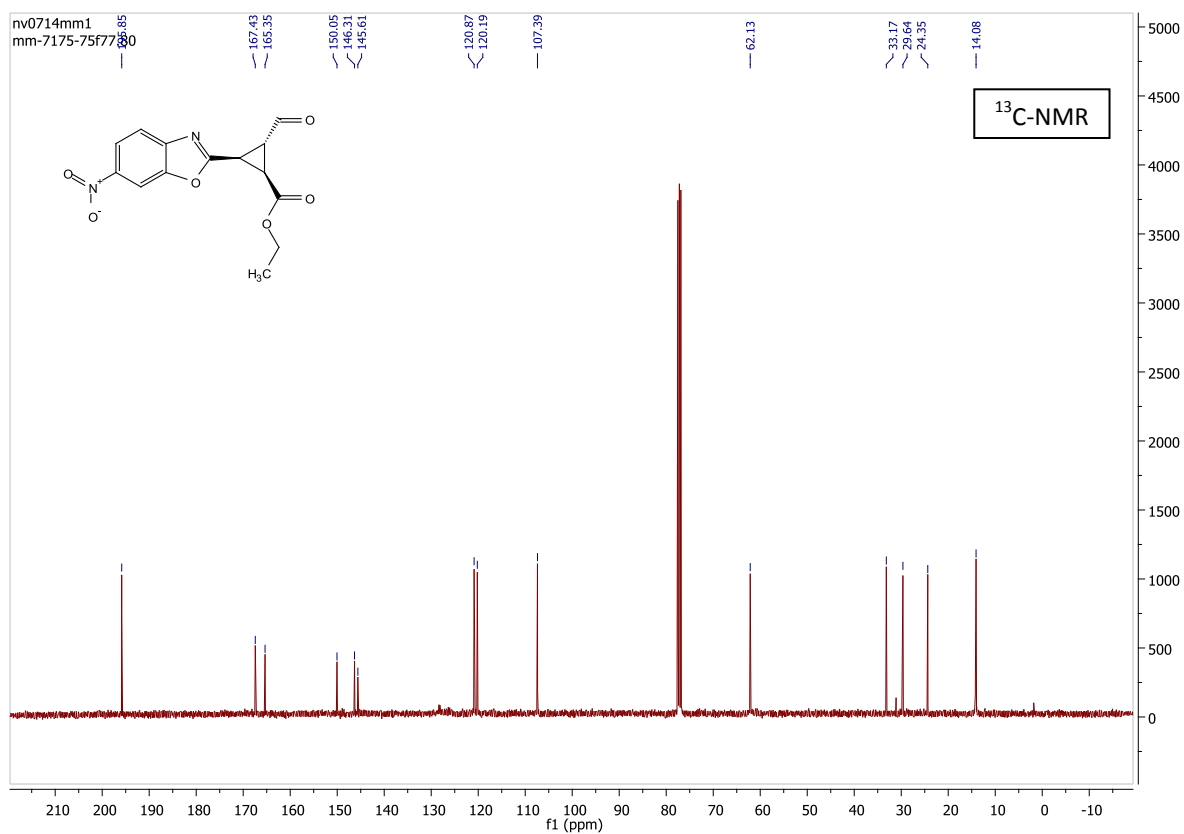


minor diastereomer + traces of minor' and major diastereomers and starting enals

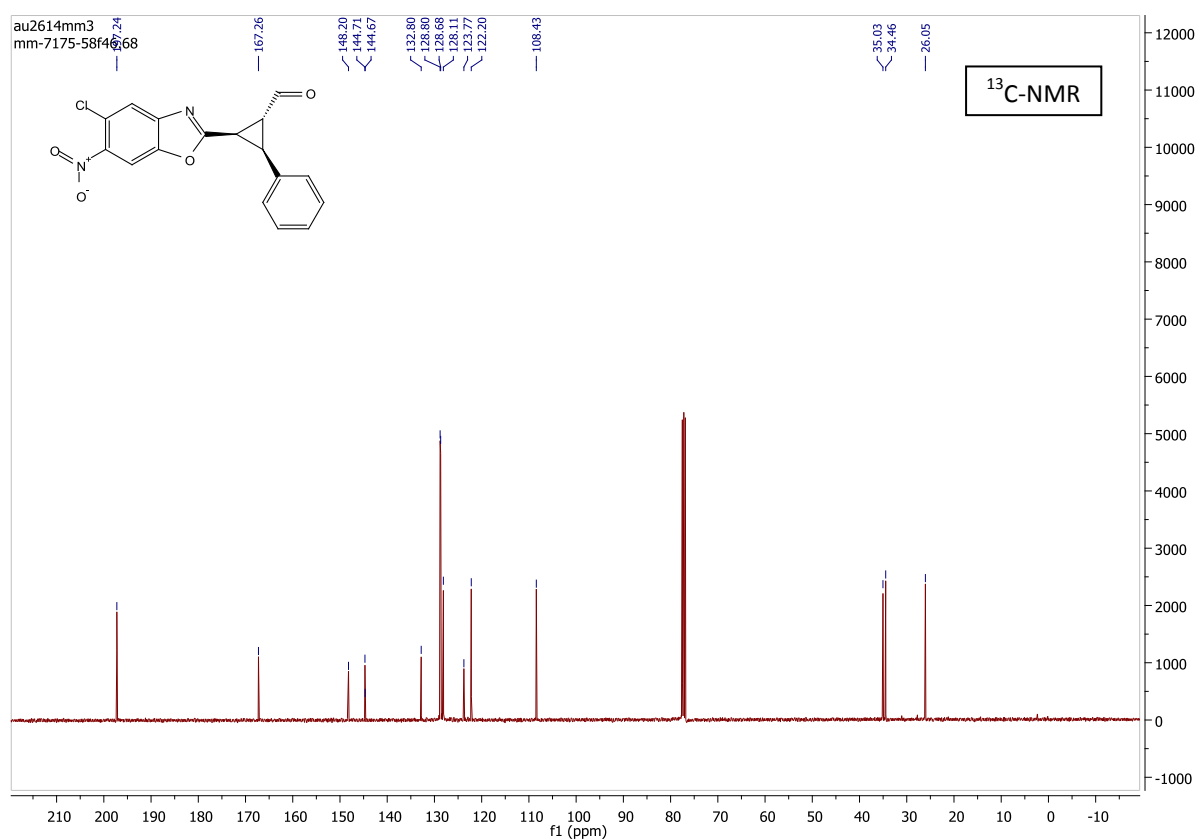
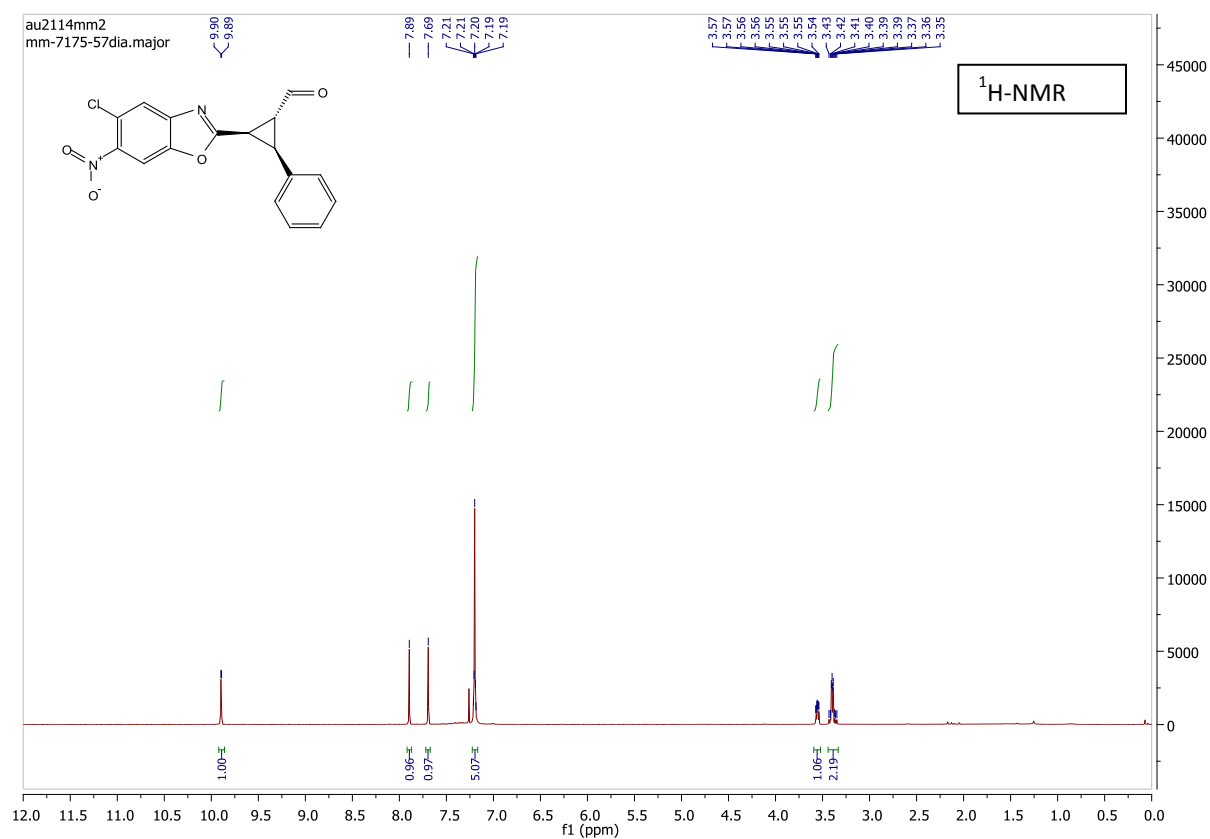


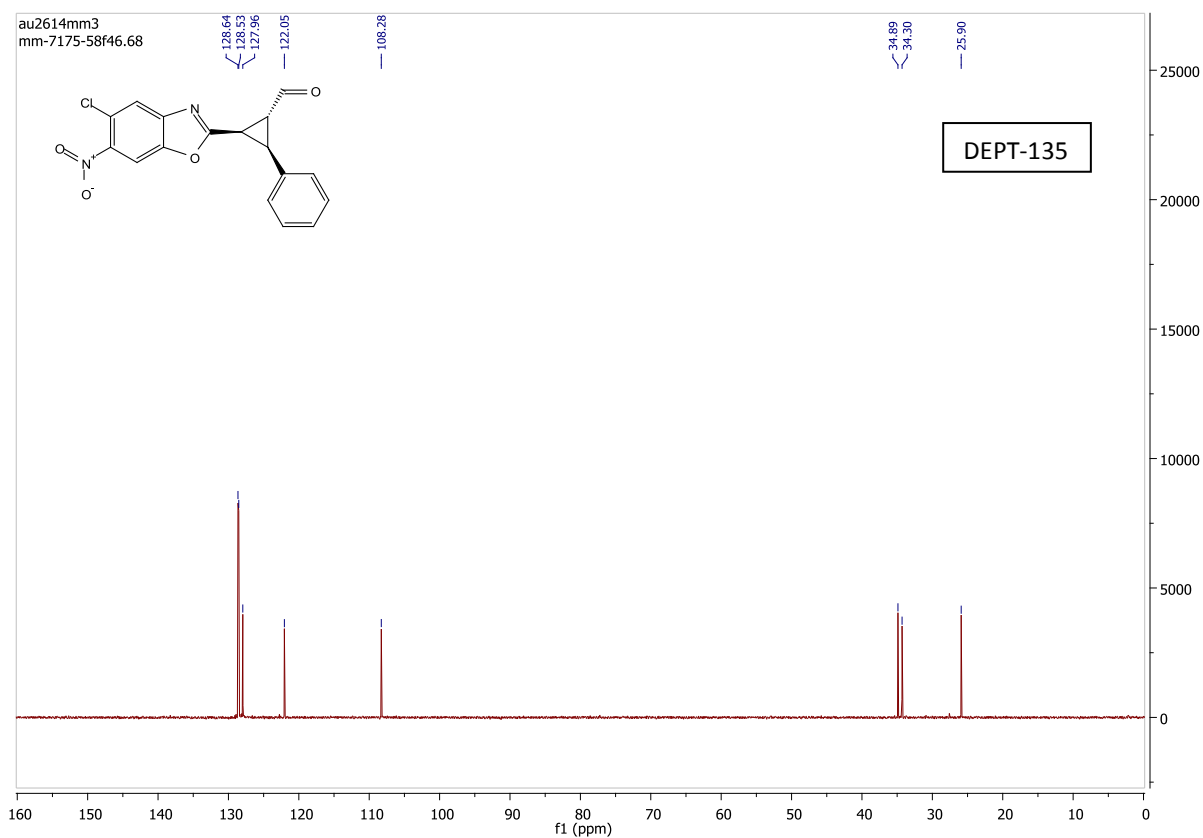
Product:



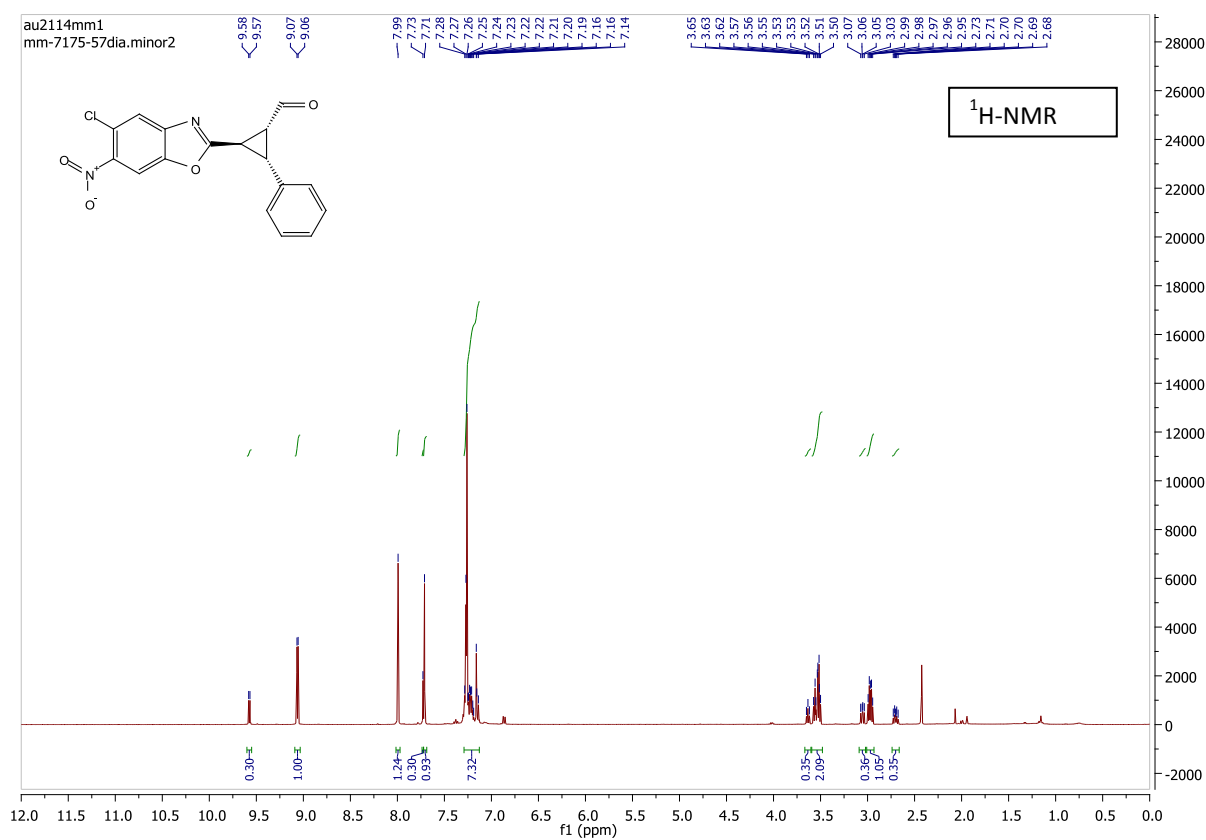


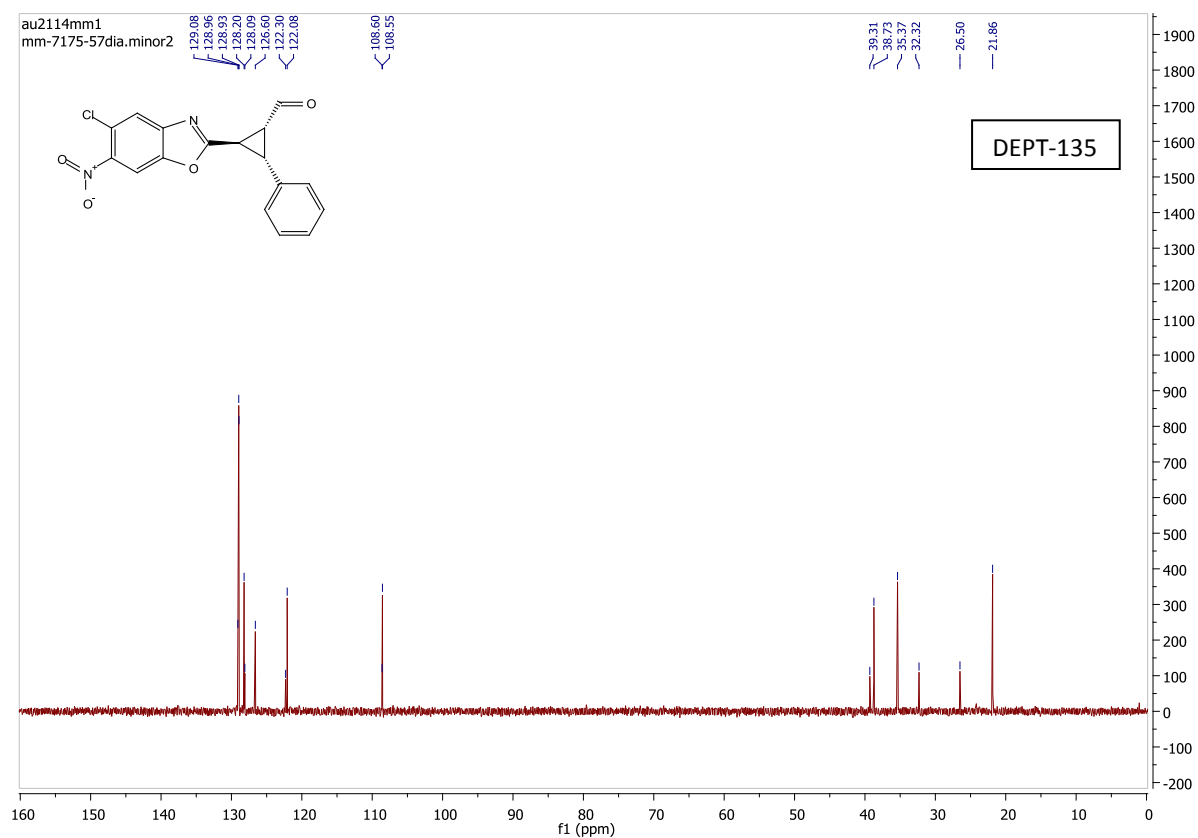
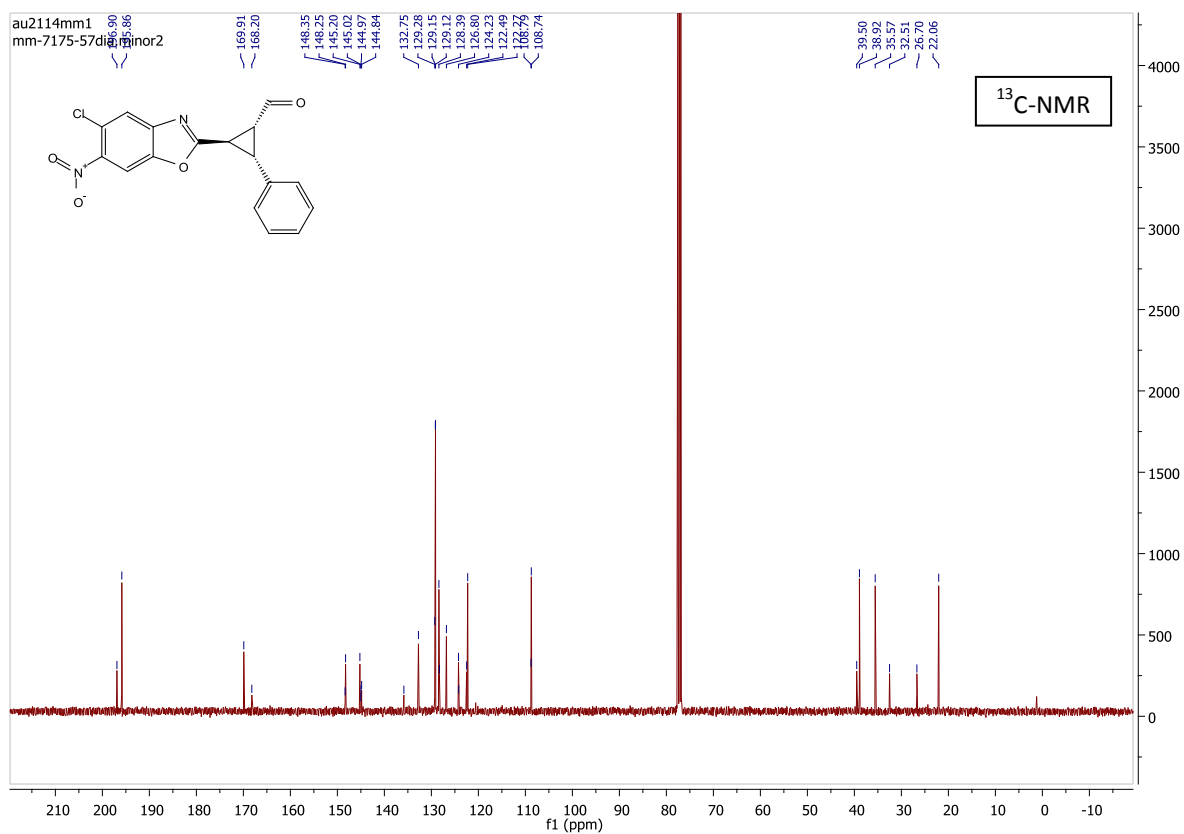
major diastereomer:



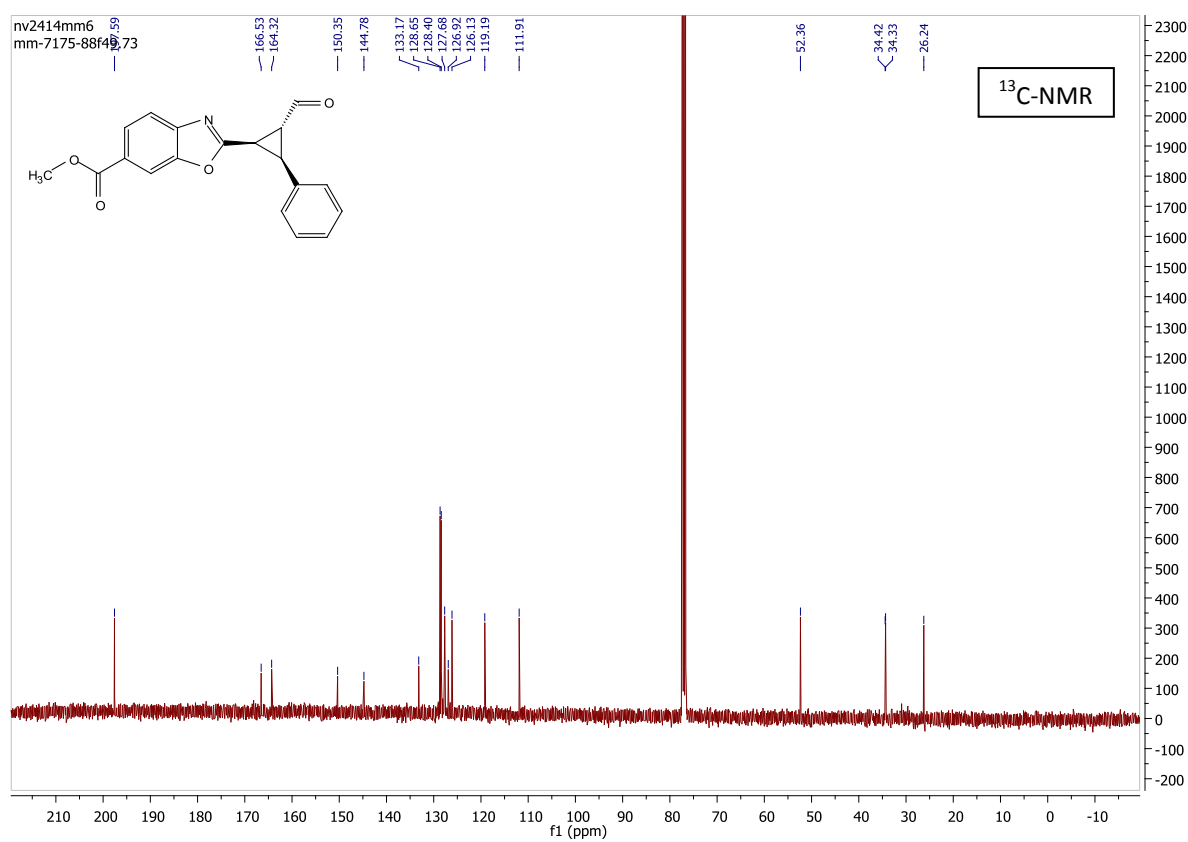
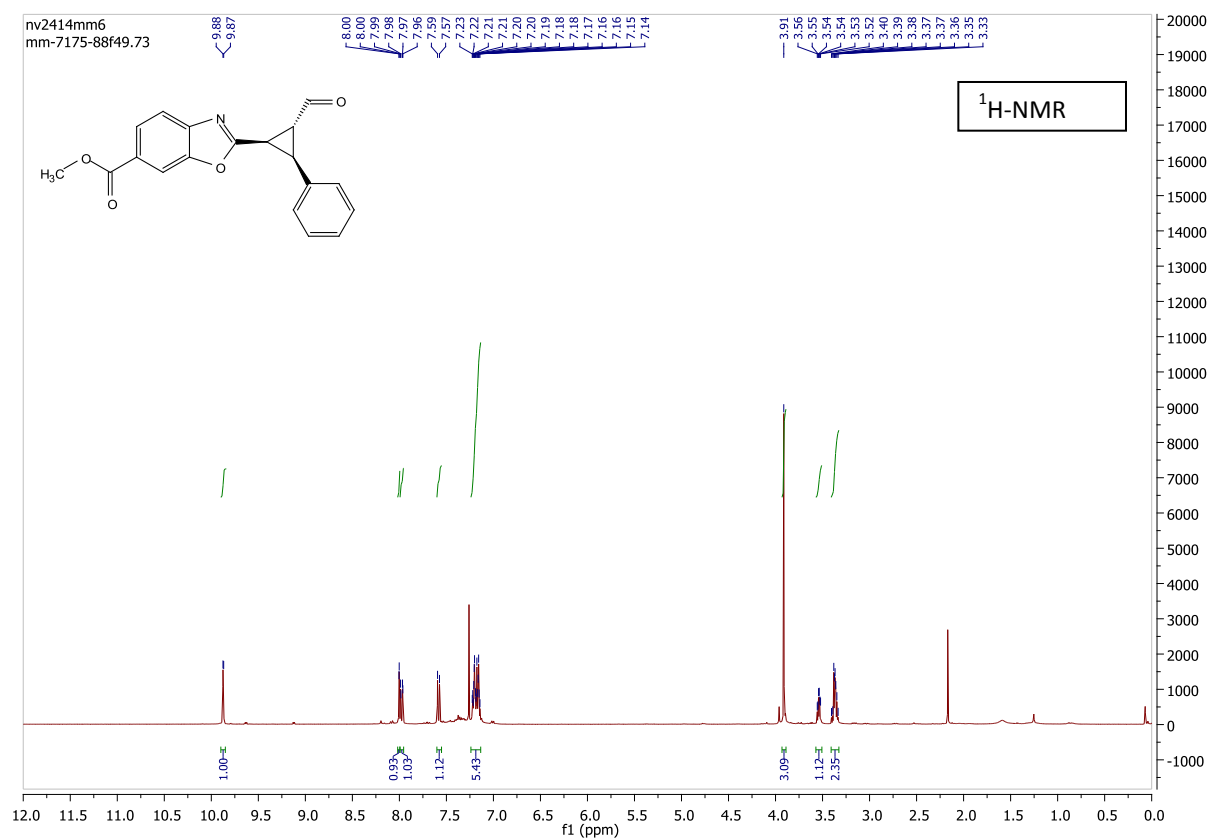


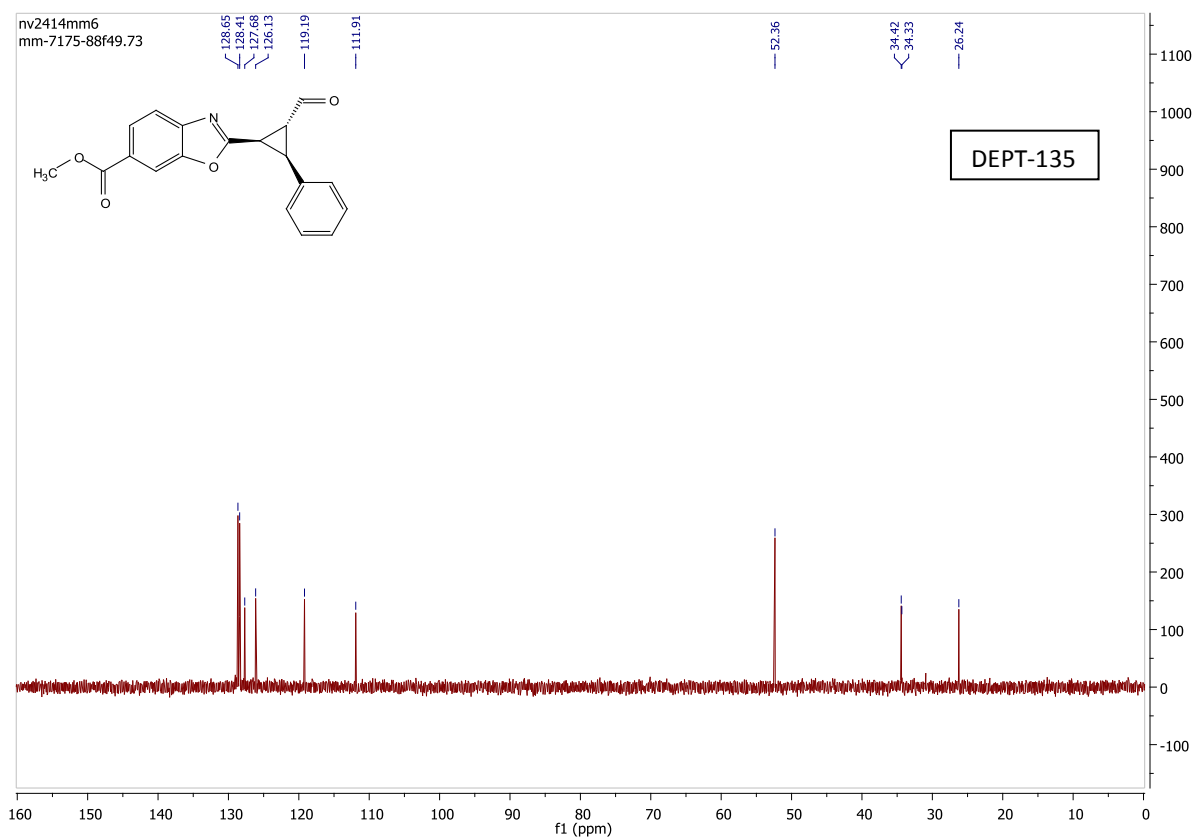
mixture of minor and minor' diastereomers:



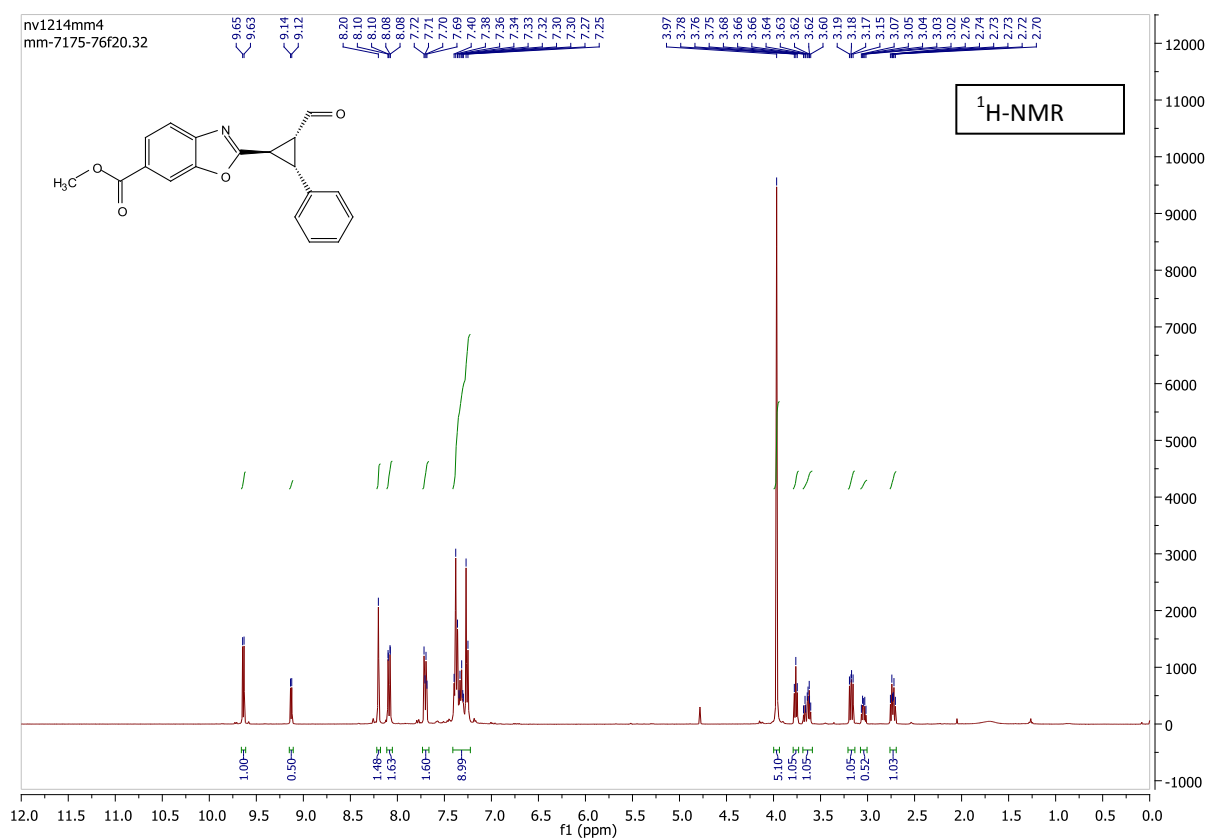


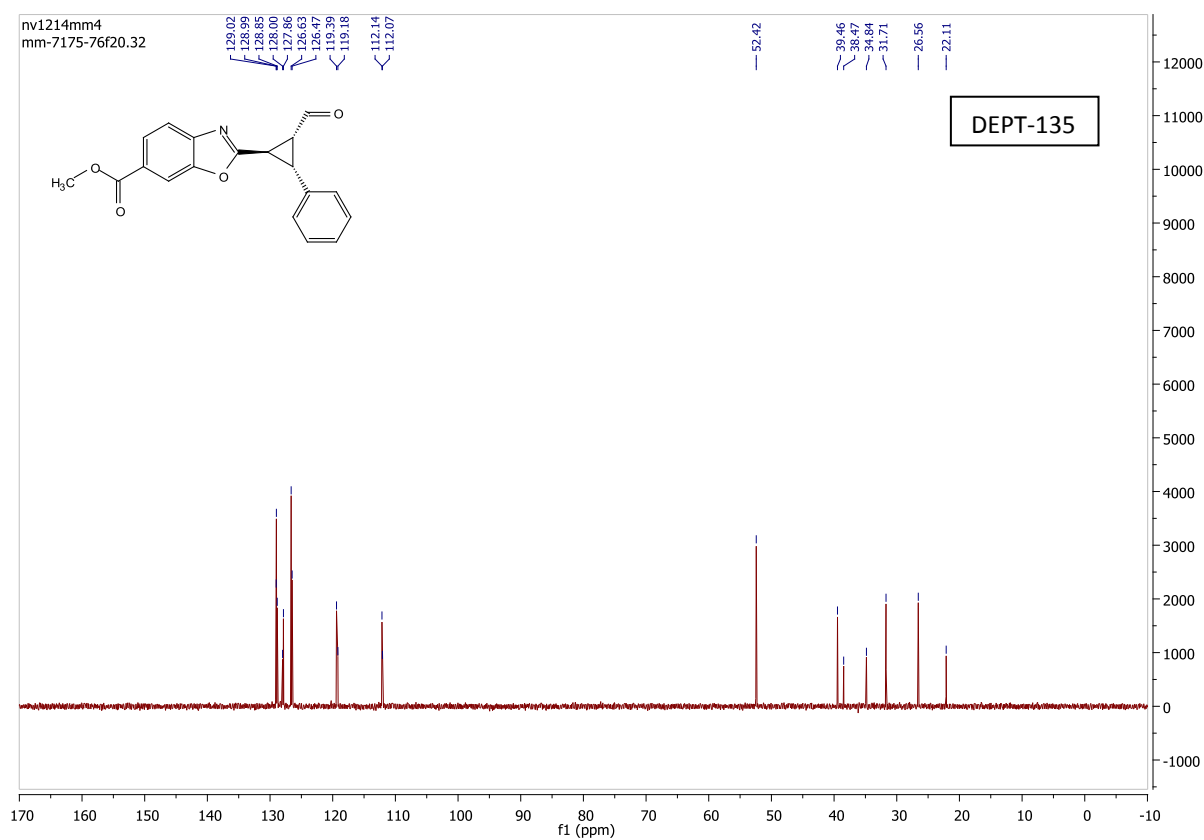
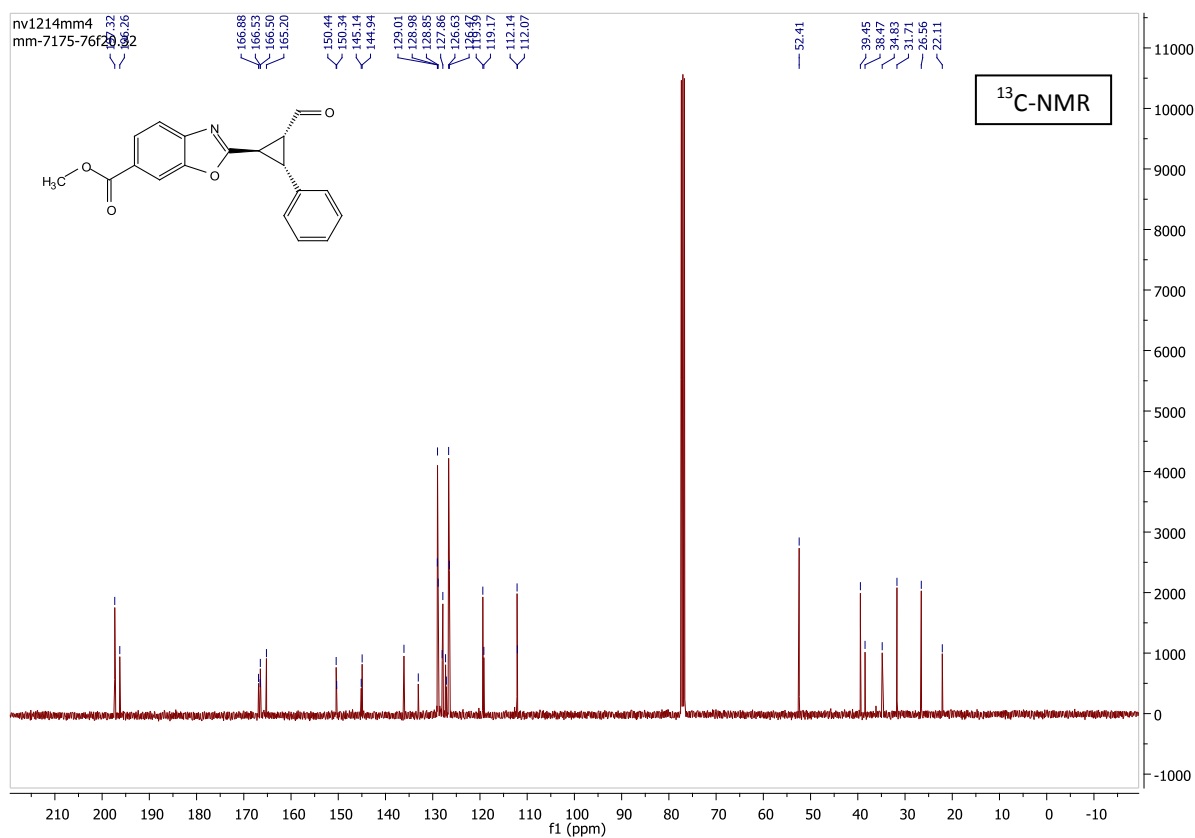
major diastereomer:



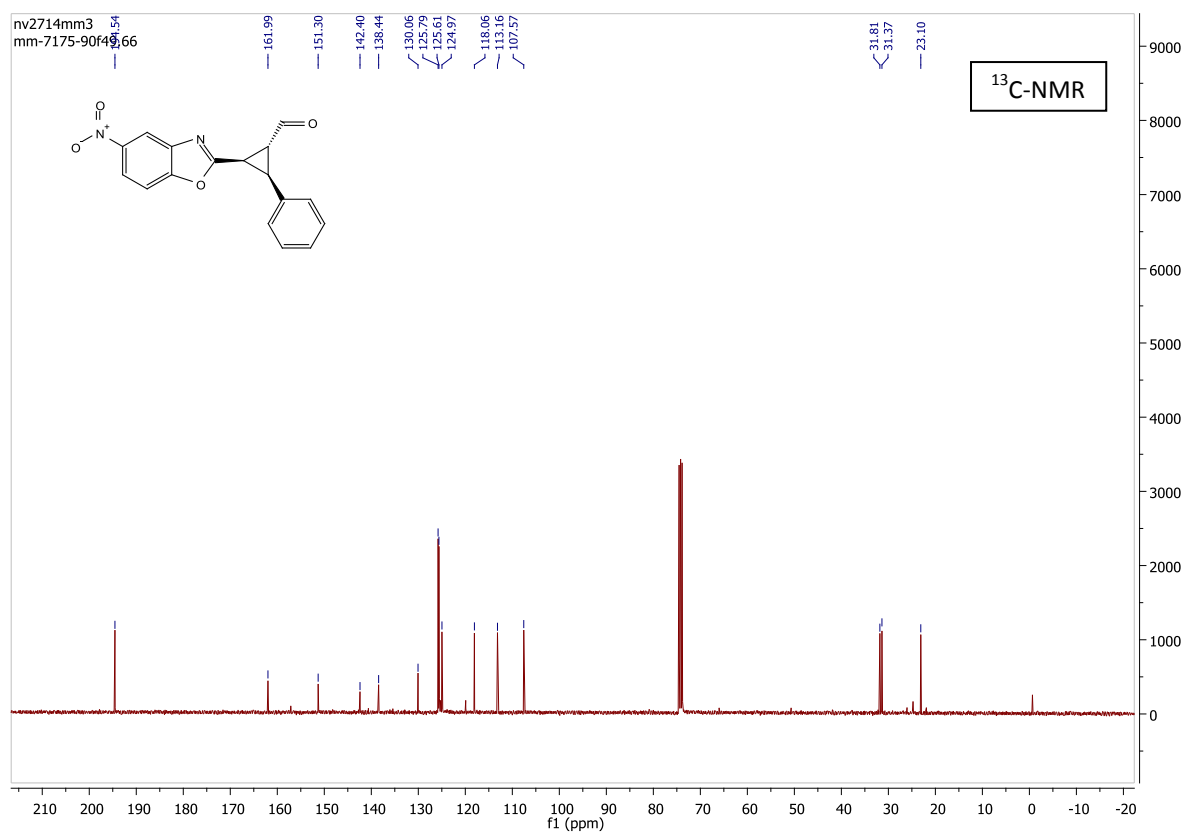
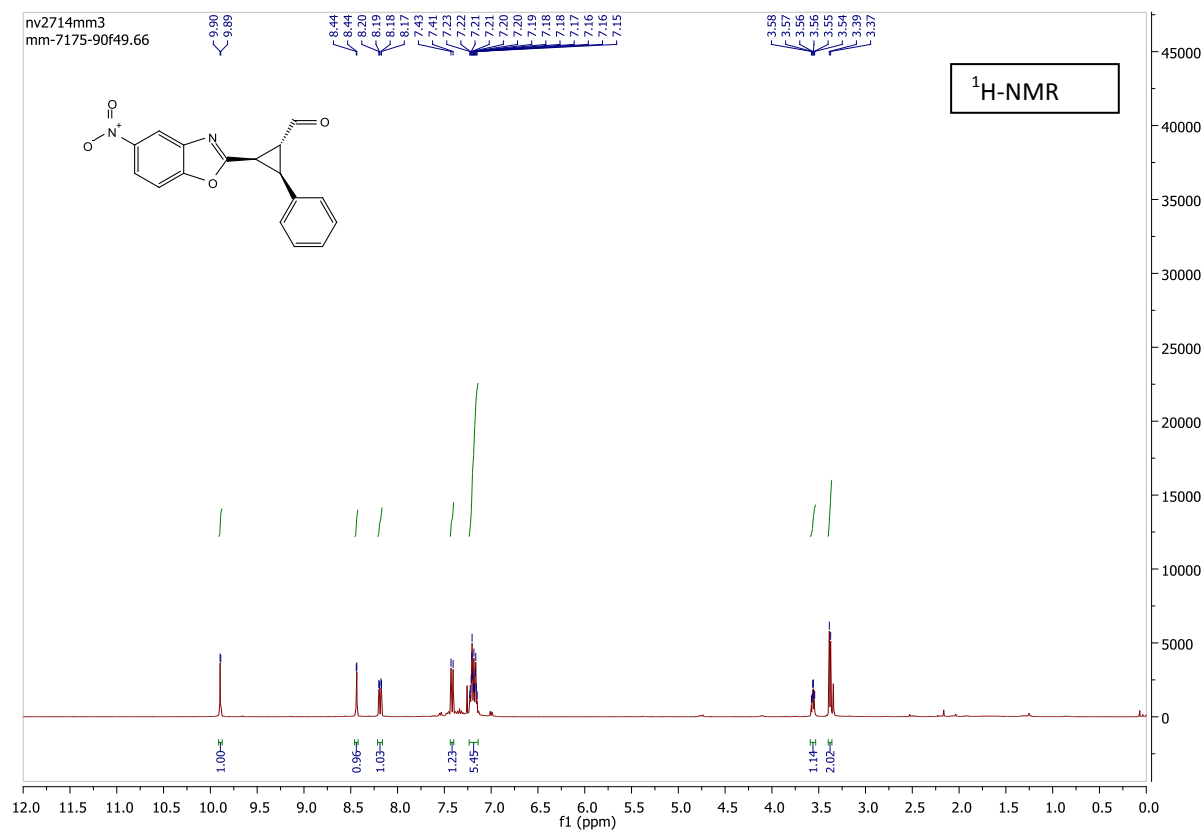


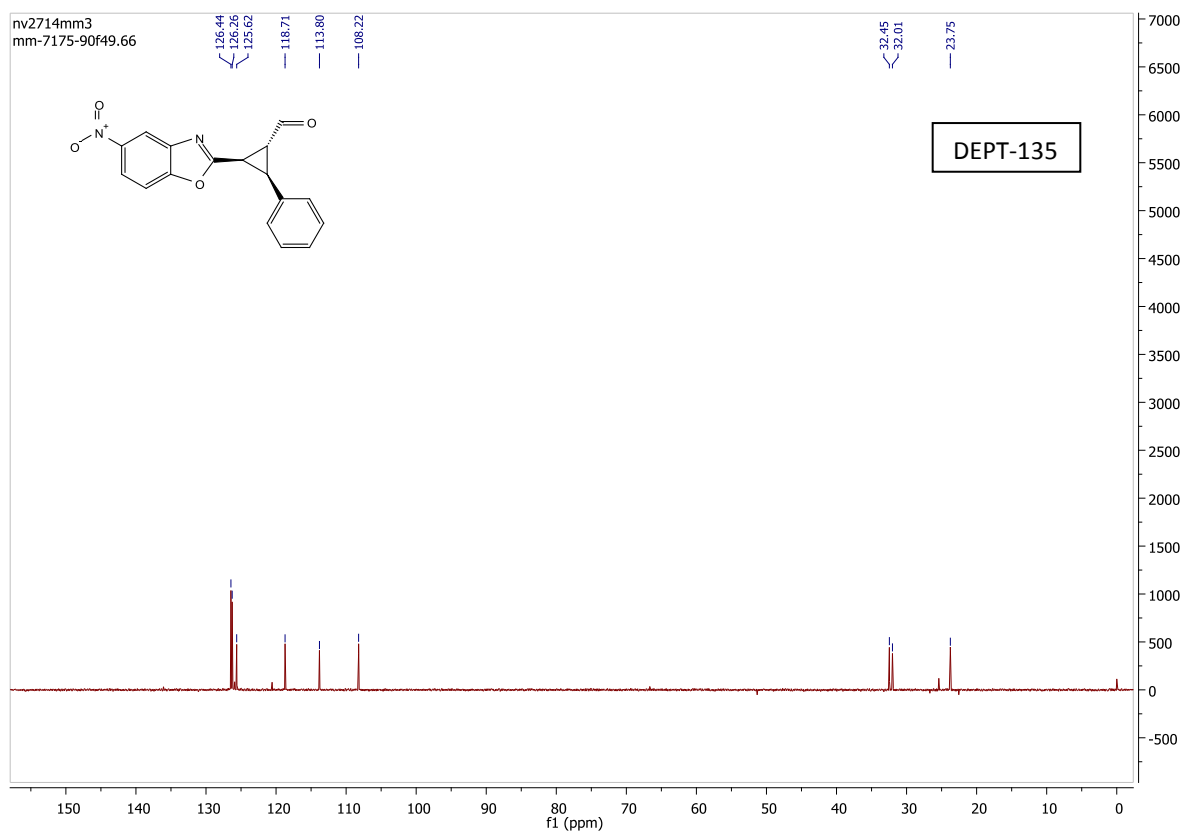
mixture of minor and minor' diastereomers:



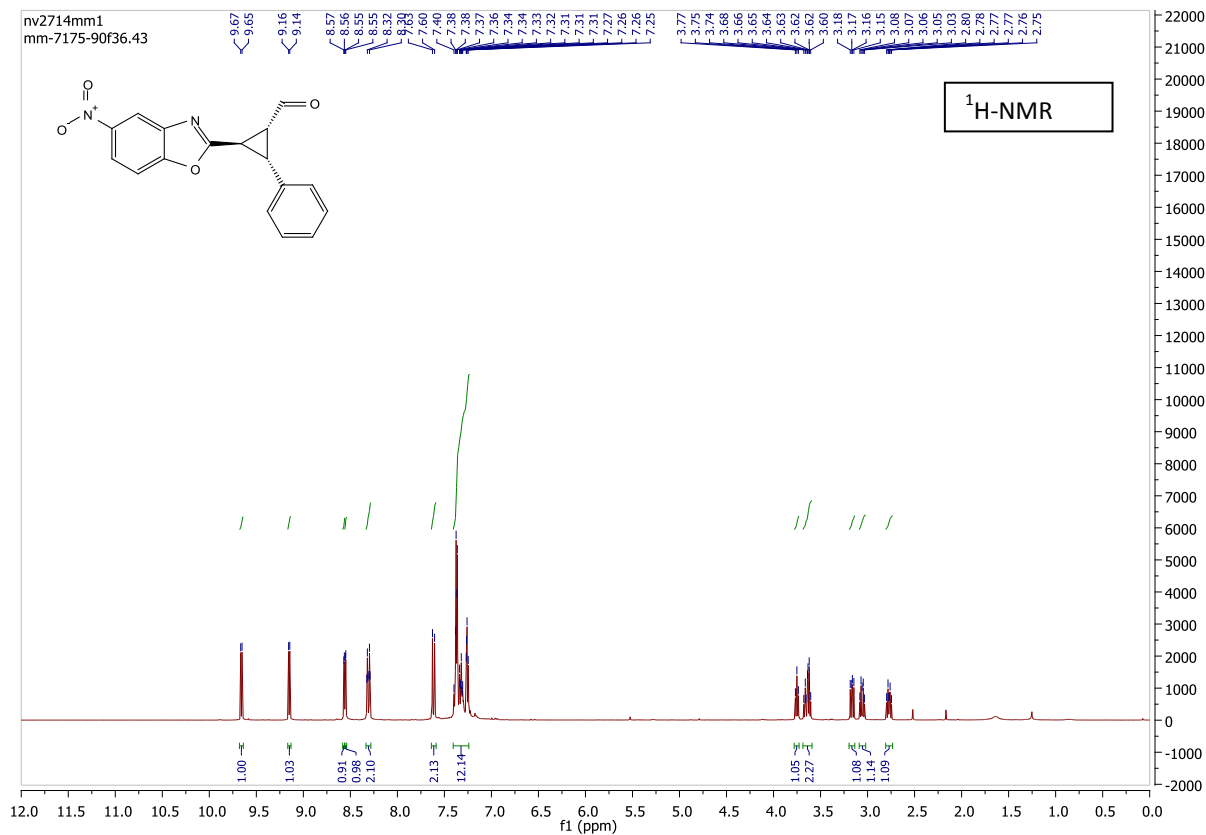


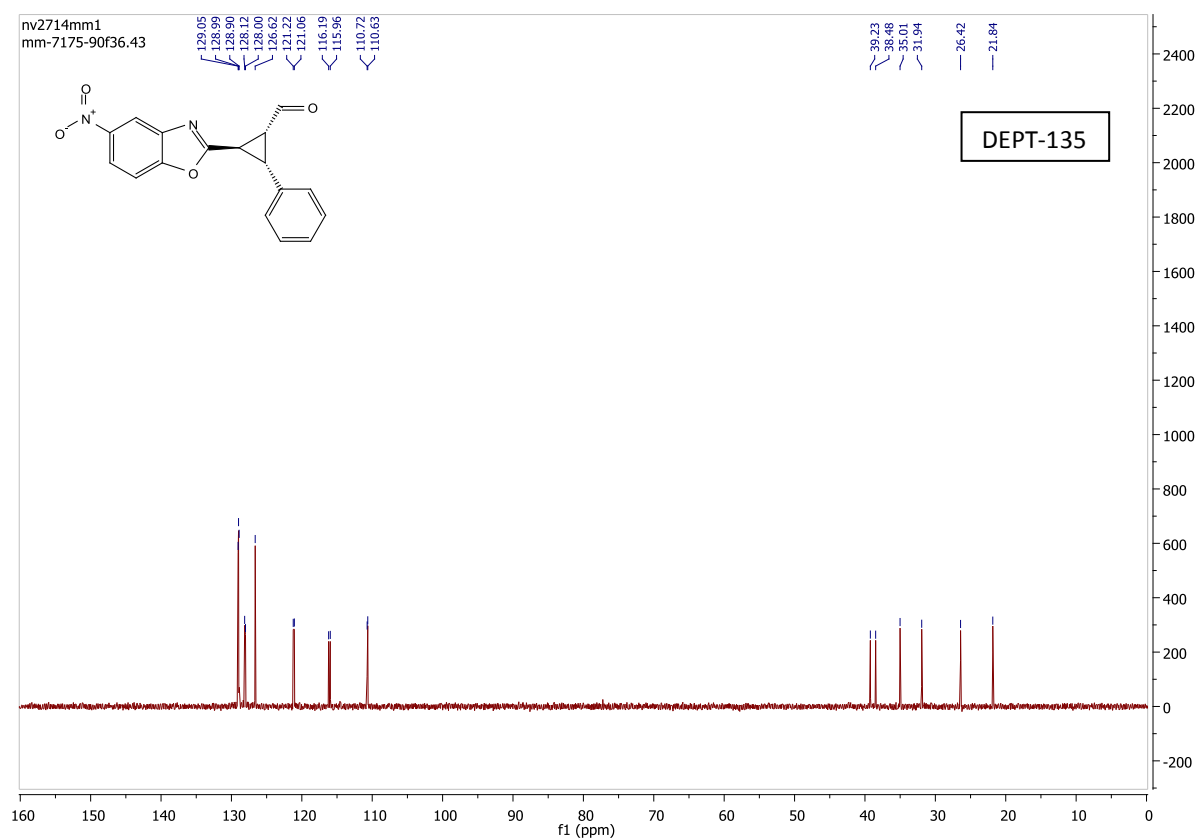
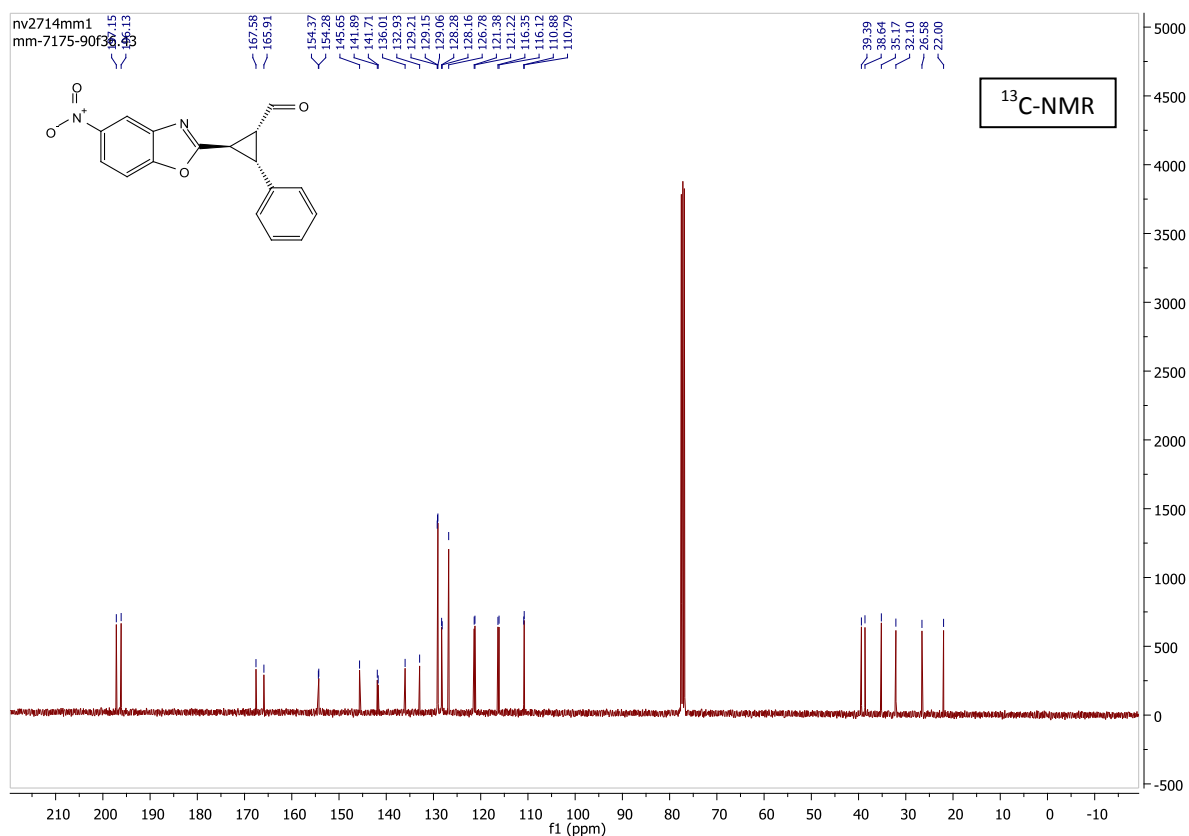
major diastereomer:



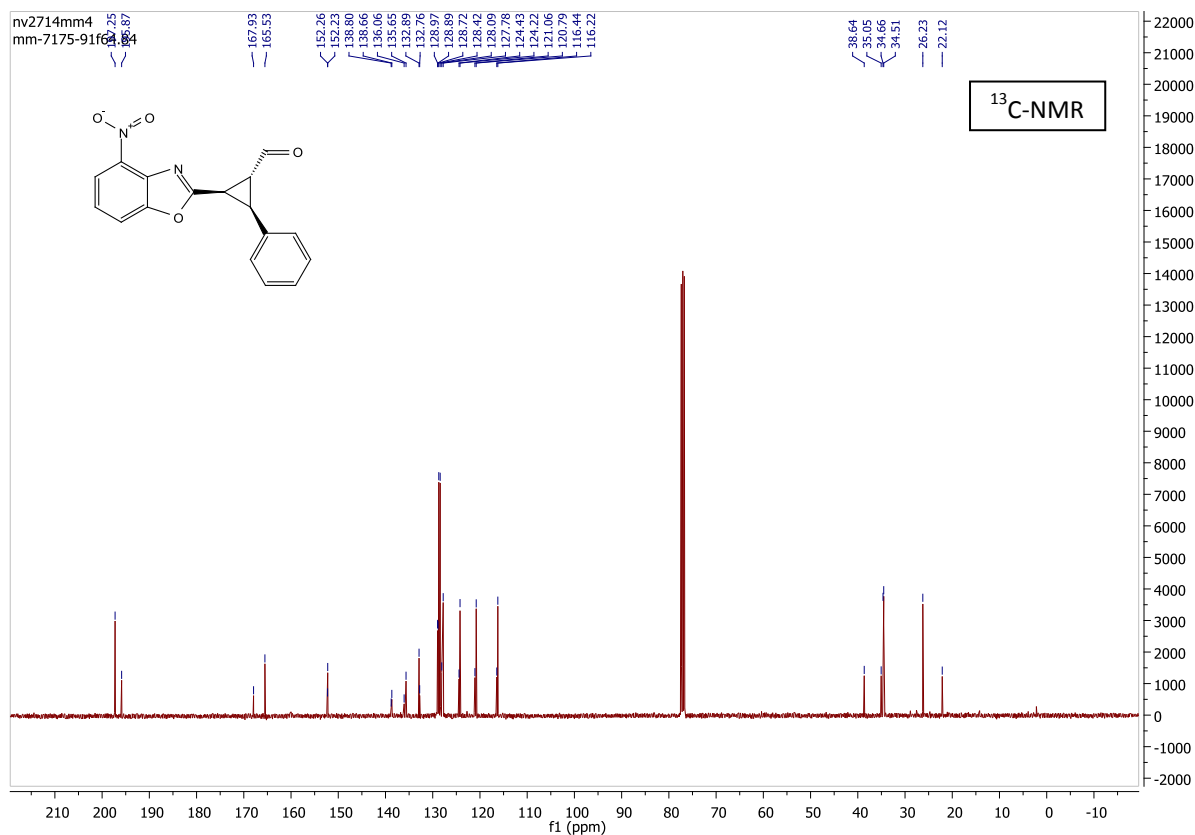
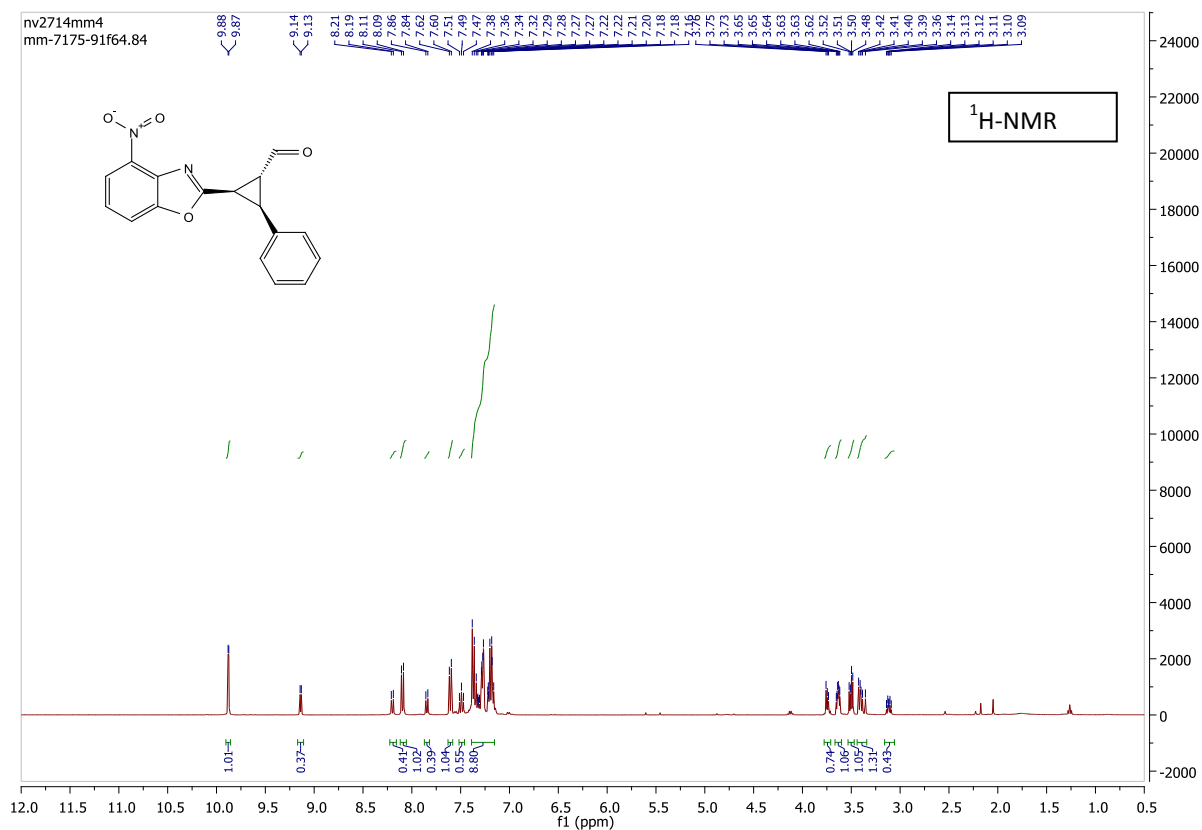


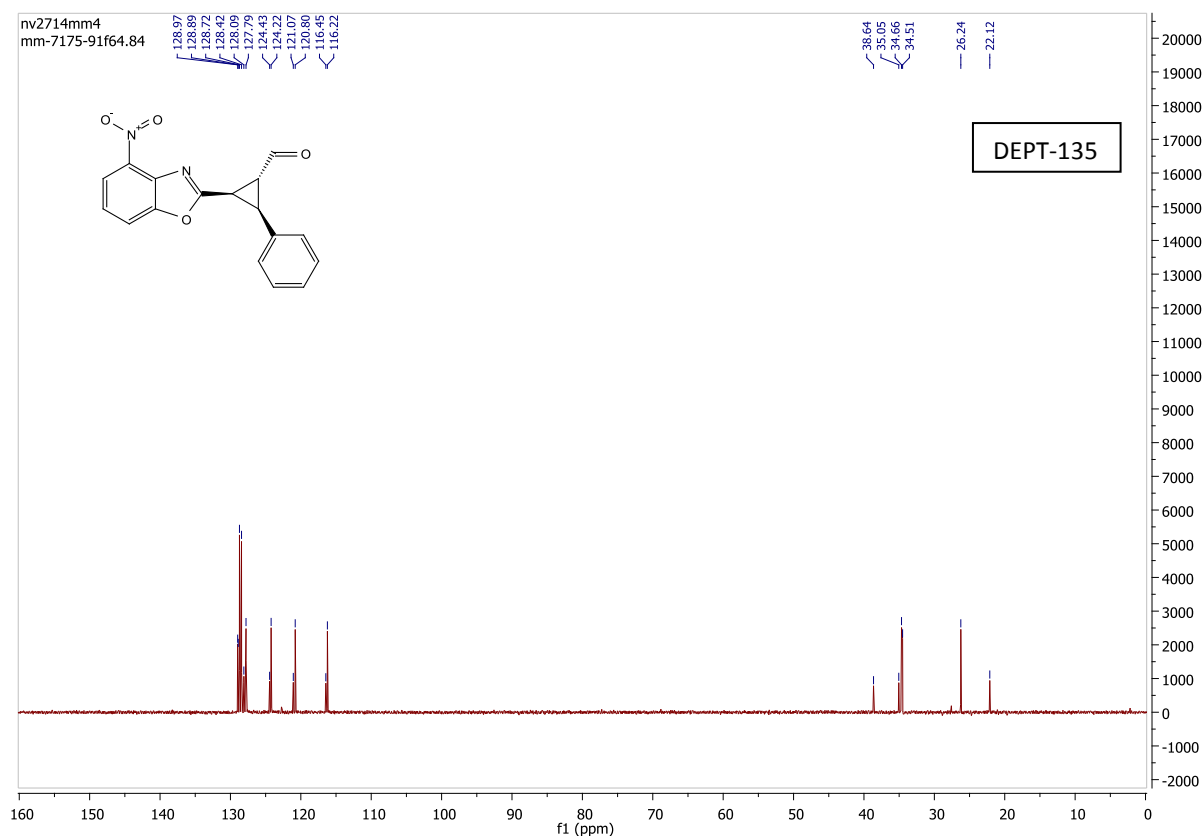
mixture of minor and minor' diastereomers:



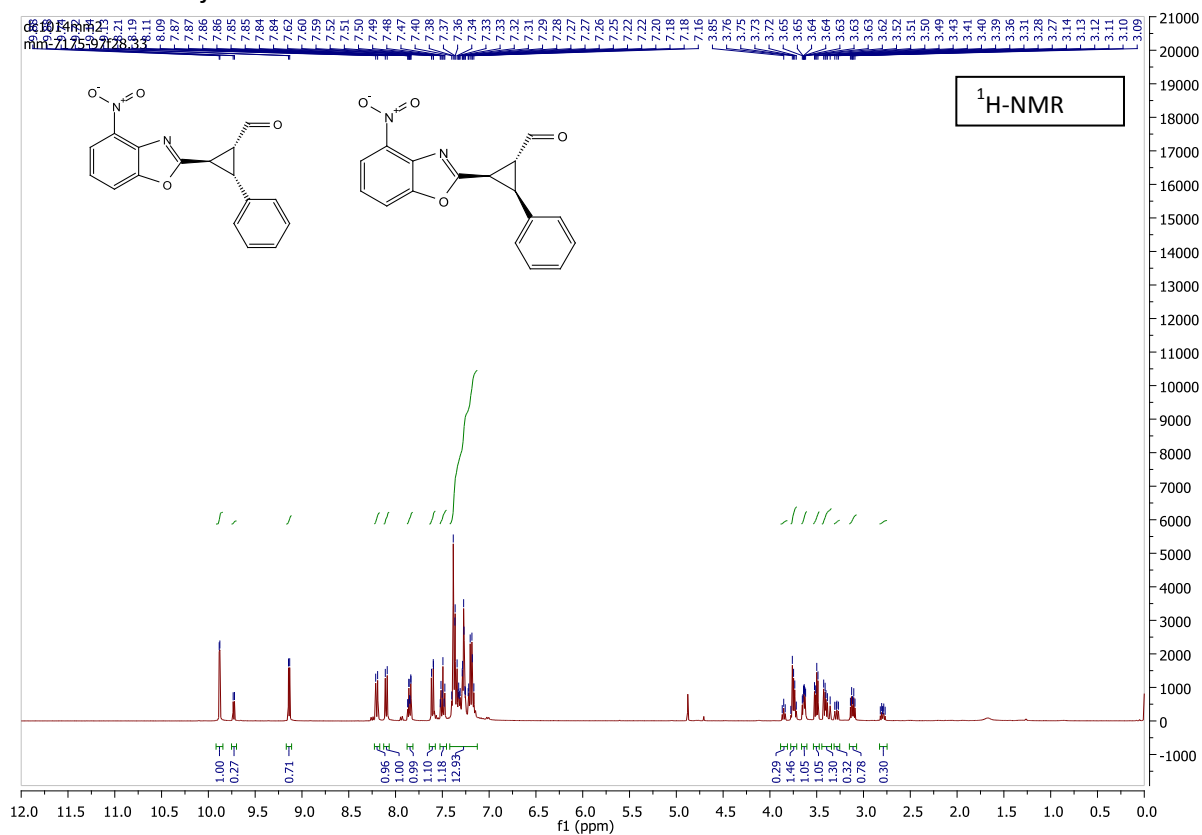


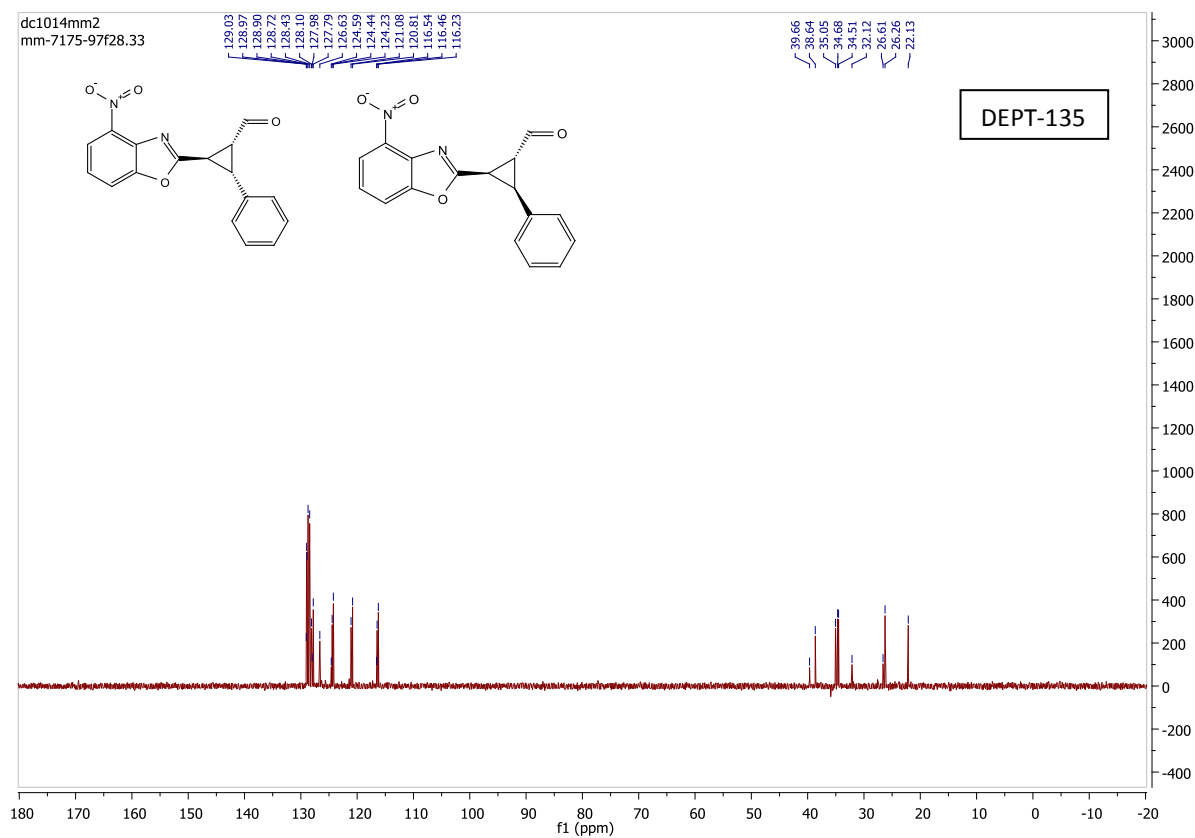
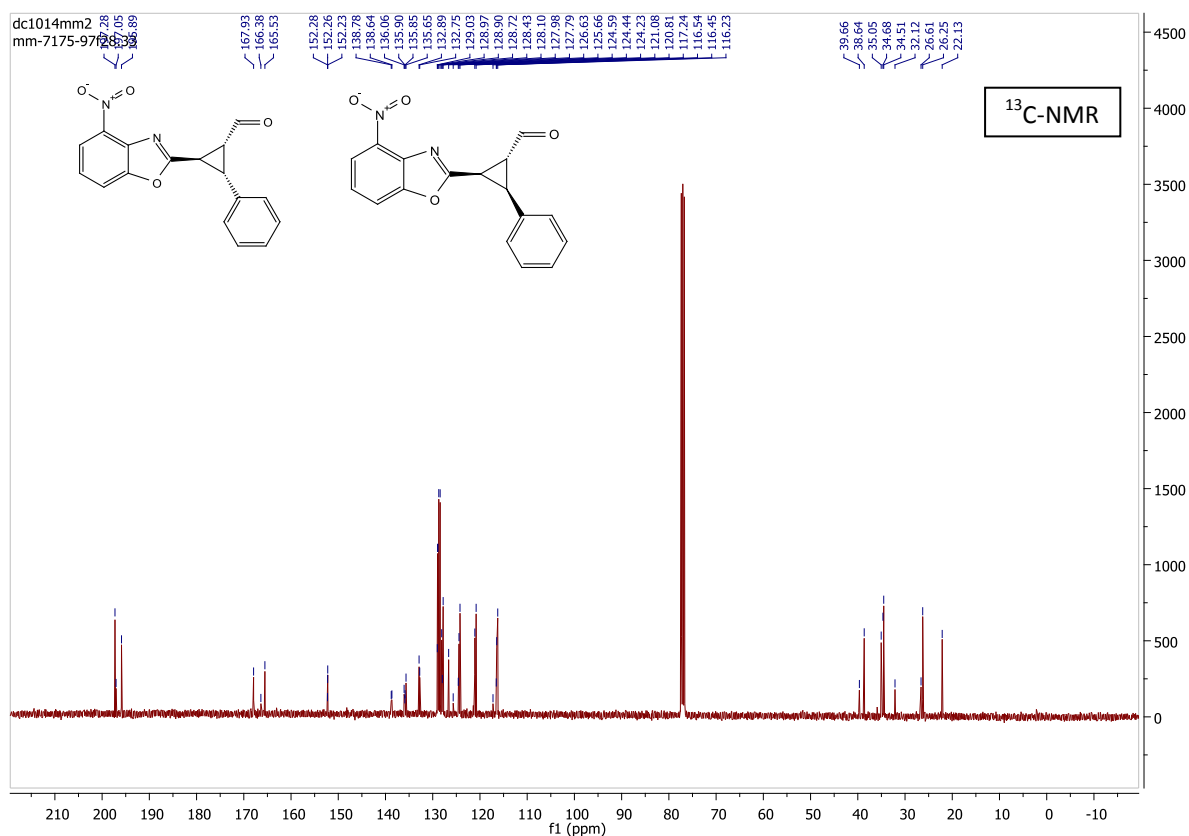
mixture of major and minor diastereomers:



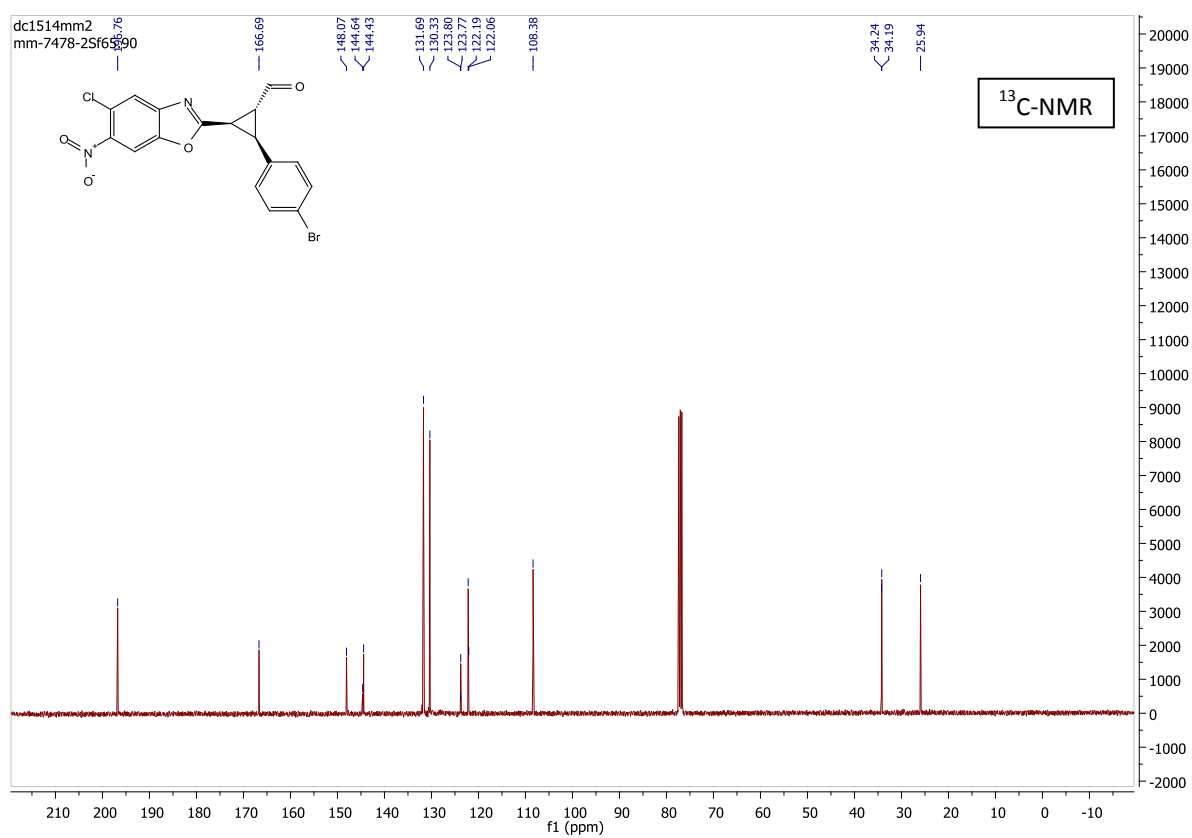
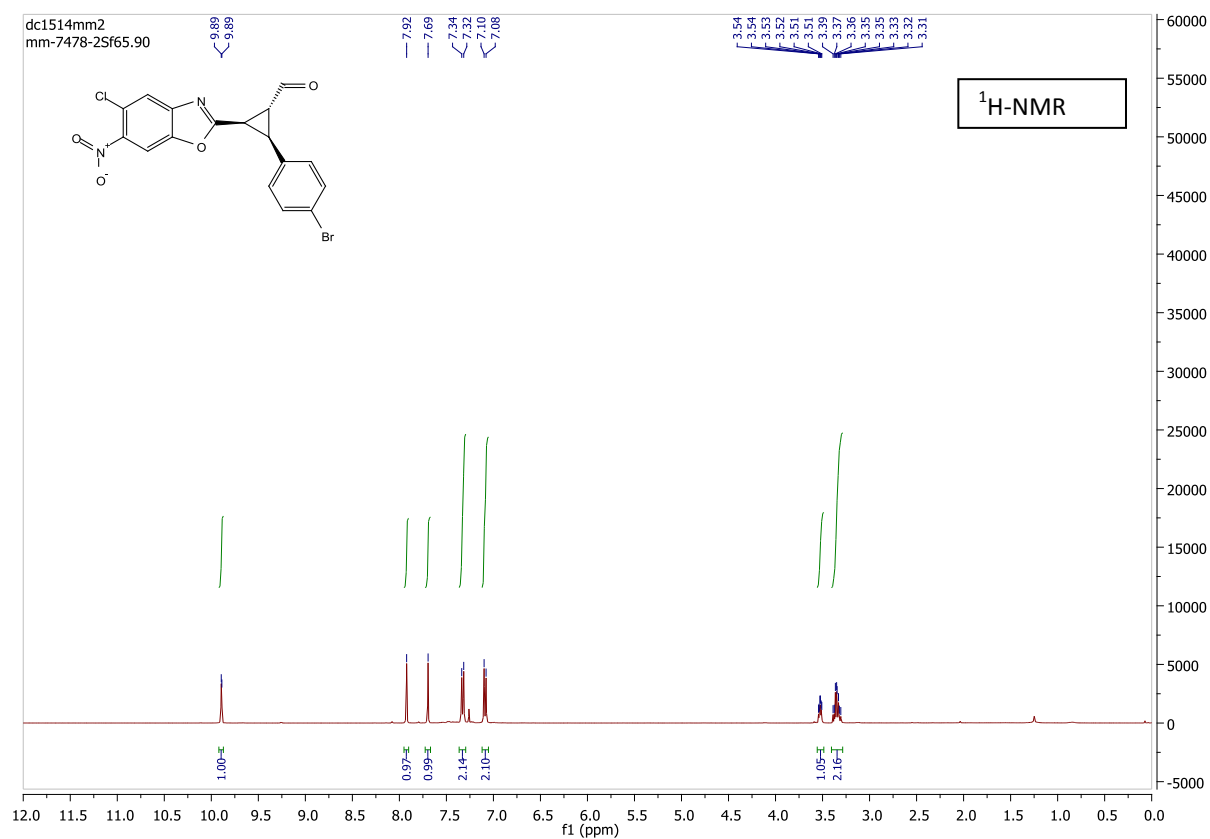


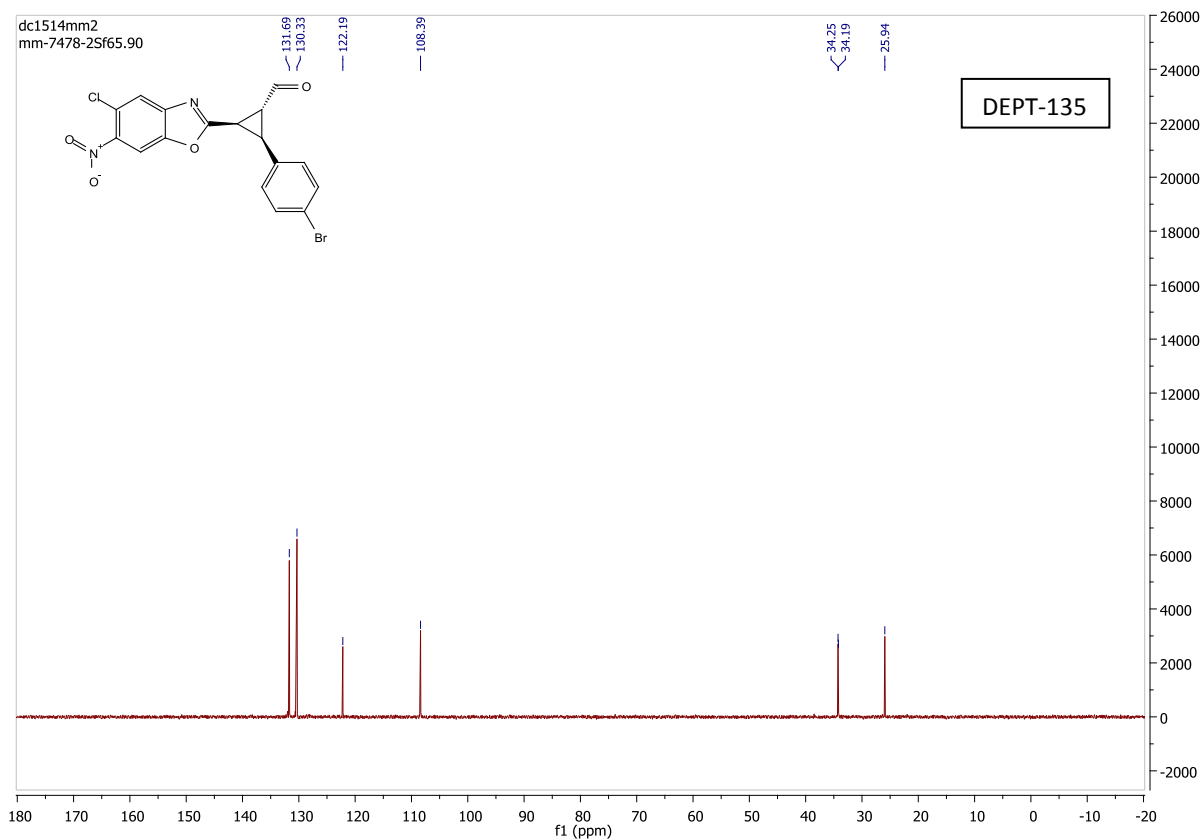
mixture of major minor ad minor' diastereomers:



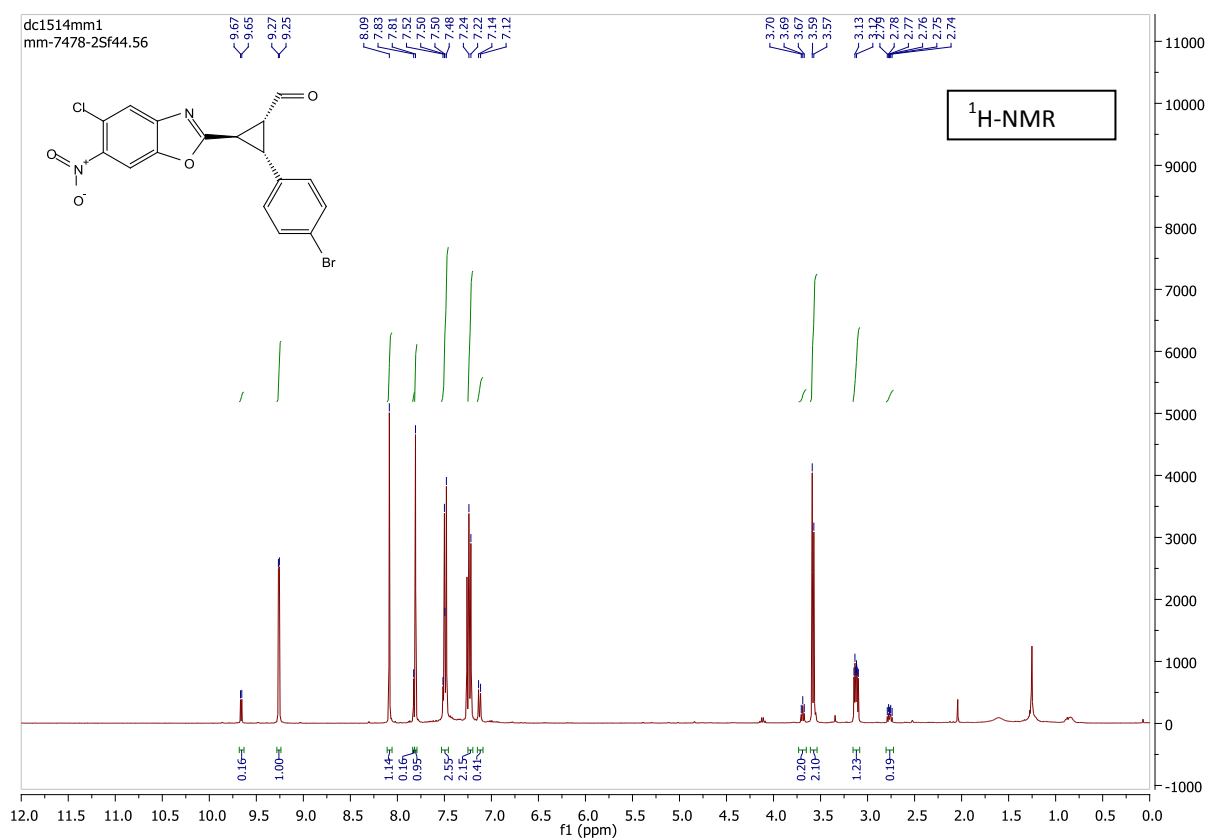


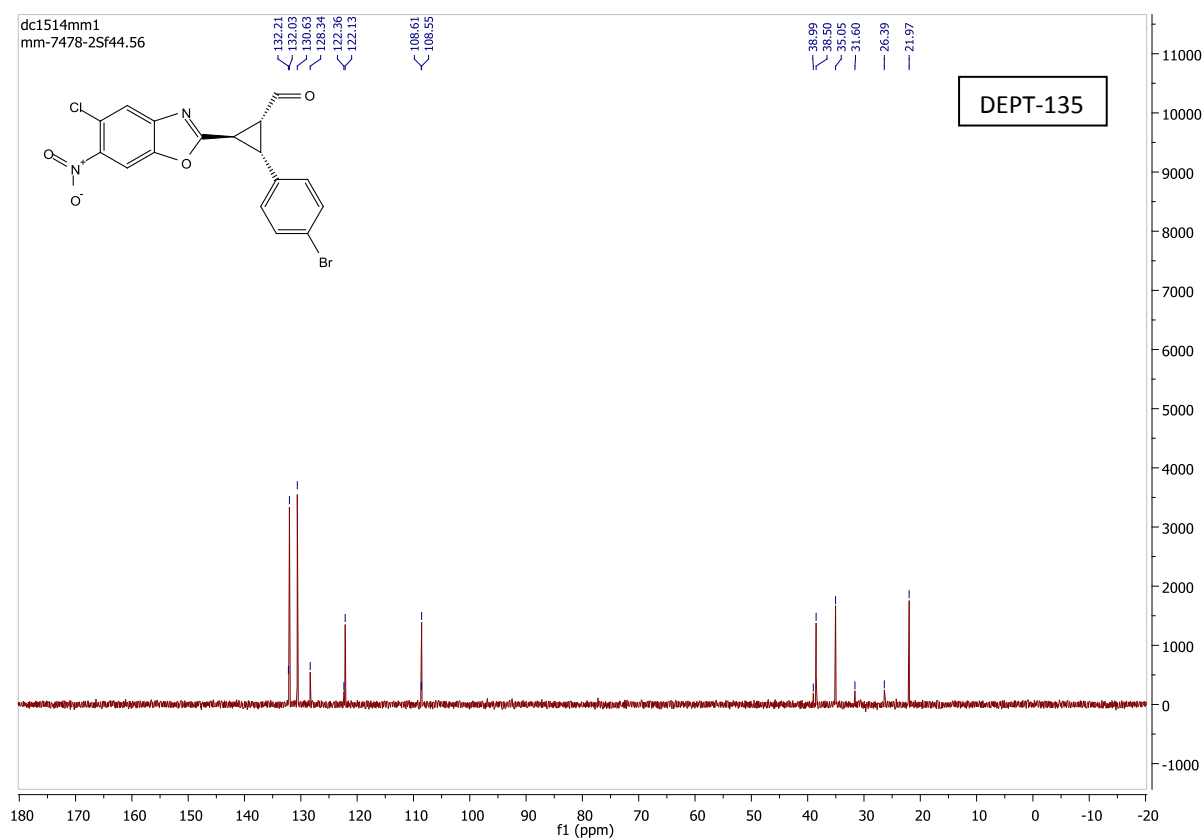
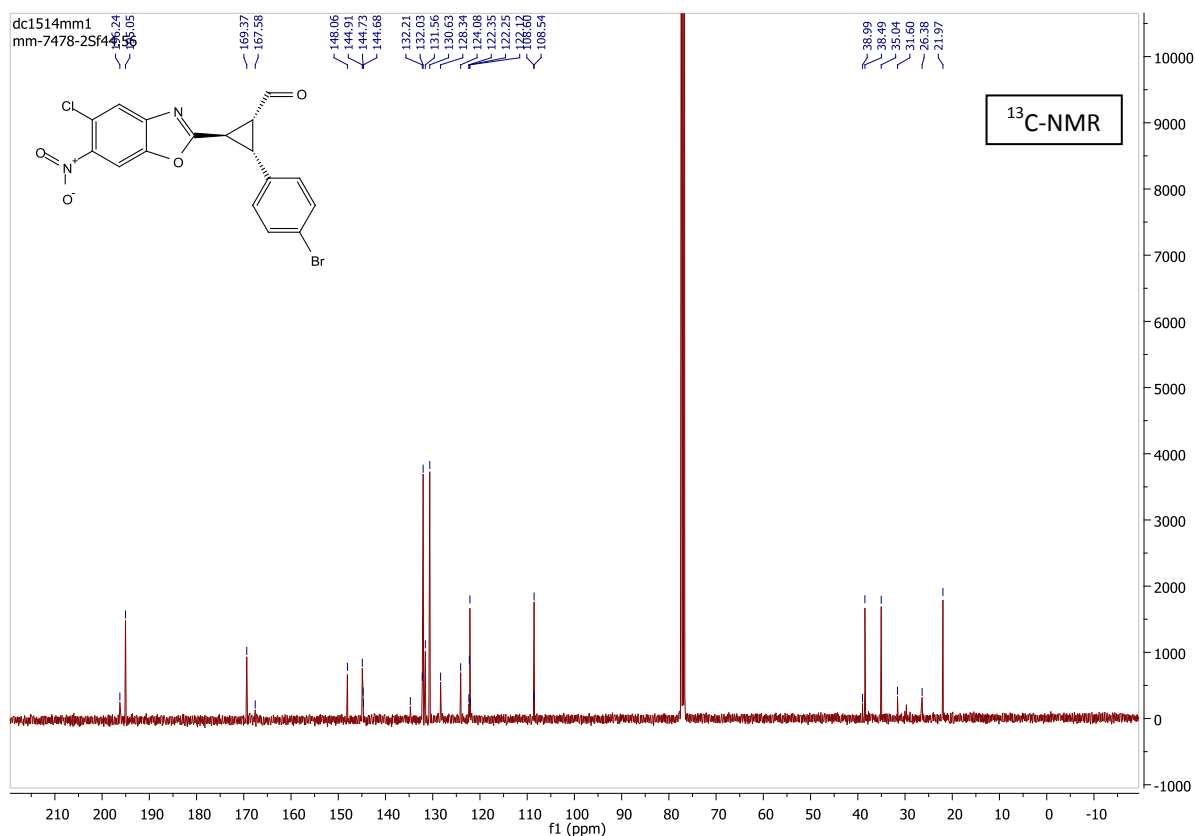
major diastereomer:



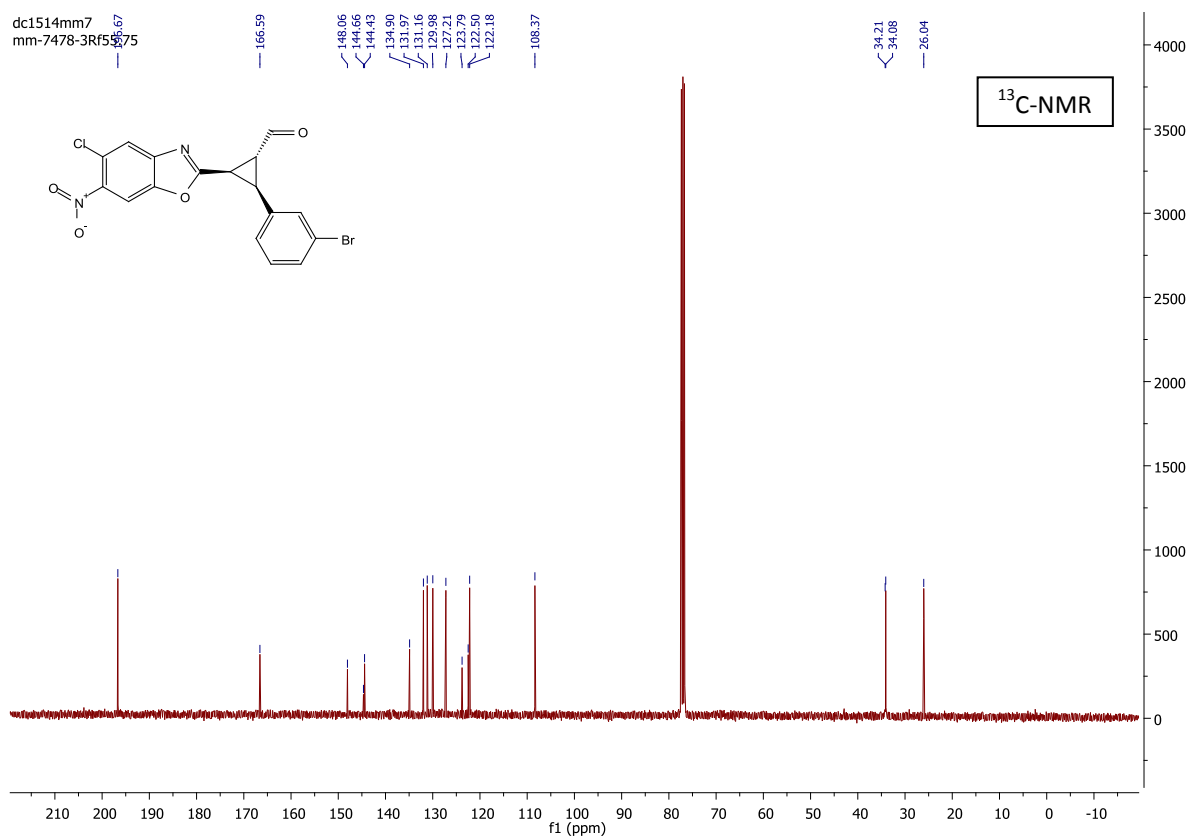
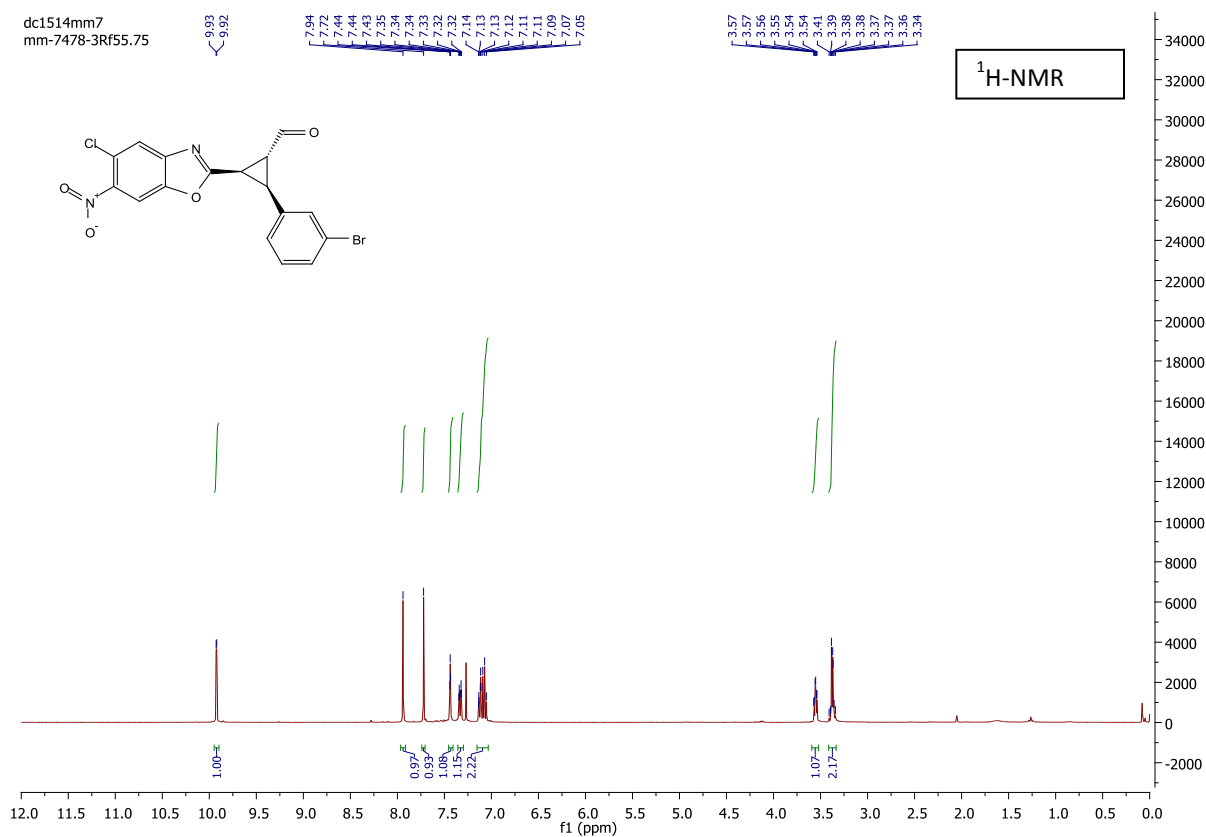


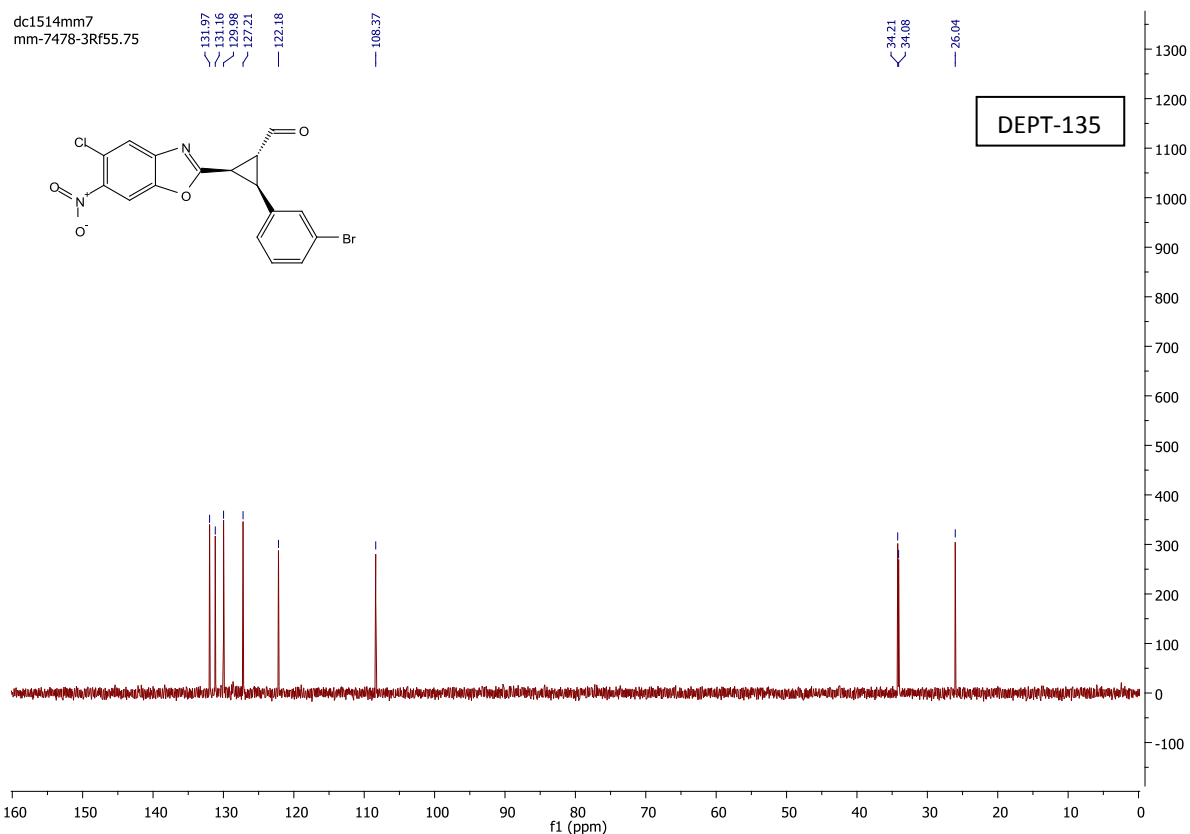
mixture of minor and minor ' diastereomers:



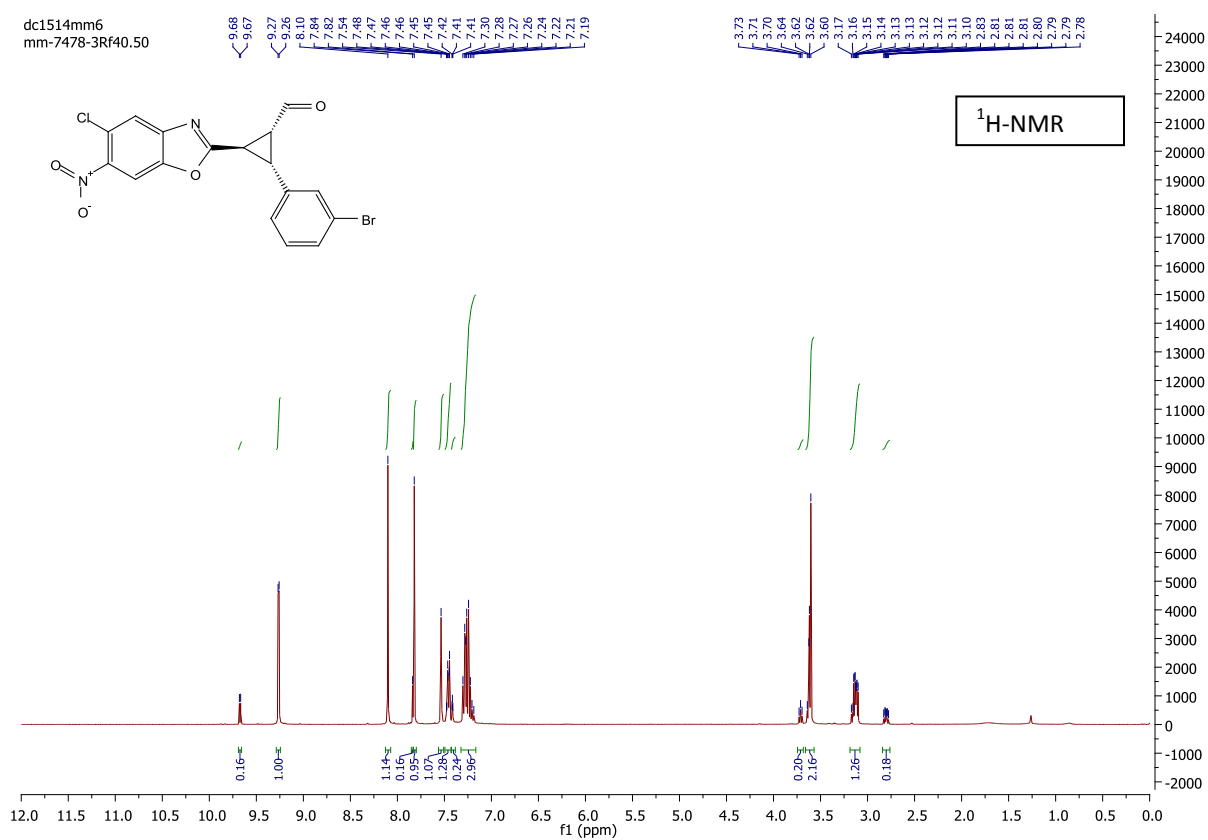


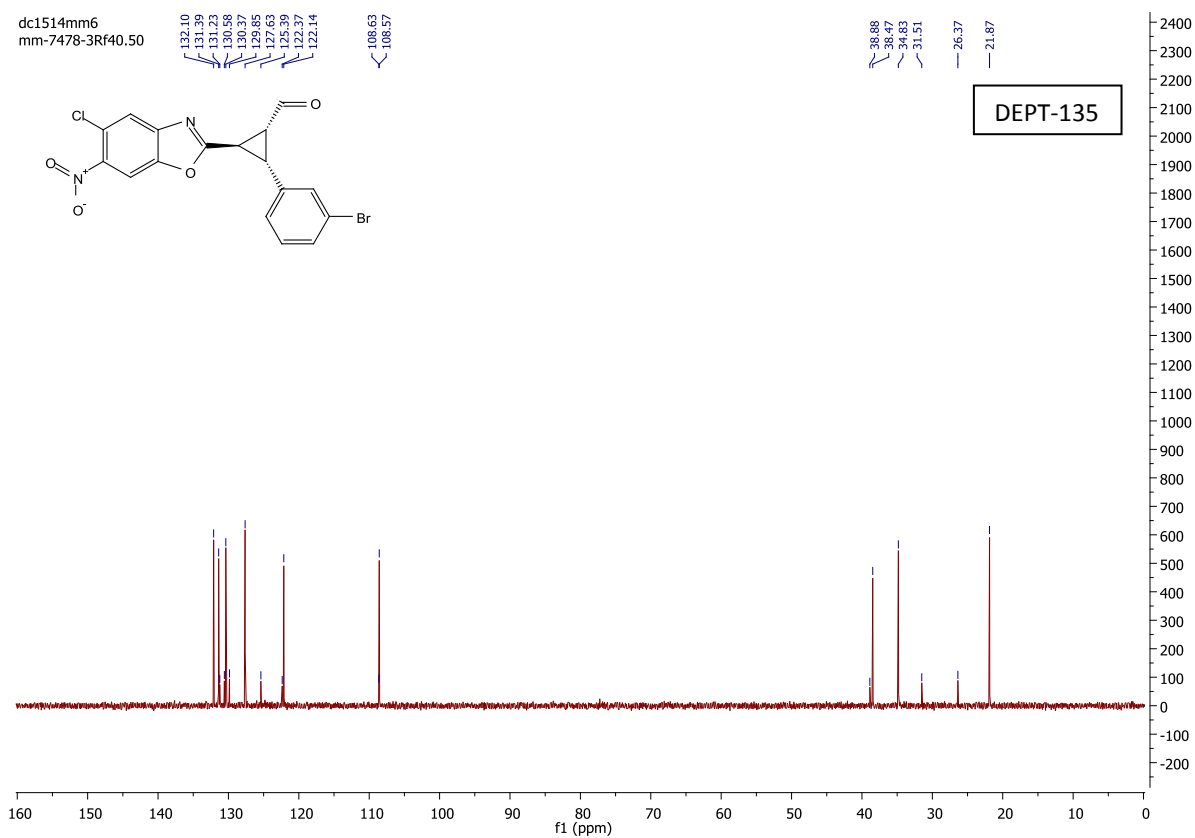
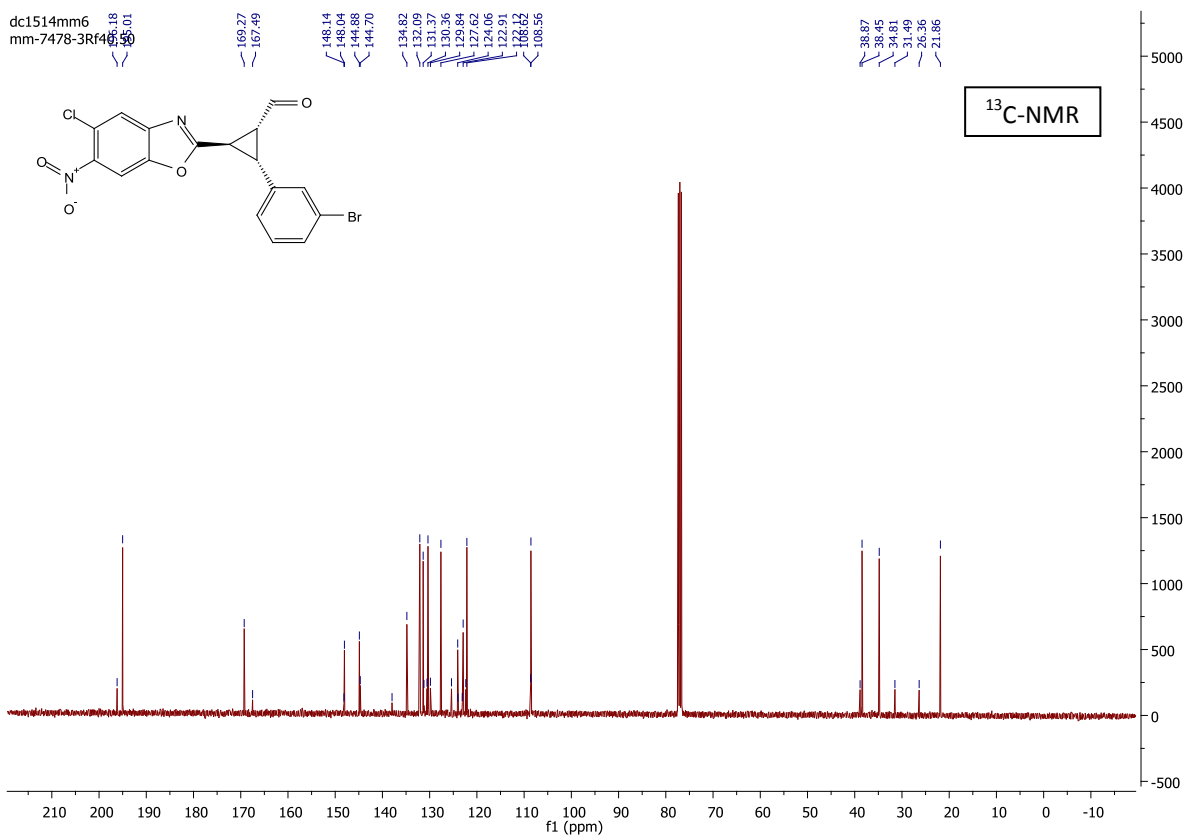
major diastereomer:





mixture of minor and minor' diastereomers:

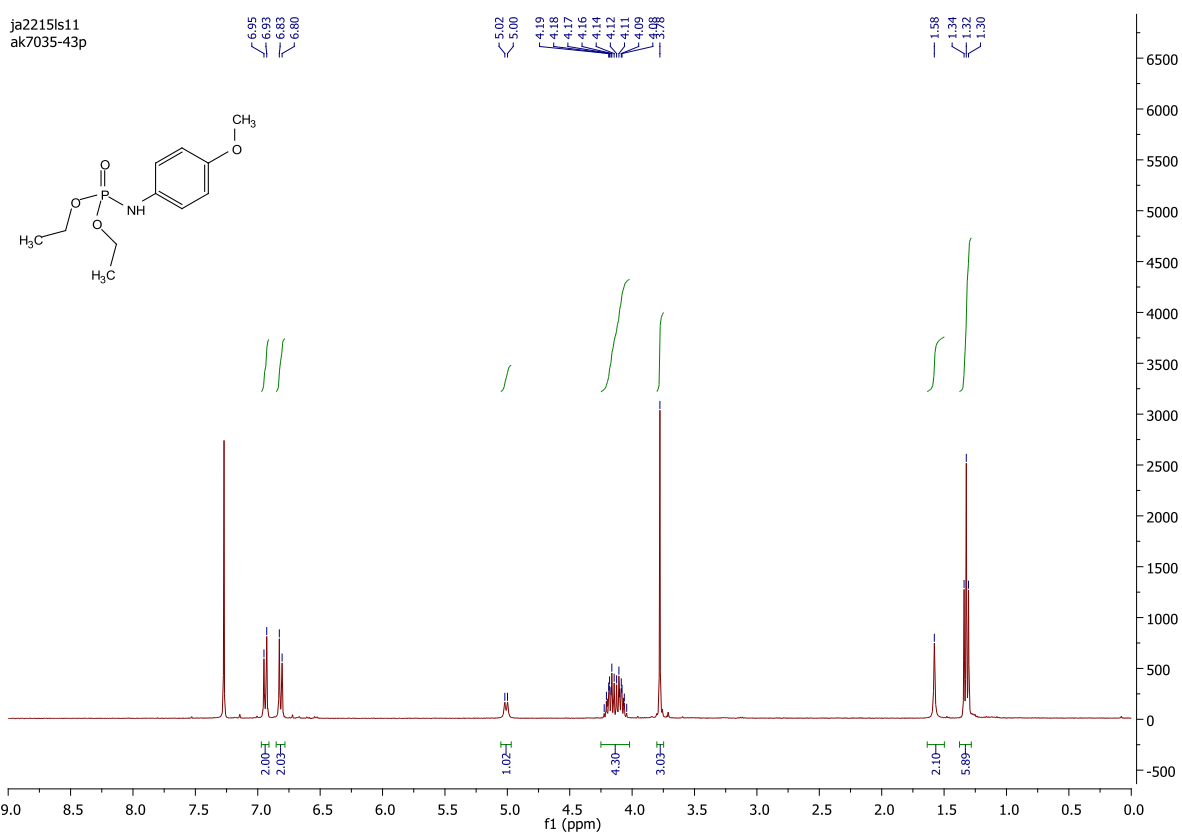




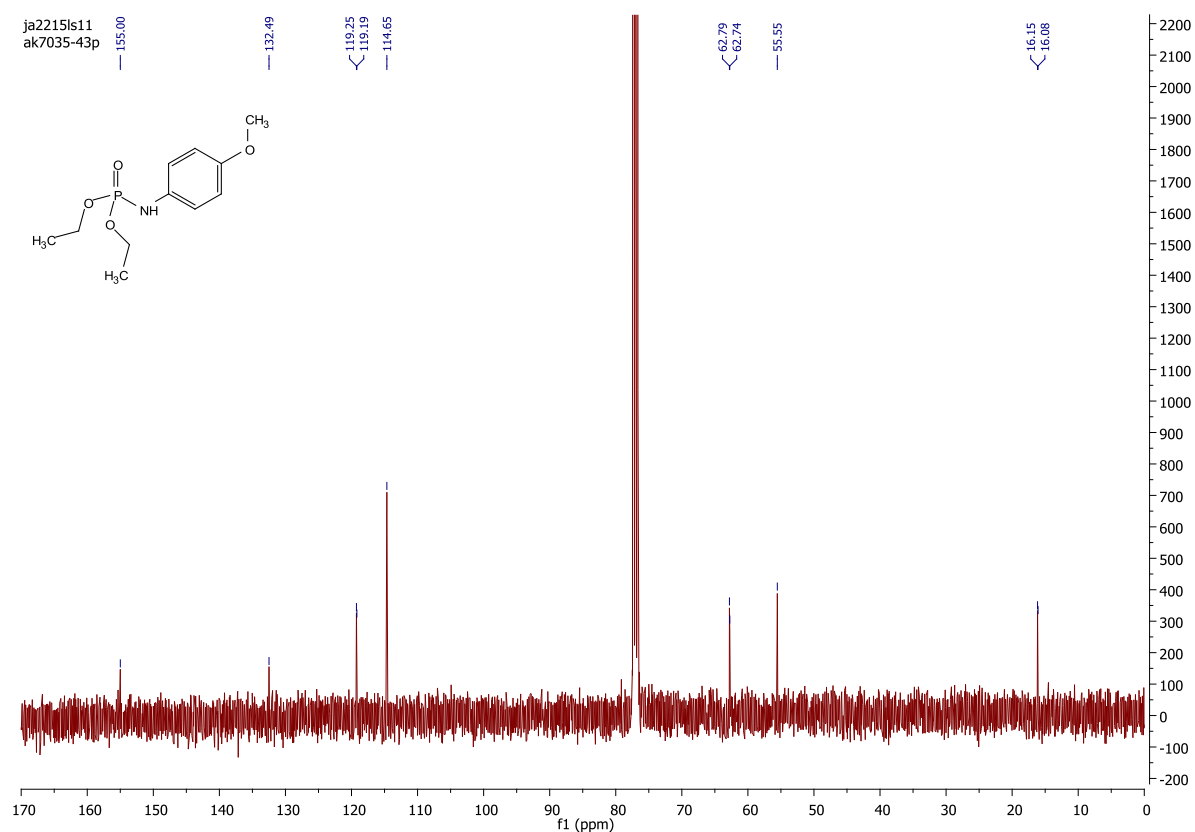
First pure organophotocatalytic synthesis of phosphoramidates

NMR

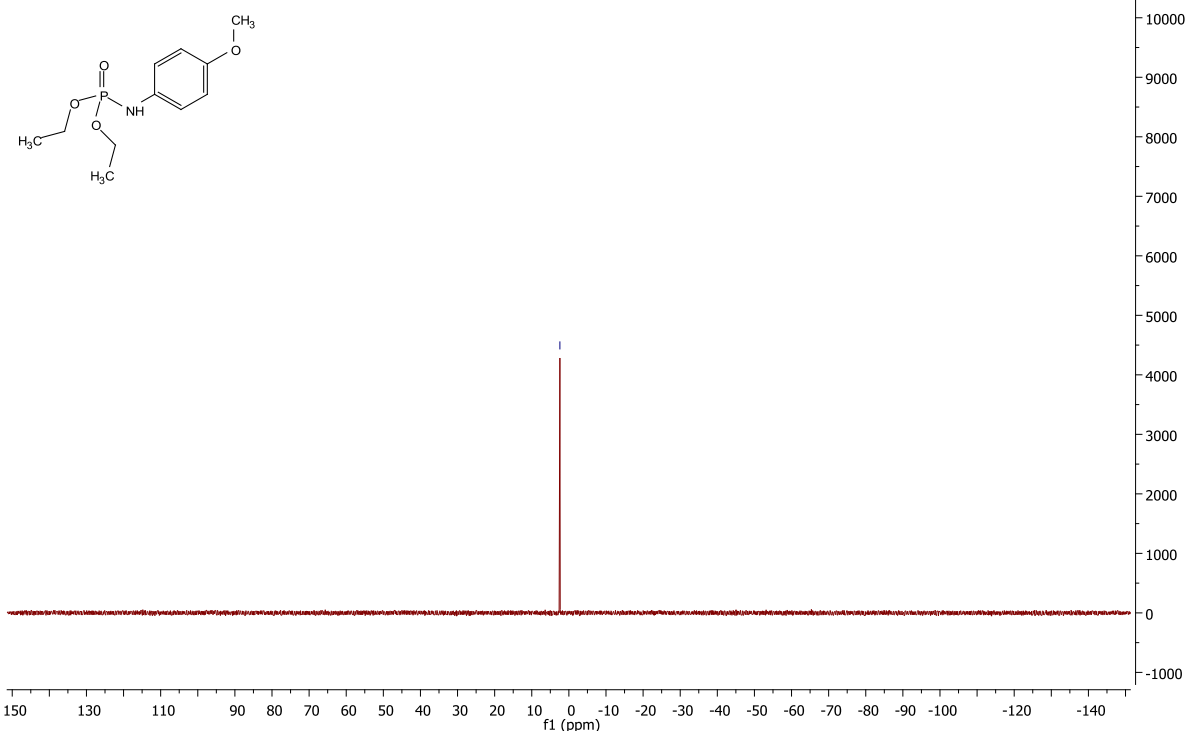
ja2215ls11
ak7035-43p



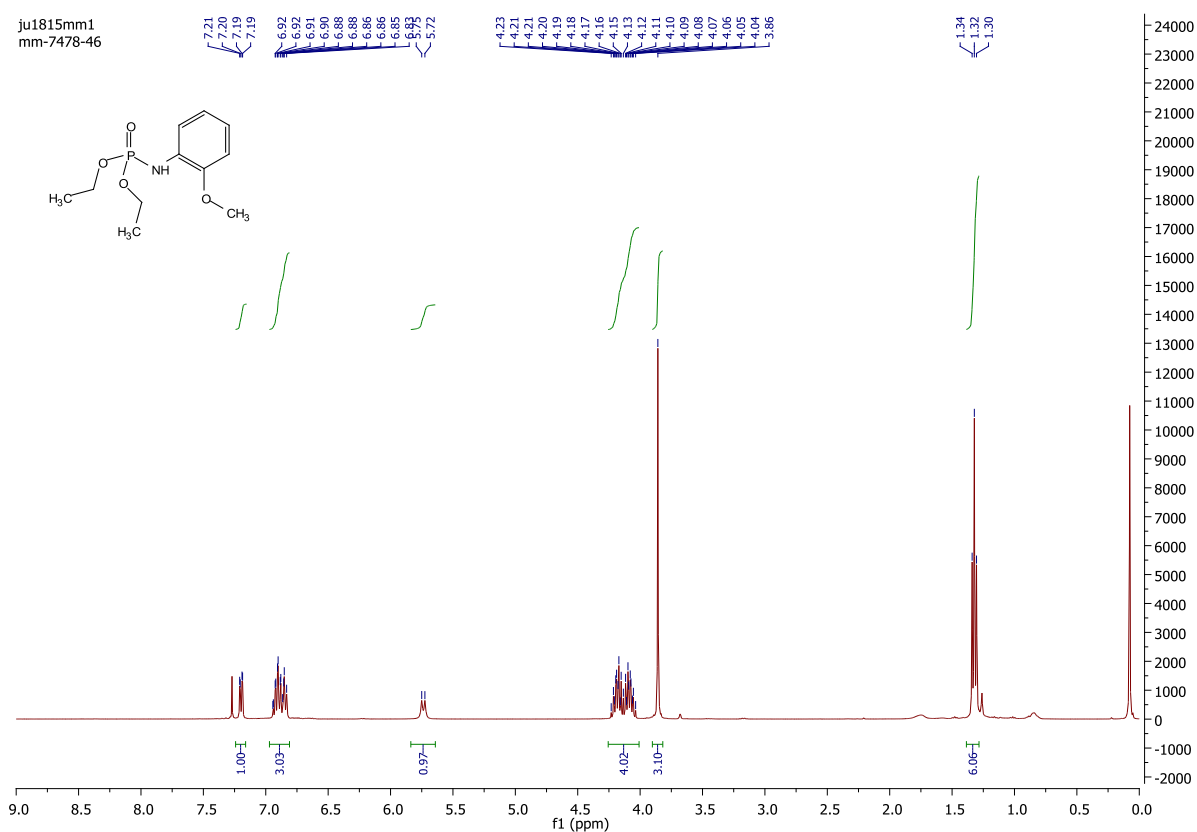
ja2215ls11
ak7035-43p

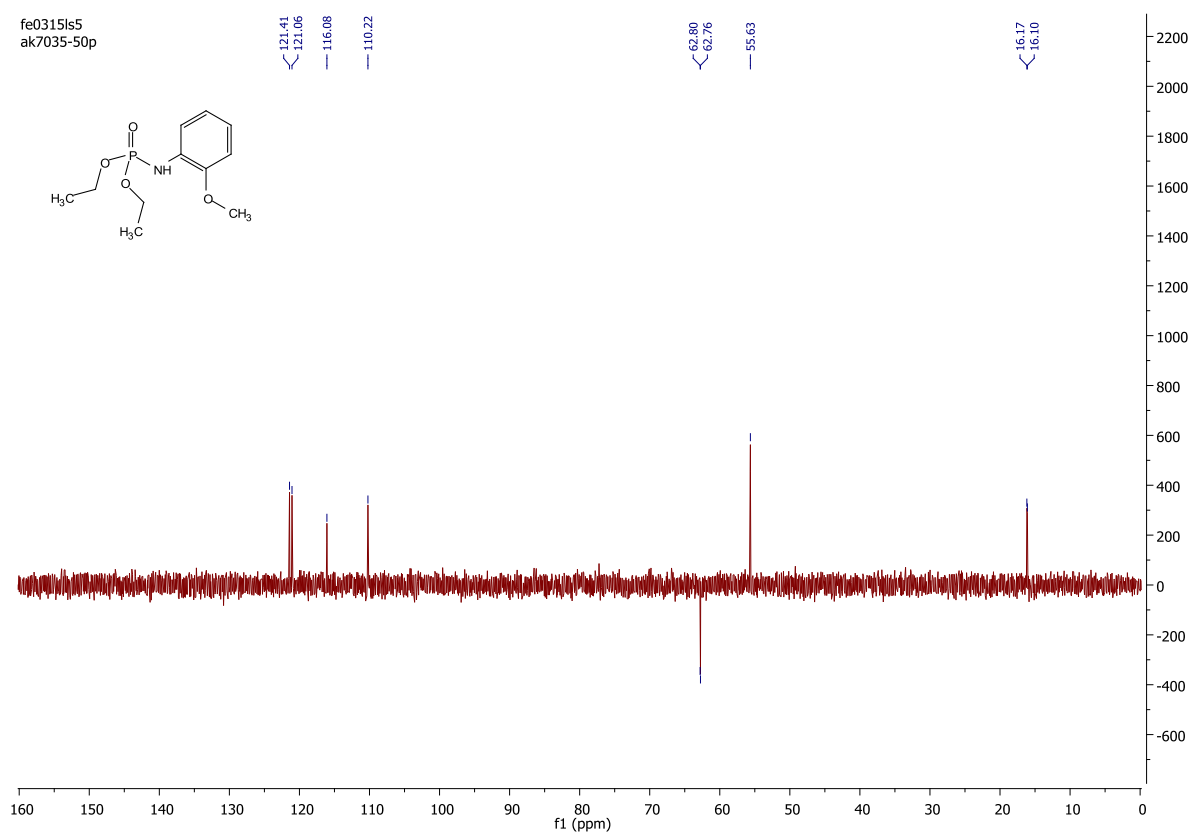
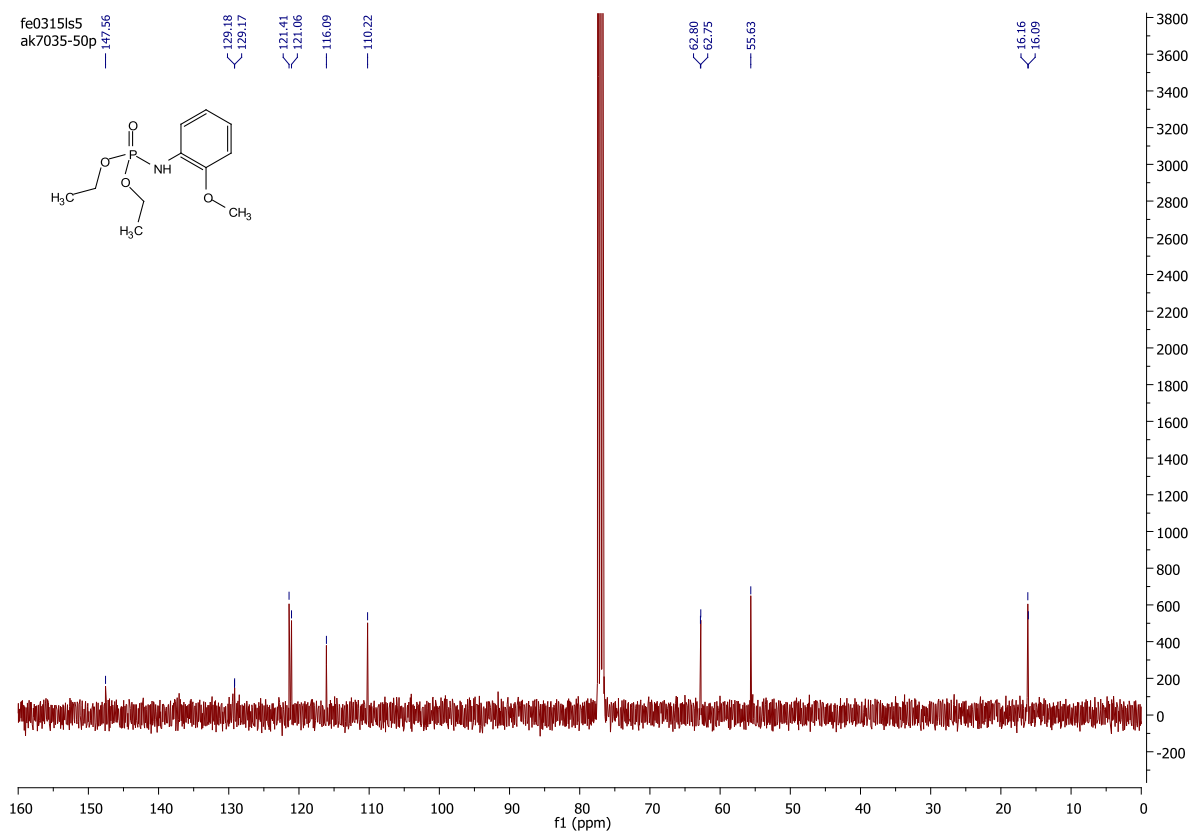


ja2215ls11
ak7035-43p

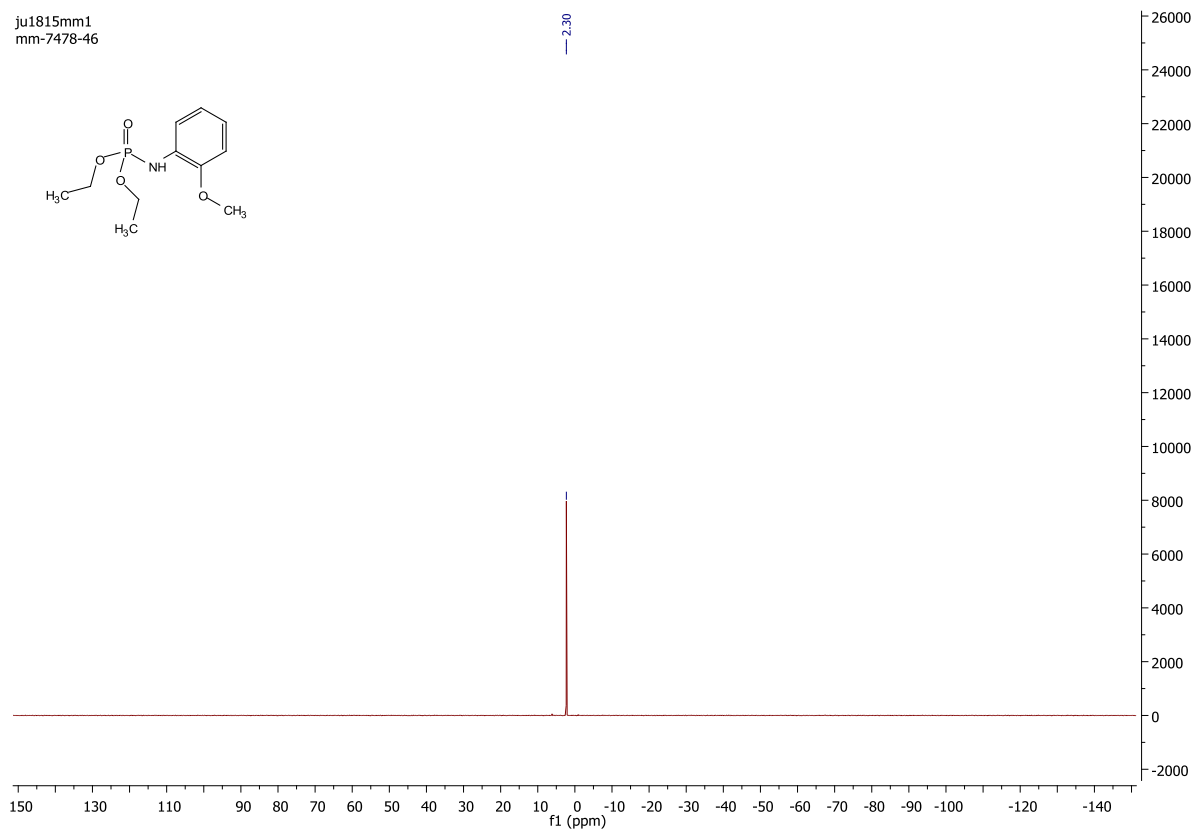
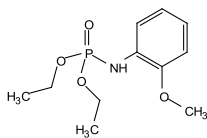


ju1815mm1
mm-7478-46

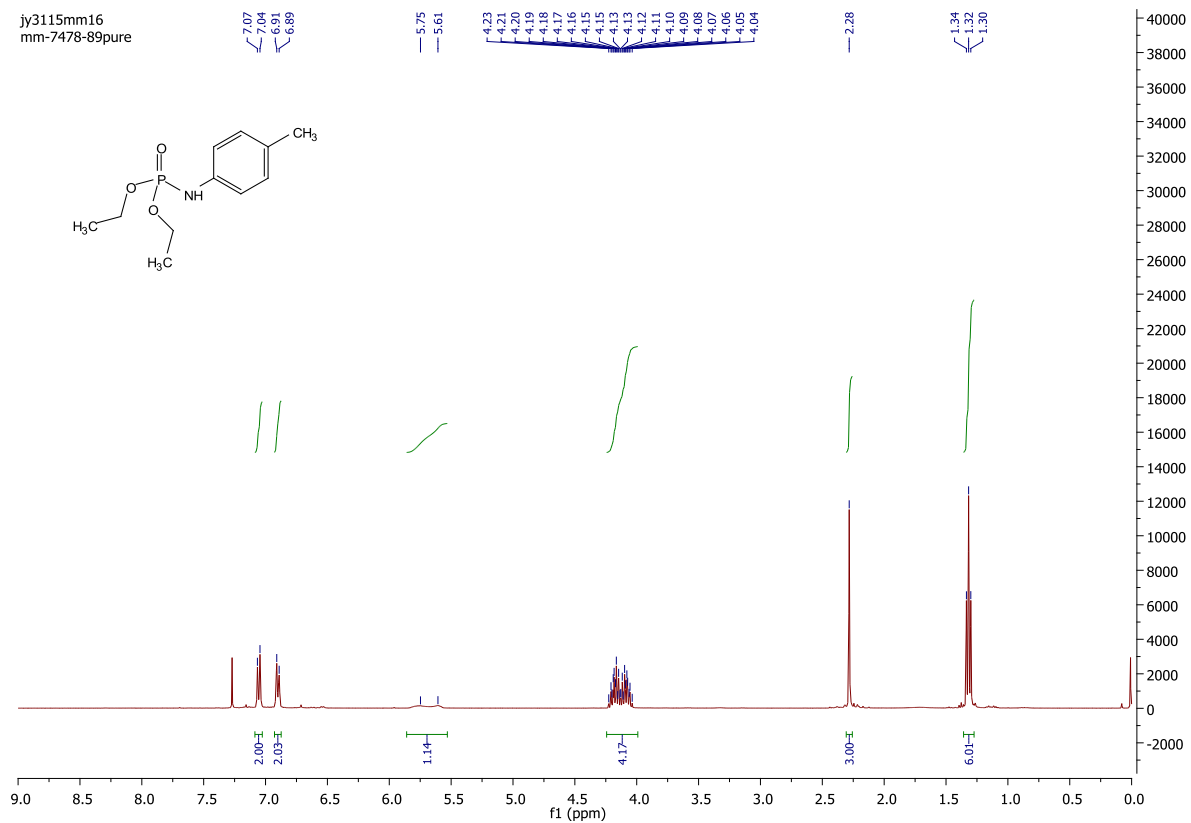
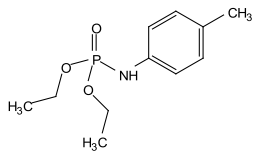


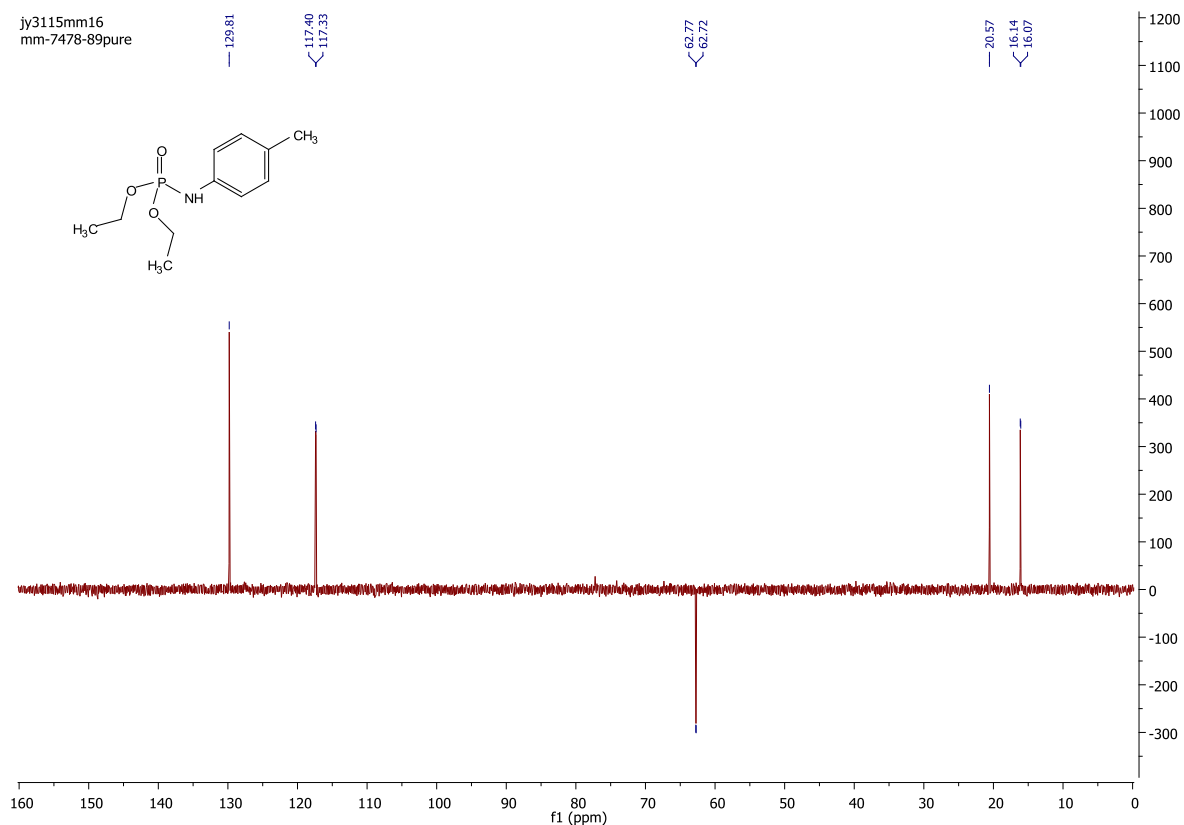
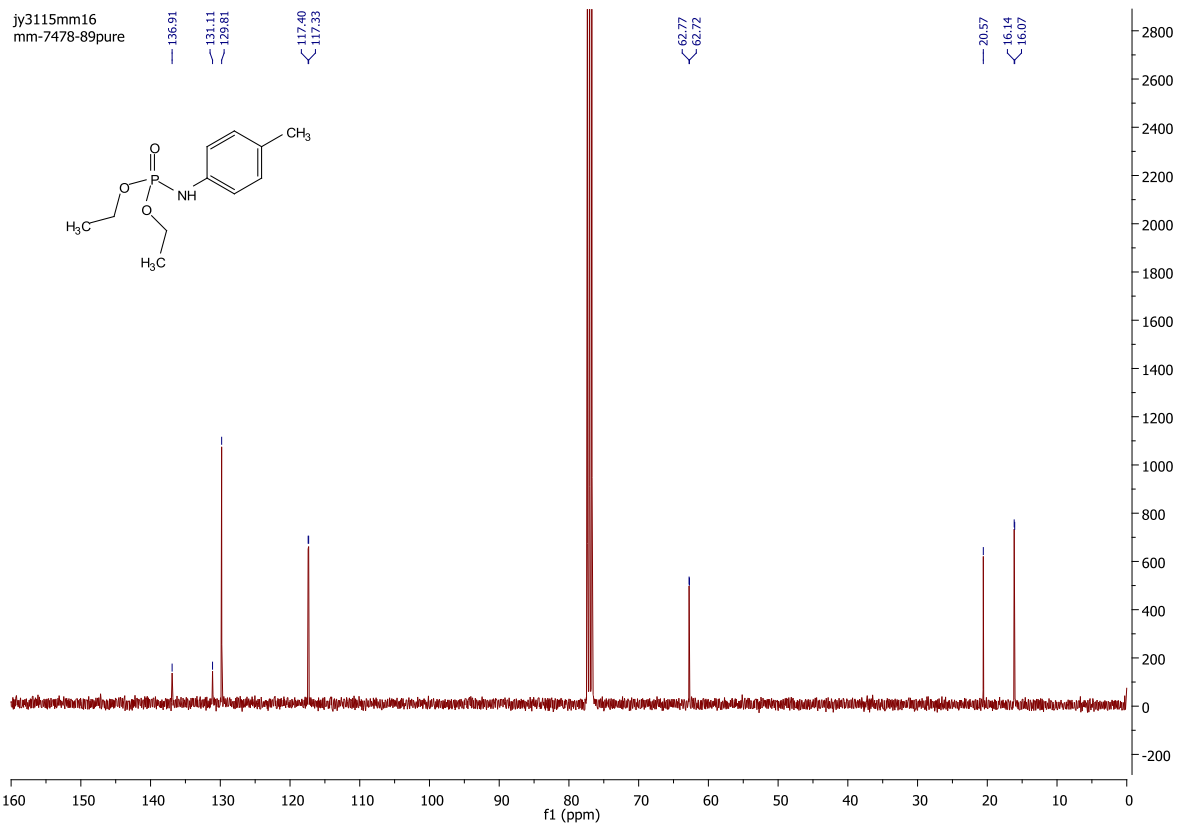


ju1815mm1
mm-7478-46

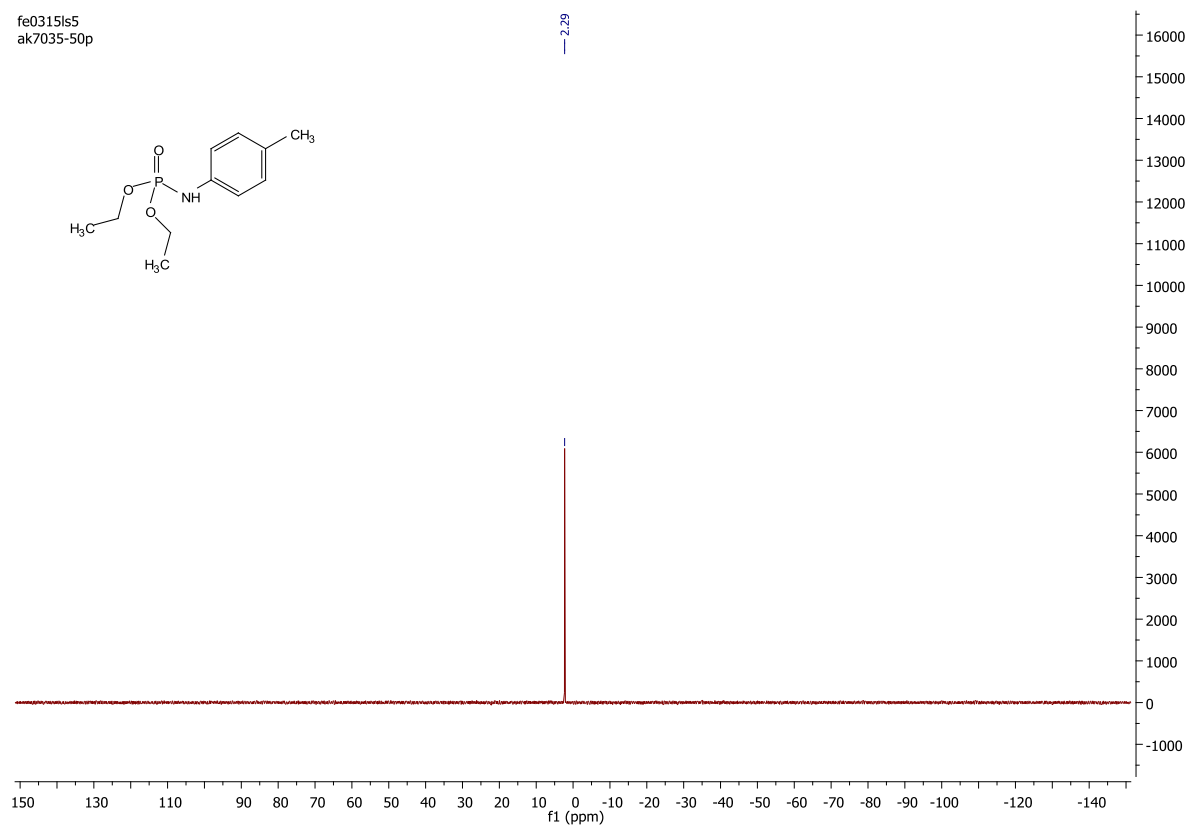
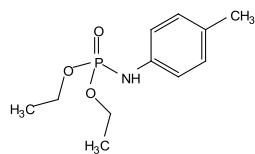


jy3115mm16
mm-7478-89pure

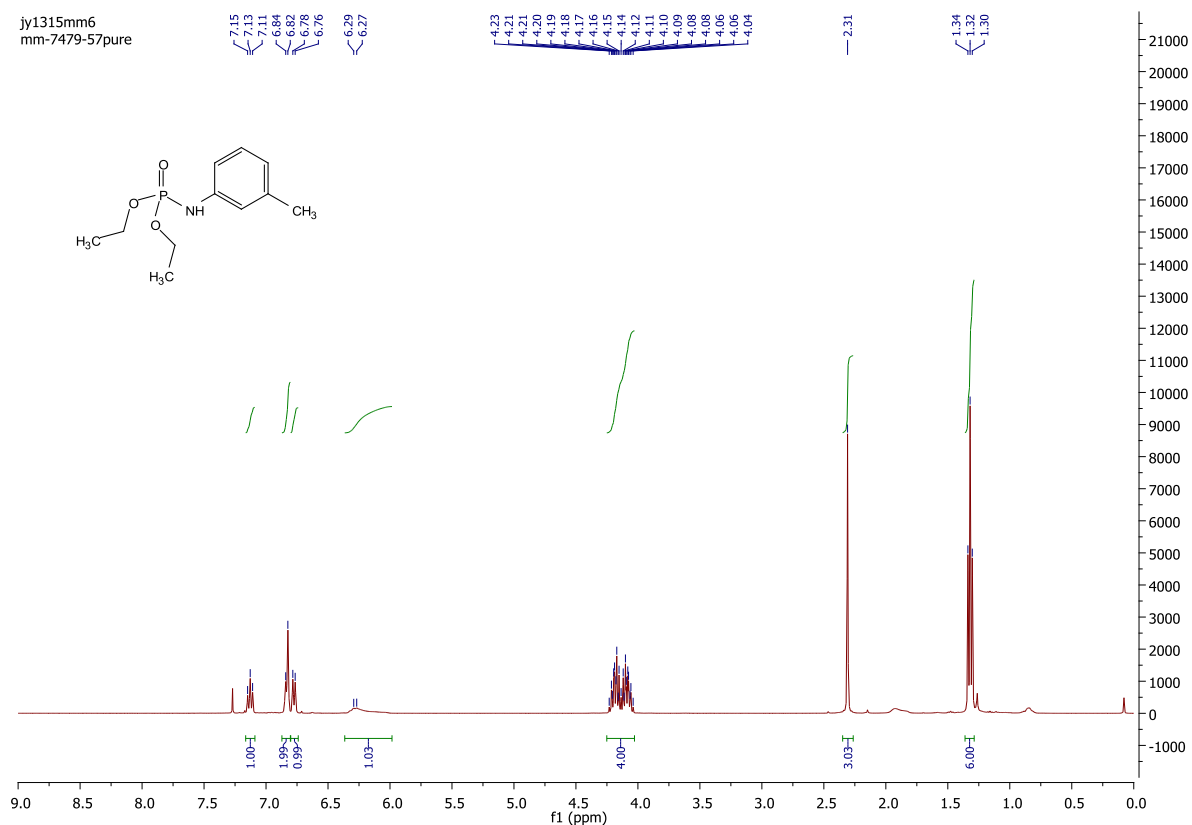
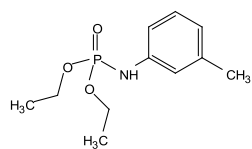


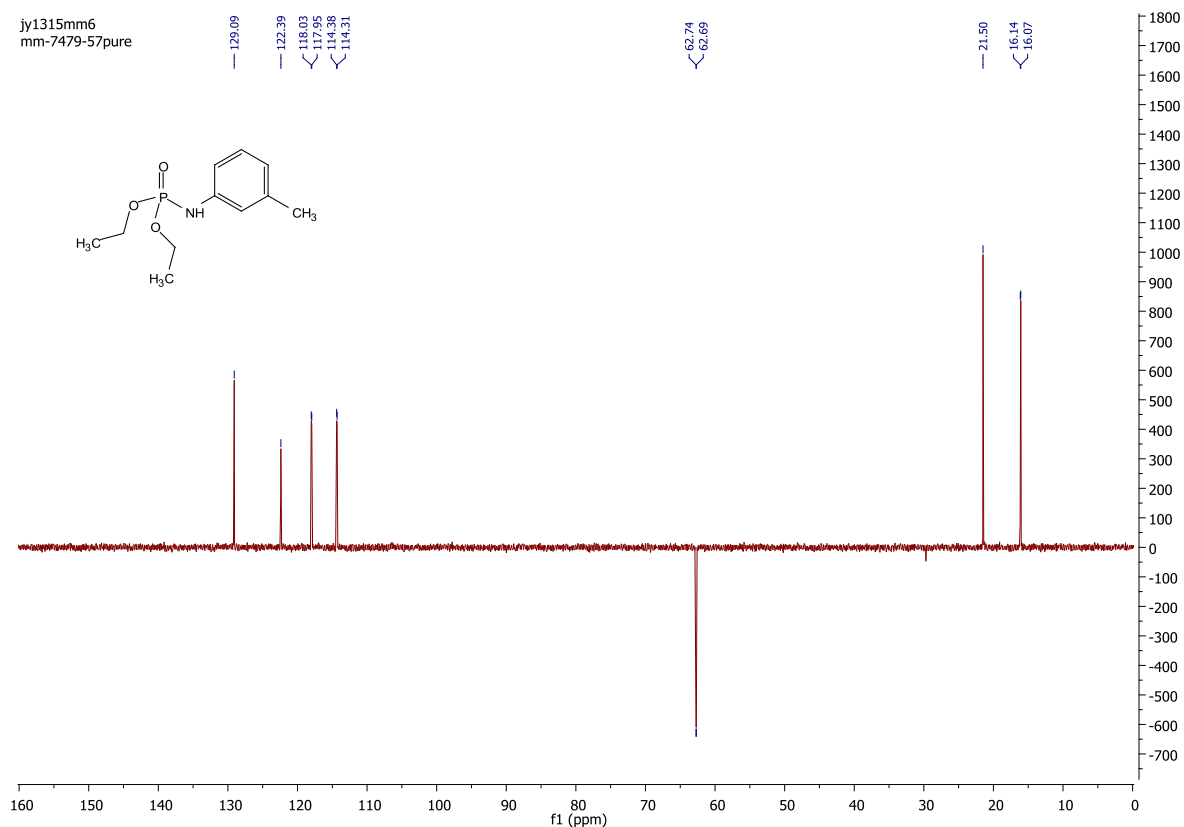
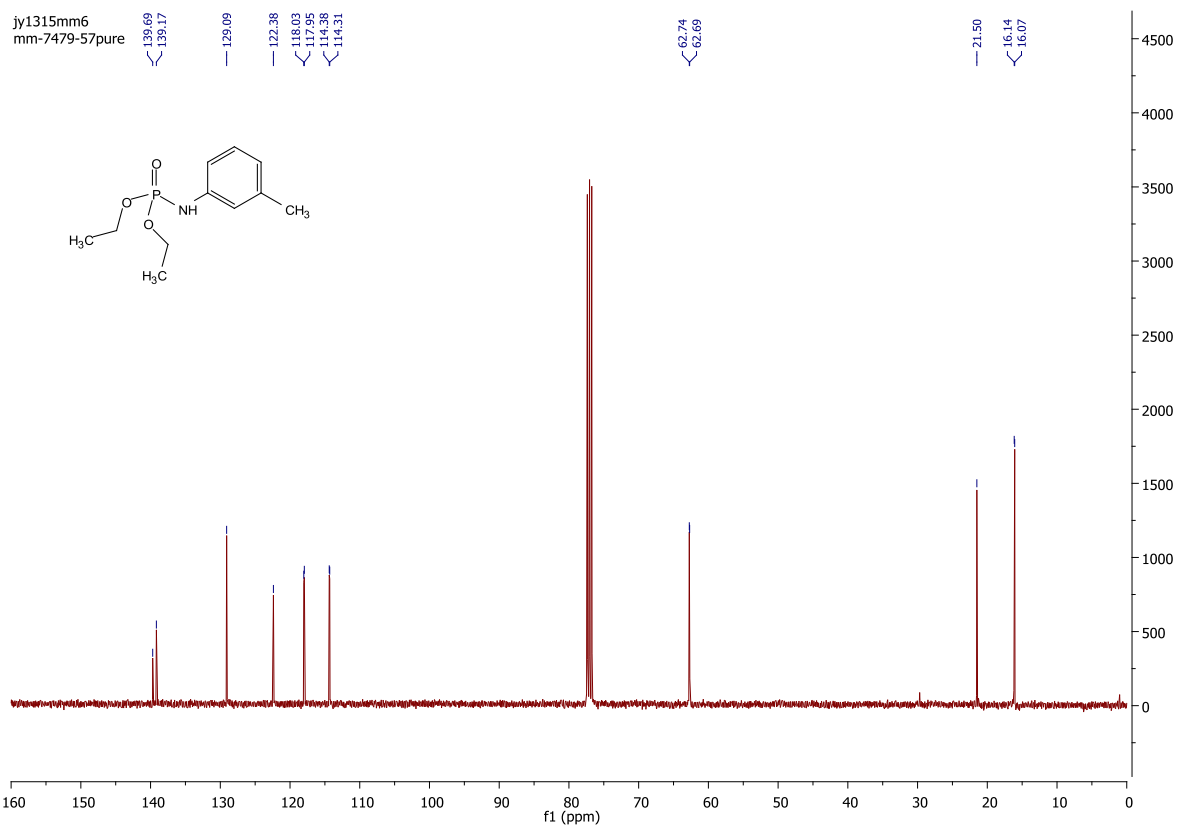


fe0315ls5
ak7035-50p

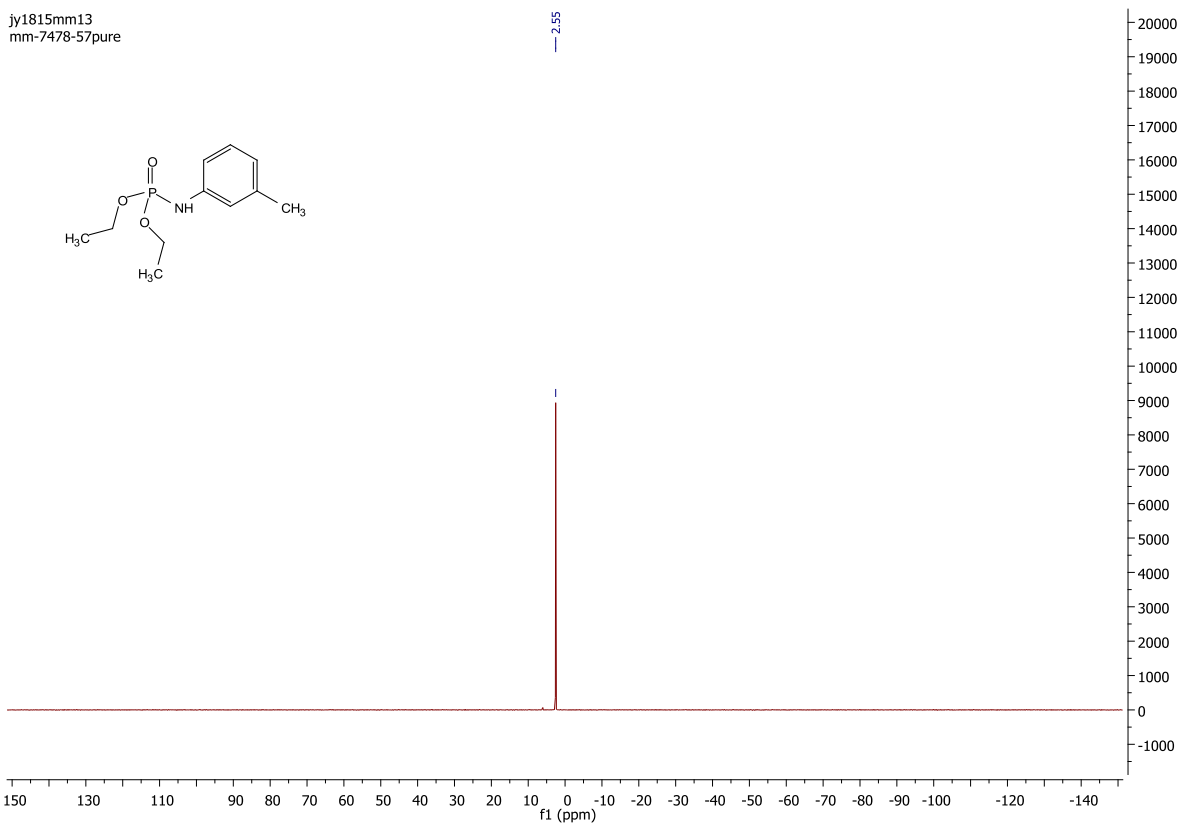


jy1315mm6
mm-7479-57pure

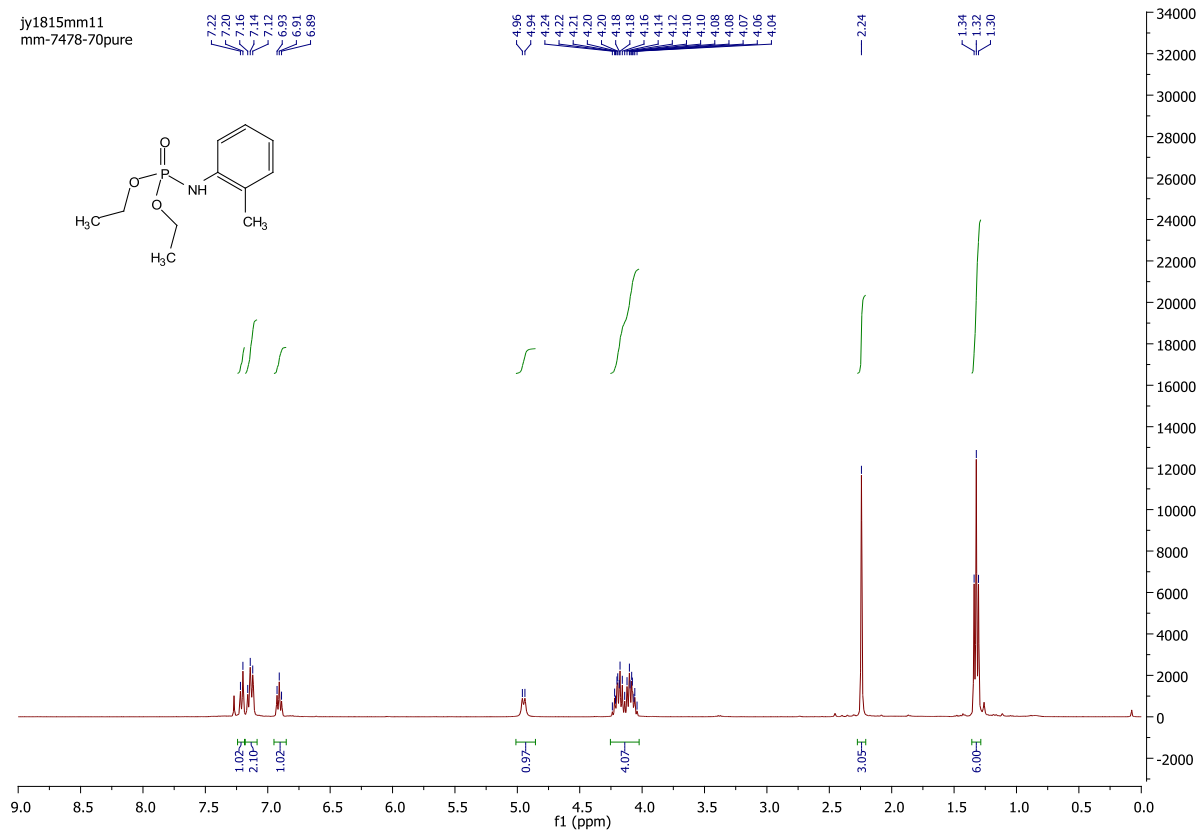




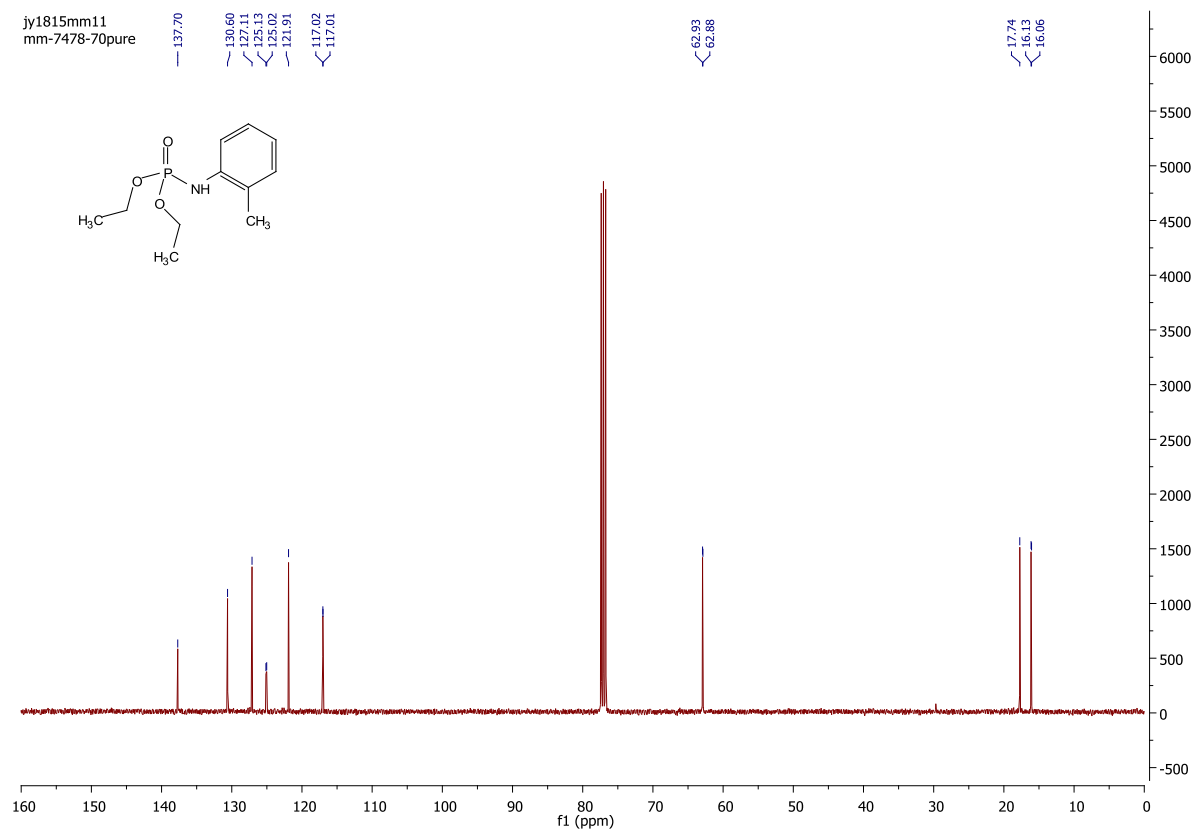
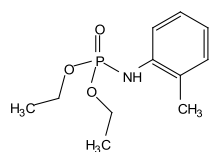
jy1815mm13
mm-7478-57pure



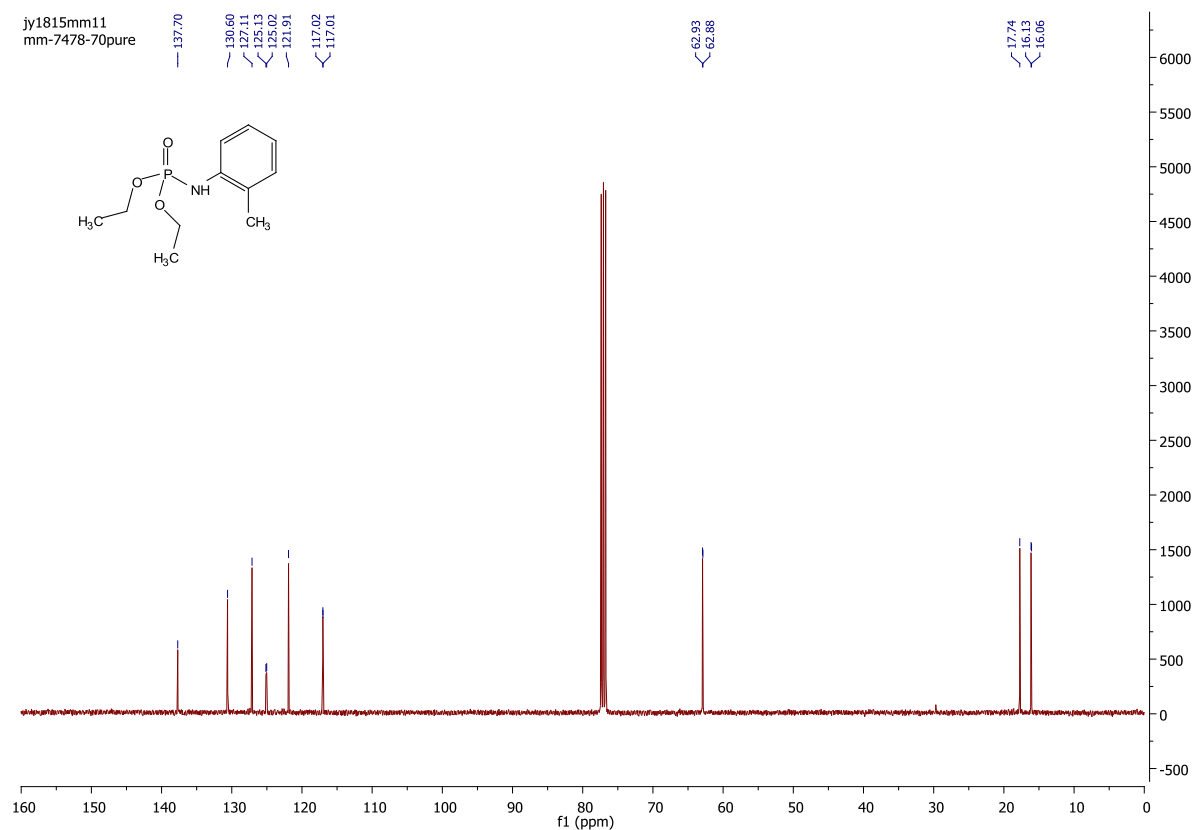
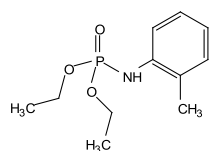
jy1815mm11
mm-7478-70pure



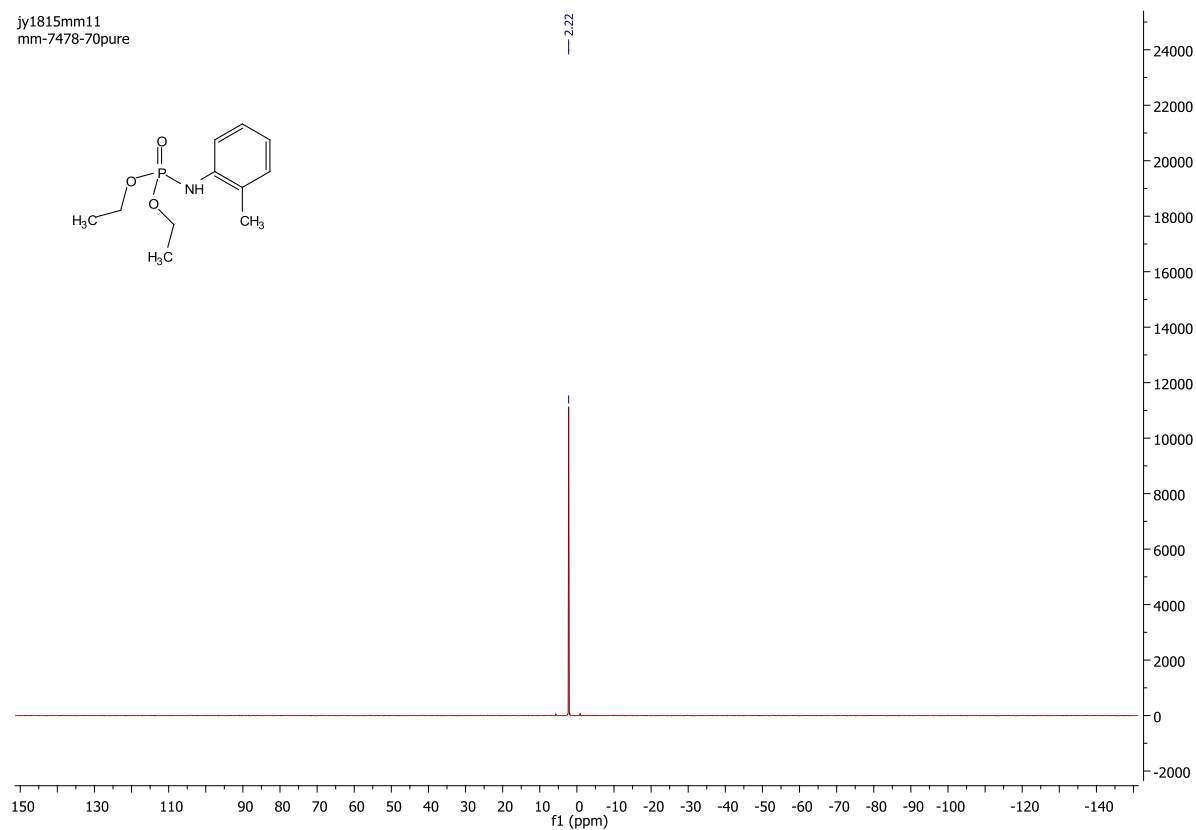
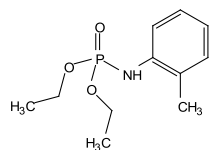
jy1815mm11
mm-7478-70pure



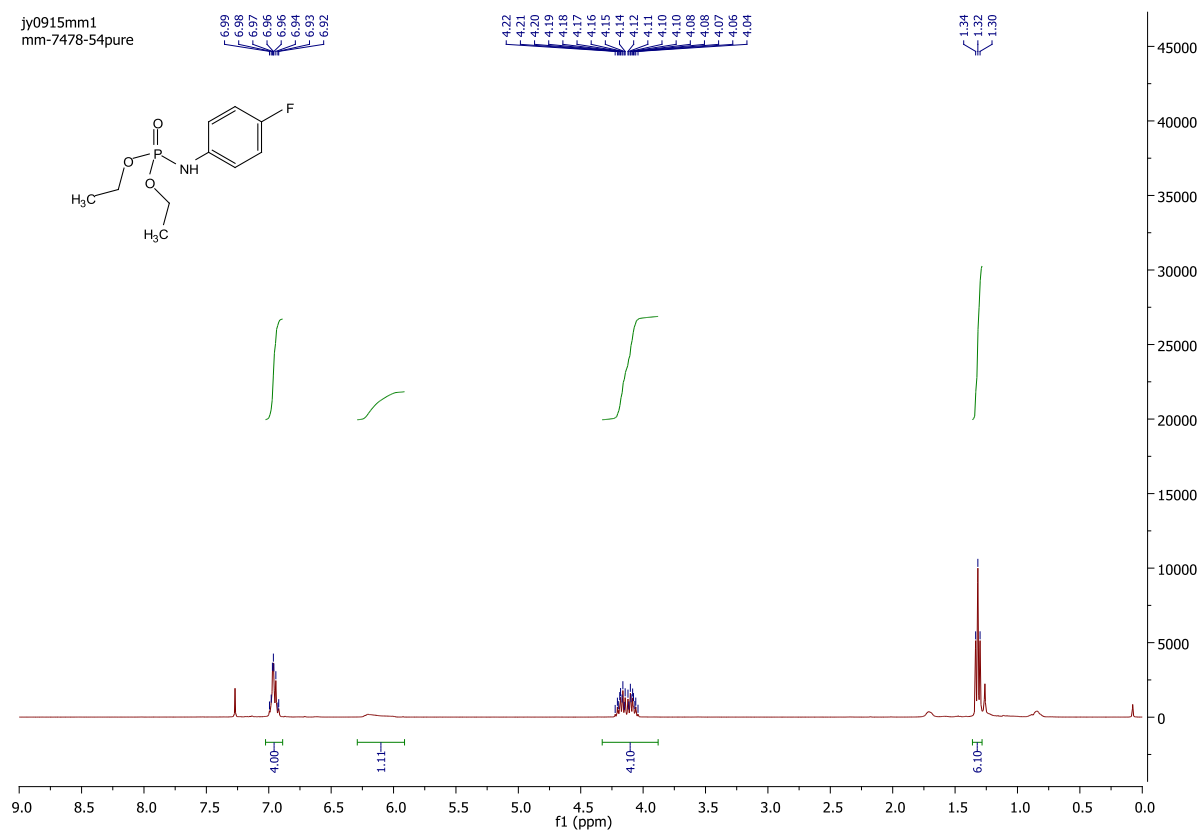
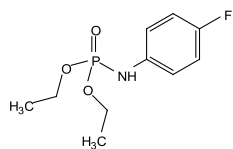
jy1815mm11
mm-7478-70pure



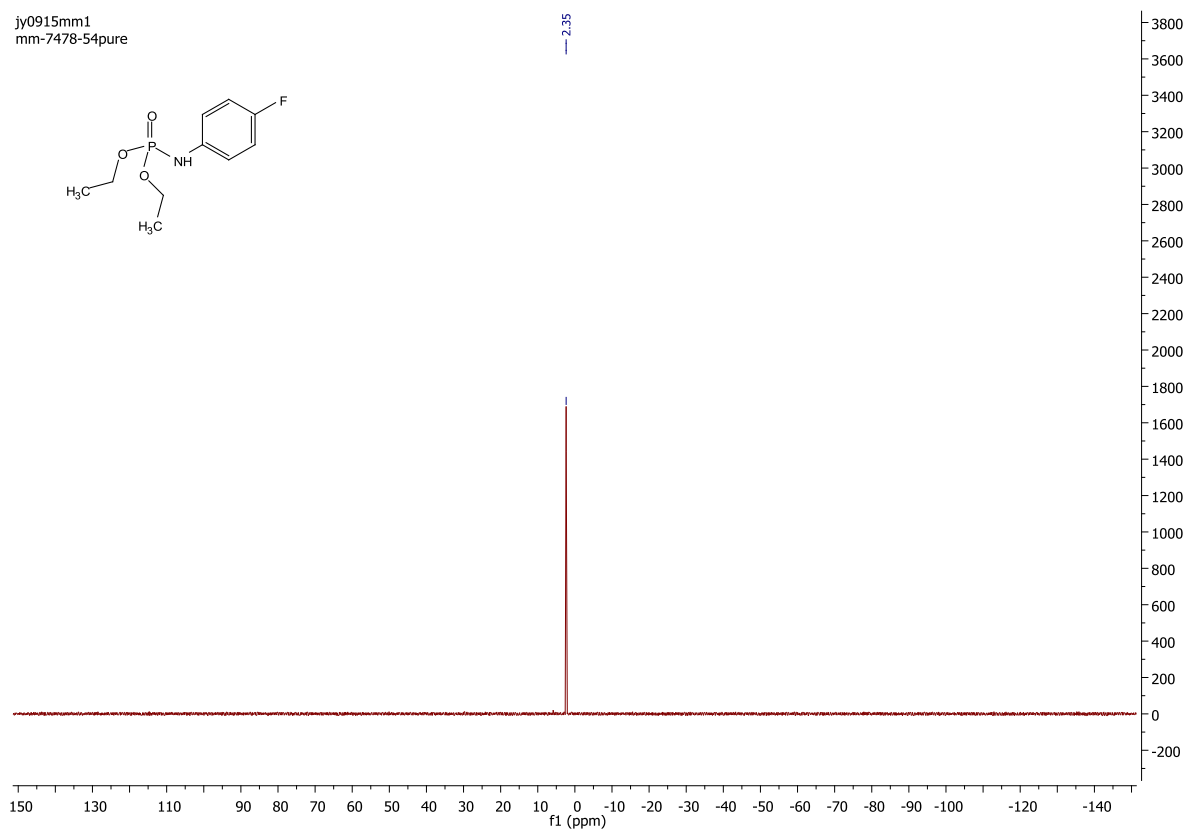
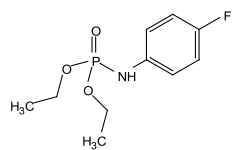
jy1815mm11
 mm-7478-70pure



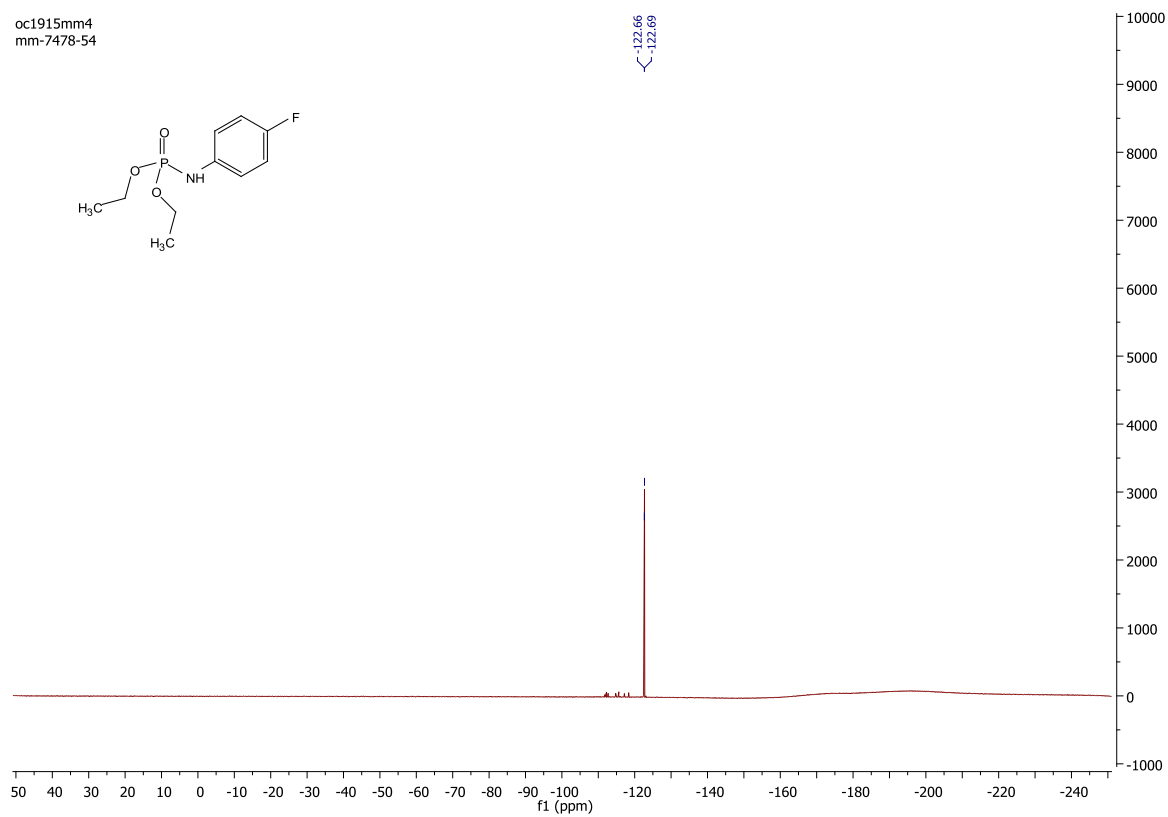
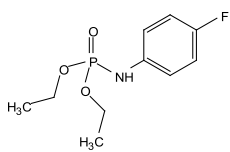
jy0915mm1
 mm-7478-54pure



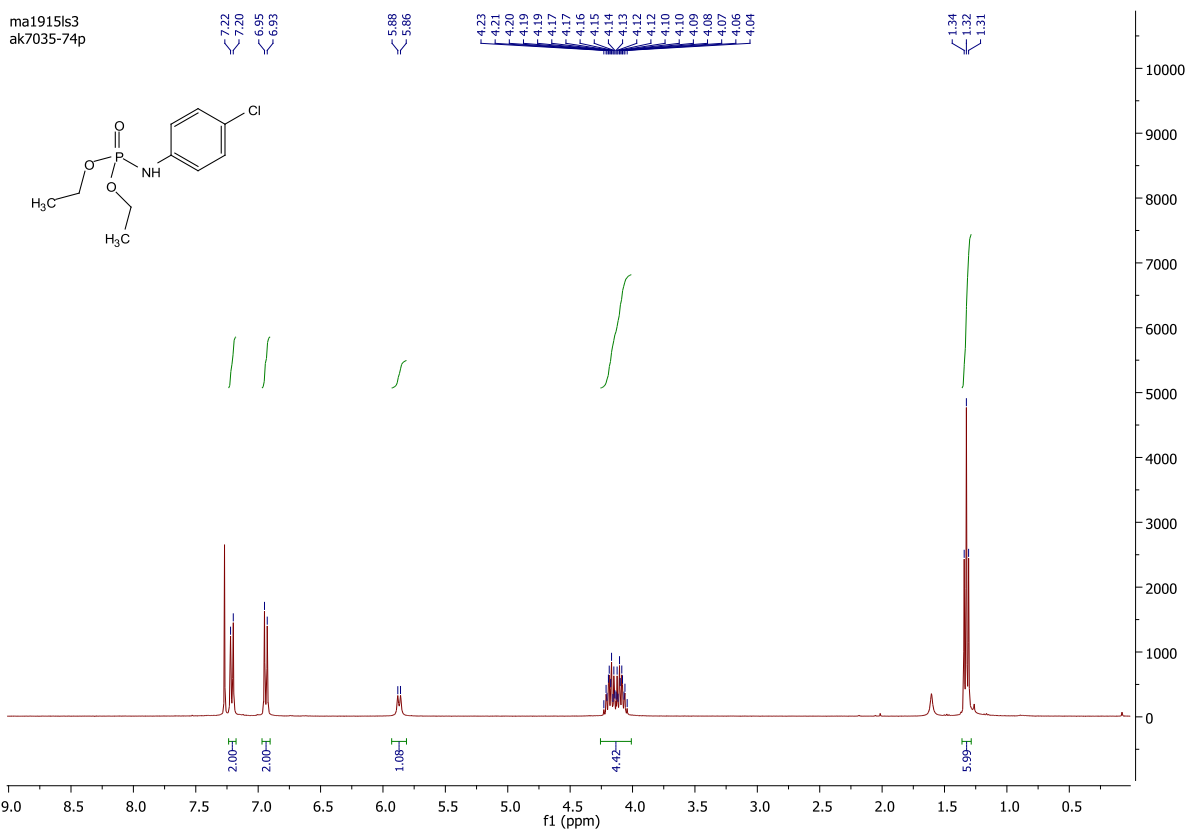
jy0915mm1
 mm-7478-54pure



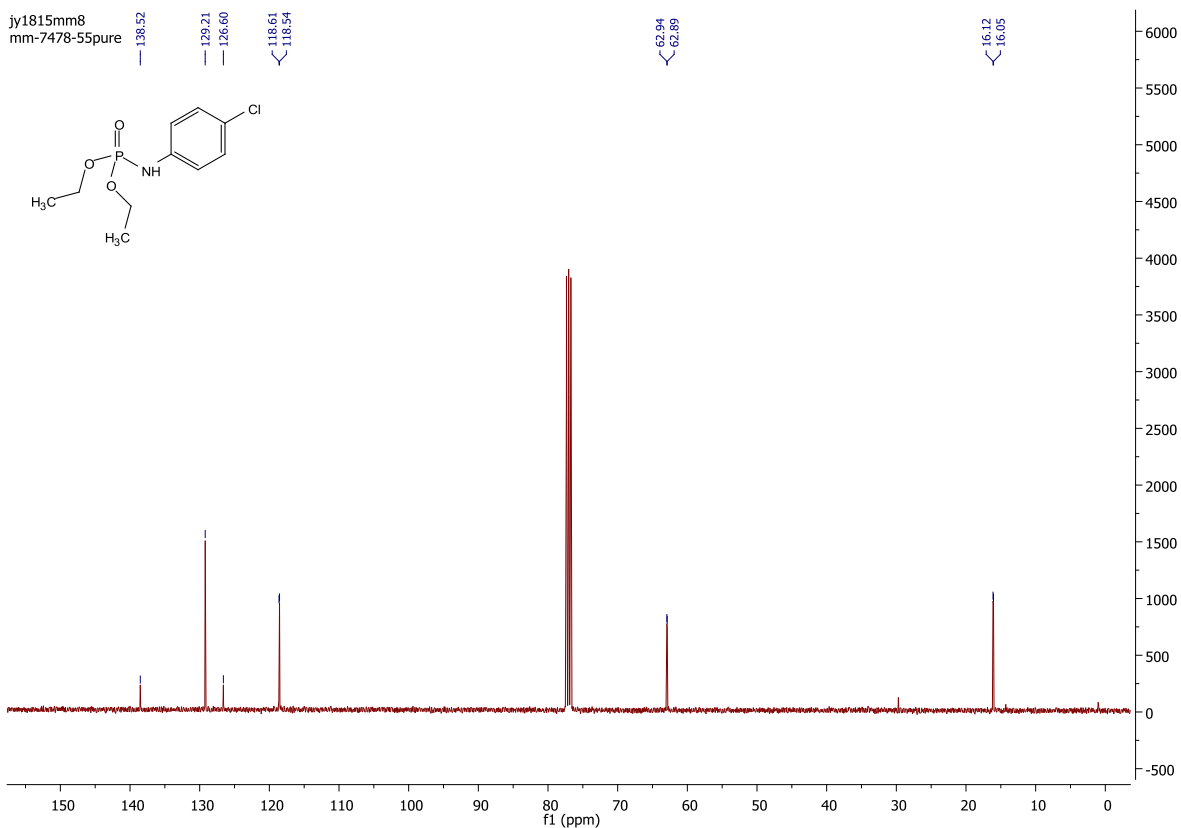
oc1915mm4
 mm-7478-54



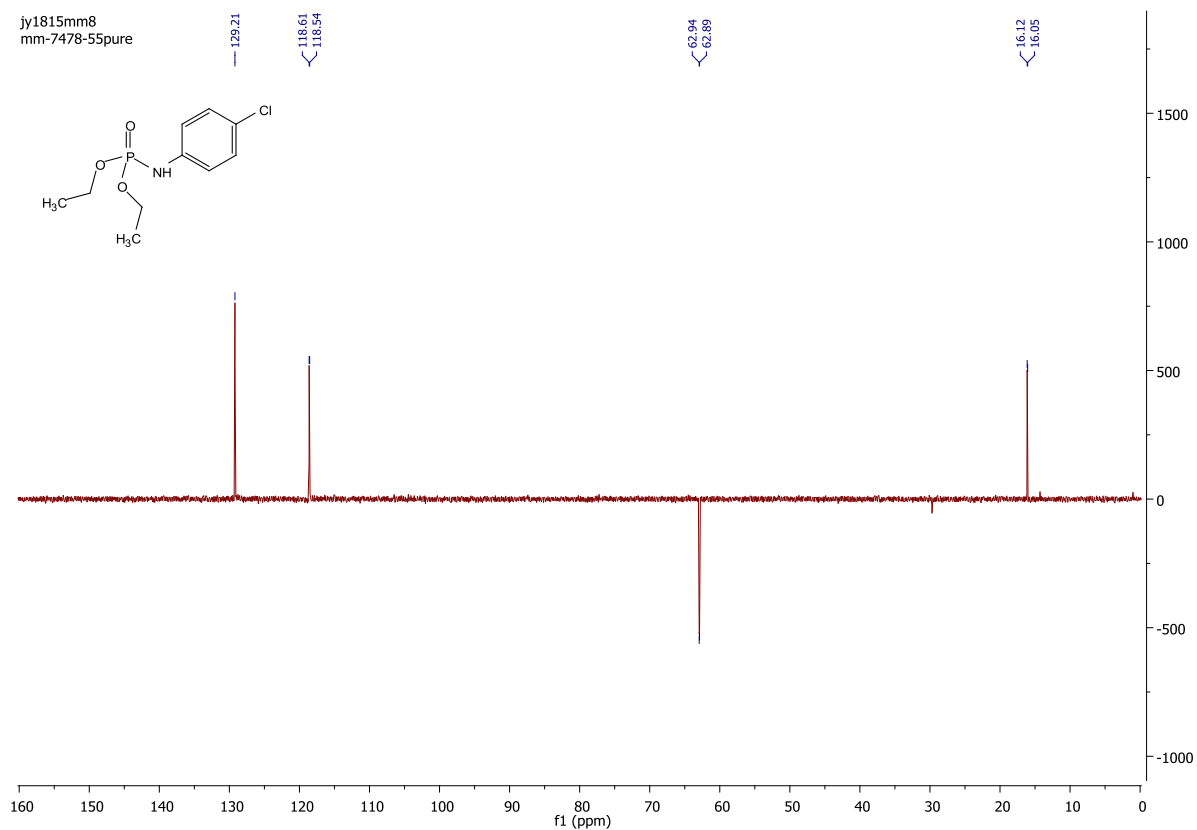
ma1915ls3
ak7035-74p



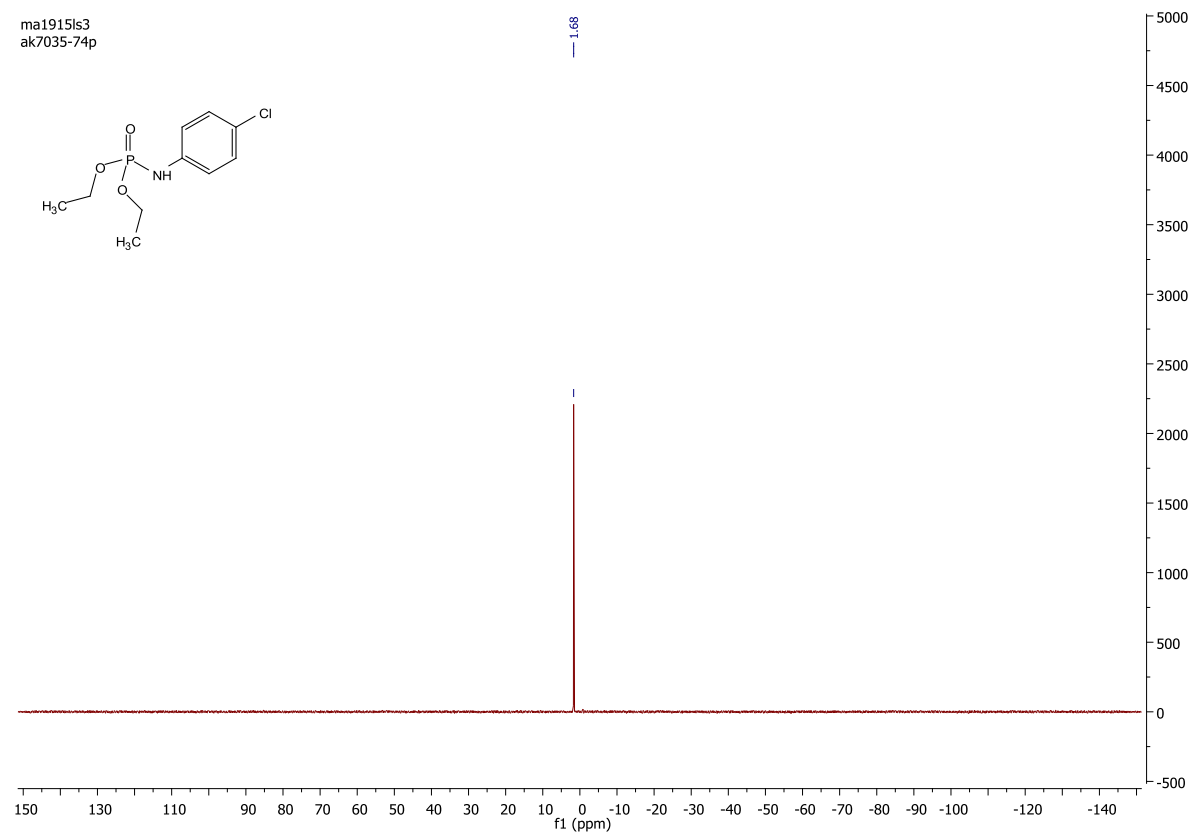
jy1815mm8
mm-7478-55pure



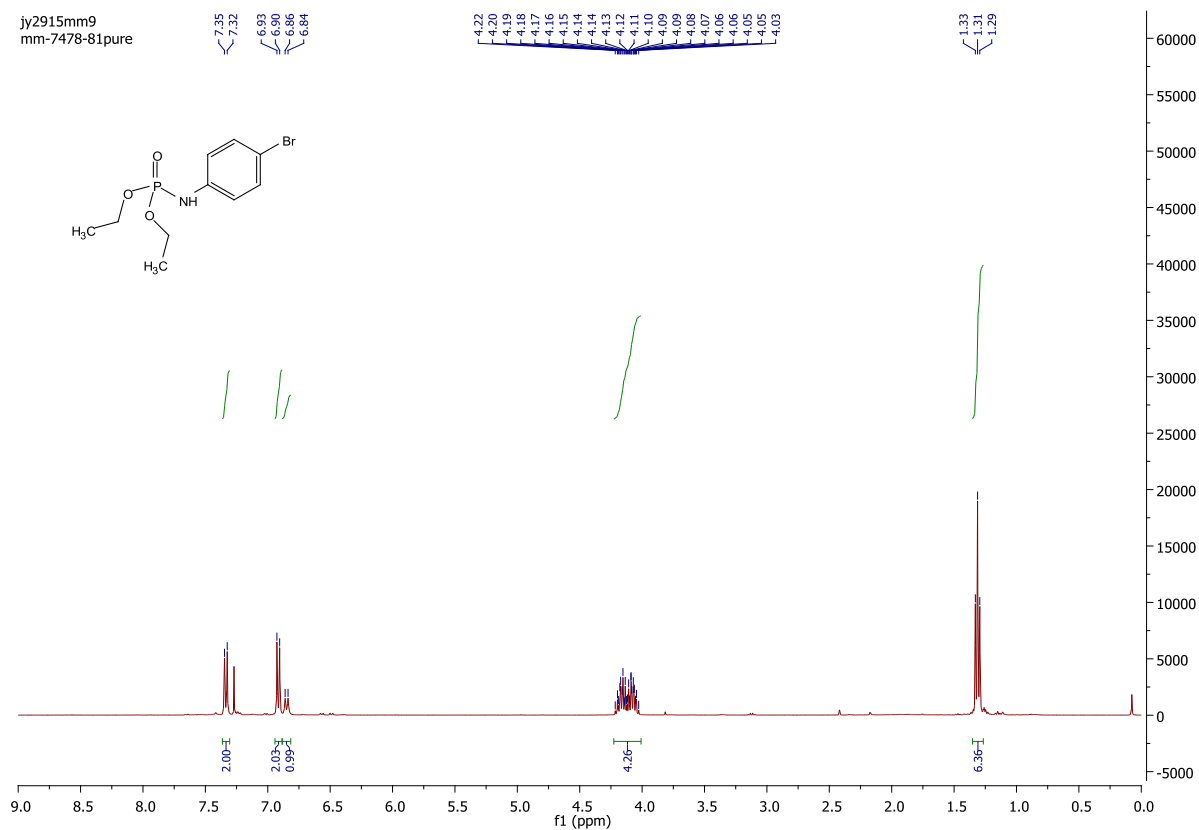
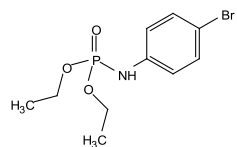
jy1815mm8
 mm-7478-55pure



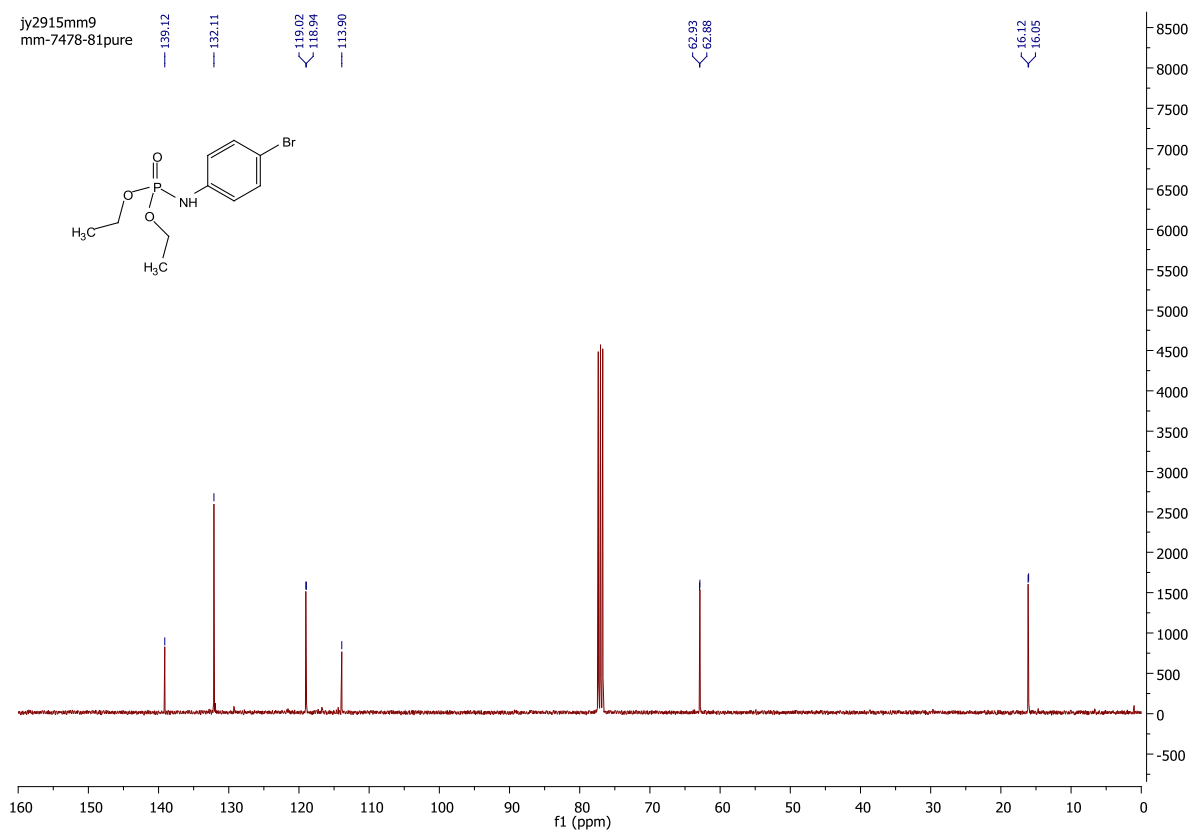
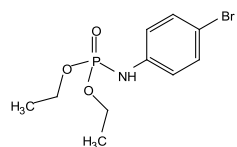
ma1915ls3
 ak7035-74p



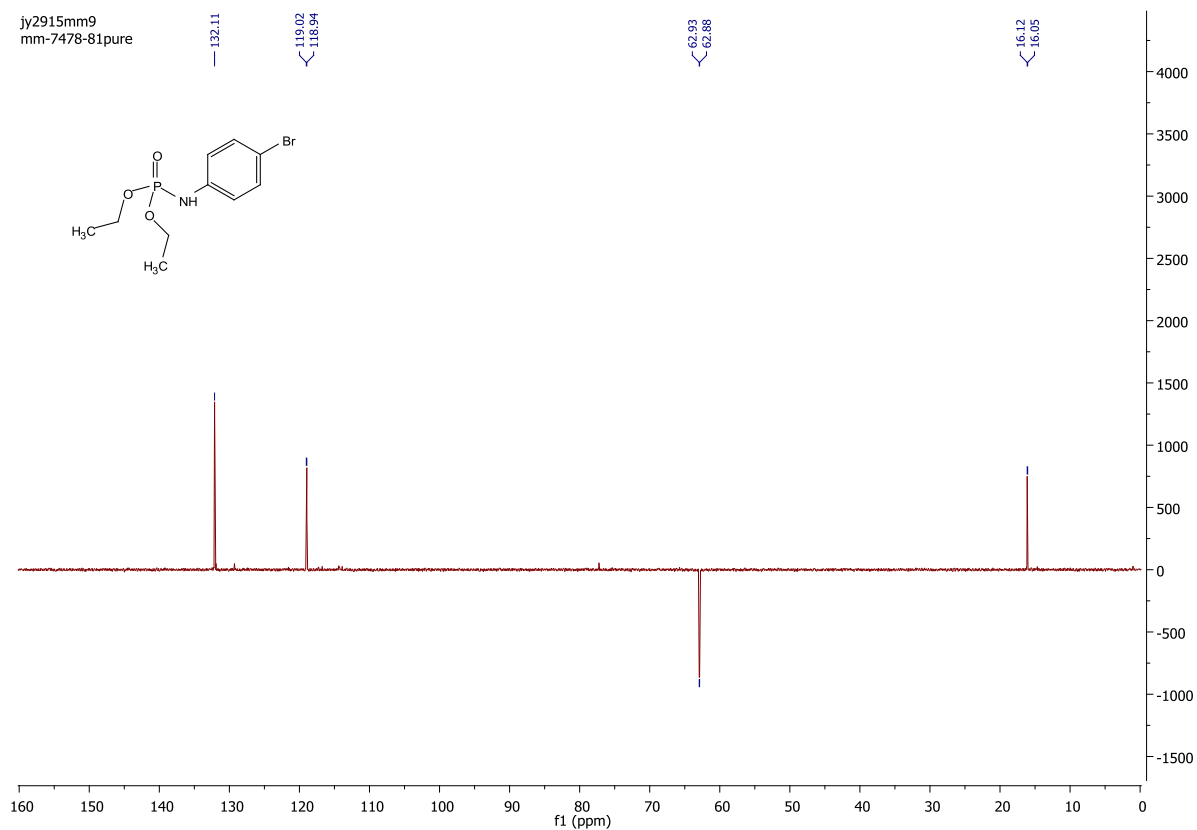
jy2915mm9
mm-7478-81pure



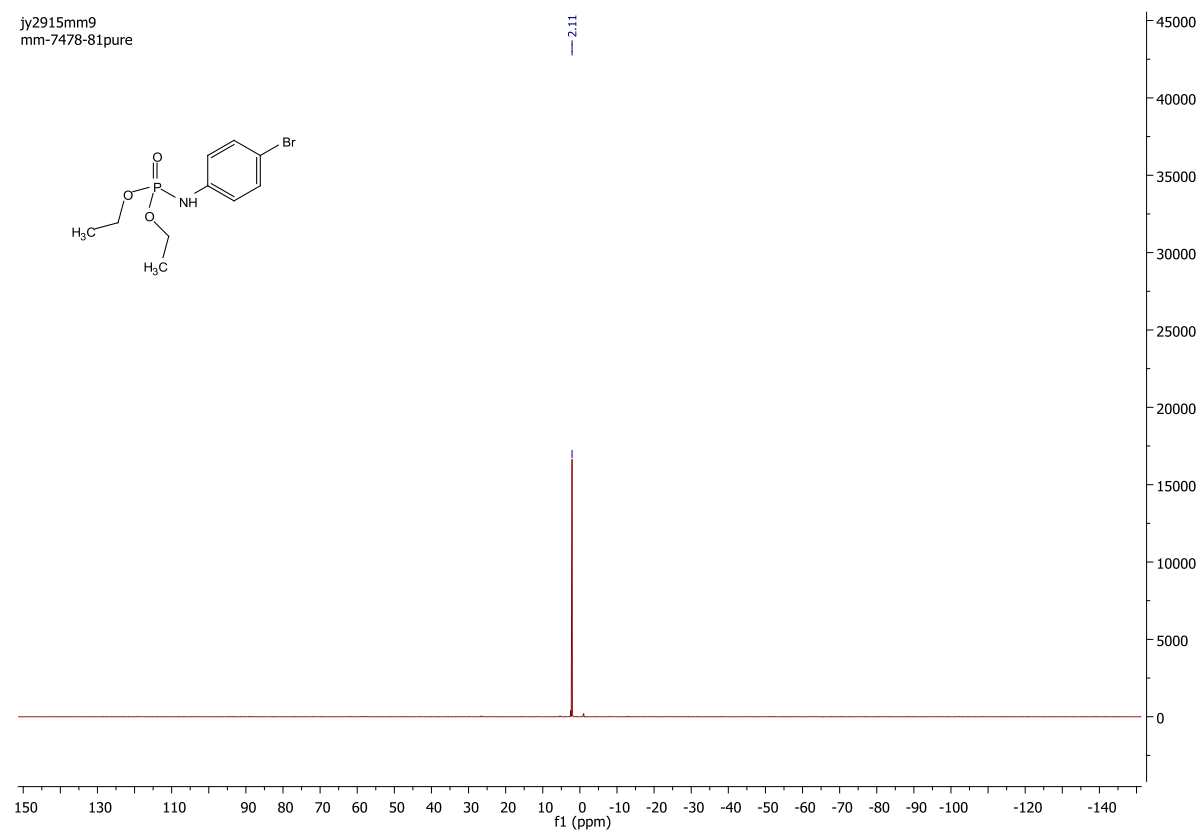
jy2915mm9
mm-7478-81pure



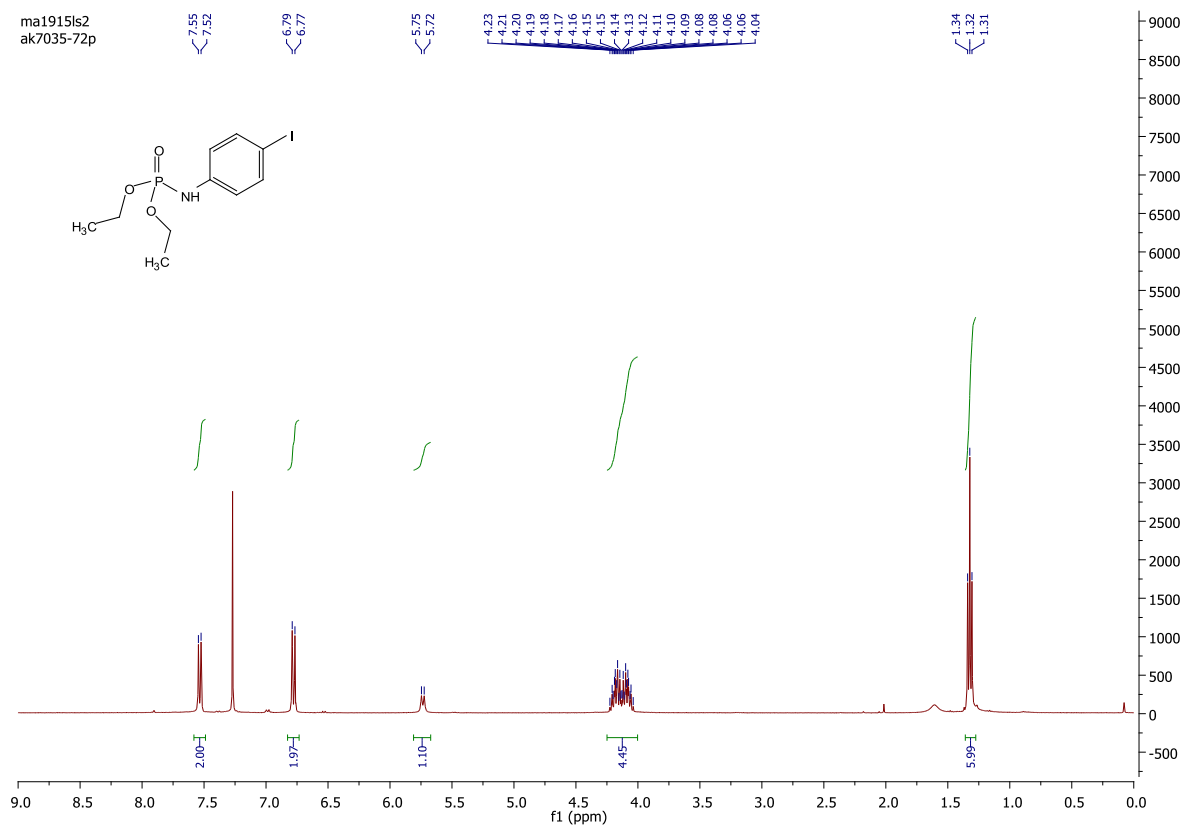
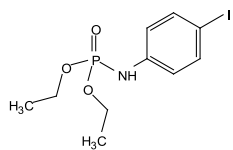
jj2915mm9
mm-7478-81pure



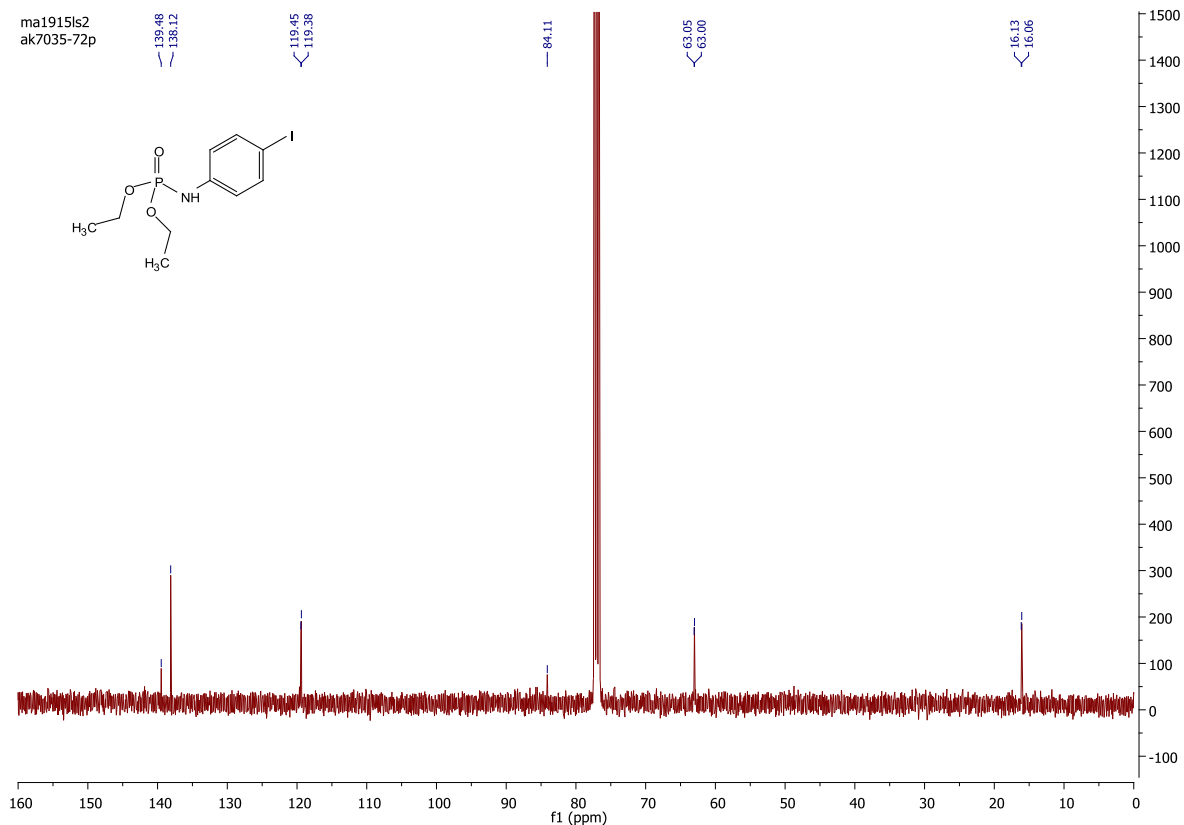
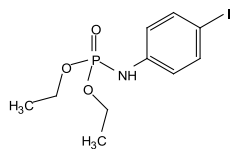
jj2915mm9
mm-7478-81pure



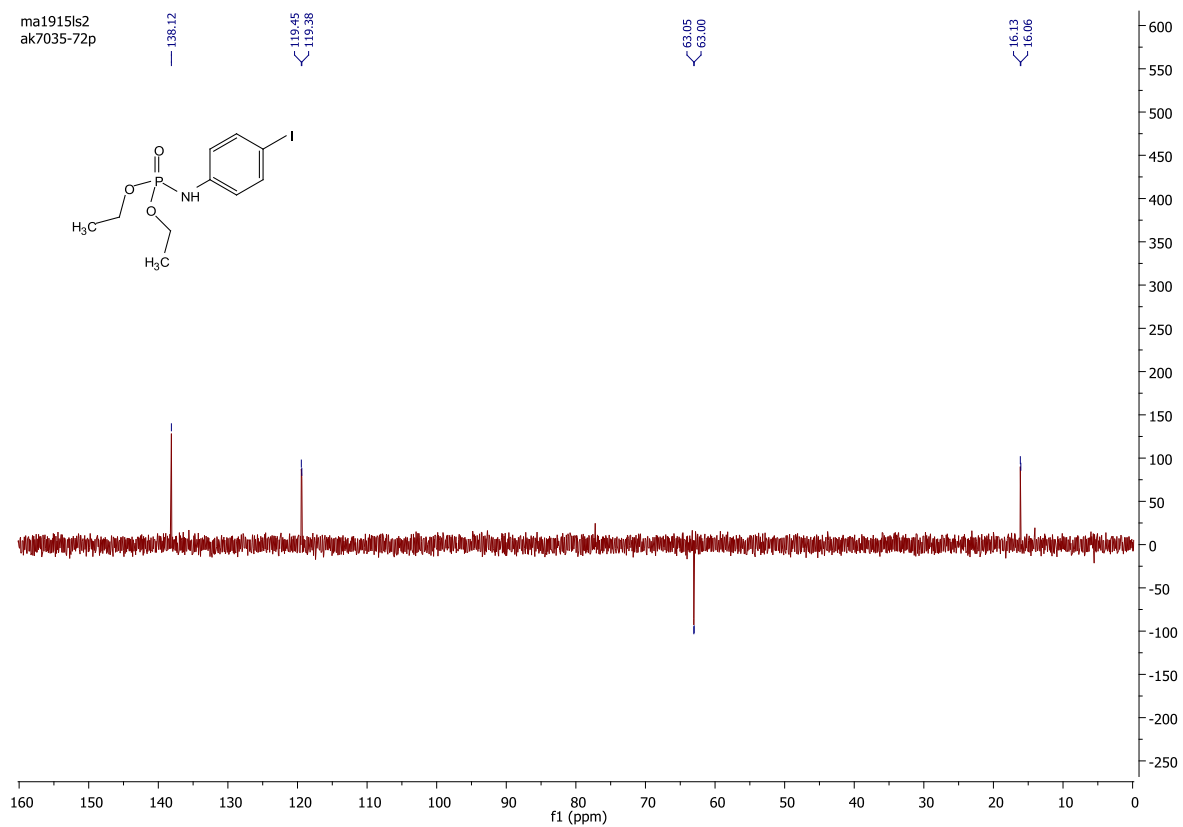
ma1915ls2
ak7035-72p



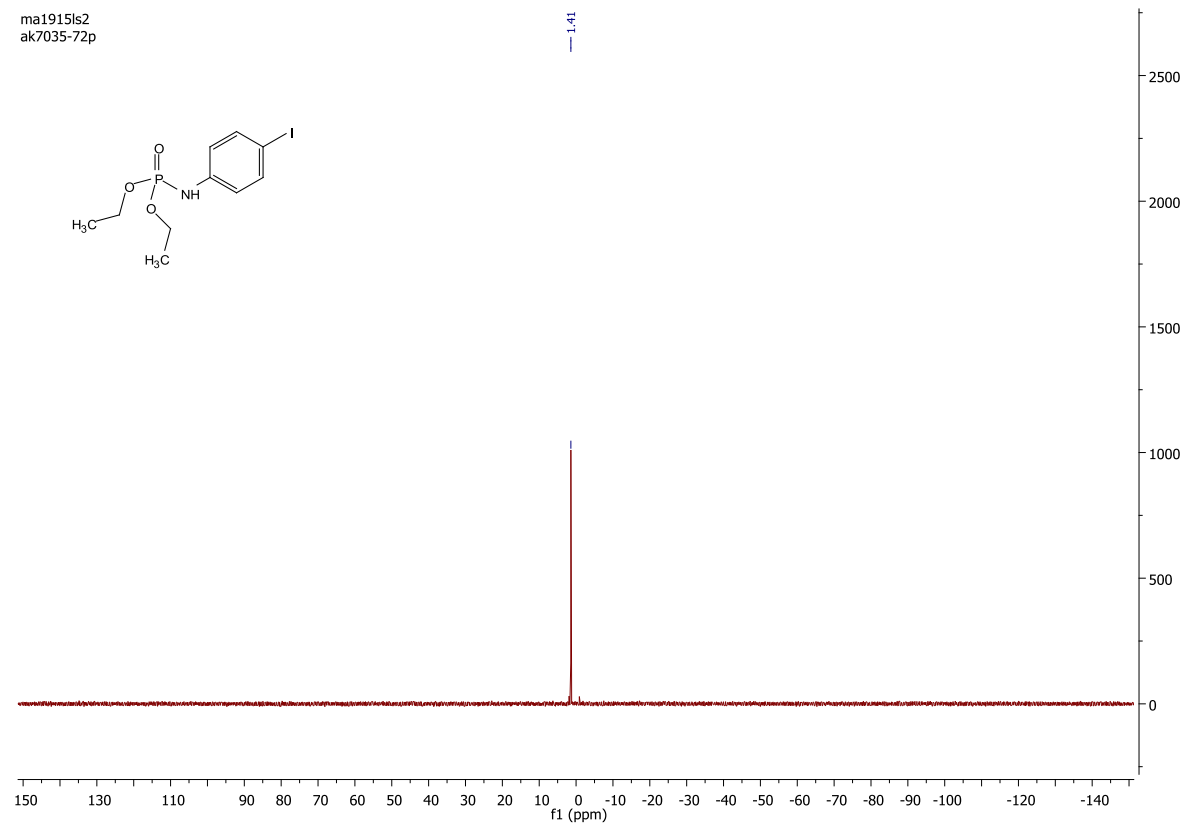
ma1915ls2
ak7035-72p



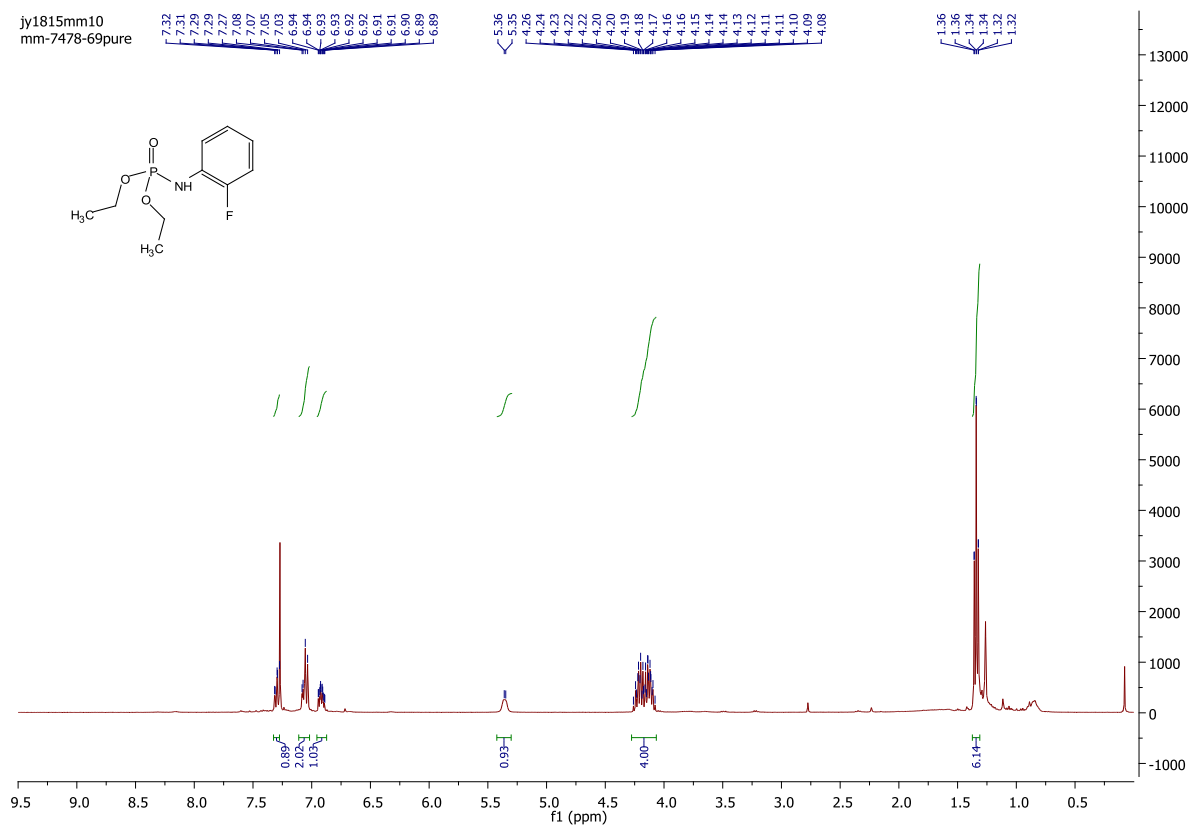
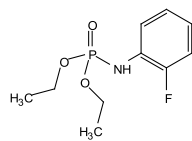
ma1915ls2
ak7035-72p



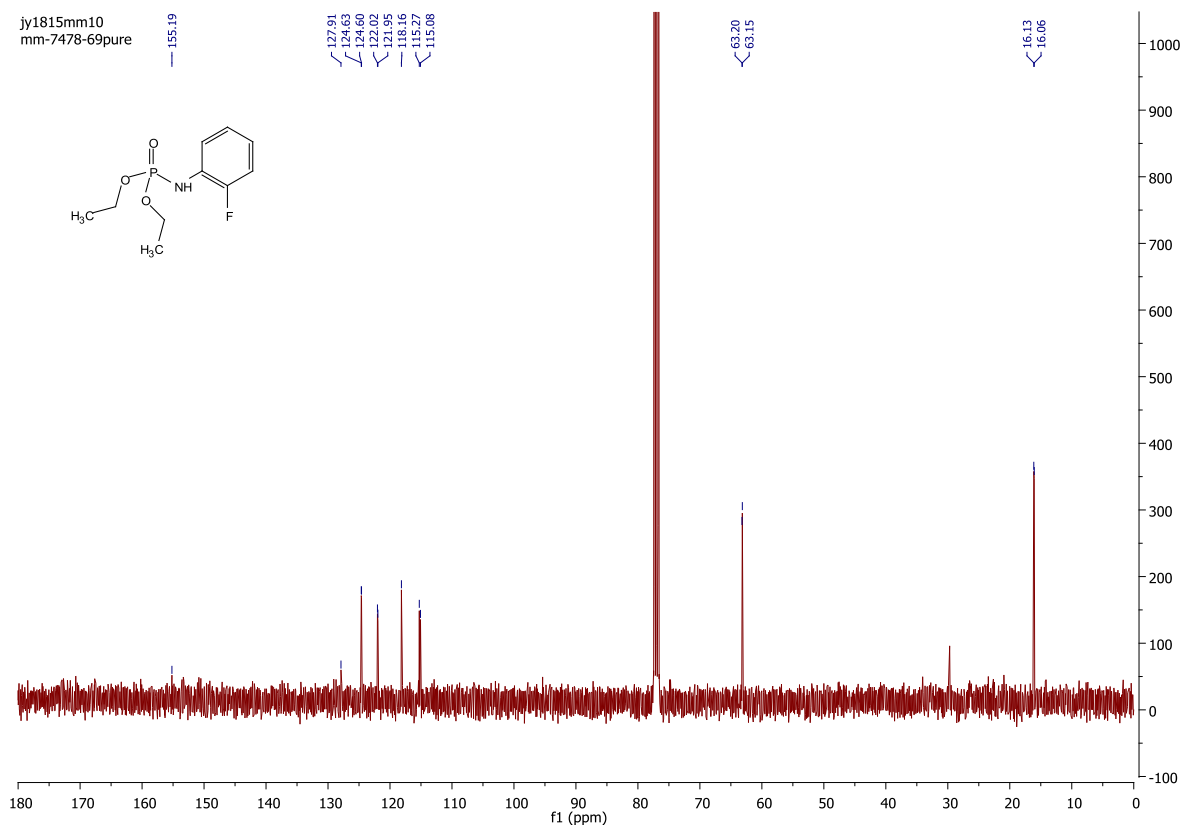
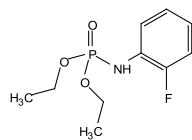
ma1915ls2
ak7035-72p



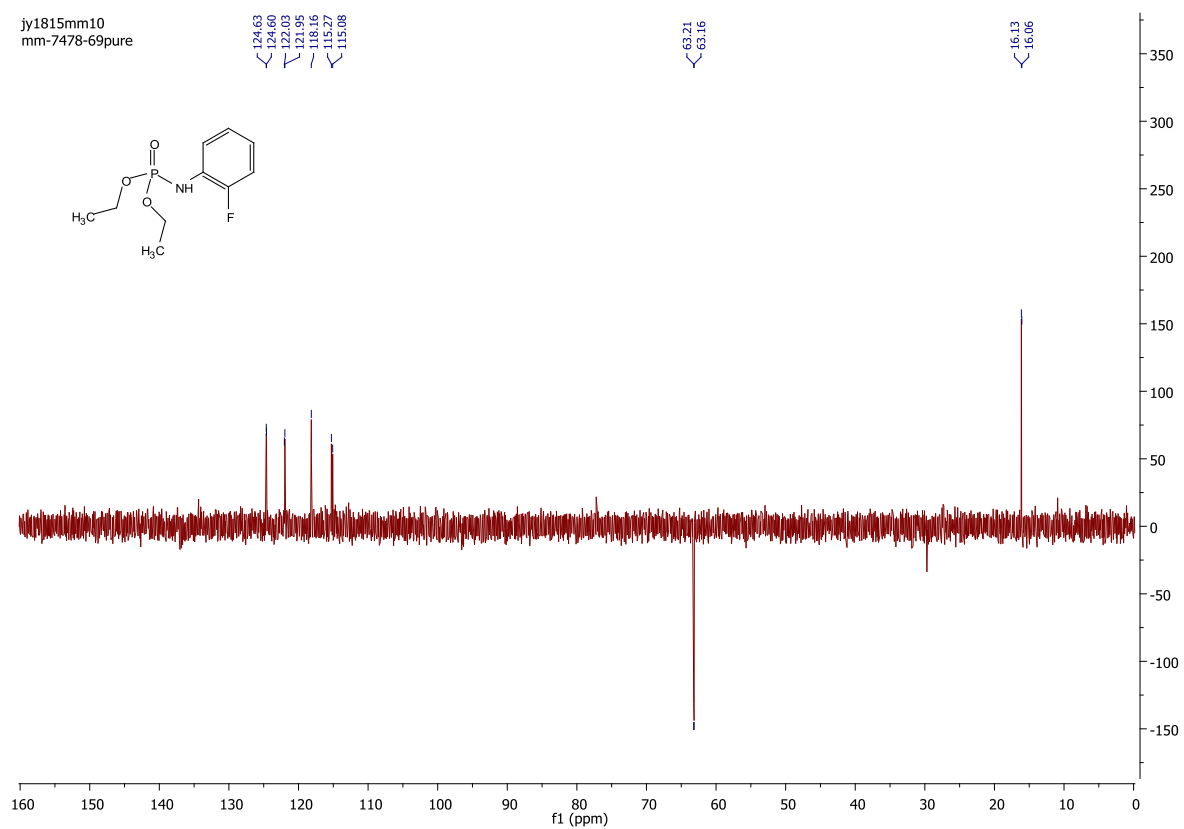
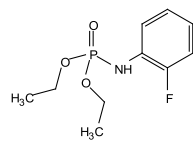
jy1815mm10
mm-7478-69pure



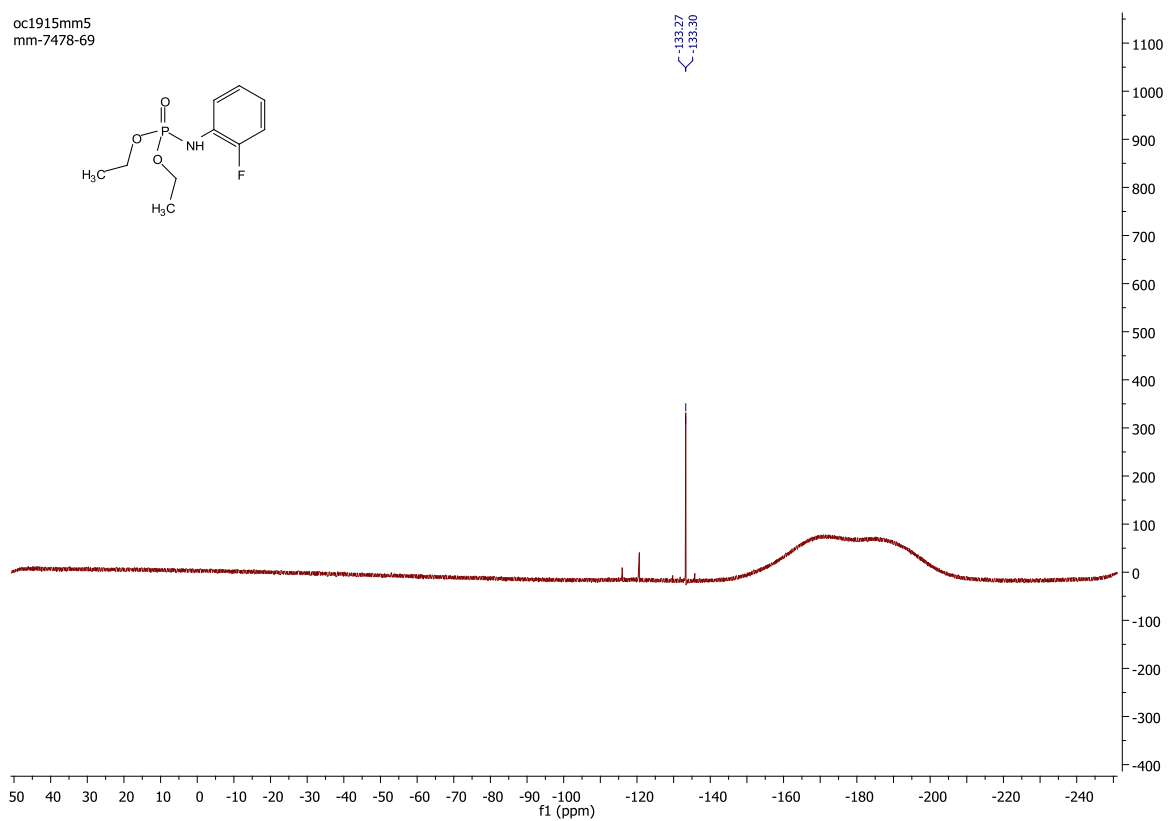
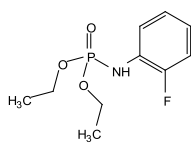
jy1815mm10
mm-7478-69pure



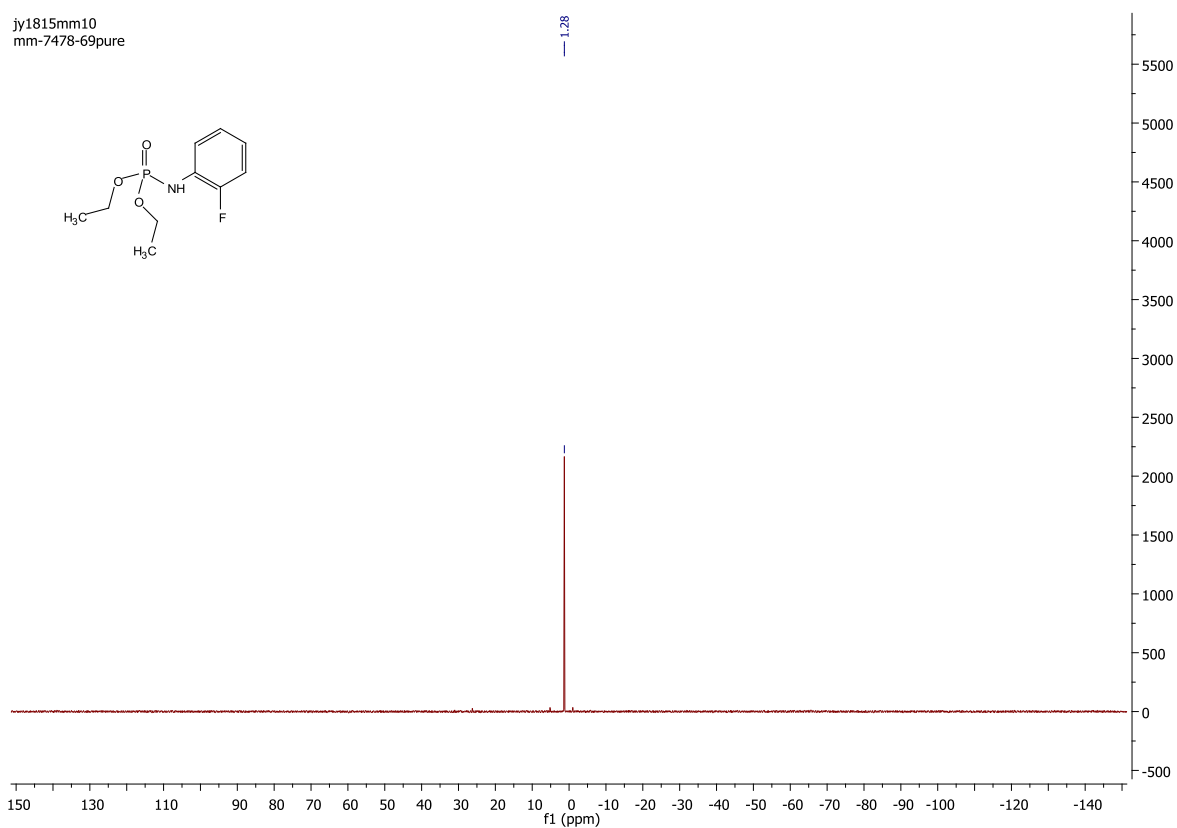
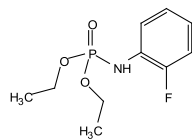
jj1815mm10
mm-7478-69pure



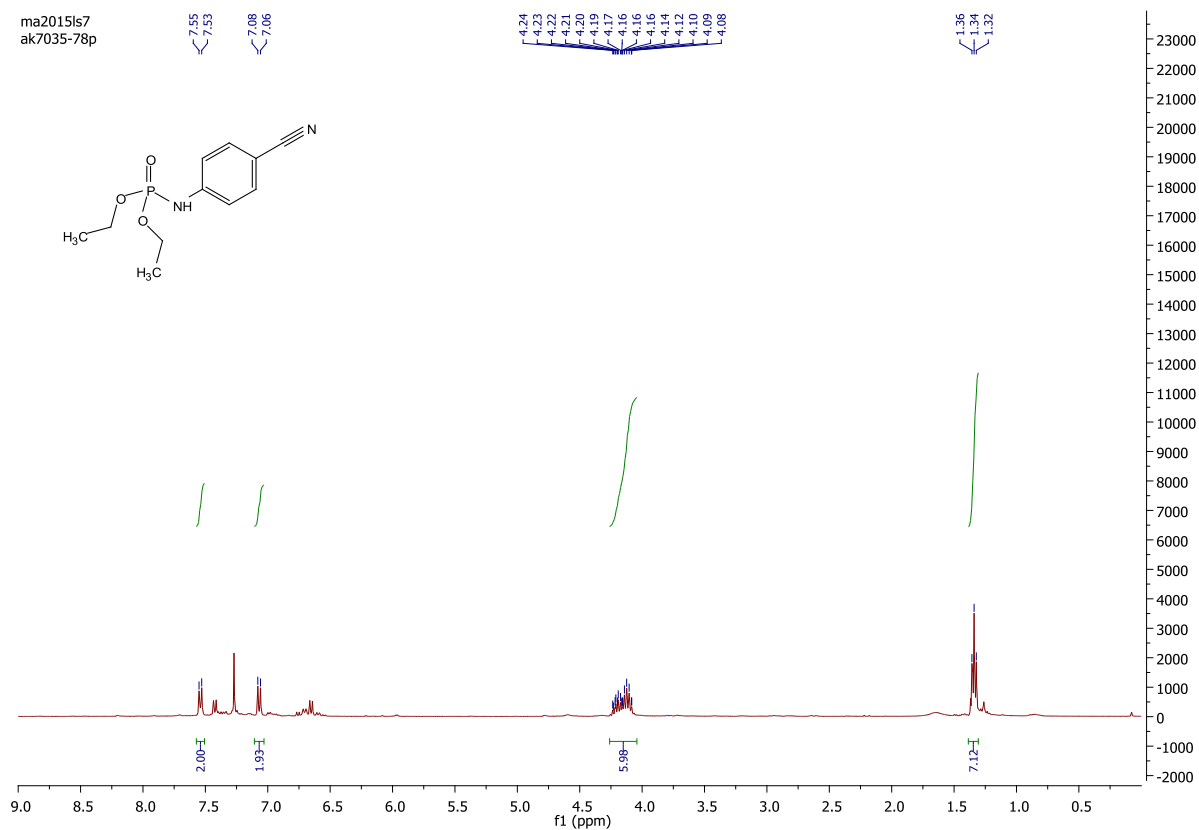
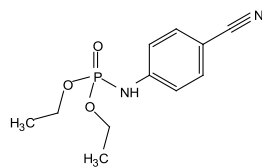
oc1915mm5
mm-7478-69



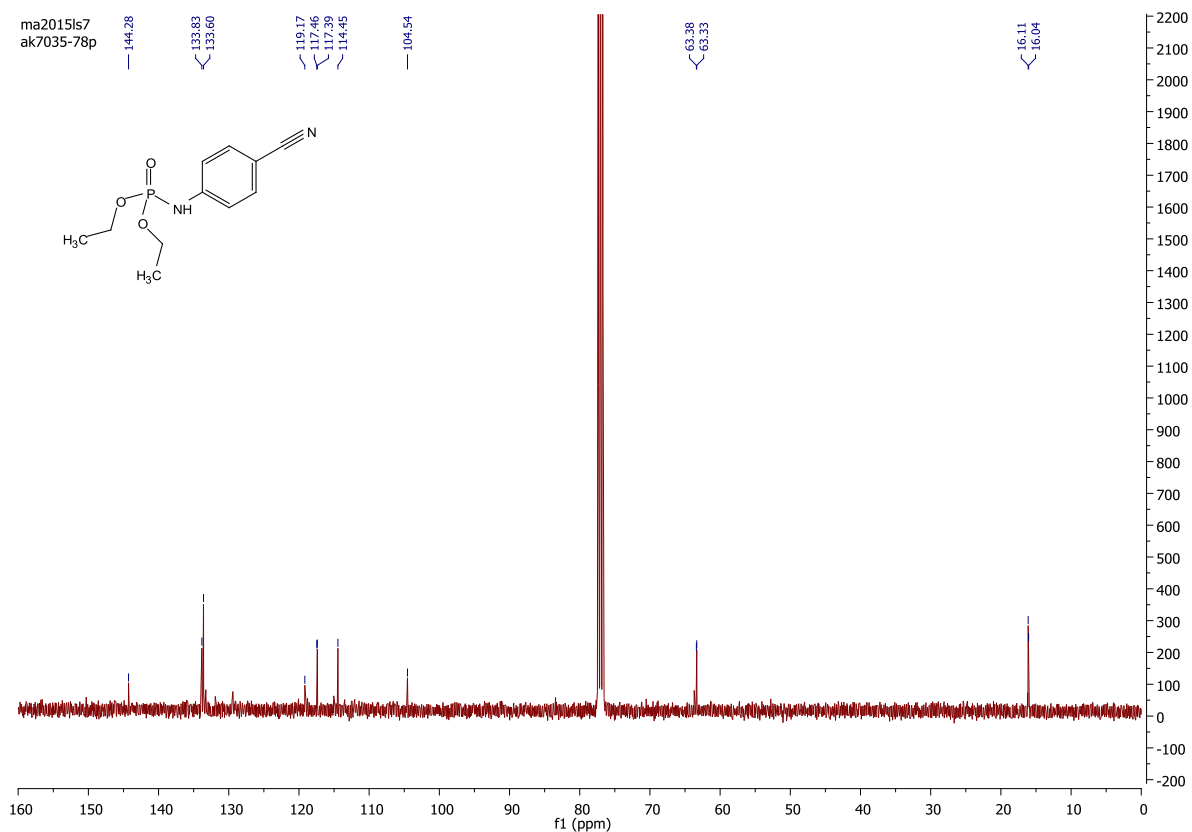
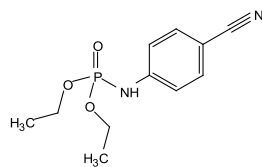
jy1815mm10
mm-7478-69pure



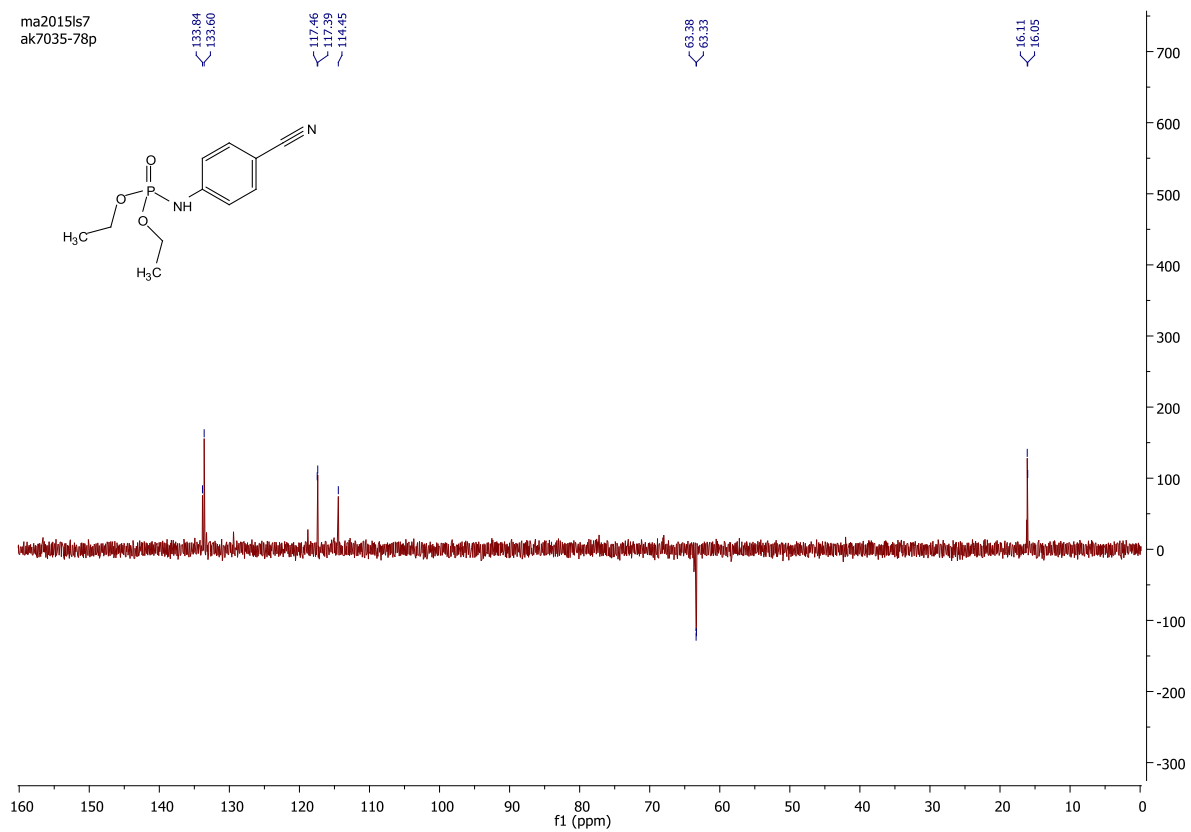
ma2015ls7
ak7035-78p



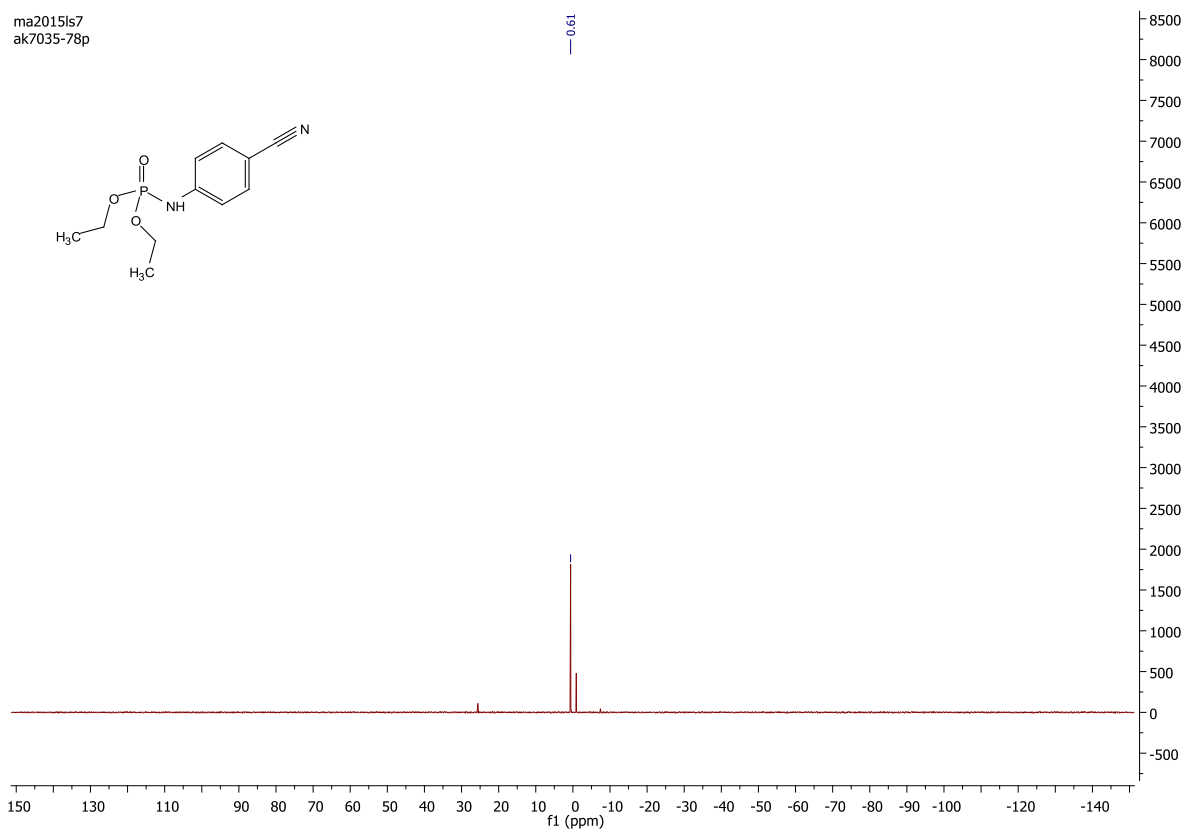
ma2015ls7
ak7035-78p



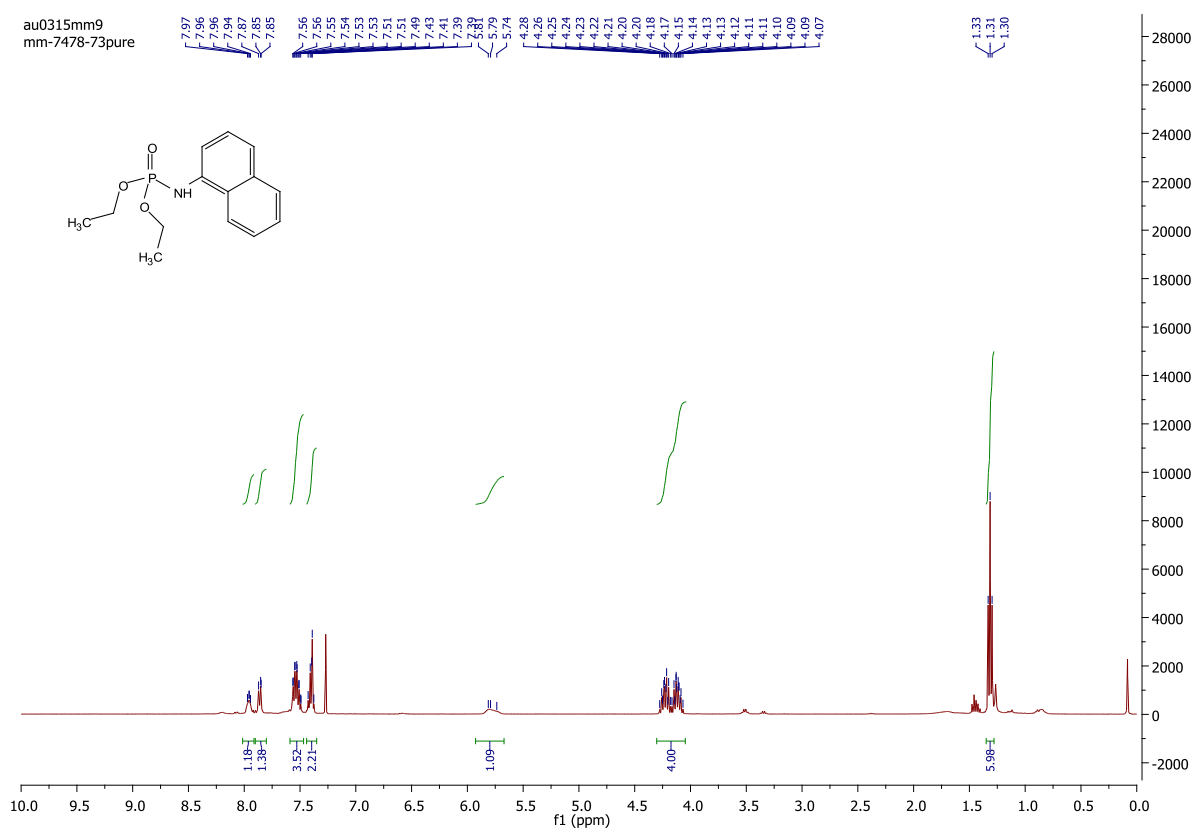
ma2015ls7
ak7035-78p



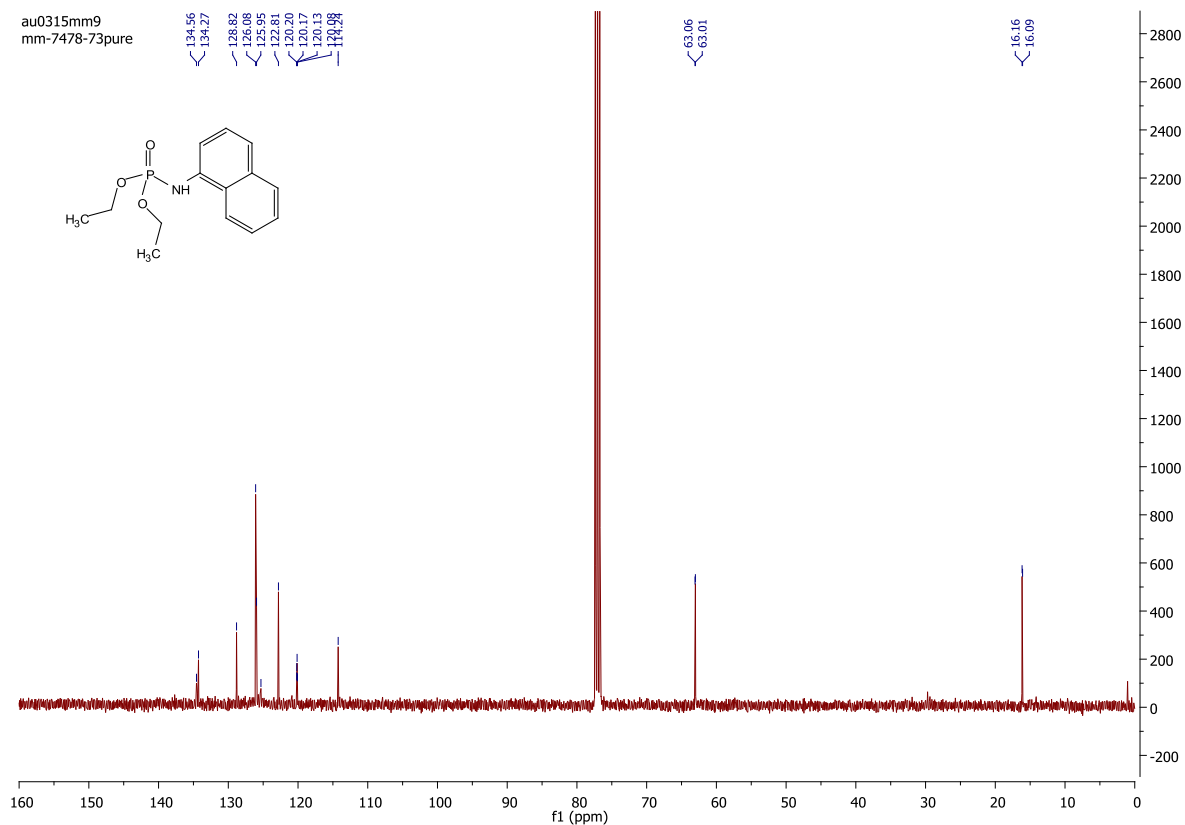
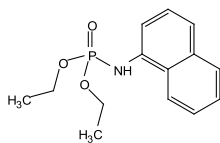
ma2015ls7
ak7035-78p



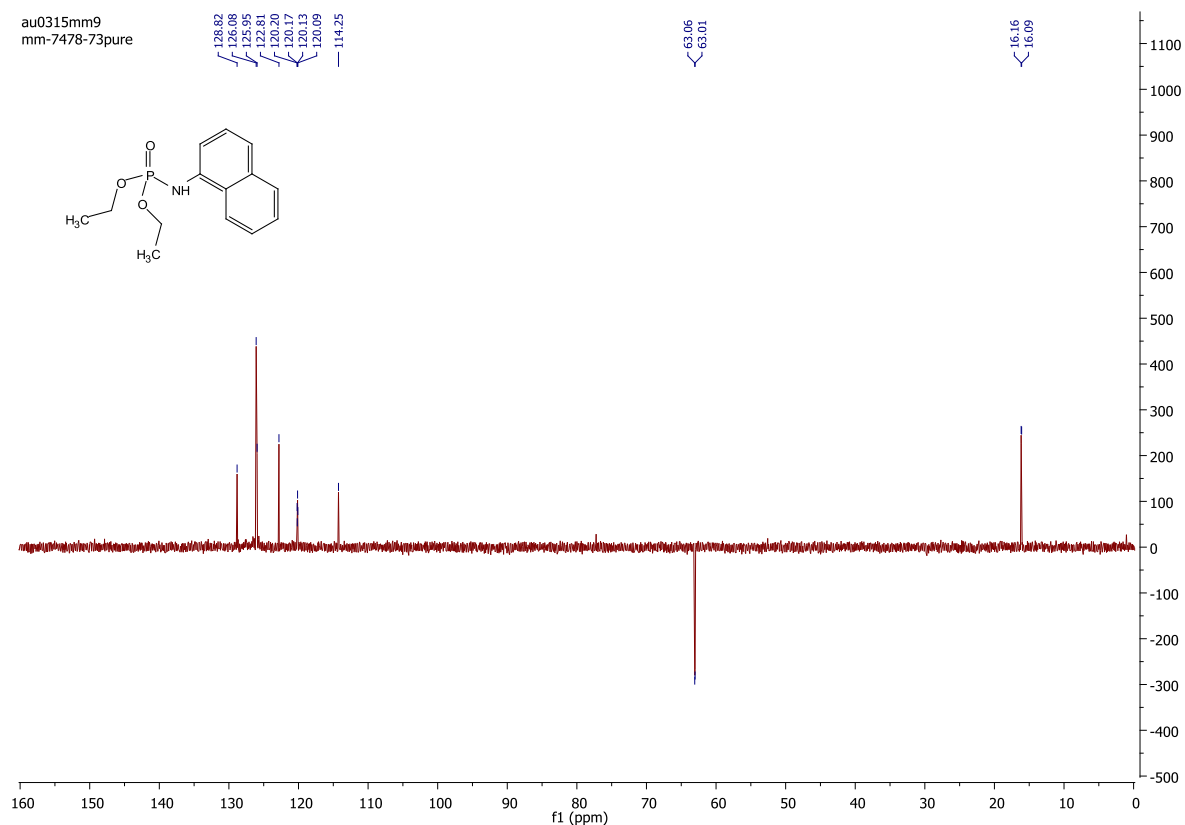
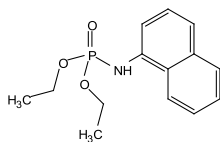
au0315mm9
mm-7478-73pure



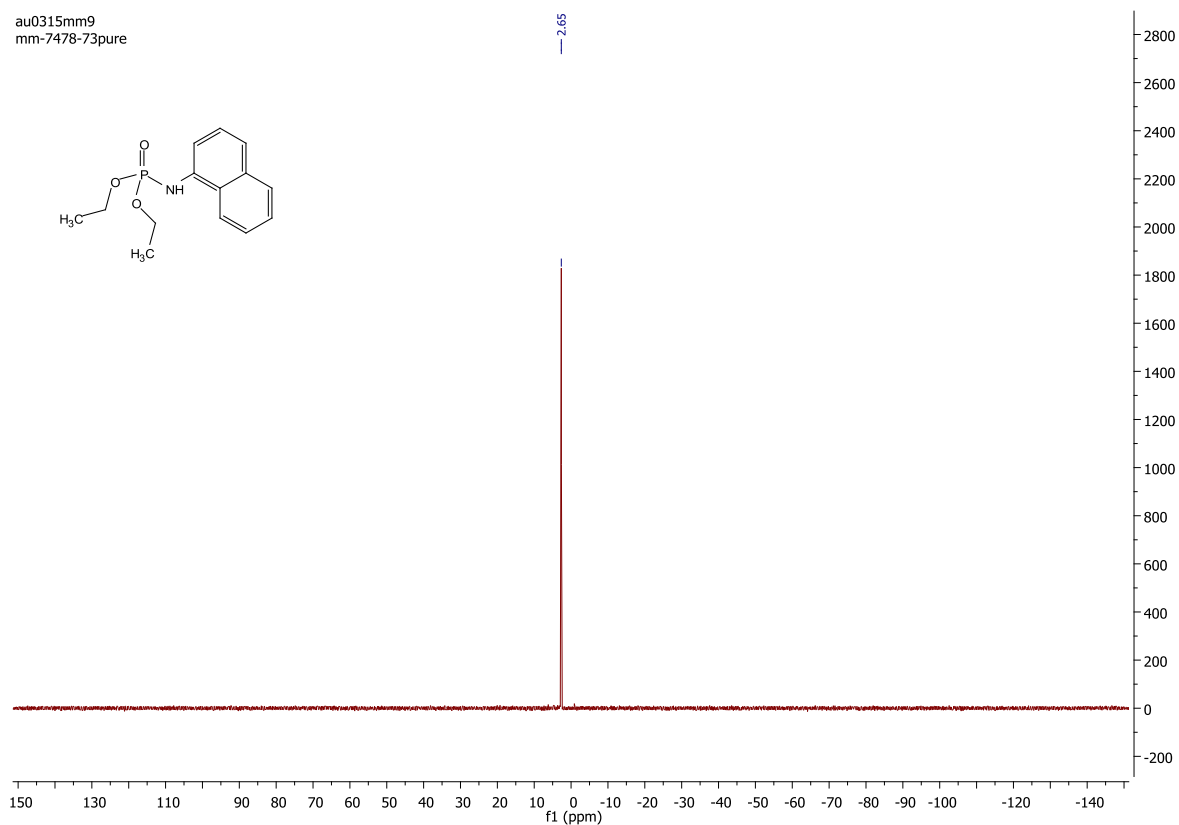
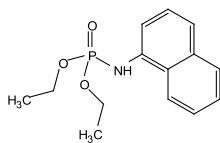
au0315mm9
mm-7478-73pure



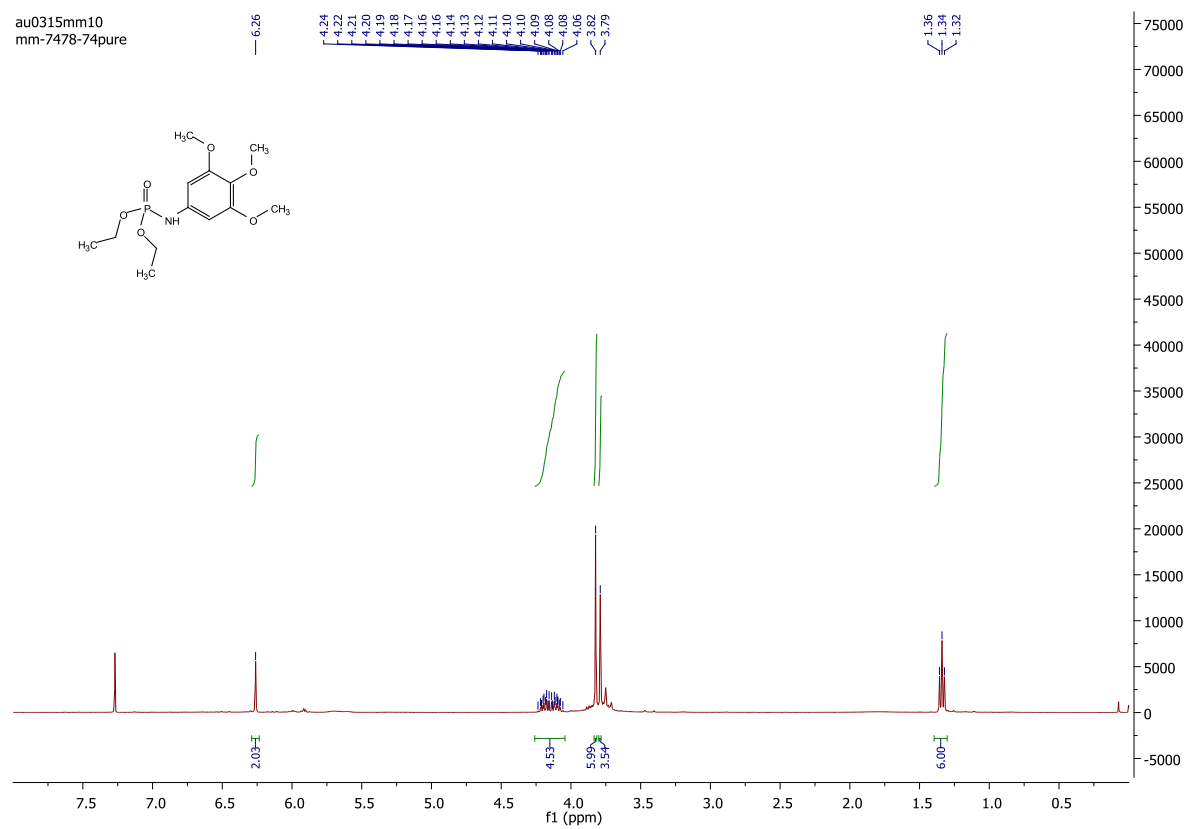
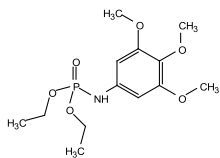
au0315mm9
mm-7478-73pure



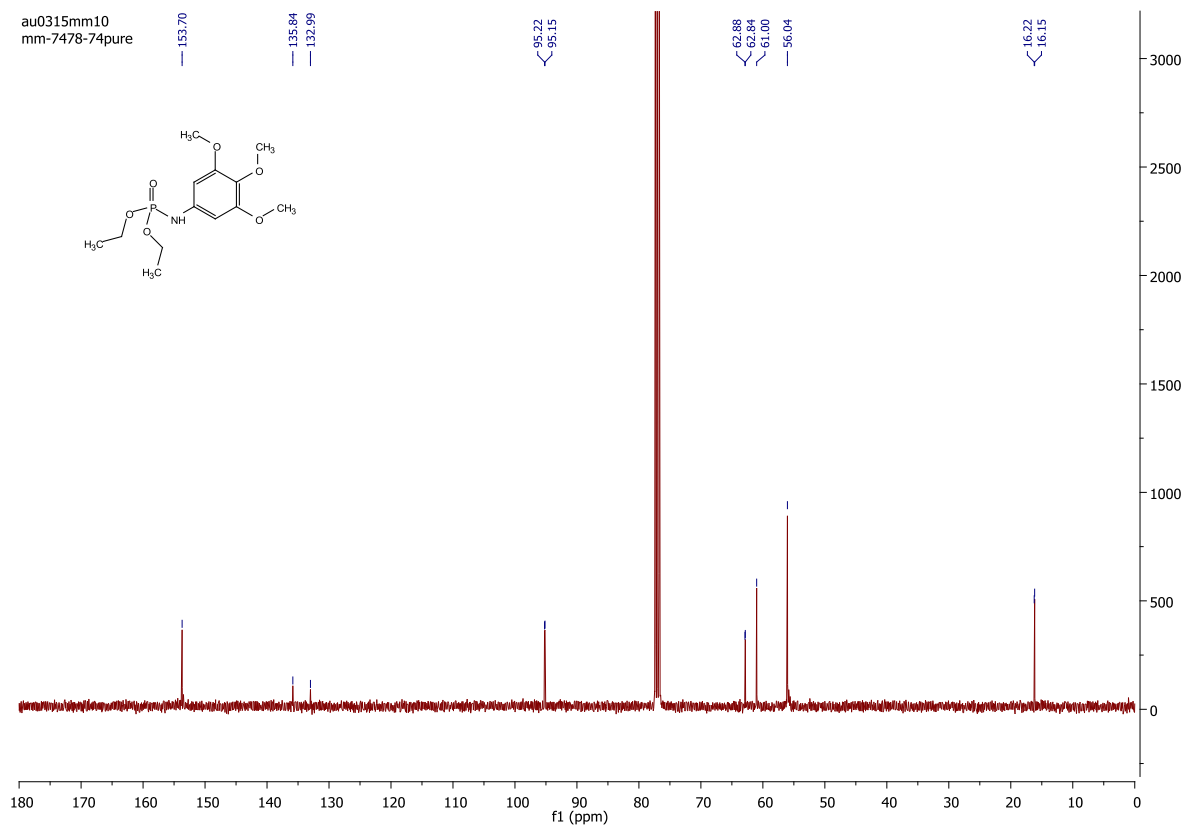
au0315mm9
mm-7478-73pure



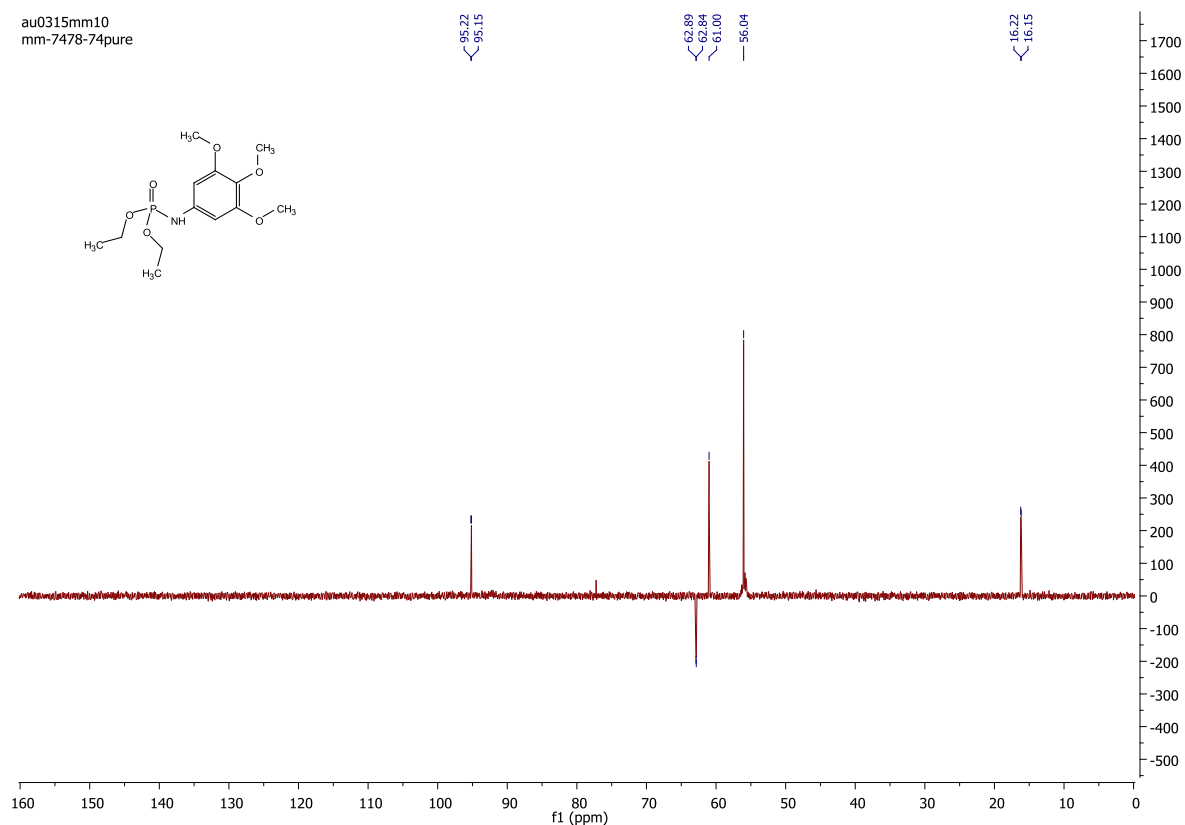
au0315mm10
mm-7478-74pure



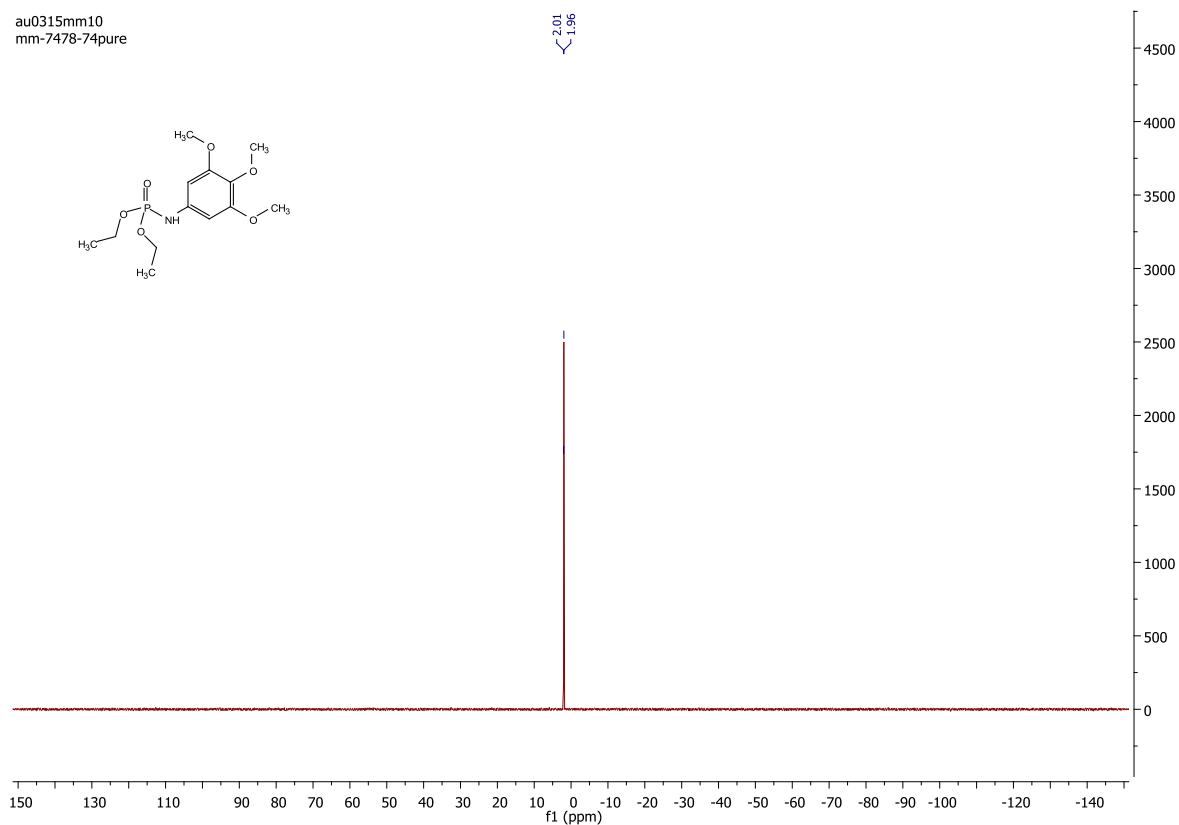
au0315mm10
mm-7478-74pure



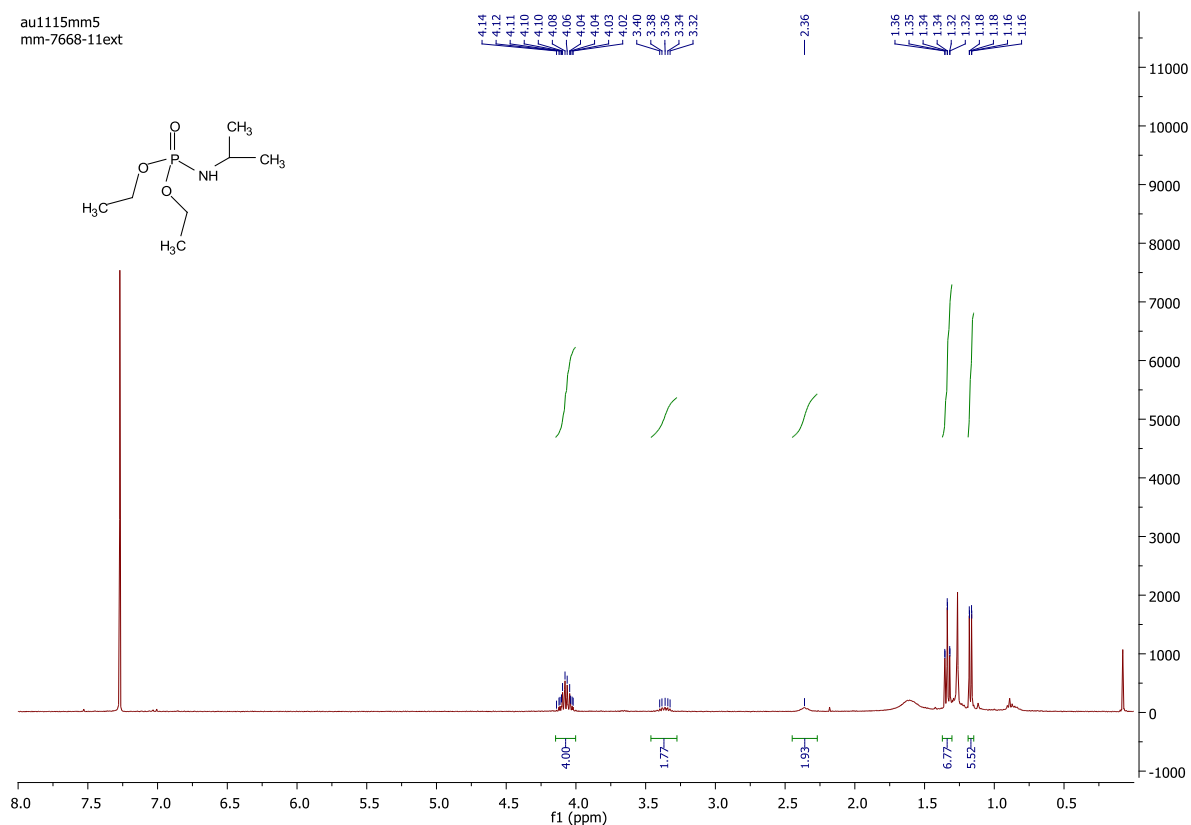
au0315mm10
mm-7478-74pure



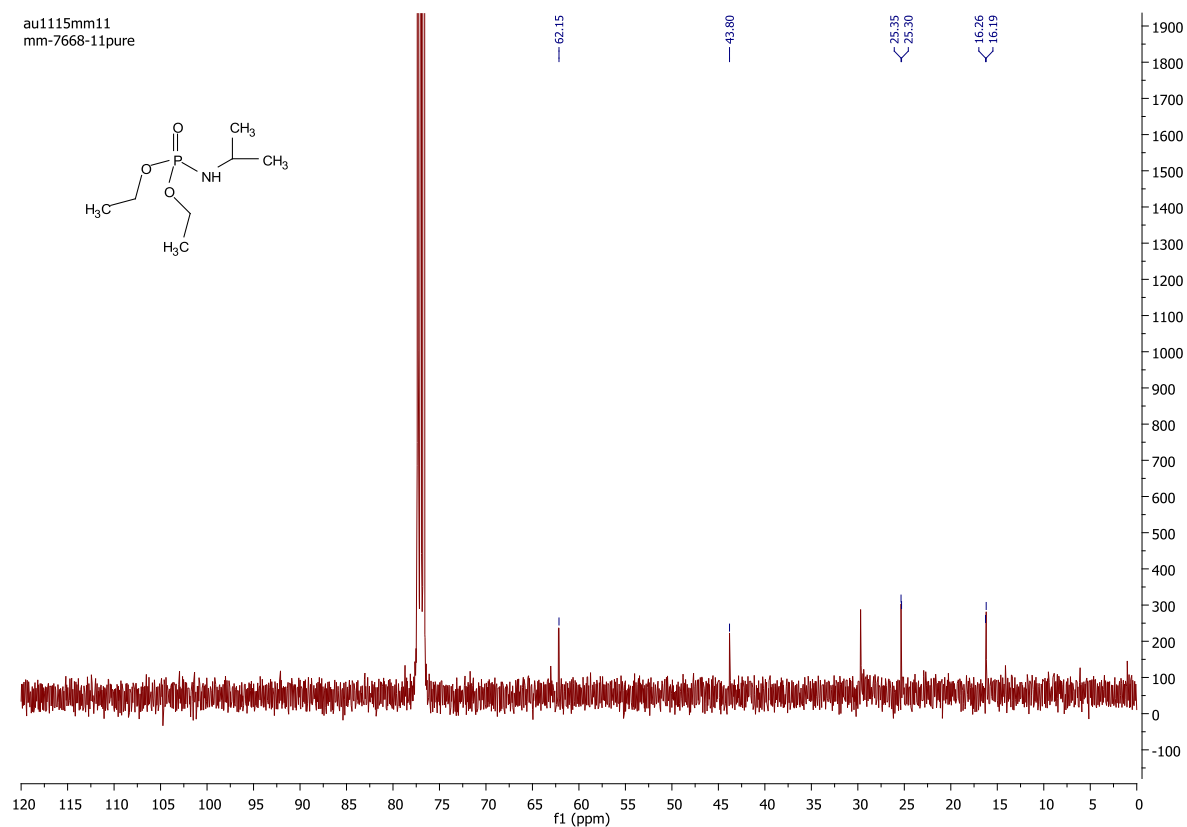
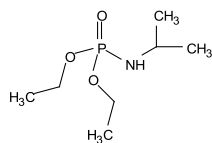
au0315mm10
mm-7478-74pure



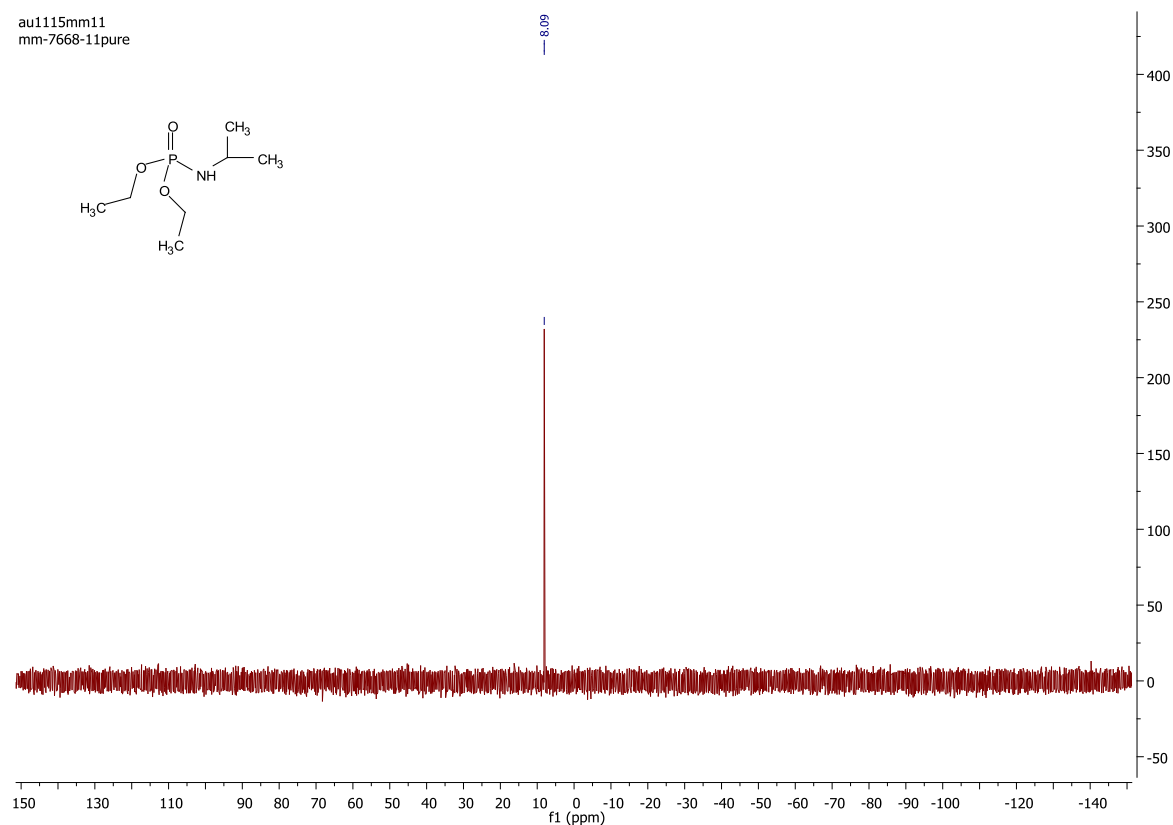
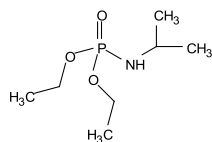
au1115mm5
mm-7668-11ext



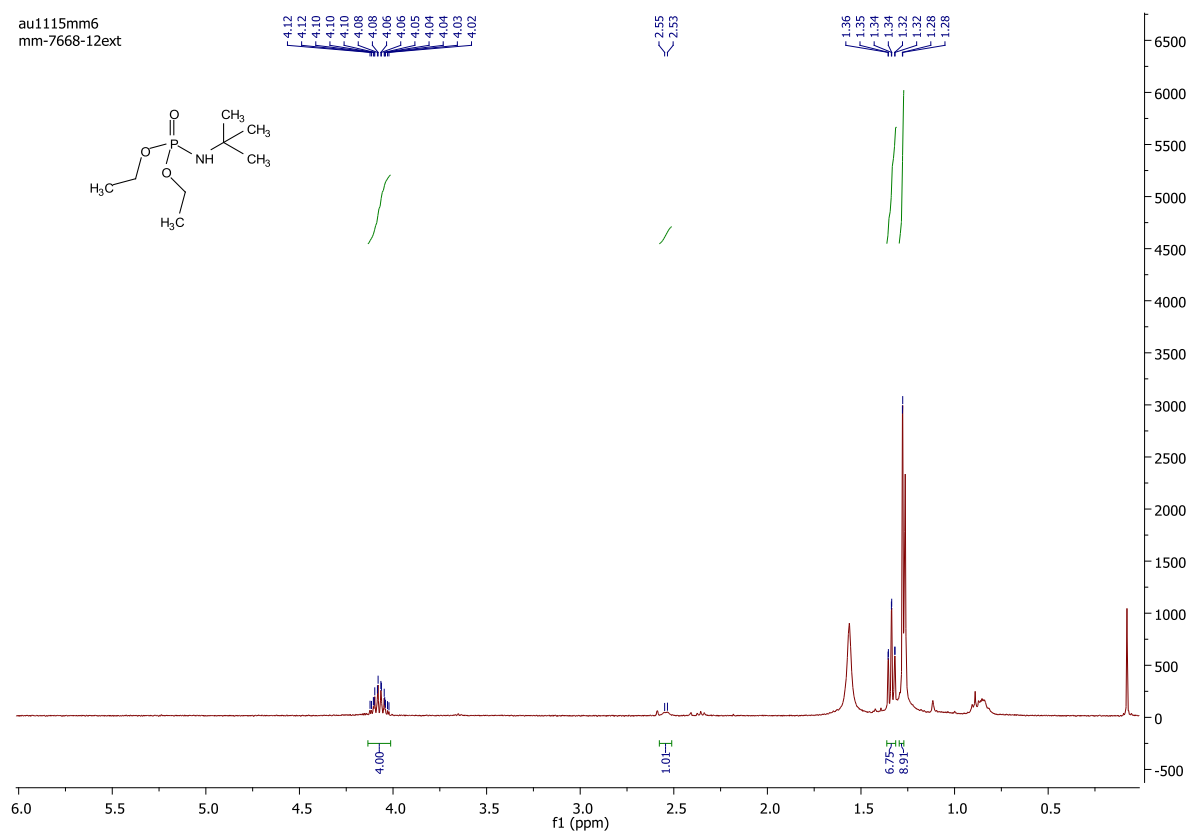
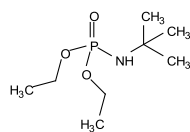
au1115mm11
mm-7668-11pure



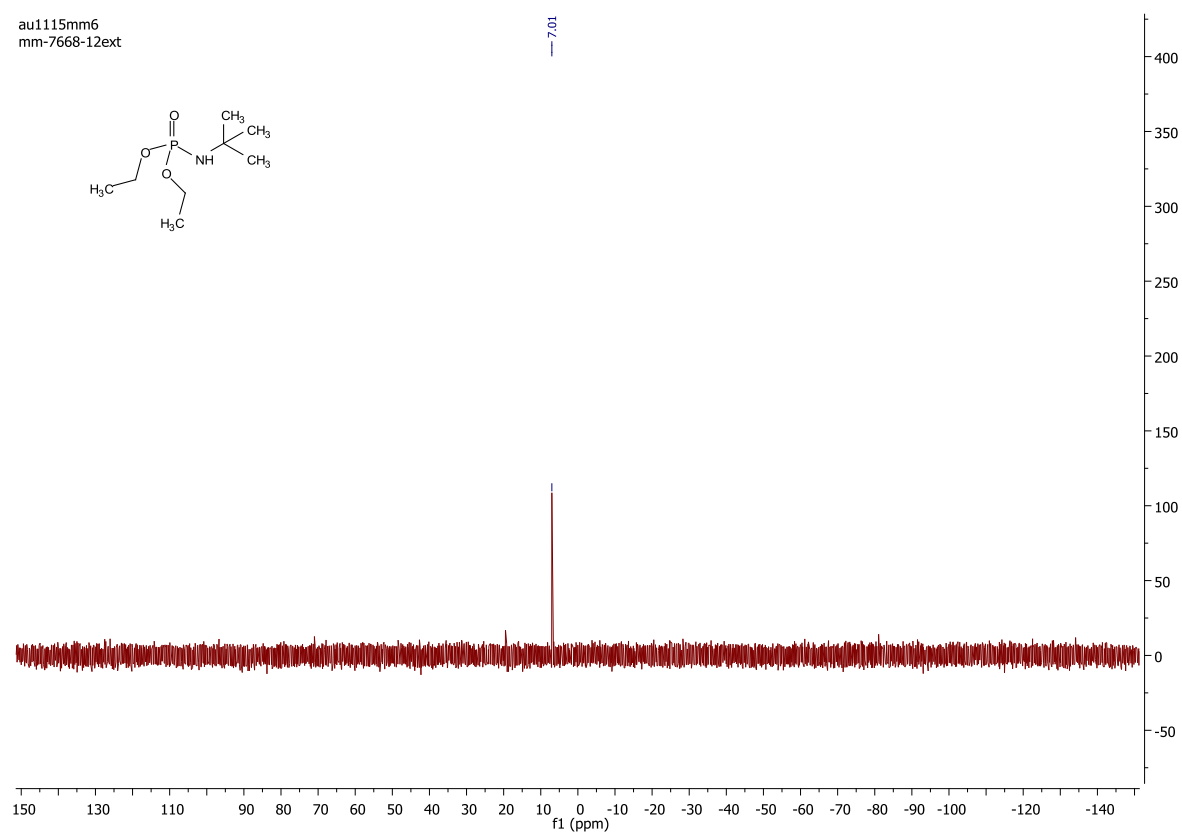
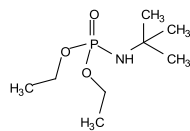
au1115mm11
mm-7668-11pure



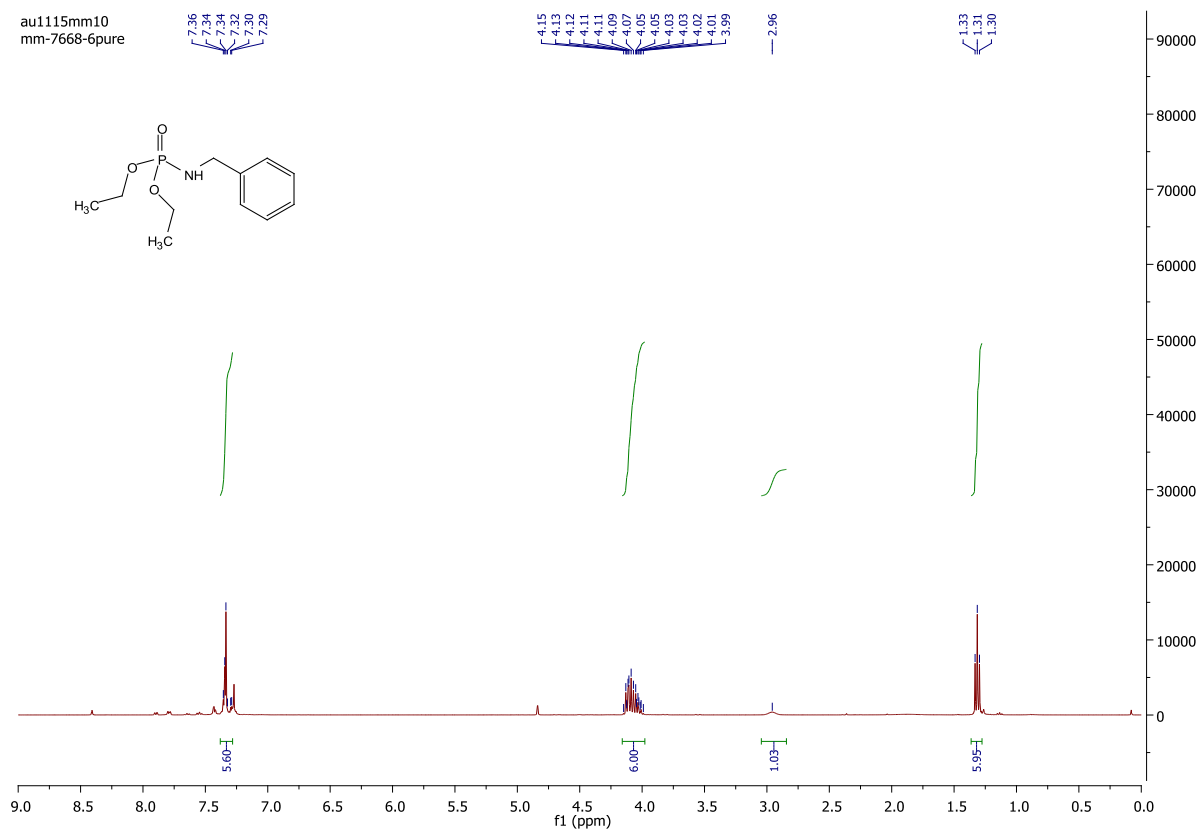
au1115mm6
mm-7668-12ext



au1115mm6
mm-7668-12ext



au1115mm10
mm-7668-6pure



au1115mm10
mm-7668-6pure

